METALLURGY AND METALLURGICAL ENGINEERING SERIES

ROBERT F. MEHL, PH.D., D.SC., *Consulting Editor*

STRUCTURE AND PROPERTIES OF ALLOYS

METALLURGY AND METALLURGICAL ENGINEERING SERIES

ROBERT F. MEHL—*Consulting Editor*

Barrett—STRUCTURE OF METALS

Brick and Phillips—STRUCTURE AND PROPERTIES OF ALLOYS, *Second Edition*

Briggs—THE METALLURGY OF STEEL CASTINGS

Butts—METALLURGICAL PROBLEMS *Second Edition*

Eckel and Raudebaugh—LABORATORY MANUAL IN METALLOGRAPHY

Heindlhafer—EVALUATION OF RESIDUAL STRESS

Kehl—THE PRINCIPLES OF METALLOGRAPHIC LABORATORY PRACTICE, *Third Edition*

Seitz—THE PHYSICS OF METALS

Williams and Homerberg—PRINCIPLES OF METALLOGRAPHY

STRUCTURE
AND
PROPERTIES OF ALLOYS

The Application of Phase Diagrams to the Interpretation and Control of Industrial Alloy Structures

BY

R. M. BRICK

Professor of Metallurgy; Director, Department of Metallurgical Engineering, University of Pennsylvania

AND

ARTHUR PHILLIPS

Professor of Metallurgy, Yale University

SECOND EDITION

New York · Toronto · London
McGRAW-HILL BOOK COMPANY, INC.
1949

STRUCTURE AND PROPERTIES OF ALLOYS

To

Champion Herbert Mathewson

PREFACE TO THE SECOND EDITION

No book in the fields of engineering and science written prior to 1942 can now be regarded as fully up to date; since that time too many developments have altered or modified previously accepted concepts. In the field of physical metallurgy, new alloys have been developed, but these do not necessarily involve new metallurgical concepts. On the other hand, further study of the transformation of austenite has elucidated the conditions for the formation of martensite with the result that the so-called *S curve* is now outmoded. The new understanding has not only necessitated a revision of fundamental theory but has made possible improved heat treatments involving martensite formation and incidentally has resulted in a new terminology supplanting the term *S curve*.

Developments of this nature have been deemed of paramount importance in writing a second edition of this book. New alloys and techniques now proved of engineering merit have been considered worthy of inclusion or expanded treatment. Examples of this are the Al-Mg-Zn-Cu alloy known as 75S, nonaging low-carbon steels, hardenability of steels, martempering, and "deep freezing" to eliminate retained austenite.

The use of the book as a text has indicated the necessity for expanding some sections originally too tersely presented for full understanding by the neophyte. A considerable amount of data has been added, mostly of laboratory type in tabular form to enable the inclusion of questions of an analytical nature, to reduce the necessity for other reference material, and to give specific dimensions to some textual statements of fundamental principles. New photomicrographs have been inserted to illustrate more fully the significance of certain metallurgical variables, and the detailed analyses of all micrographs have been rearranged to facilitate examination of structures while their descriptions are being studied. Finally, the sequence of presentation of some of the material has been altered; some rearrangement has been made to eliminate extraneous explanatory material and to enable the student to focus attention on the chief concepts under discussion.

Two entirely new chapters have been added to include alloys that by recent developments have attained industrial importance. The prep-

aration of the chapter on magnesium alloys was greatly aided by the contribution of photomicrographs of typical alloys by the Dow Chemical Company. The other new chapter on corrosion- and temperature-resistant alloys is necessarily somewhat incomplete because much of the fundamental theory is only now being developed by current research. Photomicrographs illustrating structural effects characteristic of many of these alloys have been supplied by the Universal-Cyclops Steel Corporation.

Expansion of the text has resulted in the inevitable difficulty of too much material for the usual one-semester course for engineering students. Therefore, each chapter has been set up in numbered sections to facilitate selective assignment of only a part of the text.

There has been no change in the underlying philosophy of the book: that to study alloys it is necessary to *understand* the significant phase diagrams, the structures associated with the diagrams, the properties characteristic of these structures, and the effect of processing variables on all three. The objective is not to present factual material but to present the sources of such material and enough theory for the engineering student to understand the bases and limitations of handbook data.

Lectures are a very poor educational means for attaining this type of understanding. Here, photomicrographs are designed to substitute for laboratory work or, far preferably, to extend laboratory experience beyond the scope attainable within the usual time or facility limits. The significant part of laboratory work, critical analyses of data, is represented here by questions placed at the end of each chapter. These have been increased in number and divided into two types: rather easy conventional questions or problems requiring no other reference work, and a group of more difficult questions involving use of concepts in a form not covered explicitly in the text.

The purely mental, analytical approach can save weeks and months of laborious tests, when enough fundamental data are available and all variables are properly evaluated. Yet it is seldom possible to evaluate quantitatively all variables; indeed, frequently some are forgotten or overlooked completely. The errors that then result have led to the saying, "one test is worth a thousand opinions." The plausibility of this aphorism should not exempt it from criticism—it might depend on how the test is made and who offers the opinion. Certainly the logical result of this approach would be a stultification of the imagination. On the other hand, by including a variable usually ignored, the authors in their own teaching always arrange some laboratory tests so as to yield

results different from those anticipated by the student. This does confirm the aphorism with a vengeance and ensures a more critical frame of mind on the part of the student.

R. M. BRICK
ARTHUR PHILLIPS

PHILADELPHIA, PA
NEW HAVEN, CONN.
April, 1949

PREFACE TO THE FIRST EDITION

The initiation of the Engineering, Science, and Management Defense Training Program, early in 1941, revealed a widespread interest in physical metallurgy applied to the control of metallurgical processes and the properties of industrial metals and alloys. Large plants with trained men adequate for normal production were forced to expand their technical staffs for increased production and thus faced the problem of training new men for specialized control work. Smaller plants that managed to meet the requirements of their normal peacetime production without trained metallurgists found that government contracts, or subcontracts, with definite metal specifications required men with a knowledge of the response of metals and alloys to variations in chemical composition and to mechanical and thermal treatments. Interest generally was about equally distributed between nonferrous and ferrous metals although, among the latter, tool steels were of far more importance than is represented by their percentage of the total steel production.

A course covering this field has long been given to engineering students at Yale University and was well adapted for more general purposes. The "Metals Handbook" of the American Society for Metals has been employed as a general reference and textbook, which necessarily involved supplementary lectures, mimeographed sheets, and photomicrographs. Since correlation of structures with phase diagrams is essential to an understanding of the basis of physical metallurgy and since no present textbook establishes that fundamental background in a manner readily understandable to the neophyte worker in metallurgy, it was felt that a book in this narrow field would be valuable, not only for defense training courses given to industrial employees but for general engineering students who will use metals and should understand the basis for compositions, heat treatments, structures, and properties.

The original mimeographed material which forms the basis of this book was first written in 1922 and has been subsequently revised at frequent intervals. Most of the large number of photomicrographs were prepared by Dr. D. L. Martin and Dr. R. G. Treuting, former graduate students in metallurgy. Many of the factual statements in the text

were derived from research papers by individuals working in this field, but, in view of the character of the book, few specific references to the original literature have been included.

R. M. BRICK
ARTHUR PHILLIPS

NEW HAVEN, CONN
September, 1942

CONTENTS

INTRODUCTION

> " . . . we as individuals differ to a great degree in the depth of understanding that satisfies our intellectual curiosity. A lot depends on what we have learned to accept as facts, because of frequent observation, without asking ourselves why or without being able, having asked the question, to answer why."
>
> JOHN L. CHRISTIE

Physical metallurgy is concerned with the properties of metals and alloys, as affected by composition and by mechanical and thermal treatments. Although the technological advances associated with the development of an ever-increasing number of alloys, specifically adapted for industrial usage, have received popular recognition, there is too little appreciation of the scientific approach to the problems of metal behavior.

In the short period of approximately fifty years, the metallurgist, by the accumulation and classification of voluminous data, has succeeded in establishing a systematization of knowledge that constitutes a science of metals. Certainly, present-day developments in physical metallurgy are motivated and directed by the systematic studies of the relationships between composition, structure, and properties of metallic substances. However, the status of metallurgy is not that of an independent science for its fundamental concepts have been derived by the intelligent application of three basic sciences: chemistry, physics, and crystallography.

The detailed and fragmental information acquired during the growth of a science generally leads to the adoption and standardization of forms and expressions for presenting the relatively few fundamental principles that are derived from an assembly and interpretation of experimental evidence. In physical metallurgy, the most basic expression is that embodied in the line drawings called *phase, equilibrium,* or *constitutional diagrams.* Homogeneous parts of a system that are separated from one another by definite physical boundaries are called *phases.* Although metallic phases, under nonequilibrium conditions, are not necessarily homogeneous, every phase is characterized by a distinctive atomic configuration of the material in which there may be continuous chemical and physical variations. A discontinuous change in type or spacing of atom packing is necessarily a phase change. Thus, a metal may exist in one

or more of three forms or phases; as a gas with no atomic bonds, as a liquid with loose or easily broken atomic bonds, and as a solid in which atomic bonds are strong and a fixed atomic structure exists. By using extremely high pressures, the ordinary atomic lattice or crystal structure of many pure metals may be altered, and this by definition constitutes a change in phase.

A binary alloy phase diagram shows for a system of two components (*e.g.*, chemically, water and salt, or metallurgically, copper and zinc) how changes in temperature of any specific alloy, or variations in the relative amounts of the two elements present, affect the number or composition of phases. A correlated knowledge of the crystallographic structures of the phases, of their preferred locations in the structure, and of their growth habits from the liquid or solid state makes it possible to predict in a qualitative manner the effect of temperature or concentration changes on the number, amount, size, or distribution of phases and thus the properties of the alloy. Actually, few industrial alloys consist of only two elements, since impurity elements are always present to some degree in commercial metals. However, the common impurities modify the phase diagrams only slightly, and most of the important alloys can be treated as binary.

The primary purpose of this text is to correlate, in a systematic manner, the alloy phase diagrams and property data that are available in many books, with selected photographs of the internal alloy structures at appropriate magnifications (enlarged 10 to 1,000 times). Not only are the alloy structures obtained under equilibrium conditions of extremely slow cooling, as required to conform with the phase diagrams, shown and discussed, but the more important nonequilibrium structures characteristic of many industrial alloys are reproduced. These illustrate the typical departures from a stable state frequently encountered when cooling conditions are rapid, on the order of or faster than those of sand casting or air cooling. When an understanding of the phase diagrams has been gained, it becomes possible to predict when the cooling rate is important and when it is not. Finally, some typical micrographs illustrating defective structures have been included to demonstrate the usefulness of the phase diagrams, correlated with a knowledge of the fundamental principles governing metal structures, in interpreting alloy failures. The scope of the book does not permit discussion of all metal problems or difficulties; only those specifically related to internal structures are mentioned.

Illustrative data on physical or mechanical properties have been included, in most sections of the book, in tabular rather than graphical

form. Although it is easier to grasp the significant trend of property changes with composition, etc., from drawings, the original data obtained by tests are always in tabular form, and it is believed the student may gain more by taking this material and plotting it himself than by studying charts.

The effort to focus attention upon the relationship between microstructures and properties, together with the actual application of phase diagrams in qualitatively predicting these effects, has led to a book with well-defined limits within which an attempt has been made to be reasonably comprehensive and complete for student or more general uses. At the same time, to preserve a compact treatment, it appeared undesirable to attempt either a quantitative reproduction of all the data available on alloy properties or a detailed discussion of important, related manipulative techniques such as testing and temperature measurement. The "Metals Handbook," of the American Society for Metals, which contains the most complete compilation of data on metals and alloys but is lacking in respect to microstructural effects and their causes, should be available to anyone working with metals.

For a detailed discussion of theory and practice in the field of physical metallurgy, Doan and Mahla's "Physical Metallurgy" or Sachs and Van Horn's "Practical Metallurgy" is recommended, or, in the field indicated by its title, Sisco's "Modern Metallurgy for Engineers." "Modern Uses of Nonferrous Metals" (AIME) describes the development of useful metal and alloy products in a nontechnical, narrative style. Engineers interested in metal specifications should consult the American Society for Testing Materials (ASTM) volumes of Tentative Standards or the Society of Automotive Engineers (SAE) "Specifications Handbook." Finally, if some understanding of the fundamentals of physical metallurgy is obtained from this book, men working with metals will be in a position to profit from the many technical publications of the American Institute of Mining and Metallurgical Engineers (AIME), the American Society for Metals (ASM), and, in allied fields, publications covering foundry practice, heat treating, etc., or journals of general coverage such as *Materials & Methods*.

CHAPTER 1

REQUISITE TOOLS OF THE METALLURGIST

Each section of this book devoted to specific alloy systems is subdivided into three parts entitled Phase Diagram, Structures, and Properties. An understanding of the material included under each of these headings requires a prior knowledge of methods of acquiring the significant data by direct or indirect measurements and observations. All methods employed to obtain data for the construction of phase diagrams, as well as the application of these diagrams in heat treatment procedures, require accurate measurement of temperature. Structures are visually observed by the use of polished specimens and a reflecting type of microscope. Properties are most commonly evaluated in terms of strength and hardness characteristics. The techniques used in each of these fundamental fields may influence the results obtained.

1.1 Pyrometry

Temperatures of from −40 to 400°C can be measured with thermometers having a liquid that expands in a calibrated pyrex-glass capillary tube. For temperatures below −40°C or up to about 1600°C, the thermoelectric pyrometer is generally used. This instrument includes a *thermocouple*, two wires of dissimilar metals or alloys usually welded together at one end, which is placed at the point where a temperature measurement is desired. An instrument for measuring millivoltages is connected across the other ends of the wires. As the temperature of the welded end is increased while that of the ends connected to the instrument is held constant, a current tends to flow in the wire. The voltage causing the flow increases with the temperature of the hot junction. The voltage-temperature relationship is thus the basis of measurement of temperature. Because the relationship is not linear for the useful operating range of the wires employed, tables of voltage vs. temperature for each combination of dissimilar wires, or calibration of the setup, must be used.

Table 1.1 shows temperature-millivoltage relationships for common thermocouples in their useful operating ranges. The copper-constantan

couple when used above 350°C has a rather short service life as a result of rapid oxidation of the copper. The iron-constantan couple has the advantage of a very high millivoltage change per unit temperature change. It has a short life at temperatures above 750°C in an oxidizing atmosphere but offers a longer life than chromel-alumel couples in reducing atmospheres (containing appreciable amounts of carbon monoxide or hydrocarbons) at temperatures up to 1000°C. Chromel-alumel couples are superior to iron-constantan in oxidizing atmospheres in the temperature range 650 to 1200°C and may be used intermittently up to 1300°C. Platinum-platinum rhodium or noble metal couples are expensive and, being readily contaminated, must be protected at all times. However, they are the best choice for service in the range 1100 to 1600°C. All thermocouples used near their maximum operating temperature show a drift in emf values at constant temperature even when used under normal conditions, *i.e.*, an oxidizing atmosphere.

Millivoltages may be measured with a millivoltmeter or a potentiometer. Recording-type instruments are available that will also operate controls to maintain the temperature of the thermocouple at a constant predetermined point and in addition raise to or lower from this temperature at a selected rate. Detailed information regarding these instruments may be obtained from the several pyrometer manufacturers.

Calibration of the original thermocouple and instrument and repetition of this at intervals are always desirable for the following reasons:

1. The hot-junction weld may be imperfect and result in low voltage readings with millivoltmeters.

2. No two sets of wire, even from the same source, are necessarily identical in composition, and slight variations may be responsible for voltage differences equivalent to as much as 10°C at high temperatures, *e.g.*, 1000°C.

3. The temperature-voltage relationship of thermocouples may change if the wires are contaminated by contact with certain gases (particularly carbon monoxide), by alloying upon contact with liquid metals, or simply because of inherent drift.

Calibration may be performed by comparison at various temperatures with a standardized instrument and couple or by determining the indicated freezing point of substances with known freezing points. Pure metals are customarily used, and it is essential that the calibrating substance be of the same purity as the one whose temperature is known. For example, pure copper freezes at 1083°C, but when melted in air, the liquid metal dissolves oxygen and the Cu:O alloy may freeze at as low as 1065°C.

TABLE 1.1

Temperature		Millivoltage (cold junction 0°C)				
°C	°F	Cu-constantan	Fe-constantan	Chromel-alumel	Pt:Pt 10 Rh	Pt:Pt 13 Rh
−200	−328	5.54				
−150	−238	4.60				
−100	−148	3.35				
− 50	− 58	1.81				
0	32	0.00	0.00	0.00	0.000	0.000
50	122	2.03	2.60	2.02	0.299	0.297
100	212	4.28	5.28	4.10	0.643	0.646
150	309	6.70	8.02	6.13	1.025	1.039
200	392	9.29	10.78	8.13	1.436	1.464
250	482	12.01	13.54	10.15	1.867	1.918
300	572	14.86	16.30	12.21	2.316	2.394
350	662	17.82	19.06	14.29	2.778	2.889
400	752	20.80	21.82	16.39	3.251	3.398
450	842	23.98	24.58	18.50	3.731	3.921
500	932	27.21	27.39	20.64	4.219	4.454
550	1022	.....	30.25	22.77	4.716	5.002
600	1112	....	33.16	24.90	5.222	5.561
650	1202	.....	36.13	27.03	5.737	6.135
700	1292	. ..	39.19	29.14	6.260	6.720
750	1382	.....	42.32	31.23	6.790	7.317
800	1472	.....	45.48	33.31	7.330	7.927
850	1562	....	48.65	35.35	7.878	8.546
900	1652	.....	51.82	37.36	8.434	9.177
950	1742	.....	54.99	39.35	8.998	9.817
1000	1832	.....	58.16	41.31	9.569	10.470
1050	1922	.....	61.33	43.24	10.149	11.135
1100	2012	.....	64.50	45.14	10.736	11.811
1150	2102	.....	.....	47.01	11.329	12.493
1200	2192	.....	.....	48.85	11.924	13.181
1250	2282	.....	.....	50.65	12.522	13.871
1300	2372	.....	.....	52.41	13.120	14.563
1350	2462	.....	.....	54.13	13.717	15.252
1400	2552	.....	.....	55.81	14.312	15.940
1450	2642	.....	.....	.....	14.906	16.631
1500	2732	.....	.....	.....	15.498	17.316
1550	2822	.....	.....	.....	16.087	18.000
1600	2912	.....	.....	.....	16.674	18.680
1650	3002	.....	.....	.....	17.259	19.357
1700	3092	.....	.....	.....	17.841	20.032

* From "Standard Conversion Tables," No. 31031, Leeds and Northrup Company.

In addition to the thermometer and thermoelectric pyrometer, there are resistance-wire pyrometers for use at low to moderate temperatures, and optical (disappearing filament) and radiation pyrometers for use above a moderate red heat (800°C) to 3000°C or above. The thermocouple type is by far the most widely used because of its relatively low cost, high accuracy (when properly employed), and the fact that its operating range permits it to be used in the control of most metallurgical processes. One last word as to its proper use deserves particular emphasis: the instrument records only the temperature of its "hot junction," which is not necessarily the same as that of the metal being treated. This difficulty may be avoided by setting the hot junction of the couple in the center of the charge, if possible, or by circulating the heating medium (gas or liquid) so as to obtain temperature uniformity. The wires must be insulated from each other to ensure that the active hot junction is at the welded tip. If a metal or refractory tube encloses the thermocouple to protect it from contamination by gases or liquid metals, time is necessary for the temperature to become equalized inside and outside the protection tube. There may be large differences in the temperature of metal at different points in a large furnace or a large crucible, and for uniformity of heating, tests must be made to determine if gradients exist and their extent.

1.2 Microscopy or Metallography

The word *metallography*, formerly applied to the entire field of physical metallurgy, is now generally restricted to the field of microscopic work. The internal structure of metals and alloys is revealed by magnifying a polished or a polished and etched surface. The preparation of this surface is of great importance since variations in technique may distort or exaggerate essential parts of the structure.

Essentially, polishing for structural observations requires the attainment, or approximation, of a mirrorlike surface by cutting away normal irregularities rather than by causing high areas to flow into low areas, as in buffing. Flow distorts the surface and may lead to entirely erroneous conclusions as to the characteristics of the structure (see page 243). The first stages of cutting the surface to a plane are usually accomplished by grinding with successively finer grades of abrasives cemented on paper. The direction of cutting is altered at each change to a finer abrasive to facilitate recognition of the stage when coarser or deeper scratches have been replaced by more shallow ones characteristic of the finer abrasive. Micrographs 1.1 to 1.3 show the surfaces of a cast brass, at a magnifica-

tion of 50 diameters, after grinding with Nos. 0, 00, and 000 emery papers, respectively.

Finer abrasives than No. 0000 cannot be obtained mounted on paper. It is frequently found that even this grade is not too uniform, with the result that coarser scratches may be present than those left by the No. 000 paper. The final approximation to a mirror surface must be obtained by other means, usually by use of a rotating wheel covered with a special cloth that is charged with abrasive particles, carefully sized by levigation in water or equivalent methods. Two different wheels may be used: first, one with a relatively coarse abrasive; later, a wheel charged with a finer particle size.

It is impossible to learn how to prepare a specimen for good microscopic work by reading a book. Results are obviously affected by coarse dust particles in the air settling on fine papers or cloth laps, or equivalently, by carrying coarser particles on the specimen to the next finer paper or lap. Chemical changes may affect some abrasives; *e.g.*, fine magnesium oxide used as a final polishing abrasive may pick up carbon dioxide from the air or water to form coarse particles of magnesium carbonate that ruin the surface. The type of cloth is important and, when a metallographer finds a type particularly suited for his work, he will be wise to lay in a stock of it. Finally, the pressure used by the individual in holding the specimen on the cutting papers, or laps, has a considerable influence on the results. Too little pressure retards the rate of polishing and leads to pits in the final surface. Too much pressure causes local overheating and severe distortion to an appreciable depth. The correct degree of pressure varies for different metals, and this can be learned only by actual polishing (and for a considerable time, by repolishing!).

The method of polishing outlined above was used in the preparation of all structures reproduced in this book. It can give good results when employed by experienced operators. There are other methods superior in many respects to this one. Lead laps, charged with abrasives, may largely replace the abrasive papers with a gain in speed of polishing, flatness of the specimen, and preservation of small, brittle inclusions in the structure by minimizing the time required on the cloths. Practically complete freedom from distortion is possible by electrolytically removing the flat striated surface obtained from a No. 000 emery paper or its equivalent.

The electrolytic polishing of metal specimens by controlled anodic corrosion in an electrolyte is a relatively new development requiring

special equipment that has only recently become available in a standard form. Procedures involving optimum composition and temperature of the electrolyte, current density, voltage, and time may be described in manufacturers' literature, research papers, and the ASTM Standards. Electrolytic polishing may save considerable time and labor, but its chief advantage is the absence of any surface distortion. It is, therefore, most valuable in polishing soft metals such as pure aluminum and zinc, or metals whose structures are particularly subject to alteration by distortion, such as stainless steels. The method is also being commercially employed to replace buffing where the shape of the part makes that operation difficult to perform, *e.g.*, at inside corners of rectangular sections.

The polished surface, however prepared, must be etched before any details of the structure become evident, unless there are moderately coarse sections of the surface whose hardness is very different from the remainder. If part of the structure is harder (oxide inclusions in metals, page 45), it will not wear away so rapidly as the softer matrix and will be left standing in relief. If it is softer (graphite in cast iron, page 451), it will wear away to a greater depth than the matrix and again be visible by a relief effect. Otherwise, the mirrorlike surface shows no structure until a chemical solution that reacts somewhat with the metal is placed on the surface (or the specimen may be heated in air or vacuum in some cases). The chemical will differentially attack parts of different chemical composition, or reactivity, to reveal the structural condition. The chemical agent is called an *etchant* or etching solution.

In succeeding chapters of this book, photographs of the microstructures of most of the important metals and alloys are reproduced and, in each case, the etchant employed is specified. A brief list of other etchants is also given with the particular utility of each indicated. The time or depth of etching and the type of etchant used are determined mainly by the magnification at which the structure is to be examined. If it is to be studied by the naked eye or at magnifications of less than 25 diameters (*macroscopic* examination), the specimen is usually etched deeply to increase the contrast in appearance of sections attacked at different rates. Structures magnified more than 25 diameters are called *micrographs* (micros.). If the magnification is in the range of 50 to 100 diameters, the specimen is usually given a moderately deep etch to obtain contrast. Very fine structures, that must be magnified 500 to 1,000 times, would be so roughened by a contrast etch, however, that details would be obscured. A relatively light etch is employed in these cases.

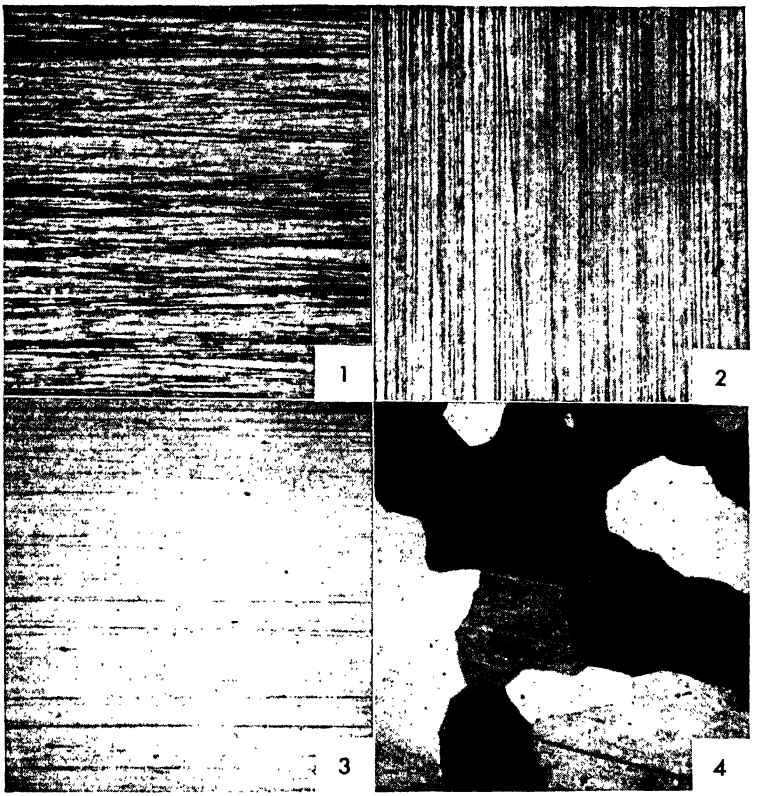

Micros. 1.1 to 1.4. Photographs of cast brass at ×50 magnification and at different stages of polishing: (1.1) after No. 0 emery paper; (1.2) after No. 00 emery paper; (1.3) after No. 000 emery paper; (1.4) after polishing on broadcloth with levigated alumina and etching with a solution of ammonium hydroxide and hydrogen peroxide.

The appearance of the unetched specimen (Micro. 1.1) is not reproduced since its uniform surface did not reveal any structural details. Etching fairly deeply in a mixture of ammonia and hydrogen peroxide has revealed a coherent group of polygonal areas, each shaded somewhat differently. The different areas are actually identical in composition and structure; each represents a crystal whose axes are at different angles with respect to its neighbors and the surface (see page 26). This particular etching solution attacks different crystal faces at a different rate and thus tends to outline a specific crystal face. A crystal in which the outlined face is parallel to the surface of polish has a maximum flatness and, relatedly, reflectivity for light, which causes it to have a bright appearance. If, in a different crystal, the outlined face is tilted away from the polished surface, that grain has a roughened or saw-tooth type of surface that does not fully reflect light to the observer's eye. Such crystals will appear dark to varying degrees, depending on the extent of etching and the actual angle of the outlined faces to the surface. Not all etching solutions have this effect of "darkening" crystals of differing orientations (*e.g.*, see photographs of iron in the next chapter). Incidentally, Micro. 1.4 shows many striations, inclined slightly from the horizontal. These are scratches that were covered by flow during the final polishing and were then revealed by the etch, which removed much of the distorted surface layer. The identification of the lines as scratches is primarily based on the fact that they cross crystalline grain boundaries with no change in direction.

Metallurgical microscopes differ only in details from those used in other types of scientific work. Light, from an electric bulb or a carbon arc, is focused by a lens (objective) on the specimen, reflected through the same lens, diverted from the original path by a prism or reflector, and passed through a second lens (ocular) to the observer's eye or to a photographic plate for permanent recording. Williams and Homerberg[1] include a detailed description of metallurgical microscopes. Assuming that the lenses are of good optical glass, ground to correct curvatures and corrected for distance and color distortions, the chief factor in preparing good photomicrographs is illumination with the proper quantity of light, correctly centered with respect to the lens system.

A few specific remarks concerning use of the metallographic microscope may be helpful. The magnifications employed most commonly, together with the lens system required, are as follows:

[1] "Principles of Metallography," McGraw-Hill, 5th ed., 1948.

a. ×75—grain size of brasses; 16 mm or ×8(0.20 N.A.)[1] objectives, ×5 or ×7.5 ocular.

b. ×100—grain size and general structures of steels; 16 mm or ×8(0.20 N.A.) objectives, ×10 ocular.

c. ×250 to ×500—details of most alloys, combining a moderately large field together with good resolution of detail; 8 mm, ×21(0.40 N.A.) or ×41(0.65 N.A.) objectives, ×10 ocular.

d. ×750 to × 1,000—fine structures; 4 mm or ×62(0.95 N.A.) objectives, ×10 to ×15 ocular.

e. ×1,000 to ×2,000—very fine structures; 2 mm or ×85(1.30 N.A.) oil immersion objectives, ×15 ocular.

Thus four objectives and three oculars could cover the useful range of photomicrographic work. In many cases, the same magnification can be attained by several combinations of objective, ocular, and bellows extension. For structural details, however, the objective lens is the critical point. Increasing the ocular or extending the bellows merely "blows up" the image, and it is usually considered that 1,000 times the numerical aperture represents the maximum useful magnification. This means that with the best apochromatic objective and blue light (the shorter the wave length, the better the resolution), about ×1,500 will give all the detail obtainable from ordinary microscopes. More significantly, the details of structure smaller than about 0.00003 cm or on the order of 1,000 atoms or less will not be directly visible.

For greater magnifications, electromagnetic waves of much shorter length than those of visible light must be used. Actually, electron beams with a wave length of about 50 to 200 Å[1 Å = $(10)^{-8}$ cm] in comparison with about 3000 Å for blue light are used. The electron waves are focused by magnetic fields and can give magnifications of transparencies on the order of ×50,000, revealing particles as small as 50 to 100 atoms in size. To study metallic structures, a transparent replica of polystyrene or similar material is produced with the thickness varying, depending on the variations in level of the etched surface. The references at the end of this chapter should be consulted for details of technique and information obtainable with the electron microscope. The method is in its infancy as yet. Although little totally new information on metal structure has been gained, it is indeed satisfying to see something clearly that was previously visualized chiefly by imaginative processes. Although the structures sometimes visible in electron

[1] N.A. = numerical aperture. See Vilella's "Metallographic Technique For Steel," ASM, 1938.

micrographs are still subject to interpretation, the disclosures of this new technique should eventually extend our knowledge of the structure and properties of metallic materials.

1.3 Hardness Tests

The word *hardness* cannot be defined except by describing the test method, and since methods may vary considerably, hardness data obtained by one method cannot be expressed in terms of another measuring system, except by the use of an empirical calibration. The hardness concept may signify resistance to cutting or abrasion, in which case a file or scratch test is applicable. It may refer to the energy absorption upon slight plastic indentation, in which event a rebound test of the scleroscope type will be informative. Usually, however, hardness is defined as the resistance of a metal to indentation. None of the usual test methods or machines successfully isolates and evaluates this property alone.

In the Brinell test, a hardened steel ball is forced by a known load into the metal being tested, the diameter of the impression is measured, and, using a formula or tables, converted into an empirical number called the *Brinell hardness number* or BHN. The Rockwell test is similar except that steel balls of various diameters or a diamond cone (Brale) may be used. The diameter of the impression of the cone is not measured; instead, its depth is automatically indicated on a dial. In both of these indentation tests, the results are affected not only by the original resistance of the metal to deformation, but by the rate at which this resistance changes at the vicinity of the indentor during the tests (see deformation hardening, page 88). The results are also affected by elastic properties of the metal since the diameter or depth of the indentation is measured after the load has been released, with an accompanying elastic recovery or slight reversed dimensional change. Another variable that should be recognized is the relative volumes of metal displaced by varying depths of indentation of a sphere and a cone. The effect of work hardening and elastic recovery in the vicinity of the indentor makes it difficult to convert data obtained by one type of test into figures obtainable by a different test. Conversion tables (Table 1.2), obtained empirically by tests of steels, may not be applicable for nonferrous metals with different work-hardening and elastic properties. Since two different combinations of load and indentor may result in different degrees of indentation by the Rockwell test, it is not possible to express hardness data obtained by one combination in terms of

TABLE 1.2. HARDNESS CONVERSION RELATIONSHIPS*

Brinell			Rockwell				
Diam. of impression		Hardness No.	C 150 kg, Brale	A 60 kg, Brale	G 150 kg, 1/16 in.	B 100 kg, 1/16 in.	F 60 kg, 1/16 in.
3,000 kg	500 kg						
....	....	...	65	84			
2.47	....	614	60	81			
2.62	....	547	55	78			
2.78	....	484	50	76			
2.95	....	429	45	73			
3.15	....	375	40	70			
3 35	....	331	35	68	96		
3.60	....	285	30	65	92		
3.80	....	255	25	63	87		
4.00	...	230	20	60	81	99	
4.20	. . .	207	15	58	74	95	
4.42	....	185	10	55	66	90	
4 67	. .	165	5	52	57	85	
4.90	2 05	150	.	49	49	80	
5.10	2 15	137	..	46	41	75	99
5.30	2.23	126	..	44	32	70	97
5.52	2.34	115	.	42	25	65	94
5.75	2.44	105	..	39	19	60	91
5.95	2.54	97	..	37	10	55	88
6.20	2.65	89	..	35	2	50	85
6.45	2.82	81	.	33	..	45	82
6.65	2.88	75	..	31	..	40	79
6.82	2.96	71	..	28	..	35	77
....	3.05	67	..	26	..	30	74
....	3.12	64	..	24	..	25	71
....	3.20	61	..	22	..	20	68
....	3.25	59	..	20	..	15	65
....	3.30	57	..	18	..	10	63
....	3.35	55	..	16	..	5	60
....	3.40	53	..	14	..	..	57

* The relationships shown here are empirical and hold accurately only for the specific metals tested in determining these data; generally steels for the Rockwell C and G ranges, brass for the Rockwell B range, and aluminum alloy for the Rockwell F range.

another, except after tests have established the correlation for the specific metal.

The empirical or arbitrary nature of the numerical hardness data

and the limitations to conversion of data from one system to another have not prevented these hardness tests from being useful. The Brinell hardness number, for example, may be multiplied by 500 to obtain a fairly good approximation of the tensile strength of most carbon steels. The Rockwell test has the advantage of ease and rapidity of measurement and a small size of indentation, which does not noticeably mar the surface or affect the usefulness of the part after testing. Most of the hardness data in this book and in metallurgical literature are expressed in terms of Brinell values or Rockwell numbers (R with another letter designating the load and indentor used; *e.g.*, B = 100 kg and $\frac{1}{16}$-in. ball; C = 150 kg and Brale).

Two other types of hardness test are of importance in research work: The Meyer hardness analysis[1] basically employs the Brinell test but operated under such conditions that intrinsic hardness and hardening from cold-work during indentation are evaluated separately. The other test, known as the *Tukon test*, employs a diamond wedge that makes very small indentations at light loads. A series of indentations may be made in a very small area and, upon examination at high magnifications, the hardness of varying structural constituents may be quantitatively evaluated. With this test, for example, it has been possible to ascertain and evaluate the local deformation at the edge of brittle fractures in cases where no deformation was previously believed to have occurred.

1.4 Tensile Tests

The hardness test is the mechanical property measurement most quickly and easily made and is consequently the most common. Probably next in frequency as an engineering specification is the tensile test where a specimen, machined to a specific shape, is subjected to an axial load tending to stretch the bar. If the extent of stretch (*deformation*, *elongation*, or *strain*) is measured and correlated with the *stress* (load per unit area), the test will give data on the following:

1. Proportional Limit. The stress beyond which strain is no longer directly proportional to load, or at which a plot of stress vs. strain (stress-strain chart) shows the first visible deviation from a straight line.

2. Elastic Limit. The maximum stress to which a metal may be subjected without suffering some permanent or plastic deformation.

3. Yield Point. The point on the stress-strain curve at which deformation starts to progress rapidly with no increase in load, or in some cases, a slight diminution in load.

[1] O'Neill, "Hardness of Metals and Its Measurement," Chapman & Hall, 1934.

4. Yield Strength. By definition, (*a*) the stress corresponding to a total deformation of 0.5% in the case of copper alloys, (*b*) the stress at which the stress-strain curve departs 0.2% from the modulus line (see point 8, below) for aluminum alloys, heat-treated steels, etc., (*c*) the stress at 0.1% departure from the modulus line, in special cases.

5. Tensile Strength. This is by custom, not by logic, the stress obtained by dividing the maximum load, sustained by the specimen before breaking, by the original cross-sectional area. It is a difficult test procedure to determine the actual specimen area at each increment of stress and particularly at the moment of maximum load, although this must be done to obtain the true stress values.

6. Elongation. The increase in length divided by the original gauge length, $(L_1 - L_0)/L_0$; (L_0 = original length, usually 2 in.; L_1 = gauge length measured after fracture).

7. Reduction of Area. The change in area divided by the original area, $(A_0 - A_1)/A_0$; (A_0 = original area = 0.2 sq in. for a 0.505 in. diameter rod; A_1 = area at point of fracture).

8. Modulus of Elasticity in Tension (Young's Modulus). The slope of the straight part of the stress-strain line, expressed in the same dimensions as stress (pounds per square inch) since it represents stress divided by strain.

In the above definitions, stress refers to the load shown by the test machine divided by the *original* cross-sectional area. Strain signifies deformation in terms of a pure number, *i.e.*, the change in length (inches) divided by the original length (inches). The strain, elongation, and reduction in area ratio values are usually multiplied by 100, to convert to percentages. Points 1 to 4 refer to the change from elastic to plastic behavior in metals.

The true proportional limit (1) can be determined only by using precision types of equipment for measuring strain; a sensitivity capable of detecting a change in length of 1 part in 100,000 may be required, and, at the same time, it is necessary that the load be uniform across the entire section being strained (axial loading) in order to calculate accurately the true stress at the point of strain measurement. With ordinary equipment, the measured proportional limit varies decidedly with the scale of plotting the stress-strain data. The elastic limit, as defined by point 2, can be determined only by loading the specimen to a given stress, relieving the load to see if the specimen returns to its original length, applying the load again with a slight increment above the previous value, again unloading to find if any permanent deformation occurred, and continuing in this manner until that point is reached. A

yield point (3) is commonly found only in soft steels, and thus the yield strength (4) is most frequently encountered in engineering specifications as the indicator of elastic strength. Whenever yield strength is mentioned, the means of determination should be specified.

The tensile test is not usually suited for brittle materials because it is extremely difficult to attain perfect alignment of the axis of the test specimen and the loading mechanism. A ductile material plastically deforms on one side or the other to achieve axiality of loading. However, a brittle substance will attain a high elastic stress on one side and a fracture start there while the opposite side is still under low or moderate stresses. The indicated fracture strength then is the mean of these values and usually will be appreciably below the true strength.

Nonaxial loading is only one of several reasons why the modulus-of-elasticity line does not usually extrapolate to zero stress at zero strain or shows deviations from linearity upon initial loading. A second reason may be the existence of a balanced set of residual stresses in the specimen before loading. If, for some reason, the metal initially had residual compressive stresses at the surface balanced by tensile stresses at the center, the superpositioning of an over-all tensile stress will not cause plastic yielding or fracture at the surface so soon as at the center. The effect of residual stresses is becoming recognized as of great engineering significance and discussions of the source of such stresses are included in Chaps. 1, 2, 6, and 10.

Finally, mention should be made of the Bauschinger effect—that straining a metal in tension beyond its yield strength decreases its compressive yield strength while increasing its tensile yield strength. This effect also is related to residual stresses, but stresses existing on a micrographic scale (microstresses) and balanced locally. On just passing the tensile yield strength, certain crystals plastically deform more than others (see page 83). When the load is released these crystals elastically compress the less strained crystals and thus induce earlier yielding upon stressing in compression.

1.5 True Stress-strain Tensile Tests and Other Mechanical Tests

The conventional tension test referred to thus far yields valuable information which, in consideration of elastic properties, particularly yield strength, is useful in design. It would be desirable, however, to have the test give more information; *e.g.*, it should distinguish between uniform strain or elongation and localized strain at the point of "necking," indicate clearly the rate of stress increase with strain during plastic

yielding, etc. This would throw light on metal-forming processes such as drawing and rolling, and could disclose information on the laws governing plastic flow and fracture of metals. However, the ordinary stress values after yielding begins are fictitious and become greatly in error near fracture. Also, after necking begins, the *strain* variation along a 2-in. gauge length is very great, and the final percentage elongation value discloses little significant information in this regard.

MacGregor[1] has been a leading exponent of carrying out the tension test in such a manner that *true stress* σ (load divided by area of specimen at that moment of loading) and *true strain* δ (change in length divided by immediately preceding length) are obtained and plotted. In engineering work, ϵ_o is employed to denote ordinary strain, $\Delta L/L_o$ (Sec. 1.4, point 6). The true strain turns out to be a summation expressed in terms of a logarithm:

$$\text{True strain } \delta \text{ (or } \epsilon) = \int_{L_o}^{L} \frac{dL}{L} = \log_e \frac{L}{L_0}$$

and for a round specimen, true strain δ = true reduction in area,

$$q^1 = 2 \log_e \frac{D_o}{D^1}$$

These are related to ordinary strain, by inspection of the above equations, as,

$$\delta = q^1 = \log_e (1 + \epsilon_o)$$

where L_o = original length
D_o = original diameter
L = length at specified period during test
D = diameter at specified period during test

True stress–true strain tests are not of great significance to engineers designing on the basis of yield strength because this form of presentation of test data does not show any noticeable deviation from the ordinary stress–strain curve until strain values reach the vicinity of 10%. However, they are vitally significant to metallurgists and others interested in fundamental mechanical properties of metals.

Figure 1.1 reproduces some true stress–true strain curves[2] obtained

[1] MacGregor, *J. Franklin Inst.*, **238**, 111–135, 159–176, 1944.

[2] Even these are not absolutely accurate true stress values since they ignore the fact that as "necking" progresses (from arrow to fracture) the originally uniaxial stress changes gradually to triaxial stress as a result of constraints to flow exerted by the shoulders of the necked portion. Taking this into account changes the flow line from straightness to a curve.

by MacGregor for a medium-carbon steel as quenched in water and drawn at increasing temperatures. The metallurgical changes involved here are discussed in Chap. 10, but attention is called to information derivable from these curves. As the drawing temperature increases, the following effects are noted:

1. Decrease in yield strength (departure of line from stress ordinate)
2. Corresponding decrease in stress at maximum load (indicated by arrows)

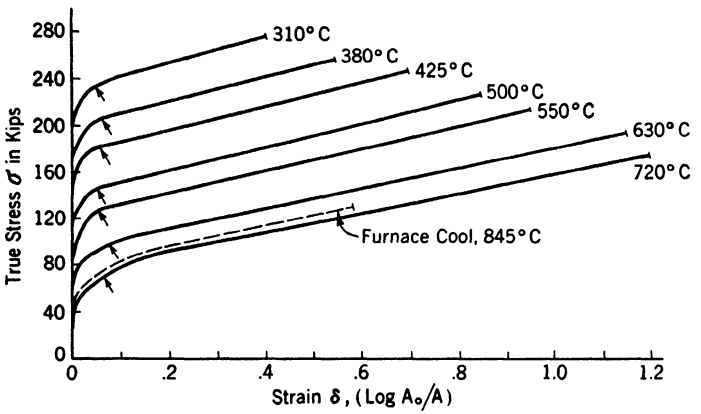

FIG. 1.1 True stress–true strain data for plain low-carbon steel (SAE 1015), quenched in water from 845°C and tempered at the designated temperatures. (*MacGregor.*)

3. Decrease in fracture stress
4. Increase in uniform strain and necking strain (line from arrow to terminus)
5. Decreased rate of hardening with increased strain (slope of the nearly straight part of lines)

Fatigue Tests. A rotating beam loaded transversely to the axis of rotation is commonly encountered in engineering service, *e.g.*, an axle. A small section of metal at the surface is alternately stressed in tension and compression during each cycle of rotation. If the stresses are completely elastic, nothing happens. If, however, the stresses are high enough for some element to be even minutely deformed, the cycle shows a closed loop when stress is plotted vs. strain. The high stress may be from overloading, from excessive vibration, or from local stress concentration at notches, keyholes, etc., when it was thought the stresses were in a safe range. A mechanical hysteresis loop such as this signifies energy absorption and, usually, its conversion into heat. Most metals

can tolerate only a certain amount of this energy absorption before a crack forms and, once this occurs, stress concentration at its root is enormously increased. This leads to crack propagation through the bar and finally a "notch" type of failure with no evidence of ductility. Such failures usually exhibit a sea-shell marking (Figs. 1.2 and 1.3) in

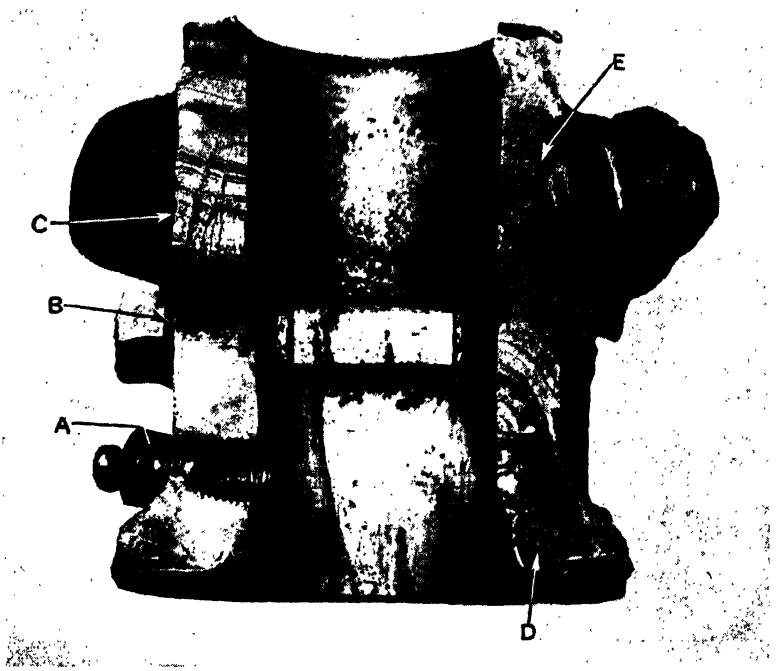

FIG. 1.2. Fatigue fracture of steering knuckle of a bus. The fracture was initiated at the lubrication fitting *A*, propagated to the hole at *B* and then around the thick section upward through *C* where the "shell" markings appear very distinctly. The fracture then started at the bottom on the opposite side, at *D* and went halfway up. At this point with only a small fraction of metal holding it together, a regular fibrous break occurred through this remainder or *E*.

the areas of crack propagation and a crystalline fracture in the section that suddenly broke in a brittle fashion after the bar cross section was sufficiently reduced.

Not much plastic strain is required to produce these failures; *e.g.*, Duralumin 24ST has a nominal tensile strength of 70,000 psi, a yield strength of 45,000 psi, and yet will break after about 100,000,000 cycles of stressing at +23,000 psi. In most steels, the endurance limit, *i.e.*, the stress that can be applied an indefinitely large number of cycles

without failure, is somewhat higher proportionately to the yield or tensile strength. However, in all metals, the engineering designer must be alert to the stress concentrations produced by keyholes, sharp internal corners, etched (pickled) surfaces, etc.[1]

Almen[2] has recently emphasized the fact that probably over 90% of fatigue failures are from tension with the crack starting at the surface.

FIG. 1.3. Fatigue fracture of an electric motor shaft, of heat-treated alloy steel 2 in. in diameter. The crack started at the left side and slowly propagated, making the "shell" markings. After going halfway across, a second fatigue crack started on the opposite face and spread towards the first crack until when final failure occurred, only a thread of metal was holding the shaft together.

Therefore, inducing residual surface stresses in compression should reduce the maximum service tensile stress at the surface and minimize the chances of fatigue failures. The residual surface stresses are induced by "shot peening" or blasting the surface with small steel balls. These plastically deform the surface and tend to increase the surface dimensions—a tendency only because the mass of undeformed metal prevents any measurable change in dimensions. The result then is

[1] Battelle Staff, "Prevention of Failure of Metals under Repeated Stressing," Wiley.

[2] Almen, *Metal Progress*, **43**, 209, 737, February and May, 1944.

that the surface is in compression, balanced by an equal tensile stress under the surface. Under such conditions, if an applied stress of sufficient intensity does start a crack, it will be initiated under the surface in the zone with residual tensile stresses. This practice of shot peening or the equivalent "surface rolling" has resulted in phenomenal increases in the service life of many metal components or enabled the use of an alloy susceptible to corrosion of a type that results in notches at grain boundaries. It is interesting to note that, until this development, engineers sought polished surface finishes to avoid the notch effects of machining marks; now they deliberately roughen the surface by shot peening.

Creep. Not only does repetition of stress affect tensile test data, but the rate of stressing and the temperature of testing are important factors. The two factors are inversely related; a higher temperature will affect results in the same way as a lower rate of stressing. The word *creep* refers to the tendency for metals to flow very slowly when subjected to steady loads for long periods of time. Since many metallic structures would be unusable if strained by more than 0.01 to 0.10%, this aspect of tensile loading is of great importance, particularly when service implies elevated temperatures as in steam and particularly gas turbines designed to operate continuously for thousands of hours. On the other hand, the high-temperature strength may be needed for only a few seconds or minutes, as in rocket propulsion units. In this case, the property desired is not *creep* strength but short-time high-temperature strength. In either case, metallurgical factors are of paramount importance. They are discussed briefly in Chap. 13.

Notched Impact Strength. The usual Izod or Charpy notched impact test is supposed to reveal the toughness of metals under impact loading conditions. Actually, the test indicates the ability of metals to absorb energy by local deformation under the biaxial stress conditions of a notch; *i.e.*, it is a *notch* test, not an impact test. For example, the energy required to break an unnotched bar in tension under impact loading (in the tensile impact test) correlates well with the area under a true stress–true strain static tensile test. In both cases, the strong but brittle metal and the weak but plastic metal show lower energy absorbed to fracture than a moderately strong, moderately plastic specimen. This energy absorption, in the absence of a notch, is considered a good evaluation of toughness.

Biaxial stresses are created in bending if the specimen is wide in comparison to its thickness. The tensile stress on one side forces an

elongation and, since volume remains constant, a corresponding lateral contraction. The compressively stressed side is shortened with a corresponding lateral expansion. In a wide thin strip or plate, the lateral expansion on one side restricts lateral contraction on the other, and this restriction effectively introduces a transverse component of stress. Thus a narrow bar may be ductile in bending, and a wide bar show brittleness.

A notch has a similar effect. In Fig. 1.4, bending across the notch tends to induce a lateral contraction as indicated by the arrows along the

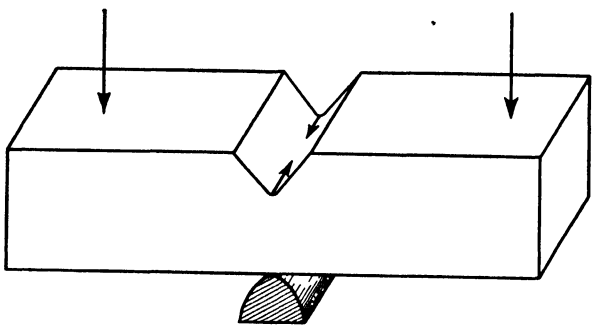

FIG. 1.4. Notched bend or impact test. The bending force indicated by the sketch would cause a tensile stress in the direction of the axis of the bar. With a notch present, however, this is not a simple uniaxial stress. Tensile deformation in the direction of this stress would require a contraction in the transverse direction as shown by the arrows. Adjacent metal, above the base of the notch, unstressed by the applied force tends to prevent this contraction and thereby effectively acts as a second stress at right angles whose intensity is controlled by the geometry of the notch and bar.

base of the notch. However, the metal immediately above the notch on either side is unstressed by the direct bending force and, therefore, is not similarly affected. Being in immediate contact with the area subjected to contraction, it tends to resist the contraction and, in so doing, effectively acts as a tensile stress along the base of the notch at right angles to the tensile stress resulting from the bending force. Therefore, the notch has introduced a second component of stress.

The relative intensity of the transverse stress at a notch depends on the geometry of the bar and the sharpness of the notch. A deeper notch, a sharper root, and a wider bar all increase the ratio of transverse stress to the longitudinal stress. For a metal with high local plasticity, these changes may not alter the energy absorbed per unit area of metal fractured. Any susceptibility to notch brittleness, however, will show up in the form of less energy absorbed per unit area of fracture as the bar is widened or the notch sharpened.

1.6 Cohesive Strength and Ductility

As hardness is changed by deformation during indentation, so tensile strength values are affected by the deformation that proceeds from the elastic limit on to fracture. It has long been a problem to find an acceptable fundamental definition for "strength" and for the deformation usually involved in experimental determinations of strength. Although yield strength, the most important strength property in design, is not affected by deformation, flow stresses during deformation and fracture stresses are important in obtaining a better understanding of mechanical properties. Since plastic deformation occurs by shear (Chap. 4), flow involves *shearing stresses* or components of the force on planes at 45 deg to the direction of extension or compression. Fracture involves *normal stresses*, components perpendicular to the plane of failure.

Fracture may be discussed in terms of the concept of cohesive strength, defined as the generalized resistance to fracture. The maximum stress required to cause tensile *fracture in the absence of any deformation* under conditions of a uniaxial or one-dimensional stress is called the *initial cohesive strength*. The maximum principal stress required to cause fracture when triaxial stresses are present, as in the case of notches, is frequently called the *technical cohesive strength*. This can vary depending on the relative magnitude of the three principal stresses, the amount of plastic deformation preceding fracture, and the temperature and rate of straining. The difficulties in evaluating these factors separately are illustrated by some original research by Kuntze who attempted to determine the cohesive strength in the absence of deformation by employing increasingly sharp notches on tensile test bars but ignored triaxial stresses[1] associated with the notches. Similarly, the effect of test temperature is difficult to study as a separate variable because ductility, or the deformation preceding fracture, also changes with temperature and affects the fracture stress.

These variables affecting cohesive strength or fracture stress have been separately determined in the case of some metals and certain generalizations may be stated:

1. Both yield and fracture stress values are markedly increased with

[1] An extremely sharp circumferential notch on a tensile test bar corresponds, in effect, to attempting to stretch a metal simultaneously in three mutually perpendicular directions. Flow or shear resulting in an extension in one direction requires a contraction in the other two. Since another component of stress at the notch prevents lateral contraction, no plastic extension may occur and rupture takes place at a high stress in a brittle manner.

increase in the ratio of transverse stresses to longitudinal stress. However, the increase in stress is usually more than offset by decreased ductility with a lower total energy absorbed in fracture.

2. Deformation increases fracture stress, but the relationship is different for different stress combinations.

3. The fracture stress or cohesive strength of all metals increases as the temperature of test decreases. This statement is postulated on the absence during cooling of any structural change in the metal and ignores, for the moment, ductility.

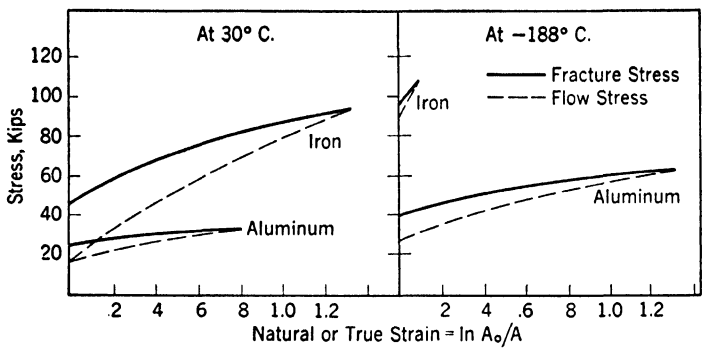

FIG. 1.5. True stress–true strain data for iron and aluminum at room temperature (30°C) and liquid-air temperature (−188°C). The increased ductility of aluminum and decreased ductility of iron at low temperatures is shown by the relative intersections of flow and fracture curves. (*McAdam.*)

The usual definition of ductility is based on the total plastic strain or elongation prior to fracture of a tensile test specimen. This is not a basic property of a metal since the strain can be altered by changing the test conditions so that the shear stress component increases in relation to the normal stress. For example, in torsion, the shear stress τ is equal in magnitude to the normal stress σ, whereas in tension the shear stress is only one-half of the normal stress. Therefore, metals of limited plasticity, or those in which the minimum flow stress approaches the fracture stress, may show ductile behavior in torsion but brittle behavior in tension.

Initial cohesive strength or the uniaxial fracture strength of undeformed metal[1] in comparison with the initial flow or yield stress is of

[1] This strength value is obtained by breaking specimens with increasingly sharp notches, which relatedly suffer less and less deformation for fracture. The extrapolated strength value so obtained must be corrected for the effect of triaxial stresses by the use of data separately obtained.

particular help in discussing ductility. This is illustrated by Fig. 1.5, from McAdam, which shows flow and fracture stresses of iron and aluminum at room and liquid-air temperatures. The relative ductilities are indicated by the difference between flow and fracture stresses at zero strain or the point of initial plastic yielding (the elastic part of the curve is not shown). From the graph, it is apparent that the lowering of the test temperature raises the flow stress of aluminum less than the fracture stress; therefore, it is more ductile at −188 than at 30°C. On the other hand, iron shows reverse characteristics; the flow stress increases with decrease of temperature more than the fracture stress so that at −188°C, they are very close together. Only a slight amount of deformation raises the flow stress to the same value as the fracture stress. As a result, iron at liquid-air temperatures breaks with little deformation or is brittle. This analysis of course delineates the facts but offers no explanation for the effects.

QUESTIONS

Group A

1. What kind of thermocouple wires would you prefer for occasional temperature measurements (employing a potentiometer to determine millivoltages) in an oxidizing atmosphere at (*a*) 400 to 500°C, (*b*) 750 to 850°C, (*c*) 1200 to 1300°C? If the thermocouple were in continuous use, or in a reducing atmosphere, would you change the wires for any of these applications? Why?

2. If distortion is encountered upon metallographic polishing with ordinary equipment, how may an undistorted surface be obtained (*a*) with the same equipment, (*b*) with no equipment limitations?

3. Give several reasons why the Rockwell test is more popular in industry than the Brinell test. What is the chief disadvantage of the Rockwell test?

4. Explain the necessity for stipulating the gauge length when specifying values for percentage elongation in the tension test.

5. From the data of Table 1.3, plot a stress-strain curve, and from it calculate values for the tensile test specifications 1 and 3 to 8 of page 12. Also calculate the fracture stress.

Group B

1. Outline a procedure for checking an industrial thermoelectric pyrometric installation. Assuming that the temperature is erroneous, outline the means for isolating the trouble among these possibilities: (*a*) thermocouple, (*b*) lead wire, (*c*) indicating instrument.

2. Explain the significance of numerical aperture of microscope objective lenses in relation to structure resolution (see Vilella).

3. Upon examination of Table 1.2, what general conclusions can you make regarding the effect of load variations for a given indentor in the Rockwell test? For what type of work would the Rockwell A be useful and for what type would it be unsuitable? Why?

4. Plot the data of Table 1.3 as true stress–true strain values. Specify the true fracture stress and the rate of strain hardening at a strain of 0.2. (Assume that volume is constant and strain is uniform over the gauge length up to the point of maximum load.)

TABLE 1.3

Load, lb	Gauge length, in.	Load, lb	Gauge length, in.
	2.00000	17,000	2.0103
1,000	2.00033	18,000	2.0118
2,000	2.00067	19,000	0.0136
3,000	2.00100	20,000	2.0156
4,000	2.00134	21,000	2.0180
5,000	2.00167	22,000	2.0208
6,000	2.00200	23,000	0.0240
7,000	2.00234	24,000	0.0285
8,000	2.00270	25,000	2.038
9,000	2.00304	26,000	2.056
10,000	2.00340	27,000	2.088
11,000	2.00380	Maximum, 39,000	2.472
12,000	2.00425	Fracture, 32,000	After fracture, 2.820
13,000	2.0047		
14,000	2.0052	Original diameter.....	0.505
13,900	2.0065	Diameter at max. load.....	0.454
15,000	2.0079	Diameter at fracture.....	0.284
16,000	2.0090		

REFERENCES

KEHL, "Principles of Metallographic Laboratory Practice," McGraw-Hill, 1943.

"Metals Handbook," sections entitled Pyrometry and Testing, including articles on the different hardness tests, Metallographic Polishing, Photomicrography.

O'NEILL, "Hardness of Metals and Its Measurement," Chapman & Hall, 1934.

SOSMAN, "Pyrometry of Surfaces and Solids," ASM.

VILELLA, "Metallographic Technique for Steel," ASM, 1938.

WILLIAMS and HOMERBERG, "Principles of Metallography," McGraw-Hill, 1939.

CHAPTER 2

COMMERCIALLY PURE METALS

In addition to a knowledge of the requisite tools used in a given field of scientific work, it is necessary to acquire a familiarity with the words commonly employed in that field. Words having special metallurgical meanings are defined when they first appear in this text in an effort to introduce gradually the special vocabulary of the metallurgist. Words having more than one common meaning are always sources of confusion and, in these cases, attempts will be made to limit the definition of terms, as far as possible, while retaining consistency with common usage.

2.1 Terminology

A *metal* may be defined as a chemical element, which in the solid form exists as a crystal or, in most cases, an aggregation of crystals characterized by two distinctive properties: free plasticity, or the ability to undergo considerable deformation without breaking, and relatively high electrical and thermal conductivity. Elements such as carbon, silicon, and boron, which exhibit some conductivity but little or no plasticity, are frequently called *metalloids*. A number of elements, including arsenic, antimony, and bismuth, are commonly classed as metals, although they are markedly deficient in these basic metallic properties in comparison with the metals of industrial importance.

The chemical processing of metal ores on a commercial scale usually produces the metallic elements with from less than 0.01 up to about 2.0%[1] of foreign elements present. If the foreign elements are present in amounts residual from the refining process, they are called *impurities*. Although impurities always affect the properties of a metal to some extent, if the magnitude of the effect is small, the metal is commonly designated as *commercially pure*. On the other hand, a small amount of an element may be added deliberately, in controlled quantities, to obtain specific property effects, in which case the metal may be called commercially pure (*e.g.*, "A" nickel) or considered an alloy (*e.g.*, low-carbon steel).

[1] Percentage by weight is used throughout this book.

The term *crystal* generally brings to mind a solid with flat, external faces at definite angles to each other. In a scientific sense, however, the word refers to a regular internal arrangement of atoms, repetitive in three chosen directions, and it is only in special circumstances that this is accompanied by external crystal faces. Metal crystals forming by solidification from the liquid state in a mold of fixed shape have to conform in external appearance to the container. If several crystals start to form in the liquid, they grow until each is in contact at some

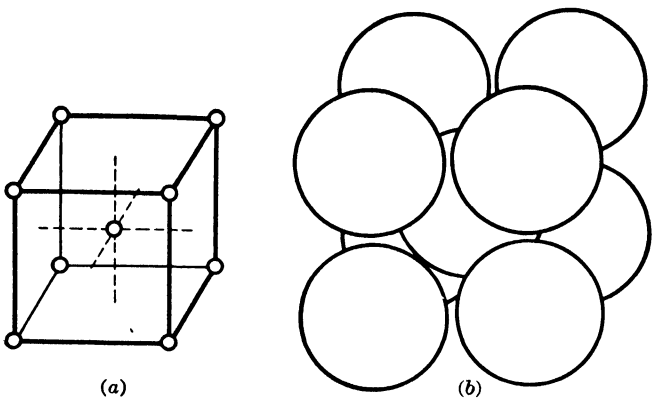

FIG. 2.1. One unit cell of the body-centered cubic structure represented by points at the left and as hard spheres at the right. The center atom touches each corner atom but these do not touch each other. Two atoms per cell (one centered atom plus one-eighth of each corner atom).

point; growth there necessarily ceases and continues at other parts of the crystal until contact at all points is completed. The size of each crystal is, of course, determined by the number in a fixed unit volume, and the shape of each is fixed by the zone of contact with surrounding crystals. Individual crystals, all of the same atomic symmetry, have their three directions (or axes) of symmetry at different angles to an external reference system, such as the surface and edge of a rolled strip. The relationship of symmetry axes to the external system is called the *orientation* of the crystal. Metal crystals, of irregular shape, in contact at all points with other similar crystals (contiguous) are called *grains*. The zones of contact are called *grain boundaries*. The word *crystallite* is commonly used synonymously with crystal or grain, but it might be desirable to confine its application to crystalline particles not in continuous contact with similar crystals. This would refer particularly to particles of a second phase for which there is, at present, no specific definitive word.

2.2 Crystal Structure

The essential characteristic of a crystal has already been specified as a regular internal arrangement of atoms, repetitive in three chosen directions. Metal crystals most frequently conform to one of the three following arrangements:

1. Body-centered cubic, abbreviated usually to b.c.c.
2. Face-centered cubic, abbreviated usually to f.c.c.
3. Close-packed hexagonal, abbreviated usually to c.p.h.

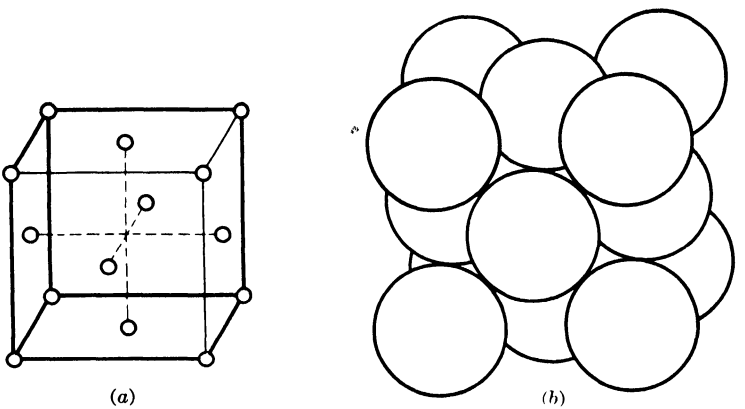

(*a*) (*b*)

FIG. 2.2. One unit cell of the face-centered cubic structure represented by points at the left and as hard spheres at the right. Each face-centered atom touches its nearest corner atom. Four atoms per cell (one-half of each face-centered atom plus one-eighth of each corner atom).

Unit cells of these are graphically shown in Figs. 2.1 to 2.3, in each case with the atom represented as a point in *a* and more accurately as a sphere in *b*. It is evident from the latter representation that, if atoms are regarded as incompressible spheres, all atoms are not in contact with each other. For example in Fig. 2.1*b*, the corner atoms of the body-centered structure all contact the centered atom but not each other; specifically, the corner atoms are closer to the centered atom than to each other. An analogous statement could be made regarding the other two arrangements.

If the arrangement in Fig. 2.1 were continued in all three directions, at 90 deg to each other, it would be found that each unit cell consisted of only two atoms—a corner atom and a centered atom—and these two are distinguished only by definition of the origin. The face-centered cubic structure of Fig. 2.2, if added to in all directions, would be found to consist of four atoms—a corner atom and three face-centered atoms.

The close-packed hexagonal structure, similarly analyzed, contains six atoms—three in the basal plane and three body-centered atoms.

The size of the unit cells of a metal lattice can be measured accurately by X-ray diffraction. For copper, the length of the edge of a unit cube is 0.000000014204 in. A straight line drawn parallel to the cube edge across a small grain, perhaps $\frac{1}{10}$ in. in diameter, would include 7,040,300 atoms in perfect alignment. A three-dimensional copper crystal in the shape of a cube $\frac{1}{10}$ in. on the edge would include $3.49(10)^{20}$ unit cubes

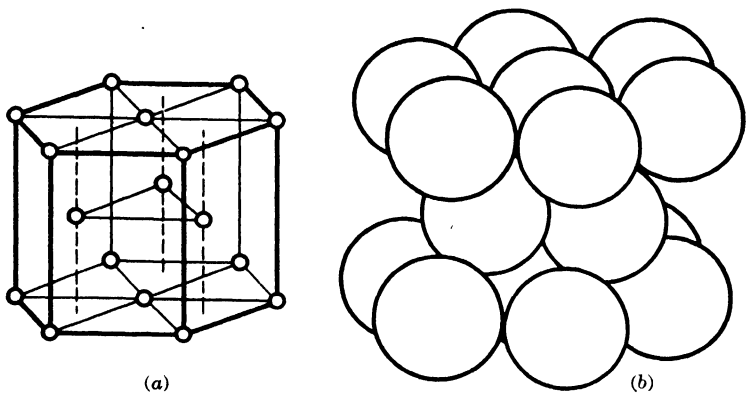

FIG. 2.3. One unit cell of the close-packed hexagonal structure represented by points at the left and as hard spheres at the right. All atoms on base planes are in contact with each other and atoms on the intermediate plane "nest" in three of the six niches so formed.

(a number making the national debt appear insignificant by comparison). There can be minute imperfections in the packing of this tremendously large number of atoms, but it is not possible to destroy the essential lattice structure except by melting the metal.

The word *molecule* is not needed in discussing metal crystal structures since the forces holding atoms in the lattice originate within the individual atoms. The word *ion* may be substituted for *atom* since electrical conductivity requires free electrons, which, in turn, means that some individual atoms must exist with positive charges. This is one point at which atomic physics and metallurgy converge, but it is outside the scope of this book.

Far more informative than any number of words about crystal structure are simple experiments in packing spheres into a closed body. It is easy to pack marbles (those used in Chinese checkers will do nicely) in a small square box. It will be necessary to have extra pieces of board to vary the size of the square when changing from one type of

packing to another. The three simplest packing methods will be found to correspond to the three commonest metal crystal forms: the body-centered cubic, and face-centered cubic, and the close-packed hexagonal. These structures appear, at first, to differ fundamentally in the character of their atomic arrangements, but closer study reveals that any one of them can be converted to either of the others by shifting the spacing of certain planes of atoms. For example, Fig. 2.4 shows two adjacent unit cells of the face-centered-cubic structure. Certain atoms of the latter structure (specifically, those on two octahedral planes) have been drawn with black centers and interconnecting lines. This configuration appears to be the same as the basal plane of the hexagonal packing (Fig. 2.3*a*), but there are two differences: (1) the distance between the basal plane of the hexagon and the one above, containing three atoms, is not fixed, while in the face-centered cube, it must be $\sqrt{2}/\sqrt{3}$ times the length of one edge of the hexagon; (2) a third plane X (not shown in Fig. 2.4) intervenes between the three-atom plane and the next hexagonal plane; *i.e.*, the order is 6, 3, X, 6, 3, X, etc., while the hexagon structure of Fig. 2.3 shows a sequence of 6, 3, 6, 3, etc.

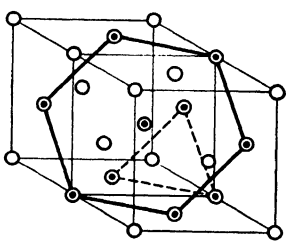

FIG. 2.4. Two unit cells of the face-centered cubic lattice (*e.g.*, Al), with atoms on the octahedral plane indicated by black centers.

In Fig. 2.5, the 12 atoms indicated by solidly outlined circles are arranged in a hexagonal pattern. Seven circles with dashed outlines represent a second layer of atoms nested on the first or bottom layer. At this stage, the atomic arrangement is like that of the centered dots of Fig. 2.4 and *the arrangement could be either close-packed hexagonal or face-centered cubic.* The third layer determines which lattice is exhibited by the packing. If the third layer is nested above the first as suggested by the small open circle, the lattice is close-packed hexagonal. If the next layer starts with the equally nested adjacent position shown by the small solid circle, the packing is face-centered cubic! Of course, it could still be called hexagonal but would logically be called cubic, since that is a more symmetrical form. The fact that it is really face-centered cubic may not be obvious and usually is visualized only by actually piling balls in this manner and then discovering and outlining the face-centered cubic faces.

The two face-centered cubic unit cells of Fig. 2.4 have again been reproduced in Fig. 2.6, but in this latter representation some of the atoms have been given black centers and connected with heavier lines.

These lines show a body-centered structure, not cubic but tetragonal since the height is greater than either edge of the square base. Again, there is no great difference between two apparently very dissimilar packings: the face-centered and the body-centered types.

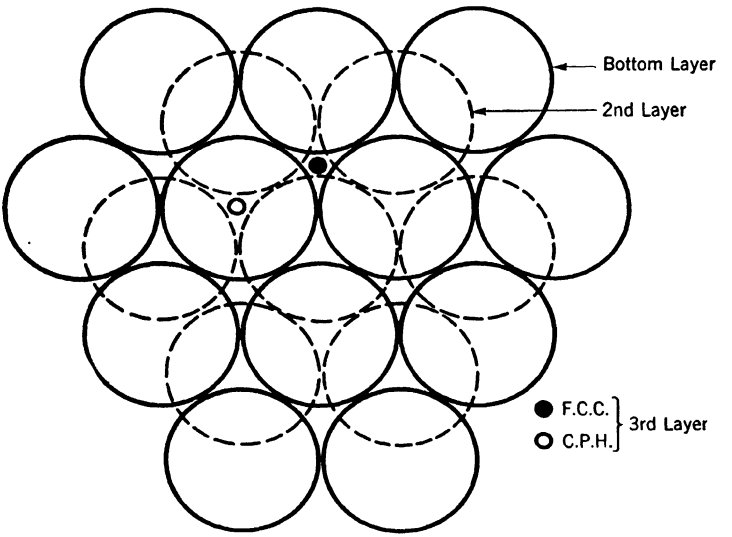

FIG. 2.5. Solidly outlined circles represent a bottom plane of atoms and dashed outlined circles represent a second plane nested on the first. If the third plane starts with an atom in the nested position of the small open circle, the packing becomes *close-packed hexagonal*. If the third plane starts with an atom in the alternative nested position of the small solid circle, the packing becomes *face-centered cubic*.

2.3 Polymorphism and Allotropy

Many metals can exist in more than one type of atom packing or crystal structure. This ability to show more than one form is called *polymorphism*. If the change in structure is reversible with change in temperature, the polymorphic change is known as *allotropy*. The most familiar example of this is iron which, upon slow heating, changes from body-centered cubic to face-centered cubic at 910°C (1670°F) and back to body-centered cubic at 1400°C (2552°F). These structure changes reverse upon cooling. The temperatures of change given are equilibrium values, and actual transformations occur at somewhat higher temperatures on heating and considerably lower temperatures on cooling

unless the cooling is very slow. The fundamental explanation of such allotropic changes is related to the tendency for a metal to exist in the form of lowest energy, although it is not known why face-centered cubic γ iron has a lower energy than body-centered cubic α iron within the temperature range 910 to 1400°C.

There is another type of allotropic change enforced by high pressures at a fixed temperature. By use of extremely high pressures, up to about 500,000 psi,[1] Bridgman has caused many metals, not ordinarily con-

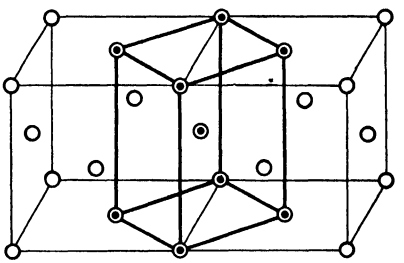

FIG. 2.6. Two unit cells of the face-centered cubic lattice (γ Fe) with specific atoms marked with black centers to indicate the structure might also be considered as body-centered tetragonal.

sidered as allotropic, to change crystal structure. In this case, the cause is usually rather simply explicable; the original structure was not one of the simple close-packed arrangement and transformation is in the direction of a denser packing of spheres.

White or ordinary tin, which is body-centered tetragonal, will tend to change to a brittle, powdery diamond cubic structure called *gray tin* when cooled below 13°C (56°F). The transformation is readily suppressed but if it does occur, an expansion of about 25% is required, which changes a solid block to a fine gray powder. This physical form is such that a reverse transformation to the original block of white tin cannot occur although the gray powder can revert to a white tin powder. Since the gray tin has a much less density than white tin, this reverse transformation is favored by high pressure. Gray tin will become white at even liquid-air temperatures if it is subjected to high compressive forces.

A truly irreversible transformation may be encountered on heating electrodeposited metals. For example, the only stable structure of nickel is face-centered cubic; yet this metal may exist in the close-

[1] This designation is employed for "pounds per square inch."

packed hexagonal form when electroplated under specific conditions. Upon heating, the metal will irreversibly change to the face-centered structure. Therefore, nickel is polymorphic but not allotropic.

2.4 Production of Commercially Pure Metals

Although this book is concerned primarily with alloys and the properties that fit them for specific services, it is desirable to describe briefly the processes by which metals are recovered from their ores. Many characteristics of commercial metals are directly related to the characteristics of the ores and their processing.

Iron. The most important ores are the oxides hematite, Fe_2O_3, and magnetite, Fe_3O_4, with which are associated varying amounts of SiO_2, MnO, P_2O_5, and other oxides. The ore is charged into a vertical shaft furnace (blast furnace[1]) with carbon in the form of coke and limestone or $CaCO_3$. In operation, preheated air is blown into the furnace near the bottom and its oxygen burns the coke, forming CO:

$$2C + O_2 \rightarrow 2CO$$

The hot CO rising through the mixture above it reduces iron, manganese, and phosphorus fairly completely to the metallic state. These reactions could be summarized as follows:

$$\begin{aligned} Fe_2O_3 &+ 3CO \rightarrow 2Fe + 3CO_2 \\ MnO &+ CO \rightarrow Mn + CO_2 \\ P_2O_5 &+ 5CO \rightarrow 2P + 5CO_2, \text{ etc.} \end{aligned}$$

The temperature in the vicinity of the combustion of the coke is sufficient to melt the iron, which trickles over unburnt coke absorbing carbon plus the metallic manganese and phosphorus. In addition, some silica in the ore is reduced to metallic Si which is also absorbed by the iron; the remainder of the SiO_2 combining with CaO from the limestone to form a slag. In addition, all commercial grades of coke contain some sulfur and in the reducing atmosphere (CO or carbon monoxide) of the blast furnace, this sulfur is only incompletely removed by forming CaS in the slag, the remainder entering the liquid iron

[1] A modern furnace has a circular hearth 26 to 28 ft in diameter, is as high as a 10-story building, produces 1,200 to 1,600 tons of pig iron a day, and uses roughly 4 *tons* of air, 2 tons of ore, 1 ton of coke, and ½ ton of limestone per ton of iron produced. Such a furnace with accessories represents an investment of several million dollars and will operate continuously for several years before the lining is worn to the point requiring rebuilding.

mixture. The metallic mixture produced by the blast furnace, called *pig iron*, is typically as follows:

Carbon: 4.–4.5% by weight
Manganese: 1.–2.5% by weight
Silicon: 0.5–1.5% by weight
Phosphorus: 0.1–1.0% by weight
Sulfur: 0.04–0.08% by weight
Any Ni, Cr, Cu, or other easily reducible, high-boiling-point metals present in ore, coke, or limestone
Iron: remainder

To produce commercially pure iron, this pig iron and steel scrap are melted under an oxidizing slag containing FeO and CaO in an open-hearth furnace fired with natural gas or fuel oil and preheated air. It is possible to oxidize out a part or almost all of these "impurities." However, traces of each of them are to be found in the ingot iron produced by the open-hearth furnace, sulfur being particularly difficult to remove. In addition, the final product, ingot iron, will always contain appreciable amounts of dissolved oxygen or included FeO. This background makes the properties of ingot iron variable from lot to lot and quite different in certain respects from really pure iron obtained by electrolytic means or by the dissociation of pure iron carbonyl.

Another type of what might be called commercially pure iron is known as *wrought iron*. To produce this, pig iron is melted in a furnace somewhat similar to the open hearth. However, as a lime-rich slag is not used, phosphorus is not removed from the iron. In addition, since the air for fuel combustion is not preheated, the temperature attained is not high enough to maintain the iron in a liquid state, and it solidifies as the impurities are oxidized into the slag. The result is that slag and metal are not completely separated; the product contains not only more phosphorus than ingot iron but also about 2 to 2.5% slag by volume.

Copper. Some metallic copper is found in nature, but most of the important ores are of copper sulfide, generally in association with other metalliferous sulfides. The copper sulfide is separated from useless minerals and other metal sulfides by a physical flotation process where the heavy sulfide, in extremely fine particles, adheres to oil-water froths, and the unwanted gangue material settles to the bottom. The copper-bearing concentrate is heated in air below its melting point to volatilize oxides of arsenic and antimony and oxidize about three-fourths of the sulfur and associated metals. After this *roasting* process,

the material is melted in a reverberatory furnace. Here some part of the iron, existing as Fe_2O_3, is reduced to FeO and slagged off with SiO_2 and CaO. The remainder, as FeS, dissolves in the copper sulfide, Cu_2S, to form a heavy *matte*, which by gravity readily settles below the slag.

Next, air is blown through the liquid matte, in a refractory vessel known as a *converter*, burning the sulfur to SO_2 and converting the iron to FeO which again is slagged off with added sand or SiO_2. These reactions may be summed up as follows:

$$2FeS + 3O_2 + 2SiO_2 \rightarrow 2FeSiO_3 + 2SO_2$$
$$2Cu_2S + 3O_2 \rightarrow 2Cu_2O + 2SO_2$$
$$2Cu_2O + Cu_2S \rightarrow 6Cu + SO_2$$

The crude copper so produced, called *blister* copper, is melted and, after partial refining, is cast into large slabs. These become anodes in an electrolytic cell containing copper sulfate in dilute sulfuric acid. Upon passage of a low-voltage, high-amperage current, copper ions are carried through the solution and deposit on the cathode, which is a thin sheet of pure copper. Some impurities do not dissolve and collect in a slime of fine particles under the anode. Au, Ag, Pt, Cu_2O, $PbSO_4$, AgCl, S, Se, Te, and salts of Bi and Sb are found in the anode slime. Fe, Ni, and Zn dissolve in the electrolyte but do not plate out on the cathode.

The electrolytic copper, of 99.95% purity, is melted and cast into bars for final use. Ordinarily, oxidizing conditions employed in melting result in the pickup of oxygen, which is reduced by stirring the molten metal with wooden poles to a final content of 0.02 to 0.05% oxygen. The final produce is known as *electrolytic tough-pitch copper*.[1] If the remelting and casting of the copper are done in a carbon-monoxide, sulfur-free atmosphere, then little or no oxygen will be present and the copper so produced has the self-descriptive trade designation, *oxygen-free high-conductivity* (OFHC) *copper*. The brittle electrolytic cathodes may be broken up, compressed, and forced through an orifice while hot (but solid) in a reducing atmosphere and this product is called *coalesced copper*. Finally, enough phosphorus may be added to eliminate all oxygen, and this product is called *phosphorized copper*. All these are generally produced from electrolytically refined copper. Some commercial copper is produced solely by fire-refining operations. This

[1] This name is of historical origin. If more than about 0.05% oxygen is present in copper, its ductility decreases and it breaks with a "dry" brittle fracture. If less than 0.02% is present, then reducing conditions will result in the pickup of sulfur, *e.g.*, from remelting fuels, and again ductility is diminished.

constitutes only a small proportion of commercial copper and will not be discussed here.

Aluminum. The element aluminum occurs in nature as an oxide in association with other oxides; its chief ore, bauxite, contains iron and silicon oxides. Finely ground bauxite is digested in an aqueous solution of sodium hydroxide. The alumina dissolves as $NaAlO_2$ whereas most of the iron and silicon oxides remain undissolved. The sodium aluminate is diluted, filtered, and then decomposed to give aluminum hydroxide which is strongly heated to drive off the water. The resulting product is Al_2O_3 of high purity. The Al_2O_3 is dissolved in a molten electrolyte consisting of calcium sodium fluoride, having a melting point of about 1000°C (1830°F). With carbon blocks for anodes and cathodes, liquid metallic aluminum is deposited on the cathode, actually the carbon lining of the electrolytic cell. Oxygen goes to the anodes—carbon blocks suspended in the electrolyte—and tends to burn these away. The liquid aluminum is tapped from the cell at intervals and cast into small ingots or "pigs." Primary metal so produced usually contains from 0.3 to 0.6% Fe, 0.2 to 0.4% Si, and from a trace to 0.2% Cu. These impurities come both from the ore and the carbon electrodes.

Other Metals. No attempt will be made to describe the processing, ore to metal, of other metals since the ones covered show, by example, that commercially pure metals aways contain some impurities in at least trace amounts, originating in the ore and the fuel. Instead Table 2.2 has been prepared to give some data on particularly important points regarding commercially pure metals.

2.5 Microstructures

The commercially pure metals discussed in this introductory chapter are generally more difficult to polish than alloys of the same metals. The pure metals are softer and are, therefore, more subject to flow and distortion during polishing. Pure aluminum in particular is almost impossible for the novice to polish properly and offers great difficulties to the expert, not so much because of flow and distortion but because of the tendency for particles of the polishing compound or abrasive to become embedded in the surface.

If the microscopist succeeds in achieving a satisfactory polish, etching is the next pitfall. The structural appearance varies widely depending on the etchant used and the depth or time of etching. Students like to be told just how many seconds or minutes are required and whether to immerse the specimen in the etching solution or swab the

TABLE 2.1 PHYSICAL PROPERTY DATA OF SOME METALS

Element	Symbol	Density, 20°C., g./cm.³	Coefficient of thermal expansion, 0 to 100°C., $\times 10^{-6}$/°C.	Electrical resistivity, at 20°C., microhm/cm.³	Electrical conductivity (compared to copper), per cent	*Lattice type at 20°C. (or indicated temperature)	Lattice parameter (length of base of unit cell), $a, \times (10)^{-8}$ cm.
Aluminum....	Al	2.70	24.0	2.65	64.	f.c.c.	4 0410
Antimony....	Sb	6.62	9.8	39.	4.3	rh. hex.	4.4974
Beryllium....	Be	1.82	12.4	5.9	13.7	c.p. hex.	2.281
Boron.....	B	2.3	2.3	18.(10)[11]	.....	complex hex.	17.86
Cadmium....	Cd	8.65	29.8	6.83	22.	c.p. hex.	2.9727
Carbon.....	C	2.22	1.2	13.(10)[3]	0.17	(graph.) hex.	2.46
						(diamond) c.	3.5597
Chromium....	Cr	7.19	6.1	13.1	12.8	b.c.c.	2.878
Cobalt.....	Co	8.92	12.8	6.24	26.4	(α)c.p. hex.	2.507
						(β-440° to 1150°C.) f.c.c.	3.546
Columbium...	Cb	8.57	7.2	13.1	8.4	b.c.c.	3.2941
Copper.....	Cu	8.96	16.7	1.68	100.	f.c.c.	3 6073
Gold.....	Au	19.3	14.3	2.19	70.	f.c.c.	4.0700
Iron.....	Fe	7.87	12.3	9.8	17.2	(α, δ) b.c.c.	2.8610
						(γ — 908° to 1400°C.) f.c.c.	3.60
Lead.....	Pb	11.34	28.3	20.65	7.2	f.c.c.	4.9389
Magnesium...	Mg	1.74	26.0	4.46	38.	c.p. hex.	3.2030
Manganese...	Mn	7.44	19.7	185.	1.	(α) complex c.	8.901
						(β—740° to 1160°C.) complex c.	6.305
						(γ—1160° to m.p.) f.c. tetrag.	3.767
Molybdenum.	Mo	10.2	4.9	5.17	35.	b.c.c.	3.1403
Nickel.....	Ni	8.9	13.3	6.9	24.	f.c.c.	3.5170
Palladium....	Pd	12.0	11.7	10.8	16.8	f.c.c.	3.8817
Platinum.....	Pt	21.45	8.9	9.83	17.1	f.c.c.	3.9158
Rhodium.....	Rh	12.44	9.6	4.5	34.	f.c.c.	3.7957
Selenium.....	Se	4.81	37.	12.(±)	14.(±)	hex.	4.337
Silicon.....	Si	2.33	3.1	23.(10)[3]	0.007	diamond c.	5.4173
Silver.....	Ag	10.5	19.7	1.60	105.	f.c.c.	4.0782
Sulfur.....	S	2.07	67.5	19.(10)[15]	.....	f.c. orthorh.	10.48
Tantalum....	Ta	16.6	6.6	12.4	11.5	b.c.c.	3.2959
Tellurium....	Te	6.24	16.8	19.(10)[2]	0.09	hex.	4.445
Tin.....	Sn	7.30	23.5	11.5	14.6	b.c. tetrag.	5.819
						(below 13.2°C.) diamond c.	
Titanium.....	Ti	4.54	8.5	80.	.....	c.p. hex.	2.953
Tungsten.....	W	19.3	4.3	5.48	30.6	b.c.c.	3.1585
Vanadium....	V	5.68	7.8	26.	6.5	b.c.c.	3.033
Zinc.....	Zn	7.14	39.7	6.0	28.	c.p. hex.	2.6600
Zirconium....	Zr	6.5	5.3	41.	4.1	c.p. hex.	3.223

* f.c.c.—face-centered cubic; rh—rhombohedral; c.p. hex.—close-packed hexagonal; b.c.c.—body-centered cubic; c—cubic; tetrag.—tetragonal. Polymorphic forms of the metals are given but not for the nonmetals S and Se. Some metals, as Cr and Ni, may exist in a different form when electrodeposited but do not show reversible, polymorphic transformations.

† Heats of formation of the oxides (from "Chemical Rubber Handbook," 22d ed.) are given in terms of a gram-molecular weight of the oxide formed. Dividing this value by the atomic weight of the element times the number of metal atoms per molecule of oxide will give relative heat data in terms of unit weight of metal oxidized.

Lattice parameter (height of unit cell), c $\times(10)^{-8}$ cm.	Specific heat (at room temperature) cal./g./°C.	†Heat of formation of lowest (metallous) oxide kilocal./g.-mol.	Heat of fusion or crystallization, cal./g.	Melting point, °C.	‡Tensile strength of annealed metal, $\times(10)^3$ p.s.i.	Tensile-test elongation of annealed metal, per cent	Brinell hardness of annealed metal, BHN	Minimum recrystallization temperature, °C	Tensile strength of cold-worked metal (reduction gen = 80 per cent), $\times(10)^3$ p.s.i.	Young's Modulus of elasticity, $\times(10)^6$ p.s.i.	Symbol
....	0.220	390.	94.6	660.	8.(Pure)	60	16.	90.	.	10.3	Al
					13.(Com.)	45.	22.	150.	24.		
57°6′	0.051	165.	39.	631.	(Brittle)					11.3	Sb
3.577	0.508	135.	262.	1284. ±	30.	0.	60	....	..	36.	Be
10.83	0.307	280.	...	2300 ±	(Brittle)		....	....	....	..	B
5.6061	0 055	65.	13.	321.	13.	48.	20.	20.	....	3.	Cd
6.6916	0.165	26.	....	3700. ±	(Brittle)		....	....	....	0.7	C
.....	0.112	267.	75.6	1830. ±	(Can be ductile)		108.	....	....	36.	Cr
4.072	0 105	57.	67.	1495.	37		124.	....	100.	30.	Co
.....	0.065	. ..	. .	2415.	50.	30.	....	....	100.	. .	Cb
.....	0.092	39.	49.	1083.	30 (Pure)	75.	. .	90.	...	. .	Cu
					32 (Com.)	48.	.	200.	64.	16.	
.....	0.031	−12	15.	1063.	16.	45.	. ..	200.	30.	11.3	Au
.....	0.107	64.	65.	1539.	38.(Pure)	45.	65.	450.	. .	30.	Fe
					41.(Com.)	42.	70.	490.	86.	30	
....	0.029	52.	6.3	327.	1.6	68.	3.	10.	.....	2.5	Pb
5.2002	0.242	146.	89.	651	28.	17	35.	150.	27.	6.2	Mg
.....	0.122	91.	64.	1242.	72.qu. (γ)	40.	30.	....	....	23.	Mn
3.526											
....	0.062	131.	70.	2500.	99.	21.	147.	900.	190.	50.2	Mo
... .	0.114	58.	70.	1455.	43.(Pure)	48.	54	...	...	....	Ni
					70.(Com.)	45.	107.	600.	120.	30.	
.. ..	0.059	21.	36.	1554.	20.	39.	46.	....	47.	17.	Pd
... ..	0.032	17.	27.	1773.	17.	30	42.	400.	34.	21.4	Pt
.....	0.059	...	. .	2500.	(Can be ductile)		101.	. .	.	42.	Rh
4.944	0.078	56.	6.6	217.	(Brittle)		....	....	....	....	Se
.....	0.176	198.	33.7	1430.	13.(Comp.)	0.	....	....	..	16.3	Si
....	0.056	6.	25.	960.	22	66.	28.	200.	57.	11.	Ag
24.55	0.175	69.	9.	113.	(Brittle)		....	..	....	..	S
...	0 035	300.	..	2996.	48	. ..	46.	1000.	169.	27.	Ta
5 912	0.048	78.	7.3	452.	(Brittle)		. .	....	....	....	Te
3.175	0.055	70	14.5	232.	2.	....	5.	15.	. .	6.	Sn
4.729	0.141	217.	....	1820.	78.	25.	....	....	112.	16.8	Ti
.....	0.032	126.	44.	3399.	145.	8.	290.	1000.	490.	60.	W
.....	0.115	209.	..	1735.	.	.	. .	. ..	....	.	V
4.9379	0.093	84.	26.	419.	16	55.		20.	22.	..	Zn
5.123	0 066	178.		1927. ±	36	31.	.	.	88.	11.	Zr

‡ Tensile strength data are given for very pure Al, Cu, Fe, and Ni and also for the commercially pure metals (com.). The strength value for brittle silicon is for compression (comp.) loading. In addition to purity, the physical state of the metal, *i.e.*, grain size and as-cast or wrought wire, rod, or sheet will markedly affect strength properties. Not all data here were on specimens in the same physical state, and therefore the values generally are only qualitatively comparable. Cr, Cb, Rh, Ti, and Zr, which are ordinarily brittle, can be produced in a ductile form, although strength data have not been published.

Most of these data were taken from the "Metals Industry [London] Handbook" for 1942, supplemented by the "ASM Handbook" (1948) and by recent research publications. Almost all the properties given here are influenced by the purity of the metal; *e.g.*, most handbooks show the melting point of Cr as 1550°C., a value obtained upon melting in air as a result of nitrogen absorption. Most properties are also crystallographically sensitive to the direction of measurement, particularly in the case of noncubic metals

TABLE 2.2

Metal	Commonest type of ore	Usual refining process	Typical impurities	Cost* per lb	Comments
Aluminum	Oxide	Electrolytic	Cu, Fe, Si, Ti	$ 0.16	Commercial grade
Beryllium	Oxide	Electrolytic	N, O, Al, Mg	65.00	Most production is directly of Cu:Be alloy
Cadium	Sulfide	Distillation, electrolytic	Bi, Zn	1.90	
Calcium	Oxide	Electrolytic		2.40 to 4.55	
Cerium	Oxide	Electrolytic	La		
Chromium	Oxide	Electric furnace	Fe, C, Si	1.10	Most production is as ferro-Cr for steels
Cobalt	Sulfides Arsenides	Electrolytic		1.70	
Copper	Sulfide	Electrolytic	O, S, Fe	0.235	
Gold	Native	Fire	Cu, Ag	35.00†	
Iron	Oxide	Fire	C, Mn, Si, S, P	0.03	Ingot iron
Lead	Sulfide	Fire, electrolytic	Ag, Cu, Cd	0.195	
Magnesium	Oxide	Electrolytic, distillation	Fe, Co, Ni, Cu	0.205	
Manganese	Oxide	Blast furnace, electrolytic		0.34 0.36	Most production is as ferro-Mn for steels, used mostly for steels
Molybdenum	Sulfide	Electric furnace		2.65	
Nickel	Sulfide	Fire, electrolytic	S, Mn, Cu	0.40	
Platinum	Native		Ir, Os, Pd	95.00†	
Silicon	Oxide	Electric furnace	Fe	0.16	
Silver	Native, sulfide		Cu, Zn	0.77†	
Tin	Oxide	Fire, electrolytic	Sb, As, Pb, Bi, Cd	1.03	
Tungsten	Oxide	Electric furnace, hydrogen reduction		2.25	Ferro-W for steels, tungsten wire
Uranium	Oxide			5.00	
Vanadium	Sulfide	Electric furnace		3.00	Used mostly for steels
Zinc	Sulfide	Electrolytic, distillation	Pb, Cd, Fe	0.19	Grade for die-casting alloys

* Approximate cost as of October, 1948. The cost in most cases depends greatly on quantity, purity and physical form.

† Per ounce, troy.

surface with cotton soaked in the solution. Generally, either immersion or swabbing methods can be employed, and the time is judged by the surface appearance—a light frosted surface for moderate to high magnifications and a longer time or deeper frost for low magnifications.

The microstructures of absolutely pure, dense metals in the cast state would show no details other than dark lines delineating grain boundaries. These appear because of the inevitable atomic lattice discontinuities resulting from attempting to fit, for example, cubic structures together at other than 90-deg. angles. Zones of slight atomic mismatching are more readily attacked by chemical agents, and the resulting narrow "valley" will not reflect light; hence the dark line. Some chemical agents also tend to etch certain crystallographic planes. If they outline cubic facets, then a grain in which the facets are parallel to the surface will appear bright. Other grains with these facets at an angle to the surface will be roughened and less reflective and, therefore, appear dark.

Beyond grain boundaries and, in some cases, differential grain darkening, micrographs of "commercially pure" metals frequently show a second constituent arising from one or more impurity elements, *e.g.*, minute FeO particles in ingot iron (Micro. 2.2), slag in wrought iron (Micros. 2.3 and 2.4), a compound of Al:Fe:Si in aluminum (Micro. 2.6), and Cu_2O in tough-pitch copper (Micros. 2.7 to 2.10).

The dispersion of impurity constituents will depend on whether the commercially pure metal is in the cast or the wrought state. If in the latter as is the case in this chapter, the impurity constituents will be aligned in the direction of flow of the metal during rolling or forging operations. A second effect of prior hot-rolling or forging is the formation of *annealing twins* in all face-centered cubic metals except aluminum. No discussion of these is presented in this text for they do not noticeably affect properties. Their real significance is that they offer positive evidence of hot deformation or of cold deformation followed by heating.

Brief information regarding the preparation of specimens for microstructural observation is given elsewhere in later chapters where alloys of a specific metal are discussed in detail.

2.6 Characteristic Properties

Metals in the pure state have relatively high plasticity or deformability and low strength. The degree to which they exhibit these properties is primarily a function of their crystal structures and the binding forces between atoms in the crystal. Drawings of the atomic

(*continued on page* 46)

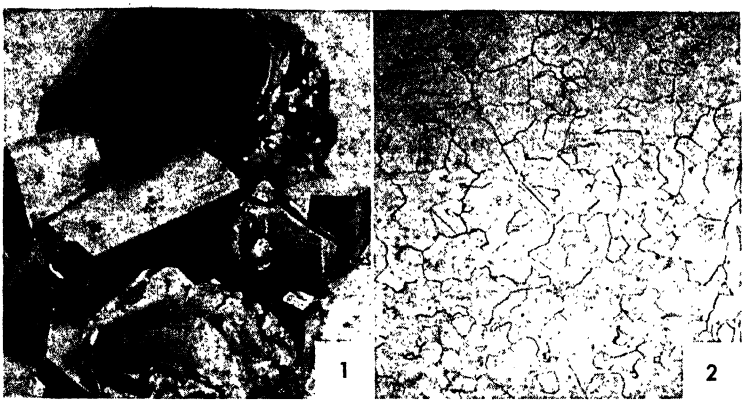

Micro. 2.1. Magnesium; photograph, at natural size, of large crystals formed directly from vapor, not by the solidification of liquid in a mold. Under this unique condition, the crystals develop external crystalline form with flat faces and true interfacial angles.

Micro. 2.2. Iron (Armco ingot iron) with about 0.13% total of impurities; ×50; 5% HNO_3 in alcohol (Nital) etch. This structure shows polygonal outlines of grains of body-centered α iron (ferrite). At the plane of contact between two crystals of differing orientation, the atoms are not firmly held in either crystal lattice. This region, called the *grain boundary*, is one of relatively low stability or high energy; reactions will generally be initiated here (see page 472), and in this region, chemical attack by the etching solution is greater. The narrow valley after etching appears as a dark line, which, outlining the grain boundaries, makes the size of individual crystals readily apparent. The black spots are sites of oxide inclusions or of localized polishing pits. The micrograph represents a cross-sectional view of a hot-rolled bar.

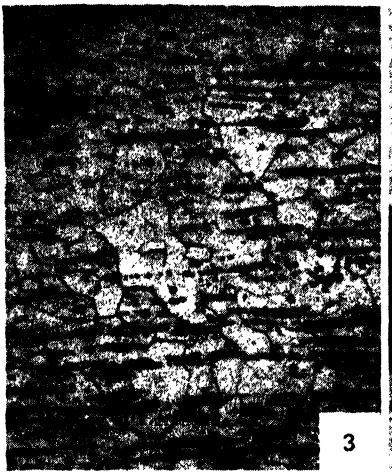

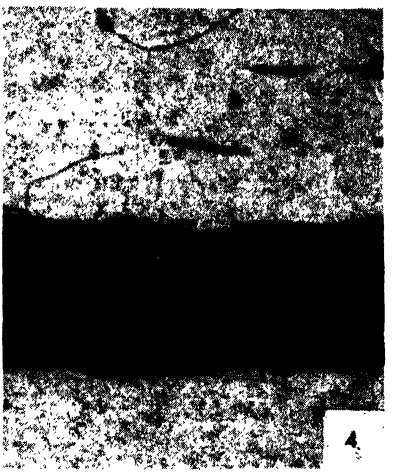

Micro. 2.3. Wrought iron; ×50; Nital etch. The matrix, or background structure, consists of ferrite grains similar to those of the ingot iron except that the dissolved impurities, particularly phosphorus, are present in somewhat greater amounts. (*Soluble impurities* means elements dissolved in the ferrite, hence not visible under the microscope and detectable only by chemical or spectographic tests.) The dark elongated stringers are inclusions of slag, largely a mixture of FeO and SiO_2. The slag is present in amounts of from 1 to 2% and is always elongated in the direction of flow from hot-rolling. Its distribution frequently is not very uniform; some areas show a lot, some very little. This micrograph is representative of a typical structure. There is no crystallographic or continuous atomic relation between atoms in the slag and in the ferrite crystals; consequently nothing but mechanical contact forces hold the metal and slag together at the contact area. The structure shows that the metal phase is much more continuous, *i.e.*, less interrupted, along a horizontal direction than along a vertical direction. As a result, strength and ductility are not uniform in all directions but depend on whether the axis of stress during testing is parallel or transverse to the direction of the slag filaments. This type of structure is fibrous and will have quite a different appearance, depending on whether the polished surface represents a section parallel, as in this picture, or perpendicular to the rolling direction.

Micro. 2.4. Same as Micro. 2.3 at ×500. This shows the duplex structure of the slag (FeO and $FeSiO_3$). The slag is harder than the metal and thus, after polishing and etching, stands in relief above the metal surface. In this picture, the slag is in focus and the metal necessarily slightly out of focus. The markings in the ferrite grains appear after moderately heavy etching and are probably related to the distribution of finely dispersed impurities.

Micro. 2.5. Cast zinc (99.99% Zn); ×50; etched with CrO_3, Na_2SO_4 solution. This structure consists of coarse grains with lenticular (lenslike) markings that are mechanical twins. The word *twin* means that, within the lens-shaped area, the crystal orientation has shifted a fixed amount, equivalent to a rotation of 180 deg about an axis normal to the crystal plane represented by the line bounding the twin. The direction of the twins thus reveals the position of a specific crystal plane in each grain. In the large dark grain, six different angular positions of the twins show six different directions of one type of lattice plane. The twin does not originate by rotation (the gross movements involved would be impossible to achieve) but from slight deformation after casting or surface flow during polishing, thus the qualifying adjective "mechanical." Carefully cast zinc polished in a manner avoiding surface distortion would show only the coarse grains.

Micro. 2.6. Commercially pure aluminum (Alcoa 2S: 99% Al + about 0.3% each of Fe, Si, and Cu); 0.5% HF etch; ×500 (photomicrograph supplied through courtesy of the Aluminum Research Laboratories). This structure is that of the metal in the worked and annealed condition. It shows rather small grains of aluminum and black particles of an Al:Fe:Si compound, originating from the impurities. The direction of these insoluble particles represents the direction of prior deformation; they are elongated in the direction of flow, similarly to the slag particle of the wrought iron. The aluminum crystals are not elongated since they re-formed during the anneal following the deformation (see Chap. 4).

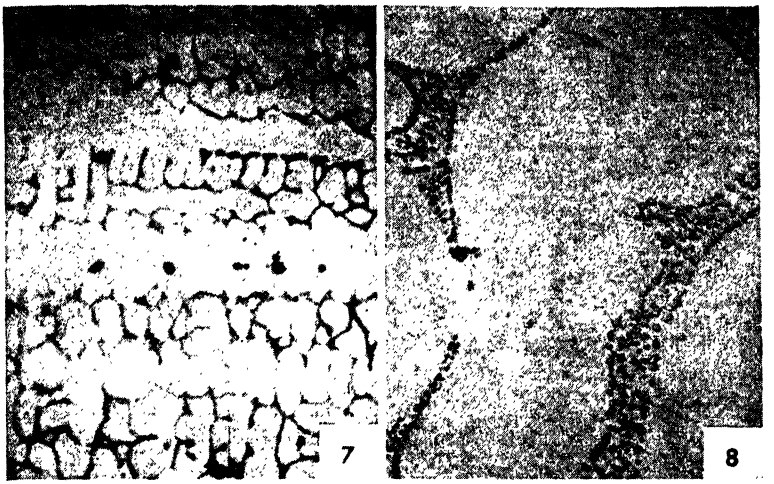

Micro. 2.7. Cast tough-pitch electrolytic copper (99.95% Cu; 0.03% O_2); ×50; NH_4OH:H_2O_2 etch. All metals solidify from the liquid state by the growth of crystals which, because of preferred growth in certain directions, form as open treelike structures called *dendrites* (see page 59). At a later stage in growth, when different dendrites are in contact, the open spaces between them are filled in with more of the crystalline element. If impurities are present, they will usually be of lower melting point or form a structure of lower melting point, which means they will be concentrated in the parts last to freeze, *i.e.*, the open spaces between dendrites. This structure of a cast wire bar shows nearly pure copper in the form of cells, actually the intersections of dendritic arms with the surface of polish. The oxygen impurity, present as Cu_2O (cuprous oxide) particles, forms with copper the dark structure of lower melting point, outlining the dendritic cells. The black spots are pores or holes in the cast metal.

Micro. 2.8. Same as Micro. 2.7 at ×500. This shows in detail the dark structure outlining the copper dendrites. The cuprous oxide particles or crystallites are seen to be globular bodies dispersed in a copper background. Note that copper is continuous and that the brittle oxide, while forming a network, actually consists of separate, discrete crystalline particles. (This alloy structure is that of a hypoeutectic; see Chap. 5.)

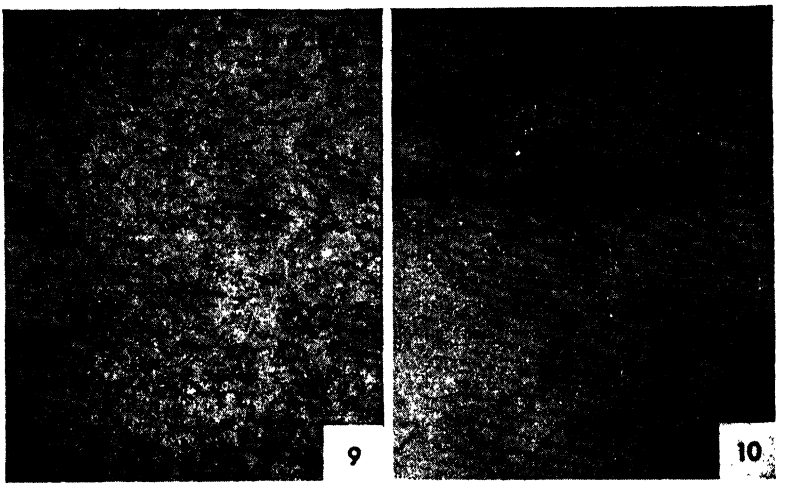

Micro. 2.9. Same as Micro. 2.7 after hot-rolling; ×50; NH_4OH:H_2O_2 etch. The dendritic structure of Micro. 2.7, showing probably only two separate crystal (or dendrite) orientations, has been completely obliterated by the hot deformation. Now the specimen shows hundreds of very small, individual crystals. Parallel straight lines extending across many of the crystals outline *annealing twins* that appear after a metal has been deformed and annealed or equivalently deformed at a high temperature. (The ingot iron, Micro. 2.2, shows what appears to be a well-defined annealing twin although body-centered cubic iron is not known to form this type of twin.) In addition to changing the grain size of the copper, the hot-rolling has destroyed the interdendritic network of Cu_2O particles and caused the oxide to be aligned as stringers of particles in the direction of hot-working (compare with the wrought iron, Micro. 2.3, and 2S aluminum, Micro. 2.6.).

Micro. 2.10. Same as Micro. 2.9 at ×500. It is apparent from a comparison of the size of these oxide particles with those in the as-cast structure, Micro. 2.8, that the hot-rolling not only changed the distribution of Cu_2O but considerably increased the size and decreased the number of the individual crystallites. This is the result of attempts by the oxide to reach a state of minimum surface. It is possible by reason of a slight solid solubility (see page 124) of Cu_2O in copper; the smaller particles of oxide dissolve, and a corresponding amount must then go out of solution by crystallizing on a particle already present. Thus there is a general tendency for particles to grow in size and decrease in number, but this is possible only when the metal is at an elevated temperature under conditions of slight solid solubility of the particle in the matrix.

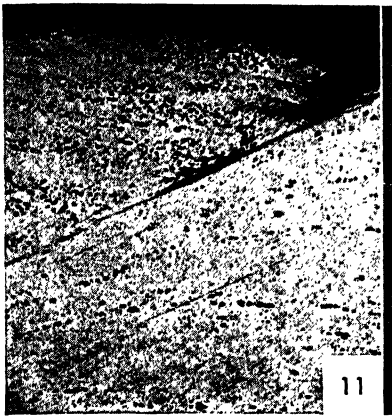

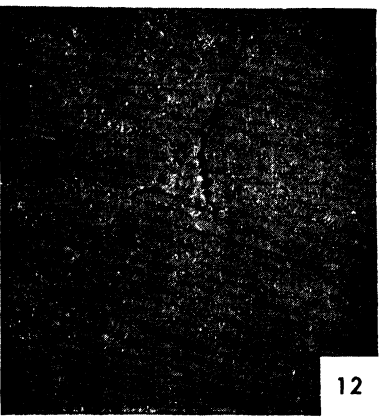

Micro. 2.11. Tough-pitch copper; ×150; no etch. This structure represents a section across a tear found in cold-rolled copper sheet. Note that the tear represents a surface with a high cuprous oxide content on one side, and a low or normal content on the other. Localized regions of high oxide content may result from insufficient "scalping" (machining) of the cast set surface of the ingot, which frequently has an oxygen content approaching 0.4%. It also may result from local overheating and melting during soaking at a high temperature for hot-working. In either event, the region adjacent to areas of high oxide content is susceptible to cracking under stress.

Micro. 2.12. Oxygen-free, high-conductivity copper, heated in an oxygen-bearing atmosphere for 2 hr at 900°C; reheated 2 hr at 900°C in hydrogen, ×200; potassium bichromate etch. Although the original copper was free of oxygen, some entered the metal during the first heat treatment, to a content of about 0.008% O_2. On reheating in H, atoms of hydrogen diffused into the copper. They reacted with cuprous oxide at the grain boundaries to form steam ($H_2 + Cu_2O \leftrightarrows 2Cu + H_2O$) at a high pressure and temperature, and the steam created a network of fine holes along the grain boundaries. (Note that the twin bands do not contain any pores. This is further evidence of the continuity of the atomic lattice at twin bands and discontinuity at grain boundaries.) Copper in this condition may show a strength of only 5,000 psi with zero elongation as compared to a normal 32,000 psi and 40% elongation.[1]

[1] Rhines and Anderson, *Trans. AIME*, **143**, 312, 1941.

lattice, such as those on page 27, are misleading in portraying atoms as small spheres widely spaced. This device is used only to permit representation of the three-dimensional lattice distribution of atoms. It should not be inferred that, having widely spaced atoms, metals might be readily compressed. They are compressible only to a slight extent, and large spheres in contact, as obtained by packing marbles in a box, better represent the actual structure. Even in this case, the stationary position of atoms is not a correct representation of the lattice, for these are only the statistical average positions of vibrating spheres. As the temperature is raised, the amplitude of atomic vibration increases and, although the configuration of atoms is unchanged, the average spacing increases and the forces between atoms become correspondingly less. Practically, this effect results in the expansion of metals and a loss in strength as the temperature increases from the theoretical absolute zero to the melting point. Although the strength-temperature relationship does not follow a straight line,[1] it suggests that low-melting-point metals should be weaker (at room temperatures) than those with high melting points. This is ordinarily true.

Plasticity of pure metal crystals is basically related to their atomic structures. Although it has been pointed out that the three common metal crystal structures (face-centered cubic, body-centered cubic, and close-packed hexagonal) are very similar, equivalent planes are not identical in respect to interplanar spacing and atomic density, two factors that determine the ease of deformability. Thus the (*octahedral*) planes, cutting off the corners of the face-centered cubic lattice, have atoms placed similarly to those on the basal plane of the close-packed hexagonal structure. However, there are four octahedral planes in the cubic lattice at different positions with reference to any outside surface or direction while the hexagonal structure has only one. Thus, if a force is applied to the two different types of lattices, the cubic crystal is certain to have at least one plane in a position that will permit slip and deformation. (These processes are discussed in detail in Chap. 4.) The hexagonal crystal, however, may have its single basal plane in such a position that it cannot function in the deformation process. Generally, it will then develop mechanical twins (see structure of zinc),

[1] Strength values are increased by the deformation that occurs during ordinary tensile testing, and the amount of this deformation is frequently a function of temperature also. However, fundamentally, strength seems to be a function of deformation and a parameter of the form $e^{Q/RT}$ where e is the natural logarithm base, Q the energy to move one atom past another, R the gas constant, and T absolute temperature.

which reorients the basal plane so that some deformation can occur. Certain positions of the basal plane with respect to the applied stress will result in cleavage of the crystal and, in general, the hexagonal metals must show considerably less plasticity than face-centered cubic metals. The body-centered cubic lattice has several potential planes of slip, like the face-centered cubic, but none so well defined, *i.e.*, densely packed and correspondingly well separated. Thus the body-centered cubic structure occupies an intermediate position in ease or possible extent of deformation.

A third important characteristic of pure metals is their electrical or thermal conductivity, both properties being apparently dependent on the presence of free electrons in the atomic structure. The solid sphere representation of this structure, although satisfactory for discussion of compressibility, is misleading in that most of the sphere is unoccupied space. As is well known, the nucleus of each atom contains most of its mass and has, as a whole, a fixed positive charge. The electrons, of generally fixed rotational orbits and energies, have low mass and, in sum, negative charges balancing the positive charge of the nucleus. Ignoring the nucleus and its energy potentialities, it is the electrons, their number, positions, etc., that determine most of the physical and chemical properties of metals.[1] When a large number of like metal atoms arrange themselves in a solid crystal form, not all the outermost electrons are tied to any particular atom. The structure actually consists of positive ions, at the specific lattice sites, immersed in an electron "gas." Under an applied potential, the electrons will flow through the metal lattice. The resistance of the metal, by Sommerfeld's theory of metals, is as follows:

$$R = \frac{mv}{ne^2l}$$

where m = electron mass
v = velocity of free electron
n = number of free electrons
e = electron unit charge
l = mean free path of electrons

Of these quantities, n will vary with the type of metal and more particularly its position in the periodic table of elements. For example,

[1] This subject is in reality in the field of physics. For a descriptive or nonmathematical treatment, see Boas, "The Physics of Metals & Alloys," Wiley, 1948, or Hume-Rothery, Atomic Structure for Students of Metallurgy, *Inst. Metals, Monograph* 3, 1946. A more extensive treatment is given in Seitz, "The Modern Theory of Solids," McGraw-Hill, 1940.

although both copper and nickel are face-centered cubic, nickel has a resistivity eight times that of copper. The mean free path l is a function of temperature, purity, and metal condition. As the temperature rises, thermal vibration of the atoms reduces the mean free path and the electrical resistivity increases; specifically, the logarithm of the free path decreases linearly as the logarithm of temperature increases. Impurities or unlike atoms that are atomically dispersed in the base metal atomic structure will in all cases decrease the mean free path by an amount depending on the relative positions in the periodic table of the two

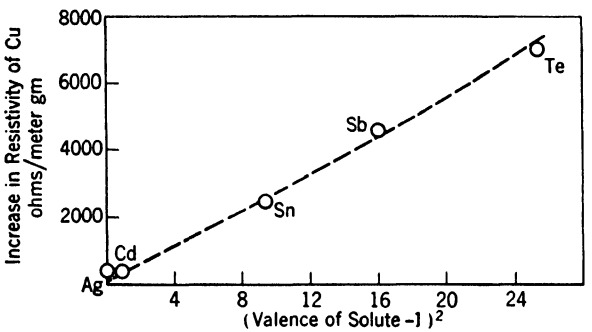

FIG. 2.7. Relation between the electrical resistivity of copper-base solid solutions and the valency of the solute (expressed as the square of the valency minus one).

elements (see page 475). Silver decreases the conductivity of copper only slightly (Fig. 2.7), while phosphorus markedly diminishes it. The metal condition has only a minor effect since severe cold-working of pure metals decreases conductivity by only 1 to 5%.

These remarks are general comparisons of pure metal crystals. The presence of impurities can markedly alter expected plasticity, strength, electrical, thermal, or other properties, as is shown in the following specific examples.

2.7 Copper

The common impurity, oxygen, slightly decreases plasticity, but this is not very noticeable, except at points of high oxide concentration (Micro. 2.11) or when the copper is heated in atmospheres containing hydrogen or in which hydrogen may be generated. Oxygen-free copper can be produced by adding phosphorus to the liquid metal, but ordinarily, the residual phosphorus content reduces the conductivity of the metal below that required for electrical applications. Oxygen-free

copper (OFHC) melted and cast in a carbon monoxide atmosphere will exhibit superior plasticity to the tough-pitch grade, although it can also be embrittled by first heating in oxygen (or air) and then in hydrogen. One other particularly dangerous impurity is bismuth which, by forming a low-melting-point structure (with as little as 0.006% Bi), causes the copper to lose all ductility at high temperatures (see hot-shortness, page 141). A lower concentration of bismuth can be tolerated on the basis of its slight solubility in solid copper.

The good electrical conductivity of copper signifies an associated high thermal conductivity. This property, together with its relatively good resistance to corrosion, accounts for numerous uses in heat-exchanger equipment, *e.g.*, in plants producing oxygen from liquid air, in all gaseous liquefaction units, in space heaters, in distillation and condensation units, etc.

One difficulty encountered frequently in the fabrication of copper is shown in Micro. 2.12 on page 45. This "hydrogen embrittlement" is a result of a chemical reaction: $Cu_2O + 2H \rightarrow 2Cu + H_2O$ (steam). The hydrogen is present in the metal as individual atoms, not as diatomic molecules. No difficulty is encountered unless the temperature is fairly high, *i.e.*, above 500°C, either because not enough hydrogen dissolves at low temperatures or because the reaction does not proceed strongly until a red heat is attained or because the H_2O or steam generated by the reaction cannot develop sufficient pressure until a sufficient temperature is reached. If the temperature is above 950°C, however, little damage occurs. Presumably this is because of the greater dissociation of H_2O or, more likely, because of self-healing or automatic self-welding of the voids created by steam pressure. The critical range of embrittlement is 650 to 850°C (1200 to 1580°F).

It is quite certain that only hydrogen causes this effect even though embrittlement has been reported when oxygen-bearing copper was heated in hydrogen-free atmospheres, *e.g.*, CO and steam. This combination of gases would be subject to the producer gas reaction, $CO + H_2O \rightarrow CO_2 + 2H$, at high temperatures and the hydrogen so evolved would cause the difficulty.

Even the use of oxygen-free copper such as OFHC does not necessarily ensure that the copper can be safely heated in hydrogen or atmospheres containing hydrogen. If the copper were first heated in oxygen, this gas would dissolve in copper, up to a maximum of about 0.01% and make the metal subject to subsequent hydrogen embrittlement.

2.8 Magnesium

The most important property of magnesium is its light weight or, in alloyed form, its high strength-to-weight ratio. Although this ratio may not be superior to that of stainless steel or strong aluminum alloys, the magnesium structure will be bulkier or thicker and, therefore, stiffer. This inherent advantage of magnesium alloys can, however, sometimes be overcome by appropriate design of aluminum or stainless-steel structures. Magnesium, a close-packed hexagonal metal, has limited ductility at room temperatures. When heated to about 500°F, it becomes very plastic and can be worked, in some cases, more severely than aluminum, brass, or steel.[1] Finally, magnesium is the world's most universally available metal, present in sea water in practically unlimited quantities. All of the metal produced in the world up to 1949 could have been taken from one-fifth of a cubic mile of sea water!

These favorable engineering characteristics are accompanied by some detrimental factors. The metal and its alloys oxidize or burn easily when liquid or in fine particles such as machined chips or powders. In addition, the cost per pound, although steadily decreasing in the past twenty years, is still higher than most competitive metals. The cost per unit volume is not always higher, and the cost of a specific fabricated article may, in some cases, be less than that for a competitive metal.

Magnesium has long been thought to have relatively poor corrosion resistance, particularly to salt-water solutions or vapors. This resulted in extremely careful surface protection (or the abandonment of use of the metal) in many applications, *e.g.*, naval aircraft. It has been found[2] that *pure* magnesium, and its important alloys are very resistant to salt-water corrosion. By keeping the amounts of iron, copper, nickel, and cobalt impurities below certain tolerance limits (*e.g.*, 0.017% Fe), or by balancing higher contents with other elements that neutralize the corrosion-stimulating effect, magnesium alloys may show far greater resistance to corrosion than was believed possible only a few years ago; *e.g.*, they withstand 3 months' alternate immersion in a 3% sodium chloride solution without significant loss of strength. This is in comparison with similar alloys made from ordinary commercial magnesium which might completely dissolve or corrode away under the same conditions. Paints following a chemical dip increase the protection of all alloys, but even the improved "pure" magnesium alloys would never

[1] Hanawalt, "Industrial Significance of the Basic Characteristics of Magnesium," *Metal Progress*, **49**, 548–552, 739–743, 1946.

[2] Hanawalt, Nelson, and Peloubet, *AIME*, **147**, 273, 1942.

be chosen solely on the basis of their resistance to salt-water corrosion.

2.9 Zinc

This metal owes one of its chief uses to the fact that it can be coated readily on the surface of iron, by immersing the iron in liquid zinc or by electrodeposition; it will thereafter protect the iron from rusting or corrosion in mildly corrosive mediums. The protection is effected by excluding contact of the mediums with iron and is electrochemical since zinc is anodic to iron and will go into solution while iron acts as a cathode and is unaffected.

Like magnesium, zinc is close-packed hexagonal and has limited ductility at room temperature, but it becomes quite plastic at elevated temperatures.

Zinc has a relatively low melting point and thus, in the alloyed form, was chosen as particularly suitable for making pressure die castings. However, the first die castings proved very unsatisfactory, particularly in warm, humid climates. They would swell enough to jam mechanisms in which they were used, and the intergranular (between grains) corrosion, which caused the swelling, greatly reduced the strength properties. Research showed that by keeping the total content of lead and cadmium impurities below 0.01%, the die castings would indefinitely resist intergranular corrosion. Thus, zinc for die-casting alloys must have a purity of 99.99%, whereas that used for alloying with copper (to make brass) or for galvanizing iron has considerably higher permissible impurity limits.

2.10 Iron

In the pure state, iron has much better corrosion resistance than in the relatively impure form of steel, even low-carbon grades. Ingot iron finds its most important applications in enameled ware and in fields where better corrosion resistance than that of steel, but not particularly high strength, is required.[1]

Iron is subject to a "hydrogen embrittlement," which is entirely different in nature from the hydrogen embrittlement of copper. Whereas copper is embrittled only when it contains oxygen (or oxide) and is

[1] There appears to be some question as to the comparative corrosion resistance of relatively pure iron and ordinary low-carbon steel. It has long been believed that, in general, metals resist corrosion better when in a pure state, *e.g.*, magnesium and zinc. This generalization appeared to be true for iron, but recently some authorities have claimed that ingot iron's only special virtue is for enameling.

heated in hydrogen, iron is embrittled even though free of oxygen and kept at room temperatures. If the iron is at room temperatures, hydrogen is absorbed in sufficiently large quantities only when the gas is present at the surface in atomic form. Thus hydrogen kept in steel cylinders does not particularly embrittle the steel. However, if iron or steel is pickled in acid or electroplated,[1] hydrogen is released in the atomic form at the metal surface and is absorbed readily by the iron. Hydrogen atoms can move freely through interstices of the iron's atomic structure. When a sufficient number come to some internal discontinuity, they tend to join up in pairs to form stable H_2 molecules and, in so doing, create a local pressure that can attain extremely high intensities. A specimen in this condition is very brittle and, relatedly, weak. The same hydrogen embrittlement will result from heating iron or steel in hydrogen[2] or from hydrogen absorbed by molten iron, in the case of certain grades of steels. Following the absorption of hydrogen, a long time at room temperature or shorter times at somewhat elevated temperatures will permit it to diffuse to the surface and escape there. This will result in regaining practically all of the original ductility of the metal.

The commonest undesirable impurity element in all iron and steels is sulfur which, with iron, forms a low-melting-point constituent and thus causes hot-shortness (see page 141). The presence of manganese in amounts of about five times the sulfur content converts the sulfur to innocuous (high-melting-point) manganese sulfide. When present in comparatively large amounts, the manganese sulfide, by interrupting the continuity of the plastic ferrite matrix, permits the steel to be machined faster, with less power, and with a better surface finish. Sulfur added to oxidized liquid steels of normal content does not seem to form the normal iron sulfide that, distributed along grain boundaries, causes hot-shortness. Ramsey and Graper[3] show that the machinability of deoxidized steels may be improved without large manganese additions by adding sulfur as a sulfite, Na_2SO_3, which, upon contact with liquid steels, decomposes to SO_2 and Na_2O. The SO_2 is absorbed by the steel, perhaps as a monoxide with the excess oxygen forming SiO_2 and Al_2O_3. These are slagged off by the Na_2O. The resulting oxysulfide inclusions, by being uniformly dispersed, increase machinability without causing

[1] See for example. Zapffe and Sims, *Trans. AIME*, **145**, 225, 1941.

[2] In one case, ductile Armco iron tensile test specimens were annealed in H at 750°C and slowly cooled in hydrogen. On being taken out of the furnace, one bar was dropped on the floor and broke into three pieces! For a full discussion of hydrogen embrittlement, some of Zapffe's papers should be consulted.

[3] Ramsey and Graper, *Trans. AIME*, **150**, 127, 1942.

hot-shortness. However, other authorities claim that the same slight increase in sulfur, added directly as sulfur rather than as sulfite, would have a comparable favorable influence on machinability.

Iron is the most strongly magnetic of all the elements, yet it is not used in the pure form in electromagnets or in permanent magnets. In electromagnets, it is too good an electrical conductor. To prevent high eddy-current losses, silicon in amounts of about 3.5% is added to reduce conductivity with little effect on magnetic permeability. Permanent magnets require characteristics that are found to the highest degree in hard alloys of iron with cobalt, aluminum, and other elements.

2.11 Aluminum

This light metal is slightly stronger and less ductile when the normal content of iron, silicon, and copper impurities are present (as in Alcoa 2S), but in most alloy applications these are relatively unimportant. They have some influence on alloy casting properties and heat treatment temperatures (for details, see page 163), and the amounts present should be controlled for reproducible optimum properties.

Aluminum has an electrical conductivity about two-thirds that of copper on a volume basis; it is a better conductor on a weight basis since it weighs only about one-third as much as copper. Since the iron and silicon impurities form constituents that are insoluble in solid aluminum and do not materially reduce conductivity, commercially pure aluminum is becoming widely used for long-distance high-voltage power transmission lines. Aluminum wires surround a steel wire, present to increase strength, and the assembly is sufficiently light to increase spans between supporting towers and materially reduce line installation costs.

The corresponding high thermal conductivity, together with cold plasticity that permits easy working, has resulted in aluminum becoming the standard material for cooking utensils. Of course, the good corrosion resistance of the metal and the nontoxic character of salts formed by any aluminum that does dissolve also have favored this field of application of the metal.

2.12 Nickel

The element in commercially pure form may contain a slight amount of sulfur from the fuel used in melting furnaces, which may form a continuous envelope of brittle sulfide at the grain boundaries and thus embrittle the entire structure. The amount of sulfide can be so small

as to be undetectable by ordinary micrographic technique. The addition of about 0.05% Mg causes sulfide to form in an innocuous dispersion of particles and permits the metal to display its inherent plasticity or malleability. Similarly, lead may be present as an impurity in gold in amounts small enough to escape detection by the microscope and yet form a thin brittle envelope at grain boundaries, which, being continuous or nearly so, embrittles the entire structure.

Nickel is the most expensive metal of those discussed so far, and its relatively high cost has limited its uses to some extent. Its very good resistance to corrosion is most often utilized by electroplating a thin layer on the base metal or on an intermediate copper plate. The nickel plate is most frequently covered with a very thin layer of chromium electroplate, the chromium being harder, brighter, and therefore more pleasing to the eye. However, the corrosion protection depends on the nickel, since the chromium deposits are always somewhat porous. When the so-called *chrome plate* on an automobile begins to rust, it is generally because too thin a layer of nickel was deposited underneath the chromium.

The electrical and electronic industries depend on nickel for various components of vacuum tubes; its electron emission and expansion (for sealing in glass) characteristics are important here. Nickel is also important as a catalyst in certain chemical industries. However, the major uses of nickel are as an alloying element, particularly in steels.

2.13 Beryllium

Although having the same type of crystal structure as zinc and magnesium, beryllium has always been considered as a brittle metal since the purest laboratory grades have shown no malleability. Recently, commercial beryllium remelted under a vacuum (to eliminate nitrogen and other gaseous impurities), alloyed with small amounts (0.2 to 0.5%) of titanium or zirconium, and then cast under vacuum, has been successfully hot-rolled. The titanium or zirconium seems to form disperse stable oxide particles which replace the former beryllium oxide films that initiated cracking. However, the hot-worked product is still deficient in cold malleability. Improvement in this direction would greatly increase the utility of this interesting metal. It is probable that small amounts of aluminum or other similar metals, by forming a low-melting phase, can make the metal hot-short in a manner similar to sulfur in iron or nickel, lead in gold, or bismuth in copper.

The only significant use of beryllium as a metal is as a window in X-ray tubes, and it was for this application that a method of hot-rolling

beryllium was developed. Beryllium, with a very low atomic number, is quite transparent to X-rays and at the same time opaque to air so that a vacuum can be maintained within the tube and X-rays are passed through the window with little loss in intensity. Apart from this, the metal is used in small amounts as an alloying constituent, particularly in copper (see page 232). It may also become important in nuclear power plants.

QUESTIONS

Group A

1. Silver used for coinage is usually alloyed by adding 10% or more of copper. Give one metallurgical and one economic reason for this.

2. The electrical conductivity of modern coppers expressed in percentage of standard is frequently given as 102% or thereabouts of standard copper. Explain the basis for conductivity in excess of 100%.

3. How could you quickly differentiate between a piece of wrought iron and a piece of identical shape and size of ingot iron?

4. Differentiate between *lattice*, *crystal*, and *grain*. What is the difference, if any, in meaning of the words *crystalline* and *granular*?

5. If you purchased iron wire electroplated with zinc and found it of variable ductility, lot to lot, what would you surmise as to the cause and, acting on this surmise, what specific tests would you make to increase and make uniform the ductility of all the wire?

Group B

1. Write brief sections on the metals tungsten, titanium, and lead, comparable to those in the text on Cu, Mg, Zn, Fe, Al, Ni, and Be.

2. The following represent typical hardness data obtained on the specified metals:

	Armco Fe	OFHC Cu	Pure (99.95%) Al	Pure (99.99%) Zn
Brinell, 500 kg, 10-sec loading	69	34	14	34
Brinell, 500 kg, 60-sec loading	69	34	14	30
Rockwell, 60 kg, 1/16-in. ball	60	23	(−30)	(−13)*
Rockwell, 25 kg, 1/16-in. ball	(111)	91	5	76 *

* 5 sec loading.

Explain why duration of loading is important in the case of zinc but less significant for the other metals.

3. If a piece of wrought iron and a piece of ingot iron were separately melted without changing compositions *e.g.*, in an electric induction furnace, and cast by pouring into similar molds, what would be the significant differences between the solidified irons? Would either of them be properly termed *cast iron*?

4. Ingot iron sometimes is difficult to hot-roll (deform between rollers at white-heat temperatures) without cracking. Explain the probable reason (based on composition).

5. Copper containing oxygen may be brought to a red heat in pure carbon monoxide without embrittlement and, if so heated for a long time, may be subsequently heated in hydrogen without embrittlement. Give a description of what probably would happen on heating in CO, remembering that atoms can diffuse through hot metals but not foreign molecules.

CHAPTER 3

SOLID SOLUTIONS: COPPER-BASE ALLOYS

Liquid solutions, *e.g.*, water and alcohol, are liquids containing two components where the temperature or the composition can be varied without the creation of a second phase. Analogously, metallic solid solutions are one-phase structures containing two or more elements in which concentration or temperature can be varied through a considerable range without changing the type of crystal structure of the alloy. Commercially important solid-solution alloys generally have the crystal characteristics of the element present in greatest amount, *i.e.*, the *solvent* metal. For example, up to about 38% of zinc can be added to copper without changing the type of crystal structure and with only moderate, continuous changes in other basic characteristics of the copper. It is impossible to distinguish between the two elements in the ordinary solid-solution phase. In the usual *substitutional* type of solutions, one type of atom, the *solute*, is substituted for the other, the *solvent*, at random points on its lattice. In the *interstitial* type of solution (see Fe:C alloys, Chap. 9), atoms of the added element are present in the interstices of the solvent lattice. It is the practice throughout this book to refer to terminal solid solutions that have the structure of one of their component metals as *alpha* (or α) phases, with a subscript added to denote the solvent metal or element when more than one such solution appears on the diagram.

3.1 Cu:Ni Phase Diagram

Charts showing the relationships between the phases present in an alloy system as a function of the temperature and composition are called *phase, constitutional,* or *equilibrium* diagrams. All the diagrams given in this textbook are "equilibrium" diagrams, meaning that the alloy phase condition indicated for a given temperature and composition will show absolutely no change or tendency to change with time. The stable or equilibrium condition is dynamic; atoms are not stationary, but the gross summation of all movements is zero. The following generaliza-

tions will be helpful in applying abstract charts to specific alloy systems, *e.g.*, the Cu:Ni system of Fig. 3.1.

1. Single-phase fields (for example, those marked *liquid* or α) must be separated by a two-phase field containing some of each single phase, *e.g.*, the field of *liquid plus* α. The upper line defining the *liquid* + α region is called the *liquidus* and the lower line, the *solidus*.

2. When an alloy of a fixed composition is heated or cooled past the temperature indicated on a diagram by a line, there is a partial (for

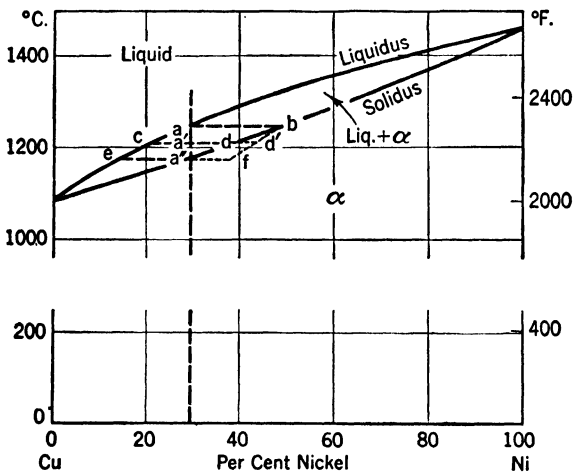

FIG. 3.1. Phase diagram of the copper-nickel alloy system.

sloping lines) or complete (for certain points on horizontal lines) change of phase and a concomitant absorption, or release of energy, in the form of heat. Thus, on cooling a 70% Cu:30% Ni alloy (composition *a*) past the liquidus, some solid crystals of the α phase start forming, and the release of their heat of formation causes a change in slope of the cooling curve. It is this effect that is utilized to determine the temperature at which solidification begins, or the minimum temperature to which an alloy must be heated to ensure complete melting.

3. In a two-phase field, the composition of each phase at a specific temperature is given by the intersections of a horizontal line, drawn at this temperature, with the phase field boundary lines. Thus, at the temperature indicated by the horizontal line *ab* the liquid has the composition of *a* (30% Ni) and the solid the composition of *b* (50% Ni); at the line *cd*, the liquid and solid phase compositions would be, respectively, 22 and 40% Ni; etc.

4. The relative proportions of each phase in a mixture of two phases,

with the temperature and composition of the alloy known, is given by the *lever rule.* This states that, for an alloy in a two-phase field the proportionate amount of each phase is given by the ratio of the *difference between the gross alloy composition and that of the other phase* to the *difference in composition of the two phases.* Thus, in the diagram, the 70% Cu:30% Ni alloy, at the temperature of the horizontal *cd*, contains α of composition d and liquid of composition c. The proportionate amounts of each would be as follows:

$$\frac{d - a'}{d - c}(100) = \frac{40 - 30}{40 - 22}(100) = 55\% \text{ liquid}$$

$$\frac{a' - c}{d - c}(100) = \frac{30 - 22}{40 - 22}(100) = 45\% \ \alpha$$

Generalization 3 requires that the composition of the solid phase must change during the interval of solidification over a falling temperature. Under equilibrium conditions, this adjustment of composition would occur throughout the solid phase, which would be forming open, treelike crystals called *dendrites.* However equilibrium is practically never achieved in commercial casting processes, and the first dendritic nuclei are richer in the higher-melting-point element than the successive layers formed at lower temperatures. The average composition of the total solid phase, in this case, will not be that shown by the phase diagram for a given temperature, *e.g.*, point d at temperature *cd* (see Fig. 3.1); it will contain more of the higher-melting-point element, perhaps that given by point d'. This difference in composition from center to edge of a dendrite may remain as a result of the slowness of atomic interchange or diffusion. (Chinese bronzes over 3,000 years old show this dendritic composition difference.) The 70:30 alloy should be completely solid when it reaches the temperature of the lower phase field boundary line (at point a''), but under nonequilibrium conditions the average solid-phase composition will be at some point near f and some liquid will remain; specifically,

$$\frac{f - a''}{f - e} = \frac{37 - 30}{37 - 15}(100) = 32\% \text{ liquid and } 68\% \text{ solid}$$

The presence of some liquid in a solid-solution alloy, cooled from the liquid state to the *solidus* line, results from the failure of diffusion, between the two types of atoms, to maintain the composition of the growing, solid-phase dendrites at the equilibrium concentration. The amount of liquid present here depends on the time permitted for diffusion

during solidification. The more rapid the freezing, the farther will be the departure from equilibrium and the greater will be the amount of liquid present. Even under relatively slow cooling conditions, such as might be employed in thermal analyses for the determination of this phase diagram, the *solidus* temperature is never well marked on a cooling curve. After the solidification of the last liquid is completed, cooling may speed up slightly, but seldom is there a well-defined change in slope at a specific temperature.

Liquidus temperatures may be depressed by undercooling because of slowness in the formation of the first dendritic crystal nuclei, but this effect can be minimized by agitating or stirring the melt or, in some cases, by artificial nucleation. The pasty condition of the nearly solidified alloy prevents stirring and, although the required diffusion would be accelerated by deformation, that is difficult to accomplish with the alloy in a crucible or mold and still partly liquid. Solidus temperatures, however, may be readily determined by heating a *homogeneous* solid solution to successively higher temperatures. If the alloy is simultaneously subjected to a slight stress, it deforms plastically while entirely solid, but as soon as the solidus temperature is reached, liquid (enriched in the lower-melting-point element) forms at the grain boundaries, and the alloy breaks with an intercrystalline failure (hot-shortness). If the alloy is quenched from just above the solidus, evidence of the existence of the liquid phase at that temperature is preserved and can be identified micrographically by reason of its different composition. This constitutes a second method of determining solidus lines.

A powerful tool in the construction of phase diagrams from experimental data is the phase rule, developed through abstract thermodynamic reasoning by Willard Gibbs, one of the greatest of American scientists. This rule, ignoring pressure as a variable,[1] is as follows:

$$F = C - P + 1$$

where F = number of independent variables
C = number of components in system; in alloys, the number of elements
P = number of coexistent phases

Applying the phase rule to the Cu:Ni system, for *each pure metal* at its

[1] The usual variables are temperature, pressure, and composition of each phase, including gas. Metals and alloys are almost always studied at atmospheric pressure and the gas phase is ignored; otherwise the general form of the phase rule would apply: $F = C - P + 2$.

melting point, there is one component and two phases, liquid and solid metal coexisting during freezing. Therefore, $F = 1 - 2 + 1 = 0$, the system is invariant, and the metal must freeze at constant temperature. If the rate of heat removal is constant near the freezing point, this means that a "cooling" curve of temperature vs. time would show a horizontal break for the duration of freezing, assuming that equilibrium exists.

The freezing of any alloy in the Cu:Ni system also involves only two phases, the α solid solution and the liquid solution. However, with two components, $F = 2 - 2 + 1 = 1$, there is one independent variable. Thus the temperature of the system may be varied while two phases coexist, but the composition of each phase is fixed for any selected temperature. If the composition of one phase, *e.g.*, the solid α, is specified, the composition of the other phase and the temperature are thereby fixed. Another means of explaining the significance of $F = 1$ is to say that the alloy freezes over a range of temperatures with compositions of both liquid and solid phases dependent on the temperature. The result of this univariance is that solidification of a solid solution is not manifested by a horizontal break on the cooling curve. The heat of crystallization of the solid α, released upon its formation in the liquid, slows the rate of temperature drop and results in a well-defined point of inflection at the start of freezing.

3.2 Cast Cupronickel Microstructures

The solidification rate of solid-solution alloys is rarely slow enough for equilibrium to be maintained through the liquidus-solidus interval. Therefore, it is characteristic for compositional gradients to exist from the center of dendritic arms to the center of interdendritic spaces. Since the rate of chemical attack varies with composition, the proper etching of polished surfaces usually reveals the dendritic structure. The degree of dendritic segregation or *coring* depends on the diffusivity of the two unlike atoms in the solid solution and the time available for diffusion. The latter in turn depends on the solidification rate, being short for chill casting and relatively long for casting in sand with its lower heat transfer rates.

The degree to which dendritic segregation is revealed by etching depends on the degree of etching and the characteristics of the specific etchant. In the case of copper-base alloys, there are many potential etchants some of which are listed on page 88. The solution of potassium bichromate listed there has been used on the cupronickel structures shown in Micros. 3.1 through 3.6.

Micro. 3.1. 85% Cu:15% Ni, as chill-cast; ×50. This structure is composed of small dendrites of a single phase, the α solid solution. There is a very considerable difference in nickel content from the central axes of the dendrites to the midspace between axes, as predicted from the considerations previously described. This is a metastable structure that is commonly described as *cored* dendrites (from the continuous differences in composition from the interdendritic spaces to the cores). Upon etching, the nickel-rich, dendritic cores are not dissolved so rapidly as the copper-rich filling; thus the surface of the etched specimen consists of a series of hills and valleys. The dendritic details obscure grain boundaries, although several differing grain orientations may be found by studying the directions of the dendrites.

Micro. 3.2. 85% Cu:15% Ni, as chill-cast and heated 3 hr at 750°C; ×50. The cored dendritic structure has changed only slightly. Counterdiffusion of copper and nickel atoms between the nickel-rich cores and copper-rich fillings has decreased the composition differences somewhat and thus slightly reduced the height of the hills and depth of the valleys. Careful examination of the structure shows some evidence now of grain boundaries.

Micro. 3.3. 85% Cu:15% Ni, as chill-cast and heated 9 hr at 950°C; ×50. This lengthy, high-temperature treatment has completely homogenized the cast structure, *i.e.*, equalized the composition at all points. Grain boundaries are clearly evident, and their irregular shape is frequently encountered in cast and homogenized solid solutions, the irregularity being related to interpenetration of dendrites growing in the liquid alloy. Black particles are copper oxide or nickel oxide inclusions. The grain size is no larger than in the original casting since grain growth does not occur in castings, except when they have been previously strained by some stress (externally applied or originating from contraction during cooling).

Micro. 3.4. 85% Cu:15% Ni, as cast in a hot mold and slowly solidified; ×50. This dendritic structure is considerably coarser than that of the chill-cast alloy (Micro. 3.1). The cells represent nickel-rich areas (low hills) and the narrow, approximately parallel, lines outline the interdendritic copper-rich valley areas. The black, vaguely outlined areas are shrinkage cavities which, it should be noted, occur in the parts last to freeze, *i.e.*, the copper-rich areas. A single grain boundary diagonally traversing the field along the interdendritic spaces is also visible.

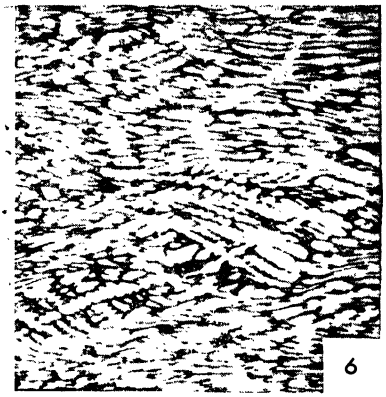

Micro. 3.5. 85% Cu:15% Ni, as cast in a hot mold, slowly solidified, and then reheated 15 hr at 950°C; ×50. In this homogenized structure the grain size is considerably coarser than that of Micro. 3.3, more so than is evident in this photograph, which was taken at the intersection of three grains. Again, copper or nickel oxides are visible and also some shrinkage cavities. The time required for homogenization of the coarse dendrites was greater than that for the fine dendrites, in spite of the smaller initial composition differences across the coarse dendrites. The reason is that the distance through which copper and nickel atoms must diffuse is so much greater in the coarse structure.

Micro. 3.6. 64% Cu:18% Ni:18% Zn; ×100. This is a longitudinal section of a wrought alloy, called *nickel silver* because its color approaches that of silver. It is frequently used as a base for plated silverware and other applications for which its color, corrosion resistance, and strength are adapted. This micrograph of commercial metal, in the hot-worked condition, shows that the cored dendritic structure has not been homogenized in spite of the fact that deformation accelerates homogenization. The increased softness of the homogenous metal in these alloys is seldom worth the costs of the prolonged, high-temperature anneals necessary to obtain complete homogeneity.

3.3 Cast Macrostructures

Upon very slow cooling of a liquid alloy with all of the metal maintained at a uniform temperature, solidification will start just below the temperature shown by the liquidus line of the phase diagram. A few nuclei, distributed throughout the liquid, will form, and each will grow in all directions (as dendrites) to form a coarse, equiaxed grain structure. If the entire liquid cools uniformly but rapidly, many more nuclei will originate in the melt and produce a finer grained equiaxed structure. If one part of the liquid cools rapidly and another slowly (as in industrial casting processes where a hot liquid is in contact with an originally cool mold), nuclei will form only where the liquidus temperature is first attained, *i.e.*, at the mold wall, and these nuclei will grow in the direction of the thermal gradient, giving elongated or columnar crystals. Later, the center, or hotter part, of the casting may reach the liquidus temperature before columnar crystals have grown into this section. Equiaxed grains may be found here.

In castings, it is possible to have combinations of coarse and fine, columnar and equiaxed crystals. By controlling liquid and mold temperatures, thermal conductivities and relative masses, it is possible to exercise considerable control of cast structures. Liquid metal temperatures just above the alloy liquidus temperature mean that removal of a small amount of heat will be sufficient for nucleation of the solid crystals to start. Nuclei will form and grow first at the mold wall but seldom can grow extensively before heat flow has brought the next layer of liquid to the initial freezing temperature. Thus new nuclei will tend to form before the first crystals have grown to this zone. Therefore, the tendency is for all crystals to be equiaxed with their size determined by the rate of heat removal, *i.e.*, the temperature, mass, and thermal conductivity of the mold.

Considerable superheat of the liquid, *i.e.*, a temperature well above its freezing point, inevitably means that steeper thermal gradients in the liquid metal are possible. Thus after the first nuclei form at the mold wall, they may be able to grow as fast as heat flows in the opposite direction. The hot liquid may not cool to the liquidus temperature appreciably in advance of the growing crystals and, therefore, no new nuclei can form. In this case, columnar crystals are certain to form but, again, their size will be determined by the rate of heat removal. It should be noted though that the long axis of the columnar crystal will always be normal to the mold wall. In addition, since a crystal does not grow in all crystallographic directions at the same rate, there is a tendency for the axis of the columnar grain to be in a specific crystallo-

graphic direction. In the case of face-centered cubic crystals, it is usually the [111] direction; *i.e.*, (111) planes will be parallel to the mold wall.

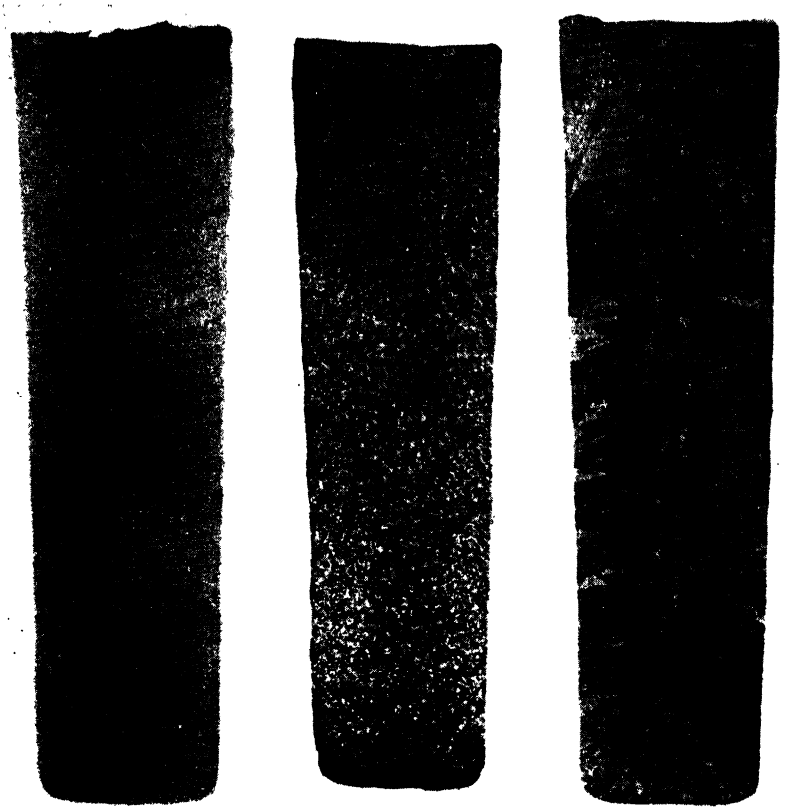

(*a*) (*b*) (*c*)

FIG. 3.2. Macrographs of aluminum-base solid solution; (*a*) fine-grained ingot obtained by pouring liquid metal at only a few degrees above its melting point into a cold iron mold; (*b*) coarse-grained ingot obtained by pouring liquid metal at only a few degrees above its melting point into a hot iron mold; (*c*) columnar-grained ingot obtained by pouring liquid metal, superheated well above its melting point, into a cold iron mold.

Typical examples of some possible ingot macrostructures are presented in Fig. 3.2. They happen to represent an aluminum solid solution but are typical of any metal solidifying quietly or without gas evolution. Figure 3.2*a* shows a very fine equiaxed grain structure; *b*, a coarser equiaxed grain structure; *c*, a completely columnar structure.

Sectioning, grinding smooth, and deep-etching of a cast metal will

not only reveal grain size and shape but also usually discloses voids. Unfortunately for illustrative purposes, but fortunately for their subsequent use, the small ingots of Fig. 3.2 are free of these voids. They may originate from gas in solution in the liquid metal that is concentrated in this liquid during solidification and evolved only when the concentration reaches a critical value. If the metal does not contain much gas, that point might be reached only in the final stages of solidification and result in a few voids in the top center or last-to-freeze part. If the original content were high, the gas bubbles might be distributed as voids in the cast metal throughout the casting.

A second source of voids appearing in the macrostructure or microstructure is the shrinkage of most metals during solidification, a result of the greater density of atom packing in the solid than in the liquid state.[1] If freezing starts at all surfaces and fixes the external dimensions at nearly the same as those of the liquid, then there inevitably will be from 4 to 8% voids in the structure, these figures representing the range of solidification shrinkage usually encountered. Shrinkage voids can be eliminated only by having an external reservoir of liquid metal to supply the deficiency represented by shrinkage. In ingots, this liquid may be supplied by insulated "hot caps" (steel) or an electric arc that keeps the top liquid (nickel) or by continually pouring liquid in the top and freezing from the bottom (aluminum alloys).[2] In sand castings, the liquid is supplied by a reservoir larger in section than the casting, which is called a *riser*, and is connected directly to the thickest section of the casting if possible.

Both shrinkage voids and gas pores are necessarily interdendritic. However, gas voids are seldom continuous. If physical conditions enable a bubble of molecular gas to form, the concentration of gas in the adjacent liquid is sufficiently diminished for normal solidification to proceed for at least some specific time interval before a critical solute concentration of gas is again attained. However, shrinkage voids are necessarily continuous throughout any area in which they occur. Shrinkage cavities are, therefore, more likely to cause "leaky" casting, *i.e.*, cast metals that permit water or other liquids under pressure to leak through the supposedly solid metal.

[1] The liquid state, at least at temperatures only slightly above the melting point, is characterized by atomic arrangements not too different from the solid lattice. For example, in a face-centered cubic lattice each atom has 12 close, equidistant neighbors. Upon melting, this changes so that each atom has 11 close neighbors. This arrangement can no longer be highly symmetrical and cubic and also necessarily involves an expansion structurally.

[2] Lippert, *Trans. AIME*, **161**, 479, 1945.

A fine equiaxed grain structure is usually desired for its greater strength and hardness (Chap. 4). If impurities are present at grain boundaries, they will be more finely dispersed in a fine-grained structure and, therefore, are less troublesome. This is particularly true when the casting is an ingot that is subsequently to be rolled; a coarse-grained structure is far more likely to crack in the early stages of working, and the brittleness is related to impurity concentrations at grain boundaries.

3.4 Segregation in Cast Alloys[1]

Dendritic segregation on a microscopic scale is called *coring* and may be explained by the use of a phase diagram in the manner already discussed. On a macrographic or full-size scale, a similar effect may be noticed in that the first parts of a casting to freeze are enriched in the higher melting phase while the parts last to solidify (generally, top center sections) are enriched in the lower melting-point constituents. The effect is statistical in nature since both sections will exhibit coring. The resulting nonuniformity of chemical composition is known as *normal segregation* and differs only in dimensions from coring. A third type of segregation is the reverse of this; *i.e.*, the parts of the casting first to freeze are enriched in low-melting-point constituents. The effect is called *inverse segregation.* It is primarily caused by the contraction of solidifying dendrites, which tends to enlarge the interdendritic channels. As these open up, a resultant suction effect draws residual liquid metal, enriched in solute atoms (or low-melting-point constituents), through the channel to the surface. The action may be aided considerably by an internal pressure from the release of dissolved gases. Thus "tin sweat," exudations rich in tin, may form on the surface of tin bronze castings when the liquid metal contains appreciable amounts of dissolved hydrogen which is released as gas in a late stage of solidification and forces the tin-rich liquid at the center of the casting through the interdendritic channels to the surface.

Coring may be completely eliminated by diffusion (homogenization) treatments at high temperatures as shown by the photomicrographs. Normal and inverse segregation are little affected by such treatments because of the tremendous distances (on an atomic scale) involved.

3.5 Homogenization by Diffusion

Diffusion is an important factor in many metallurgical problems. At the moment, it is apparent from the Cu:Ni phase diagram and the accompanying discussion of solidification, that the composition of the

[1] For a more complete discussion, see Brick, *Trans. AIME*, **161**, 65, 1945.

solid phase must change during solidification under equilibrium conditions. Micrographs 3.1 to 3.6 give evidence that, if diffusion does not occur during solidification, it can occur subsequently by heating to a temperature near the melting range. It might be helpful to show graphically the most probable means of doing this.

In the discussion of the crystal structure of metals in Chap. 2, the statement was made that millions or billions of atoms are present in an orderly repetitive three-dimensional arrangement. Also, a statement

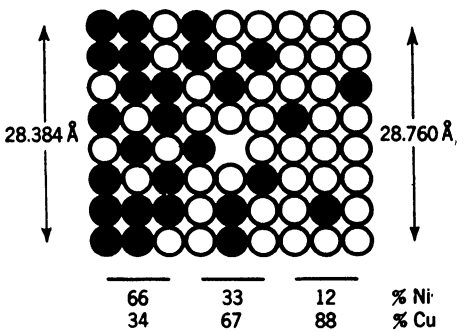

FIG. 3.3. Atomistic picture of an exaggerated sharp compositional gradient in a solid solution, *e.g.*, strong coring in a chill-cast cupronickel. Accompanying the compositional gradient will be a gradient in the size of the unit cube with extremes suggested on the sketch in Angstrom units (10^{-8} cm.). A vacant atom site in the center is postulated and this permits atom movements which would make the distribution of nickel atoms (black) and copper atoms (white) uniform, *i.e.*, the solid solution homogeneous, if time and temperature permitted.

was made to the effect that, since metals are nearly incompressible, the arrangement is best portrayed by using solid spheres to represent atoms. If these statements were strictly true, homogenization or counter-diffusion of copper and nickel atoms through a cored dendritic lattice would be impossible.

The modern view regarding atomic lattices is that they are imperfect and that not all possible atom sites are occupied. The unoccupied sites or vacancies are not observable by any means now available, and it is a temptation to deny their existence. However, they provide the best explanation of diffusion in substitutional solid solutions.

On examining Fig. 3.3, it is postulated that the left-hand zone is nickel rich and the right-hand zone is relatively low in nickel. If the nickel atom to the left of the vacancy moves into the vacant site and the two copper atoms below it move as indicated, then the net movement would be describable as one nickel atom being moved one unit distance to the right and vice versa for one copper atom. Operating

this as a puzzle board or a problem in Chinese checkers, it is possible to continue the movements and finally achieve a uniform distribution of copper and nickel atoms without trying to squeeze any relatively incompressible atom between two adjacent and equally incompressible atoms.

The pertinent facts on diffusion may be summed up as follows:

1. Diffusion increases exponentially with temperature as follows:

$$D = Ae^{-Q/RT}$$

where D = diffusion rate
A = parameter (constant for one pair of atom types and concentration gradient)
Q = energy required to move one atom past another
R = gas constant
T = absolute temperature

2. The diffusion rate varies with the concentration gradient. (This affects the parameter A above.)

3. Diffusion is most rapid when the diffusing element forms an interstitial solution for, then, only the small interstitial atoms need migrate.

4. In substitutional solutions, diffusion rates are higher the greater the difference in melting points of the two elements, the greater the difference in size or, relatedly, the more restricted the solid solubility.

Refer again to Fig. 3.3. If a mirror image of this occurred alongside the section shown, it might represent the area from the center of one dendrite to the center of another. Repetition of this across equally spaced dendrites would give a sinusoidal or cyclical curve for a plot of composition vs. distance. The interdendritic spacing, the concentration difference, and the diffusion coefficients being known, it is possible to calculate the time required for homogenization.[1]

3.6 Properties, General

The effect of solute concentration on some mechanical and physical properties of two copper-base solid-solution alloys, the Cu:Ni and α brass series, is indicated by the data of Table 3.1.

The properties of annealed solid solutions are so affected by the grain size of test specimens and by soluble impurity elements that it is difficult to obtain comparable data for specimens representing concentrations across an alloy diagram. Recrystallization temperatures and grain-growth characteristics are affected by both solute concentra-

[1] Masing, Z. Metallkunde, **34**, 10, 1942.

tion and impurities. Consequently, the data given here are not necessarily the same as would be obtained with industrial alloys and should be taken only as qualitatively indicative of the effects of dissolved

TABLE 3.1 PROPERTIES OF ANNEALED COPPER SOLID-SOLUTION ALLOYS*

Solute concentration	Tensile strength, psi	% elongation in 2 in.	BHN, 10 mm, 500 kg	Lattice parameter, $\times 10^{-8}$ cm	Electrical resistivity, microhms per cm³	"Self-potential," mv, (see p. 74)
Per cent Ni:						
0	30,000	53	36	3.6073	1.7	− 65
10	35,000	47	51	3.5975	14	− 45
20	39,000	43	58	3.5871	27	− 25
30	44,000	40	67	3.5770	38	+ 10
40	48,000	39	70	3.5679	46	+ 55
50	50,000	41	73	3.5593	51	+105
60	53,000	41	74	3.5510	50	+150
70	53,000	42	73	3.5432	40	+185
80	50,000	43	68	3.5350	30	+205
90	48,000	45	61	3.5265	19	+215
100	43,000	48	54	3.5170	6.8	+225
Per cent Zn:						
0	32,000	46	38	3.6073	1.7	
5	36,000	49	49	3.6176	3.1	
10	41,000	52	54	3.6275	3.9	
15	42,000	56	58	3.6378	4.7	
20	43,000	59	56	3.6488	5.5	
25	45,000	62	54	3.6612	6.3	
30	46,000	65	55	3.6735	6.6	
35	46,000	60	55	3.6864	6.7	
40($\alpha + \beta'$)	54,000	45	75	3.6940(α)		

* Mechanical property data for high-purity Cu:Ni alloys from Broniewski and Kulesza (*Métaux & corrosion*, **12**, 67, 1937). Data in "Metals Handbook" show decidedly higher strengths for Cu:Ni alloys because soluble impurities (*e.g.*, Mn) are present and the alloys probably had a finer grain size. Mechanical property data for brass alloys are from a Chase Brass & Copper Company *Bulletin* for commercial alloys of moderate grain size. Lattice parameter data (from Owen and Pickup) indicate changes in the size of the unit cells of the alloys effected by the solute atoms. "Self-potential" data for Cu:Ni alloys and the discussion of related corrosion properties on p. 74 are from the Research Laboratory of the International Nickel Co. The 40% Zn alloy marked ($\alpha + \beta'$) is a two-phase alloy, as hot-rolled (see p. 222).

elements. These, and other data not reproduced here, lead to the following general conclusions:

1. *Mechanical properties* show moderate, *gradual* changes, generally of considerably less magnitude than those effected by cold deformation. Strength and hardness (by indentation tests) are always increased, although not necessarily in a parallel manner. In a continuous series,

such as the Cu:Ni alloys, this requires maximum values for strength and hardness, although the two maxima do not necessarily come at the same concentration. The changes in these properties are not linear in most cases. Considerable effort has been devoted to find an explanation for the differences in solid-solution hardening as effected by different solute elements. No consistent correlation has been found between the hardness increase and the type or size of the solute atom, although usually the hardening effect is greatest when the solubility is restricted. For example, to increase the hardness of pure copper from Vickers DPN 40 to 54, the following atomic concentration of each of the respective solute elements is required: 0.6% Sb, 3.6% As, 4.6% Mn, 4.6% Si, 4.7% Al, 12.1% Zn, 13.2% Ni (data by R. P. Angier on pure binary alloys annealed to a uniform, 0.035-mm grain size). It appears that the most rapid hardness increases are found when the potential solubility is least, although there are some exceptions to this generalization (*e.g.*, manganese).

Table 3.1 shows that the effect of solid-solution elements may be to increase or decrease ductility in so far as that rather vaguely defined property is indicated by tensile-test elongation values. In most cases, the trend of elongation values probably varies inversely with that of strength and hardness, but silicon, zinc, or tin seems to increase the ductility of copper.

2. *Physical properties* also vary with solute concentration. Electrical conductivity is always decreased, or conversely, resistivity increased, although to a different extent by different solutes. In a complete alloy series, such as Cu:Ni, this requires a maximum in resistivity at some intermediate alloy concentration. Other characteristics, such as the size of the lattice, as indicated by the length of the edge of the unit cube or *lattice parameter*, vary linearly or approach a straight-line relationship (Vegard's law). Both Cu:Ni and Cu:Zn alloys show a negative deviation from linearity, but the difference is not known to have any significance.[1]

The lattice parameter relationship is important in consideration of the effect of coring, and its elimination, on mechanical properties. A specimen such as Micro. 3.1, with a fine dendritic, heavily cored structure cannot have a uniform slip system existing across one grain for, as the lattice periodically is contracted and expanded by the variation in nickel content, the potential slip planes must exhibit a related non-

[1] In both systems, there is reason to believe that special interaction forces between unlike atoms result in departures from random atomic arrangements and, relatedly, a denser packing than would be predicted by strictly additivity considerations.

uniformity. Thus a greater stress is required to cause deformation, and the metal is relatively harder and stronger than it would be in the homogenized condition with a uniform lattice. The coarse dendritic structure of the specimen in Micro. 3.4 would show intermediate strength or hardness values.

Solid-solution alloys are not customarily used where strength or hardness is of paramount importance. Their basic properties are ductility approaching or, in some cases, surpassing that of the pure solvent metals, plus moderately increased strength properties and other special properties derived from one or more of the components. Alpha brasses are cheaper than copper (since the addition agent, zinc, is cheaper), stronger, and yet show good corrosion resistance and excellent ductility. Cupronickels have much improved corrosion resistance as compared to both copper and brasses. In all other cases, comparable compromises of special properties may be obtained in solid-solution alloys.

It is interesting to list alloy systems that show complete solid solubility at all temperatures. The more important ones, together with their lattice arrangements, include:

Ni:Cu, Ni:Co, Ni:Pt, Ni:Pd (face-centered cubic)

Ag:Pd, Ag:Au, Au:Pd, Pt:Rh, Pt:Ir (face-centered cubic)

W:Mo (body-centered cubic); Bi:Sb (rhombohedral hexagonal)

Another group of alloy systems includes elements which are completely soluble at some elevated temperature in the solid state but which, in some range of concentration, change structures at lower temperatures. Frequently, the structural change does not involve any change in lattice type, which remains that of original solid solution. However, in this lattice, the two types of atoms do not remain randomly dispersed but occupy preferred lattice sites. For example, the face-centered cubic lattice contains four atoms per unit cell, one corner atom (eight unit cells share the atom at each of the eight corners per cell) and three face-centered atoms (each of the six face-centered atoms is shared by two cells). In a random solid solution, the four atoms in each cell may be of either solute or solvent elements, but at a concentration of three atoms of element *A* to one of element *B* (*e.g.*, 75 atomic % Cu and 25 atomic % Au), three atoms of type *A* may, at some temperature, occupy the face-centered positions and the one atom of *B* may occupy the corner positions of each unit cube. This lattice is no longer a simple solid solution but is called an *ordered* solid solution. Since ordering is strongest at simple atomic ratios and usually results in marked abnormalities of properties, usually an increase of electrical conductivity, of

strength and a loss of ductility,[1] ordered structures are sometimes thought of as intermetallic compounds and their development considered to be a change in phase. The present tendency, however, is to use the specific descriptive term *ordered structure* or sometimes *superlattice* and to show the effect on phase diagrams by dotted lines, since a strict definition of the word *phase* does not require ordering to be a phase change. Systems which are completely soluble at elevated temperatures (below the solidus) but which show, at some concentration, either true phase changes or ordered structures include:

Fe:Cr, Fe:Mn, Fe:Ni, Fe:Co, Fe:V, Fe:Pt (solution range is either body-centered cubic or face-centered cubic, depending on the solute element, see Chap. 13).

Au:Ni, Au:Cu, Au:Pt, Pt:Cu (face-centered cubic).

The α copper-base solid-solution alloys are necessarily all face-centered cubic structures and have a rather high degree of ductility or plasticity at room temperatures. Associated with this characteristic is the property of ready formability. Thus, although this chapter is primarily concerned with the cast structures of solid-solution alloys, the materials are usually employed in the wrought state, *i.e.*, the alloys are cast into large ingots or slabs that are rolled, hot or cold, into sheet, strip, or rod. The ingots may also be pierced or extruded and drawn into seamless tubing or pipe. The effect of working on structure and the properties of these copper-base solid solutions will be covered in the following chapter, but the alloys are discussed here as typical solid solutions.

3.7 Copper-base Engineering Alloys

Cu:Ni. The electropotential values for Cu:Ni alloys, shown in Table 3.1, are the basis of a particularly interesting illustration of a compromise in properties that results in an alloy of specific industrial use. The data are not true self-potential values but actually represent, at each alloy concentration, the millivoltage difference, measured in an aerated 3% sodium chloride solution, between a large clean sheet and a small sheet in contact with its products of corrosion.[2] The plot of potential vs. percentage of nickel gives a curve that passes through a zero value at a concentration near 70% Cu and 30% Ni. Similarly, if a series of Cu:Ni alloys were suspended in sea water near a harbor and if the change in weight were determined and plotted against nickel concentration, it would be found that the copper-rich alloy lost weight

[1] Nix and Shockley, Revs. Modern Phys., 10, 1, 1938.

[2] Research Laboratory, International Nickel Co.

through general corrosion, while the nickel-rich alloys had gained weight, by barnacle growth on the metal. Again, the 70:30 composition would show approximately no change in weight. The problem, like most corrosion effects, is quite complex but, stated in the simplest manner, may be explained in terms of the copper ion concentration required to prevent barnacle growth. The high-copper alloys corrode, or dissolve, rapidly enough to maintain the copper ion concentration sufficiently high at the surface to poison marine growths. The nickel-rich alloys do not dissolve so rapidly, and although pitting corrosion occurs at the point where barnacles attach themselves to the metal, there is a net gain in weight when that of the barnacles is included. Aside from the question of barnacle growth, the 70% Cu:30% Ni alloy is specifically adapted for use in contact with salt water, *e.g.*, in marine condensers.

Two alloy compositions other than the 70:30 combination are of industrial importance. The data of Table 3.1 show a maximum in electrical resistivity at 55% Cu:45% Ni, and an alloy of approximately this composition, known as *constantan*, is widely used for precision resistance units and rheostats because of its low change in resistance with temperature as well as the relatively high magnitude of resistivity. The third alloy in this series is known as *Monel metal*. The same table shows that this alloy, containing two parts of nickel to one part of copper, is at the strength maximum of the Cu:Ni series. Industrial Monel metal, containing slight amounts of other elements, is stronger than the pure alloy of Table 3.1. Increased strength, with little loss in corrosion resistance or pleasing color, may be obtained by further alloying to attain precipitation hardening effects (page 138).

Cu:Zn. Up to about 35% Zn can be added to copper without changing the face-centered cubic structure other than dimensionally, as indicated in Table 3.1 by the lattice parameter data. The many α solid-solution alloys of this system are differentiated by gradual changes in color, strength, ductility, corrosion resistance, and cost.

1. The 5% Zn alloy, known as *gilding metal*, has a golden color and is used for cheap jewelry or gilding purposes.

2. The 10% Zn alloy, known as *commercial bronze*, has a bronze color and is cheaper than the tin bronzes.

3. The 15% alloy has a red tint somewhat like copper and logically is called *red brass*. It is like copper and the preceding alloys in being resistant to cracking under the combined action of elastic stresses and corrosive agents such as ammoniacal solutions or vapors and mercury salts.

4. The 30% Zn alloy has higher strength and ductility than any of these alloys and this combination makes the 70:30 solid solution particularly well suited for severe cold-forming operations. One of the most severe operations is drawing a deep cup shape such as a cartridge from a flat circular blank. The ease of fabrication by cold-drawing to such shapes plus cold-worked strength (see Chap. 4) and the general resistance to corrosion have caused this alloy to be universally used for cartridge shells which hold the propellent powder and the missile or shot. The chief objections to the use of this alloy are the tendency of the alloy to crack when subjected to stress and ammonia or amines and the usual relative scarcity of copper and zinc in wartime.

Cu:Si. Copper containing up to about 4% Si remains a single-phase terminal solid solution. The silicon increases both strength and ductility, as shown in Chap. 4, and also increases resistance to certain types of corrosive mediums. Usually ¼ to 1% of iron and frequently other elements besides silicon are added for purposes of further strengthening, grain-size refinement, or avoidance of patent infringement. The important characteristics of these alloys are ease of welding combined with the strength of mild steel and the corrosion resistance of copper.

Cu:Sn. When 2% or less of tin is added to copper, the alloy is considered to be a solid solution. Most Cu:Sn *bronzes* contain more than this amount of tin and are, therefore, two-phase alloys. As such they are discussed in Chap. 8. However within the limited range of solubility, tin is a potent strengthener of copper. Whereas both zinc and silicon are automatic deoxidizers of copper, removing oxygen as ZnO and SiO_2 respectively, tin, like nickel, requires the addition of a separate deoxidizing agent when added to liquid copper. Phosphorus is the usual agent, and residual phosphorus (beyond that which is removed with oxygen as P_2O_5) further increases the strength of bronzes. The tin-bronzes deoxidized with phosphorus are commonly known as *phosphor bronzes*.

Cu:Al. Like the Cu:Sn alloys, one-phase solid solutions of Cu:Al are restricted to a maximum of about 5% Al.[1] This α aluminum bronze[2] has good tensile strength with considerable ductility although it work-hardens (see Chap. 4) rapidly. The alloy resists oxidation as a result of the initial formation of a relatively impervious Al_2O_3 surface film and also resists attack by many acid solutions. It has a pleasing golden

[1] Industrially useful alloys may contain from 5 to 10% Al. These two-phase alloys are discussed in Chap. 8.

[2] The word *bronze* originally referred only to Cu:Sn alloys but has come to have a more general connotation of recent years.

color similar to that of 18-carat gold and has some decorative applications.

Complex Solid Solutions. In many cases, more than one solid solution element is added to copper. In the alloy once known as *German silver*, now generally as *nickel silver*, no silver is present at all; instead the proper amount of nickel and zinc combine to give a color (or lack of it) quite similar to silver. It is widely used for plumbing fixtures, as a base for silver-plated jewelry, table, and flatware. Like the brasses, these alloys are solid solutions when the combined nickel and zinc contents are less than about 36%.

The Cu:10% Zn alloy may have ½% tin added which slightly increases its strength and corrosion resistance. The 30% cartridge brass may have 1% tin added for the same purpose. This solid solution is called *admiralty metal* and with about 0.04% As present, the material is widely used, in the form of tubing, for steam condenser units. Arsenic seems to reduce "dezincification."[1]

Aluminum brass is essentially cartridge brass with the zinc content lowered to about 22% and about 2% Al added. The aluminum, in solid solution in the α brass, increases resistance to corrosion, particularly pitting and impingement attack by high-velocity water. Again, arsenic may be added to minimize dezincification.

A new solid-solution alloy[2] has been developed with 10% Zn and 20% Mn. When made with high-purity manganese, this alloy has properties and a color quite similar to the nickel silvers.

3.8 Solid Solutions of Iron

Soft magnetic alloys are those which develop strong magnetism when in a magnetic field, *e.g.*, inside a coil carrying an electric current, and lose their magnetism almost completely on removal of the field, *e.g.*, stoppage of the electric current. Mention has been made of the addition of about 3.5% Si to iron, which increases the resistance of the iron to electric eddy currents with related heating and electrical losses at no real loss in magnetic strength. Other solid solutions are used in this same field of materials, notably Fe:Ni solid solutions called *Permalloys*. For example, 78.5% Ni in iron results in an alloy with a high ratio of flux density (B) to the magnetizing force (H) producing it; more specifically, the permeability or ease of magnetization is initially very high and makes this alloy ideal for armatures and the cores of

[1] Dezincification is a selective form of corrosion where zinc atoms are preferentially dissolved from the surface of the alloy.

[2] *Trans. AIME*, **161**, 244, 1945.

sensitive relays. *Perminvars* are Fe:Co:Ni alloys (ratios of 30:25:45) possessing constant permeability over a range of low flux densities.

Studies of solid solutions in which pure ferrite or body-centered cubic iron is the solvent have shown strengthening effects similar to those for copper-base solutions. Lacy and Gensamer[1] found that both

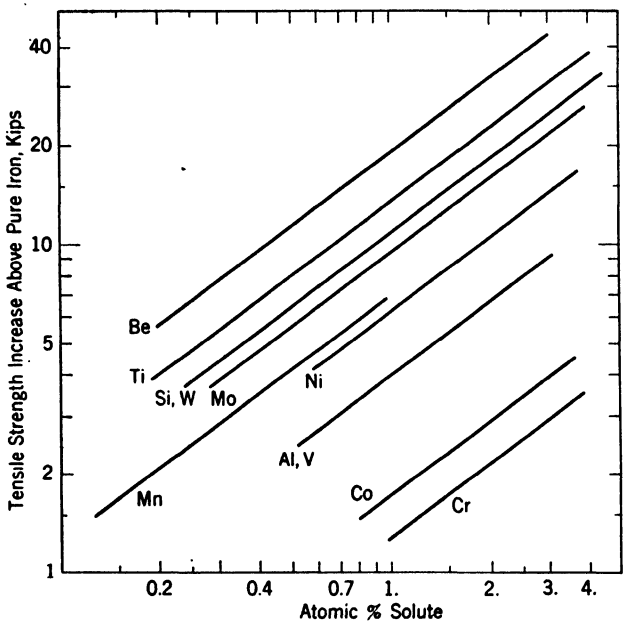

FIG. 3.4. Strengthening effect of different solute elements in ferrite or body-centered cubic iron; Kips = thousands of pounds per square inch. (*Lacy and Gensamer.*)

tensile and yield strengths were increased as shown in Fig. 3.4. The exponential rate of strengthening as a function of solute concentration can be expressed as follows:

$$S - S_0 = kX^{0.71}$$

where S = strength of the alloy
S_0 = strength of the unalloyed ferrite
X = concentration of alloying element
k = strengthening coefficient (Table 3.2)

The data of Table 3.2[1] show that, as in the case of copper-base solid solutions, a greater difference in atom size of solute and solvent and an accompanying lesser solid solubility result in a greater hardening or strengthening of the body-centered cubic ferrite. Silicon is an excep-

[1] Lacy and Gensamer, Properties of Alloyed Ferrites, *Trans. ASM*, **32**, 88–115, 1944.

tion, but there are additional reasons for believing that it does not form a simple, random solid solution with iron.

Stainless irons are essentially solid solutions of iron with from 15 to 30% Cr. These alloys are body-centered cubic like iron and, in the absence of carbon, are not susceptible to hardening by heat treatment. Their usefulness lies in the corrosion and oxidation resistance conferred by chromium or more specifically by the initial chromium oxide protective film formed on the surface of the alloy (Chap. 13).

TABLE 3.2. ORDER OF EFFECTIVENESS OF SOLID-SOLUTION STRENGTHENING OF FERRITE*

Order based on wt. %	Order based on atomic %	Strengthening coefficient for tensile strength	Solubility atomic %
Be	Be	19,000	
Si	Ti	14,000	4
Ti	W	11,000	1
Mn	Si	11,000	26 (or 9?)
Al	Mo	9,600	2
Mo	Mn	7,000	12
Ni	Ni	6,100	19
V	Al	4,000	25
W	V	4,000	32
Co	Co	1,800	77 (?)
Cr	Cr	1,400	42

* Lacy and Gensamer, Properties of Alloyed Ferrites, *Trans. ASM*, **32**, 88-115 1944.
NOTE These data apply only to carbon-free iron, not steels.

Stainless steels are most commonly face-centered cubic solid solutions of iron with from 15 to 30% Cr and 8 to 20% Ni (Chap. 13). Again, the important characteristic is resistance to corrosion although these alloys also have much greater cold ductility than the stainless irons (as would be expected from the face-centered cubic structure as compared to the body-centered cubic structure), and can be cold-worked to attain high strength (Chap. 4). In order to ensure a single-phase solid solution with optimum resistance to corrosion and satisfactory working and welding properties, the carbon content must be restricted to less than about 0.10%.

QUESTIONS

Group A

1. Specify three general effects of a rapid rate of solidification on solid solution micro- or macrostructures.

2. What would be the differences, if any, in microstructure between the following alloys when chill-cast and then homogenized: (*a*) 85% Cu:15% Zn, (*b*) 70% Cu:30% Zn, and (*c*) 50% Cu:50% Ni?

3. In comparison with their base metal or solvent, are solid solutions always (*a*) stronger, (*b*) less ductile, (*c*) more resistant to corrosion, (*d*) poorer electrical conductors, (*e*) larger in atomic spacing?

4. If insoluble impurities are present in a solid-solution alloy, where in the microstructure will they be found if the alloy is in (*a*) the cast condition, (*b*) the wrought condition (see micrographs of Chap. 2)?

5. If a specific casting has too coarse a grain size, what can be done about it?

Group B

1. Construct a complete metastable solidus for the alloy constantan assuming no diffusion in the solid dendrites during solidification. Describe the basis for construction, particularly below the equilibrium solidus and specify the temperature at which solidification is complete.

2. How can ordering of atoms in a solid-solution alloy be surmised or detected? Why is ordering in a body-centered cubic structure most likely to be found at a 50:50 atomic per cent composition while, in a face-centered cubic structure, it is equally likely at a 75:25 atomic per cent composition?

3. Which is greater in intensity (*a*) microsegregation or macro (normal) segregation, (*b*) hardening by coring or by straight solid-solution effects?

4. If internal voids are found in the microstructure of a solid-solution alloy casting, how could their origin be specified as between these possibilities: (*a*) shrinkage cavities from inadequate "feeding" during solidification, or (*b*) blowholes from gas evolved from the liquid because of a solubility decrease upon solidification?

CHAPTER 4

COLD-WORKING AND ANNEALING

Plasticity of metal crystals is synonymous with deformability—the ability to be strained or to undergo a considerable change in shape or dimensions without cracking or breaking. When the deformation occurs below a certain minimum temperature, the hardness and strength properties increase, *i.e.*, *strain hardening* occurs, while ductility properties correspondingly decrease. Under these conditions, the deformation process is generally called *cold-working*. Ductility may be restored to its initial value and the strain hardening eliminated by *annealing* the metal, *i.e.*, reheating above the minimum temperature previously mentioned. If the deformation proceeds at temperatures in the annealing range, no strain hardening occurs and the process is called *hot-working*.

4.1 Mechanics of Deformation

It has already been pointed out that plasticity in metals is related to crystal structure; more specifically, it depends on the existence of parallel planes of high atomic density and correspondingly wide spacing, together with the special interatomic forces binding metal atoms in a lattice. The three simplest planes in a cubic lattice are reproduced in Fig. 4.1. In both the face-centered cubic and body-centered cubic lattices, cube planes spaced $\frac{1}{2}\,a$ (the edge distance being a) account for all atoms. The dodecahedral or (011) planes accounting for all atoms are spaced twice as far apart in the body-centered cubic lattice as in the face-centered cubic lattice; therefore, (011) is a widely spaced plane for iron and similar metals but not for aluminum, copper, etc. The octahedral or (111) planes cutting all three axes show the reverse relative spacing. In order to account for all atoms, the (111) plane in the body-centered cubic lattice has half the relative spacing of the face-centered cubic lattice and, therefore, in copper, aluminum, etc., this widely spaced family of octahedral planes is the important one in deformation processes.

Blocks of the crystal on either side of a specific plane, or group of

planes, can move in opposite directions, come to rest with atoms on either side of the plane in *nearly* equilibrium positions, and thus change the external shape of the crystal without destroying it. The atoms cannot be in exactly normal positions after the deformation for then the properties of the crystal should be unchanged and no strain hardening would have occurred. Atomic conformity cannot have been entirely destroyed across the plane or subsequent movements at right angles would not be possible (Micro. 4.2). The mechanics of the movement are not known with certainty. It may occur by a shearing movement

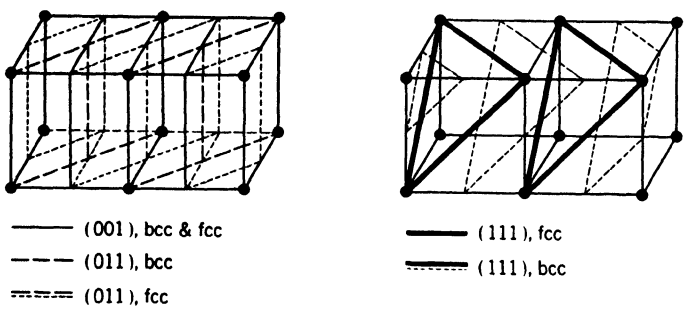

FIG. 4.1. Two cells of a cubic lattice showing only the corner atoms. The cube plane (001) spacing (left figure) is the same for both body-centered and face-centered cubic structures. The dodecahedral or diagonal plane (011) spacing necessary to account for all atoms is twice as great for the body-centered as for the face-centered cube. The reverse is true of the actahedral planes (111) as shown by the right-hand drawing.

of entire blocks at adjacent planes or by migration of atoms through vacant sites of the lattice structure, starting at one side of the crystal and crossing it like a wave on the specific plane and in the requisite direction. In either event, the individual crystal is not isotropic; *i.e.*, it cannot flow in any direction, as do tar or other noncrystalline (amorphous) solids, but moves only according to the crystallographic slip planes and directions available. The slip process also requires a rotation of the slip plane and direction toward the direction of stress or plastic flow, Fig. 4.2. (This rotation may be visualized by placing some flat pieces of a hard, sheet material in a ball of plastic clay and forcing the ball to elongate in a direction of about 45 deg to the plates; they will be found to rotate during the deformation toward parallelism with the flow direction.) Although the individual atomic movements during the plastic deformation of a single crystal are uncertain, the gross movements of large blocks of the crystal are predictable.

When a relatively fine-grained commercial metal is cold-rolled, the simple picture of slip and rotation becomes more complicated in that

the operative slip systems of the aggregate are at different angles to the flow direction. The applied stress is resolved in each crystal to a stress on the slip plane and in the slip direction and another component normal to the plane. The normal stress tends to cause cleavage along the plane, and, since this does not ordinarily occur in ductile metals, the normal stress is generally ignored. The stress acting along the slip planes is the cause of shearing movements and flow. Since the resolved stress is a function of the orientation of each crystal and since a minimum elastic shearing stress limit[1] must be exceeded before flow begins, it is

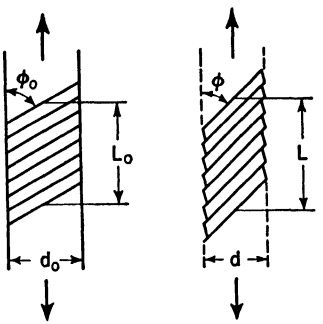

FIG. 4.2. Schematic drawing of shear deformation on a given set of slip planes in a single crystal. Upon deformation, an extension from length L_0 to L occurs and a decrease in thickness from d_0 to d (the third dimension is unchanged). Individual lamina remain unchanged in size. The slip process is necessarily accompanied by a rotation decreasing angle ϕ_0 to ϕ.

apparent that all crystals do not start to flow at the same time and that, if the maximum stress is near the gross elastic limit, some crystals will have deformed plastically and some only elastically. This is one source of *residual* or *internal stresses* (on a micro scale) after releasing the applied stress and is also why most commercial metals do not show

[1] The stress at which single crystals of a specific metal start to deform plastically at a specific temperature may vary widely; *e.g.*, Schmidt (*Z. Elektrochem.*, **37**, 447, 1931) found a variation from 210 to 1,500 psi for the yield points of magnesium crystals. However, when these figures are vectorially calculated in terms of the stress on the slip plane and in the slip direction, the *critical resolved shear stress was found to be the same.* This resolved shear stress τ is calculated as follows:

$$\tau = \frac{F}{A} \cos \phi \cos \lambda$$

where F = load
A = cross section area
ϕ = angle between specimen axis and normal to slip plane
λ = angle between specimen axis and slip direction

a sharp, well-defined, yield point (page 12). A second complication in the deformation of polycrystalline metals enters when neighboring crystals of differing orientation tend to flow in slightly different directions, yet must maintain contact at all points or a crack will form and spread. To ensure contact at all grain boundaries of an aggregate of crystals during flow, each crystal is forced to use more than one slip system (one plane and one direction) and, consequently, some bending of the lattice structure is bound to occur, particularly at grain boundaries. Rotation of the slipping "blocks" will not be uniform and, as a result, deformation creates a series of crystal block fragments, often arranged in parallel, curved bands having slightly varying orientations within each band and mirror image rotations from band to band, all derived from an initial crystal of uniform structure.

A fine-grained metal containing crystals with a random distribution of orientations will, in most respects, behave as an isotropic substance despite the nonisotropic behavior of its individual component grains. After considerable plastic deformation, however, with crystallite fragments in each grain rotating toward a common position with respect to the flow direction, the metal ceases to be isotropic, both crystallographically and mechanically. It will show somewhat different properties depending on the direction of measurement, *i.e.*, the position of the axis of the test specimen with respect to the flow direction or direction of rolling.

In this discussion, deformational processes have been considered as applied to metals with a uniform crystal structure. This would include any pure metal or solid solution. Most of the actual structures employed to illustrate this discussion are of a solution-type alloy, α brass (in this case 70% Cu:30% Zn), which has a crystal structure nearly identical to that of copper. It might also be pertinent to point out that a hard, insoluble constituent, such as Cu_2O in copper (Micro. 2.9, page 44) or Al:Fe:Si compound in aluminum (Micro. 2.6, page 42), will be strung out in the direction of flow without very seriously affecting the mechanics of deformation of the ductile matrix crystals.

4.2 Microstructures of Cold-worked Brass

The α brasses whose structures are reproduced in this section offer no particular difficulties for metallographic polishing. Etching of brasses is customarily done with mixtures of hydrogen peroxide and ammonia, frequently somewhat diluted with water. Staining may be eliminated by wiping the polished surface lightly during etching. The ammonia peroxide must be freshly mixed.

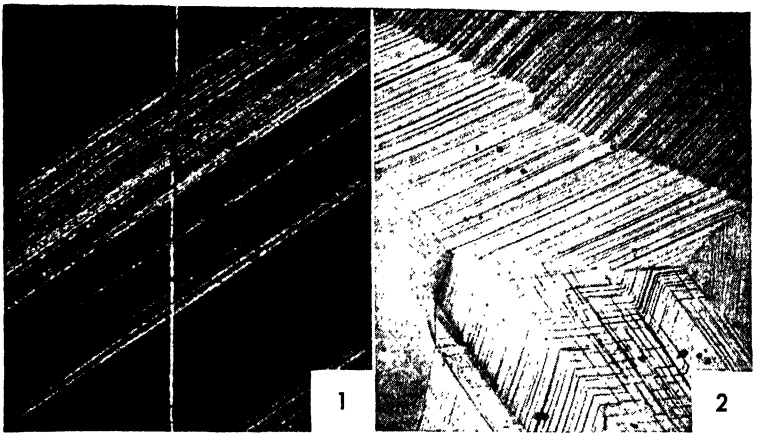

Micro. 4.1. Single crystal of α brass strained 0.2% in tension; ×200. This specimen was polished, etched with ammonia peroxide, strained, and then photographed with the light at an oblique angle. The undisturbed surface of the crystal is dark, but light has reflected from the sides of steplike discontinuities or lines indicating the planes of block slip. The single longitudinal line was scratched on the polished surface before straining. The slight deviation from the original straightness indicates that the amount of plastic displacement at each visible slip line amounts to about 700 to 800 atoms.

Micro. 4.2. Polycrystalline annealed brass, polished, etched with ammonia peroxide, and then squeezed slightly in a vise; ×100. With normal illumination, the color variations of this grain structure are related to orientation differences (page 39). The parallel, dark lines are steplike discontinuities resulting from block slip. Note that, when these reach grain boundaries, they stop or change direction. In some cases, they are parallel to annealing twins (the planes of slip in brass are also potential twinning planes). Where the active slip plane is not parallel to the twin but intersects it, note the change of direction at the twin and resumption of the original direction on the other side. This is further evidence of the change of orientation in twins and yet the atomic conformity between the twin and original crystal. Note also that the bottom crystal shows two sets of intersecting lines within some of the twin bands, indicating that more than one set of the potential slip planes functioned during this slight deformation. All these markings appear only by reason of a difference in surface level on either side of the slip plane; repolishing of the specimen would remove the line markings.

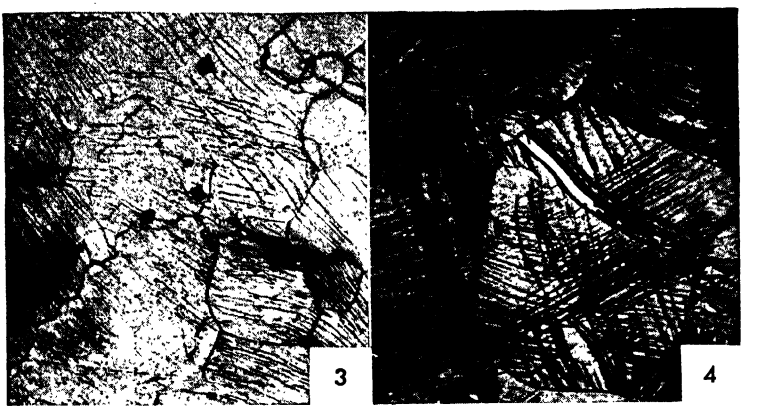

Micro. 4.3. Armco iron polished, etched with Nital, and then squeezed in a vise; ×100. Body-centered cubic iron has no single set of well-defined slip planes. That, rather than any lesser perfection of the crystal structure, is the probable explanation of these characteristically forked and wavy slip lines.

Micro. 4.4. α brass cold-rolled to a 30% reduction; $NH_4OH:H_2O_2$ etch; ×200. This structure of a surface parallel to the rolling plane (with the rolling direction vertical) shows grains somewhat elongated in the direction of rolling. The formerly straight twin bands now show curvature indicative of lattice bending. The numerous curved, dark lines in the crystals are parallel to the active slip planes but appear for an entirely different reason than those of Micro. 4.2; after the relatively high reduction of 30% (Micro. 4.2 was deformed less than 1%) atomic nonconformity at the active slip planes, or possibly fragmentation or other localized atomic changes, has created a zone of high, localized instability where etching attack proceeds more rapidly, in a manner analogous to attack at grain boundaries. Three sets of markings in one crystal indicate that three different sets of octahedral planes were active in the deformation process. Since these markings cannot be removed by repolishing, they are called *noneffaceable deformation lines, etch markings*, or simply *strain markings.*

5

6

Micro. 4.5. α brass cold-rolled to a 60% reduction; NH_4OH:H_2O_2 etch; ×200. After a greater reduction, this structure of the rolling plane (rolling direction again vertical) shows strain markings that are less well defined and more wavy, curved, or branched, indicating greater lattice distortion and fragmentation. It is also evident that the strain markings (on the active slip lines), instead of being randomly disposed, grain to grain, as a result of random crystal orientation, are now tending to assume a common general position on the sheet surface, approaching perpendicularity to the rolling direction. Thus the rotation of individual crystals, or banded sections of crystals, into symmetry positions with respect to the direction of flow is generating a preferred orientation.

Micro. 4.6. Same as Micro. 4.5 but photographed at ×200 on a plane parallel to the rolling direction and normal to the rolling plane (longitudinal section). The markings that tended to be perpendicular to the rolling direction in Micro. 4.5 are now seen to represent twisted and warped planes tilted at approximately 45 deg to the surface of the rolled sheet.

A potassium bichromate etch is also satisfactory. It is made up of 2 g of $K_2Cr_2O_7$, 4 cc of a saturated solution of NaCl, 8 cc of concentrated H_2SO_4, and 100 cc of H_2O. This solution has the advantage of stability; it can be made up and kept indefinitely. Among other etches, a chromic acid solution may be mentioned, *viz.*, 50 cc of 10 to 15% CrO_3 solution with 1 or 2 drops of HCl added at the time of use.

In any micrographic examination of a cold-worked metal, the plane of polish with relation to the direction of cold-working is important. For example, in cold-rolled metals, the crystals on the rolling plane appear elongated with the width unchanged; on a transverse cross section, they appear thinned with the width unchanged and on the longitudinal cross section, they appear both elongated and thinned. Thus the deformation is most obvious when examined on the longitudinal cross section.

4.3 Property Changes from Cold-working

Strain hardening has already been defined as the change in mechanical properties, *i.e.*, increases in hardness and strength, decreases in ductility, that accompanies cold deformation. There is no single, universally accepted explanation for strain hardening, but it seems certain that the visible distortion of the crystal lattice, manifested by curved and warped lines of deformation, and the accompanying fragmentation of the crystal must increase the force required to cause further deformation *on any set of slip planes*, as compared to the force required to initiate slip in a crystal with a relatively perfect lattice.

The extent of the various property changes is of more immediate importance in evaluating potential engineering applications of cold-worked metals. Although both hardness and strength increase, they do not follow parallel courses when plotted against the reduction by cold-rolling (see Fig. 4.3, page 89). Strength generally increases more or less linearly, whereas hardness increases very rapidly in the first 10% reduction and then more slowly at successively higher reductions. In Fig. 4.3, for example, the increases of Rockwell B hardness, and tensile strength of 70:30 cartridge brass are shown for increments of reduction up to about 70% total deformation. The very steep initial increase of the hardness values and later leveling off may be partly explained in terms of two factors: the Rockwell scale and the depth of indentation. Table 1.1 shows how all Rockwell scales are very sensitive in the low numerical ranges and relatively insensitive as they approach 100. Second, cold-rolling of most metals involves a greater elongation (and lateral spread) at the surface layers than in the center as is evidenced

by the common observation of concavity of ends and edges. Since the Rockwell impression is made on the surface, this would also magnify initial increases.

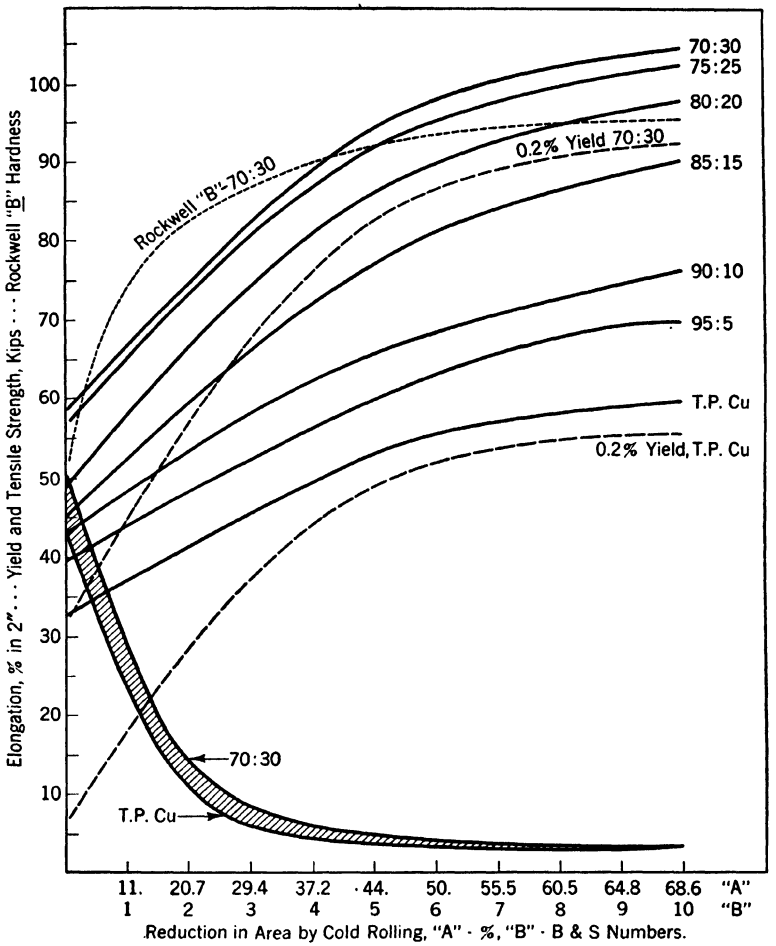

FIG. 4.3. Effect of cold-rolling on the tensile strength of copper and the alpha solid-solution brasses, from 95:5 to 70:30 Cu-Zn alloys. All tensile test elongation values fall within the shaded area. Yield-strength changes are also shown for copper and the 70:30 brass and Rockwell-hardness changes for the 70:30 alloy. (*Wilkins and Bunn.*)

Ductility, as shown by the elongation in a tensile test, follows a course opposite to that of hardness, a large initial decrease in the first

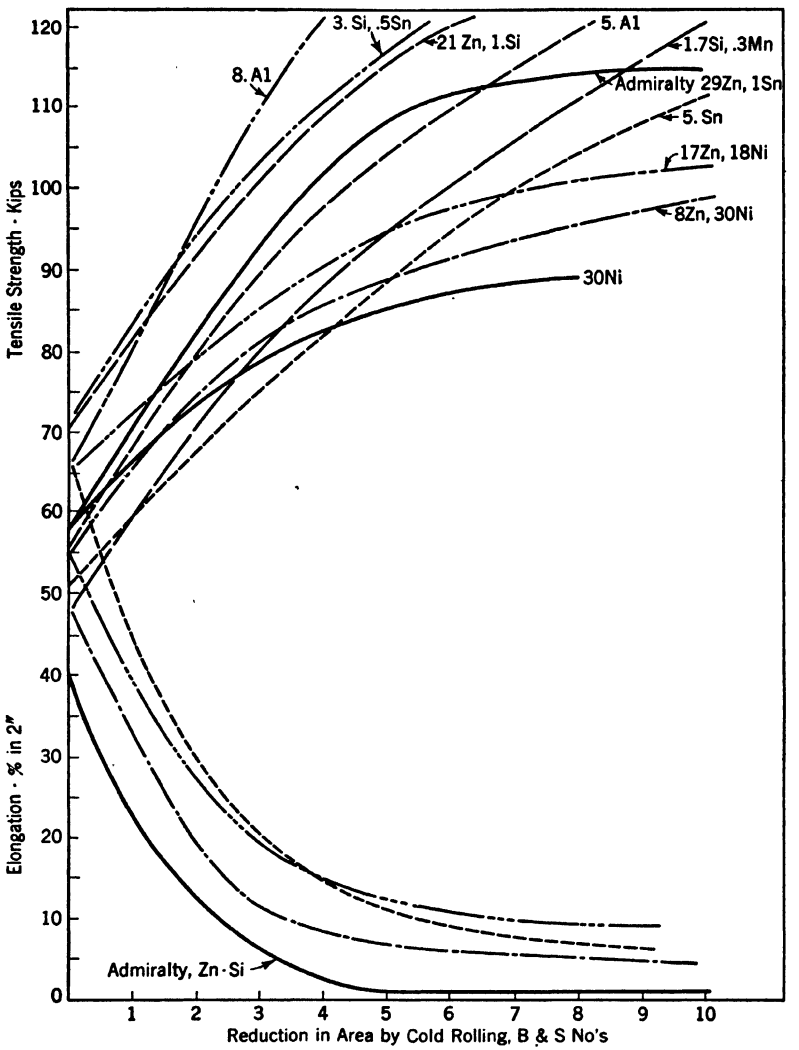

FIG. 4.4. Effect of cold-rolling on the tensile strength and test elongation of several copper-base wrought solid-solution alloys, *i.e.*, 5% and 8% aluminum bronzes, silicon brass (Zn, Si) 3% and 1¾% silicon bronzes, admiralty metal, 5% tin (phosphor) bronze, two grades of nickel silver (Zn, Ni) and 30% cupronickel. (*Wilkins and Bunn.*)

20% reduction and then a gradually slower rate, asymptotically approaching zero. The data of Fig. 4.3 show the effect of increased zinc content in increasing both the solid-solution tensile strength (initial ordinate values) and the strain hardening response. The relative effect of zinc in solid solution on plasticity or ductility is shown in two ways, by the elongation values and by the yield strength (at a 0.2% offset) for tough-pitch electrolytic copper and the 70:30 cartridge brass. The elongation data show a slight beneficial effect of zinc at low and intermediate reductions. The yield strength data in comparison with the corresponding tensile strength data are more significant in discussing ductility. The yield strength of the copper, although very low in the annealed state, more closely approaches the tensile strength of the copper from reductions of 40% on, than is the case with cartridge brass.

The greater spread between yield strength and tensile strength for cartridge brass than for copper means that cold-drawing can be carried out more readily without danger of cracking. Cold-rolling is not so affected because of the absence of tensile stresses, but in cold-working where tensile stresses are present the cartridge brass is notably superior to copper and, indeed, to almost all metals.

Changes in tensile strength and tensile test elongation upon cold-rolling of other copper-base solid solutions are shown by the curves of Fig. 4.4. The cupronickels and nickel silvers are moderately strong initially, in the annealed state, but strain-harden less than the tin, silicon, and aluminum "bronzes."

Typical data for hardness changes of several commercial metals and solid-solution alloys are reproduced in Table 4.1.

In addition to mechanical properties, cold-working changes physical properties; *e.g.*, it has a deleterious effect on the magnetic properties of soft iron and decreases electrical conductivity of pure metals slightly (about 2 to 5%) and of some alloys, such as α brass, strongly (about 20%, see Fig. 4.5, page 93). The distorted lattice of cold-worked metals is of an unstable character and contains stored energy, which means that chemical reactivities of cold-worked metals are also affected (as shown by the increased rate of attack by etching solutions).

4.4 Mechanics of Annealing

The process of changing the distorted, unstable, cold-worked lattice, which may have residual macro- or microstresses, back to a strain-free structure by the application of heat is termed *annealing*. *Macro-* and *micro-* have the same significance here as when applied to photographs

TABLE 4.1. HARDNESS CHANGES OF VARIOUS METALS AND SINGLE-PHASE COPPER-BASE SOLID SOLUTIONS UPON COLD-ROLLING

Metal			Reduction %						
Designation	Condition	Type of Test	0	10	20	30	40	50	60
Armco iron	Annealed 725°C	Rockwell G*	5	36	45	52	57	59	60
		BHN (1000 kg)	76	100	114	126	132	138	142
Aluminum 2S	Annealed 400°C	Rockwell H*	6	45	53	59	64	69	73
		BHN (500 kg)	13	16	19	22	24	27	29
Zinc, 99.99%	Annealed 300°C	Rockwell Y*	(—13)	10	19	17	10	5	1
		BHN (500 kg)	34	40	45	42	39	37	35
Copper, OFHC	Annealed 600°C	Rockwell F*	26	80	84	87	89	91	92
		Rockwell F	40	78	83	86	89	92	94
Gilding metal, 95:5	Fine grain	Rockwell F	58	83	90	94	98	100	102
	Coarse grain	Rockwell F	40	70	83	89	94	97	99
Commercial bronze, 90:10	Fine grain	Rockwell F	62	86	96	98	100	102	104
	Coarse grain	Rockwell F	48	79	90	95	97	99	101
Red brass, 85:15	Fine grain	Rockwell B*	..	60	70	77	82	86	88
	Coarse grain	Rockwell B	..	48	62	70	77	82	85
Spring brass, 75:25	Fine grain	Rockwell B	48	72	82	87	90	92	94
	Coarse grain	Rockwell B	5	42	64	75	83	86	89
Cartridge brass, 70:30	Fine grain	Rockwell B	48	74	82	87	90	93	95
	Coarse grain	Rockwell B	6	60	73	79	84	87	90
High brass, 65:35	Fine grain	Rockwell B	48	69	80	86	89	92	94
	Coarse grain	Rockwell B	5	54	68	77	83	87	90
Admiralty, 70% Cu; 29% Zn; 1% Sn	Fine grain	Rockwell B	57	77	87	91	95	97	99
	Coarse grain	Rockwell B	10	60	71	79	86	90	93
Si brass, 77% Cu; 22% Zn; 1% Si	Fine grain	Rockwell B	73	88	83	96	98	99	100
	Coarse grain	Rockwell B	22	65	78	86	90	93	95
Ni silver, 65% Cu; 17% Zn; 18% Ni	Fine grain	Rockwell B	67	79	88	91	93	94	95
	Coarse grain	Rockwell B	35	53	69	81	85	88	90
Cupro-Ni, 70:30	Fine grain	Rockwell B	45	70	82	85	87	88	89
	Coarse grain	Rockwell B	30	58	77	81	83	85	87
Monel metal, "A" Ni	Fine grain	Rockwell B	58	76	88	93	96	98	100
	Coarse grain	Rockwell B	50	71	80	87	92	96	98
Si bronze, "B" Cu; 1.7% Si; 0.4 Mn	Fine grain	Rockwell B	30	76	82	86	88	90	92
	Coarse grain	Rockwell B	..	68	77	82	85	87	89
Al bronze, 95% Cu; 5% Al	Fine grain	Rockwell B	47	75	82	87	90	92	94
Phosphor bronze, 4% Sn; 0.03% P	Fine grain	Rockwell B	47	69	80	86	91	94	97
	Coarse grain	Rockwell B	18	56	70	77	83	88	92

* Rockwell scales. G—1/16 in., 150 Kg; H—1/8 in., 60 Kg; Y—1/8 in , 25 Kg; F—1/16 in., 60 Kg; B—1/16 in., 100 Kg.

of structures. The word *macrostresses* refers to elastic stresses existing, in a balanced state, over large areas of the metal. When the balance is upset by machining away part of the metal, the unbalanced stresses will redistribute themselves by a distortion of the metal; *e.g.*, a slit cold-drawn tube may open up at the cut, increasing the diameter of the tubing. On the other hand, microstresses, while also of necessity in a balanced state, are so localized in extent that they cannot cause a

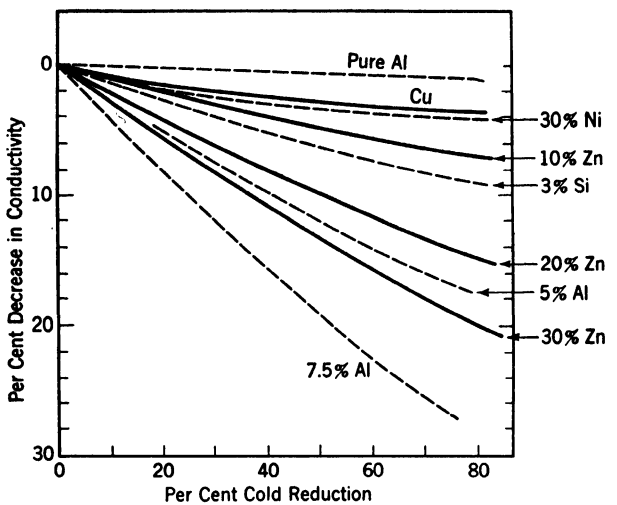

FIG. 4.5. Effect of cold-working on the electrical conductivity of pure aluminum, tough-pitch copper, Cu + 30% Ni; Cu + 3% Si; Cu + 5% and 7.5% Al; Cu + 10%, 20% and 30% Zn.

change of dimensions upon machining of the metal and are detectable only by X-ray diffraction or comparable methods.

At some relatively low temperature of heating, residual stresses are relieved: measurable macrostresses by plastic flow or creep, and microstresses by the movement of some atoms, forced out of stable lattice positions with respect to their neighbors, toward localized equilibrium positions. Since the gross lattice distortions are unaffected, hardness and strength may not be noticeably decreased; in fact, in some solid-solution alloys, such as the α brasses, the hardness and strength may increase slightly. [Placing a test specimen of cold-rolled brass on a hot radiator for a couple of hours may bring its strength up to specifications, if it originally was a little below the minimum. This slight increase in hardness and strength is believed by some to be caused by precipitation (see page 138) of a phase, soluble in the stable lattice and insoluble in the

distorted lattice.] Heat treatment in this relatively low temperature range is called a *stress-relief* anneal. The residual stresses in a cold-worked metal may approach the strength of the material and exceed it, if localized surface notches are formed by the attack of certain specific corrosive agents, *e.g.*, ammonia or mercurous nitrate solutions for brasses. When the localized stresses exceed the strength of the material, cracks start forming. Since the corrosive attack usually creates notches at grain boundaries, the cracks start and propagate along grain boundaries, resulting in intergranular failure of the type known as *season-cracking* or, more accurately, *stress-corrosion cracking*. The temperature range of stress-relief annealing is called the *recovery* range. Besides the property changes already mentioned, there may be some very minor structural changes but, at most, these will be only the partial disappearance of etch or strain markings. Their removal takes a considerably longer time than is possible to employ commercially, but the tendency illustrates the decrease in localized stresses that had given the original etching effect.

At the upper temperatures of the recovery range, hardness may start to decrease markedly. Simultaneously, minute new crystals, identical in composition and lattice structure to the original undeformed grains, make their appearance in the microstructure. These crystals are not elongated, as are the fragmented, deformed grains, but appear to be approximately *equiaxed; i.e.*, their diameters are about the same in whatever direction measured. The crystals appear first in the most severely distorted part of the worked structure, which would usually be at former grain boundaries. Presumably the re-formation of atoms into the uniform lattice of a new crystal requires a certain minimum energy, and since areas of maximum distortion are regions of maximum instability or of high energy content, they require less energy from an outside source, *i.e.*, heat from the annealing process. The atoms, or groups of atoms, from which the new grains start to form are *nuclei*, and the process of their formation and growth to a visible size is called *recrystallization*. The process is not completed instantaneously at a fixed temperature. As in all crystal structural changes involving nucleation and growth, the process is a function of both temperature and time. The other variable to be considered is that of the initial instability, and factors affecting that are the degree of prior deformation and the prior grain size.

After recrystallization begins, the use of longer times at a specific temperature, or slightly higher temperatures (generally, doubling the time is equivalent to raising the temperature 10°C), results in growth

of the first new crystals from strained material surrounding them and the formation of additional nuclei in the somewhat less distorted sections of the cold-worked lattice. Strictly speaking, the word *recrystallization* refers only to the process by which nuclei form and grow *at the expense of the distorted lattice*, resulting in the gradual disappearance of the cold-worked structure. The temperature range in which this occurs is one of sharp changes of mechanical properties, unless the prior reduction was very small and the recrystallization temperature range correspondingly wide. However, a multitude of new crystals (Micro. 4.7) usually will completely fill one area while an appreciable amount of the distorted lattice remains unaffected. In this case, some of the new crystals will *grow larger at the expense of other new crystals adjacent to them.* This process is called *grain growth.* It is clear that the grain-growth and recrystallization processes overlap and cannot be cleanly separated in a temperature or time chart.

Grain growth in a completely recrystallized structure (or section of a structure) occurs by boundary migration; *i.e.*, atoms at the boundary plane between two crystals, A and B, are not in stable positions with respect to either crystal. If they become attached in normal lattice positions for grain A, the next adjacent layer of atoms is pulled slightly from symmetry positions with respect to B. The boundary then has migrated one atom distance, A has grown larger and B smaller. Which crystals are marked by what force to grow and which are to disappear are interesting questions but unanswerable at the present time.

4.5 Microstructures of Annealed Brass

All wrought and annealed brass structures show annealing twins. In making grain-size determinations, it is necessary to avoid mistaking twin-band boundaries for grain boundaries. The distinction is usually readily made on the basis of the straightness of twin-band edges and the fact it is a band, *i.e.*, has parallel sides. Use of an etch that differentially colors grains of different orientations facilitates grain-size determinations. These may be made in four different ways: (1) by taking a section of known area, counting all grains contained within that area, and adding half of those intersected by the edges. This gives the average number of grains per unit area. (2) The number of grains per unit area can be converted to a figure representing average grain diameter by making certain assumptions as to the shape of the grains. (3) The number of grains intersected by a straight line of fixed length, drawn at random across the image (or micrograph) of the structure may be taken as representative of the grain size. This method, which is

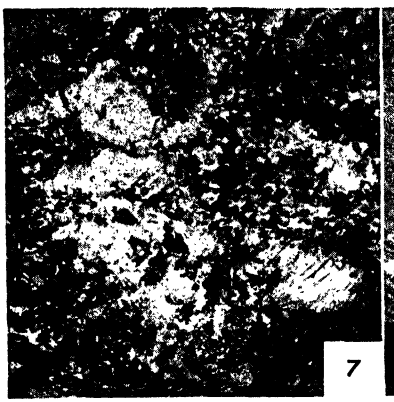

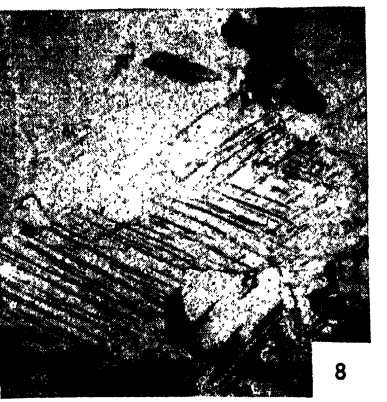

Micro. 4.7. α brass, cold-rolled 60% and heated to a temperature in the recrystallization range (30 min at 300°C); ×75. This structure shows masses of tiny new crystals, not very well resolved here, and some areas of the old deformed structure containing strain markings.

Micro. 4.8. Same as Micro. 4.7 at ×500. The structure of the new crystals is somewhat better resolved at this magnification. The average diameter of the new crystals is about 0.002 mm.

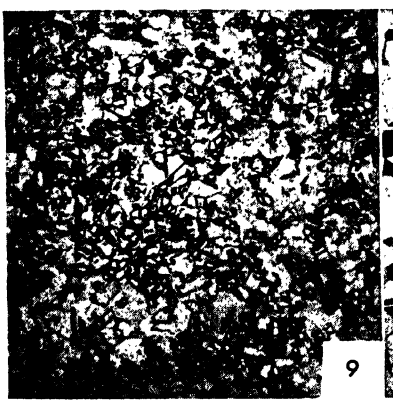

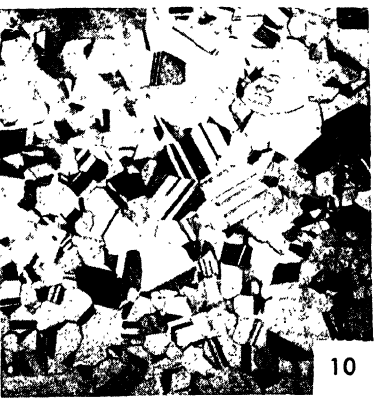

Micro. 4.9. Same specimen as Micro. 4.8 reheated 30 min at 400°C; ×75. After recrystallization has been completed and after some crystal growth, the average grain diameter is about 0.020 mm.

Micro. 4.10. Same specimen, reheated 30 min at 500°C; ×75. Additional growth has increased the average grain diameter to about 0.045 mm.

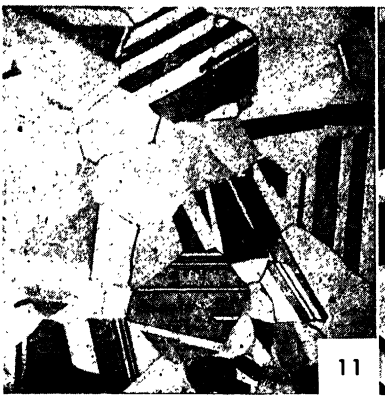

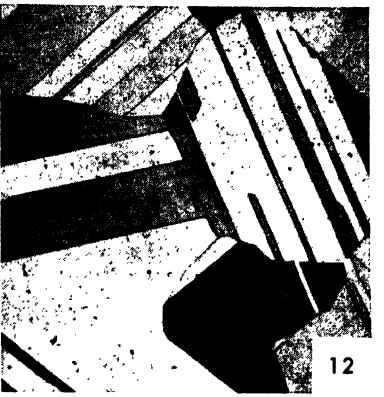

Micro. 4.11. Same specimen, reheated 30 min at 650°C; ×75. The average grain diameter is now about 0.15 mm.

Micro. 4.12. Same specimen reheated 30 min at 800°C; ×75. Inspection of a larger area at a lower magnification is required to determine that the average grain diameter is now about 0.25 mm.

Micro. 4.13. Annealed 70:30 brass subjected to a tensile stress of 10,000 psi in an atmosphere containing some ammonia vapor; ×250; $NH_4OH:H_2O_2$ etch; courtesy F. H. Wilson, American Brass Co. The specimen failed in 244 hr. This microstructure, at some distance from the point of final fracture shows a crack that follows grain boundaries of the α solid solution. Failures of this character always involve intercrystalline (between crystals) cracks although part of the final fracture may be of the shear or normal type (transcrystalline or across crystals), once the intercrystalline crack has sufficiently reduced the effective cross section.

coming to be employed for tool steels (page 376), is useful in a qualitative sense. The grain structure at a specific magnification can be compared with standard structures of known grain size (reproduced in the "Metals Handbook," ASTM Standards, etc.) at the same magnification or, by use of a conversion factor, at a different magnification. This last method is quickest and about as accurate as the other, more tedious methods. It is equally useful in most work since, by all methods, measurement is made on a two-dimensional view of a three-dimensional object, and the resulting data are not absolutely quantitative. Another method, less quantitative than the previously listed types, employs the appearance of a fractured specimen, usually obtained by impact stressing of a notched bar. If the notch prevents the localized deformation that usually accompanies a metal fracture, the appearance of the surface is indicative of the grain size. This quick test will give a very useful qualitative indication of grain size. A standard set of fractures of tool steels is available to enable a more quantitative description of results for these materials.

It is desirable here to record some of these comparative systems of reporting grain size. The ASTM number system is based upon the formula: number of grains per square inch at $\times 100 = a^{N-1}$, where N = ASTM number. The various systems are compared in Table 4.2. Of these, average grain diameter is used with brasses, grains per square millimeter for magnesium alloys, ASTM numbers for most steels, and grain intercept for tool steels.

4.6 Property Changes upon Annealing

The recovery range of annealing has already been defined as one where hardness and strength are little affected, but stresses are at least partially removed and thus susceptibility to stress-corrosion cracking is diminished or eliminated. Residual stresses are undoubtedly related to nonuniform positions of individual atoms in the lattice with respect to one another (microstresses), or very large blocks of atoms to other blocks (macrostresses). In either case, the atomic displacements must be elastic. When the temperature is increased, the elastic strength of the metal is diminished, and the stresses cause plastic flow, or block movement toward equilibrium positions, that reduces the stress. The temperature-time relationships required to reduce the stresses to a given value may be calculated from creep (flow vs. time) data, but they are more readily determined experimentally by forcing a strip of material to assume a specific curvature (using three pins with the center one out of line) with a resultant calculable tensile stress on the convex side, bal-

anced by an equal compressive stress on the concave side. If the stresses are elastic, the beam will spring back to straightness when removed from the fixture. If the bent beam is heated for various times in the recovery range, the degree of stress relief can be measured by the tendency to spring back to straightness. When stresses are completely removed, the strip will remain permanently in the curved position.[1]

TABLE 4.2. COMPARATIVE SYSTEMS OF REPORTING GRAIN SIZE

ASTM No.	Grains per sq. in. at ×100*	Grains per sq. mm	Average grain diameter, mm
−3	.06	1	1.00
−2	.12	2	0.75
−1	.25	4	0.50
0	.5	8	0.35
1	1	16	0.25
2	2	32	0.18
3	4	64	0.125
4	8	128	0.091
5	16	256	0.062
6	32	512	0.044
7	64	1,024	0.032
8	128	2,048	0.022
9	256	4,096	0.016
10	512	8,200	0.011
11	1,024	16,400	0.008
12	2,048	32,800	0.006

* For ×50, report 2 ASTM numbers lower; for ×200 report 2 ASTM numbers higher.

It has been experimentally observed that the troublesome macrostresses in cold-worked metals can be largely diminished by plastic flow in the recovery range without materially reducing the microstresses, altering the appearance of the cold-worked structure, or reducing strength and hardness properties.

The recrystallization range, in which the deformed structure is replaced by new, undistorted crystals of the same type, is a range of rapid transition of properties from those of a strained to a strain-free structure. Thus hardness and strength diminish, and ductility, as shown by elongation values in the tensile test, increases (Fig. 4.6). Higher annealing temperatures which increase the grain size, corre-

[1] Kempf and Van Horn, *Trans. AIME*, **147**, 250, 1942.

spondingly decrease the number of grain boundaries, which, it will be recalled, offer discontinuities to slip or deformation. Thus, grain coarsening is accompanied by further decreases in strength and hardness and by increases in plasticity. The effects of the factors of prior deformation and temperature are shown in Table 4.3, and the effect of the time factor may be indicated by saying that doubling the time

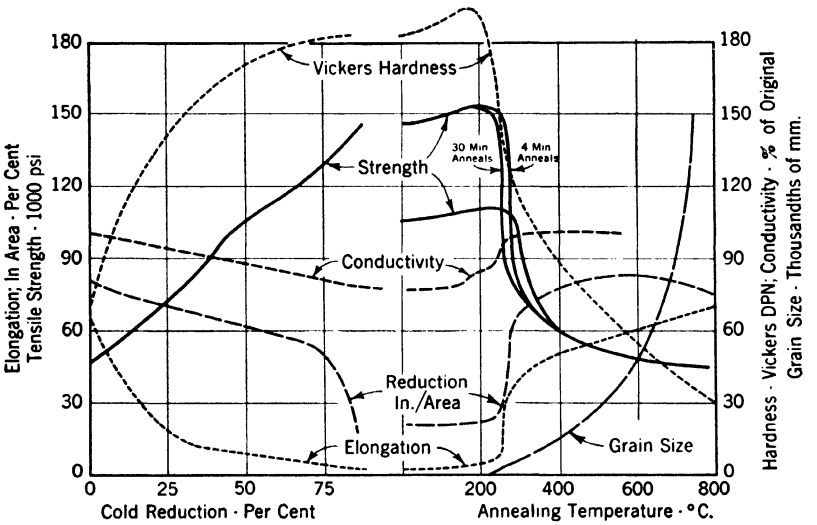

FIG. 4.6. The effect of cold-working and annealing on some properties of common high brass (65% Cu, 35% Cu : Zn).

would probably give about the same data for temperatures 10°C lower than those shown.

A more detailed discussion of the factors affecting recrystallization temperatures and grain-growth characteristics is given in the "Metals Handbook." A summary of the more important influences follows:

1. Recrystallization starts at a lower temperature and is completed within a narrower temperature range:
   a. The greater the prior deformation
   b. The finer the prior grain size
   c. The purer the metal
   d. The longer the time of annealing
2. The recrystallized grain size will be smaller:
   a. The lower the temperature (above that required for recrystallization)
   b. The shorter the time at temperature

c. The shorter the time heating to temperature (increased nucleation)
d. The heavier the prior reduction
e. The more insoluble particles present, or the more finely they are dispersed

It is evident from statements 1*c* and 2*e* that soluble impurities or alloying constituents, such as zinc in copper, raise the recrystallization temperature while insoluble constituents, such as Cu_2O in copper, do not noticeably affect the temperature of recrystallization but decrease

TABLE 4.3. ANNEALING OF SPECIMENS FROM TABLE 4.1

	Copper, OFHC			70:30 brass*				
	Prior reduction							
	30%	50%	80%	50% F.G.	50% C.G.	T.S.	El.	G.S.
Initial	RH86	RH91	RH95	RX99	RX97	80,000	8	
30 min:								
150°C	85	90	94	101	98	81,000	8	
200°C	80	88	93	102	100	82,000	8	
250°C	74	75	65	103	101	82,000	8	
300°C	61	54	42	82	98	76,000	12	
350°C	46	40	34	66	80	60,000	28	0.02
450°C	24	22	27	50	58	46,000	51	0.03
600°C	15	17	22	38	34	44,000	66	0.06
750°C				20	14	42,000	70	0.12
Final grain size	0.15	0.12	0.10	0.08	0.12			

* F.G. = originally fine grained, C.G. = originally coarse grained; T.S. = tensile strength in pounds per square inch; El. = elongation, per cent in 2 in.; RH = Rockwell scale, ⅛-in. ball, 60-Kg load; RX = ⅛-in. ball, 75-Kg load; G.S. = grain size in millimeters.

the recrystallized grain size. This latter effect is widely used commercially to obtain fine-grained structures in annealed metals.

The grain size obtained after holding a specific time will be increased if the metal is reheated to a higher temperature, but will be stable, unaffected by all lower temperatures, unless the time is increased very considerably (*e.g.*, multiplied by about 1,000 for 100°C lower).

The effects of some of these variables are also shown in Fig. 4.7, annealing curves of a high-purity copper. Changing the annealing time from 1 to 24 hr lowers the softening or recrystallization temperature range of 50% cold-rolled metal from 150–160°C to 110–120°C. Changing the reduction from 50 to 88% reduces the softening temperature, for 24-hr anneals, from 110–120°C to 80–95°C. Figure 4.8 shows the effect of changing the grain size, prior to cold-working, on the annealing of OFHC copper. It will be observed that softening is more rapid or

that recrystallization takes place within a narrower temperature range, for the material that was fine grained (dashed lines) with prior reduction and annealing times the same in both cases. This would be anticipated

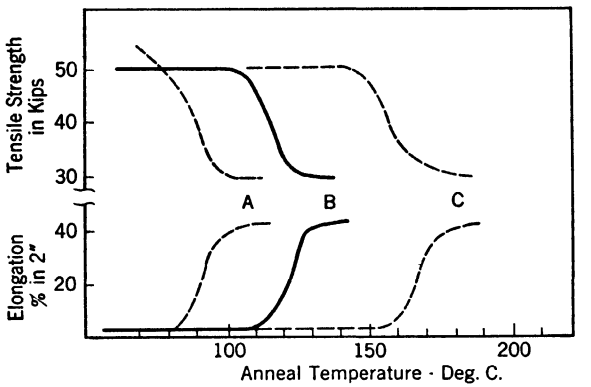

FIG. 4.7. Annealing curves of tensile strength and elongation for high-purity copper, showing the effect of prior reduction and annealing time on the recrystallization temperature; (*A*) prior reduction of 88%, 24-hr anneals; (*B*) prior reduction of 50%, 24-hr anneals; (*C*) prior reduction of 50%, 1-hr anneals. (*Smart, Smith, and Phillips.*)

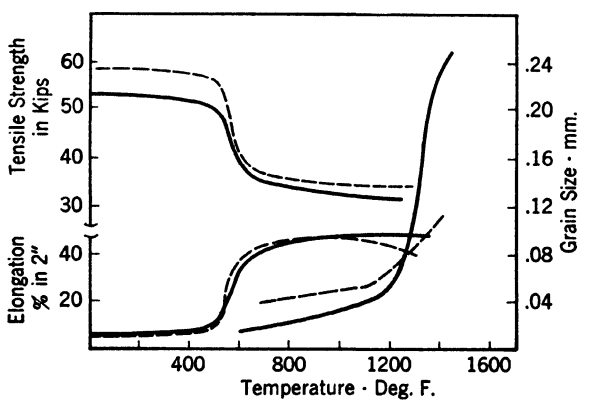

FIG. 4.8. Annealing curves of tensile strength, elongation and recrystallized grain size for OFHC copper rolled 50% from two different initial grain sizes; dashed line—originally 0.015 mm grain size; solid line—originally 0.045 mm grain size, 1-hr anneals. (*Wilkins and Bunn.*)

in view of Table 4.1 where it was shown that fine-grained material strain-hardens more for a given reduction, *i.e.*, requires less reduction by rolling for the same strain-hardening effect.

The grain sizes of Fig. 4.8 show that the originally coarse-grained

material (solid lines) has a finer grain size within a specific temperature range but coarsens much more above about 1250°F. The same degree of coarsening would not be observed in tough-pitch copper which has Cu_2O inclusions to restrict grain growth. (Iron or chromium in brass has a similar function.) It is interesting to note the effect of metal purity on annealing as shown by the much higher softening temperature

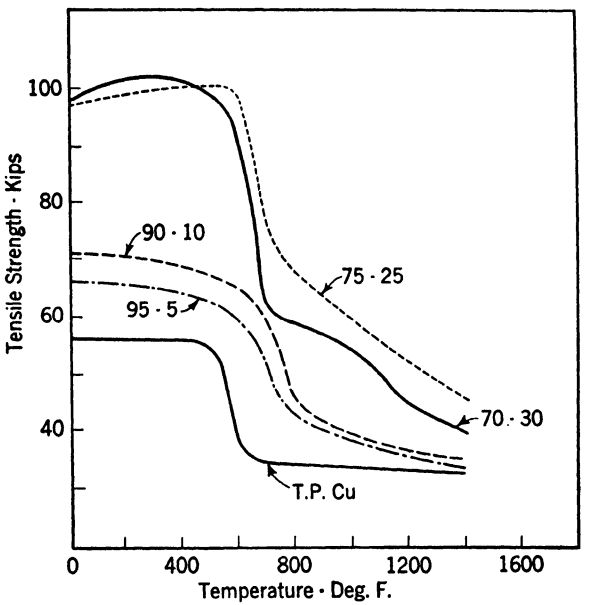

FIG. 4.9. Annealing curves of tensile strength vs. annealing temperature for tough-pitch copper and 95:5, 90:10, 75:25 and 70:30 copper-zinc brasses. All alloys were originally 0.015 mm grain size, were cold-worked 40% and annealed for 1 hr at temperature. (*Wilkins and Bunn.*)

of OFHC copper in Fig. 4.8, 290 to 315°C (550 to 600°F) as compared to the ultrapure copper of Fig. 4.7 with 150 to 160°C for 50% reduction and 1-hr anneals.[1]

The effect of solid-solution alloying elements on annealing curves is shown by the graphs of Figs. 4.9 and 4.10. The first one shows how zinc, when added to copper, particularly in amounts up to 10%, raises the recrystallization temperature as well as the solid-solution hardness

[1] In several of the figures in this chapter, it will be observed that the properties are given for two different "ready-to-finish" grain sizes. Mill terminology includes this term to designate the anneal or the grain size resulting from the anneal that immediately precedes final cold-working. In scientific work, it is common to speak of the "penultimate" anneal or grain size for this same stage.

(*e.g.*, annealed at 1400°F) and cold-worked hardness (initial values). This figure also shows that it is only in the higher zinc-content alloys, 25 to 35% zinc, that an increase in hardness is noted on stress-relief annealing.

Figure 4.10 shows annealing curves for several ternary solid solutions. It is quite evident that nickel greatly raises the softening or recrystallization temperature but does not have such a pronounced effect on the

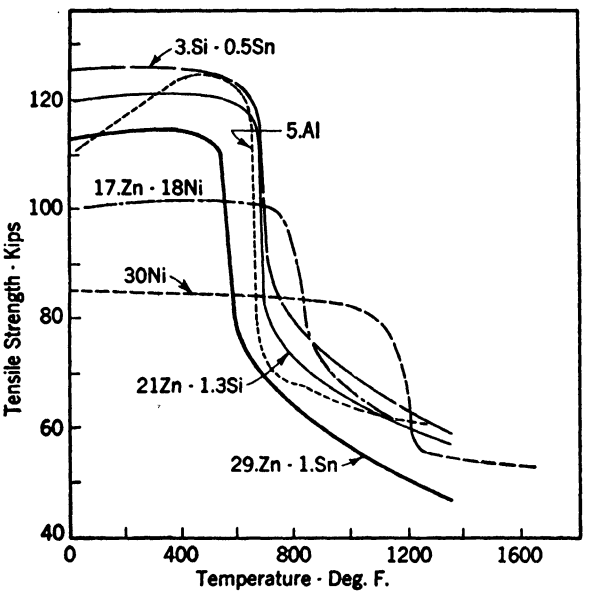

FIG. 4.10. Annealing curves of tensile strength vs. annealing temperature for various copper-base solid-solution alloys: admiralty metal (Cu + 29% Zn + 10% Sn), silicon brass (Cu + 29.% Zn + 1.3% Si), cupronickel (Cu + 30% Ni), nickel silver (Cu + 17% Zn + 18% Ni), aluminum bronze (Cu + 5% Al) and silicon bronze (Cu + 3% Si + 0.5% Sn). All alloys were of comparable initial grain size, cold-worked about 40% and annealed 1 hr at temperature. (*Wilkins and Bunn.*)

strength of the cold-worked alloy. Silicon and aluminum, whether added to an α brass or to copper, greatly increase the cold-worked strength but have little effect on softening temperatures. Incidentally, the pronounced hardening of the 95% Cu:5% Al alloy in the stress-relief annealing range is evidence of some change other than merely macrostress relief (see page 178). Presumably it is a precipitation hardening effect (to be discussed in Chap. 6).

4.7 Hot-working

It is now possible to define hot-working more positively: plastic deformation at temperatures and rates such that recrystallization

occurs and the final structure is substantially free of strain hardening. Although it is usually stated that hot-working is the equivalent of cold-working and annealing, it must be appreciated that time and rate factors may cause very appreciable differences in structures. For example, very pure copper when severely cold-worked may recrystallize and soften completely within 24 hr at 100°C, as shown by Fig. 4.7. However, the same copper probably could never be considered as hot-worked if rolled at any temperature close to 100°C because of time and rate limitations. Laboratory tests have shown that cast tough-pitch copper hot-rolled at 800°C had the same hardness and strength as similar copper cold-rolled the same degree and annealed for 1 hr at 350°C. However the Cu_2O inclusions in the two samples were distributed somewhat differently, and the ductility was less in the cold-rolled and annealed structure. Recommended hot-working temperatures for copper-base alloys and softening temperatures for the same alloys as cold-rolled are given in Table 4.4.

It has already been pointed out that, upon cold-rolling, deformation is greater at the surface in contact with the rolls, particularly in the early stages of deformation, and results in concave ends and edges. The opposite is true of hot-working. Since the rolls or other working surfaces are usually cooler than the metal, the surface layers of the metal become cooler and harder. Therefore, deformation is greater in the center and, consequently, the ends and edges of sections are apt to be convex or bulged.

In all deformational processes, a large part of the energy employed to change the shape of the metal is transformed to heat. In hot-working with no strain hardening, practically all of the energy becomes heat. If the surface-volume ratio of the metal being worked is large, heat is lost to the surroundings faster than it is generated in the metal, and cooling will occur during working. However, large sections with a relatively small surface-volume ratio may become appreciably hotter and may even partially melt if deformed too rapidly. This factor limits the maximum deformation temperature. The minimum limit may be the danger of strain hardening or of cracking in the case of metals and alloys that have limited ductility at ordinary temperatures.

Metal crystal lattices are expanded at elevated temperatures, and the specific lattice planes to which slip during cold-working processes is limited are not the sole planes participating in the flow process at high temperatures. For example:

1. Magnesium, a close-packed hexagonal metal, has limited ductility at room temperatures where only the basal plane functions in the slip process. However, at elevated temperatures it becomes very plastic.

This marked increase in deformability is related to the fact that a new set of slip planes becomes operative in addition to the basal plane.[1]

TABLE 4.4. HOT-WORKING TEMPERATURES OF COPPER-BASE SOLID-SOLUTION ALLOYS COMPARED TO THEIR SOFTENING TEMPERATURES

Alloy	Softening temperature range after the usual cold-rolling, °F	Recommended hot-working temperature range, °F
Tough-pitch copper	500–600	1400–1600
95% Cu:5% Zn	600–700	1400–1600
90% Cu:10% Zn	650–750	1400–1600
85% Cu:15% Zn	650–750	1450–1650
80% Cu:20% Zn	600–700	1500–1650
70% Cu:30% Zn	600–700	1450–1650
Nickel Silver		
65% Cu:18% Ni; 17% Zn	750–850	
80% Cu:20% Ni	1000–1100	1700–1900
70% Cu:30% Ni	1100–1200	1700–1900
Sn bronze, 5% Sn	.....	1500–1650
Si bronze, 3% Si, 1% Sn	600–700	1250–1600
Al bronze 5% Al	600–700	1350–1600

2. Iron, which is moderately plastic at room temperatures, has three different sets of slip planes that may function during deformation. However, at liquid-air temperatures and below, iron becomes quite brittle (Chap. 13), and at the same time slip becomes limited to one set of crystal planes.[2]

3. Similar changes of operative slip planes with change in temperature have been found for the metals tin, molybdenum, and aluminum.

4.8 Preferred Orientation and Directional Properties

The process of cold-working, as depicted in Fig. 4.2, calls for a rotation of crystals with respect to the direction of flow. As was indicated in Sec. 4.1, this rotation in polycrystalline alloys does not occur in the form of entire crystals rotating uniformly but as sections, fragments, or bands. Furthermore, the sketch of Fig. 4.2 is misleading in suggesting that the slip planes necessarily tend to become parallel to the flow direction. In face-centered cubic metals, at least, a second

[1] Bakarian and Mathewson, *Trans. AIME*, **152**, 226, 1943.

[2] Barrett, Ansel, and Mehl, *ASM*, **25**, 702, 1937.

slip plane begins to function when the first one reaches an angle of about 55 deg from the flow direction, and the position of stability is reached where the actual position of crystal blocks is as indicated in Fig. 4.11. Not all crystals are in exactly that position (or its symmetrical mirror image), but there is a tendency to approach the orientation shown. Body-centered cubic and close-packed hexagonal metals, with different slip mechanisms, would have different end positions of the crystals or crystal fragments.

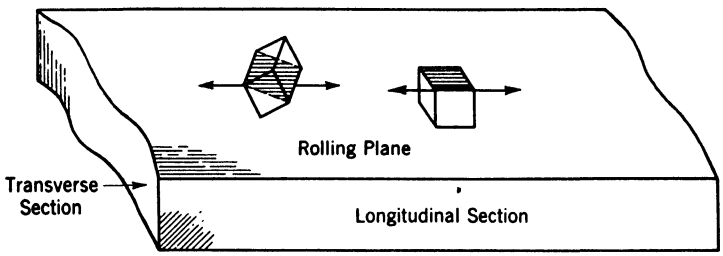

FIG. 4.11. The usual preferred orientation in cold-rolled copper is shown by the left-hand cube which has a body diagonal plane parallel to the rolled surface, oriented in the direction shown or the mirror image thereof. After annealing, this copper sheet would show the preferred orientation indicated by the right cube—having a cube face parallel to the rolled surface and a cube edge in the rolling direction. Different preferred orientations are shown by brasses, aluminum, etc.

The development of a cold-rolled or drawn preferred orientation is very greatly dependent on the state of the metal—random or preferred orientation—before cold-working. In any event, a new cold-worked orientation does not usually become pronounced until the cold reduction exceeds 50%. Consequently, there is no direct relationship between strain hardening and preferred orientation.

Since most metal crystals are individually anisotropic, if the crystalline blocks all tend to align themselves in the same position with respect to the direction of flow, it would be anticipated that mechanical and other properties would vary depending on the direction of testing with respect to the direction of flow. The data of Table 4.5 for rolled sheet of the 90% Cu:10% Zn alloy show the variations in strength and elongation in different directions and for different rolling techniques. These data are not completely representative of real property differences as is realized when one tries to bend cold-rolled sheet in different directions. If the axis of bending is parallel with the rolling direction, the tendency to crack along the bend is far greater than when the axis of bending is at right angles to the rolling direction. The difference

is so great that it seems probable that preferred orientation is not the sole explanation, although no better one has yet been advanced.[1]

The preferred orientations found in deformed metals after relatively high reductions are frequently changed but never obliterated by the recrystallization and grain growth accompanying subsequent anneals; in fact, the directionality of properties may be greater. It is certain to be more troublesome, since disks blanked from rolled and annealed

TABLE 4.5. DIRECTIONAL PROPERTIES OF COLD-ROLLED 90% Cu:10% Zn ALLOY

	Tensile strength, psi			% elongation in 2 in.		
	Angle, specimen axis to rolling direction, deg					
	0	45	90	0	45	90
A. Light reductions and anneals + 37%	59,000	60,000	63,000	5.0	4.0	3.0
B. Moderate reductions and anneals + 56%	74,000	74,000	77,000	4.0	3.0	3.0
C. One heavy reduction, 95%	82,000	87,000	95,000	2.7	2.7	3.2

sheet are frequently drawn into cups or tubes, and, if the crystals are oriented in preferred directions, the *flowability* of metal will be greater in certain directions and, correspondingly, the drawn cups will not be uniform at the top edge but will have high sections (*ears*) of less wall thickness. The directional properties of different metals vary; upon cupping, some show four ears at 0 and 90 deg to the rolling direction, others four ears at the 45-deg position, while hexagonal and, occasionally, cubic metals may show six ears. Since the directional properties generally increase, not only with increased prior reduction but with increased temperature of annealing, it would seem that not only do nuclei during recrystallization tend to show a preferred orientation but, more important, during grain growth, crystals oriented close to certain positions are favored and absorb their less fortunately situated neighbors. Data on the extent of the property variations, Table 4.6 (these are from the same commercial bronze as tested, in the cold-worked state, for the data of

[1] In cases such as wrought iron, covered in Chap. 2, the fibrous slag inclusions that intercept the continuity of matrix metal much more in one direction than in the other offer a plausible explanation for transverse weakness. The same explanation is not tenable for wrought brasses.

Table 4.5), indicate that, in annealed metal, elongation values are more sensitive to directionality than strength.

The considerable amount of research in the field of preferred orientations in annealed metals has not defined in a quantitative sense the mechanism of their origin and development, but has revealed the conditions that tend to increase directionality, *i.e.*, heavy penultimate

TABLE 4.6. DIRECTIONAL PROPERTIES OF ANNEALED 90% CU:10% ZN ALLOY

	Tensile strength, psi			% elongation in 2 in.			Height of ears, in.†
	Angle, specimen axis to rolling direction, deg						
	0	45	90	0	45	90	
*A.** Ann. 500°C; 0.01 mm grain size	42,000	41,000	42,000	41	44	44	
A. Ann. 800°C; 0.07 mm grain size	36,000	36,000	37,000	39	45	44	0.01
B. Ann. 500°C; 0.01 mm grain size	47,000	45,000	45,000	37	41	42	0.01
B. Ann. 800°C; 0.04 mm grain size	39,000	36,000	38,000	37	44	45	0.03
C. Ann. 500°C; 0.01 mm grain size	48,000	45,000	44,000	38	41	40	0.01
C. Ann. 800°C; 0.05 mm grain size	40,000	33,000	34,000	32	47	48	0.05

* *A*, *B*, and *C* are same specimens listed in Table 4.5.

† Ears on cups 0.6 in. deep by 1.12 in. diameter occurred at 45 deg to the rolling direction.

(next to last) reductions, and low penultimate annealing temperatures and high temperatures of final annealing.[1]

The change of properties with direction of testing is also known as *fiber* or *texture*. The fiber of these rolled and annealed metals, based on preferment of crystallographic orientations, should not be confused with the fiber of wrought iron or similar metals, where the effect is mechanical, caused by the presence of slag stringers all distributed in the rolling direction.

4.9 Engineering Considerations

The nonferrous metals, copper, aluminum, nickel, and their solid-solution alloys are commonly furnished in various conditions of "tem-

[1] Burghoff and Bohlen, Palmer and Smith, *Trans. AIME*, **147**, 144, 164, 1942.

per" obtained by cold-working after annealing. Cold-working by rolling, drawing, etc., to decreasing thickness, is frequently measured in Brown and Sharpe gauge numbers, and the temper of brass mill products is commonly designated in terms of the reduction by gauge numbers.

The cold-worked structure of solid-solution alloys gives much higher strength without any pronounced impairment of corrosion resistance. The diminished ductility is not detrimental in many uses and is of pronounced benefit where machinability is a factor. The harder, more brittle structure results in a tendency for shear cracking of the metal ahead of the cutting tool and easy breakage of the chips resulting

TABLE 4.7. TEMPER DESIGNATIONS FOR COLD-ROLLED COPPER ALLOYS

Commercial temper, cold-rolled stock	Brown and Sharpe No. reduction	Reduction of area, %
Soft (annealed)	0	0
Quarter hard	1	10.9
Half hard	2	20.7
Three-quarters hard	3	29.4
Hard	4	37.1
Extra hard	6	50.0
Spring	8	60.5
Extra spring	10	68.7

from machining. These two factors result in less wear at the edge of the cutting tool and a better surface finish on the machined sections.

The alloys shown in the different figures in this chapter include some of the most important copper-base solid-solution alloys, but not all are represented. The most comprehensive listing of alloys in this field together with tabulations of properties and the effects of cold working and annealing is given by Wilkins and Bunn.[1]

Grain size has been shown to be a significant factor, although not a major one, in determining the hardness strength and ductility of annealed structures. It has a particular industrial significance where sheet-metal blanks are being cold-worked into some specific shape. Although the coarse-grained structures are softer and, therefore, more easily deformed, they are more apt to show a rough "orange-peel" surface in sections not subject to pressure on both faces by the deforming tool. This results from the crystallographic nature of slip and the related necessity for certain crystals to deform differently, depending on the orientation of the slip plane with respect to the flow direction.

[1] Wilkins and Bunn, "Copper-base Alloys," McGraw-Hill, 1943.

In fact a fairly good idea of grain size may be obtained simply by stretching or bending a piece of strip metal.

Lead and tin do not strain-harden at ordinary room temperatures but recrystallize spontaneously following cold plastic deformation. Zinc, when very pure, behaves similarly, but commercial grades can be hardened somewhat by cold-working. This behavior results from a recrystallization temperature at or below room temperature.

The plain carbon steels containing very little carbon, such as SAE 1010 and 1015 (0.10 and 0.15% carbon), are very commonly cold-worked to raise their strength and improve surface finish and machinability. This is also done with higher carbon steels in certain applications, such as cold-rolled shafting or cold-drawn wire for wire cable. The George Washington Bridge across the Hudson River, for example, is borne by four 36-in. cables, each composed of 61 strands of 434 wires each, 0.192 in. in diameter, cold-drawn from $\frac{3}{8}$-in. patented (sorbitic) rod containing about 0.8% carbon. The rod has a tensile strength of about 170,000 psi and elongation value of 8% before drawing, compared to 240,000 psi and 2 to 3%, respectively, after drawing. In most other applications, however, steels containing 0.3% or more carbon are usually heat-treated to develop optimum strength properties. The familiar 18%Cu:8% Ni (low-carbon) stainless steel is not improved by heat treatment but can be approximately doubled in strength by cold-working and is used extensively in this condition.

QUESTIONS

Group A

1. How can you distinguish between (*a*) slip lines, (*b*) lines of deformation (strain markings), (*c*) annealing twins, (*d*) mechanical twins?

2. Explain the course of the cold-rolling data for zinc given in Table 4.1. Assume that the rate of rolling is such that the zinc does not get noticeably warmer during the rolling operation.

3. If a 70:30 brass strip were to be annealed and blanked into disks which were to be drawn to shape as reflectors, what would be the most desirable annealing temperature? Why?

4. Give at least two reasons why the brass for question 3 would probably be annealed at a much higher temperature at the penultimate or ready-to-finish stage.

5. Both cold-worked and cast metals may have elongated grains. What is the difference (*a*) in the direction of elongation, (*b*) in the lattice structure within the elongated grains?

Group B

1. Assume that a cast brass part had numbers stamped on the surface and then filed off. How would you identify the original stamped numbers? If the numbers were cast in the mold, would it be possible to identify them once they were filed off?

2. Assume that aluminum sheet, after cold-rolling presumably to final size and annealing, was found to be 2% oversize in thickness. What would be the effect of cold-rolling to size and annealing to remove the hardening effects of this slight cold reduction?

3. If a metal tube is reduced in diameter by drawing through a die without an internal die, it will have severe residual tensile stresses present. If this is given a reversed bending operation (as in roller straightening), the residual stresses are diminished. Describe the basis for this mechanical reduction of residual stresses.

4. Assume that silicon bronze parts stressed in service, while wrapped with friction tape, are found to break with an intercrystalline failure. Diagnose the probable cause of the trouble and suggest means of checking the diagnosis and of eliminating the trouble.

CHAPTER 5

CAST EUTECTIC ALLOYS: LEAD-BASE SYSTEMS

There are at least two requirements that must be met for an alloy system to show *complete* solid solubility: (1) The two metals must have atomic lattices of the same type; *e.g.*, both should be face-centered cubic or body-centered cubic. (2) The two atoms must be of nearly the same size. In the Cu:Ni and Au:Ag solutions, copper and nickel atoms differ in size by less than 3%; gold and silver atoms differ by less than 1%; and all four of these metals have face-centered cubic lattices. If the component metals of an alloy system do not meet the requirement of similar lattice types, complete liquid solubility is, of course, possible, but the alloy system must show two solid phases. These frequently originate in a reaction known as a *eutectic*. The metal lead forms eutectic systems with several other metals. The industrially significant systems to be discussed here are Pb:Sb, Pb:Sn, and Pb:Sn:Sb.

5.1 Pb:Sb Phase Diagram

The α phase, at the left end of the horizontal line of Fig. 5.1, represents solid lead with about 3.5% Sb in solid solution. This solubility decreases with temperature, as shown by the course of the left-hand line (solid solubility or *solvus* line), which drops steeply with temperature and also veers to the left, indicating a solubility limit at room temperature of 0.3% Sb. Under equilibrium conditions, an alloy of lead with 2% Sb will solidify as a solid solution (see Cu:Ni alloys, Chap. 3), which is stable until the temperature falls to about 220°C. Upon further cooling, the alloy crosses the *solvus* line and enters a two-phase field with a resultant formation of $\alpha_{(Sb)}$ crystals in the solid $\alpha_{(Pb)}$ phase (see generalization 2 on page 471). The change from a one-phase solid to a two-phase structure on cooling, as related to this type of solvus line, is essential for age-hardening (discussed in more detail in Chap. 6). Under equilibrium conditions, then, this 2% Sb alloy would show a two-phase structure at room temperatures but no eutectic.

Means of determining the liquidus lines of a phase diagram by thermal analyses of slowly cooled liquid alloys and of determining the

solidus lines by reheating homogeneous solid solutions have already been described. The temperature-concentration course of the solvus line cannot be determined by thermal analyses, since only a small amount of heat is liberated by the separation of a minute amount of a second phase, and the separation is very slow and subject to undercooling, requiring as it does diffusion of solute atoms through the solvent lattice to nuclei of the new phase. The solubility relationship may be

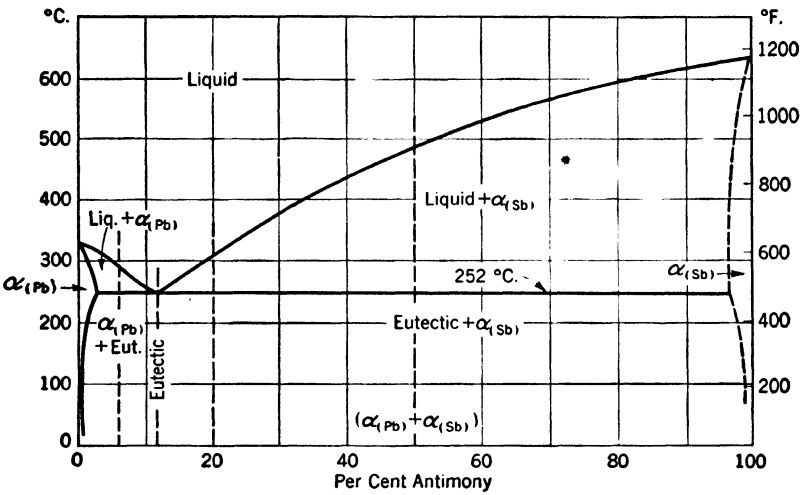

FIG. 5.1. Phase diagram of the Pb : Sb alloy system.

determined micrographically by heating alloys of several concentrations at specific temperatures for long periods of time (in some cases, for weeks), quenching the specimen, and examining the structure for evidence of the presence of a second phase. If the change of solvent lattice parameter with solute concentration (page 72) is first measured (by X-ray diffraction), then, by reheating a saturated alloy at several temperatures in the two-phase field until equilibrium is attained, quenching, and measuring the lattice size of the solvent, the solute concentration at each temperature may be obtained. Finally, since electrical resistivity is strongly affected by an element in solid solution and only slightly by an element present as a disperse, second phase, resistivity measurements may be employed for solid-solubility determinations. The course of the solvus line, based on data from any of these methods, may be checked by the *log (solubility)* vs. *reciprocal of the temperature* plot described on page 137.

The $\alpha_{(Sb)}$ phase, at the right end of the horizontal line, represents solid antimony with some lead in solution. (It is called an α phase since the convention has been adopted, here, of calling all terminal solid solutions *alpha*.) The actual degree of this solubility is not definitely known and is of no commercial importance since antimony and thus the $\alpha_{(Sb)}$ phase are relatively weak and brittle.

Along the horizontal line at 252°C, three phases may exist in equilibrium and, in accordance with Gibbs's phase rule, three phases can exist in a binary system *under equilibrium conditions* only at a constant temperature and with a fixed composition of each phase. This situation is best represented by the reversible reaction:

$$\text{Liquid}_{(Pb+11.1\%Sb)} \rightleftarrows \alpha_{(Pb)\ (3.5\%Sb)} + \alpha_{(Sb)\ (3\%Pb)} + \text{heat}$$

The reaction proceeds to the right upon cooling, releasing the heat of crystallization of the $\alpha_{(Pb)}$ and $\alpha_{(Sb)}$ phases and, under equilibrium conditions, solidification takes place at a constant temperature, 252°C. (For many years, eutectics were thought to be definite chemical compounds since they froze at a constant temperature and exhibited fixed concentrations, *i.e.*, in this case, Pb + 11.1% Sb.) On heating, the reaction goes to the left, absorbing the heat of crystallization of $\alpha_{(Pb)}$ and $\alpha_{(Sb)}$ phases and forming the liquid phase containing 11.1% Sb. Since the eutectic alloy (11.1% Sb) melts at a constant temperature, the Greek word *eutectic* meaning "well-melting" has come into use to describe this type of reaction or phase change. It has been logical, then, to apply the Greek prefix *hypo-*, meaning "less than," to alloys having less than the eutectic concentration of an alloying element and more than the solid-solution limit (here, 3.5 to 11.1% Sb), and to use the prefix *hyper-*, meaning "more than," to alloys to the right of the eutectic (here, 11.1 to about 97% Sb).

Under equilibrium conditions, hypoeutectic alloys solidify from the liquid state as follows: (1) On reaching the liquidus, nuclei of *primary* crystals of $\alpha_{(Pb)}$ form with the composition given by rule 3 on page 58. (2) Cooling through the $\alpha_{(Pb)}$ + liquid field results in growth of the primary dendrites of $\alpha_{(Pb)}$ while their composition changes with temperature, as shown by the *solidus* line; at the same time, the formation of a lead-rich phase causes the residual liquid to become enriched in antimony so that its composition changes along the liquidus line. (3) At 252°C, primary $\alpha_{(Pb)}$ crystals and liquid exist in the ratio given by the lever rule; the eutectic liquid freezes, forming $\alpha_{(Pb)}$ and $\alpha_{(Sb)}$ phases in a rather fine mechanical dispersion. The dispersion is called *mechanical* since

there is no continuous atomic conformity nor necessarily any relationship between atoms of the two phases at their interfaces or planes of contact.

Under nonequilibrium conditions, freezing begins not at the liquidus line but at a temperature a few degrees under it (super-cooling).[1] The average composition of the primary crystals does not lie on the equilibrium solidus but on a "metastable" solidus (see page 58) and, consequently, the percentage of liquid at 252°C will be somewhat greater than that shown by the diagram. The low concentration of alloying element in the primary dendrites requires a metastable, leftward prolongation of the eutectic horizontal to intersect the metastable solidus. As a result, an alloy containing only 1.5% Sb, which should show no eutectic structure, usually will do so when solidified at rates encountered in normal castings. The eutectic freezing may be delayed by undercooling as well as the crystallization of the primary crystals; if one phase of the eutectic undercools more than the other, there can be a displacement of the eutectic concentration as well as temperature (see Al:Si alloys, page 133).

Undercooling of the eutectic liquid has a dual effect. Thermally, it causes the eutectic reaction to occur at a temperature of several degrees (perhaps 5 to 30°C) under that shown by the equilibrium diagram. Structurally, it causes a refinement of the particle size of the phases participating in the reaction, in the same way as solid-solution dendrites (page 62) are refined by chill casting. When $\alpha_{(Pb)}$ containing 3.5% Sb and $\alpha_{(Sb)}$ containing about 97% Sb form from a homogeneous liquid, there must be a counterdiffusion of the two kinds of atoms in the liquid to each nucleus of the two phases. The rate of solidification when the liquid is suddenly chilled does not permit much time for even relatively rapid liquid diffusion and, simultaneously, there is a very great increase in nucleation points for the reaction. Both factors operate to change the size of crystallites in the eutectic.

5.2 Pb:Sb Microstructures

Lead- and tin-base alloys are so soft that plastic flow readily occurs during polishing. This makes it sometimes difficult to prepare specimens for examination. It is necessary to lubricate the emery papers with a solution of paraffin dissolved in kerosene to prevent particles of lead or tin from adhering to the paper and subsequently causing smearing and distortion of the surface layers. Wet polishing is done in the normal way but, if a black smudge appears on the surface, the cloth

[1] Blumenthal, *Trans. AIME*, **156**, 240, 1944.

must be kept wet with alumina and soap and polishing must be continued until the surface appears bright.

A microtome may be used if it is sufficiently rigid and the knife maintained sharp and smooth. The instrument should be capable of removing a layer only 2 microns thick. With proper handling, the microtomed surface may be etched directly for immediate examination with no further polishing.

Etching solutions include the following:

1. Three parts glacial acetic acid + 1 part 30% hydrogen peroxide. Etching time, 6 to 15 min, for Pb:Sb, Pb:Sn, etc.
2. Various dilutions of HNO_3, for Pb:Sb alloys.
3. One part glacial acetic acid + 1 part HNO_3 + 4 parts glycerol. Etching time, 10 to 15 sec, for Pb:Sb, Pb:Ca, and low Sn alloys.

5.3 Pb:Sn Phase Diagram

The equilibrium features of the Pb:Sn system can be described in the same terms employed for the Pb:Sb system. Solid lead can dissolve up to a maximum of 19.5% Sn, at 183°C, and following our previous convention, this solid-solution phase will be called $\alpha_{(Pb)}$. Solid tin can dissolve a maximum of 1.6% Pb at this same temperature, the solid solution being termed $\beta_{(Sn)}$.[1] The two solid solutions can form simultaneously from a homogeneous liquid containing 62% Sn as it cools past 183°C, the eutectic reaction being

$$\text{Liquid}_{(Pb+62\%Sn)} \rightleftarrows \alpha_{(Pb)(19.5\%Sn)} + \beta_{(Sn)(1.6\%Pb)} + \text{heat}$$

Hypo- and hypereutectic alloys freeze in a manner analogous to the previous description. For example, soft solder containing 50% Pb and 50% Sn will cool to the hypoeutectic liquidus at about 210°C. Under equilibrium conditions, lead dendrites containing about 18% Sn in solid solution will then start to form and continue to grow, becoming slightly richer in tin as the temperature drops to 183°C. At this temperature, again under equilibrium conditions, the dendrites will contain 19.5% Sn and represent as a proportion of the structure:

$$\%\alpha_{(Pb)} = \frac{62 - 50}{62 - 19.5}(100) = 28.2\%$$

[1] In this case the convention of α for terminal solid solutions must be abandoned because $\alpha_{(Sn)}$ has long been the designation for *gray* tin, the allotropic form that is stable below 13.2°C. The ordinary solid ductile tin, called *white* tin, is by custom called β tin.

(*continued on page* 122)

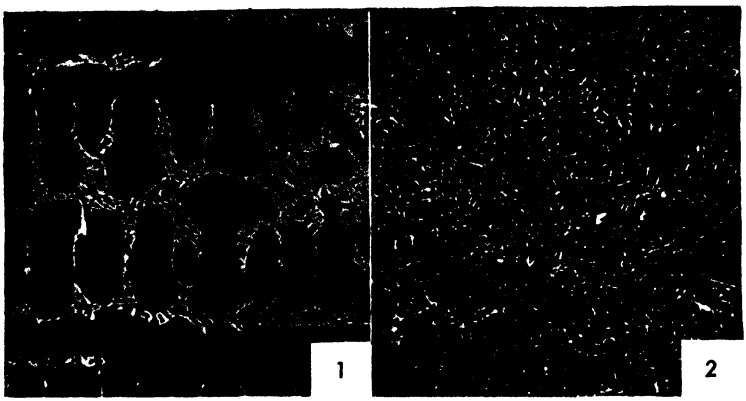

Micro. 5.1. Pb + 6% Sb; ×50. This is a typical hypoeutectic structure consisting of primary $\alpha_{(Pb)}$ dendrites (black), plus an *interdendritic* filling of eutectic. The white particles are $\alpha_{(Sb)}$ crystals, which, together with the black $\alpha_{(Pb)}$ in which they are embedded, comprise the two-phase structure. There is a difference in appearance of primary $\alpha_{(Pb)}$ and the eutectic $\alpha_{(Pb)}$, but both form a continuous plastic structure.

Micro. 5.2. Pb + 11.1% Sb; ×50. At this concentration, the structure is completely eutectiferous with white brittle crystallites of $\alpha_{(Sb)}$ dispersed in a *continuous* matrix of plastic $\alpha_{(Pb)}$. Differently oriented "colonies" of $\alpha_{(Sb)}$ particles indicate different starting points for the eutectic reaction.

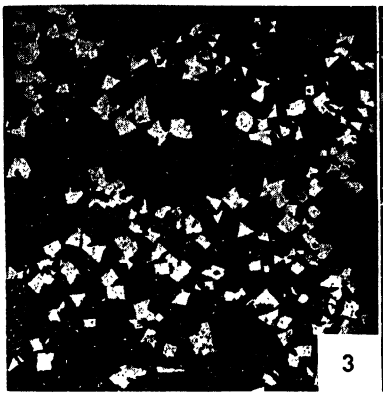

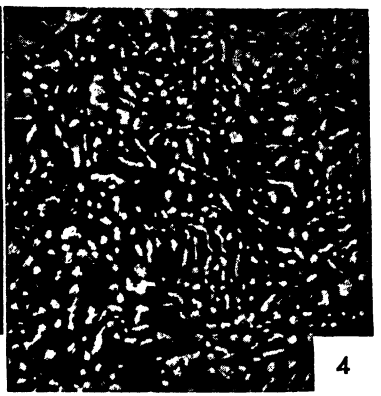

Micro. 5.3. Pb + 20% Sb; ×50. The hypereutectic structure shows primary $\alpha_{(Sb)}$ crystals in a eutectic matrix. The primary $\alpha_{(Sb)}$ crystals are angular rather than rounded like primary $\alpha_{(Pb)}$, presumably because of lower surface-tension forces. Note the clear-cut distinction in appearance, not in structure or composition, between the primary and the eutectiferous crystallites of antimony. There is a striking difference in the size of the eutectiferous $\alpha_{(Sb)}$ particles of this structure and those in Micro. 5.1. This is caused by a difference in solidification rate; the 20% Sb alloy was chill-cast whereas the 6% Sb alloy solidified slowly in the melting crucible. If the 20% alloy were slowly cooled in the same manner, it would be found to show a marked *gravity* segregation; the lower half would be a completely eutectiferous structure with 11.1% Sb while the upper part would be crowded with the primary $\alpha_{(Sb)}$ crystallites and might contain from 50 to 60% Sb.

Micro. 5.4. Pb + 20% Sb; ×500. This microstructure of the same alloy as Micro. 5.3 is deceptive (photographs can lie!) in that it shows just the eutectic part of the structure. Highly significant is the contrast in the *shape* as well as size of the eutectiferous $\alpha_{(Sb)}$ particles here and those in Micro. 5.1. Rapid solidification not only has caused the eutectic particles to be much smaller but has prevented them from becoming platelike. Here they are much more rounded in shape.

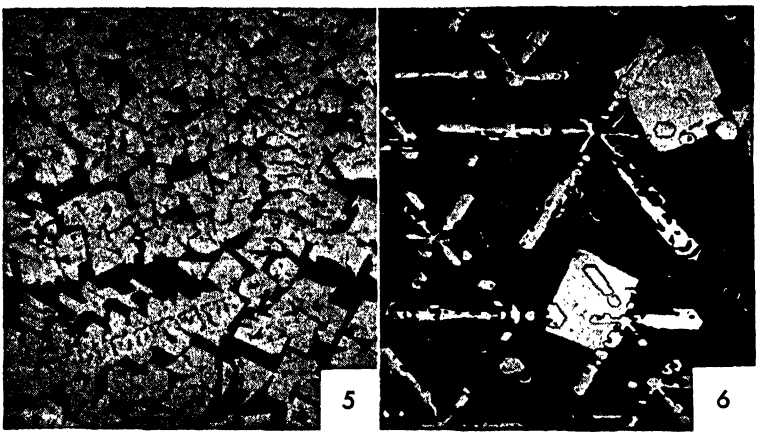

Micro. 5.5. Pb + 50% Sb; ×50. This hypereutectic alloy contains more of the primary $\alpha_{(Sb)}$ crystals in a eutectic matrix. Note that the primary crystals, although characteristically sharply angular, now show a distinctly dendritic pattern or arrangement.

Micro. 5.6. Hard babbitt of 84% Sn, 7% Cu, 9% Sb; ×50. This hypereutectic *ternary* (three-component) alloy shows primary clusters of CuSn (an intermetallic compound) crystals, arranged in a star-shaped dendritic pattern, and large rectangular crystals of primary SnSb compound in a ductile ternary eutectic consisting of these compounds and a tin-rich solid solution. The CuSn compound has a higher freezing point than the SnSb, since it seems to exist inside the latter phase; *i.e.*, during solidification, the SnSb formed on some of the CuSn crystals already present.

Micro. 5.7. Eutectic alloy of 68% Sn and 32% Pb; etched with mixed acid (1 part HNO_3, 3 parts glacial acetic acid, 5 parts glycerol); ×500.[1] This is an unusual photomicrograph since the soft Sn:Pb alloy used for solders is extremely difficult to polish. The lamellar structure evident here would be anticipated on the basis of the proportionate amounts of $\alpha_{(Pb)}$ and $\beta_{(Sn)}$ phases present. The tin phase constitutes the continuous background with the $\alpha_{(Pb)}$ phase appearing in the photograph as lines but existing as laminations or warped plates in three dimensions. This structure is of the alloy slowly solidified in a hot mold.

[1]Photomicrograph by H. Kalish.

The remaining 71.8% of the structure will be liquid containing 62% Sn which solidifies as a eutectic of $\alpha_{(Pb)}$ and $\beta_{(Sn)}$ surrounding the primary $\alpha_{(Pb)}$ dendrites.

This system like the Pb:Sb alloys again shows the eutectic composition to be nearer the lower melting point phase in the eutectic, here the tin phase rather than the lead phase.

The diagram in Fig. 5.2 is not a complete representation of the system because there is a phase change in the $\beta_{(Sn)}$ phase, *i.e.*, the allo-

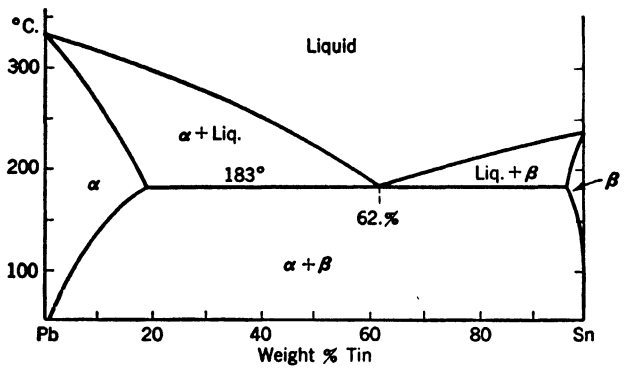

FIG. 5.2. Phase diagram of the Pb:Sn system. The beta ⇄ alpha transformation of tin at 13.2°C is not shown nor the way this allotropic change affects the phase diagram although the transformation can occur in alloys from at least 60% Sn to the pure metal.

tropic change from body-centered tetragonal to diamond cubic structures, which occurs in pure Sn under equilibrium conditions at 13.2°C. The effect of a slight amount of lead in solid solution in the tin on this allotropic change is not known with certainty at the present time, nor the form of the phase diagram below the transformation temperature below 13.2°C.[1]

Only one photomicrograph of the Pb:Sn alloys is included, Micro. 5.7, primarily because of the difficulty in obtaining a good polish with standard procedures. Both the $\alpha_{(Pb)}$ and $\beta_{(Sn)}$ phases are soft and subject to severe flow during polishing. The alloy shown is of eutectic composition. Ordinary soft solder (50% Sn, 50% Pb) would show some $\alpha_{(Pb)}$

[1] Information concerning tin-base systems below 13°C is of considerable potential value to some industries, particularly those concerned with soldered structures that are subjected to low temperatures, such as parts of liquid-air plants producing industrial oxygen or even of refrigeration systems since the transformation is most rapid at −30 to −40°C.

dendrites of primary origin. Soldered joints would solidify more rapidly and show a finer eutectic structure.

5.4 Cu:O System

It is pertinent now to return to one of the commercially pure metals discussed in Chap. 2, specifically, tough-pitch copper. At that time, this commonest grade of copper was specified as having about 0.035%

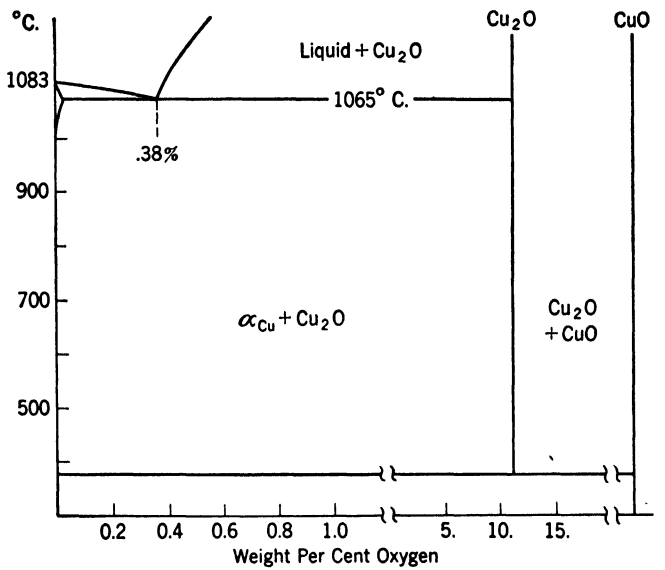

FIG. 5.3. Phase diagram of the copper end of the Cu:O system. The indicated decomposition of Cu_2O to copper and CuO at about 360°C rarely occurs in the low oxygen coppers.

oxygen present as cuprous oxide, equivalent to about 0.3% Cu_2O. The Cu:O phase diagram is quite complex when the oxygen content exceeds about 1.5% by weight; below that concentration this system forms a eutectic, not between copper and oxygen, however, but between copper and cuprous oxide as shown by Fig. 5.3.

It is evident from this diagram that tough-pitch copper is actually an hypoeutectic $Cu:Cu_2O$ alloy. When in the cast form, this grade of copper exhibits the typical hypoeutectic structure, primary dendrites of copper surrounded by from 5 to 10% of a eutectic of $\alpha_{(Cu)}$ and Cu_2O. Micrographs 7 and 8 on page 43 show the cast structure of a tough-pitch electrolytic copper wire bar.

The eutectic composition is, fortunately, much closer to the ductile copper phase than to the brittle Cu_2O phase. The eutectic structure has copper as the major and continuous phase and is, therefore, essentially ductile. The effect of hot-working is clearly shown by comparing these two micrographs with those of the hot-rolled copper on page 44. Considerable deformation at a high temperature completely destroys the eutectic structure of Cu_2O as well as recrystallizing the copper dendrites into new smaller grains containing twin bands. The eutectiferous Cu_2O particles are much larger after hot-working. This agglomeration effect is discussed on page 44.

Oxygen is slightly soluble in solid copper[1] as would be expected in view of the agglomeration of excess Cu_2O particles that occurs upon hot-working of tough-pitch copper. The presence of excess or eutectiferous Cu_2O assures that the matrix copper is saturated with oxygen. If deoxidized copper is heated in air, Cu_2O forms on the surface in contact with the matrix metal. Continued heating makes it possible for this Cu_2O to supply oxygen atoms, which can diffuse inward and in time saturate the matrix. If the saturation temperature is high, the previously deoxidized copper becomes nearly as susceptible to hydrogen embrittlement (page 49) as ordinary tough-pitch copper.

5.5 Ternary Pb:Sn:Sb Phase Diagram

Three metals can form a eutectic system as well as two metals. To represent the phasial conditions, three dimensions may be utilized as shown schematically in Fig. 5.4. Here it is postulated that three metals, A, B, and C, form binary eutectic systems with each other. They also form a ternary eutectic that could be given as follows:

$$\text{Liquid}_{(ABC)} \rightleftarrows \text{solid } \alpha_{(A)} + \text{solid } \alpha_{(B)} + \text{solid } \alpha_{(C)} + \text{heat.}$$

From Fig. 5.4 it is apparent that the binary liquidus lines in three dimensions form three liquidus surfaces intersecting in three valleys that meet at a low point somewhere within the bounding binary sides. Thus the addition of a third element depresses the freezing point of each binary eutectic and may also alter the relative proportions of the constituent metals. The ternary eutectic is necessarily at the minimum temperature where a liquid phase containing all three components can exist.

Compositions are shown on the sides of the equilateral triangle of Fig. 5.4. For accuracy in establishing quantitative relationships, the

[1] Phillips and Skinner, *Trans. AIME*, **143**, 1941.

ternary phase diagram must be represented by several two-dimensional triangular graphs, one to show the liquidus temperatures of the system and others to show the equilibrium at specific temperatures in the solid state.

This book will generally be restricted to binary alloys or alloys that can be discussed in terms of a binary phase diagram. This brief section

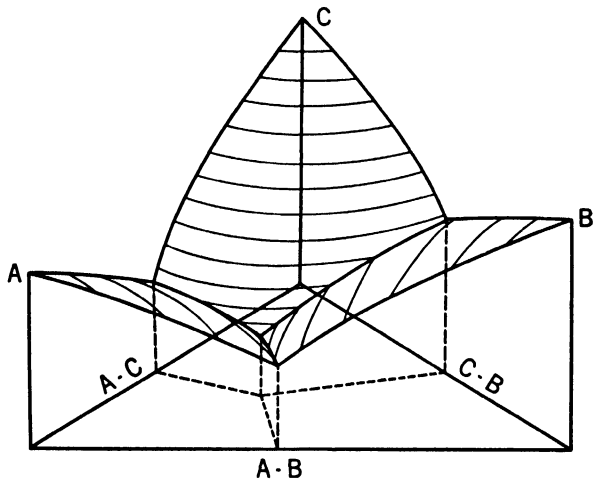

FIG. 5.4. Isometric sketch of three-dimensional phase diagram showing a ternary eutectic between metals *A*, *B*, and *C*. Temperature is plotted vertically; composition is plotted in the equilateral triangular base. The liquidus surface has curved isothermal contour lines meeting at binary eutectics which converge to a low point, the ternary eutectic. Projections of the binary eutectic valleys are dashed in on the base.

serves only to show the extensions in principles from binary to more complex systems.

5.6 Characteristic Properties of Eutectic System Alloys

The properties of a series of alloys across a eutectic horizontal will naturally be a function of the two solid phases present. In the Pb:Sb system and in a majority of all commercially important eutectiferous alloys, one phase is relatively weak and plastic, the other relatively hard and brittle. As the antimony content is increased from 3 to about 97%, the proportionate amount of $\alpha_{(Sb)}$ crystallites increases linearly, but the strength does not increase in the same way because of the difference in dispersion or size of the $\alpha_{(Sb)}$ solid-solution crystals, depending on whether they are primary or eutectiferous. There is a rapid rate of increase in strength from 3 to 11%, and a diminution from 11 to 97% Sb. In the former range, fine, eutectiferous crystallites of $\alpha_{(Sb)}$ are

increasing in amount; in the latter range, the amount of small particles (or the amount of eutectic) is decreasing, with a corresponding increase in the number and size of large primary crystallites of antimony. The result is an inflection at the eutectic point in the plot of any mechanical property against alloy concentration across a eutectic series; in fact, it may be not only an inflection but a maximum, particularly of strength. Strength and ductility of cast Pb:Sb, Al:Si, and Al:Cu alloys are reproduced graphically in Fig. 6.4 on page 160.

Examination of the microstructures shows that in all hypo- and hypereutectic alloys, the eutectic structure is continuous, as would be expected since, during freezing, eutectic liquid surrounds the primary dendrites. If in the eutectic structure the plastic phase is continuous as in the Pb:11.1% Sb alloy, then the entire series of alloys must have some plasticity. If, on the other hand, the brittle phase is continuous as in Al:Cu alloys, the entire series will be brittle. It seems to be generally true that, if one phase is present in a considerably greater proportion in the eutectic, it will be continuous in the duplex structure. Thus, if the eutectic concentration is much closer to that of a plastic phase, the eutectic generally will be plastic, and vice versa.

In addition to these considerations, an increase in cooling rates during solidification generally will result in smaller primary dendrites, a finer particle size (and perhaps different shape) in the eutectic, and perhaps a greater amount of eutectic. These factors may influence mechanical properties of eutectic alloys to a very considerable degree.

5.7 Properties and Uses of Pb:Sb Alloys

It is evident from the data of Table 5.1 that, in 1947 at least, the hypoeutectic Pb:Sb alloys used in storage batteries constituted the largest market for lead and that the solid-solution alloy, Pb + 1% Sb, used to cover electrical or telephone cables, was the next most important alloy. In the case of batteries, the Pb:Sb alloy is used because of the electrochemical properties of the lead and the good casting properties and comparative strength of this alloy. For example, the die-cast 10% Sb alloy has a tensile strength of 7,600 psi as compared to 1,800 psi for pure lead.[1]

The 1% Sb alloy is used for cable coverings because its low melting point and softness permit easy extrusion over the cable wires without destroying their insulation. The metal has a high resistance to cor-

[1] No yield strength values can be reported on these soft metal alloys since they will deform plastically at very low stresses if these are applied for months. In fact, rate of loading will affect strength data almost as much as alloying.

rosion, and the strength properties are fairly good. By heat treatment, *viz.*, heating at 250°C to obtain uniform $\alpha_{(Pb)}$ solid solution, quenching, and "aging" by allowing the alloy to stand at room temperature, the strength of the 1% Sb alloy will increase from some 2,500 psi for the extruded metal to about 6,000 psi. The metallurgical explanation of this age-hardening process is covered in detail in Chap. 6. It is not too important here since in the lead alloy, over-aging or softening will later occur as the aging process continues over a period of years. For the same basic reason—the low melting point of the metal—none of

TABLE 5.1. METALLURGICAL USES OF LEAD*

Product	Tons Pb 1947	Tons Pb 1937	Alloy
Storage batteries	360,000	192,000	Pb + 7 to 12% Sb
Cable covering	155,000	93,000	Pb + 1% Sb
Plumbing and building uses	65,000	45,000	Pb + 0 to 8% Sb or Sn
Ammunition	40,000	39,000	Pb + 1% As
Solder	56,000	22,000	Pb + 15 to 60% Sn
Foil	3,600	21,500	Pb + Sn
Type metal	26,000	17,000	Pb + Sn + Sb
Bearing metals	42,000	15,000	Pb + Sn + Sb + Cu
Other uses	200,000	92,000	
Tetra ethyl lead	63,000		

* Exclusive of oxides used for pigments, etc.

the lead-base alloys are susceptible to strengthening by cold-work. They spontaneously recrystallize and "self-anneal" at room temperatures.

Data on the properties of extruded Pb:Sb alloys are introduced in Table 5.2. The chief point of interest here is the relatively low strength of extruded alloys containing 8 to 12% Sb in comparison with similar cast alloys. The probable reason is the form of the second phase. In cast alloys, the $\alpha_{(Sb)}$ is present as eutectiferous crystallites in a randomly distributed interdendritic network. In the extruded alloys, the network is broken up, and the $\alpha_{(Sb)}$ particles are isolated and aligned with the flow direction, which is also the test direction. In this dispersion, they are less effective in strengthening the metal. A second factor is the coarse grain of the cast alloys and, for stresses in the vicinity or above the recrystallization temperature, a coarse cast structure is almost always stronger than a wrought fine-grained structure (see Chap. 13).

The plumbing applications of Pb:Sb alloys as listed at the beginning of this section recall an interesting point. Lead resists corrosion by all

kinds of waters, as shown by the fact that lead water pipes are found, in good condition, in Roman cities and settlements. The Latin word for lead then, *plumbum*, not only gives us the usual abbreviation for the

TABLE 5.2. MECHANICAL PROPERTIES OF Pb:Sb ALLOYS

% Sb	Cast alloys*			Extruded alloys†		
	Tensile strength,psi	% elongation in 2 in.	BHN	Tensile strength,psi	% elongation in 2 in.	BHN
0	1,780	..	3.0	1,740	110	2.0
1	.....	..	4.2	2,920	58	5.1
2	.....	..	4.8	3,200	56	6.5
3	4,700	15	5.3	3,100	55	7.7
4	5,660	22	5.7	3,100	58	8.9
5	6,360	29	6.2	3,150	59	9.9
6	6,840	24	6.5	3,300	65	10.7
7	7,180	21	6.8	3,240	68	11.4
8	7,420	19	7.0	3,330	75	12.4
9	7,580	17	7.2	3,400	76	12.8
10	7,670	15	7.3	3,700	64	13.7
11	7,620	13	7.4	3,800	74	13.7
12	7,480	12	7.4	3,800	65	14.3
13	7,280	10	...	4,000	57	14.6
14	7,000	9	...	3,930	48	14.6
15	6,800	8	...	4,180	41	14.9
16	6,620	8	...	4,110	36	14.9
17	.....	..	...	4,180	34	14.9
18	.....	..	...	4,340	22	15.3
19	.....	..	...	4,300	20	15.3
20	.....	..	...	4,460	23	15.9

* Vinal, "Storage Batteries," Wiley.
† Schumacher, "Metals Handbook," 1937.

element, Pb, but also has given us our word for water and sewer connections, *plumbing*.

A relatively new lead alloy, now competitive with Pb:Sb alloys, contains from 0.04 to 0.08% Ca. Like the 1% Sb alloy, the Pb:Ca alloy develops high strength by aging at room temperature. It is of interest primarily for its creep and fatigue strength as given in Table 5.3.

While discussing the binary-eutectic alloys of lead, it is pertinent to mention Pb:Mg alloys. Lead forms a eutectic with the compound Mg_2Pb with a eutectic composition of about 3% Mg. Thus a 1% Mg alloy is hypoeutectic with the eutectic structure of Pb:Mg_2Pb continuous. Since the compound and the matrix have far different electrochemical potentials, the alloy disintegrates rapidly when immersed in water. This lack of resistance to corrosion makes the alloy potentially useful for shot used in hunting. There has always been a rather high mortality among ducks feeding in marshy areas that are hunted frequently. The ducks accidentally get bird shot in their intestines and subsequently die of lead poisoning. If the shot were made of the Pb:1% Mg alloy,

TABLE 5.3. RELATIVE STRENGTHENING OF LEAD BY CA, SB, AND SN

Alloy	Stress for 2% creep in 1 yr, psi*	Endurance limit, psi†
Pb + 0.04% Ca	840	1,020
Pb + 1.0% Sb	630	500
Pb + 2.0% Sn	405	
Pure Pb	320	250

* Moore, Betty, and Dollins, *Univ. Illinois Exp. Sta. Bull.* 272, 1935.
† Schumacher and Bouton, *Metals & Alloys*, **1**, 405, 1930.

they would disintegrate after being fired and lying in wet marshes a short time and thus reduce accidental mortality among ducks.[1]

5.8 Properties and Uses of Pb:Sn and Pb:Sn:Sb Alloys

The binary Pb:Sn alloys are used chiefly for soft solders. Since both constituents in the eutectic are soft and ductile, alloys over the entire range of compositions, from 0 to 100% Sn, are readily workable. They can easily be extruded, rolled, or stamped even in the cold state. The tensile properties of the binary alloys are unimportant; instead melting point or melting range, surface tension in the liquid state, solidification shrinkage, and bonding characteristics (probably, alloying properties with metal to be soldered) are significant. The ordinary soft solders are as follows:

85% Pb:15% Sn—relatively high melting range; low cost (relatively little of the more expensive tin).

60% Pb:40% Sn—solder with an extensive melting range used as a wiping solder to join lead pipes, cable sheaths, etc. 2.5% Sb may replace an equal amount of tin.

[1] Dowdell and Green, *Mining and Met.*, **18**, 463, 1937.

50% Pb:50% Sn—general-purpose and most popular solder.

40% Pb:60% Sn—fine solder; sharp melting and freezing.

Fluxes have to be used during soldering to promote chemical bonding, *i.e.*, alloying between the solder and the metal being soldered, and, therefore, to attain best strength of the joint. If the metal has been precleaned, rosin will prevent oxidation during heating to the soldering temperature but will not remove oxides already present. A surer flux

TABLE 5.4. TYPICAL COMPOSITIONS OF TYPE METAL AND WHITE BEARING METALS

Alloy	% Sn	% Sb	% Cu	% Pb	% As	BHN
Electrotype	3	3	...	Diff.	...	14
Linotype	4	11.5	...	Diff.	...	22
Monotype	7	16.5	...	Diff.	...	26
Lead babbitt, No. 12	..	10	0.5	90	0.2	14.5
Lead babbitt, No. 11	..	15	0.5	85	0.2	15
Lead babbitt, No. 10	2	15	0.5	83	0.2	17.5
Lead babbitt, No. 8	5	15	0.5	80	0.2	20
Lead babbitt, No. 7	10	15	0.5	75	0.2	22.5
Lead babbitt, G	1	12 5	0.5	Diff.	3.0	22
Lead babbitt, S	1	15	0.5	Diff.	1.0	20
Tin babbitt, No. 5	65	15	2.0	18.0	...	22.5
Tin babbitt, No. 4	75	12	3.0	10	.	24.5
Tin babbitt, No. 3	83.3	8.3	8.3	...	. .	27
Tin babbitt, No. 2	89	7.5	3.5	....	. .	24.5
Tin babbitt, No. 1	91	4 5	4 5	...	. .	17.0

is a eutectic mixture of zinc and ammonium chlorides. (Metal systems are not the only ones to show eutectics.) $ZnCl_2$ has a melting point of 365°C, but a eutectic mixture of 71% $ZnCl_2$ and 29% NH_4Cl melts at 180°C, fortunately just below the melting point of the Pb:Sn eutectic at 183°C. The chlorides tend to clean the surface chemically as well as to prevent oxidation.

Ternary Pb:Sn:Sb alloys are used for type metals and, occasionally, as bearing metals. The alloys listed in Table 5.4 represent typical ternary compositions. In type metals service, the desired properties are low melting point, good casting characteristics, such as fluidity to reproduce details sharply, and sufficient hardness to minimize the wear and deformation that seriously reduce clarity of printing. The wear resistance is frequently improved by electroplating chromium on the surface, but high antimony content is also effective in this regard.

QUESTIONS

Group A

1. Draw cooling curves for alloys of lead with 1, 6, 11, 20, and 50% Sb. The significant temperatures should be correlated with the phase diagram. Assume that equilibrium is attained.

2. Calculate the percentages of structural constituents (*i.e.*, primary $\alpha_{(Pb)}$ or $\alpha_{(Sb)}$ and eutectic) present in each of the alloys of question 1.

3. In discussion of the microstructure of the Pb:20% Sb alloy, it was pointed out that chill-casting was required to prevent a gravity segregation effect. Why is this true for the 20% Sb alloy and not for the Pb:6% alloy?

4. In a ternary eutectic system, is it possible to have an alloy that will show two different types of (*a*) primary crystallites, (*b*) eutectiferous crystallites?

5. Many soldered joints are "wiped" by employing a solder that in the "mushy" state can be pushed around with a gloved hand. Why would the Pb + 52% Sn alloy be specifically suited or unsuited for this usage?

Group B

1. If the microstructure of a Pb:Sb alloy showed only traces of fine eutectiferous antimony crystallites in an interdendritic dispersion, what would be the probable composition of the alloy? If the few eutectiferous $\alpha_{(Sb)}$ particles were coarse, would the composition be any different? Why?

2. Explain the origin of the black areas immediately contiguous to the primary $\alpha_{(Sb)}$ crystallites in Micro. 5.3, page 119. (HINT: Preferred nucleation.)

3. Why would it be difficult to obtain a hypereutectic structure in a slowly solidified, overoxidized copper?

4. Would an increase in the tin content of Wood's metal affect its final solidification temperature? Explain your answer.

5. Explain the presence and type of coring in (*a*) Pb + 6% Sb alloy, (*b*) Pb + 11% Sb alloy. Your answer should explain the error in a definition of coring as "a greater concentration of higher melting point element in the center of dendrites."

CHAPTER 6

AGE-HARDENING: CAST- AND WROUGHT-ALUMINUM ALLOYS

None of the industrially important aluminum alloys is strictly binary since the base metal, as commercially produced, always contains about 0.3% each of copper, iron, and silicon. The iron and silicon usually combine with aluminum to form an intermetallic compound that is almost completely insoluble in the solid alloy and thus always visible in the microstructure. The Al:Fe:Si compound not only complicates the appearance of the alloy microstructures but, since it forms a low melting eutectic with aluminum, the presence of iron and silicon affects melting-point and heat treatment temperatures. However, the binary diagrams remain useful in discussing the general structural and property characteristics of most of these alloys.

6.1 Al:Si Phase Diagram

Aluminum is a soft and ductile metal with a moderately low melting point at 660°C, while silicon is a brittle, high-melting-point (1420°C) metalloid. The Al:Si system has a phase diagram almost identical in appearance to the Pb:Sb system except for temperature differences. Figure 6.1 shows that the eutectic concentration, 11.7% Si, is nearly the same. Again, the eutectic composition is nearer the ductile, lower melting-point metal, which therefore is the chief constituent and, relatedly, the continuous phase.

The silicon crystallites, primary or eutectiferous, are markedly affected by the solidification rate and casting temperature. If an alloy of eutectic composition, 11.7% Si, is chill-cast, it will have a hypoeutectic structure. Formation of silicon crystallites is suppressed by rapid freezing more than the formation of $\alpha_{(Al)}$. These latter crystallites start to form just under the eutectic temperature, and their growth is not accompanied immediately by any eutectiferous silicon crystallites. Therefore, the $\alpha_{(Al)}$ phase forms dendrites that grow over a falling range of temperatures like ordinary primary crystallites. When the eutectic reaction does begin, or equivalently, when it is no longer possible further to undercool the silicon crystallite formation, the

remaining liquid that solidifies eutectically contains more than 11.7% Si; it may be as high as 13 or 14% Si.

This situation, a greater undercooling of one phase in a eutectic than of the other, results in a displacement of phase diagram lines in the manner shown in Fig. 6.1 by dashed lines. *Here the dashed lines do not represent equilibrium* but actually the *furthest departure from equilibrium* that has been observed in this system.

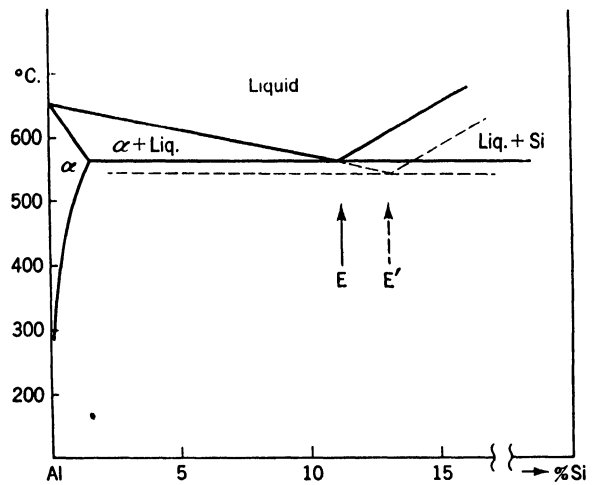

FIG. 6.1. Aluminum-silicon phase diagram under equilibrium conditions (solid lines) and as chill-cast or sodium-modified (dashed lines) showing eutectic temperature and composition displacement resulting from preferential undercooling of the silicon phase.

The undercooling effect in Al:Si alloys is more readily obtained by means other than chill casting. It was first discovered in alloys melted under a sodium fluoride flux. Later research showed that the addition of about 0.1% metallic sodium, stirred into the liquid Al:Si alloy 15 or 20 min before casting, gave a similar effect of changing a slightly hypereutectic alloy of, *e.g.*, 13% Si, to a slightly hypoeutectic one.

Much more important than the shift in eutectic temperature and composition is the correlated change in eutectic structure. As mentioned in the discussion of the microstructures of Pb:Sb alloys, chill casting greatly refines the eutectic particle size. Addition of sodium to Al:Si alloys or *modification* of these alloys gives a much greater refinement of the silicon particles and a change to a much more rounded, less platelike structure.

The exact mechanism of sodium modification of Al:Si alloys has not

been completely discovered. Practically all the sodium added before pouring volatilizes, and only traces of it remain in the alloy, but these traces presumably are essential for the modification effect or suppression of silicon crystallite formation. At present, the modification process is of minor interest since, as will be shown later, other alloys have largely replaced the modified Al:13% Si alloys for high-strength aluminum castings.

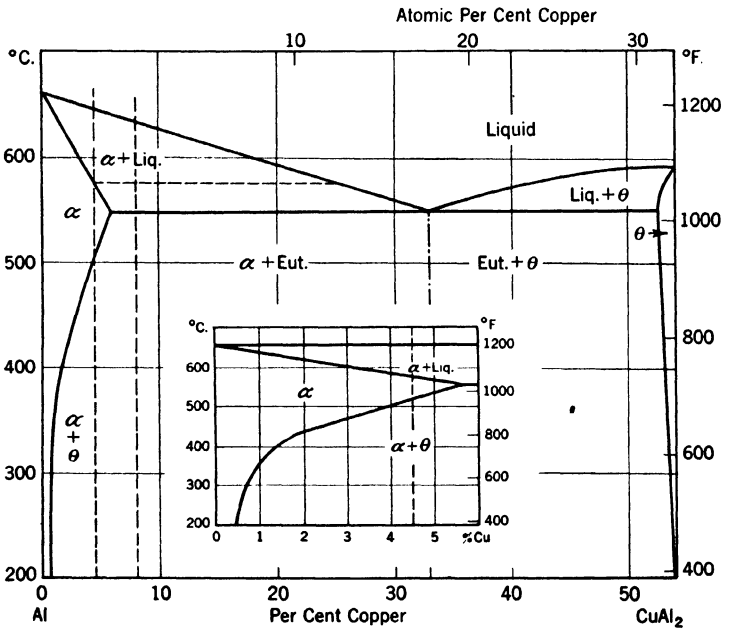

FIG. 6.2. Phase diagram of the Al:Cu alloy system, from 0 to 54% Cu.

6.2 Al:Cu Phase Diagram

The Al:Cu system diagram from 0 to 54% Cu, as reproduced in Fig. 6.2 above, differs from the Pb:Sb diagram (page 114) in only two essential respects: the eutectic contains more than 50% of the right-hand phase, and this phase is not a terminal solid solution but an intermediate alloy structure θ, which is hard, brittle, and of a narrow range of compositions approximating that of the intermetallic compound $CuAl_2$, *i.e.*, a structure containing one atom of copper for every two atoms of aluminum. (The binding forces in intermetallic com-

pounds differ from those holding chemical compounds in a specific crystal form. In salts, such as NaCl, the binding force arises from ionic or electrostatic fields resulting from exchanges of valency electrons. In intermetallic compounds, ordinary valency rules do not always determine the atomic ratios.) The aluminum ends of the Al:Mg, Al:Ni, Al:Mn, and Al:Fe systems are like the Al:Cu in showing eutectics between an $\alpha_{(Al)}$ solid solution and an intermediate limited solid-solution phase or intermetallic compound, while the Al:Si eutectic is between the two terminal solid solutions. All these alloys show the same constitutional features that were discussed in detail in Chap. 5 (Pb:Sb alloys). In all except the Al:Fe system, the solubility of the second phase in the $\alpha_{(Al)}$ solid solution is distinctly greater at the eutectic temperature than at room temperature, and, in the Al:Cu and Al:Mg systems, this feature is utilized to obtain high-strength alloys by a controlled dispersion of the second phase.

The extent of solid solubility of one element in another was stated on page 113 to depend on the relative types of lattices and atomic sizes of the solute and solvent metals. Atomic sizes are not fixed quantities; a large atom, randomly dispersed at lattice points of a solvent metal having a smaller atom, must contract somewhat to fit in the solvent lattice, which, simultaneously, necessarily is expanded (Vegard's law, page 72). Contrariwise, a smaller atom may be enlarged if present in solid solution with a larger atom whose lattice is thereby contracted. The difference in sizes of solute and solvent atoms (measured when present in their own form) is an important factor in determining the extent of solubility that may exist. If the two atoms differ by more than 15%, extensive solid solutions are not usually found, although Table 6.1 shows that the converse of this statement is not always true (*e.g.*, Ti). For example, two atoms may be of nearly the same size but differ greatly in electrochemical characteristics. Here compound formation and only slight solubility in the solid state are to be anticipated.

It is quite evident that the lattice type and atomic size of the solute are not the only factors affecting the maximum solubilities. Generally, however, a high solid solubility appears to be favored either by a low eutectic temperature or by a favorable atomic-size ratio. The effect of a low eutectic temperature is shown by the close-packed hexagonal metals, zinc and magnesium, which have greater solubilities in face-centered cubic aluminum than face-centered cubic metals with a smaller atomic-size difference, silver and copper, respectively.

6.3 Correlation of Phase Diagrams[1]

Since the phase diagrams of all alloy systems are based fundamentally on physical chemistry, many attempts have been made to verify equilibrium data by physical chemical laws. Reference has been made to Gibbs's phase rule (page 60) defining the number of variables F, usually temperature and concentration, which can be altered in an alloy

TABLE 6.1. ATOM-SIZE FACTOR IN ALUMINUM-BASE SOLID SOLUTIONS

Solute		Reaction and temperature, °C	Maximum solubility		Atomic size,* Å	% atomic size difference
Element	Lattice		% by weight	Atom, %		
Al	f.c.c.†				2.86	
Zn	c.p.h.‡	eutectic-380	82	66	2.75	− 3.8
Ag	f.c.c.	eutectic-558	57	25	2.88	+ 0.7
Mg	c.p.h.	eutectic-451	14.9	16.3	3.19	+11.5
Cu	f.c.c.	eutectic-548	5.65	2.48	2.55	−10.8
Mn	complex c.	eutectic-659	1.82	0.90	2.37	−17.1
Si	diamond c.	eutectic-577	1.65	1.59	2.35	−17.8
Cr	b.c.c.§	‖peritectic-661	0.77	0.40	2.49	−12.9
Ti	c.p.h.	peritectic-665	0.28	0.16	2.93	+ 2.4
Zr	c.p.h.	peritectic-661	0.28	0.08	3.19	+17.7
Ni	f.c.c.	eutectic-640	0.05	0.023	2.48	−13.3
Be	c.p.h.	eutectic-645	0.05	0.15	2.25	−22.7
Fe	b.c.c.	eutectic-655	0.02	0.009	2.48	−13.3
Co	b.c.c.	eutectic-657	0.02	0.009	2.50	−12.6

* From Hume-Rothery "Structure of Metals and Alloys," Institute of Metals, London.
† f.c.c.—face-centered cubic.
‡ c.p.h.—close-packed hexagonal.
§ b.c.c.—body-centered cubic.
‖ The peritectic reaction is described on p. 213.

having a known number of component metals C without changing the number of phases P present. Ignoring pressure as a variable, the relation is

$$F = C - P + 1$$

A second equation, developed by Le Châtelier, gives the relation between the concentration of an ideal solution (solid or liquid) and its temperature when the precipitating phase is of constant concentration (an element or compound):

[1] Fink and Freche, Trans. AIME, 111, 304, 1934.

$$\log (\text{solute concentration in solvent}) = \frac{\text{constant}}{\text{temperature}} + \text{constant}$$

According to this equation, all solid solubility curves for ideal solutions should become straight lines when the logarithm of the solubility is plotted against the reciprocal of the temperature (Kelvin or absolute scale). The solid solubility or solvus curves for most of the aluminum alloys of Table 6.1 have been so plotted and, in almost all cases, show a linear relationship. Furthermore, by definition of terms, this equation is equally applicable to hypereutectic liquidus curves, as has been demonstrated, at least for many aluminum alloys. A third equation, which is not reproduced here, has successfully established a relationship between the eutectic concentration, the solid solubility at the eutectic temperature, and the actual temperature of the eutectic for many of the systems listed in Table 6.1. Other correlations of an empirical nature have been discovered in the aluminum-base-alloy phase diagrams. For example, the logarithm of the lowering to the eutectic temperature seems to be linearly related to the solute concentration of the α solid solution at the eutectic temperature and, furthermore, both of these quantities are linearly related to the slope of the solid solubility curve. These and other relationships satisfactorily generalize the data on a series of alloy systems. It is also evident that, where these relationships hold, the equilibrium diagrams at one end of an alloy system can be constructed with very few experimental data. Two points on the hypereutectic (or hyperperitectic) liquidus, the eutectic temperature, and one point on the solid solubility curve could suffice.

6.4 Coherency Theory of Age-hardening

Ordinarily, concentrations of the hardening constituent approaching maximum solid solubility in the α phase at the eutectic temperature are chosen. The first step in the heat treatment is to heat the alloy to a temperature in the α phase field in order to obtain a solid solution of uniform composition. The saturated solution thus formed is quenched or at least cooled at too rapid a rate to permit the separation of the second phase that would normally occur with slow cooling. As a result of the rapid cooling, the alloy is in a state of supersaturation and is, therefore, thermodynamically unstable. The subsequent age-hardening of the alloy is a result of the decomposition of the solution, which in some alloys occurs at ordinary room temperatures but usually requires a relatively low-temperature heat treatment.

The hardening of Duralumin (basically, Al + 4½% Cu), the alloy earliest known to be capable of age-hardening (1911), was first attributed

(Merica *et al.*, 1919) to the precipitation of the compound $CuAl_2$ in the form of particles too small to be visible under the microscope. According to the theory rather generally accepted prior to 1930, the particles of the compound hardened and strengthened the alloy by making slip along crystallographic planes more difficult. In other words, the uniformly dispersed particles were considered to have a keying action, thereby obstructing movement along planes of ready slip.

As correlated data accumulated from age-hardening studies, this simple mechanical conception of hardening by compound precipitation appeared to become inadequate. Anomalous increases in electrical resistivity during aging at ordinary temperatures (resistivity should decrease as the concentration of solute atoms decreases, see page 71), intermediate peaks in hardness-time curves, and other comparable data led to postulates of preprecipitation changes such as the formation of knots of segregated solute atoms that affected the properties of the alloy independently of any subsequent precipitation.

Critical studies of the last few years have led to a more complete understanding of the age-hardening process, which appears to proceed in the following sequential stages:[1]

1. Segregation of solute atoms on a specific crystallographic plane of the matrix (tetragonal $\theta_{(CuAl_2)}$ forms with its square, basal plane parallel to the cube plane of the $\alpha_{(Al)}$ phase, or the hexagonal γ precipitate in Al:Ag alloys forms with its basal plane on the corresponding octahedral plane of the face-centered cubic matrix).

2. Formation of a new lattice of the precipitating phase. The precipitate is only from 2 to 50 atoms thick and may be from 20 to several hundred atoms long or wide; in other words, it is a thin plate. There must be atomic conformity between the lattices of the precipitating phase and the matrix, which requires that growth occur laterally along the plane of precipitation. The new phase, at this stage, is under high elastic stress (calculated to be about 115,000 psi in Al:Ag alloys) as a result of the enforced atomic conformity between lattices of somewhat different spacings, and thus it may have abnormal dimensions. It then is usually found to be a metastable or transition phase (θ' for Al:Cu alloys or γ' for Al:Ag alloys). The enforced lattice conformity between precipitate and matrix that results in a high elastic stress on the precipitate also requires a balancing localized elastic stress and deformation in the matrix phase.

3. Shearing along the plane of conformity occurs when the elastic stresses, increasing with precipitate particle size, reach a critical value.

[1] Barrett, Geisler, and Mehl, *Trans. AIME*, **143**, 134, 1941.

Then atomic coherency over the entire plate ceases, and the precipitate phase assumes its stable lattice dimensions and form.

In this picture of sequential changes, it should not be assumed that all precipitate particles during aging are, at the same time, in the same stage of growth. Nucleation does not start all particles at the same time and, therefore, some particles may be in the transition stage while others are in the segregation stage 1 and still others have assumed the stable form of stage 3. However at sufficiently low aging temperatures, *e.g.*, room temperature for aluminum alloys, no particles will ever reach stage 3 because diffusion of copper at this temperature is too slow for growth of the θ' to a sufficient size. At subzero temperatures, *e.g.*, $-50°C$, even stage 1 will not be attained and the soft, supersaturated condition characteristic of the as-quenched, unaged alloy may be preserved indefinitely. Aging at too high a temperature, on the other hand, may result in only stage 3 ever being detected. At 350°C, the Al:Cu alloy would never show any evidence of the segregation of stage 1 or the θ' of stage 2 and, if these occur, their existence is fleeting as a result of very rapid diffusion of copper atoms and resulting precipitate particle growth.

It seems probable, from the evidence now at hand, that maximum age-hardening and strength are associated with the localized lattice deformations characteristic of stage 2 or the transition phase. This brings in a new requirement for age-hardening beyond the decreasing solubility with decreasing temperature. The additional requirement is that lattice conformity between precipitate and matrix must be enforced for at least a certain period. Supporting evidence for this requirement is offered by the Mg:Pb system.[1] Magnesium can dissolve 46 wt. % Pb (9 atomic %) at the eutectic temperature of 468°C but only about 2 wt. % Pb at room temperature. This system shows the anticipated microstructural effects of solution and precipitation upon proper heat treatment, *but no age-hardening occurs.* It has been found that the precipitate is crystallographically so unlike the matrix that no detectable stage of lattice conformity and localized distortion exists during precipitation.

The abnormalities that caused abandonment of the first simple theory of age-hardening have now been satisfactorily explained. Electrical conductivity decreases rather than increases in stage 1, and perhaps in stage 2, because the wave length of the electron flow constituting the electrical current is such that the small particles are so spaced as to interfere with flow and this effect overbalances the tendency

[1] Geisler, Barrett, and Mehl, *Trans. AIME*, **152**, 201, 1943.

5. Micros. 6.28–6.35: Effect of cooling rate from a solution treatment, on the structure of a wrought pure Al:10% Mg alloy—precipitation and also recrystallization in the solution-treated and cold-worked 10% Mg alloy during aging at varied times and temperatures. The pertinent phase diagram for this alloy is on page 186.

6.6 Hot-shortness and Burning

Any tensile stress applied to an alloy while it is in the two-phase, *solid* + *liquid*, condition will naturally cause the metal crystals to

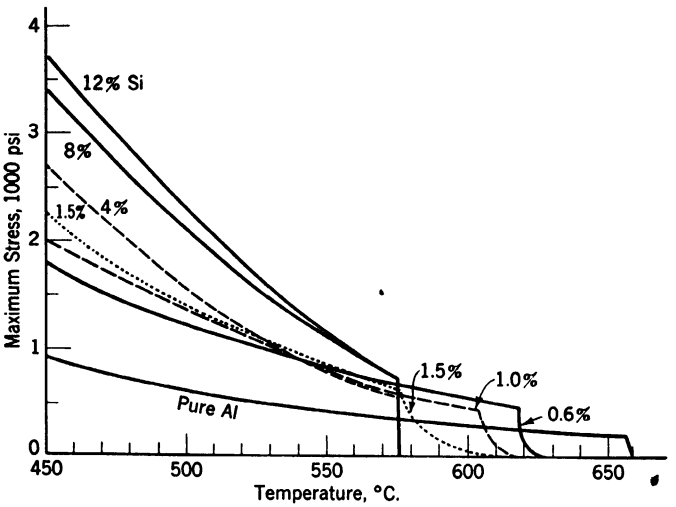

FIG. 6.3. High-temperature tensile tests of Al:Si alloys of the indicated silicon contents. The 4, 8, and 12% Si alloys lose all strength sharply at the eutectic temperature, 577°C. The 0.6, 1.0, and 1.5% Si alloys have a range of partially melted structures that show a definite although small strength.

separate where there is no solid-to-solid contact. The stress may come from rolling, forging, or other form of hot-work, or it may originate in the contraction or shrinkage of a hollow casting about a strong core. In the latter case, the amount of liquid is critical, and Sachs and Van Horn show that, with more than about 15% present, the structure is sufficiently open for more liquid to flow or be sucked in from hotter portions (*e.g.*, the riser) to fill any openings. The susceptibility to damage while at the high temperature of the α + *liquid* field is known as *hot-shortness*.

For example, the strength of Al:Si alloys upon rapid stressing at high temperatures is shown in Fig. 6.3.[1] The data of Table 6.2 show

[1] Singer and Cottrell, *J. Inst. Metals*, **73**, 33, 1946.

(*continued on page* 159)

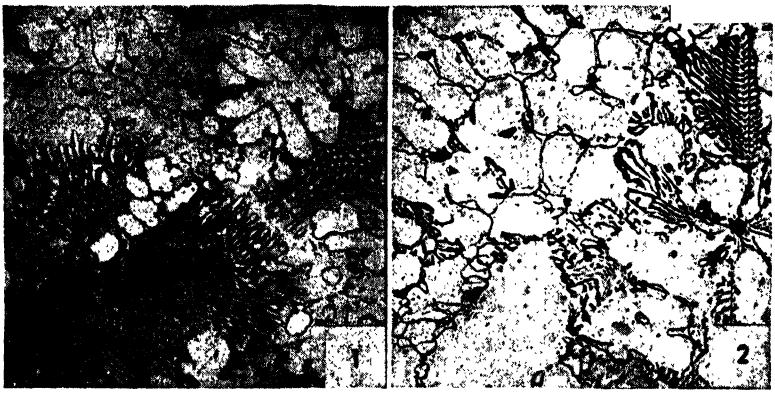

Micro. 6.1. Al + 30% Cu; ×100; 0.5% HF etch. This slightly hypoeutectic alloy is used as a hardener to make the usual 4 to 5% Cu content alloys. The structure shows a few aluminum solid-solution dendrites in the $\alpha + \theta$ eutectic. In this eutectic, θ is the darker (generally), continuous phase. It is very fine and lamellar in nature in spots where freezing started. As the heat of the eutectic solidification was released locally, solidification slowed up and the eutectic structure became coarser.

Micro. 6.2. Alloy No. 112 (7% Cu, 1.7% Zn, Fe and Si impurities); ×100; 0.5% HF and then 20% hot H_2SO_4 etchants. The θ phase is the clearly outlined particles that form a nearly continuous network. The adjacent α, which shows coring, constitutes the eutectiferous α, connected with and indistinguishable from primary α. The iron and silicon impurities with aluminum form an Al:Fe:Si compound, here blackened by the H_2SO_4 etch. The delicate tracery of this constituent has led to the descriptive name "Chinese script." The zinc is in solution in the α phase.

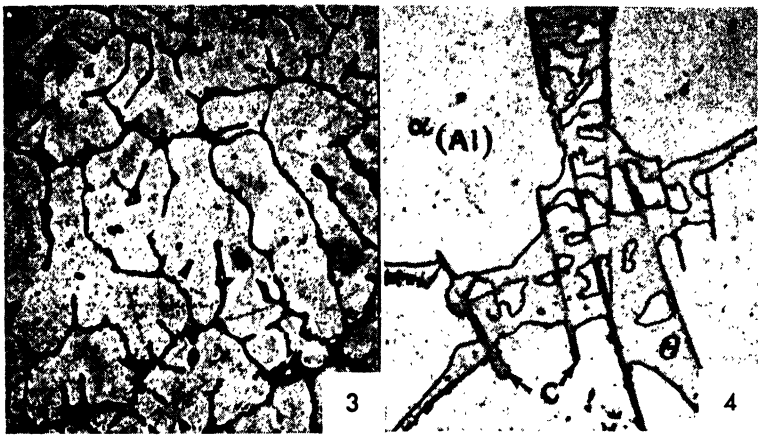

Micro. 6.3. Al + 8% Cu + about 1 to 1½% Fe and Si as impurities (Alcoa 12); ×50; 0.5% HF, then 20% hot H_2SO_4 etch. This is a hypoeutectic structure consisting of cored primary $\alpha_{(Al)}$ dendrites (the dendritic characteristic is not very evident) surrounded by the eutectic of $\alpha_{(Al)}$ and θ (or $CuAl_2$).

Micro. 6.4. Same alloy (8% Cu) at ×1,000; 0.5% HF, then hot 20% H_2SO_4 etch. A greatly magnified view of the $\alpha_{(Al)}$ and θ_{CuAl_2} eutectic shows that the brittle θ phase is continuous, probably because this eutectic consists of 58% θ and 42% $\alpha_{(Al)}$ (proportions calculated on a weight basis). The needles (marked *C*) extending through the eutectic are an Al:Cu:Fe compound originating from the iron impurity.

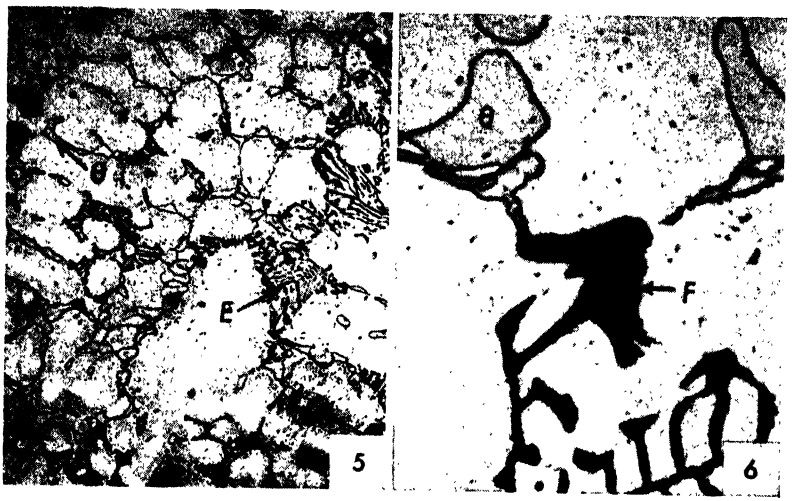

Micro. 6.5. Al + 4½% Cu with controlled impurities (1 to 1½%) of Fe and Si (Alcoa 195); ×75; 0.5% HF etch, then hot 20% H_2SO_4. The as-cast structure reproduced here shows cored dendrites of $\alpha_{(Al)}$ surrounded by the $\alpha_{(Al)} + \theta$ eutectic and a eutectic structure of $\alpha_{(Al)}$ and Al:Fe:Si compound (E) originating from the impurities. Although the copper content of this alloy lies to the left of the $\alpha_{(Al)} + \theta$ eutectic horizontal, some eutectic is found in the cast structure because of the metastable position of the solidus on rapid cooling of the casting (page 116).

Micro. 6.6. Same alloy (4½% Cu) at ×1,000; 0.5% HF etch, then hot 20% H_2SO_4. Again the θ present does not appear to be a part of a eutectic structure since the $\alpha_{(Al)}$ of the eutectic is not inside the θ but outside, in contact with, and indistinguishable from the primary $\alpha_{(Al)}$. The θ and Al:Fe:Si compound appear to be isomorphous since there is a continuity from one structure to the other with a gradation in the coloring or degree of attack by the etchant.

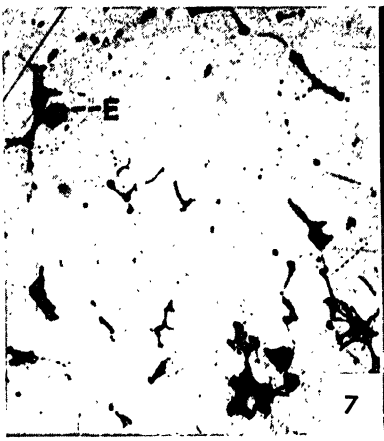

Micro. 6.7. Same alloy (4½% Cu) at ×75; 0.5% HF etch, then hot 20% H_2SO_4; structure after heat treatment (ASTM No. 3) as follows: 15 hr at 510°C, followed by a water quench; reheated 15 min in high-pressure steam. This structure should be compared with that of Micro. 6.5. It is evident that the heat treatment at 510°C has caused the $CuAl_2$ to dissolve in the $\alpha_{(Al)}$ matrix (thus the high-temperature treatment is called a *solution anneal* or *solution heat treatment*). Quenching in water after the high-temperature soak prevented precipitation of the dissolved θ upon cooling the alloy to temperatures at which two phases exist according to the diagram. Reheating this metastable or supersaturated solid solution has not caused particles of $CuAl_2$ to form in a size visible at this magnification. Particles of the Al:Fe:Si compound (*E*) are still present, since this phase has no measurable solubility in $\alpha_{(Al)}$ and remains substantially unchanged through the heat treatment.

Micro. 6.8. Same alloy (4½% Cu) at ×500; etched with HCl, HNO_3, and HF in water (Keller's reagent); structure after heating to 575°C and quenching. According to the Al:Cu phase diagram, when this alloy is heated above about 565°C, it is in a two-phase field, $\alpha_{(Al)}$ + liquid, and the liquid has an almost eutectic concentration of copper. The liquid phase forms at the $\alpha_{(Al)}$ grain boundaries and, upon quenching, must solidify there, in large part as a eutectic, which in this system is brittle. With a nearly continuous brittle structure enveloping each grain, the total structure is now weak and brittle. The etch used for this micrograph has brought out coring in the aluminum matrix, *i.e.*, variations in the amount of dissolved copper. Although the binary Al:Cu diagram shows the safe solution annealing temperature range to be 510 to 565°C, the presence of a eutectic network in the original casting of this alloy would set the upper limit at 545°C. More importantly, the presence of iron and silicon impurities means that a ternary or quaternary eutectic exists with a melting point of about 525°C, so that the safe heat treatment temperature range is quite narrow, 505 to 520°C. The lower limit is set by the necessity for dissolving all the copper in order to obtain optimum properties, while the upper limit is set by the melting point of any eutectic present in the structure.

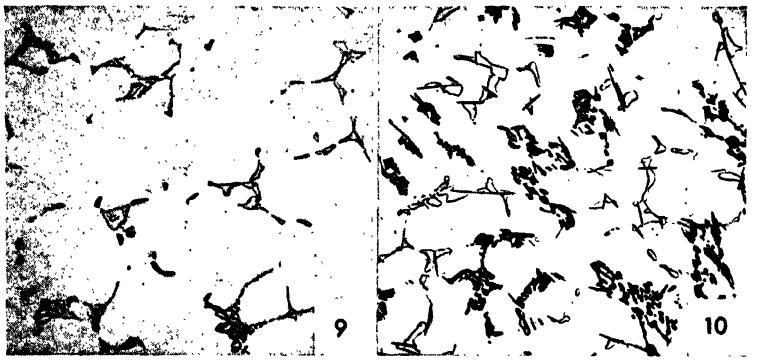

Micro. 6.9. Same 195 alloy (4.5% Cu; Fe and Si impurities) heated only 6 hr at 510°C and quenched; ×100; 0.5% HF, then 20% H_2SO_4 etchants. The θ compound, here a light clear gray, has not been completely dissolved because of too short a solution treatment. The amount present has decreased and the interdendritic continuity broken up, however. Less than optimum properties would be shown by this structure.

Micro. 6.10. Alloy 122 (10% Cu, 0.2% Mg; Fe and Si impurities); chill-cast, heated 8 hr at 510°C and quenched; ×100; 0.5% HF then 20% H_2SO etchants. The solution treatment of this alloy cannot, of course, dissolve all the θ phase, but the alloy becomes somewhat tougher when the continuity of the eutectiferous θ is broken up. Furthermore the hardness of the alloy is increased and dimensional stability gained by a subsequent precipitation treatment.

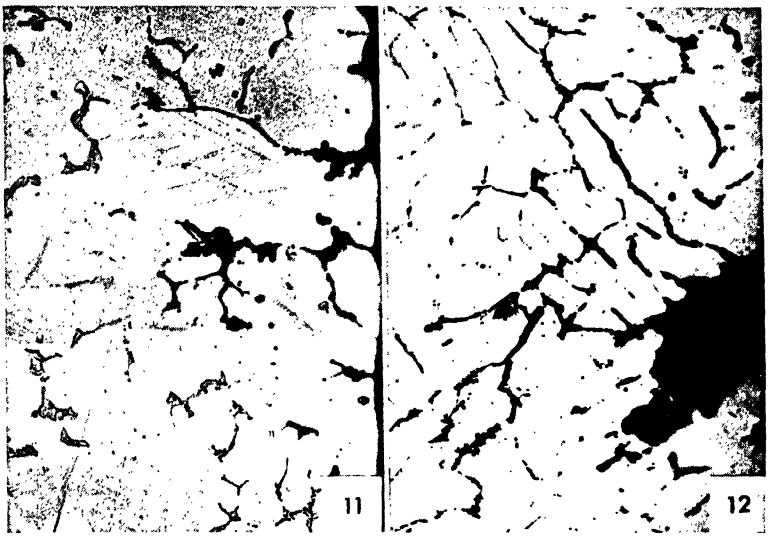

Micro. 6.11. Alloy 195-T4 (4.5% Cu; Fe and Si impurities) solution heat-treated, hot-water quenched then immersed in a 3% aqueous NaCl solution for 12 months; ×100; 0.5% HF etch. This micrograph of the alloy, etched more heavily to bring out individual grains of the α phase, shows how corrosion has chiefly been intergranular or along grain boundaries.

Micro. 6.12. Alloy 195-T62; sand-cast, solution treated 8 hr at 510°C, quenched and aged 16 hr at 160°C; then immersed in 3% aqueous NaCl for 12 months; ×100; 0.5% HF etch. In the aged condition, corrosion has been more severe, resulting in pitting and strong interdendritic penetration.

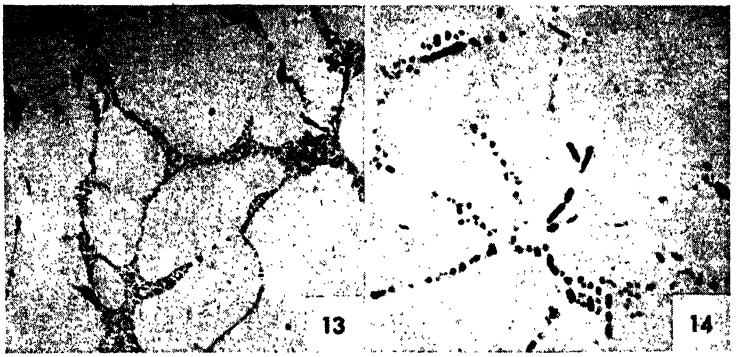

Micro. 6.13. Al + 3% Si + 0.3% Mg, sodium modified sand casting, as cast; ×100; 20% H_2SO_4 etch. The low silicon hypoeutectic alloy shows primary aluminum and a very fine interdendritic eutectic network containing silicon crystallites and also Mg_2Si (black).

Micro. 6.14. Alloy of Micro. 6.13, heat-treated 20 hr at 540°C; ×100; 0.5% HF etch. The long-time solution heat treatment has dissolved some silicon crystallites and the Mg_2Si. Its most marked effect, however, has been to agglomerate the undissolved silicon crystallites. After the α phase is saturated, remaining silicon particles continue to grow in a spheroidal manner. This occurs by smaller ones dissolving and an equal amount of silicon precipitating from the now oversaturated α on to other silicon particles that grow.

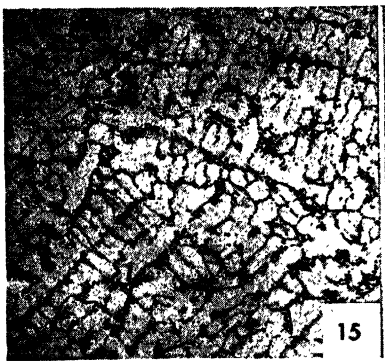

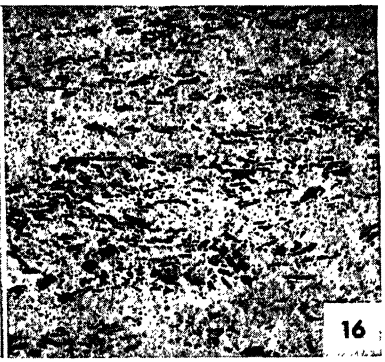

Micro. 6.15. Al + 6% Si, chill-cast; ×100; 0.5% HF etch. In this chill casting, the amount of eutectic is greater, naturally, than in the 3% Si alloy, Micro. 6.13. Note that chill casting has given fine eutectiferous silicon particles, but they are not so fine and are more platelike than those in the modified alloy.

Micro. 6.16. Al + 6% Si, hot-forged at about 500°C; ×100; 0.5% HF etch. Forging has broken up the eutectic structure, and aligned silicon crystallites in the flow direction. The temperature of hot work has also induced growth of the eutectiferous crystallites. Slow cooling from the forging temperature has caused precipitation of silicon from solid solution which gives the "dirty" background.

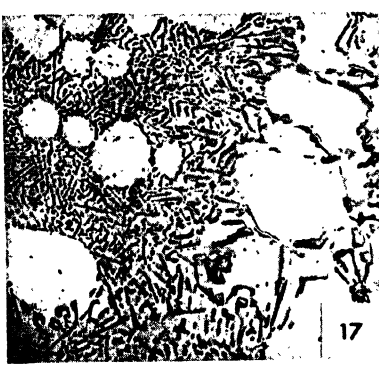

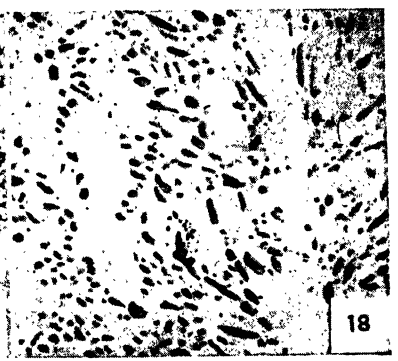

Micro. 6.17. Al + 11% Si + 0.3% Mg, chill-cast; ×100; 0.5% HF etch. There is less primary α now, and the eutectiferous silicon is finer in some places than in others for the reason presented in the case of the Al:Cu eutectic (Micro. 6.1, page 142).

Micro. 6.18. Same specimen as Micro. 17, heated 20 hr at 540°C and quenched; ×100; 0.5% HF etch. As in Micro. 14, the solution heat treatment has resulted in a pronounced agglomeration of undissolved silicon crystallites.

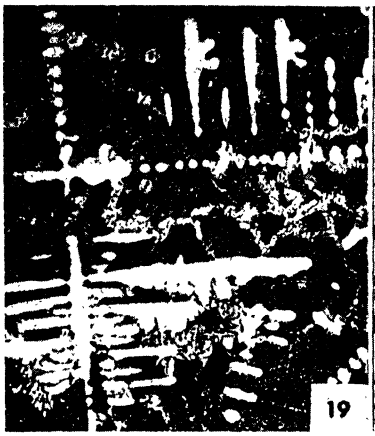

Micro. 6.19. Al + 13% Si + about 0.8% Cu and Fe as impurities (Alcoa 47); ×75; 0.5% HF etch. This is a hypoeutectic structure showing a few primary dendrites of $\alpha_{(Al)}$ in a fine eutectic structure. Since the equilibrium eutectic composition is at 11.6% Si, this alloy would normally be hypereutectic, but the addition of 0.25% sodium, 15 min before casting, suppresses both the formation of primary silicon crystals and the eutectic reaction. The liquid cools until it reaches the temperature of the *metastable* prolongation of the hypoeutectic liquidus to form a few primary $\alpha_{(Al)}$ dendrites after which the eutectic reaction starts. The undercooled eutectic liquid forms a very finely dispersed two-phase structure (at about 564°C rather than the equilibrium temperature of 578°C).

Micro. 6.20. Same alloy (13% Si) at ×1,000; 0.5% HF etch. Dark gray particles, such as that marked *A*, are eutectiferous silicon crystallites; lighter gray needles, marked *B*, are an Al:Fe:Si compound originating from the iron impurity. Note that the $\alpha_{(Al)}$ phase is *continuous*, as predictable from the approximate relative proportions of $\alpha_{(Al)}$ and silicon in the eutectic.

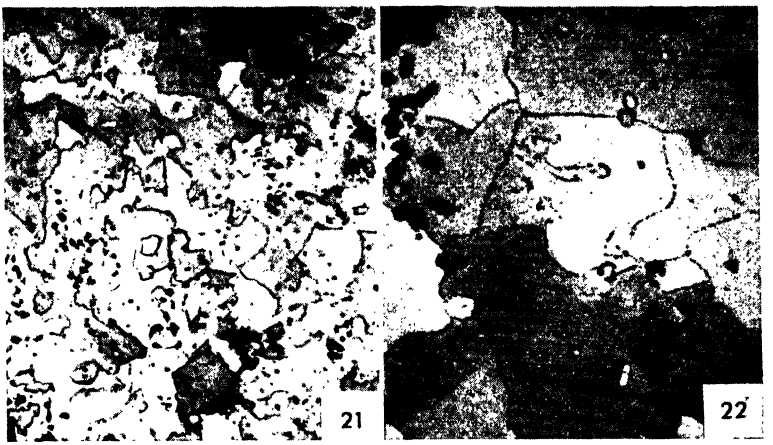

Micro. 6.21. Al + 4.4% Cu, 1.5% Mg, 0.6% Mn, and about 0.5% Fe and Si as impurities (Super-Duralumin or 24ST); the alloy in sheet form was quenched from 500°C and aged at room temperature; ×75; HCl, HNO_3, and HF in water (Keller's etch). The etch employed in this case differentially attacks the aged $\alpha_{(Al)}$ solid-solution matrix to show the typical, irregularly shaped grains of the structure on a section parallel to the rolling plane. Insoluble Al:Cu:Fe:Mn intermetallic compounds are again extended in the direction of flow during hot-working. Only traces of copper or magnesium compounds are visible since they were almost completely dissolved during the heat treatment and now cannot be seen in the extremely fine precipitated form characteristic of the aged alloy.

Micro. 6.22. Same as Micro. 6.21 (24ST) at ×500. At the higher magnification, the clear, white particles of residual $CuAl_2$ are visible as well as the black and dark gray Al:Mn and Fe:Si compounds. In addition, a series of small, dark particles along the grain boundaries are now resolved. They probably originated upon cooling the alloy somewhat too slowly from the solution treatment, *i.e.*, by quenching in hot water. The hot-water quench diminishes distortion and quenching stresses, but the grain-boundary precipitate (of θ or $CuAl_2$) results in a susceptibility to intergranular corrosion. This may be avoided by coating the alloy with pure aluminum (Alclad 24ST).

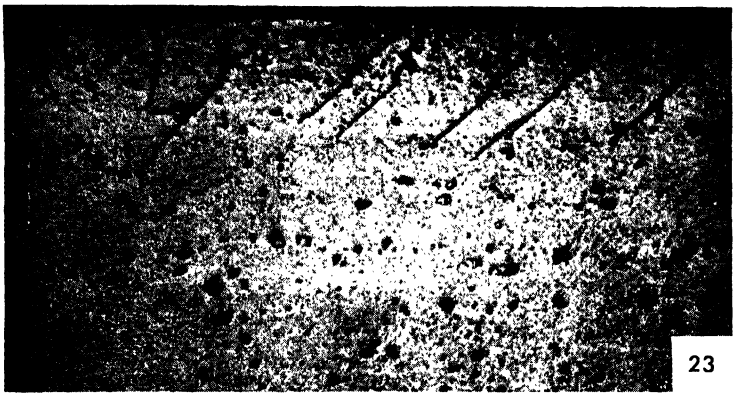

Micro. 6.23. Same alloy (24ST) in the Alclad form; the sheet was carried through 900,000 cycles of stress (by bending) which attained a maximum intensity of about 18,200 psi at the surface; ×500; 0.5% HF etch. The bottom of the micrograph shows the structure of the alloy core, and the upper ¾ in. shows the structure of the aluminum coating. The line of delineation between the core and originally pure aluminum layer is based on the absence of the insoluble constituents in the latter zone. However, some copper and magnesium have diffused from the core into the coating during the hot-rolling and solution heat treatment stages of processing of the sheet. Al in the diffusion zone is harder and has polished cleanly. The outer zone of the coating is probably still pure aluminum and so soft that polishing abrasive has adhered to this part of the specimen, resulting in a "dirty" appearance. It is important so to control the hot-rolling and heat treatment times and temperatures that copper and magnesium atoms are not permitted to diffuse to the surface, or the benefits (see page 174) of the aluminum coating will be lost. In this micrograph, the rounded, clear particles in the core may be residual $CuAl_2$ or θ, left undissolved when the solution treatment was shortened sufficiently to avoid alloy diffusion to the surface.

The black lines at approximately 45 deg to the surface of the sheet are shear cracks developed by repeated application of a stress with a maximum value far below the ordinary, axially determined tensile strength (62,000 psi) or even yield strength (40,000 psi). These cracks would eventually cause the sheet to break if the stressing was repeated often enough (this difficulty is minimized by design, see page 18). Failures of this type are called *fatigue* failures but are popularly (and erroneously) known as failures resulting from *crystallization* of the metal, since it is not generally realized that metals are always crystalline. The deformation accompanying an ordinary tensile fracture destroys the crystalline appearance of the broken surface. However, when a fatigue crack has reduced the effective cross-sectional area of the metal sufficiently, the remainder of the section breaks suddenly without any noticeable deformation and thus frequently has a crystalline appearance.

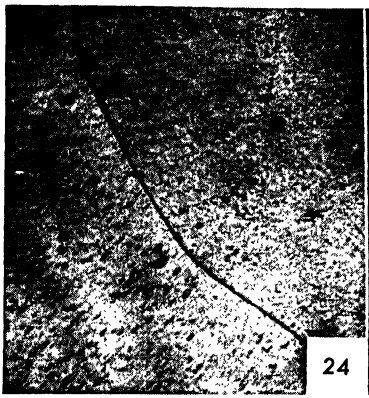

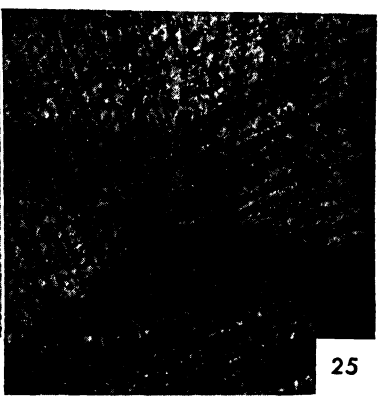

Micro. 6.24. Al + 5% Cu; alloy of pure materials (less than 0.05% Fe + Si); quenched from 540°C, reheated 30 min at 200°C; ×1,000; 0.5% HF etch. The heat treatment given this alloy resulted in maximum hardness (see Table 6.2), but there is no readily visible precipitate. The grain boundary has etched more deeply than it would in the as-quenched (from 540°C) structure, and there are a few markings within the grains, indicative of some change in the solid solution. Special etches have revealed more positive indications of precipitation in equivalent structures, but this is representative of the structure shown by the usual micrographic technique.

Micro. 6.25. Al + 5% Cu; ×1,000; 0.5% HF etch. A specimen similar to Micro. 6.24 was quenched in cold water from a solution treatment at 540°C and reheated 1 hr at 250°C. Distortion from the cold-water quench caused a slight plastic deformation of the alloy matrix, and the subsequent aging treatment resulted in precipitation of the θ phase, which occurred preferentially on the slip planes that were active in the plastic movement. Nucleation of the precipitation (or more generally, of any solid phase change) occurs first at the least stable part of the matrix lattice, normally at grain boundaries but, in the case of prior or simultaneous plastic deformation, at slip planes. Note that precipitation is not uniform in all grains (in slight deformations, plastic movement is not uniform in all crystals). Particles of the precipitated θ are very fine and not clearly resolved here.

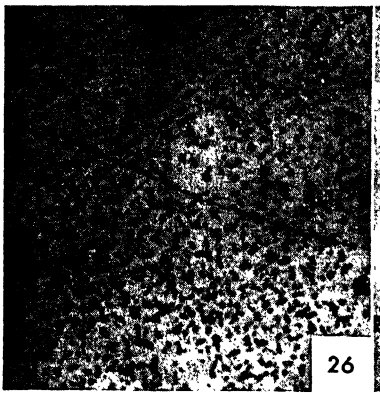

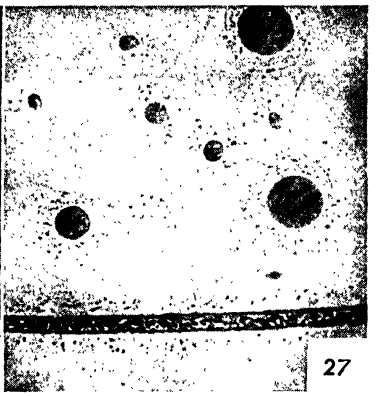

Micro. 6.26. Al + 5% Cu; ×1,000; 0.5% HF etch. A specimen similar to Micro. 6.24 was quenched from 540°C and reheated 1 hr at 400°C. At this high aging temperature, the precipitated particles are very coarse and, partly as a result of their size and partly as a result of re-solution of θ (1.5% Cu is soluble at 400°C and only 0.6% at 250°C), there are fewer particles. Upon close examination, some needles are visible and these, in the third dimension, would of course be plates. The plates show the genetic relationship between matrix and precipitate lattice orientations, as mentioned in the previous section on theory of age-hardening. These visible plates, however, are tremendously larger than the "platelets" present at an early stage of aging. Notice the lineup of θ particles along the $\alpha_{(Al)}$ grain boundary.

Micro. 6.27. Same Al + 5% Cu alloy quenched from 620°C and reheated at 400°C; ×1,000; 0.5% HF etch. The high-temperature treatment was well above the solidus temperature for this alloy (see Fig. 6.2), and "burning" occurred. Not only did a eutectiferous liquid form at the grain boundary (the horizontal eutectic structure), but a similar liquid formed in spherical globules within the grains, resulting in the circular eutectic "rosettes" shown above the boundary. Coring in the adjacent solid solution is revealed by the precipitate adjacent to the boundary eutectic and the rosettes; the $CuAl_2$ was precipitated in these regions upon the subsequent reheating to 400°C. The thin lines visible in parts of the structure are new grain boundaries, formed by recrystallization, at 400°C, of metal plastically deformed during the previous quench.

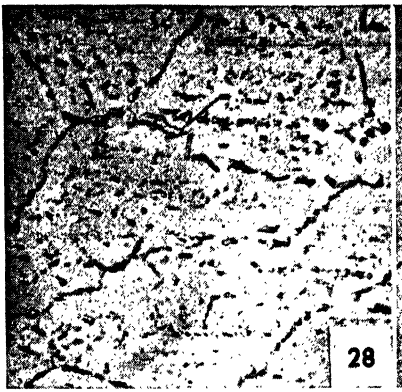

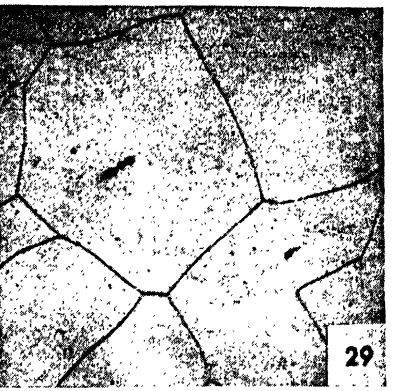

Micro. 6.28. Wrought Al:10% Mg alloy, solution-treated at 430°C and furnace-cooled; ×500; 0.5% HF etch. Slow cooling permitted almost complete precipitation of the second phase, here a β or Al_2Mg_3 compound, which shows some tendency to align in the flow direction of the hot-rolling. The β phase also shows a tendency to precipitate at grain boundaries and thus reveal the matrix grain size.

Micro. 6.29. Wrought high-purity Al:10% Mg alloy, solution-treated 10 hr at 430°C and quenched, heated 5 days at 100°C; ×500; 0.5% HF etch. The solid solution shows no structure other than polygonal grains. Five days at 100°C has caused no visible precipitation. (For the phase diagram appropriate for this and succeeding micrographs, see page 186.)

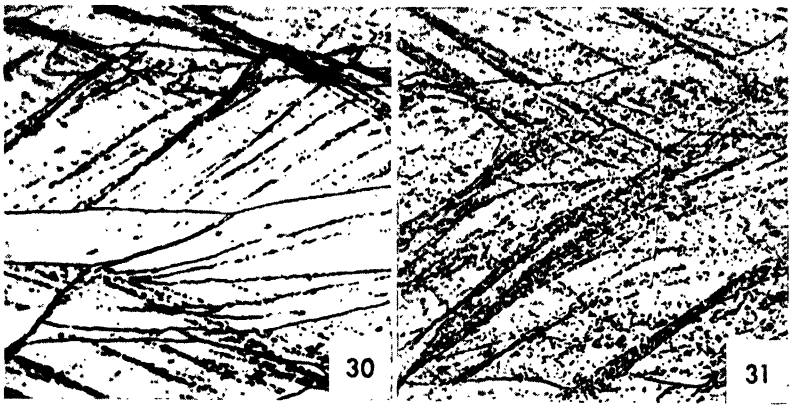

Micro. 6.30. Wrought Al:10% Mg alloy, solution-treated at 430°C, quenched, cold-rolled 50%, and aged 1 hr at 160°C; ×500; 0.5% HF etch. This longitudinal section clearly shows the elongated α grains. Precipitation at this slightly higher aging temperature (as compared to Micro. 6.28) has occurred heavily on the octahedral shear planes participating in the cold deformation. The active slip planes tend to orient themselves at an angle of 45 deg to the rolling plane. There is no evidence of grain-boundary precipitation.

Micro. 6.31. Same as Micro. 6.30 but aged 1 hr at 260°C. The Mg_2Al_3 precipitate at this higher temperature not only is coarser with individual particles clearly resolved, but it is also more generally distributed throughout the structure. Shear planes are still in evidence, however, and show a slight tendency to cross α grain boundaries, but for only a short distance. Again, there is no evidence of grain-boundary precipitation.

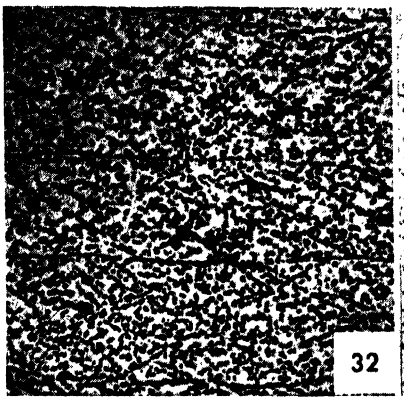

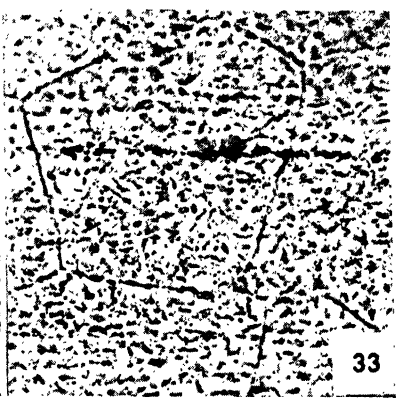

Micro. 6.32. Wrought Al:10% Mg alloy. Same as Micro. 6.31 but aged 6 days at 260°C rather than 1 hr; ×500; 0.5% HF etch. Precipitation is so general after this protracted period of aging that the shear lines are no longer very evident. β particles are much coarser too, but the elongated α crystals are still evident.

Micro. 6.33. Wrought Al:10% Mg; after cold-rolling the alloy was reheated to 430°C, quenched, and aged 6 days at 260°C as in Micro. 6.32; ×500; 0.5% HF etch. This micrograph shows that reheating to the solution range *recrystallized* the $\alpha_{(Al)}$ to an equiaxed structure. Precipitation now is definitely favored at grain boundaries (see Micro. 6.36).

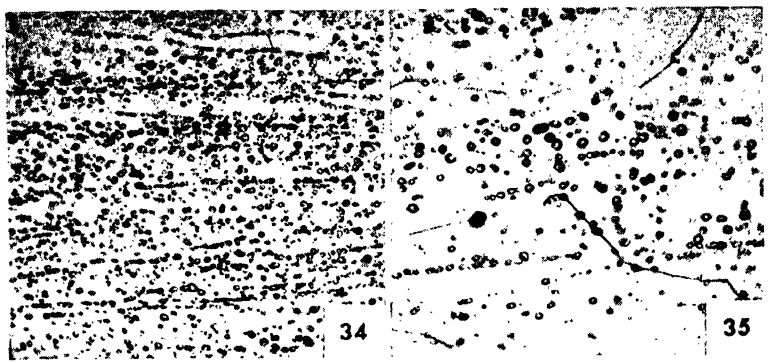

Micro. 6.34. Wrought Al:10% Mg; solution-treated, cold-worked and aged 1 hr at 350°C; ×500; 0.5% HF etch. This higher aging temperature has resulted in a very coarse globular precipitate, but there is no evidence of recrystallization of the α matrix.

Micro. 6.35. The alloy of Micro. 6.34 aged 1 hr at 365°C. The slightly higher aging temperature has caused a marked decrease in the quantity of the precipitated phase as a result of re-solution. Also, the structure shows recrystallization of the α matrix and a further growth of undissolved β.

Micro. 6.36. Wrought Al:10% Mg alloy; solution-treated at 430°C, aged at 200°C; tensilely stressed, elastically, in 3% NaCl solution; ×100; 0.5% HF. Precipitation of β in the α is evident even at this low magnification. Grain-boundary precipitation, discussed in Micros. 6.29 to 6.33, has created a susceptibility to the intergranular stress-corrosion cracking shown here so beautifully.

that the ductility drops to zero while an appreciable strength remains. The strength results from mechanical interlocking of dendritic arms, but the intervening liquid completely destroys plasticity under tensile

TABLE 6.2. MECHANICAL PROPERTIES OF AL AND AL:SI ALLOYS UPON SHORT-TIME TENSILE TESTS IN THE VICINITY OF THE SOLIDUS TEMPERATURE*

Pure Al (99.9%)			Al:1.0% Si		
Temp., °C	Max stress, psi	% elongation in 2 in.	Temp., °C	Max stress, psi	% elongation in 2 in.
430	1,070	133	520	1,010	55
498	660	161	549	775	53
571	340	160	587	530	69
610	270	142	597	425	22
652	185	138	601	425	0
656	155	0	605	395	0
657	81	0	607	295	0
658	0	0	612	63	0
659	0	0	617	32	0

* Singer and Cottrell, *J. Inst. Metals*, **73**, 33, 1946.

TABLE 6.3. CRITICAL PROPERTIES OF AL:SI ALLOYS UPON SHORT-TIME TENSILE TESTS AT TEMPERATURES IN THE VICINITY OF THE HYPOEUTECTIC SOLIDUS*

Alloy	Strength at critical point (*i.e.*, solidus) psi	Temp. of sudden decrease in strength, °C	Temp. of loss of all strength, °C	Temp. range for hot-shortness, °C
Superpure Al	180	655	659	4
Al:0.25 Si	410	641	653	12
Al:0.6 Si	420	622	652	30
Al:1.0 Si	400	607	649	42
Al:1.5 Si	590	578	637	59
Al:2.0 Si	590	577	635	58
Al:4.0 Si	600	575	606	31
Al:8.0 Si	630	574	578	4
Al:12.0 Si	660	576	578	2

* Singer and Cottrell, *J. Inst. Metals*, **73**, 33, 1946.

stressing. This effect, previously described (page 60) as a means of experimentally determining solidus temperatures, has been further tabulated for a series of Al:Si alloys in Table 6.3. It is clear that the widest temperature range in which the alloy has no ductility but some strength occurs in alloys with from 1.5 to 2.0% Si. Hot-shortness would be greatest for these alloys and least for the eutectic alloy.

The structure shown by Micro. 6.8 is commonly called a *burnt* structure; the word as here used does not signify an oxidation reaction but heating into a two-phase, *solid* + *liquid*, field during solution heat treatments or hot-working operations. Deformation within this temperature range, of course, will cause the alloy to crack and be ruined. If the alloy has a plastic eutectic, as in the Al:Si alloys, the damage to the quenched

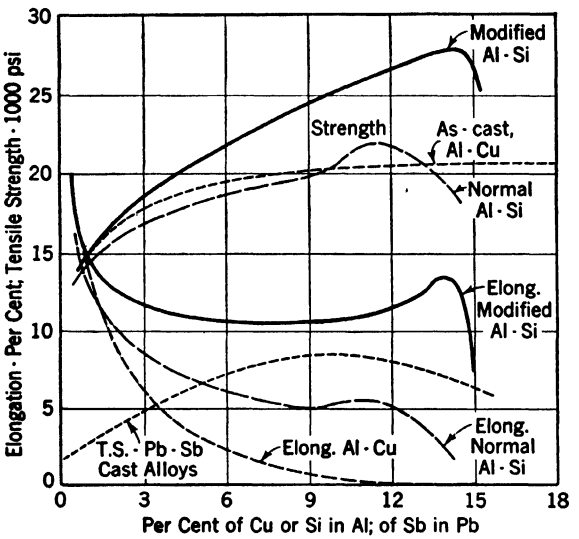

FIG. 6.4. Strength properties across the hypoeutectic sections of the Al:Cu, Al:Si, and Pb:Sb systems; effect of modification on the strength and elongation of the Al:Si alloys.

metal (in the absence of deformation) is negligible. If the eutectic envelopes around the grains are brittle, as in the Al:Cu alloys, both strength and ductility are seriously impaired. Although the bad effects could largely be eliminated by a solution anneal, the time required to redissolve the eutectic is so long that it is not generally profitable commercially to do other than scrap the overheated alloy.

6.7 Properties of Alloys, General

The properties of the eutectiferous alloys can be qualitatively evaluated on the basis of the proportionate amounts of primary crystals and eutectic structure and the physical characteristics of the eutectic.

All the Al:Si alloys show some ductility since α_{Al} is the *continuous* phase in the eutectic. The superior ductility of the modified

alloys is related to the shape as well as the size of the eutectiferous silicon crystallites. In the normal alloys, they tend to be angular plates whose sharp edges act as internal notches in the structure, whereas this effect is nearly absent with the rounded silicon particles of the modified alloy (Micro. 6.20).

The Al:Cu system (page 134) has a eutectic composition nearer the brittle θ phase ($CuAl_2$) than the plastic $\alpha_{(Al)}$ phase, and thus the $\alpha_{(Al)} + \theta$ eutectic structure is inherently brittle. The effect of fairly rapid cooling in casting and the related position of the metastable solidus result in

TABLE 6.4. AGING OF AL:5% CU ALLOY AS-QUENCHED FROM 540°C, RF61

Time	Temperature, °C	Hardness	Time	Temperature, °C	Hardness
0	25	RF61	1 hr	150	RF80
2 hr	25	RF72	1 hr	200	RF90
1 day	25	RF85	1 hr	250	RF84
1 week	25	RF87	1 hr	300	RF73
1 month	25	RF88	1 hr	350	RF56
1 year	25	RF88	1 hr	400	RF44
¼ hr	200	RF78	¼ hr	300	RF83
1 hr	200	RF90	1 hr	300	RF73
5 hr	200	RF87	5 hr	300	RF65
24 hr	200	RF83	24 hr	300	RF43

some eutectic in cast alloys with as little as 2% Cu present. Figure 6.4 shows that there is a moderate increase in strength and strong decrease in ductility (as shown by test elongation values) as the amount of copper in aluminum is increased. When the eutectic structure becomes continuous (Micro. 6.3; 8% Cu), the strength is almost at a maximum and the ductility nearly zero. Further increases in the amount of eutectic have little effect on the strength properties, within the range of commercial alloys of aluminum and copper, although the 12% Cu alloy has greater hardness and wear resistance as a result of the increased amount of θ present in the structure.

Strength, ductility, and hardness properties of two-phase alloys are related to the size, number, distribution, and properties of the crystals of both phases. The effect of an added element in solid solution was discussed in Chap. 3, of matrix grain size in Chap. 4, and of a relatively coarse dispersion of a second phase in Chap 5. Very fine dispersions cannot be obtained from the liquid state but can form in the solid by reason of the greater order of magnitude of nucleation in the latter case.

The process involved has been discussed from the standpoint of the phase diagram under theory of age-hardening. Precipitate structures have been shown, which should be examined with relation to the data of Table 6.4.

It is evident that, even when the precipitate is as fine as that shown in Micro. 6.25, the alloy has passed its point of maximum hardness and

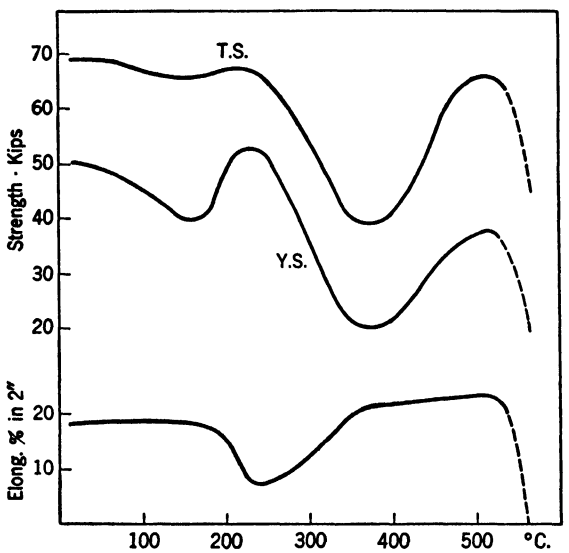

FIG. 6.5. Tensile strength, yield strength, and tensile-test elongation values for aluminum alloy 24ST (quenched and aged at room temperature) sheet specimens. They were reheated to varying temperatures for one hour, quenched and aged at room temperature. The difference between initial values at the left and the equivalent condition of 500°C reheat is presumably due to a slower original mill quench (*e.g.*, in hot water) and the slight working resulting from a pass through straightening rolls; both factors would increase yield-strength values particularly. (*Sachs and Van Horn.*)

would be in a condition known as *over-aged*, while the coarse precipitate of Micro. 6.26 would represent a structure of minimum strength and hardness, designated as the *annealed* or SO condition by the Alcoa system. The precipitate present in the condition of optimum strength and hardness is not readily detected by ordinary micrographic technique for many alloys, although special care in polishing and the use of special etches generally will reveal some structural alteration as compared to the initially as-quenched supersaturated condition.

Strength properties generally show the same trends as hardness, but ductility may not show the usual inverse trend. The decrease in tensile-test elongation values during early stages of aging may be slight. At

about the point of maximum hardness or slight over-aging, a sharp drop in ductility values is frequently observed. This stage seems to correspond to a very heavy and almost continuous grain-boundary precipitation of the brittle θ. When the precipitate has coarsened considerably, brittleness diminishes and, at the point of minimum strength and

TABLE 6.5. EFFECT OF IRON IMPURITY ON THE PROPERTIES OF MODIFIED CHILL-CAST AL:10% SI ALLOY*

% Si	% Fe	Tensile strength, psi	% elongation in 2 in.	% reduction in area	BHN
10.8	0.29	31,100	14.0	15.3	62
10.8	0.79	30,900	9.8	11.6	65
10.3	0.90	30,000	6.0	6.2	65
10.1	1.13	24,500	2.5	2.2	66
10.4	1.60	18,000	1.5	1.0	68
10.2	2.08	11,200	1.0	0.2	70

* Stockdale and Wilkinson, *J. Inst. Metals*, **36**, 313, 1926.

TABLE 6.6. DISPOSITION OF IRON IMPURITY IN AL:CU ALLOYS, QUENCHED FROM THE SOLID-SOLUTION FIELD

% Cu	% Fe	Al lattice parameter	% Cu in solution	% Cu in compound	Max. BHN
4.48	0.01	4.0310	4.48	....	114
4.44	0.18	4.0321	4.08	0.36	109
4.35	0.32	4.0330	3.67	0.68	104
4.47	0.47	4.0335	3.45	1.02	101
4.46	0.61	4.0343	3.08	1.38	92
4.40	0.74	4.0351	2.73	1.67	75
4.43	0.90	4.0358	2.41	2.02	65
4.43	1.05	4.0364	2.16	2.27	60

hardness, the alloy again shows good ductility, the boundary precipitate now consisting of a few discrete, large particles of θ. As the heat treatment temperature is further increased, to the vicinity of the solvus line, re-solution of the θ phase causes a slight additional increase in ductility and a simultaneous increase in strength. These changes are illustrated by the curves in Fig. 6.5 for properties of alloy 24S.

6.8 Cast-aluminum Alloys, Problems and Properties

Aluminum alloys may be cast in sand molds, in gravity-fed iron molds (permanent molds), or in steel dies under pressure. Solidification

is much more rapid when the alloys are cast in metal molds and, therefore, a given alloy will be finer grained and stronger as a permanent mold casting. Since more sand castings on a weight basis are made (55%)[1] than permanent mold castings (27%)[1] or pressure die castings (18%),[1] the discussion and data will be confined largely to sand castings.

The alloys are usually obtained, made up to proper composition, in the form of pigs although virgin aluminum may be alloyed with rich alloys (*e.g.*, Al + 33% Cu) to obtain the specified composition. In addition, there is usually from 25 to 75% secondary metal or scrap to be used up. Melting is customarily done in iron pots with the iron protected by a lime or similar ceramic coating to prevent the pickup of iron by liquid metal. The deleterious effect of iron on the properties of a cast 10% Si alloy is shown by the data of Table 6.5. The diminution in both strength and ductility is caused by an increasing amount of coarse Al:Fe:Si crystallites in place of fine eutectiferous silicon. The data of Table 6.6 indicate that iron impurity combines with copper and aluminum, forming an insoluble Al:Cu:Fe compound. This reduces the amount of copper that can dissolve in aluminum and, therefore, has an adverse effect on the properties of heat-treated Al:4.5% Cu alloys. The curves of Fig. 6.6 show how 1% Fe in a 4.5% Cu alloy reduces the age-hardening response to somewhat the same increment as shown by a 1.5% Cu alloy containing no iron.

When melting aluminum alloys, it is necessary to avoid overheating for two reasons: (1) As discussed in Chap. 4, overheated metal, when cast into a mold, solidifies more slowly because of the additional heat to be removed and, therefore, a coarser grain and weaker structure will be obtained. (2) Aluminum at high temperatures reacts readily with water vapor to form aluminum oxide and hydrogen. This gas is avidly dissolved by the liquid metal. As the temperature decreases, the hydrogen becomes less soluble and during freezing the solubility drops very sharply. At the same time, there are physical factors such as dendrites to encourage hydrogen bubble formation and, unfortunately, simultaneously prevent the escape of the bubbles. Therefore, aluminum alloys melted on humid days or in furnaces fired with city gas (yielding considerable water vapor in the products of combustion) are always more porous than castings made on dry days or melted in electric furnaces.

It would be too expensive to melt with electricity in air-conditioned foundries and, therefore, hydrogen pickup is minimized by avoiding overheating and then removed, if necessary, by flushing with a neutral

[1] Figures for December, 1945, for United States production.

gas. Dried nitrogen bubbled through the liquid before pouring the castings will remove hydrogen by physical means. Chlorine gas is more expensive but, if bubbled through the liquid, not only removes hydrogen but also chemically purifies the bath by removing oxide or dross films that are entrapped during melting.

The casting of the alloys follows normal practice. Although overheating is undesirable, the liquid must be sufficiently hot to fill the mold

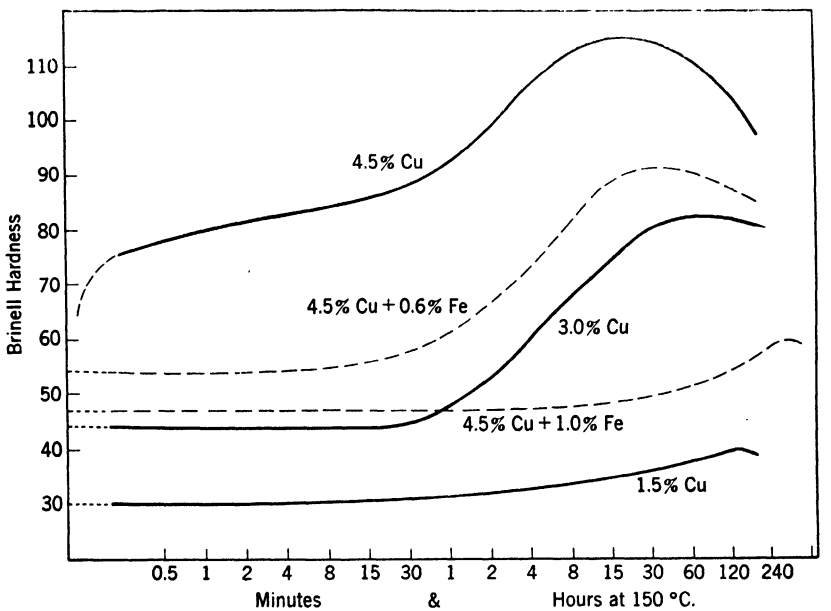

FIG. 6.6. Effect of iron impurity in alloy of aluminum + 4.5% Cu on the response to age-hardening at 150°C following a solution heat treatment and quench. The aging response indicates that 0.6% Fe makes the ternary alloy age-harden like a binary 3% Cu alloy and 1% Fe reduces the aging response to that of a 1.5% Cu alloy. (*Hunsicker.*)

before solidification begins, to avoid *cold shuts* or *misruns*. These are discontinuities arising from streams of metal coming from different directions that make physical contact without completely fusing because of heavy oxide films and lack of fluidity.

The casting characteristics of pure aluminum are improved by alloying even more than the mechanical properties. The higher silicon-content alloys listed in Table 6.7 all exhibit very good fluidity in the liquid state, are not hot-short nor susceptible to hot cracks, and are also less susceptible to shrinkage cavities. Since these cavities tend to be interdendritic and structurally connected, this means that the Al:Si

alloys such as Nos. 43, 108, 319, and 356 are all well suited for pressure-tight parts, and the choice between them might depend primarily on the mechanical properties required and the cost, these usually being directly proportional. Relative properties are given by the data of Table 6.8.

The higher copper-content alloys, *e.g.*, Nos. 112 and 212 in Table 6.7, are characterized by good casting characteristics and also better machinability than the silicon alloys. They are not so suitable, how-

TABLE 6.7. COMPOSITION OF SOME COMMON ALUMINUM CASTING ALLOYS*

Alcoa designation	Composition†				Heat-treatable	Characteristics
	% Cu	% Si	% Mg	% other elements		
112	7.0	....	....	1.7 Zn	‡	General-purpose castings
212	8.0	1.2	....	1.0 Fe	‡	Better castability than 112
195	4.5	....	....	....	Yes	High strength
43	...	5.0	....	....	No	Excellent castability
108	4.0	3.0	....	....	‡	Strength and castability
319	3.0	6.0	....	....	Yes	Strength and castability
356	...	7.0	0.5	....	Yes	Strength and castability
220	...	....	10.0	....	Yes	Highest strength
142	4.0	....	1.5	2.0 Ni	Yes	Good hot strength
132	0.8	12.0	1.0	0.8 Fe: 2.5 Ni	Yes	Hot strength, low thermal expansion

* From "Alcoa Aluminum and Its Alloys," 1946 ed. Alloys 112 and 212 not listed in 1948 edition.
† Small quantities of Fe and Si plus traces of other impurities are present in alloys.
‡ Alloy not usually heat-treated although some improvement in properties is possible.

ever, for pressure-tight castings or where both thick and thin sections adjoin in the same casting. These alloys are not heat-treated although they would respond favorably as could be anticipated from the phase diagram. The discussion of Micro. 6.14 would lead one to guess that, although the embrittling interdendritic eutectic network of α:$CuAl_2$ could not be completely eliminated, the continuity of the $CuAl_2$ phase could be disrupted by spheroidizing effects with an improvement in ductility.

The 4.5% Cu alloy, No. 195, is more difficult to cast but, when heat-treated, has the best mechanical properties of any of the common sand-casting alloys. As Table 6.8 shows, its mechanical properties are poorer than those of the 10% Mg alloy, No. 220, and in addition, the latter alloy is lighter, more resistant to corrosion, and more machinable. Unfortunately the No. 220 alloy, like magnesium base alloys, requires

TABLE 6.8. TYPICAL PROPERTIES OF SOME COMMON ALUMINUM CASTING ALLOYS IN SAND-CAST FORM*

Alcoa designation	Condition	Tensile strength, psi	Yield strength, psi	%Elongation in 2 in.	BHN	Endurance limit, psi	Thermal expansion, 30-100° C
112	As-cast	24,000	15,000	1.5	70	9,000	12.2
212	As-cast	23,000	14,000	2.0	65	8,000	12.2
195-T4	12 hr, 515°C, qu.	32,000	16,000	8.5	60	6,000	12.2
195-T6	12 hr, 515°C; 4 hr, 155°C	36,000	24,000	5.0	75	6,500	12.2
195-T62	12 hr, 515°C; 14 hr, 155°C	40,000	30,000	2.0	95	7,000	
43	As-cast	19,000	9,000	6.0	40	6,500	12.2
108	As-cast	21,000	14,000	2.5	55	8,000	12.2
319	As-cast	27,000	18,000	2.0	70	10,000	
319-T6	12 hr, 515°C; 4 hr, 155°C	36,000	24,000	2.0	80	10,000	
319-T6†	12 hr, 515°C; 4 hr, 155°C	40,000	27,000	3.0	95		
356-T51	8 hr, 228°C	25,000	20,000	2.0	60	7,500	11.9
356-T6	12 hr, 540°C; 4 hr, 155°C	33,000	24,000	4.0	70	8,000	11.9
356-T7	12 hr, 540°C; 8 hr, 228°C	34,000	30,000	2.0	75		
356-T71	12 hr, 540°C; 3 hr, 245°C	28,000	21,000	4.5	60		
356-T7†	12 hr, 540°C; 4 hr, 155°C	40,000	27,000	5.0	90		
220-T4	Sol'n and qu.	46,000	25,000	14.0	75	7,000	13.6
142-T21	3 hr, 345°C	27,000	18,000	1.0	70	6,500	12.5
142-T77	6 hr, 520°C; 2 hr, 345°C	32,000	28,000	0.5	85	8,000	
132-T551†	16 hr, 170°C	38,000	28,000	0.5	105		10.5
132-T65†	8 hr, 515°C; 14 hr, 170°C	47,000	43,000	0.5	125		

* From "Alcoa Aluminum and Its Alloys," 1947 ed. The mechanical properties here are of separately cast bars, tested without machining the gauge section. Since the skin of the casting is strongest, these properties would not necessarily represent accurately those of machined test bars nor sections much thicker or thinner than ½-in. test bars.

† Alloy cast in permanent mold.

special inhibitors in the sand to prevent deep surface defects and in general shows poorer castability. These difficulties plus the high cost have prevented the 10% Mg alloy from being used extensively.

Returning again to the effects of impurities, the data of Table 6.9 in comparison with those of Table 6.8 show how noticeably superior are the

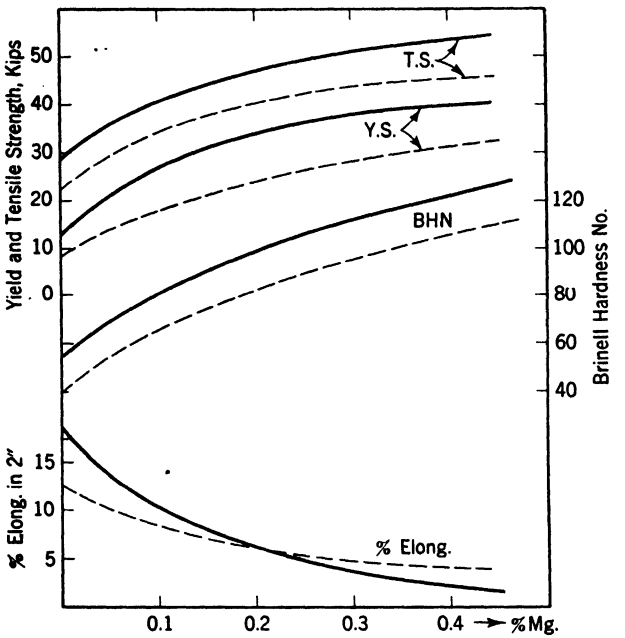

FIG. 6.7. Effect of variation of magnesium content upon the mechanical properties of Al:5% Si alloy (dashed lines) and Al:13% Si alloy (solid lines). These data are based on tests of chill-cast test bars, solution heat-treated 2 hr at 550°C, quenched and aged 20 hr at 155°C. The alloys here are of the Alcoa 356 type (7% Si, 0.5% Mg).

properties of the 4.5% Cu alloy when made from high-purity aluminum. However, since the higher purity base metal costs about 50 cents a pound as compared with 16 cents a pound for ordinary primary aluminum, there is little industrial interest in the high-purity alloys.

The effect of magnesium variations, at three different silicon contents, on alloys of the No. 356 type is shown by the graphs of Fig. 6.7. It is apparent that magnesium is more potent as a strengthener than is silicon. In these alloys, the response to heat treatment is associated with the solution of the compound Mg_2Si and its precipitation during the aging heat treatment.

The heat treatments given in Table 6.8 follow the system of designations shown below:

T2—Annealed. Usually performed at 345°C, this treatment relieves macrostresses and stabilizes dimensions by complete precipitation. Microstructural changes are slight when the alloy is in the as-cast condition, *i.e.*, has not been given a solution treatment.

T4—Solution Treatment. The temperature must be above the solvus line but below the solidus to avoid "burning." The time will depend on the identity and size of the soluble second-phase crystallites.

TABLE 6.9. EFFECT OF HEAT TREATMENT ON THE PROPERTIES OF SAND-CAST AL:4.5% CU ALLOY MADE OF HIGH PURITY (99.93%) AL*

Condition of alloy	Tensile strength, psi	Yield strength, psi	% elongation in 2 in.	BHN
As-cast, aged r.t.†	20,100	8,800	7.5	45
1 hr at 540°C, quenched, aged r.t. 2 days	32,200	22,600	5.5	76
8 hr at 540°C, quenched, aged r.t. 2 days	40,200	22,400	14.6	74
40 hr at 540°C, quenched, aged r.t. 2 days	42,300	24,000	19.0	83
40 hr at 540°C, quenched, test immed.	35,800	17,400	20.7	62

* Data from Jeffries and Archer, *Proc. IMD, AIME*, p. 35, 1927.
† Room temperature.

Thick sections that solidified more slowly will require longer solution times to attain maximum properties. Quenching ordinarily is in hot or boiling water (65 to 100°C) to minimize quenching stresses (see page 176).

T5—Artificially Aged Only. Rapid solidification and a cored microstructure result in some parts of the structure that are supersaturated in the as-cast and unheat-treated alloy. Thus aging at an elevated temperature will result in some increase in strength and hardness.

T6—Solution Treated and Artificially Aged. This heat treatment is designed to attain maximum strength and hardness.

T7—Stabilized. If the artificial or elevated temperature aging is carried out at a temperature and time that result in over-aging beyond the point of maximum hardness, then the precipitate phase is in its stable form and the alloy is not subject to dimensional changes upon

service at lower temperatures. This treatment is particularly important in parts like automotive pistons operating at elevated temperatures to close dimensional clearances.

6.9 Properties of Wrought-aluminum Alloys

Aluminum alloys in hot- or cold-worked form are identified by numerical designations with the suffix S and another letter which, like those just described, specifies the condition. These designations follow the scheme below:

Non-heat-treatable Alloys (hardenable only by cold work):

S-O—annealed, *i.e.*, recrystallized to a medium grain size.

S-H18—cold-worked to the hard temper (*i.e.*, about a 40% reduction); S-H14 means half hard.

Heat-treatable Alloys:

S-O—annealed, to a coarse precipitate of the second phase, a structure of maximum softness and workability (for bending, etc.).

S-T4—solution-treated, quenched, and then naturally aged (formerly SW). The old W designation was not applicable to alloys that age at room temperature but was used for those which require artificial aging at an elevated temperature to attain desired properties. It could be applied to 24S, for example, only when the solution-treated and quenched alloy was cooled and maintained at dry-ice temperatures immediately after quenching.

S-T3—solution-treated and then cold-worked. This designation applies to those products where cold-work is performed to improve strength properties or to indicate the effect of straightening or flattening operations.

S-T36—solution-treated, cold-worked, and naturally aged.

S-T6, S-T81, S-T86—solution-treated and artificially aged. It has recently been found that artificial aging treatments of alloys such as 24S, which formerly were aged only at room temperature, result in desirable increases in yield strength at not too great a sacrifice in ductility and corrosion resistance. Elevated temperature aging (8 hr at 190°C) of 24S is designated by -T6; if cold-working is also employed previous to artificial aging, designations -T81 and -T86 apply.

The compositions of the common wrought alloys are listed in Table 6.10 and typical mechanical properties for non-heat-treatable alloys in Table 6.11. Typical properties of some forging alloys are listed in

TABLE 6.10. COMPOSITIONS OF SOME COMMON WROUGHT-ALUMINUM ALLOYS

Alcoa designation	Composition *					Chief characteristic
	% Cu	% Si	% Mg	% Mn	% others*	
2S	...	...	...	...	...	Commercially pure Al
3S	...	...	...	1.2	...	Slightly stronger but like 2S
11S	5.5	...	...	...	0.5 Pb, 0.5 Bi	Free machining and strong
14S	4.4	0.8	0.4	0.8	...	Strongest forging alloy
17S	4.0	...	0.5	0.5	...	Oldest strong alloy, forgings
24S	4.5	...	1.5	0.6	...	High strength
25S	4.5	0.8	...	0.8	...	Good forgeability and strength
32S	0.9	12.5	1.0	...	0.9 Ni	Strength at high temperatures
A51S	...	1.0	0.6	...	0.25 Cr	Very good forgeability
52S	...	...	2.5	...	0.25 Cr	Intermediate between 3S and 24S
61S	0.25	0.6	1.0	...	0.25 Cr	Corrosion resistance, formability, low cost
75S	1.6	...	2.5	0.2	5.6 Zn, 0.3 Cr	Strongest alloy

* All alloys contain about 0.3% Fe and Si, each.

TABLE 6.11. TYPICAL PROPERTIES OF NON-HEAT-TREATABLE WROUGHT-ALUMINUM ALLOYS*

Alcoa designation†	Tensile strength, psi	Yield strength, psi	% elongation in 2 in.		BHN	Endurance limit, psi
			Sheet	Rod		
2S-O	13,000	5,000	35	45	23	5,000
2S-H14(½H)	17,000	16,000	9	20	32	7,000
2S-H18 (H)	24,000	22,000	5	15	44	8,500
3S-O	16,000	6,000	30	40	28	7,000
3S-H14 (½H)	21,500	19,000	8	16	40	9,000
3S-H18 (H)	29,000	26,000	4	10	55	10,000
4S-O	26,000	10,000	20	25	45	14,000
4S-H34 (½H)	34,000	27,000	9	12	63	15,000
4S-H38 (H)	40,000	34,000	5	6	77	16,000
52S-O	27,000	12,000	25	30	45	17,000
52S-H34 (½H)	37,000	31,000	10	14	67	18,000
52S-H38 (H)	41,000	36,000	7	8	85	19,000

* Data from "Alcoa Aluminum and Its Alloys," 1948 ed.

† New temper designations given with former designations in parentheses.

TABLE 6.12. TYPICAL MECHANICAL PROPERTIES OF ALUMINUM FORGING ALLOYS*

Alcoa designation†	Tensile strength, psi	Yield* strength, psi	% elongation in 2 in.	BHN	Endurance limit, psi
A51S-O	16,000	6,000	30	28	
A51S (W)	35,000	20,000	24	64	
A51S-T6 (T)	48,000	43,000	17	100	11,000
32S-T6 (T)	55,000	46,000	9	120	16,000
25S-T6 (T)	58,000	37,000	19	110	18,000
14S-O	27,000	14,000	18	45	13,000
14S-T4 (W)	62,000	44,000	20	105	18,000
14S-T6 (T)	70,000	60,000	13	135	18,000

* Forgings up to 4 in. in thickness, tested parallel to direction of grain flow. Data from "Alcoa Aluminum and Its Alloys," 1948 ed.

† New term per designations given with former designations in parentheses.

TABLE 6.13. TYPICAL MECHANICAL PROPERTIES OF HEAT-TREATABLE ALUMINUM-ALLOY SHEET (0.065 in.)*

Alcoa designation†	Tensile strength, psi	Yield strength, psi	% elongation in 2 in.	BHN	Endurance limit, psi
61S-O	18,000	8,000	22	30	9,000
61S-T4 (W)	35,000	21,000	22	65	13,500
61S-T6 (T)	45,000	40,000	12	95	13,500
24S-O	27,000	11,000	19	47	13,000
24S-T3 (T)	70,000	50,000	16	120	18,000
24S-T36 (RT)	73,000	57,000	13	130	18,000
Alclad 24S-O	26,000	11,000	19		
Alclad 24S-T3 (T)	64,000	44,000	15		
Alclad 24S-T36 (RT)	67,000	53,000	11		
Alclad 24S-T81	65,000	60,000	6		
Alclad 24S-T86	70,000	66,000	6		
75S-0	33,000	15,000	17	60	
75S-T6 (T)	82,000	72,000	11	150	21,000
Alclad 75S-O	32,000	14,000	17		
Alclad 75S-T6 (T)	76,000	67,000	11		

* Data from "Alcoa Aluminum and Its Alloys," 1948 ed.

† New temper designations given with former designations in parentheses.

Table 6.12 and for other heat-treatable types in Table 6.13. The strength and ductility values, as for all metals and alloys, depend to some extent on the section size of the metal being tested, and these strength values would be appreciably higher for thin sheet or wire and lower for very thick plates or rods.

The alloys hardenable only by cold-work are all characterized by very good corrosion resistance and good formability. The latter decreases, and the alloy cost increases, proceeding from 2S through the increasing strength series to 3S and 52S. Decreasing ductility and

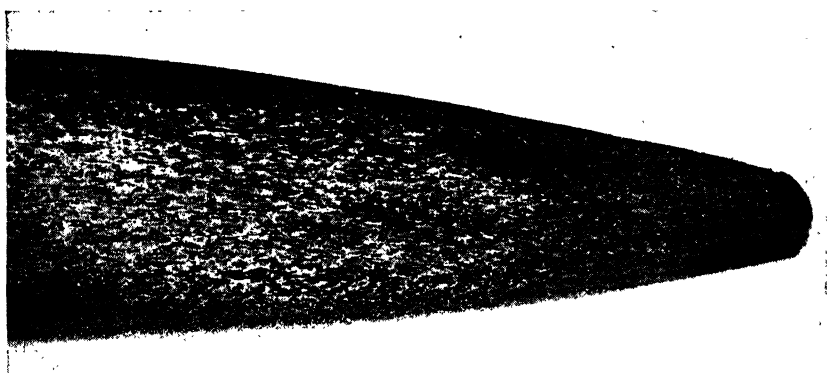

FIG. 6.8. Macrostructure of a longitudinal section of an aluminum alloy 25ST propeller as hot-forged and heat-treated, showing grains retained in elongated shapes by insoluble microconstituents and a finer grained structure nearer the surface, resulting from a lower hot-working temperature; ×6; hot NaOH etch followed by HNO_3 dip.

increasing fatigue strength accompany increasing strength, whether by alloy or by cold-work.

Among the forging alloys, A51S is so soft at high temperatures that very intricate forgings can be produced and although moderate strength values are obtained by heat treatment, they are low in comparison with the other alloys. Alloy 14S represents the other extreme; it develops very good strength properties but is not suitable for complicated shapes because of its relative stiffness even at forging temperatures. The other alloys are intermediate in these regards. The tip of a heat-treated propeller of 25ST is reproduced in the macrograph of Fig. 6.8, which shows how grain flow is revealed by grain shape even after subsequent heat treatment. Equiaxed grains cannot grow in these alloys containing insoluble constituents from the manganese addition as well as the inevitable iron and silicon impurities.

The data of Table 6.13 hold several points of interest. Alloy 61S is relatively low in cost, is readily formable, and has a high corrosion

resistance. The 24S alloy, available also in extruded forms, etc., offers a tensile strength five or six times that of annealed commercially pure aluminum with fairly good ductility in the ordinary tensile test. It does have poor local plasticity and is sensitive to notches so that a sheet test specimen of 24ST will frequently break at a scratched gauge mark. The alloy, except when quenched in cold water or cold-worked and aged, also is sensitive to intercrystalline corrosion from grain-boundary precipitation of the second phase. The matrix phase at grain-boundary areas, after precipitation, is depleted in solute atoms and in a corrosive solution acts as an anode. The rest of the grain serves as a cathode and as current passes, the grain-boundary areas are selectively dissolved. Under these circumstances, a small amount of corrosion (small in terms of total amount of metal corroded away) may be accompanied by a large decrease in strength and ductility, the ductility being particularly reduced by the notch effect of grain-boundary attack.

For use in corrosive environments, the alloy 24ST is protected by a surface layer of pure aluminum, which is integrally attached by hot-rolling and a related pressure welding effect. The deformation breaks the aluminum oxide layer always present to some degree on aluminum alloys and permits atomic structural continuity to be developed across the interface. Although slightly reducing strength and endurance properties, particularly in bending fatigue, the pure aluminum is anodic to the alloy and prevents intercrystalline corrosion, even at cut edges. Furthermore, the highly plastic aluminum surface layer eliminates notch sensitivity so that minor scratches are no longer sources of brittle failure.

The atomic continuity across the alloy-aluminum interface permits diffusion to occur, and if copper diffuses to the surface, most of the advantages of the Alclad form are lost. The diffusion may be minimized by restricting the heat treatment to the shortest effective time (see Table 6.14). Knowing the diffusion rate of copper in aluminum at the heat-treatment temperatures and making certain assumptions about the initial state of the alloy, it is possible to calculate the maximum time the Alclad alloy could be held at the solution heat-treatment temperature. Practically, it is customary to take test specimens of Alclad annealed sheet and heat-treat in a liquid salt bath for increasing increments of time, *e.g.*, 2, 5, 10, 20 min, and determine the minimum time required to develop substantially standard mechanical properties. There are chemical and metallographic methods[1] for determining whether or not this time permitted copper to diffuse to the surface of the Alclad to an unfavorable extent.

[1] Keller, *Metal Progress*, **41**, 63, January, 1942.

In Table 6.13 it is seen that the relatively new 75S alloy shows appreciably higher strengths than 24S; its *yield* strength (75S-T) is frequently higher than the *tensile* strength of 24S-T. The alloy is not so readily formed as 24S-T, and it shows more sensitivity to cracking under the combined influence of a tensile stress and corrosive environ-

TABLE 6.14. RECOMMENDED HEAT TREATMENTS FOR WROUGHT-ALUMINUM ALLOYS*

Alloy	Annealing temperature			Solution treatment			Precipitation treatment		
	Temp., °F	Time, hr	Temper.	Temp., °F	Time, hr	Temper.	Temp.	Time, hr	Temper.
2S	650	†	−0						
3S	775	†	−0						
4S	755	†	−0						
52S	650	†	−0						
14S	775	3†	−0	940	§	−T4	340	10	−T6
17S	775	3‡	−0	940	§				
24S	775	3‡	−0	920	§	−T4	375 375	9 12	−T84 −T81
75S	775	3†	−0	870	§		250	24	−T6
25S	775	3‡	−0	960	§	−T4	340	10	−T6
32S	775	3‡	−0	950	§	−T4	340	10	−T6
A51S	775	3‡	−0	960	§	−T4	340	10	−T6
61S	775	3‡	−0	970	§	−T4	320 or 350	18 8	−T6 −T6

* From "Alcoa Aluminum and Its Alloys," 1948 Ed.

† Time in furnace need be only enough to bring all parts to the annealing temperature; cooling rate is unimportant.

‡ To obtain full softening, cooling should be at a rate of no faster than 50°F per hour down to 500°F; the subsequent rate is unimportant.

§ Time may vary from 10 min for sheet in a salt bath, 60 min for plate in air to at least 4 hr in air for average forgings. Time for Alclad products should be minimized to prevent diffusion of alloying elements from core to surface. Rapid transfer from the furnace to a cold-water quench is recommended except for large forgings which may be quenched in hot water.

ment. The latter tendency may be minimized or eliminated by surface peening, usually with steel shot. This treatment induces a residual compressive stress as shown by Fig. 6.11 and thus reduces the actual surface tensile stress that may result from a given bending force.

6.10 Residual Stresses and Relaxation

Aluminum alloys are subject to distortion and residual stresses when quenched in cold water as a result of the temperature gradients developed during cooling. Contraction of the more rapidly cooling

surface compresses the interior, which plastically deforms to conform to the shrunken exterior. As the center cools to the same temperature as the surface, it attempts to contract, but by this time the surface metal is cold and not very plastic. As a result, it is under an elastic compressive

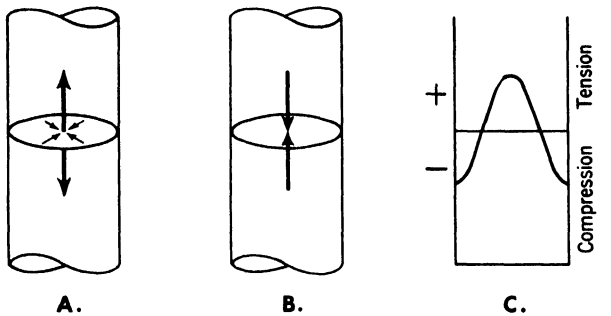

FIG. 6.9. Origin of residual stresses upon quenching: (*A*) cylinder immediately after immersion in quenching fluid; surface contracts and, being colder and stronger than the hot center, squeezes this section plastically along axis; (*B*) later stage of quench when center cools and contracts, a movement resisted by the now cold and relatively stiff surface; (*C*) residual stress distribution in a longitudinal direction across the cylinder; compression at the surface changing to tension at the center.

TABLE 6.15. LENGTH CHANGES UPON BORING AND RESIDUAL STRESSES OF ALUMINUM ALLOY 122 CYLINDERS, 2½ IN. IN DIAMETER BY 10 IN. LONG, WHEN QUENCHED FROM A SOLUTION TREATMENT AT 480°C*

Cooling condition	Contraction in total length, in.	Surface stress, psi	Center stress, psi
Annealed alloy	0.0004	−600	+600
Quenched, boiling water	0.0010	−2,300	+1,300
Quenched, ice water	0.0120	−19,500	+16,100
Above, annealed at 225°C	0.0066	−5,700	+8,500

* Kempf, Hopkins, and Ivanso, *Trans. AIME*, **111**, 158, 1934.

stress, and since the rigidity of the surface prevents the interior from attaining its stable dimensions, there is a balancing tensile stress in the central region. The development of residual or macrostresses as a result of differential plastic deformation caused by the thermal gradients of quenching is illustrated for cylindrical shapes by Fig. 6.9. The intensity of the stresses that may be developed in some common alloys is given by the data of Table 6.15. These data were obtained by machining away part of quenched cylinders, measuring the deformation that

occurs when the stress system is thus unbalanced, and calculating the stress associated with the deformation by the equations of Sachs.[1]

Comparable residual stresses may result from forming operations that involve differential plastic deformation, *e.g.*, bending. The

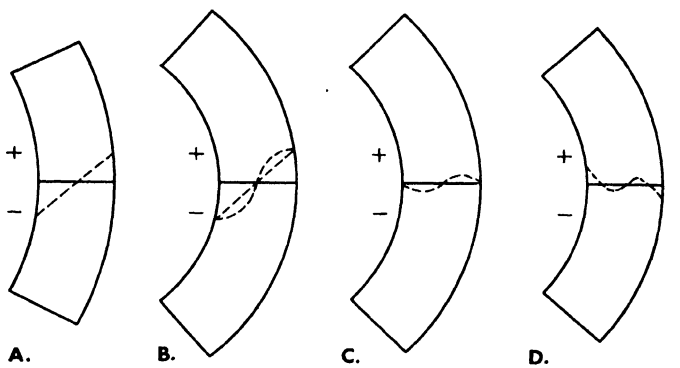

FIG. 6.10. Origin of residual stresses upon cold bending: (*A*) strip bent so that surface stresses (dotted line) just reach elastic limit of the metal at the surfaces; (*B*) continued bending causes plastic flow at surfaces, raises stress at inner zones nearer to the elastic limit; (*C*) release of the bending force causes elastic spring back, here shown carried to point where surface stresses are zero but stress distribution makes this position unstable; (*D*) further springback to balance the stresses on either side of the neutral axis results in residual *tensile stress on the compression surface* and vice versa.

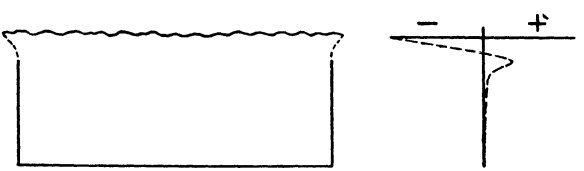

FIG. 6.11. Shot peening of the immediate top surface of the block (left side) tends to spread it. Rigidity of the metal underneath prevents bending or spreading; thus the surface is in compression (right-hand schematic stress plot) with a balancing layer underneath in tension.

schematic drawing of Fig. 6.10 shows that the surface that was deformed in *compression* upon bending subsequently has a residual *tensile* stress and vice versa.

A third source of residual stresses is differential plastic deformation deliberately imposed by surface rolling or peening, which tensilely deforms the surface as in Fig. 6.11 and subsequently leaves it in a state of elastic compression. This has already been referred to in the previous section as a means of preventing tensile stress-corrosion cracking in

[1] Kempf, Hopkins, and Ivanso, *Trans. AIME*, **111**, 158, 1934.

certain susceptible alloys such as 75S-T. The introduction of favorable compressive stresses by this means is also common practice in highly stressed steels and other alloys.

Residual stresses, whatever their source, may be reduced or virtually eliminated by a slight reheating, which, as described in Chap. 4, lowers

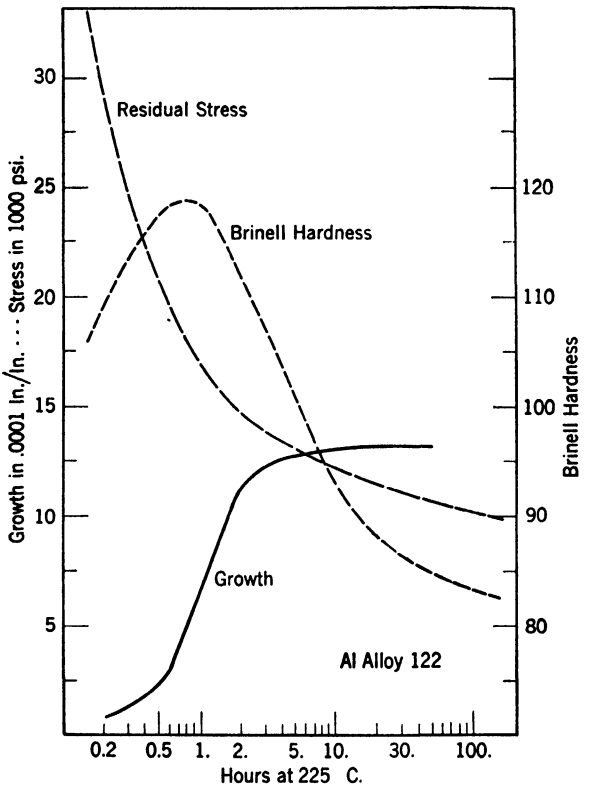

FIG. 6.12. Rate of stress relief at 225°C of aluminum alloy 122 as-quenched from a solution treatment. The accompanying precipitation-hardening and later "overaging" or softening is shown and also the growth which accompanies precipitation.

the elastic limit and permits elastic stress to be reduced by a differential plastic flow. The data of Fig. 6.12 show a typical stress relieval or *relaxation* curve showing the effects of time at a constant temperature on residual stress, Brinell hardness, and growth[1] of aluminum alloy No. 122.

[1] Growth is the increase in dimensions or volume resulting from the formation of the stable θ phase as a precipitate from supersaturated α and the related change in lattice dimensions of the α phase.

To minimize the distortion and residual stresses resulting from drastic quenches, many alloys are quenched in hot water which cools the metal more slowly and, relatedly, minimizes the temperature gradients that cause residual stresses. The slower rate of cooling is still rapid enough to retain the solute in a supersaturated matrix solution *except at grain boundaries.*

Grain-boundary precipitation during cooling (or aging) may not adversely affect the mechanical properties attained by the alloy but may have serious consequences on its resistance to corrosion and on the physical properties shown by corroded specimens. A uniform chemical composition throughout the structure generally assures a uniform rate of corrosion which, in aluminum alloys, is quite slow. Alloys of aluminum with 4 to 5% Cu, as quenched in cold water, are substantially in this condition, for, if precipitation occurs, it takes place throughout the structure upon the planes of plastic movement during the quenching (Micro. 6.25), and, as a result, corrosion is uniform. When these alloys are quenched in hot water to avoid distortion and stresses, the subsequent precipitation is concentrated at grain boundaries with a related concentration gradient of copper from the boundary regions to the remainder of the grains. The boundary area, of purer aluminum (since precipitation of copper is more complete), acts as an anode in an electrolyte, with the large area of the grain acting as a cathode, when this alloy is subjected to corrosion. As a result, the attack is chiefly at grain boundaries and, if the alloy is in relatively thin sheet as in aircraft structures, it can be seriously embrittled. The difficulty can be overcome by having the alloy coated with pure aluminum that, by the electrolytic effect mentioned above, tends to protect the alloy even at the edges of the sheet or at regions of cracks or other surface damage.

QUESTIONS

Group A

1. Why is the corrosion resistance of all Al:Cu alloys, as-cast or heat-treated, poorer than that of pure aluminum or the Al:Si alloys?

2. Why are the Al:Cu alloys more machinable than the Al:Si alloys?

3. If a complex shape is to be formed at room temperature from 24S and high strength in the final shape is required, what condition of heat treatment should the alloy be in if (*a*) the shape can be heat-treated subsequently and (*b*) no heat treatment (above room temperature) is possible after forming?

4. Specify the advantages and disadvantages of quenching alloy 25S aircraft propellers in cold water.

5. If an alloy is "burnt" during heat treatment, why are some voids usually found in the zones that were liquid at the high temperature?

Group B

1. Take the plots of tensile strength and percentage elongation vs. percentage copper of as-cast copper alloys (Fig. 6.4, page 160) and superimpose graphs for the *probable* tensile strengths and percentage elongations vs. percentage copper for the alloys as solution heat-treated and aged.

2. Assume that alloy 2SO sheet, upon cold-drawing into a deep rectangular box, showed cracking at the corners. How would you change (*a*) the box design or (*b*) the alloy or condition, to avoid corner cracking?

3. Alloy 24S-T can be formed into shape by bending, etc., much more easily if the deformation is performed at 200 to 230°C and if the time at this temperature is short, the alloy will not over-age.[1] Why is forming easier at this temperature? Would the deformation be hot-working or cold-working?

4. Why are solution heat-treatment times greater for castings than equivalent wrought alloys and, among wrought alloys, greater for forgings than for sheet?

[1] Finch, Wilson, and Dorn, *Trans. ASM*, **36**, 254, 1946.

CHAPTER 7

ALLOYS OF MAGNESIUM

The ready availability of an important "ore" of magnesium, *i.e.*, sea water, the light weight of the metal, the excellent machinability and good strength properties of its alloys—these factors ensure an ever-increasing utilization. The two chief drawbacks to its more general use are the relatively high cost and chemical reactivity of magnesium, both of which are being overcome by increased production and research, respectively. The tremendous demand for this metal during the Second World War was responsible for a great expansion in primary production facilities and a widespread dissemination of knowledge regarding the fabrication of its alloys by casting, welding, forming, etc. Now, the metal is no longer regarded as a hazardous and unreliable material but as a common engineering metal, which in alloyed form is competitive for many applications with aluminum, copper and ferrous alloys.

7.1 Fundamental Alloying Nature of Magnesium[1]

Crystallography. Magnesium has a close-packed hexagonal structure (Fig. 2.3, page 28) and would be expected to form complete solid solutions only with similar structures of nearly the same atom size and electrochemical characteristics. Actually the other common close-packed hexagonal metals, zinc, cadmium, and beryllium, do not form continuous solid solutions with magnesium, although cadmium most nearly meets the requirements for unlimited solid solubility.

Relative Atomic Sizes. It was pointed out earlier that alloying elements must have an atomic size within 15% of that of the solvent metal for extensive solid solutions to form. The atomic sizes of metallic elements are shown in Fig. 7.1 with a band showing the 15% limit of favorable atomic sizes for solution in magnesium. The atomic diameters shown are not fixed values since a magnesium atom, for example, will be much smaller when it combines with chlorine to form $MgCl_2$ and loses two electrons than when it is present with other magnesium atoms

[1] From an article under this title by Carapella, *Metal Progress*, August, 1945.

in the metallic structure. Likewise in view of the change of lattice parameters with composition, as discussed in Chap. 4, the atom in solid solution appears to show a still different size. In Fig. 7.1, the most probable value of atomic diameters or the limits are shown. It is apparent that about half of the elements are within the favorable zone, about one-tenth are on the border lines, and the remainder are outside. The size factor thus initially limits the solid-solution possibilities. Its effect on solid solubility where electrochemical and valency factors are

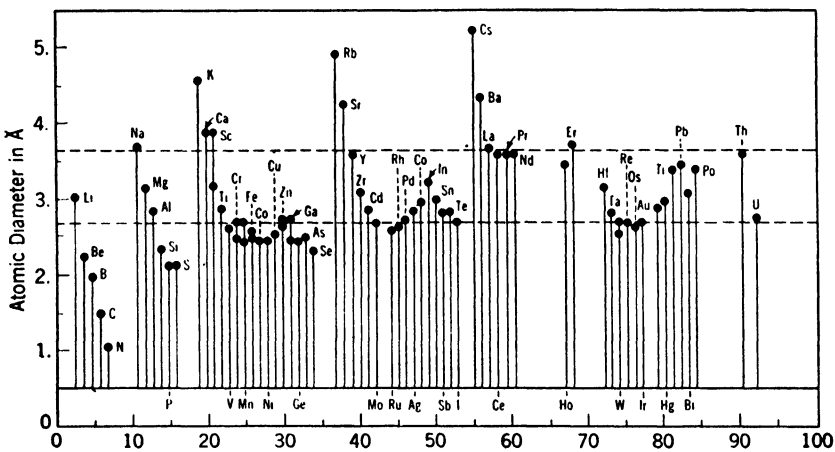

FIG. 7.1. Atomic diameters of the elements with the zone within plus or minus 15% of the nominal size of the magnesium atom shown by dashed lines.

constant is shown in Fig. 7.2; phase diagrams of the magnesium-rich alloys with periodic table Group IIIB elements, Al, Ga, In, and Ti.

Valency Factor. It seems to be a general rule[1] that, as valencies of solvent and solute become more unlike, solid solubility is more restricted. This is shown by Fig. 7.3, phase diagrams of magnesium-rich alloys with Ag, Cd, In, Sn, and Sb, elements in the Long Period 5B of the periodic table. All are within the favorable zone with regard to atomic size.

The figure also illustrates the *relative valency effect, i.e.*, that an element of higher valency is more soluble in a metal than one of comparable lower valency. Thus, although the valency difference between Mg:Ag and Mg:In is the same, univalent silver is less soluble in divalent magnesium than is trivalent indium.

[1] Hume-Rothery, "Structure of Metals and Alloys," *Inst. Metals Monograph.*

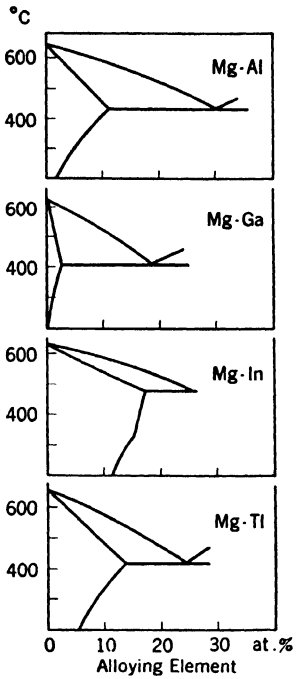

FIG. 7.2.

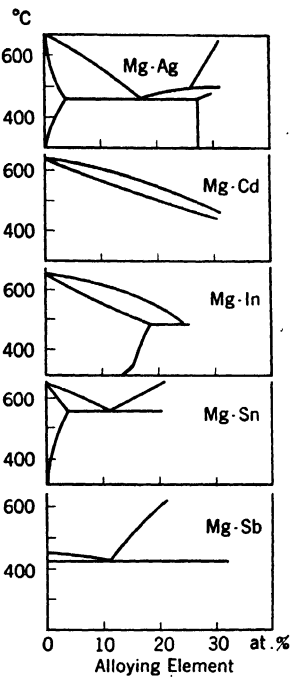

FIG. 7.3.

FIG. 7.2. Influence of size factor on the solid solubility of periodic table Group IIIB elements in magnesium as shown by the binary phase diagrams:

	Period	Lattice	Valence	Size factor, %
Aluminum	3	F.c.c.	3	10
Gallium	4	Orth.rh.	3	13
Indium	5	F.c.t.	3	6
Thallium	6	H.c.p.	3	10

FIG. 7.3. Influence of valence on the solid solubility of Long Period 5 elements in magnesium as shown by the binary phase diagrams:

	Group	Lattice	Valence	Size factor, %
Silver	IB	F.c.c.	1	10
Cadmium	IIB	H.c.p.	2	7
Indium	IIIB	F.c.t.	3	6
Tin	IVB	B.c.t.	4	12
Antimony	VB	Rhomb.	5	10

Electrochemical Factor. Magnesium is a strongly electropositive element and, when alloyed with electronegative elements, compounds are almost invariably formed despite occasionally favorable size factors.

These compounds are practically always of the ionic or NaCl type and have compositions in accord with normal chemical valency rules.[2] For example,

1. Mg + Group VIIB elements: $MgCl_2$, $MgBr_2$
2. Mg + Group VIB elements: MgS, MgSe, MgTe
3. Mg + Group VB elements: Mg_3P_2, Mg_3As_2, Mg_3Sb_2, Mg_3Bi_2
4. Mg + Group IVB elements: Mg_2Si, Mg_2Ge, Mg_2Sn, Mg_2Pb.

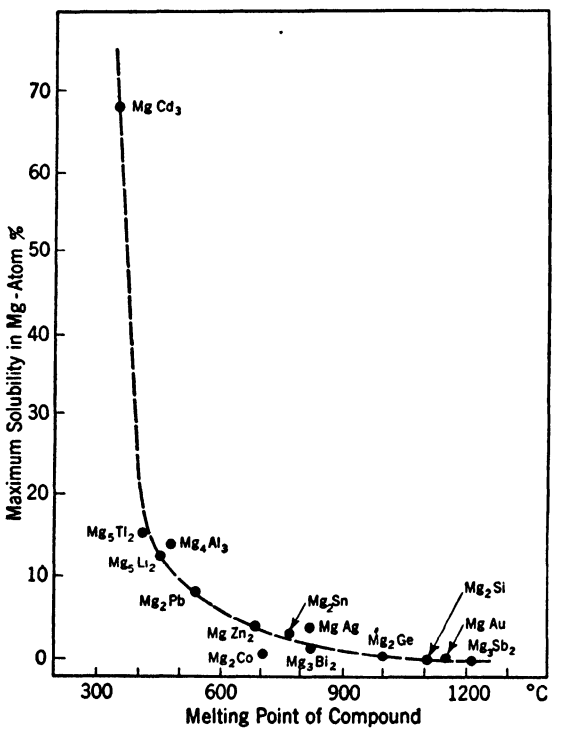

FIG. 7.4. Relationship between the stability of compounds, as indicated by their melting points, and the maximum solid solubility of the second element in magnesium.

Compounds may also be formed when the metal is alloyed with weakly electropositive or weakly electronegative elements. However, the compositions of these compounds do not correspond to normal valencies. They are less stable and have lower melting points. How-

[2] It should be emphasized that in intermetallic compounds, formulas corresponding to the normal valencies of the elements are comparatively rare, except for compounds of strongly electropositive metals with elements from Groups IVB, VB, VIB, and VIIB.

ever, the elements involved are the more important alloying agents. There is a fairly good relationship between the stability of the compound as shown by its melting point and its influence on the metallurgically important phase diagrams. Since most magnesium alloy systems show eutectics between the compounds and the terminal or magnesium-rich solid solution, the effects discussed are best summarized by Figs. 7.4 to 7.7, which show the following:

Figure 7.4: The higher the melting point of the compound, the less its solid solubility in magnesium.

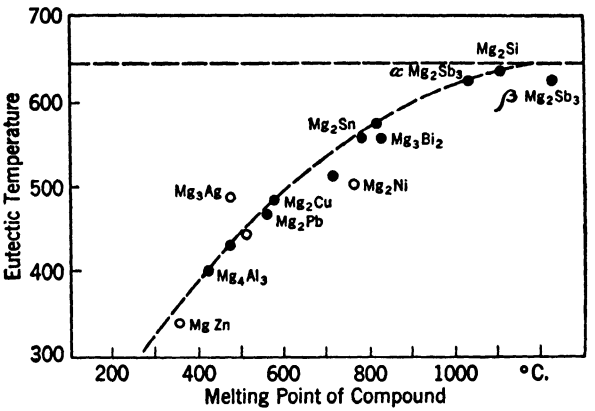

FIG. 7.5. Relationship between stability of compounds, as indicated by their melting points, and the eutectic temperature (solid points) or equivalently the peritectic temperature (circles) in case where the compound forms by the latter type of reaction (see Chap. 8).

Figure 7.5: The higher the melting point of the compound, the higher the melting point of the eutectic.

Figure 7.6: The higher the eutectic melting point, the lower the solute element content of the eutectic (or the nearer the eutectic composition is to the magnesium end of the diagram).

7.2 Pertinent Phase Diagrams

The most important alloys of magnesium contain aluminum, and it seems desirable to reproduce the binary phase diagram with more details than are evident in Fig. 7.2. The entire system is reproduced in Fig. 7.7 since alloys at the aluminum-rich end are also important, as indicated in the previous chapter.

At each end of the diagram, there is a eutectic between a brittle compound and a terminal solid solution. The compound in each case is of relatively low stability having a relatively low melting point;

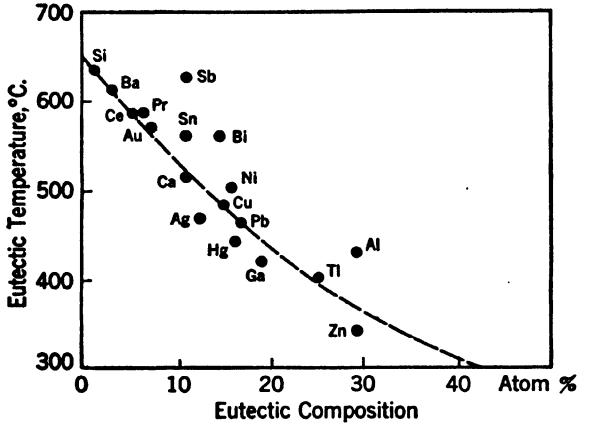

FIG. 7.6. Relationship between the eutectic temperature and eutectic composition for a number of binary alloys of magnesium.

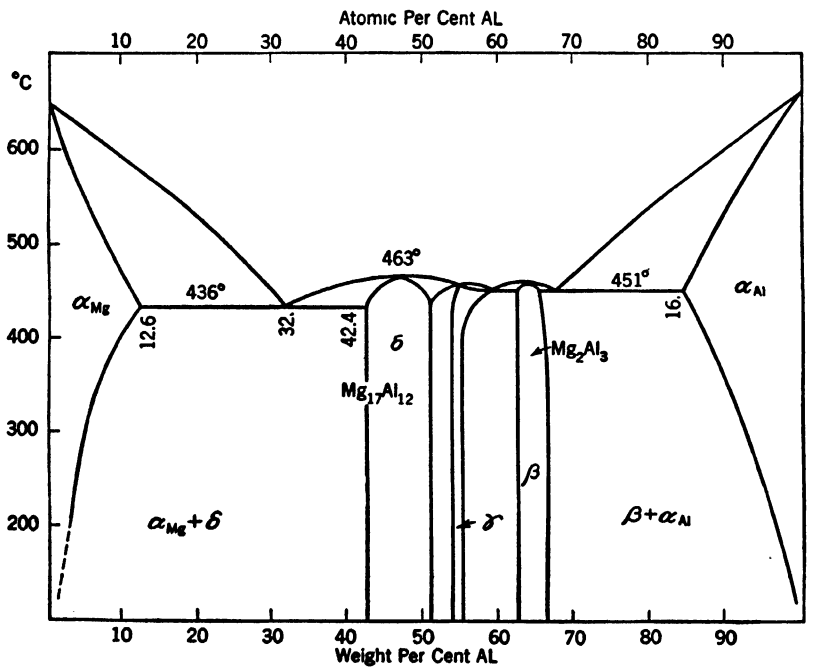

FIG. 7.7. Magnesium-aluminum phase diagram. The δ phase is also known as the compound $Mg_{17}Al_{12}$—a designation based on crystallographic evidence rather than composition since Mg_2Al_3 would be simpler and within the delta homogeneity field. The β phase is also sometimes called Mg_2Al_3.

necessarily, therefore, the eutectic melting points are moderately low. The eutectic structures, as shown by the lever rule, contain more compound than α solid solution and, since the compounds are brittle, alloys with a eutectic network are brittle. Also, in each case, the solid solution has a relatively high solute content at the eutectic temperature and

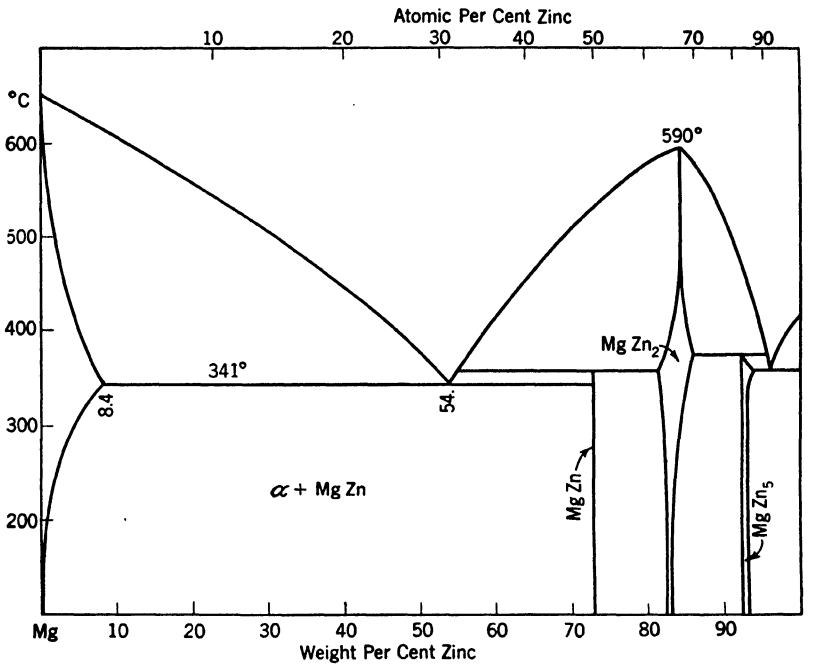

FIG. 7.8. Magnesium-zinc phase diagram. The three intermediate phases have narrow composition bands and are satisfactorily described by the compound designations MgZn, $MgZn_2$, and $MgZn_5$.

a decreasing solubility with decreasing temperature. Consequently, age-hardening possibilities exist.

Zinc and manganese are also frequently alloyed with magnesium and the binary Mg:Zn phase diagram is reproduced in Fig. 7.8. Again, a eutectic is found between a terminal solid solution and a brittle phase MgZn. Both the Mg:Zn and Mg:Mn systems show solid solubility decreasing with decrease in temperature.

Since the useful alloys contain appreciable concentrations of both aluminum and zinc, a ternary diagram is required to show the phasial conditions of these complex alloys. Not all data for the magnesium-

rich alloys of Mg:Al:Zn can be shown in a single diagram, but the change of solid solubility with temperature and the identity of the second phase in cast alloys, data of most value in the discussion of heat treatment and structures, are shown in Fig. 7.9 together with the

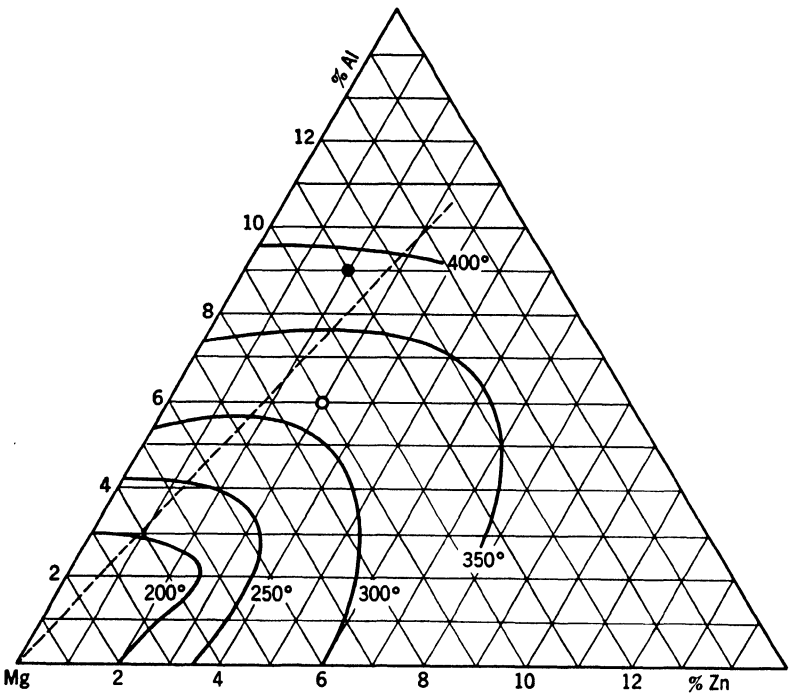

FIG. 7.9. Ternary section at the magnesium corner of the Mg:Al:Zn system with isothermals showing the solid solubility limits at the indicated temperatures (*Busk and Marande*). The dotted line separates structural fields in as-cast alloys. To the left, structures consist of the solid solution and massive $Mg_{17}Al_{12}$; this area includes Dow alloy C at the solid black circle. To the right of the dotted line, as-cast structures consist of the solid solution, massive $Mg_{17}Al_{12}$ and the ternary compound $Mg_3Zn_2Al_3$ as, for example, in Dow alloy H at the open circle composition.

compositions of two commercial sand-casting alloys.[1] Alloy C shows only the binary compound $Mg_{17}Al_{12}$ while alloy H shows in addition to this some ternary compound $Mg_3Zn_2Al_3$. The composition of the ternary compound is such that five Mg atoms in $Mg_{17}Al_{12}$ have been replaced by eight Zn atoms.

[1] Busk and Marande, *Trans. AIME*, **166**, 346, 1946. This paper gives other data on the ternary system, data of importance in the choice of specific ternary alloy compositions.

7.3 Microstructures of Magnesium Alloys

Magnesium is a soft metal, and most second-phase structures are relatively hard compounds. The usual precautions to avoid flow and relief effects during polishing must be observed. The customary technique[1] includes carrying through the No. 0 and 000 emery papers, then on a Vel-Chamee cloth with 600 alundum, and finally a similar rotating lap and cloth with levigated alumina in a soap solution.

Standard etches are as follows:

Macro etches: 10 sec to 2 min in 10% acetic or 10% tartaric acid in water.

Micro etches: For cast alloys, the "glycol" etch is preferred when applicable. When heat-treated castings or wrought structures are to be examined, the modified acetic-glycol etch is generally satisfactory. The phospho-Picral etch is useful because it darkens the magnesium solid-solution areas and, leaving other phases white, permits a quick estimate of the amount of undissolved compound in heat-treated alloys. The compositions of these etches are as follows:

Glycol etch: Ethylene glycol, 75 pt by volume
Conc. HNO_3, 1 pt by volume
Distilled water, 24 pt by volume

Acetic-glycol etch: Ethylene glycol, 60 pt by volume
Glacial acetic acid, 20 pt by volume
Conc. HNO_3, 1 pt by volume
Distilled water, 19 pt by volume

Phospho-Picral etch: Orthophosphoric acid, 0.7 cc (sp. gr. 1.7)
Picric acid, 4.0 g
Ethyl alcohol, 100 cc

Special etches have been newly developed[2] to show differences in aluminum content of the solid-solution magnesium phase, *e.g.*, concentration gradients associated with the solution of $Mg_{17}Al_{12}$ and subsequent diffusion of the aluminum atoms. Another etch makes it possible to distinguish between microshrinkage during casting and voids that originate from "burning" or partial fusion of the cast structure.

The beautiful photomicrographs in this section, illustrating the structures of the important cast and wrought alloys of magnesium, were contributed by P. F. George of the Dow Chemical Co.

[1] Hess and George, *Trans. ASM*, **31**, 423, 1943.
[2] George, *Trans. ASM*, **38**, 686, 1947.

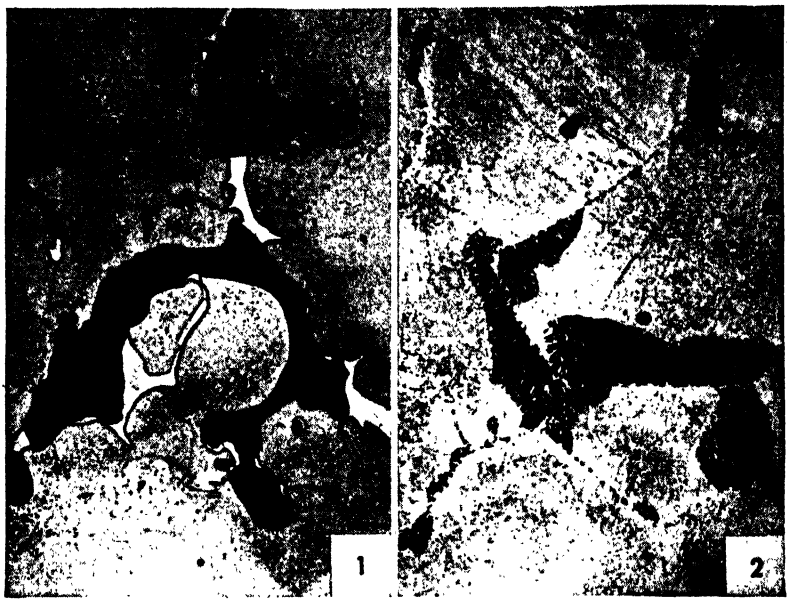

Micro. 7.1. Alloy H (6% Al, 3% Zn, 0.2% Mn) in the as-cast condition; etched with (*a*) 5% Picral (50 cc) and H_2O (50 cc), then (*b*) 1% HF, and (*c*) 5% Picral (10 cc) and H_2O (90 cc); ×500. The first etch slightly stained the hexagonal crystal of Mg_2Si and protected it from attack by the second etch. The HF then blackened the $Mg_{17}Al_{12}$ compound. The third etch then darkened the matrix leaving the ternary compound $Mg_3Al_2Zn_3$ clearly evident as the white constituent. The small lamellar particles in the matrix adjacent to the massive compound are $Mg_{17}Al_{12}$ particles that precipitated upon relatively slow cooling following solidification in the mold.

Micro. 7.2. Alloy H-HTA (6% Al, 3% Zn, 0.2% Mn) in the heat-treated and aged condition; etched with glycol reagent; ×500. After the solution heat treatment, the structure consisted of polygonal grains of the supersaturated magnesium solid solution with a few particles of rounded manganese compound (gray). Aging induced precipitation of two types: general, continuous precipitation of particles here not clearly resolved; the lamellar or pearlitic (see Chap. 9) discontinuous precipitate of $Mg_{17}Al_{12}$, which started at the solvent grain boundaries and progressed only a short distance.

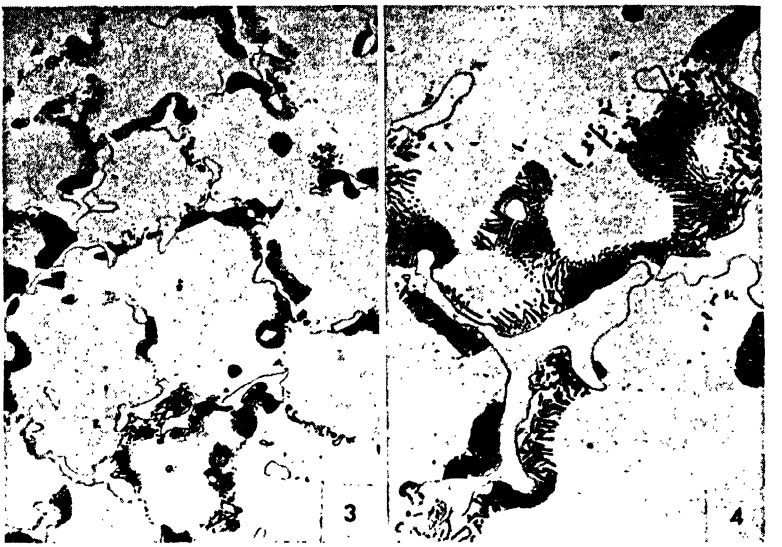

Micro. 7.3. Alloy C (9% Al, 2% Zn, 0.1% Mn) in the as-cast condition, glycol etch; ×250. The structure shows massive eutectiferous $Mg_{17}Al_{12}$ as the clearly outlined and more or less continuous network. The eutectic has "separated' '; *i.e.*, the α Mg phase of the eutectic is connected to and indistinguishable from the primary α Mg dendrites leaving massive compound. Slow cooling after solidification permitted precipitation of fine $Mg_{17}Al_{12}$ in lamellar form from the aluminum-rich (cored) α Mg near the compound. Note the absence of the ternary compound $Mg_3Al_2Zn_3$ in this alloy.

Micro. 7.4. Alloy C, same as in Micro. 7.3 but at a higher magnification; ×500. The small gray particle of manganese compound, the massive eutectiferous $Mg_{17}Al_{12}$ and the lamellar precipitate of this compound all show up more clearly here.

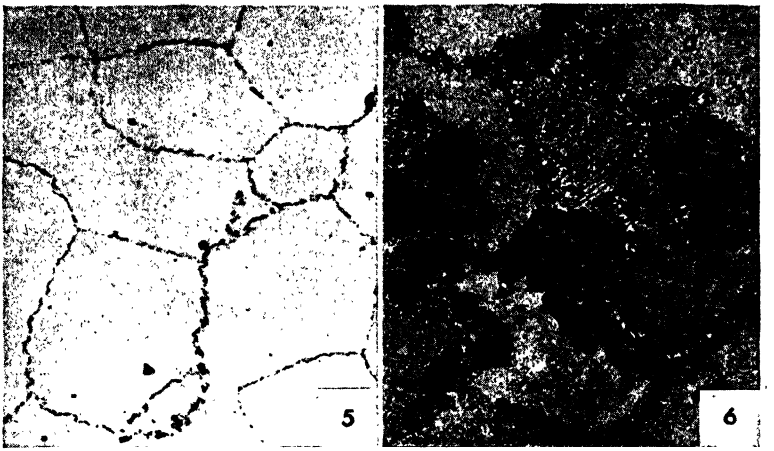

Micro. 7.5. Alloy C-HT (9% Al, 2% Zn, 0.1% Mn), cast and solution heat-treated; acetic-glycol etch; ×250. This is a typical solution-treated structure with all $Mg_{17}Al_{12}$ from the cast structure in solution. The casting was air-cooled from the solution temperature, and the wavy irregular grain boundaries are characteristic of this cooling rate. Probably localized precipitation occurs during cooling (see improvement possible by water quenching, page 199).

Micro. 7.6. Alloy C-HTA (9% Al, 2% Zn, 0.1%Mn) cast, heat-treated, and aged; etched with 5% Picral (100 cc) and H_2O (10 cc); ×250. The solution heat treatment dissolved all the $Mg_{17}Al_{12}$ compound without affecting the particles of manganese (outlined and gray in color). Aging has caused two types of precipitate: lamellar particles adjacent to grain boundaries and a very fine distribution within the matrix grains.

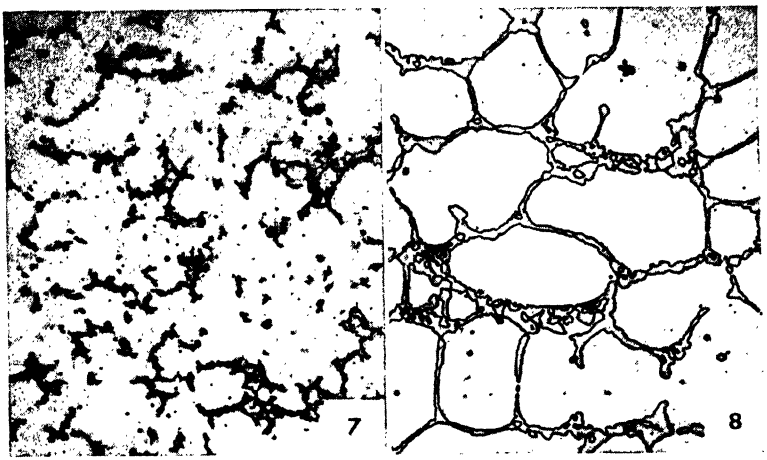

Micro. 7.7. Alloy R (9% Al, 0.6% Zn, 0.2% Mn) in the die-cast condition; etched with glycol reagent; ×500. This die-cast structure should be compared with Micro. 7.4, the somewhat similar C alloy sand-cast and also at ×500. The great refinement in $Mg_{17}Al_{12}$ eutectic particle size achieved by chill casting is self-evident. Rapid cooling also accounts for the absence, in this structure, of any precipitated $Mg_{17}Al_{12}$.

Micro. 7.8. Alloy EM62 (6.0% Ce or Misch metal, 2% Mn); in the as-cast condition, etched with acetic-glycol reagent; ×250. This newly developed alloy, important for its creep strength at elevated temperatures, owes its rigidity to the eutectic network where the second phase, Mg_9Ce, is continuous and resists solution or agglomeration except at temperatures close to the solidus.

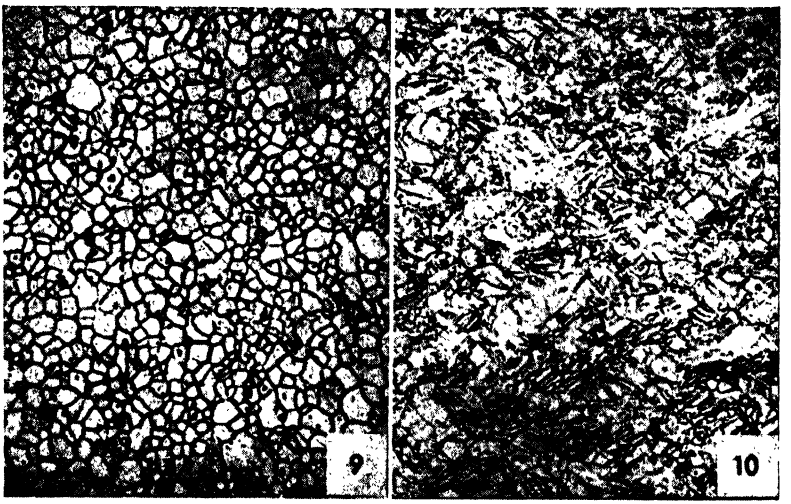

Micro. 7.9. Alloy FS-1a (3% Al, 1% Zn, 0.3% Mn) as annealed sheet; etched with 5% Picral (100 cc), H_2O (10 cc), and glacial acetic acid (5 cc); ×250. A slight color contrast between grains of the uniform solid solution is caused by orientation differences. The absence of mechanical twins is typical of wrought close-packed hexagonal metals after annealing.

Micro. 7.10. Alloy FS-1h (3% Al, 1% Zn, 0.3% Mn) as cold-rolled or hard sheet; same etch and magnification as Micro. 7.9. This view of the rolling plane, parallel to the sheet surface, shows the anticipated *apparently* larger grains (with abundant mechanical twins). A propensity for the twins in different grains to assume similar angles to the edge suggests preferred orientation of the sheet prior to cold-rolling.

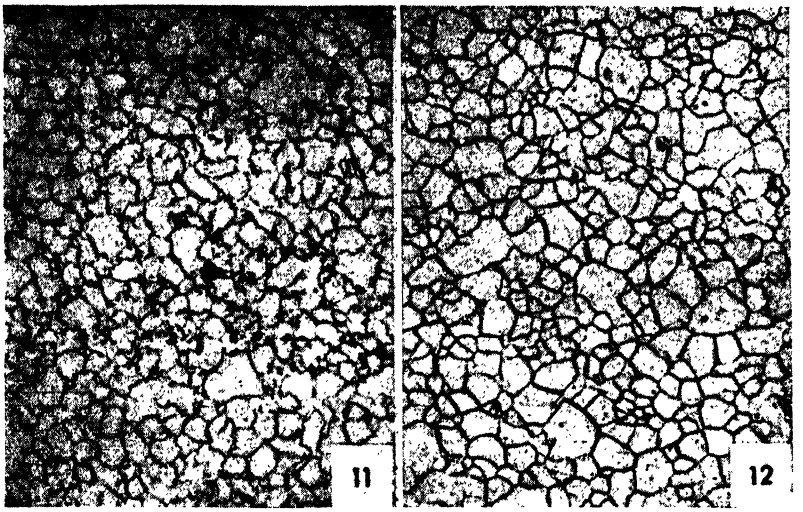

Micro. 7.11. Alloy J-1 (6% Al, 1% Zn, 0.2% Mn) in the extruded condition; acetic-glycol etch; ×250. The extruded alloy shows less precipitate "banding" from microsegregation and also, in this case, a finer grain size than the forged alloy. Like Micro. 7.6, the wavy grain boundaries are characteristic of air cooling from the solution (extrusion) temperature and are associated with localized precipitation.

Micro. 7.12. Alloy M-a (1.5% Mn) as annealed sheet; acetic-glycol etch; ×250. Uniform equiaxed grain characteristic of an annealed structure with some extremely fine precipitated particles of manganese compound.

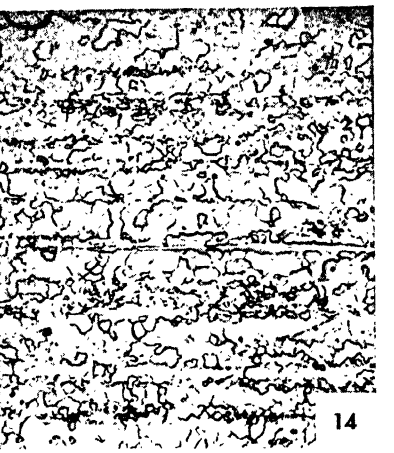

Micro. 7.13. Alloy O-1 (8.5% Al, 0.5% Zn, 0.2% Mn) as extruded and aged; glycol etch; ×250. The structure of this alloy, the strongest of the older standard alloys, is comparable with that of the similar cast alloy C-HTA. Lamellar $Mg_{17}Al_{12}$ has precipitated in most of the grains with one particle of manganese (gray) visible also.

Micro. 7.14. Alloy ZK-60 (6% Zn, 0.5% Zr) as extruded, etched with 5% Picral (100 cc), H_2O(10 cc), and glacial acetic acid (5 cc); ×250. This new zirconium alloy, combining the toughness of FS-1 or J-1 with a better strength than even O-1, has a fine-grained structure showing the flow direction. No second constituent can be definitely identified here.

7.4 Properties of Sand-cast Magnesium Alloys

Magnesium is a highly reactive metal under certain conditions, yet it can safely be melted in iron or graphite crucibles. Clays are unsatisfactory since the SiO_2 present is readily reduced with the silicon to form Mg_2Si as $4Mg + SiO_2 \rightarrow 2MgO + Mg_2Si$. Usually the primary producer markets alloys in the forms of ingots and "hardeners" made up to chemical specifications although the principal alloying elements, aluminum and zinc, have sufficiently low melting points to be conveniently added at the foundry in amounts needed.

The liquid metal should be protected from direct contact with the air. This can be done by sprinkling the metal with sulfur, forming heavy SO_2 gas above the charge, and also by adding a flux. Usually a refining flux[1] is added and stirred in the metal to remove oxide dross films. This flux has nearly the same density, when melted, as the liquid alloy and some settles to the bottom while some surrounds the sides and partly covers the top. A covering flux, somewhat lighter, is added for superheating the alloy (see page 202).

The reactivity of the metal causes reactions between the metal and water in the sand of "green" sand molds or oxygen in dry sand cores. These reactions result in blackening of the skin to an appreciable depth with local porosity and gray oxide powder effects, called *burning*. To avoid these defects which markedly reduce strength properties, the sands are mixed with addition agents such as sulfur, boric acid, ammonium silicofluoride, specifically known as *inhibitors*. For example 0.5% of boric acid and an equal amount of sulfur[2] in dry sand cores gives castings that are clean and bright on the surface and on fractured sections right up to the surface.

The two alloys most frequently used for sand castings are Dowmetal C and Dowmetal H,[3] both heat-treatable Mg:Al:Zn alloys containing a little manganese. Nominal compositions and typical properties (not specification minima) are given in Table 7.2. The heat treatments ordinarily employed to obtain these properties are shown in Table 7.1. The slightly lower solution treatment for alloy H results from the increased zinc content, which lowers the eutectic melting temperature.

Burning during heat treatment of magnesium alloys may occasionally

[1] Typical refining flux: 52.5% KCl + 40% $MgCl_2$ + 6% $BaCl_2$ + 1.5% CaF_2.
Typical covering flux: 34% KCl + 42% $MgCl_2$ + 14% CaF_2 + 10% MgO.

[2] Myers, *Trans. AIME*, **161**, 253, 1945.

[3] These are designations by the Dow Chemical Co., the major producer of primary magnesium; corresponding designations by the American Magnesium Corp., a large fabricator of magnesium alloys, are also shown in Table 7.2.

occur. It manifests itself in three ways: (1) surface exudations, (2) a gray-black powder on the surface, and (3) voids on the surface and in the interior.

The cause of burning may be too high a solution-treatment temperature, an effect comparable to burning of aluminum alloys. It may also

TABLE 7.1

	Dowmetal C (9% Al, 2% Zn)	Dowmetal H (6% Al, 3% Zn)
Solution treatment	2 hr, 260–410°C, hold 18 hr at 410°C	2 hr, 260–390°C, hold 10 hr at 390°C
Aging treatment	18 hr at 180°C	18 hr at 180°C

TABLE 7.2. TYPICAL PROPERTIES OF CAST-MAGNESIUM ALLOYS*

Specification		Condition	Compositon			Tensile strength, psi	Yield strength, psi	% elongation in in.	Rock. E
Dow Chem. Co.	Amer. Mag. Corp.		% Al	% Zn	% Mn				
C-AC	AM260-C	As-cast	9	2	>0.1	24,000	14,000	2	77
C-HT	AM260-T4	Solution treatment				40,000	16,000	10	75
C-HTA	AM260-T6	Solution quenched, aged				40,000	23,000	2	90
H-AC	AM265-C	As-cast	6	3	>0.15	29,000	14,000	6	59
H-HT	AM265-T4	Solution treatment				40,000	14,000	12	66
H-HTA	AM265-T6	Solution quenched, aged				40,000	19,000	5	83
M-AC	AM403	As-cast	..	..	1.5	14,000	4,500	5	3
R	AM263	Die-cast	9	0.7	>0.13	33,000	22,000	3	72
EM-6	.....	As-cast	6 Ce	..	.0	19,000	16,000	1	58

* Dowmetal Data Book, 1944.

be caused by too rapid a heating to the proper temperature; the microsegregation typical of the cast structures is then responsible. A third cause of burning may be the presence of water vapor in the surrounding atmosphere and the absence of sulfur dioxide.[1] Even 1% SO_2 has an inhibiting effect on the H_2O:Mg or H_2O:$Mg_3Al_2Zn_3$ reaction (in alloy H). For this reason, sulfur dioxide is customarily used as an atmosphere during solution heat treatment of magnesium alloys.

From the phase diagrams and previous microstructures, it is evident that these alloys have brittle, interdendritic, eutectiferous networks in

[1] Thomson, Burks, and Jominy, *Metal Progress*, **50**, 67, July, 1946.

the as-cast structure, which are eliminated by the solution treatment. Thus the solution-treated alloys, C-HT or H-HT, have far better ductility than the as-cast alloys, and at the same time the tensile strength is very considerably increased. The aging treatment does not affect tensile strength but notably increases yield strength, which, as earlier remarked, is the more important property in engineering design. The decrease in ductility that occurs on aging is related to heavy precipitation, but this treatment leaves the casting with sufficient ductility for most uses.

TABLE 7.3. EFFECT OF COOLING RATE FROM THE SOLUTION TREATMENT ON PROPERTIES OF SUBSEQUENTLY AGED SAND-CAST MAGNESIUM ALLOYS*

Cooling time, 410–190°C	Alloy C-HTA			Alloy H-HTA		
	Tensile strength, psi	Yield strength, psi	% elongation in 2 in.	Tensile strength, psi	Yield strength, psi	% elongation in 2 in.
190 sec (air cool)	40,000	24,100	2.0	40,000	19,200	5.0
65 sec (oil quench)	41,900	25,000	1.8	40,400	23,400	3.4
5.5. sec (water 90°C)	45,900	30,000	2.2	42,400	21,700	5.7
0.5 sec (cold-water spray)	48,200	29,900	3.5	45,100	21,600	7.3

* Busk and Anderson, *Trans. AIME*, **161**, 278, 1945.

The comparative properties of alloys C and H show that C has somewhat better yield strength and less ductility. However, the relative casting characteristics are also important in choosing between the two alloys. Since alloy C is less subject to microporosity (very fine pores rather uniformly distributed through the structure) and has generally a better castability, it is the more generally used alloy.

The solid solution obtained by the solution heat treatment is generally air-cooled to avoid distortion and cracking. However, it has been found that, as in the case of aluminum alloy 24S, more rapid cooling eliminates the tendency for grain-boundary precipitation, which occurs to some extent upon air cooling. The subsequent aging results in more uniform precipitation, less boundary concentration of the precipitant, and correspondingly better strength and ductility. These effects are shown by the data of Table 7.3.[1]

[1] Busk and Anderson, *Trans. AIME*, **161**, 278, 1945. Also Flanigan *et al.*, *Metals Technol., Tech. Pub.* **2282**, September, 1947.

Water quenching of the cast magnesium alloys may cause cracking if the alloy is quenched from within the hot-short range, *i.e.*, from too high a temperature, or if the water is too cold. The resulting thermal gradients give rise to cooling stresses of a high magnitude. Figure 7.10 shows the limits of the relationship of metal and water temperatures within which cracking may or will not occur. Quenched within these limits, the alloy will show residual stresses, but the subsequent aging treatment will reduce the macrostresses to a negligible value. After

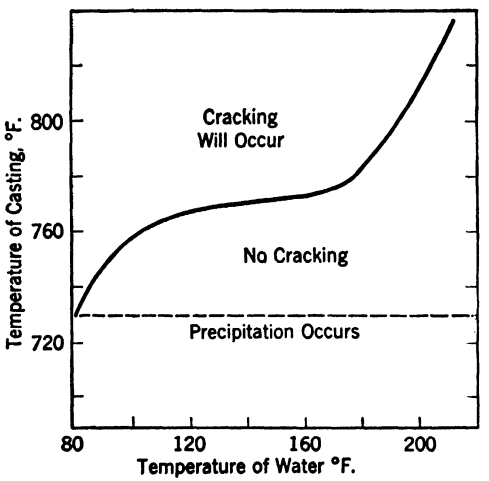

FIG. 7.10. The cracking tendency of Dow casting alloy C upon water quenching from the solution heat treatment as related to the temperature of the casting and of the quenching water. (*Busk and Anderson.*)

aging, as shown in Table 7.3, the properties are usually at least 10% better than those obtained with the usual air-cool and aging treatment.

Microporosity in magnesium castings has been troublesome in attempting to obtain maximum properties for aircraft use. The fairly uniformly distributed minute voids *may* be basically caused by shrinkage on solidification and inability to feed all sections of the metal. However, it is now certain that hydrogen dissolved in the liquid metal seriously increases microporosity[1] and leads to lowered tensile properties and leakage under pressure. The source of the hydrogen may be moisture in the air on humid days or moisture in the products of combustion of city gas during the melting. As in the case of aluminum, degassing can be accomplished by bubbling an insoluble gas through the liquid alloy. Helium and chlorine have been used, with chlorine

[1] Baker, *J. Inst. Metals* (London), **71**, 165, 1945. Busk and Bobalek, *Trans. AIME*, 1946. Burns, *Trans. AIME*, **166**, 328, 1946.

somewhat superior from a cost and rate standpoint. The formation of $MgCl_2$ permits chlorine to be added more rapidly, and this compound simultaneously removes MgO in a fluxing manner.

The effect of microporosity on properties of the Dowmetal C is shown by the graphs of Fig. 7.11, in which the porosity index is an arbitrary number assigned on the basis of radiographic data. It is clear why microporosity is regarded with disfavor, and attempts to minimize this condition are standard foundry procedures.

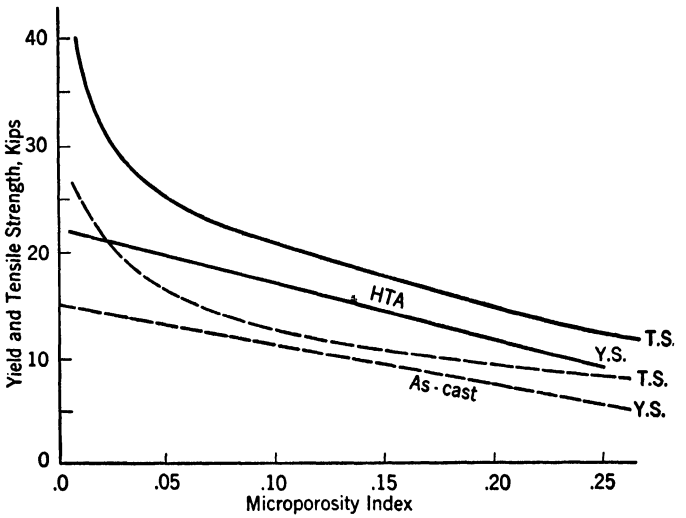

FIG. 7.11. Effect of microporosity on the yield and tensile strength of cast-magnesium alloy C in the as-cast condition (dashed lines) and the solution heat-treated and aged condition (HTA, solid lines). The microporosity index number is based on the density of radiographs made under standardized conditions. (*Burns.*)

A new cerium alloy, EM62 has poorer room-temperature properties than the standard casting alloys as is evident from the data of Table 7.2. However, the continuous eutectic network of Mg_9Ce, shown in Micro. 7.8, which does not dissolve at elevated temperatures, gives this alloy remarkably good strength at elevated temperatures, *e.g.*, 500°F, as is shown by the data of Fig. 7.12.

7.5 Grain Size Control of Cast Alloys

Magnesium alloys containing appreciable amounts of aluminum are customarily superheated in the liquid state before casting in order to obtain a very fine as-cast grain size. This is in direct contradiction to the generalization in Chap. 3, that overheating a liquid metal before

casting results in a coarser grain since all potential nuclei in the liquid are dissolved (assuming subsequent cooling to the same pouring temperature). Later, in Chap. 6, overheating of aluminum alloys was shown to be further undesirable because of hydrogen absorption by the liquid and the resulting gas porosity of the casting. Yet Mg:Al casting alloys after being heated several hundred degrees Fahrenheit above

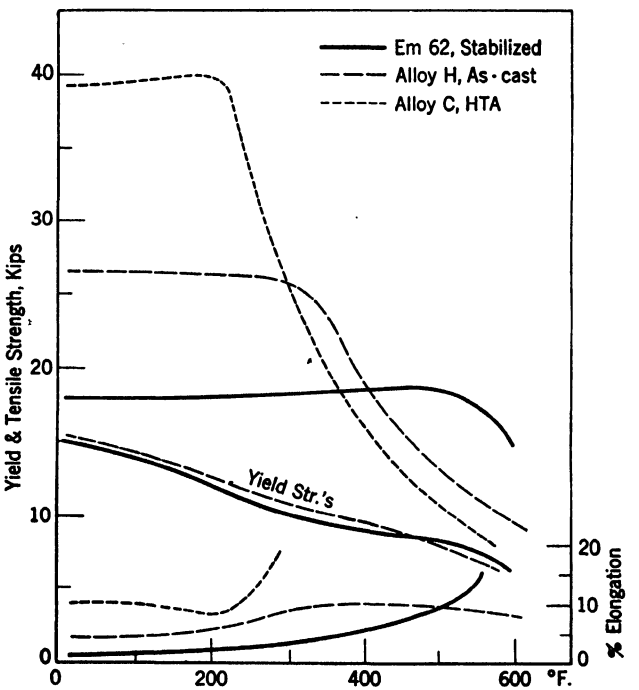

FIG. 7.12. Retention of strength at elevated temperatures, *e.g.*, 500°F, of the magnesium-cerium cast alloy EM62 as compared to the loss shown by standard casting alloys H and C; based on short-time tensile tests at elevated temperatures.

their melting points and then cooled to their proper pouring temperatures, show a much finer as-cast grain size than when just barely melted and cast.[1]

The usual procedure is to melt the alloy and, at about 730°C, refine by treating with a flux that is stirred with the metal to remove oxide dross films. Then a covering flux is added and the temperature raised to between 870 and 930°C. No holding time at this temperature is necessary beyond that required to equalize the temperature. The

[1] Pure magnesium and the alloy Dowmetal M containing only manganese are exceptions and do not show the superheating grain refinement.

liquid metal is cooled in the furnace pot to the proper pouring temperature of about 730°C, again held only to equalize the temperature, and the metal poured into the mold. The process of superheating is obviously expensive by reason of fuel costs, the long nonproductive time required for heating and cooling, and the decreased life of furnace refractories and melting pots.

Many researches,[1] instigated by the need of increased and more rapid production during the Second World War, have shown that other methods may be equally effective in achieving grain refinement of magnesium alloy castings. Some of these methods are as follows:

1. Vigorous stirring at 760°C (applicable only to small melts).
2. Bubbling acetylene, methane, propane, or carbon tetrachloride through the liquid at about 760°C.
3. Stirring into the melt about 0.003% carbon as graphite, lampblack, or aluminum carbide, Al_4C_3.

Metal refined by superheating loses most of its fine-grained characteristics upon remelting but, when refined by carbon additions, a good part of the effect is retained upon remelting scrapped parts of castings, etc.

Some of the voluminous data on this subject have been collected and are presented in Table 7.4. Parts *A* and *B* are not directly comparable. *A* represents tests on alloy from ordinary electrolytic magnesium, and *B* represents alloy made from special carbothermic metal. The data of part *A* under Heating show that heating this alloy from its melting point, about 610°C, up to 800°C and *casting from the actual temperature* results in the expected coarser grains, but that heating from 800 up to 900°C gives a pronounced grain refinement. When cast from varying temperatures on the cooling cycle, the data under Cooling show that some of the grain refinement effect is lost. However, it would usually be impracticable to pour the metal from the superheat temperature into the mold. Also in part *A* are data showing the effects of stirring in carbon. Here superheating also shows some grain refinement, but the superheat temperature is much lower, only 800°C. The data of part *B* show that longer holding at near the usual refining temperature of only 750°C will give grain refinement if the metal already contains some carbon. Presumably similar effects would be found if carbon were added instead of being present from the production process. *B* also shows very clearly the effect of the type of mold. It is evident that castings made in permanent molds of iron or in steel dies would not require superheating of the metal to the same degree as sand castings.

[1] Papers by Hultgren, Mitchell, and York, by Hultgren and Mitchell, and by Mahoney, Tarr, and LeGrand appear in *Trans. AIME*, **161**, 315–348, 1945.

The fact that grain refinement by superheating or carbon additions is possible only in aluminum-bearing alloys such as C or H makes it seem probable that Al_4C_3 is the responsible nucleating agent in heats

TABLE 7.4. GRAIN REFINEMENT OF MAGNESIUM ALLOY C BY SUPERHEATING

A. Ordinary Electrolytic Magnesium Cast from Specified Temperature

Casting temp. °C	Time at temperature, min	Grains per sq mm*			
		Superheated melts		Carbon-treated melts	
		Heating	Cooling	Heating	Cooling
650	5	40	↑ 110	130	↑ 110
700	5	16	130	90	130
750	5	8	160	100	160
800	5	6	190	↓ 180	180
850	5	16	225		
900	5	200 ↓	200		

* All cast in permanent mold. Data by Mahoney, Tarr, and LeGrand, *Trans. AIME*, **161**, 315–348, 1945.

B. Carbothermic Magnesium Contains Some Carbon from Production Process

Temp., °C	Time, min	Grains per sq mm†		Super temp., °C	Heat time, min	Grains per sq mm‡	
		Cast-iron mold	Sand mold			Thin section	Thick section
760	2	94	8	700	30	40	32
760	60	615	105	700	180	25	18
815	15	455	157	750	30	35	30
870	2	402	153	750	180	75	72
930	1	320	131	800	30	50	40
980	1	360	91	800	180	98	75
				850	5	285	270
				850	180	292	265
				900	30	240	224
				980	30	95	80

† Data by Hultgren, Mitchell, and York, *Trans. AIME*, **161**, 315–348, 1945. The cast-iron mold was at 180°C, the sand mold at room temperature.

‡ Data by Tiner, *Trans. AIME*, **166**, 242, 1946.

where carbon is present. Presumably the carbide is slightly soluble in the liquid and, since a critical dispersion is required, slight superheating or longer holding is required to dissolve coarser Al_4C_3 particles while too high a temperature dissolves most or all of them. The basis of the

effect of just superheating of the electrolytic metal, presumably carbon-free, relates to the effect of high temperatures on Mn:Al compounds that are present in the liquid alloy. Nelson[1] shows that, in the grain-refinement temperature range, $MnAl_4$ is present and has the proper close-packed hexagonal structure to act as a nucleating agent.

The property effects of grain size for the two casting alloys are given by the data of Table 7.5. The range of grain sizes is what might be encountered under usual casting conditions. The data show the decidedly detrimental effect of coarser grains, but much greater effects can be observed if extreme grain growth occurs upon heat treatment. In the latter case, grains may grow to be from 3 to 15 mm in diameter

TABLE 7.5. EFFECT OF GRAIN SIZE ON THE TENSILE PROPERTIES OF HEAT-TREATED AND AGED MAGNESIUM-ALLOY CASTINGS*

Aver. grain diam., mm	Alloy C-HTA			Alloy H-HT		
	Tensile strength, psi	Yield strength, psi	% elongation in 2 in.	Tensile strength, psi	Yield strength, psi	% elongation in 2 in.
0.08	40,900	25,100	1.5	40,400	22,100	4.9
0.15	37,200	24,000	1.6	38,000	18,500	5.2
0.32	35,000	23,400	2.6	36,800	18,000	4.2
0.60	32,000	21,900	0.9	33,300	18,000	4.0

* Busk and Phillips, *Trans. AIME*, **161**, 266, 1945.

and, in these cases, the tensile strength will decrease to about 20,000 to 25,000 psi.

The addition of about 0.05% Be to magnesium or its alloys decreases the combustibility of the alloy in the liquid state. This very desirable property, which makes alloys containing beryllium safer to work with, is offset somewhat by the tendency of cast alloys containing beryllium to show a coarse grain size. This detrimental effect may in turn be eliminated by the addition of a small amount (0.05%) of zirconium, through use of a zirconium chloride flux. The zirconium addition is not effective for all magnesium alloys but is successful in the case of the C alloy. The advantages of beryllium additions are at present insufficient to justify the greater cost of alloys containing even the small quantity of 0.05%.

[1] Nelson, Hoyt Memorial Lecture; *Trans. AFS*, **56**, 1, 1948.

7.6 Properties of Wrought-magnesium Alloys

There are five alloys of magnesium that are produced in wrought forms. Alloys with the suffix -1 are made from high-purity magnesium and contain not more than 0.05% Cu, 0.005% Ni, 0.005% Fe, and a total of less than 0.3% of other impurities.

Designation		Analysis			Forms available
Dow Chem. Co.	Amer. Mag. Corp.	% Al	% Zn	% Mn	
FS-1	AMC52S	3.0	1.0	0.3	Extrusions, plate, sheet
J-1	AMC57S	6.5	1.0	0.2	Extrusions, forgings, sheet
M	AM3S	...	...	1.5	Extrusions, forgings, plate, sheet
O-1	AMC58S	8.5	0.5	0.2	Extrusions, forgings
ZK-60	.....	...	5.0	(0.7 Zr)	Extrusions

Typical mechanical properties of the first four alloys, extruded in rod form, are given in Table 7.6. Of these alloys, only O-1, with the highest aluminum content, shows an age-hardening response upon heat treatment. Since the extrusion process is carried out at approximately the solution heat treatment temperature and the extruded shape cools in air fairly quickly, it is usually necessary only to age the alloy after extrusion. The same is generally true of forgings and other wrought forms although, if hot-working is carried out at too low a temperature, the regular solution heat treatment may be employed prior to aging. The aging treatment does not markedly affect the properties listed in Table 7.6, but it is effective in increasing the creep strength of the alloy at elevated temperatures.

In the discussion of wrought alloys of magnesium, the close-packed hexagonal structure of the metal becomes significant. Cold-working of the alloy is possible to a rather limited extent. By slow and repeated deformations, more extensive total cold-working has been reported at room temperatures, probably because of reorientation of crystals and mechanical twinning, but it is not possible to double the strength of annealed magnesium sheet by 50% cold reduction as is the case with most metals. In magnesium, the chief benefit is in increased yield strength.

At elevated temperatures, slip planes other than the basal plane become active, and most of the alloys in sheet form can readily be drawn into complex or deep shapes if the metal is deformed at about

200°C. In this case, the properties of the metal are little affected. Forging is performed at a higher temperature, about 300 to 400°C, starting with extruded bar stock and forging slowly by presses rather than hammers.

TABLE 7.6. TYPICAL MECHANICAL PROPERTIES OF WROUGHT-MAGNESIUM ALLOYS

Alloy	Form	Tensile strength, psi	Yield strength, psi	% elongation in 2 in.	Rock.E hardness	Electrical resistivity, microhm per cm	Notch bend strength, in.-lb
FS-1	Extruded	40,000	30,000	15	57		
FS-1a	Annealed sheet	37,000	22,000	21	67	10	15.3
FS-1h	Hard-rolled sheet	43,000	33,000	11	83		
J-1	Extruded	45,000	32,000	15	70		
J-1a	Annealed sheet	43,000	26,000	16	70	12.5	15.6
J-1h	Hard-rolled sheet	47,000	34,000	9	83		
M	Sand-cast	14,000	4,500	5	3		
M	Extruded	38,000	26,000	10	41		
M-a	Annealed sheet	33,000	15,000	17	55	5.7	
M-h	Hard-rolled sheet	37,000	29,000	8	67		
O-1	Extruded	49,000	33,000	11	77		
O-1A	Extruded and aged	50,000	34,000	7	87	14.5	3.1
ZK-60*	Extruded and aged	49,000	40,000	9.5	..	....	15.0

* New alloy of 5% Zn and 0.7% Zr. Doan and Ansel, *Trans. AIME*, **171**, 286, 1947.

Included in Table 7.6 are data on a new alloy of magnesium containing no aluminum but about 5% Zn and 0.7% Zr. This alloy may supplant O-1 as the high-strength alloy since it has a higher yield strength plus a much greater resistance to notch brittleness with toughness equal to that of the lower strength alloys FS-1 and J-1. The superior properties of the new alloy are accompanied by a greater cost, which somewhat limits its application.

The cerium-type alloy, EM62 (6% Ce, 2% Mn) may also be produced in wrought form with the cerium content reduced. Again, the advan-

tage is in high temperature strength. The creep rates for this type alloy are of a new order of magnitude. For example, the regular high-strength alloy O-1, HTA creeps at a rate of 0.7% in 1,000 hr under 4,000 psi stress at 300°F, while forged alloy EM22 (2% Ce, 2% Mn) creeps only 0.3% in 1,000 hr at 20,000 psi stress—less than half the rate at five times the stress. The same remarkable high-temperature strength of this alloy is shown by the stress-rupture data of Fig. 7.13.

Forgings may be directly compared to castings in the case of the binary Mg:Mn alloy, M (see Table 7.6). This alloy is utilized occa-

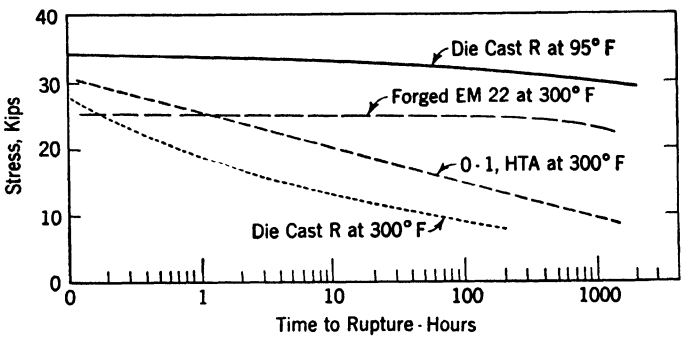

FIG. 7.13. Stress-rupture data showing the exceptional high-temperature (300°F) strength of a new Mg, EM22, (2% Ce, 2% Mn alloy) as compared to the standard strong magnesium-forging alloy, O-1 HTA, and die-casting alloy R.

sionally in cast form because of its superior weldability, but it is obvious that at room temperatures the wrought structure is more than 2½ times as strong and also considerably more ductile.

7.7 General Characteristics of Magnesium Alloys

1. Corrosion Resistance. The first important uses of metallic magnesium were in the field of pyrotechnics and for chemical reagents, such as the Grignard reagent, used in the synthesis of organic compounds. These applications take advantage of the chemical activity of the finely divided metal. With the introduction of alloys having favorable weight-strength ratios, serious problems regarding the stability of the material arose. From the standpoint of corrosion resistance to ordinary outdoor atmospheres, substantial improvement over the earlier alloys has been attained by the use of higher purity magnesium and by modifications of foundry practice, particularly with respect to fluxing treatments. Unfortunately, many of the earlier tests of magnesium products were made by subjecting the material to the direct action of

salt-water solutions or salt-bearing atmospheres—tests that had little significance for most normal usages of the alloys. Although the better commercial alloys are reasonably stable under inland atmospheres, unless it is definitely known that the exposure conditions are not unfavorable, it is well to protect the metal with a paint system. Seacoast locations involving direct contact with salt products are definitely corrosive to magnesium alloys. If used under such conditions, the metal should be adequately protected by one of the modern finishes, such as a chrome pickle followed by an elaborate paint schedule. However, adequate protection lasts only as long as the protective coating is maintained, and for this reason magnesium alloys are not generally recommended for applications involving contact with salt water.

2. Formability. The crystal structure that limits the cold forming of magnesium allows the attainment of excellent plasticity at slightly elevated temperatures. Hanawalt[1] cites some shapes which are made in one draw from magnesium alloy sheet but which would require two draws if made of steel or aluminum.

3. Notch Sensitivity. The strength properties of magnesium alloys, both wrought and cast forms, may be impaired by notches or sharp discontinuities that serve as stress raisers. Some values for notch bend strength are given in Table 7.6. The marked notch sensitivity of these alloys calls for particular care in the design of stressed parts to avoid abrupt changes in cross section, to provide ample fillets of smooth curvatures, etc. Stressed magnesium parts may be also dangerously weakened by faulty machining operations that produce notch effects.

4. Modulus of Elasticity. The tensile elastic modulus for magnesium is 6,500,000 psi as compared to 10,300,000 for aluminum alloys and 29,000,000 for steel. Thus for the same dimensions, an elastically stressed magnesium alloy will deflect over four times as much as steel and 50% more than aluminum. Since the relative densities are 1.8, 2.8, and 7.9, equal *weights* of the three materials would show magnesium to be the stiffest while steel would show the greatest deflection. The extreme lightness of the metal, therefore, more than compensates for its low modulus. Many structures of magnesium, if made to the same weight as a comparable aluminum alloy, may be sufficiently bulkier or thicker to avoid the use of stiffening ribs or members, thus simplifying design and lowering fabrication or assembly costs.

5. Machinability. The low plasticity, particularly local, of the metal at room temperatures makes this metal the most machinable of all. It can be cut at high speeds to a beautiful finish with little tool

[1] Hanawalt, *Metal Progress*, **49**, 548, 739, 1946.

heating or wear. One large firm lists machining costs of aluminum castings as 25% higher, bronze castings 35% higher, and iron castings 50% higher than for magnesium castings.[1] The combustibility of magnesium dust and chips constitutes a hazard that can be eliminated by proper safety precautions: washing fine cuttings away continually, collecting and disposing of dust, etc.

6. Weldability. Alloys of magnesium can be readily fusion-welded with a gas torch, by the use of a filler rod of the same composition as the alloy being welded. A chloride flux must be employed. This means that *welding is confined to joints that can be thoroughly cleaned of flux afterward.* The alloy can also be arc-welded with a tungsten electrode, a filler rod, and a neutral gas such as dry helium. The gas protects the weld metal from oxidation, and thus no flux and subsequent cleaning are required. With this so-called *heli-arc* welding, all welding operations used for steel welding can be performed on magnesium alloys. The usual welding problems of residual stresses and the tendency for certain alloys to be hot short can be overcome by care, preheating, and post-heating for stress relief.

7. Cost. Magnesium in alloyed form costs more per pound than its chief industrial competitors, steel, aluminum, and copper. It cannot compete with other metals except when one or more of its most important characteristics can be employed to advantage, but at those times, it may be cheaper than a competitive metal. Hanawalt cites an aircraft stabilizer, which when made of aluminum alloy weighed 60 lb and cost $40 for material and $191 for labor. Fabricated in magnesium with a simpler and bulkier design of the same weight, the stabilizer cost $60 for material but only $78 for labor. Relative total costs may not usually be so favorable to magnesium, but there undoubtedly are many as yet undeveloped engineering applications where a magnesium alloy will be uniquely suitable and cheaper from an over-all cost standpoint.

QUESTIONS

Group A

1. Calculate the tensile and yield trengths of a round test bar of Dow alloy C-HTA whose cross-section area was such that its weight per unit length was identical to that of the comparable cast aluminum alloy Alcoa 195-T. Which alloy, C-HTA or 195-T, is stronger?

2. Make the same calculation and comparison as in question 1 for the strongest wrought alloys of aluminum, 75S-T, and of magnesium, 0-1a.

3. Why is it that wrought magnesium alloys, particularly sheet, are produced from high-purity magnesium whereas cast alloys are made up with ordinary electrolytic metal?

[1] Hanawalt, *Ibid.*

4. Flux inclusions in magnesium castings are very detrimental. Explain why.

5. Explain why, if a magnesium alloy is attached to another metal, *e.g.*, copper, it should be electrically insulated from that metal.

Group B

1. Explain in fundamental terms why magnesium alloy parts require more generous fillets at angles than do comparable aluminum alloy parts.

2. Would wrought-magnesium alloys be expected to show greater or less directionality of properties than wrought-aluminum or copper alloys?

3. Discuss the probable reasons why M alloy castings are more weldable than C alloy castings.

4. When magnesium alloy parts are joined by riveting, aluminum alloy rivets are almost always used. Discuss the reasons for the choice of aluminum rather than magnesium or copper alloys.

CHAPTER 8

PHASE TRANSFORMATIONS: TWO-PHASE COPPER ALLOYS

Copper-zinc alloys or brasses containing up to about 35% Zn are one-phase solid solutions whose structural and property characteristics were described in Chaps. 3 and 4. The phase transformations occurring with temperature changes in brasses of higher zinc content are of industrial importance in their own right but they introduce the subject of transformations in the solid state, which are of fundamental significance in studies of the structural features of steels. Only the Cu:Zn system will be treated in detail, but the principles governing these alloys may be applied to structural studies of Cu:Sn bronzes or other copper-base alloys.

8.1 Cu:Zn Phase Diagram

The solid solubility of zinc in copper follows a course opposite to that shown by age-hardening alloys; it increases with decreasing temperatures from 32.5% at 905°C to about 38% at 453°C (see Fig. 8.1). There is some recent, but inconclusive, evidence that it changes course and decreases below this temperature, but since there is no evidence of age-hardening in 38% zinc brasses after quenching from 450°C (except in "recovery" anneals of unstable, cold-worked alloys, see page 103), the solubility limit has been indicated by a dashed line in the low-temperature range. The line on the phase diagram showing this solubility limit as a function of temperature is approximately paralleled by another line showing the solubility limit of a solid phase labeled β above 453°C and β' below this temperature. Between the uniform α solid solution and the β solid solution, there is a field of mixed α and β phases.

The horizontal line bisecting the $\alpha + \beta$ field at 453°C is dotted to indicate that it is not related to a true phase change and thus need not conform to the phase rule generalization (page 115) of three phases existing in equilibrium at constant temperature. At this temperature, β becomes unstable and changes to β'. The latter phase has a crystal structure identical to that of its parent, β, a body-centered solid solution, but whereas above 453°C zinc and copper atoms are dispersed at random

on points of the lattice, below 453°C the copper and zinc atoms tend to occupy specific, fixed positions relative to each other, *e.g.*, copper atoms at the corners of the unit cubes, zinc atoms at their centers. The latter condition is termed an *ordered* solid solution (see page 73). The ordered structure is one of smaller free energy and, therefore, of greater stability

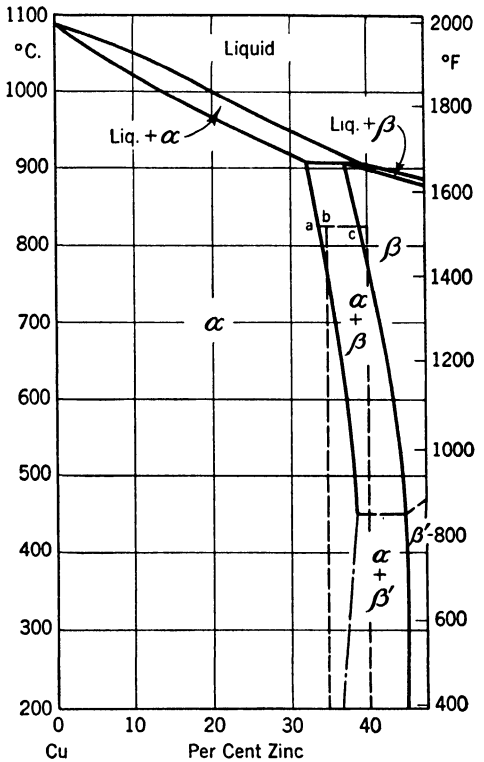

FIG. 8.1. Phase diagram of the Cu : Zn system, from 0 to 50% Zn.

and, in this case, has considerably different properties from the equivalent "random" solid solution, particularly, much less plasticity.

In liquid alloys containing from 32.5 to 38.5% zinc, the β phase originates at 905°C with a composition of 37% zinc, as a result of a reaction between α (32.5% Zn) and liquid (38.5% Zn) written in the form α + liquid $\rightleftarrows \beta$. It is called a *peritectic*, from the Greek form *peri* which means "around," since, during the reaction, α crystallites will be surrounded by the reaction product, β, which in turn is surrounded by liquid. It is very unusual, however, for a peritectic structure to be visible in the microstructure as such. Consequently, it does not rank

in industrial importance with the eutectic. Alloys containing from 50 to 95% zinc contain other phases resulting from peritectic reactions, but these brittle structures are not useful industrially. For this reason only half of the Cu:Zn phase diagram, from 0 to 50% zinc, has been reproduced.

An alloy of 65% Cu:35% Zn, under equilibrium conditions, consists of homogeneous grains of α up to about 780°C. Upon heating above this temperature, the alloy enters the two-phase field, $\alpha + \beta$, which means that β crystals of a higher zinc content (about 39% Zn) form with a corresponding decrease in zinc content of the remaining α. On heating to increasingly higher temperatures, the amount of α decreases and that of β increases, as may be quantitatively estimated by use of the lever rule (see page 59). At the same time, the concentration of zinc in both phases changes in accordance with the slope of the phase boundary limits. At 905°C, some α remains

$$\%\,\alpha = \frac{37 - 35}{37 - 32.5}\,(100) = 44\%;\ +\ 56\%\ \beta$$

and, by supplying additional heat, the peritectic decomposition of the β forms more α and some liquid,

$$\%\,\alpha = \frac{38.5 - 35}{38.5 - 32.5}\,(100) = 58\%;\ +\ 42\%\ \text{liquid}$$

All these changes are reversible under equilibrium conditions as approached by very slow cooling.

The 60% Cu:40% Zn alloy contains some β (or β') at all temperatures; at room temperatures, this amounts to about $[(40 - 38)/(45.5 - 38)]$ (100) or 26%, but on heating above 453°C the proportion of β increases while that of α decreases and the zinc concentration in both phases decreases. At about 780°C, the alloy enters the single β phase field, and it will remain a completely β structure up to the temperature of the solidus line where melting begins in the manner previously described as "burning." Again, these changes are reversible under equilibrium conditions of cooling, or the nearest approach to that almost unattainable state. It is unattainable during a cooling cycle because the diagram requires that, under equilibrium conditions, both the relative amounts of α and β and, simultaneously, their composition (or zinc contents) shall change. This requirement means that zinc and copper atoms must travel continually through the lattice (in opposite directions), not merely at the boundaries

of the two phases but through each large crystallite in order to maintain homogeneity of the phases. The metastable position of the solidus line (page 58) encountered in the simple solid-solution diagram has already been described as originating from incomplete diffusion, or atomic interchange, between two elements in a single phase. In a similar manner, the boundaries of the $\alpha + \beta$ field are subject to displacement to the left under ordinary cooling conditions. Thus the 60:40 alloy, after cooling in air to room temperature, may show considerably more than the calculated 26% of the β' phase. In addition, an alloy of 67.5% Cu:32.5% Zn, which according to the diagram should show no β', will probably contain some on air-cooling relatively small sections.

Since normal cooling rates tend to result in metastable positions of the phase field boundaries of the diagram, very fast cooling rates, by preventing diffusion, may make them appear vertical; *i.e.*, the equilibrium structural condition for a high temperature may be at least partially preserved, by quenching, for observation at room temperature.

An alloy of 62.5% Cu:37.5% Zn is of particular interest in that, under equilibrium conditions, it has a completely β structure at 900°C, and a uniform α structure below about 500°C. Upon extremely slow cooling from 900°C, it will gradually transform to α on passing through the $\alpha + \beta$ field, and this transformation will be of a diffusion type, *i.e.*, accompanied by continual changes in the zinc concentration of the α and β phases. On more rapid cooling to room temperature, there will be some residual β (or β') in a metastable condition, and the amount of β will increase with increase in cooling rate. However, an extremely drastic quench from 900°C into an iced brine solution results in an entirely different structure. There is no opportunity for the time-consuming diffusion type of α formation in the temperature range 900 to 500°C, but the unstability of β at the low temperature causes it to transform at about −14°C to a face-centered structure similar to α but differing in that one edge of the cube is longer than the other two. It is then called a *face-centered tetragonal* structure. The high-temperature β and the room-temperature α are of the same composition, and the change from body-centered cubic β to face-centered cubic α requires only a slight contraction of the lattice in two directions and an expansion in the third. If the dimensional readjustment is incomplete (because of lattice rigidity at low temperatures), the intermediate, unstable tetragonal lattice is found.

The atomic adjustments required may be visualized by reference to Fig. 8.2 showing four unit body-centered cubic cells, *i.e.*, four cells of the β structure, drawn in light lines. The face diagonal of each cube

on the top and bottom of the structure, with connecting vertical lines, will be found to outline a tetragonal structure where the length of the side of the base (face diagonal of the cube) is $\sqrt{2}$ times the height of the tetragon. Furthermore, the body-centered atoms of each of the four β cubes may also be considered as centered in the four side faces of the tetragon, while the top and bottom shared corner atoms of the cubes may be considered as centered in the top and bottom faces of the tetragon. (The atoms that make up the tetragonal structure are shown with black centers.) Thus a body-centered cubic structure may be

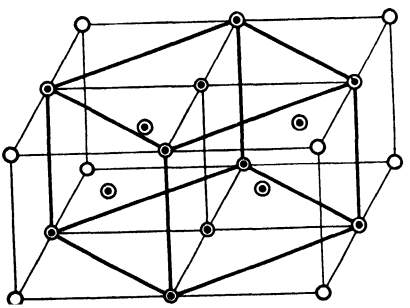

FIG. 8.2. Four unit cells of the body-centered cubic structure β with specific atoms marked with black centers to indicate the structure might also be considered as face-centered tetragonal.

considered as a face-centered tetragonal structure. It is merely customary to designate it by its more symmetrical form (see page 29).

The diffusionless transformation of the 62.5:37.5 brass is of no commercial importance since the requirement of heating to within a few degrees of the melting point gives very coarse grains, and the drastic quench required can be obtained only for relatively thin metal sections. However, the structure and its origin are quite similar to the martensitic structure of steels (page 270), which is of paramount industrial importance.

8.2 Cu:Sn Alloy System

Tin bronze is one of the oldest alloys used by man. Many commercial wrought bronzes are essentially single-phase alloys containing about 5% Sn in solid solution. A study of the phase diagram shown in Fig. 8.3 indicates that even these wrought 5% Sn bronzes should show two phases at ordinary temperatures, α plus precipitated ϵ or Cu_3Sn. Presumably, the temperature at which the α becomes unstable and tends

to precipitate Cu_3Sn, 300°C for the 5% alloy, is so low that the precipitate does not form, at least in visible size. This precipitation hardening potentiality may well be an explanation of the high strength properties of cold-worked tin bronzes. Deformation would presumably accelerate precipitation in the metastable, supersaturated α matrix.

Most cast binary tin bronzes contain approximately 10% Sn. According to the phase diagram, a 90% Cu:10% Sn alloy should solidify

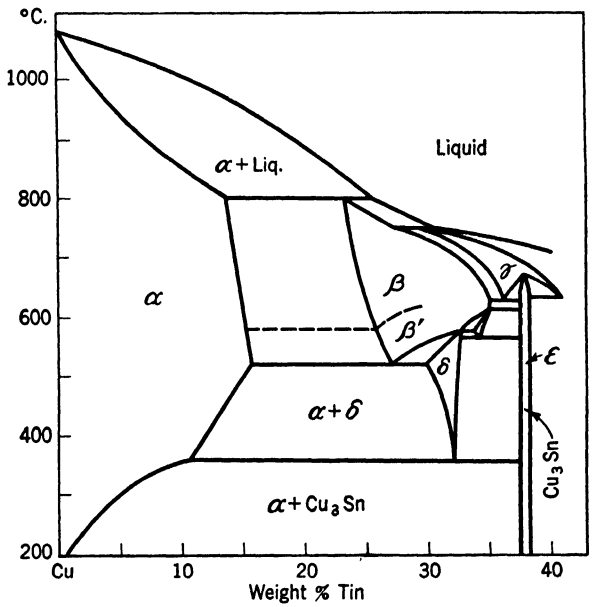

FIG. 8.3. Phase diagram of the Cu:Sn system up to 40% Sn. The ϵ phase is also called Cu_3Sn, with an electron: atom ratio of 7:4.

as a single-phase alloy and remain unchanged to just below 360°C where, again, a supersaturated condition would be developed with the tendency for precipitation of Cu_3Sn limited or suppressed by the low diffusion rate at these temperatures. This theoretical structure, all α for the 10% Sn alloy, is practically never observed because the alloy almost never solidifies under equilibrium conditions. Coring during dendritic solidification of α results in a metastable solidus (see page 58) placed to the left and under the equilibrium solidus. Therefore, at 798°C some interdendritic liquid remains, and this peritectically reacts with α to form interdendritic β, *viz*, α + liquid $\rightarrow \beta$.

The phase diagram for the higher tin-content alloys, 15 to 37% Sn, is quite complicated, but a discussion of what happens to the β on cooling

below 798°C requires a brief discussion of this part of the diagram.

During cooling from 798 to 520°C, the changes are similar to those for high brasses: β diminishes in quantity as part of it changes to α; simultaneously the β becomes richer in tin. These changes are predicted by the slope of the lines separating the α:$\alpha + \beta$:β phase fields. At 580°C, the β changes to β', an internal ordering of copper and tin atoms.[1] Thus far, the changes are exactly analogous to those described earlier for the Cu:Zn system.

At 520°C, the β' phase disappears completely, undergoing the reaction $\beta' \rightarrow \alpha + \delta$. The two sloping lines from above converge to meet the horizontal line at a composition of 26.8% Sn. This construction is identical to that of the eutectic discussed in Chap. 5, the only difference being that there is a solid phase above the horizontal rather than a liquid. Transformations of this type, called *eutectoids*, will be covered in detail in Chaps. 9 and 10. At the moment, discussion will be limited to pointing out that cooling through 520°C results in the disappearance of β with an increase in the amount of α already present in the 10% Sn alloy postulated at the start, and the appearance of a new phase of higher tin content called δ, which is a brittle compound, of composition equivalent to $Cu_{31}Sn_8$.[2] This compound is still mechanically distributed in the structure, of necessity, in the interdendritic spaces where β was originally formed peritectically.

As the alloy cools from 520 to 360°C, the α should change in composition, becoming lower in tin content, while the δ phase becomes richer in tin. These changes, predicted by the slopes of the boundaries of the $\alpha + \delta$ field, would not ordinarily be realized because of the slowness of the diffusion required to permit these compositional adjustments.

The δ phase field boundaries converge at a horizontal line at 360°C. The construction of the diagram and the reaction here are practically

[1] The structural change at 580°C is not yet fully understood. Some research papers have advanced the view that the 580°C change is a eutectoid transformation, $\beta \rightleftarrows \alpha + \gamma$, in a manner analogous to the transformations at 520 and 360°C. This view requires a somewhat different construction of the phase diagram in the vicinity of 580°C.

[2] Ordinary valency rules do not hold for intermediate phases in alloy systems except for alloys of Periodic Table Group I and Group II metals with Groups IVB, VB, VIB, and VIIB elements (see back cover). In other cases, notably copper alloys, structures are formed with specific electron-to-atom ratios, approximating 3:2, 21:13, and 7:4. β brass, Cu:Zn, has three electrons for two atoms or a 3:2 ratio. In this Cu:Sn system, the diagram shows Cu_3Sn and $Cu_{31}Sn_8$. Taking Sn as having four valency electrons, these two compounds correspond to ratios of 7:4 and 21:13, respectively. For further information on this systemization of intermediate alloy phases and their structures, see Hume-Rothery, "Structure of Metals and Alloys."

identical to those just discussed; here the eutectoidal reaction on cooling is

$$\delta \rightarrow \alpha + \epsilon_{(Cu_3Sn)}$$

Whereas the β' eutectoid reaction is difficult to suppress, the δ eutectoid reaction is sluggish and difficult to achieve completely because of low

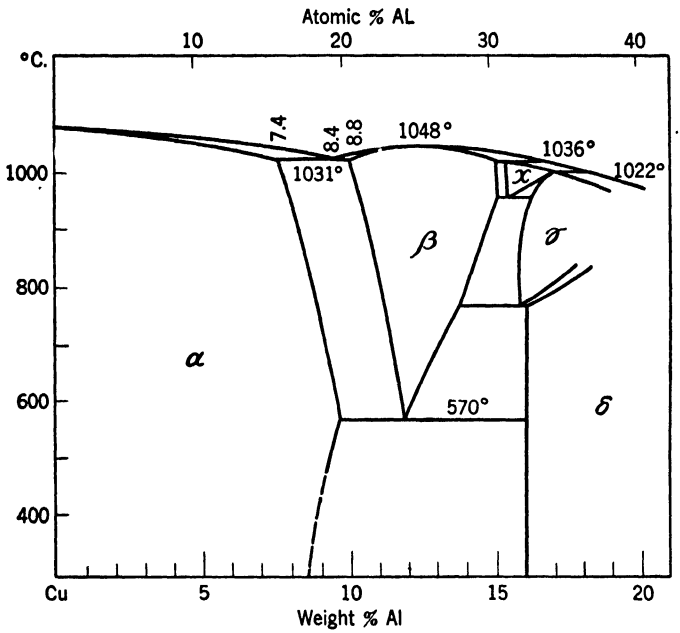

FIG. 8.4. Phase diagram of the copper-rich end of the Cu : Al system. The solid solubility of Al in α_{Cu} below 570°C is somewhat uncertain, hence the dashed line.

atomic mobility at this relatively low temperature and the greater compositional changes involved. The new phase ϵ is close-packed hexagonal, brittle, and of a composition equivalent to the compound Cu_3Sn.

8.3 Cu:Al Alloy System

Following standard terminology where the first word indicates the base metal, Cu:Al alloys are not light alloys but ones in which copper is the major constituent. The phase diagram for alloys with from 0 to 50% Cu is given on page 134; part of the other end of the system is reproduced in Fig. 8.4.

Particularly notable in this diagram is the closeness of liquidus and solidus temperatures. The short freezing interval minimizes or eliminates segregation difficulties, in contrast to the Cu:Sn system. There is a eutectic at 1031°C and 8.4% Al but, in this case, the eutectic is not of much significance since solid state changes at lower temperatures eradicate eutectic structures. The 12% Al alloy solidifies to the β phase at 1048°C in a manner similar to a pure metal. The peritectic at 1036°C, forming χ phase of 15.3% Al, and the peritectic at 1022°C, forming γ of 17% Al, are of little significance with regard to structures or properties of useful alloys.

The β phase reacts eutectoidally upon slow cooling, about 1°C or less per minute, to form a mixture of α and δ phases, comparable to the analogous reaction in the Cu:Sn alloys. The dispersion of α and δ in parallel layers gives a "pearlitic" structure (see Chap. 9). This transformation is of considerable importance with respect to heat treatment of the 10 to 12% Al alloys and also because it is so analogous to the comparable eutectoid in steels.[1]

In the Cu:Al alloys, the regular eutectoid transformation can be suppressed by quenching, but the β phase is not retained. Instead it changes first to an ordered body-centered cubic structure (β_1) and then, as the temperature decreases, to an acicular or needlelike ordered close-packed hexagonal structure (β'). This quenched structure forms with no counterdiffusion of Cu and Al atoms such as is required to form α and δ of different compositions. The needlelike aggregate is called *martensite*, a generic name for structures formed during cooling of a metastable eutectoidal solid solution.[2] Martensitic structures are possible from both the Cu:Zn and Cu:Sn β structures just discussed but are commonly observed only in Cu:Al alloys and, of tremendously greater industrial importance, in steels.

The solubility of aluminum in copper has been assumed to remain constant at 9.5% Al below 570°C, but there is reason to suspect that it may decrease, hence the dashed line. The atom percentages expressed at the top of Fig. 8.4 indicate that, analogously to β in the Cu:Zn and the Cu:Sn systems, the β phase here could be called Cu_3Al with the same electron-atom ratio of 3:2 (3 Cu electrons + 3 Al electrons for 4 atoms) and the same body-centered cubic structure. Likewise in all

[1] For example, see Smith and Lindlief, *Trans. AIME*, **104**, 69, 1933; cf. with Chap. 10.

[2] Greninger and Mooradian, *Trans. AIME*, **128**, 337, 1938. Greninger, *Trans. AIME*, **133**, 204, 1939.

three systems, the δ phase has a 21:13 electron ratio and a complex cubic structure.

8.4 Phase Diagram of Cu:Be Alloys

The highest strength copper-base alloys presently available contain about 2.0 to 2.25% Be as the significant alloying element. Although the alloy is not important tonnage-wise because of its high cost, it is important for certain uses, chiefly as a spring material. The phase diagram, Fig. 8.5, again shows a β phase, which eutectoidally forms α and, in this case, δ or CuBe on slow cooling. However, in view of the composition cited, it should be evident that the eutectoid reaction here is not the important part of the diagram but rather the decrease in solid solubility with decrease in temperature. At the peritectic temperature of 864°C, the alloy is a straight α solid solution. At room temperature, the alloy under equilibrium conditions will contain δ precipitated from the α solid-solution structure. By controlling the temperature at which the second phase forms, the alloy can be made soft (furnace cooling from the α field) or hard (quenching and aging at the optimum temperature).

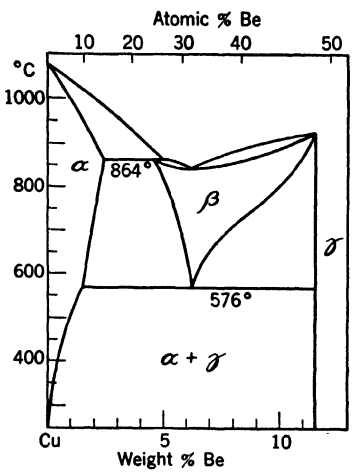

FIG. 8.5. Phase diagram of Cu: Be system up to 11.5% (by weight) Be, the composition of the γ phase. Note the very great difference in atomic and weight percentages in the heavy metal —light metal alloy series.

8.5 Microstructures

Polishing and etching of two-phase copper-base alloys may offer a few more difficulties than are encountered with single-phase structures. Lead globules in leaded brasses or bronzes are so soft that they are removed by the nap of the polishing cloth. Abrasive particles collecting in the pits so formed will drag out and form streaks or "comet tails" from each inclusion. This is minimized by using cloth with a short nap, by limiting the time of polishing on the nap, and by frequently changing the direction of polishing on the cloth.

A second problem, particularly in the Muntz metal type of alloys, is to show up the second phase clearly and to distinguish between the α

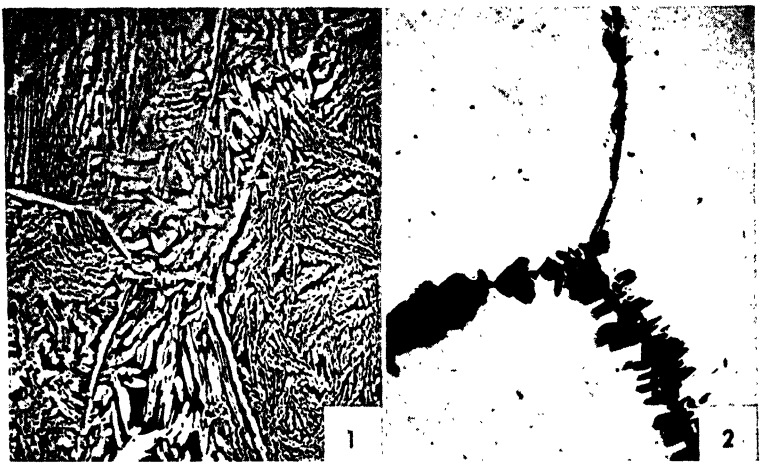

Micro. 8.1. Extruded and air-cooled section of 60% Cu, 40% Zn alloy (Muntz metal); ×50; $FeCl_3$ etch (black phase is β'). At the extrusion temperature, the alloy was completely β and, upon deformation and cooling, α (white) formed in the β structure, first at the β grain boundaries and then inside the β grains. The α formation at the β boundaries indicates the size of the β grains at the high temperature; parts of about six of the *former* β grains are visible. The α crystals, during initial formation in the β structure, must have their atoms in conformity with atoms of the β crystals. This is a general rule for the formation of any new solid phase in a solid matrix of different crystal structure (*cf.* precipitation of $\theta_{(CuAl_2)}$ from $\alpha_{(Al)}$ during age-hardening, page 138).

Usually, only one type of plane of the matrix and one type of plane of the new phase have atoms in a similar pattern when compared in a specific direction. For example, Fig. 8.2 shows that the base plane of the face-centered tetragon (cube plane when it shifts to face-centered cubic α) matches the cube plane of the body-centered cubic β when the edge of the base of the tetragon is in the direction of the face diagonal of the body-centered cube. This conformity results in an alignment of the new phase, α, in only certain planar directions of the β phase. Sometimes these planes are clearly outlined by the new phase, and the structure may then be said to show a *Widmanstätten pattern*,[1] as is evident here to some extent. Frequently, later growth stages of the new phase may form an equiaxed shape, which obscures its crystallographic relationship to the matrix.

Micro. 8.2. The same Muntz metal quenched (in a ⅛-in. thick section) in water from 825°C; ×50; etched with $NH_4OH:H_2O_2$ so that α is dark and β' light (colors reversed from previous specimen). At the high temperature, this structure was completely β (see phase diagram). The quench preserved most of the β but did not suppress completely the formation of α, particularly at the β grain boundaries. Note the directional character of the α forming as plates extending from the boundary into the β' grains (a Widmanstätten characteristic). The relationship is also shown by a few, very small, isolated platelets of α within the β' grains. The β grain size is very coarse, as a result of grain growth in the single-phase range, 780 to 825°C. It was difficult to find sections showing as many as three grains for this micrograph.

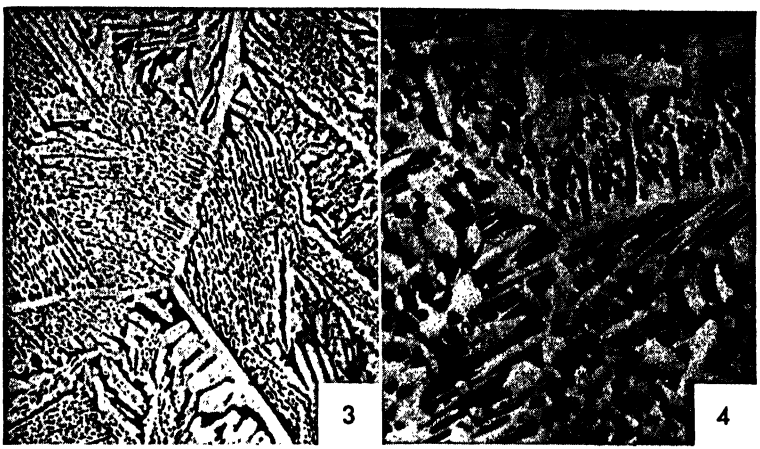

Micro. 8.3. Same as Micro. 8.1 (quenched from 825°C) after reheating 1 hr at 450°C; ×50; etched with $FeCl_3$ (colors again reversed so that α is light and β' dark). The unstable β' of the quenched alloy changed over to α upon heating in the low-temperature range, resulting in the attainment of approximately equilibrium proportions of the two phases. The initial platelets of α at the grain boundaries have grown farther into the former β grains, and their shape, as plates, is still evident by the shape of residual β crystallites between the α plates. The very small plates or needles of α visible in Micro. 8.2, have grown in a similar manner so that the quenched and annealed structure resembles that of the extruded stock (Micro. 8.1).

Micro. 8.4. A different 60% Cu:40% Zn alloy quenched from 825°C and reheated at 500°C; ×200, $FeCl_3$ etch. This structure differs from Micro. 8.3, in that, while α crystals initially grew in a needlelike structure from the β grain boundaries, at a later stage, the α formed in more or less equiaxed shapes and the residual β' crystallites do not show any crystallographic pattern or relationship of origin. This is frequently although not universally true: that the new phase formed at a high temperature under equilibrium cooling conditions will show a crystallographic pattern while that formed by annealing a quenched metastable structure is equiaxed (*cf.* carbide structures from various heat treatment of steels, page 284). Almost always, however, it is fairly easy to distinguish between structures formed at high or low temperatures. Note the twin bands, faintly visible, in the α crystals of this structure, formed as a result of strain accompanying the transformation.

[1] The orientation of the lattice in a new phase, forming from a parent solid phase, is related crystallographically to the lattice of the parent phase. On a polished and etched surface, the traces of the plates, needles, or polyhedra of the new structure exhibit a geometrical pattern. Familiarly seen in cast steel or overheated wrought steel but a possibility in any alloy subject to a phase change in the solid state.

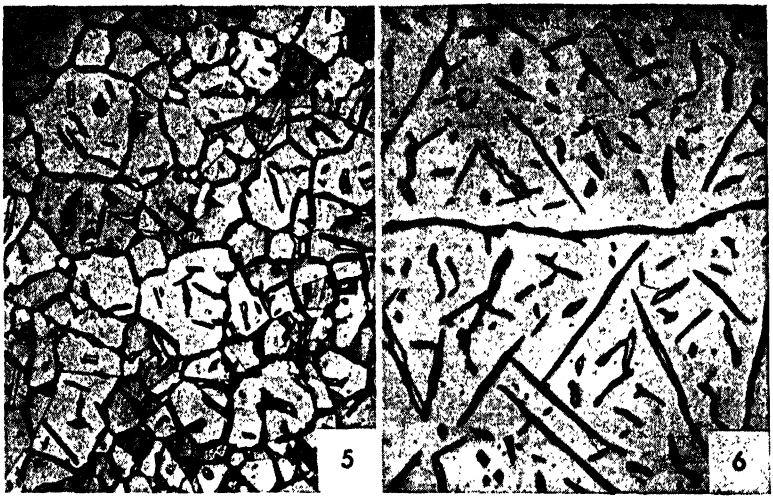

Micro. 8.5. Worked and annealed 65% Cu:35% Zn alloy (common high brass) quenched from 825°C; ×50; ammonium persulphate etch. As ordinarily worked and annealed, this brass will have a uniform α structure showing annealing twins and a grain size characteristic of the specific rolling and annealing schedule. However, upon heating to 825°C, it enters the $\alpha + \beta$ field (see phase diagram). The new phase, β, forms predominantly at the α grain boundaries and, to a somewhat less extent, within the α grains. That forming inside the grains shows the crystallographic relationship required of β forming in α; the β is in lens-shaped plates on specific crystal planes of the α. Quenching from the high temperature has preserved most of the β as β'.

Micro. 8.6. A cast 65:35 brass quenched from 825°C; ×50; ammonia peroxide etch. The very coarse-grained cast structure shows no twins, but the Widmanstätten pattern of β' platelets in two grains of α is beautifully illustrated.

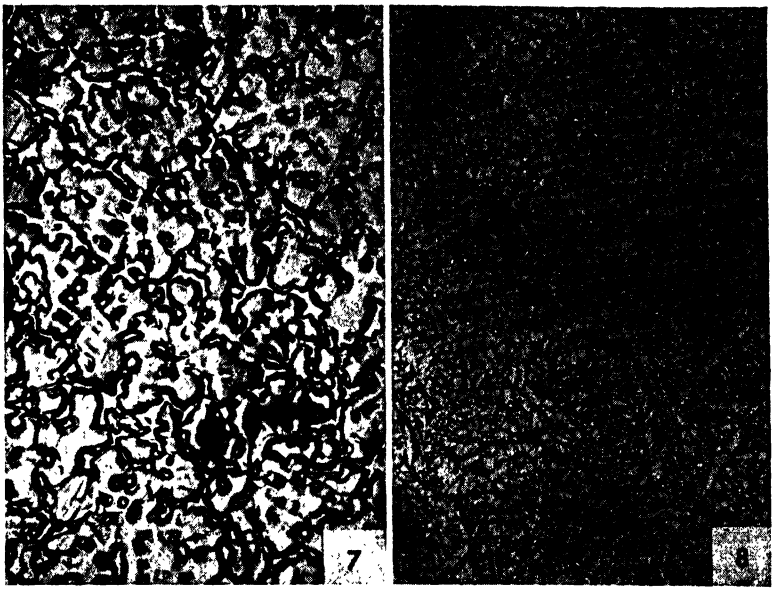

Micro. 8.7. Phosphor bronze with 6% Sn; ×75; dichromate etch[1]. A typical cast microstructure showing cored dendrites of α and interdendritic δ constituent.

Micro. 8.8. Aluminum bronze (trade name, Avialite, of composition 89.4% Cu, 9.2% Al, 0.51% Fe, 0.49% Ni, 0.35% Sn); ×75; dichromate etch.[1] This wrought structure is of a rod normally used for forging stock. The structure shows white α and a dark matrix that consists of a fine mixture of α and δ formed eutectoidally from the high-temperature β phase upon slow cooling.

[1] Courtesy F. H. Wilson, American Brass Co.

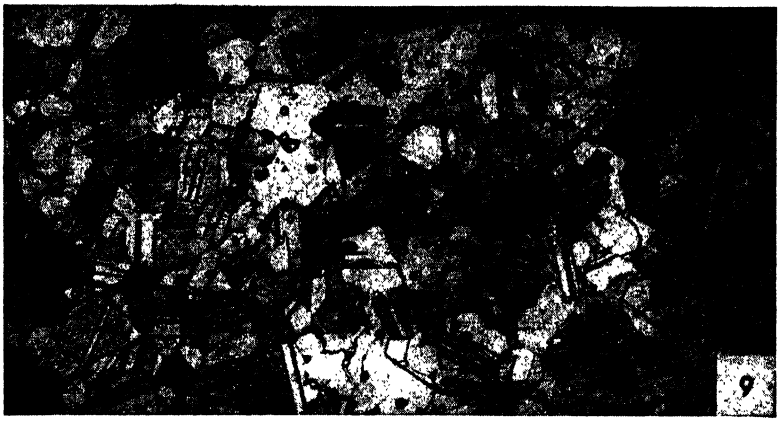

Micro. 8.9. Cu:Be, nominally 97.5% Cu, 2.25% Be, 0.25% Ni; ×250; dichromate etch.[1] This structure represents the solution-treated condition (called, erroneously, the *annealed* state) obtained by a quench from 800°C. It is apparent that not all of the second phase is in solution; the beryllium content here is in excess of that required for precipitation hardening and the presence of the undissolved β constituent is not necessarily a critically important consideration. The supersaturated α shows abundant evidence (annealing twins) of the prior hot-working.

[1] Courtesy F. H. Wilson, American Brass Co.

and the β' phases. Ferric chloride solutions will blacken β' in a structure that is predominantly α, but its effect is somewhat different in a structure that is mostly β'. Uncertainties as to which crystallites are α and which are β' can usually be resolved by a knowledge of the phase diagram and the crystallographic habits of the structure. For example,

1. Any grain containing an annealing twin must be face-centered cubic α rather than body centered cubic β'.

2. Grain-boundary crystallites in a normally all α brass (*e.g.*, high brass or 65:35) must be β'.

TABLE 8.1

Heat treatment	60:40 brass (arsenical)	65:35 brass		
	Rock. E hardness 1/8 in., 100 kg	Rock. E	Tensile strength, psi	% elongation in 2 in.
Quenched 650°C (10 min)	76	32	44,000	64
Quenched 700°C (10 min)	83	27	43,000	67
Quenched 760°C (10 min)	86	23	42,000	70
Quenched 825°C (10 min)	93	40	50,000	52
Quenched 825 + 250°C (60 min)	106	38	49,000	58
Quenched 825 + 325°C (60 min)	100	34	47,000	62
Quenched 825 + 400°C (60 min)	93	30	45,000	65
Quenched 825 + 450°C (60 min)	85	27	44,000	67
Quenched 825 + 500°C (60 min)	79	24	43,000	69

8.6 Properties of Brasses

The mechanical properties of brass specimens with the microstructures shown here can be qualitatively estimated on the basis that α is rather soft and plastic, particularly when moderately coarse-grained, that β' is a rather hard and brittle phase, and that the *continuous* phase will have an effect out of proportion to the relative amount present. Instead of a discussion of the properties of the individual specimens, data pertaining to corresponding structures are reproduced in Table 8.1, as typical of the properties developed upon heat treatment of small sections.

Annealing the 60:40 brass at low temperatures following the 825°C quench results in an increase in hardness. At first it might seem anomalous for this alloy to become harder as the amount of the soft α phase increases. However, when the α forms at very low temperatures

in a very disperse form, it causes precipitation hardening of the β' matrix. There is a continual decrease in hardness as the α particles increase in size. Low-temperature annealing of the 65:35 brass, quenched from 825°C, is accompanied by a gradual decrease in the amount of β' although minute amounts are still present after the 500°C anneal. The properties change more rapidly than the change in the amount of β present because these anneals first tend to interrupt the continuity of the β network (*cf.* Micro. 8.5) while longer times or higher temperatures are required to eliminate completely the disperse β' particles.

Although face-centered cubic α brass is considerably softer and more plastic than the ordered body-centered β' at temperatures up to about 450°C, at very high temperatures, the β structure is much more plastic than the α and is, therefore, preferred for hot-working. If up to 3% lead is added for machinability, it is present as insoluble globules and, presumably, as a result of the change of crystal structure of the 60:40 brass with temperature, the lead does not impair hot-working properties. In α brass, however, as little as about 0.04% lead will make the metal hot-short since it is present as an intercrystalline film in the cast billet.

Brass screws and various small fittings machined from rod in high-speed automatic machines are usually of Muntz metal (60:40) containing up to about 3% of lead. For hot forgings, a similar alloy is employed although the lead content is somewhat lower and the copper content a little higher—chiefly to ensure better ductility at room temperatures while retaining hot-working properties and machinability. If higher strength is desired, Muntz metal is alloyed with 1% Sn (naval brass). The regular hot-forging grade may show 54,000 psi tensile strength, 20,000 psi yield strength, and 45% elongation, while the naval brass will average about 58,000 psi tensile, 27,000 psi yield strength, and 45% elongation.

Castings are seldom produced from plain Cu:Zn brasses but frequently from 60:40 brass to which has been added small percentages of aluminum, manganese, and iron; *e.g.*, 58% Cu, 39% Zn, 1% Al, 1% Mn, 1% Fe. The name commonly used for this alloy is *manganese bronze*, a complete misnomer inasmuch as little or no tin may be present and manganese is not a major alloying element. As is evident from the data in Table 8.2, the alloy is strong and ductile. In addition, it possesses excellent resistance to corrosion by sea water and many other corroding agents. Therefore, it is widely used for marine applications, including ship propellers and hydraulic machinery. It is also produced in wrought form with properties as given in Table 8.2.

8.7 Properties of Tin Bronzes

Whereas the two-phase brasses are employed mostly for wrought products, two-phase tin and aluminum bronzes are employed chiefly in the cast form. The tin bronzes are not binary products since zinc or lead are usually present. Three alloys, listed in Table 8.2, are most common in engineering use:

TABLE 8.2. TYPICAL PROPERTIES OF TWO-PHASE BRASSES AND BRONZES

Alloy	Composition				Condition	Tensile strength, psi	Yield strength, psi	% elongation in 2 in.
	% Zn	% Sn	% Pb	% others				
Wrought Form								
Muntz metal	39	....	....	.....	Annealed	54,000	20,000	45
Muntz metal	39	.	....	.....	Cold-rolled	80,000	60,000	10
Arch. bronze	38.8	..	3 2	.....	Extruded	54,000	18,000	30
Mn bronze	39	1.0	. .	1% Fe, 0.03% Mn	Annealed rod	72,000	32,000	35
Mn bronze	39	1.0	. ..	1% Fe, 0.03% Mn	Half hard	83,000	60,000	20
Naval brass	39.2	0.8	....	.....	Annealed rod	58,000	27,000	45
Naval brass	39.2	0.8	. .	.....	Half hard*	80,000	57,000	20
Leaded naval brass	37.8	0.8	1 5	.....	Annealed rod	57,000	25,000	40
Leaded naval brass	37.8	0.8	1.5	.....	Half hard	75,000	53,000	15
Phos. bronze	..	8.0	..	0.2% P	Annealed strip	60,000	....	65
Phos. bronze		8 0	...	0.2% P	Spring†	111,000	....	5
Cast Form								
Mn bronze	40	1.5	....	2% Mn, 1% Al, 1% Fe	As-cast	70,000	32,000	30
Bearing bronze	..	10	10	.....	As-cast	31,000	21,000	13
Gun metal	2	10	....	.... ..	As cast	40,000	20,000	25
Three-fives	5	5	5	. .	As-cast	40,000	20,000	25

* Cold-worked 2 Brown and Sharpe Nos. † 8 Brown and Sharpe Nos.

Three-fives, a name of obvious origin since it consists of copper with 5% Sn, 5% Zn, and 5% Pb. The most widely used copper-base cast alloy, it has the following attributes: fairly low cost, fair mechanical properties, good casting characteristics, excellent machinability, and good resistance to corrosion. Under equilibrium conditions it would be all α with lead inclusions, but actual castings usually show a small amount of $\alpha + \delta$ eutectoid in the cored α, plus interdendritic lead inclusions.

Gun metal, also known as *G bronze,* is an ancient alloy that is still popular and important. Its composition may be 10% Sn + 2% Zn or

8% Sn + 4% Zn. As would be anticipated, the higher tin-content alloy contains more $\alpha + \delta$ eutectoid with a corresponding greater hardness and greater tendency toward segregation and hard spots due to masses of the δ constituent. The alloy is subject to "sweating" or exudation of a tin-rich liquid on the surface during solidification. The solution of hydrogen during melting followed by hydrogen bubble formation during solidification results in an interdendritic flow of the last liquid phase. The hydrogen bubbles exert an internal pressure that pushes the interdendritic liquid, which is quite high in tin content, toward the surface, leaving internal voids at the center. This difficulty may be eliminated to a significant extent by oxidizing the charge after melting (*e.g.*, with Cu_2O) and subsequently removing excess oxygen by phosphorus additions. The excess of oxygen is required because of chemical equilibrium considerations, specifically the mass action law.

Castings of gun metal usually have a dense fine-grained surface but, if the surface layer is removed by machining, the casting may not be pressure tight when used for valves, etc. Annealing at 760°C improves ductility by tending to spheroidize the interdendritic δ eutectoid, and the treatment also reduces or eliminates leaky castings. Whether this desirable result is caused by growth associated with solution of more δ constituent or with oxidation of the interdendritic voids is not known with certainty. At any rate, it is the combination of properties—moderate strength and toughness, bearing-metal qualities, good casting characteristics, and resistance to salt-water corrosion—that makes this alloy well adapted for steam and marine uses.

10:10 bronze, with 10% Sn and 10% Pb, structurally consists of a cored α matrix with interdendritic $\alpha + \delta$ eutectoid and dispersed lead globules. The alloy is best fitted for heavy-duty bearings since the α matrix provides strength and toughness, the eutectoid contributes hardness and wear resistance, and the lead improves the antifriction characteristics.

8.8 Properties of Aluminum Bronzes

There is no technical justification for calling these Cu:Al alloys bronzes inasmuch as tin is not employed as an alloying element. Instead, iron is added with the aluminum to increase the yield strength. The alloys have a pleasing color and a range of properties from moderate strength with good ductility to high strength and hardness with little ductility. As would be anticipated from the phase diagram, the alloys containing 10% or more of aluminum respond to heat treatment, and either the yield strength or the ductility of cast structures can be

increased. Data on a series of alloys marketed by one prominent producer specializing in aluminum bronzes are given in Table 8.3. The heat treatments used here give *martensitic*-type structures.

The first two, softer grades of these alloys are used for bushings, bearings, and parts subjected to impact and corrosion. The 10 and 12% Al alloys are used for bushings, bearings, and gears running against steel. The wear resistance of the alloy makes it suitable for many

TABLE 8.3. TYPICAL PROPERTIES OF CAST-ALUMINUM BRONZES

Composition		Sand-cast		Properties		
% Al	% Fe	Tensile strength, psi	Yield strength, psi	% elongation in 2 in.	BHN	Structure*
9.0	3.0	80,000	30,000	40	131	All α
10.0	3.5	90,000	32,000	22	146	Primary α and eutectoid
10.6	3.6	90,000	37,000	14	174	Primary α and eutectoid
10.6	3.6†	90,000	33,000	18	156	Primary α in coarse eutectoid
10.6	3.6‡	100,000	53,000	6	223	Precipitate α in β'
10.6	3.6§	100,000	45,000	14	187	Precipitate α in β'
12.0	4.0	85,000	40,000	4	207	Primary α in β
12.0	4.0†	85,000	35,000	6	202	Primary α in β
13.0	4.2	75,000	55,000	1.5	285	δ in β and eutectoid
14.0	4.6	85,000	70,000	0.5	331	δ in β and eutectoid

* Relative quantities of constituents depend on the cooling rate as well as on composition.
† Tempered at 1100°F, water-quenched.
‡ Heated at 1650°F, water-quenched, aged at 1150°F.
§ Heated at 1650°F, water-quenched, aged at 1200°F.

specialized parts of machinery. The 13 and 14% alloys can be used for forming and drawing dies where their high compressive strength and anti-seizing properties result in long life.

All these aluminum bronzes are somewhat difficult to handle in the foundry as they are prone to develop aluminum oxide dross films and shrinkage cavities. These tendencies are minimized by reducing turbulence during flow of the liquid in the mold and by employing amply large feeding reservoirs above heavy sections.

8.9 Properties of Cu:Be Alloy

This alloy, like so many other copper-base alloys, bears a misleading name—*beryllium copper*—and nonmetallurgists are likely to assume that

it is essentially a beryllium metal whereas it actually contains only 2 to 2.25% Be. From ¼ to ½% nickel or small concentrations of iron or cobalt are present, primarily as a grain refiner. The alloy is expensive for several reasons: the alloying element beryllium is rather expensive to produce, the alloy is handled in small lots of a few hundred pounds and tends to tie up expensive mill facilities installed for volume products, and, finally, beryllium oxide is poisonous and several fatalities have resulted from working with the molten alloy without adequate safety precautions.

TABLE 8.4. TYPICAL PROPERTIES OF Cu:Be ALLOY (2¼% Be, ¼% Ni)*

Condition	Tensile strength, psi	Yield strength, psi	% elongation in 2 in.	BHN	Tensile modulus
1. Solution-treated and quenched	70,000	25,000	45.0	110	$18.0\ (10)^6$
2. Same, then aged at 275°C	175,000	120,000	6.3	340	$18.9\ (10)^6$
3. Solution-treated, quenched, rolled 2 Nos	103,000	68,000	8.0	200	$17.5\ (10)^6$
4. Same as 3, aged at 275°C	173,000	125,000	4.8	340	$18.5\ (10)^6$
5. Solution-treated, quenched, rolled 4 Nos	118,000	78,000	4.3	220	$17.2\ (10)^6$
6. Same as 5, aged at 300°C	193,000	145,000	2.0	365	$18.4\ (10)^6$

* "Metals Handbook."

The alloy is given a solution treatment at 800°C, a temperature that would cause marked grain coarsening if it were not for the small amount of nickel or equivalent addition element present. If the metal had been hot-worked in its proper hot-working range, 575 to 775°C with an $\alpha + \beta$ structure, subsequent holding at 800°C for 3 hr before quenching is required to eliminate the duplex structure or at least to saturate the α matrix. If the 800°C treatment is to soften the alloy after cold-working, 15 min at temperature is adequate. A nonoxidizing atmosphere, *e.g.*, hydrogen at 800°C, is desirable. Otherwise scaling necessitates pickling the surface, and oxygen may diffuse inward, oxidize the beryllium, and thereby cause the surface to remain soft after the subsequent precipitation treatment. The soft surface has a severely lowered fatigue strength, which is particularly detrimental when the alloy is employed for corrosion-resistant springs, subject to reversed stresses that are of highest magnitude at the surface.

As quenched from 800°C, the alloy is soft and readily cold-worked;

therefore, common terminology lists this treatment as an anneal. (Again—the purist protests—it should be called a *solution heat treatment.*) After being quenched from 800°C, the alloy remains soft indefinitely at room temperature. This might appear to be in contrast to Duralumin or Al 24S alloy, but room temperature for the Cu:Be is roughly equivalent to −80°C for Duralumin.

The response of the soft, solution-treated alloy to elevated temperature aging and also, when so treated and then cold-worked, is shown by the hardness graphs of Fig. 8.6. The data, based on 1- and 5-hr treat-

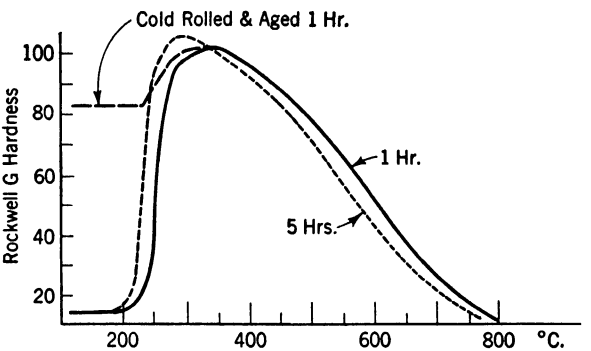

FIG. 8.6. Age-hardening curves for industrial beryllium-copper alloy (2.2% Be, 0.25% Ni) following a quench from a solution heat treatment at 800°C. In one curve, the alloy was cold-rolled 37% before the aging treatment. Aging treatments for 1 or 5 hr were followed by a quench.

ments, show a sharp hardness maximum at 300°C, with no effects of heating below 200°C and steady softening beyond 325°C. The choice of longer or shorter precipitation treatment times would result in similar graphs but with the hardness maxima displaced to lower or higher temperatures. In practice, it is customary to precipitation-harden by heating the metastable supersaturated solid solution for about 4 to 5 hr at 275°C.

Mechanical properties of the Cu:Be alloy are given in Table 8.4 and in comparison with data on other copper-base alloys, the tensile strength of nearly 200,000 psi and Brinell hardness of 365 are notable. The alloy can be used for nonsparking tools and, more importantly, for springs. It has spring properties approaching that of spring steels together with nonrusting characteristics and the generally high corrosion resistance of copper alloys. It has very much higher strength and fatigue resistance than the other important copper-alloy spring material, phosphor bronze.

QUESTIONS

Group A

1. Describe two methods of varying the relative proportions of α and β in Muntz metal by heat treatment.

2. Explain the course of the hardness vs. temperature data in Table 8.1 for the 65:35 brass and the 60:40 brass, as quenched from 650 to 825°C.

3. Explain why the composition 61% Cu, 37% Zn, and 2% Pb is particularly suitable for brass forgings. The comparison might be made with 70:30 brass or nonleaded 60:40 brass.

4. How may the β' structure in wrought Muntz metal be distinguished from α, regardless of the prior hot-working or heat treatment by (*a*) microstructure appearance without regard to the particular etch and (*b*) by use of a special etch?

5. Copper containing 2% Be in supersaturated solid solution looks like ordinary copper. How could you readily distinguish it from copper (*a*) without chemical or micrographic tests and (*b*) without the microscope?

Group B

1. Nickel is used as an alloying agent in tin bronzes. Draw the appropriate phase diagram (ternary or quasi-binary) to show, for an alloy of 8% tin and 8% nickel, the probable heat treatment ranges, etc.

2. Redraw the Cu:Sn diagram (Fig. 8.3) for the area from 30 to 40% Sn and from 500 to 750°C. Enlarge the abscissa scale, particularly, to show the appropriate reactions at horizontal lines. Be sure that the drawing is in accord with Gibbs's phase rule; *i.e.*, where three phases coexist, no degrees of freedom are possible, and the system is invariant.

3. Describe the changes that should occur in the Cu:2¼% Be alloy if it were slowly cooled from 800 to 550°C, held long enough for equilibrium to be attained, then quenched and reheated at 275°C. Sketch the probable microstructure.

CHAPTER 9

IRON-CARBON ALLOYS: NORMALIZED AND ANNEALED STEELS

Commercial steels are never binary alloys of iron and carbon, for manganese, silicon, sulfur and phosphorus are always present in the Fe:C alloy, as produced from pig iron by any of the industrial refining processes. Plain-carbon steels, produced in the open-hearth furnace using from 25 to 50% scrap metal, may also contain residual elements such as copper, nickel, chromium, and tin, to name but a few, in amounts up to 0.1%. All these elements affect some property of the steel but, in general, the effects are small. The Fe:Fe_3C phase diagram is not noticeably changed by the presence of any of these residual impurities, or addition agents, such as manganese or silicon, in the amounts usually found in carbon steels. Modifications in the diagram, in the properties of steels, or in their response to heat treatment, as affected by larger additions of other elements, will be discussed in later sections.

9.1 Fe:Fe_3C Phase Diagram

The phase diagram (Fig. 9.1) has been reproduced with the carbon-concentration scale plotted so as to expand the area including commercial steels, 0 to 1.4% carbon, and compress the area of cast irons, 2 to 4% carbon, in which the exact carbon content is of less importance. The basis of the differentiation between steels and cast irons is found in the phase diagram and may be expressed in two ways. From a practical standpoint, steels have such a high melting point (above 1440°C) that special and expensive equipment is required to melt them, whereas cast irons melt at 1350°C or less, a temperature much more readily attained with inexpensive equipment. However, since the decrease in melting point (or liquidus temperature) with increase of carbon content is continuous from 1525 to 1130°C, this reasoning, although of practical importance, leads to no specific demarcation limit. A second means of distinguishing between the two classes of materials is on the basis of structure and properties; iron containing up to 1.7% carbon can be heated to a temperature at which it will show only one phase, face-

centered cubic γ, while alloys containing more than 1.7% carbon always contain γ + Fe_3C eutectic structure.[1] The eutectic has some 50% by weight (more by volume) of the brittle Fe_3C phase which tends to be

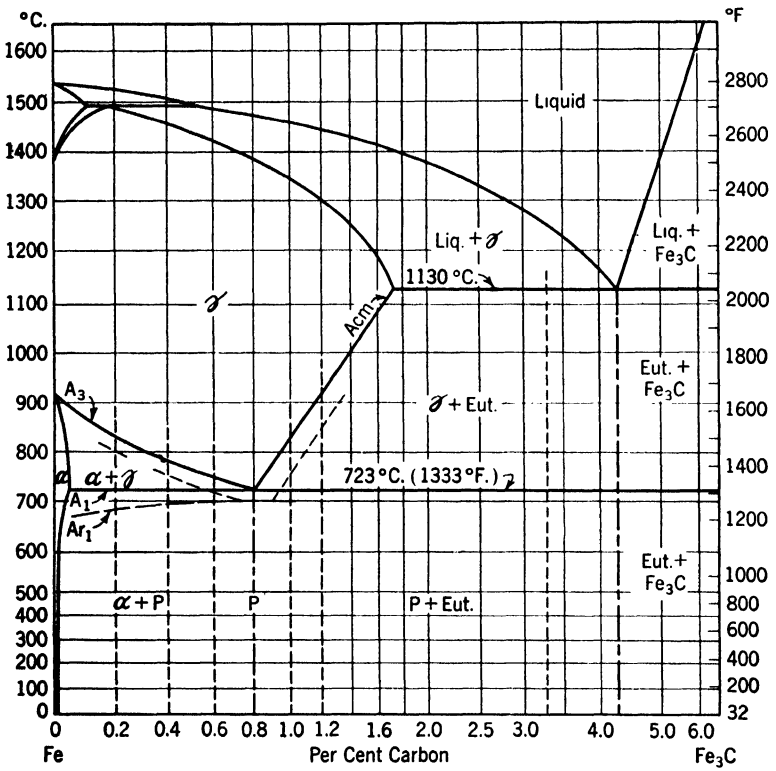

FIG. 9.1. Phase diagram of the $Fe:Fe_3C$ (metastable) alloy system.

continuous, and thus alloys above 1.7% carbon, containing eutectic at all temperatures, are somewhat brittle. The eutectic in alloys of less

[1] Although the $Fe:Fe_3C$ diagram as revised in 1946 and published by the ASM shows a 2% carbon solubility limit, the previously accepted solubility maximum was 1.7% carbon in austenite at the γ + Fe_3C eutectic temperature. The lower figure of 1.7% carbon is primarily based on metallographic work employing solid-state saturation. When austenite or γ is exposed to gaseous atmospheres containing carbon, *e.g.*, CH_4 in hydrogen or CO, the solubility limit seems to be in the vicinity of 2% C as shown by Gurry (*AIME*, **150**, **147**, 1942) and more recent work by G. V. Smith and separately by Toensing. It seems possible that the discrepancy between the old-established figure of 1.7% and the newer figure of 2% is based on the fact that the latter actually involves a ternary system, Fe:C:H or Fe:C:O.

than 1.7% carbon, resulting from undercooling, can be dissolved in γ which, being face-centered cubic, is plastic. This distinction, that steels can be hot-rolled and cast irons cannot, is not absolutely clear-cut however nicely it ties up with the phase diagram. For example, cast irons (white) of about 2.25% carbon, which contain only 20% of the eutectic and 80% of the γ phase at about 1100°C, can be hot-rolled if the initial soaking at the high temperature before rolling is effective in breaking the continuity of the carbide in the eutectic (by agglomeration, see page 148), and if the initial breakdown passes are moderate. Alloys in the range from 1.5 to 2.5% carbon, then, are intermediate between steels and cast irons. This should not lead to their being termed semi-steels (page 457) for the reason that the latter designation has been used for such a wide variety of Fe:C alloys that it has become practically meaningless.

The phase diagram shows three horizontal lines, each representing a reaction involving three phases and occurring at a constant temperature. The reactions may be represented as

(1) At 1492°C, δ (0.08% C) + liquid (0.55% C) $\rightleftarrows$ γ (0.18% C)
(2) At 1130°C, liquid (4.2% C) $\rightleftarrows$ γ (1.7% C) + Fe_3C (6.7% C)
(3) At 723°C, γ (0.80% C) $\rightleftarrows$ α (0.025% C) + Fe_3C (6.7% C)

The solidification process, through the peritectic range (0.1 to 0.5% C), solid-solution range (0.5 to 1.7% C), or hypoeutectic range (1.7 to 4.2% C) of carbon content, proceeds as it does in any alloy system showing comparable conditions. For example, an alloy of iron and 1.2% carbon upon cooling from the liquid state to 723°C behaves exactly like an Al:4% copper alloy; solidifies in the form of a solid solution, γ, and, as this cools past the line marked A_{cm}, the decrease of solubility of Fe_3C causes the carbide phase to precipitate from solid solution in γ, which correspondingly becomes depleted in carbon. The carbide precipitation occurs chiefly at the γ grain boundaries, although, if a large amount of Fe_3C must separate, it forms Widmanstätten plates within the grains. When the γ phase reaches a carbon content of 0.80% at 723°C (under equilibrium conditions), reaction (3) occurs. This reaction is missing from the Al:Cu diagram although, again, the construction of the phase diagram is identical if the γ field is taken to represent liquid alloys. Because of the essential similarity of reaction (3) to the eutectic (2), the former is known as a eute*ctoid*. Whereas a eutectic represents the formation of a mechanical dispersion of two new solid phases, here γ + Fe_3C, from a liquid, a eutectoid represents the formation of a dis-

persion of two new solid phases, $\alpha + Fe_3C$, from a solid γ. In both cases, the two-phase dispersed structure has a distinctive appearance as compared with either phase that may have formed in a different manner.

The term "hypoeutectoid" has the same significance as hypoeutectic. On cooling a 0.4% carbon steel past the line equivalent to the liquidus in eutectics, here called the A_3 line, crystals of α begin to form at the γ grain boundaries and continue forming until, at 723°C, they represent $(0.80-0.40)/0.775 = 52\%$ of the structure (under equilibrium conditions), after which the residual γ, now of 0.80% carbon content, goes through the eutectoid reaction. Hypereutectoid alloys behave in an identical manner, except that the phase separating from γ at its grain boundaries is Fe_3C.

9.2 Solubility of Carbon in Austenite and Ferrite

Austenite with a face-centered-cubic structure represents a denser packing of atoms than ferrite, the body-centered cubic room-temperature form of iron. This is forcefully demonstrated by the substantial contraction that occurs upon heating iron past 910°C and causing ferrite to change to austenite. A comparable expansion occurs during the reverse transformation upon cooling past the A_3 temperature. Assuming that iron atoms are or at least act as incompressible spheres, it is simple to calculate the percentage of unfilled space in the two lattice types and it is found that

$$\text{Voids in body-centered cubic} = 32\%$$
$$\text{Voids in face-centered cubic} = 25\%$$

The carbon atom is dissolved in either lattice interstitially; *i.e.*, it occupies voids between the iron atoms. It seems somewhat anomalous that so many more atoms of carbon can dissolve in austenite that has less "empty" space to contain them. However, this discrepancy is easily resolved by a study of Fig. 9.2 and calculations based thereon.

The body-centered cube of ferrite has its largest hole on the cube face, such as the front but not at the obvious position in the middle. The body-centered atom has another atom in line with it, normal to the front face and the same short distance away as that separating two adjacent corner atoms. Therefore, the largest hole is halfway between the center of the face and the mid-edge or space between the two corner atoms. Two of the four possible sites for a carbon atom on the front face of a body-centered cube are shown in the left-hand sketch of Fig. 9.2. With the distance between atom centers along a cube edge known

to be $2.86(10)^{-8}$ cm, the largest interstitial sphere that would just fit has a radius of $0.36(10)^{-8}$ cm.

In the face-centered cube of austenite, the right-hand side of Fig. 9.2, the largest interstitial hole is midway along the edge between the two corner atoms (these atoms are of the same size as in the body-centered cubic structure). This hole will contain a sphere of radius

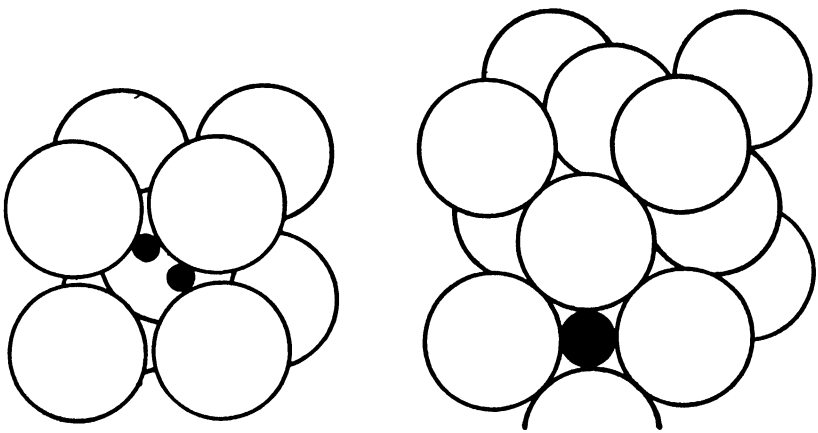

FIG. 9.2. Interstices of the body-centered cubic (left) and face-centered cubic lattices. The maximum diameter foreign sphere (black) that can enter the body-centered cubic lattice is indicated by the black atom with two of the four possible positions on one face shown here as filled. The face-centered cubic lattice has far fewer interstices, one per face, but as shown by the black sphere, the hole is much larger.

Body-centered Cubic Lattice
Holes at ½, 0, ¼; ¼, 0, ½, etc., for atom radius (α Fe) = 1.23 Å: edge of cube = 2.86 Å
Radius, interstitial hole = 0.36 Å

Face-centered Cubic Lattice
Holes at ½, 0, 0; 0, 0, ½, etc., for atom radius (γ Fe) = 1.26 Å: edge of cube = 3.56 Å
Radius, interstitial hole = 0.52 Å

$0.52(10)^{-8}$ cm or almost 50% greater than the sphere fitting in ferrite interstices. Thus it is reasonable that austenite has a much greater solubility for carbon. However, since the carbon atom, at least in diamond crystals, has a radius of $0.77(10)^{-8}$ cm, even the austenite lattice is strained by the solution of carbon and a maximum of only about 10% of the interstices (corresponding to 1.7 wt. % carbon) can be filled. The distortion of ferrite by carbon solution is so much greater that solubility is much more restricted.

Note that the solubility of Fe_3C in the α phase decreases from 0.025% carbon at 723°C to about 0.007% at room temperatures. This indicates that low-carbon alloys are susceptible to age-hardening when cooled

rapidly from the vicinity of the eutectoid temperature (page 236), an effect known as *quench-aging*.

9.3 Terminology

The Fe:Fe_3C diagram was one of the first metallic systems to be studied. This fact, plus the predominant commercial production and use of steels among all alloys, has led to the application of special names for phases and structures, in addition to the basic Greek-letter designations. The common ones are as follows:

Austenite = γ, the face-centered cubic structure that can dissolve up to 1.7 (or perhaps 2.0) % carbon at 1130°C.

Ferrite = α, body-centered cubic iron dissolving a maximum of 0.025% carbon at 723°C.

Cementite = Fe_3C = iron carbide or simply "carbide."

Eutectic = the word may refer to the *reaction* at 1130°C: liquid $\rightleftarrows$ γ + Fe_3C, or to the liquid *composition* participating in the reaction; *i.e.*, 4.2% carbon is the *eutectic* alloy, or to the *structure* resulting from the reaction on cooling, known as *ledeburite* (see page 448).

Eutectoid = again the word may refer to the *reaction* $\gamma \rightleftarrows \alpha$ + Fe_3C, or to the *alloy* whose composition is that of the austenite in the reaction; *i.e.*, 0.8% carbon is the *eutectoid* steel, or the word may refer to the lamellar *structure* resulting from the reaction on cooling, pearlite.

Pearlite = the distinctive two-phase lamellar structure resulting from the eutectoid reaction upon relatively slow cooling.

A_{cm} = line showing thermal arrest resulting from precipitation of carbide from austenite (on cooling).

A_3 = line showing thermal arrest resulting from formation of ferrite in austenite (on cooling, A_{r_3}; on heating, A_{c_3} indicates the reverse, *i.e.*, solution of ferrite in austenite).

A_2 = line at about 768°C showing a magnetic change in ferrite; not a phase change and not shown on this phase diagram.

A_1 = horizontal line representing eutectoid reaction (on cooling, A_{r_1}, and on heating, A_{c_1}).

Normalizing = heating into the austenitic field followed by air cooling.

Annealing (full) = heating above the A_{c_3} for hypoeutectoid steels or above the A_{c_1} for hypereutectoid alloys (for reason, see page 251) followed by furnace cooling.

Annealing (process) = heating to a temperature below but close to the A_1 line. This temperature does not result in any phase change but will soften work-hardened ferrite and spheroidize lamellar Fe_3C.

9.4 Equilibrium and Nonequilibrium

The phase diagram shown for $Fe:Fe_3C$ alloys cannot be called an equilibrium diagram, for that would imply no change of any phase with time. However, even relatively pure $Fe:Fe_3C$ alloys will change; a low-carbon steel, 0.08% carbon with low silicon content, held several years at 650 to 700°C (in an oil distillation system), was found to consist of ferrite and graphite, not ferrite and carbide as the diagram would lead one to expect. Since a long time at an elevated temperature is known to be conducive to the establishment of equilibrium, it is concluded that iron carbide is always a transitional or metastable phase. However, extraordinary temperature and time conditions (or a relatively high silicon content, see page 444) are required to decompose carbide into graphite and ferrite:[1]

$$[Fe_3C \rightleftarrows 3Fe(\alpha) + C \text{ (graphite)}]$$

Although the $Fe:Fe_3C$ diagram is known to represent metastable conditions, the temperature-composition limits of phase changes shown by various lines can be considered as having equilibrium positions under normal heating and cooling conditions. Liquidus and solidus lines will be depressed by undercooling in the same manner as those on true equilibrium diagrams. The lines on the diagram outlining the eutectoid transformation are particularly subject to displacement from overheating or undercooling, since transformations requiring diffusion in the solid state are necessarily slower than those involving a liquid. (For example, the "metastable" solidus in solid solutions is not usually accompanied by a detectable metastable liquidus since atomic diffusion is so much more rapid in the liquid than in the solid state.)

The displacement of the A_3 and A_1 lines of the phase diagram has caused the use of the designation A_c

(c = "chauffage" = heating)

for their positions on ordinary heating cycles or A_r

(r = "refroidissement" = cooling)

on ordinary cooling cycles, as indicated under Terminology. A more

[1] Above the A_1 temperature, carbide will break down to graphite and austenite when the alloy is to the right of the A_{cm} line. The eutectoid composition of the iron graphite system is 0.69% carbon and the eutectoid temperature is 738°C.

complete discussion of these effects is given in Chap. 10, but it is desirable to point out here that the A_3 and A_{cm} lines are subject to greater displacement, as a result of reluctance by the ferrite or cementite to form in austenite, than the A_1 line at which pearlite forms from austenite. The positions of all three of these important lines upon air-cooling of moderate-sized sections are shown in the diagram. The result of undercooling is immediately evident in the composition of the eutectoid; it is no longer fixed at 0.80% carbon but includes a range of concentrations of from 0.7 to 0.9% carbon. Older books on this subject often show carbon contents for the eutectoid different than the 0.80% given here, and the basis for past confusion is related to undercooling. The 0.80% value was obtained by heating and cooling tests of alloys between 0.7 and 0.9% carbon in which the change of temperature was only $\frac{1}{8}$°C per min.[1] The effect of undercooling on the carbon concentration and temperature of this eutectoid should be compared with the effect on the silicon content and temperature of the Al:Si eutectic, although in the latter case, since only the formation of silicon is suppressed by undercooling, the eutectic concentration is displaced in only one direction.

The construction of that part of the Fe:Fe_3C diagram (Fig. 9.1) shown by the dashed A_{r_1} line is patently in violation of the Gibbs phase rule. With three phases present, γ, α, and Fe_3C, the temperature of the system and compositions of the phases should all be fixed, yet the austenite shows a range of compositions. The answer to this apparent discrepancy is that the phase rule applies only to equilibrium conditions while the A_{r_1}, A_{r_3}, and $A_{r_{cm}}$ lines represent nonequilibrium conditions.

The concentration of the carbon content of the eutectoid is important in applying the lever rule to hypo- or hypereutectoid structures, *i.e.*, in predicting whether a specific alloy should show excess ferrite or carbide and how much or vice versa, in estimating carbon content on the basis of the presence and amount of an excess of one of these phases. The lever rule can be useful in both of these ways but is quantitatively applicable only when the structures are obtained under conditions approaching equilibrium, *i.e.*, very slow furnace cooling.

9.5 Microstructures

While the entire two-phase field between 0.007 and 6.7% carbon, at room temperatures consists of the phases, ferrite and carbide, the structural appearance of different alloys varies with the state of aggregation of the ferrite and carbide as a function of their origin. The follow-

[1] Mehl and Wells, *Trans. AIME*, **125**, 429, 1937.

ing ranges in slowly cooled alloys can be differentiated, chiefly on the basis of five types of carbide distribution:

a. 0.007 to 0.025% carbon; ferrite with carbide precipitated in a very fine form, usually invisible.

b. 0.025 to 0.8% carbon; ferrite + pearlite.

c. 0.8 to 1.7% carbon; pearlite + carbide precipitated from austenite.

d. 1.7 to 4.2% carbon; pearlite in a dendritic structure (from hypoeutectic primary austenite) + carbide precipitated from austenite (usually attached to and indistinguishable from eutectic carbide) + ledeburite.

e. 4.2 to 6.7% carbon; primary carbide crystals + ledeburite. Of these structures, (*a*) is not reproduced although the "Metals Handbook" gives methods of detecting this form of carbide precipitation; (*b*) and (*c*) are shown in this chapter; (*d*) is given in Chap. 14 on cast irons; and (*e*) is not reproduced since no commercial alloys fall within this range.

Polishing of steels is quite simple with one important qualification. Surface flow usually considerably distorts the lamellar pearlite structure and, if this is relatively fine as in normalized steels, flow may completely efface the lamellar characteristics. The surface flow is reduced but not eliminated by the use of light pressure during polishing. However, too light a pressure so increases the required polishing time that greatly increased surface pitting is encountered. The problem is readily solved by etching after the first polish, repolishing on the last lap, and re-etching. This removes the distorted surface layer. Two repolishings may be required to reveal the structure clearly.

The common etching reagents are Picral—usually a 4% solution of picric acid in alcohol, or Nital—from 2 to 10% concentrated HNO_3 in alcohol. Picral is somewhat superior in revealing carbides and is best employed to bring out details of carbide structures. The Nital will also reveal pearlitic structures although not quite so nicely and, since Picral stains the fingers or hands, Nital is more generally used. The more concentrated Nital is used for lower carbon-content steels or for quenched structures (Chaps. 10 to 12).

Microstructures in this chapter include Micros. 9.1 to 9.4, 0.2% or low-carbon steel as normalized and annealed, low and high magnifications.

Micros. 9.5 to 9.8, 0.4 to 0.8% carbon steels in the normalized or annealed state.

Micros. 9.9 to 9.10, hypereutectoid steels air- and furnace-cooled from above the A_{cm}.

Micros. 9.11 to 9.16, low-carbon steel, cold-rolled and process-annealed.

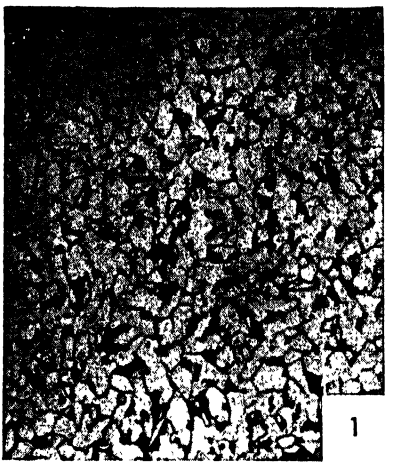

Micro. 9.1. 0.15% C normalized steel; ×100; Nital etch. The structure is about 80 to 85% ferrite (white) as predicted by the phase diagram. The black areas are pearlite whose two-phase lamellar structure is not resolved at this magnification. The black lines in the ferrite are grain boundaries, which delineate the ferrite grain size.

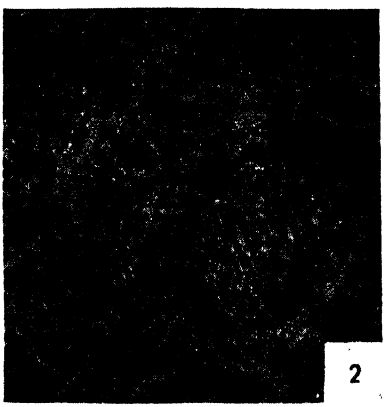

Micro. 9.2. 0.20% C+ 0.42% Mn steel, normalized from a higher temperature (1000°C) and cooled faster in air (by using a smaller section); ×100 Nital etch. This structure is of the Widmanstätten type where α formed not only at γ grain boundaries but to an equal degree along certain crystallographic planes of the γ. Austenite remaining at the Ar_1 was in layers between ferrite plates and thus the fine pearlite (unresolved here) has that form. The former austenitic grain size is somewhat evident, and it clearly was coarser than that of Micro. 9.1.

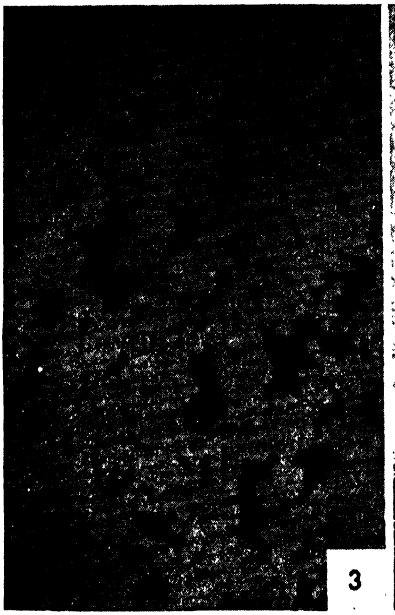

Micro. 9.3. 0.20% C + 0.42% Mn steel, annealed by furnace cooling from 1000°C; ×100; Nital etch. At a low magnification the relative quantities and distribution of ferrite and pearlite are evident as well as the ferrite grain size.

Micro. 9.4. Same as Micro. 9.3 at ×1,000. At the higher magnification, the coarse lamellar carbide of the pearlite is resolved. Black spots are oxide inclusions.

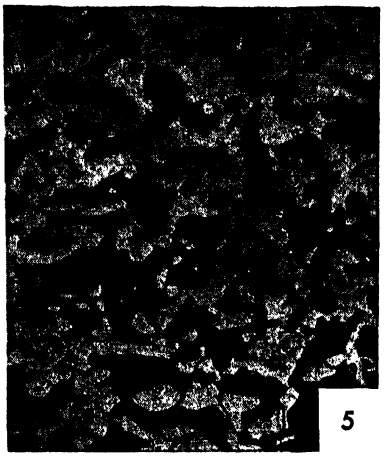

Micro. 9.5. 0.40% C normalized steel; ×100; Nital etch. This structure is also composed of white ferrite crystals and dark areas of pearlite. (It is inaccurate to speak of *grains* of pearlite when it actually consists of two different types of crystals, α and Fe_3C, in a fine lamellar dispersion.) Ferrite here amounts to noticeably less than the expected 50% of the structure, for the reason that upon air-cooling of the specimen in the normalizing treatment, separation of hypoeutectoid ferrite is not complete and the carbon content of the pearlite consequently is diminished.

Micro. 9.6. 0.60% C normalized steel; ×100; Nital etch. Moderately rapid air-cooling of this specimen has resulted in somewhat less than the expected 25% ferrite. As the ferrite forms preferentially at the austenitic boundaries, with the center of the austenite grains later transforming to pearlite, the ferrite crystals outline the former austenitic grains. This specimen showed considerable variation in the size of the austenite grains; some are quite small, others are large. Ferrite formation is not confined completely to austenitic grain boundaries since some white crystallites are visible inside the present pearlitic areas. Slow cooling from a very high temperature, as in castings of hypoeutectoid steels, sometimes gives a pronounced Widmanstätten pattern of ferrite plates in a pearlitic background. Color variations in the pearlite are associated with variations of the angular position of the ferrite-carbide lamellae with respect to the surface of polish.

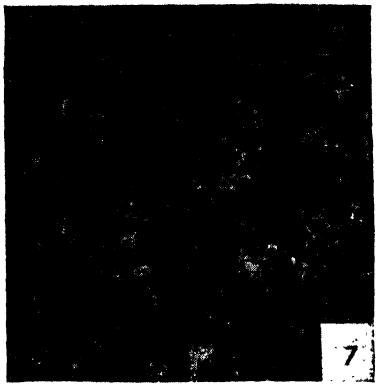

Micro. 9.7. 0.8% C + 0.65% Mn steel, annealed by furnace cooling from 810°C; ×100; Picral etch. The absence of any structural constituent other than pearlite results in a dark appearance at low magnification with variations in shading that are associated with variations in the angle between carbide lamellae and the polished and etched surface.

Micro. 9.8. Same structure as Micro. 9.7 at ×1,000. Details of the lamellar pearlite show that ferrite, the background, is the continuous phase, representing (6.7 − 0.8)/6.7, or 88% by weight of the structure. When the carbide lamellae are normal to the surface (near upper right corner), the *apparent* spacing is less than when they approach parallelism to the surface.

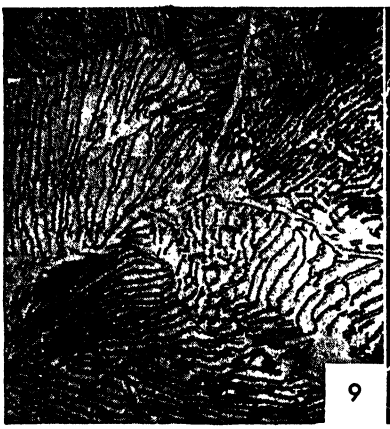

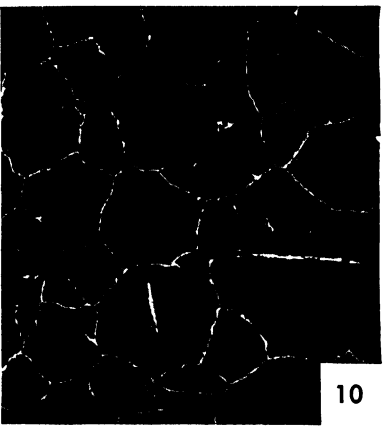

Micro. 9.9. 1.0% C annealed steel; ×1,500; Picral etch. For the reasons previously discussed, this slightly hypereutectoid steel would show little or no excess cementite if a relatively small section were air-cooled. When furnace-cooled from the austenitic field past the A_{cm} line, iron carbide forms at the grain boundaries of the austenite. This micrograph shows the intersection of three former austenite grains, outlined by a thin, continuous cementite envelope at their boundaries. The remainder of the structure is similar to the straight eutectoid steel. Note particularly that, although ferrite and carbide lamellae are approximately parallel in some sections, in other areas within the same former austenite grain they are arranged in a different pattern. This demonstrates that, in normalized or annealed steels, the orientations of pearlitic areas do not reveal the austenitic grain size; some excess carbide (or ferrite) is required.

Micro. 9.10. 1.3% C annealed steel; ×100; Nital etch. With a greater amount of excess carbide present, a high magnification is not required to show the structure of the steel. The white carbides outline former austenitic grain boundaries and reveal the size of the grains existing at the high temperature, *viz.*, about ASTM No. 2 (see page 97). With the increased amount of excess carbides, some large plates of Fe_3C have formed within the former γ grains and outline the specific crystal plane on which they necessarily formed. The dark background structure is pearlite.

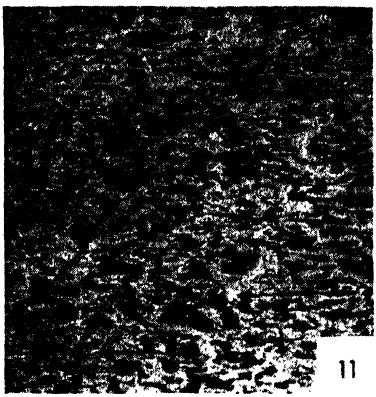

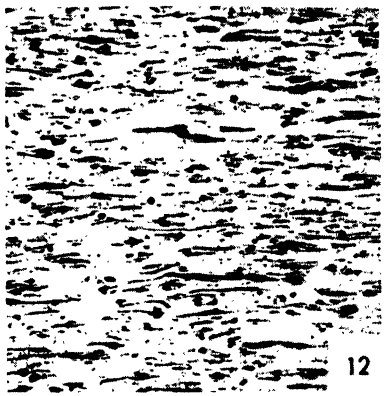

Micro. 9.11. 0.20% C steel, annealed and cold-rolled 40%; ×100; Nital etch. This longitudinal section most clearly shows the cold-work by a combined thinning and elongation of both ferrite grains and pearlite areas.

Micro. 9.12. 0.20% C steel, annealed and cold-rolled 80%; ×100; Nital etch. Again the longitudinal section shows the extreme "fibering" or elongation and thinning of the ferrite and pearlite structure, which has been cold-worked far more than is customary in mill operations.

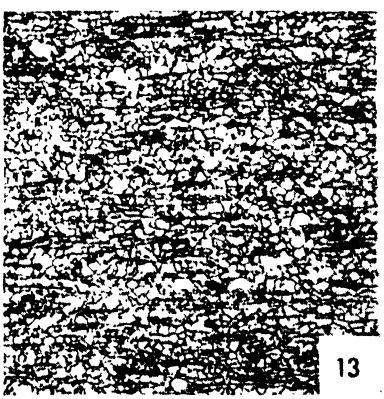

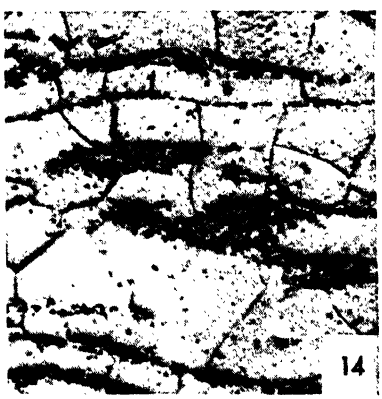

Micro. 9.13. 0.20% C steel, annealed and cold-rolled 80% and annealed 30 min at 700°C; ×100; Nital etch. The subcritical anneal has obviously recrystallized the ferrite grains into equiaxed shapes but has not changed the distribution of pearlitic areas, which still show elongation.

Micro. 9.14. Same structure as Micro. 9.13 at ×1,000. At the high magnification, it is evident that the former pearlitic areas no longer show lamellar carbides. The subcritical anneal has changed the lamellar carbides into groups of spheroidal carbides that occupy the elongated former pearlitic areas. (Compare agglomeration and spheroidization of eutectiferous silicon plates in Al:Si alloys, page 148.)

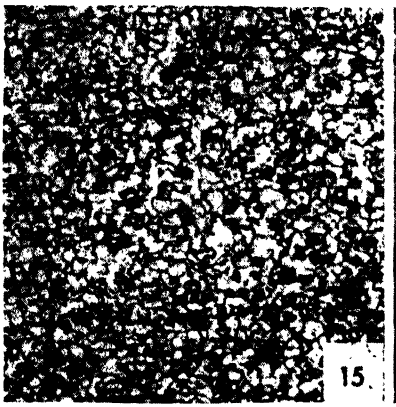

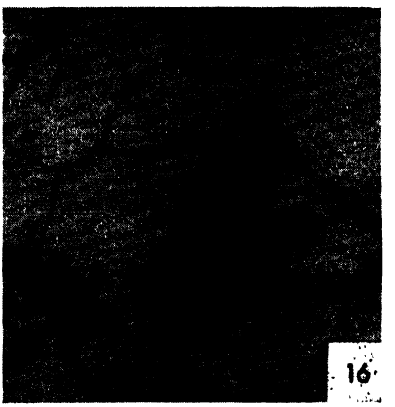

Micro. 9.15. Low-carbon steel, cold-rolled 80%, annealed 1 hr at 800°C, and furnace-cooled; longitudinal section; ×100; Nital etch. Heating above the A_1 temperature caused the distorted pearlitic areas to form austenite and change in shape from elongated to more or less equiaxed shapes. Some growth of ferritic grains has occurred on heating to 800°C, a temperature well below the A_3 temperature of the steel.

Micro. 9.16. Same low-carbon steel as Micro. 9.15 but at ×1,000. At a high magnification, it is clear that not only has the shape of the pearlitic areas been changed but the normal lamellar carbide structure has been restored. This is in contrast to the subcritical or process anneal of Micro. 9.14, which resulted in spheroidal carbides.

9.6 Properties

The mechanical properties of normalized steels, as those of any alloy, are determined by the phases present and their distribution. Ferrite, relatively pure, body-centered cubic iron, has moderately good plasticity and strength, while the carbide is very hard and brittle. In the aggregate or structural constituent called *pearlite*, the ferrite is nearly continuous. Consequently the eutectoid structure has some plasticity combined with moderately high hardness and strength. Hypoeutectoid alloys show a continuous ferrite grain structure containing islands of pearlite; therefore, these steels show good plasticity and strength, the plasticity decreasing and the strength increasing as the amount of ferrite decreases and the amount of pearlite increases with carbon content.

Hypereutectoid alloys, when slowly cooled past the A_{cm} line, show carbide envelopes at the former austenitic grain boundaries and, with this continuous brittle phase, structures such as those in Micros. 9.9 and 9.10 are inherently brittle. It is for this reason that, in commercial practice, hypereutectoid steels must be annealed *below* the A_{cm} line. The two structures shown would be very undesirable for an industrial alloy. Since the more rapid air-cooling of a normalizing treatment suppresses the formation of hypereutectoid carbide envelopes, normalizing can be and is carried out above the A_{cm} line. Quantitative data showing these effects are presented in Table 9.1. For hypoeutectoid steels, the changes in properties are so nearly linear that they can be expressed with reasonable accuracy by a simple equation, which relates the specific property to carbon content by means of the properties of ferrite and pearlite and the proportion of each present in the structure. Thus the tensile strength of annealed hypoeutectoid steels (using the data of Table 9.1 and the lever rule) is related to carbon content by

$$\text{Tensile strength} = \frac{41{,}000\ (\%\ \text{ferrite}) + 115{,}000\ (\%\ \text{pearlite})}{100}$$

$$= 41{,}000\left(1 - \frac{\%\ \text{C}}{0.8}\right) + 115{,}000\left(\frac{\%\ \text{C}}{0.8}\right)$$

A more accurate empirical equation has been developed for the tensile strength of hot-rolled carbon steels:

$$\text{Tensile strength} = 38{,}000\ (1 + 0.024 \times \%\text{C})\ (1 + 0.0009 \times \%\text{Mn} + 0.00001 \times \%\text{Mn}^2)\ (1 + 0.015 \times \%\text{P})\ (1 + 0.004 \times \%\text{Si})\ (1.07 + 0.22G + 0.10G^2)$$

where C, Mn, P, Si signify the weight percentage of the element and G is the gauge expressed in inches.

TABLE 9.1. MECHANICAL PROPERTIES OF NORMALIZED AND ANNEALED STEELS

% carbon	Yield point, psi (000)	Tensile strength, psi (000)	% elongation in 2 in.	Reduction in area, %	BHN
Hot-rolled steel:					
0.01*	26	45	45	71	90
0.20	45	64	35	60	120
0.40	51	85	27	43	165
0.60	60	109	19	28	220
0.80	70	134	13	18	260
1.00	100	152	7	11	295
1.20	100	153	3	6	315
1.40	96	148	1	3	300
Annealed:					
0.01*	18	41	47	71	90
0.20	36	59	37	64	115
0.40	44	75	30	48	145
0.60	49	96	23	33	190
0.80	52	115	15	22	220
1.00	52	108	22	26	195
1.20	51	102	24	39	200
1.40	50	99	19	25	215

* Data on Armco iron. Other specimens represent killed, commercial steels of similar compositions except for carbon content (Nead). The "hot-rolled" state is taken to be equivalent to the normalized state, assuming air-cooling from the γ field.

The other basic factors influencing properties of these alloys will be discussed later, ferrite grain size in the next section and size of the lamellae of pearlite in Chap. 10.

9.7 Grain Size of Steels

Grains have been defined in this book as contiguous crystals of the same phase. In the Fe:Fe_3C system, it is possible to have ferrite grains or austenite grains. It is not possible to have carbide "grains" since the carbide crystallites are not contiguous, except to a very minute degree, with other carbide crystallites. Likewise, it is not possible to have pearlite grains since ferrite crystals are in contact with carbide crystals, and vice versa.

From a glance at Micros. 9.1 through 9.6, it is clear that in normalized or annealed steels, ferrite grain size is significant only in steels with less than about 0.4% carbon; above this value, the amount of free ferrite

becomes so small that at most there are excess or pro-eutectoid ferrite crystallites in contact with pearlite areas.

Austenite grain size is never observed directly in the plain-carbon steels here considered since austenite as a phase disappears at the A_{r_1} temperature. Micrographs 9.3 and 9.6 show the grain size of the austenite that existed in the γ field by the evidence of the small amount of free ferrite or carbide that separated at the austenitic grain boundaries during the relatively slow cooling. There are other methods of determining, at room temperature, the grain size of austenite previously existing at a high temperature (see pages 275 and 376).

Ferrite grain size is controllably varied in the same way as α brass grain size as discussed in Chap. 4. The grain size obtained on heating to 600°C may be increased by heating to a higher temperature. However, here there is a limit well below the melting point; on heating above 723°C, any pearlitic areas present will transform to austenite grains, which, upon continued heating, will grow at the expense of ferrite grains even as the latter are growing at each other's expense. The process is complete, of course, at the A_{c_3} temperature when all ferrite disappears.

In connection with ferrite grain size, there is another variable to be considered in addition to the ones previously discussed in connection with brass: *viz.*, degree of cold-work, annealing temperature (subcritical) and time, purity of ferrite, etc. The new variable is that a given set of ferrite crystals can come into existence in the solid state by other than a recrystallization process. Ferrite crystals form by the $\gamma \rightarrow \alpha$ transformation in pure iron or low-carbon steels upon cooling from the austenitic state. It is not possible to state the relationship mathematically but, since the ferrite grains are nucleated and grow, their size will depend on time and temperature or, specifically, on the cooling rate. Slow cooling of low-carbon austenite will give a much coarser ferrite grain size than fast cooling. The austenitic grain size itself is a variable since, for a given cooling rate, a coarse-grained austenite will give a coarser ferrite grain size than a fine-grained austenite. Factors such as a finely dispersed insoluble phase are important; such a dispersoid would be conducive to a fine-grained austenite and, necessarily then, a fine-grained ferrite.

The usual rules of grain size apply to austenite as well as to ferrite. Although it is not possible to cold-work a plain-carbon-steel austenite, hot-working involves recrystallization and grain growth to a degree dependent on the hot-working temperature. If the austenitic grains do not form in this way, they form in pearlite upon heating a steel containing this structure. Since they form eutectoidally, both ferrite and

carbide must be present at the site of nucleation, but obviously this is no limitation in a pearlitic area where α and Fe_3C are everywhere in contact. This being the case, heating rate through the A_{c_1} temperature only slightly affects the resulting initial austenitic grain size. The coarseness of the pearlitic lamellae will also have only a slight effect.

The newly formed γ grains, just above the A_{c_1}, are of minimum size which increases slightly with time but markedly with temperature. Austenitic grain-growth curves are greatly influenced by the presence

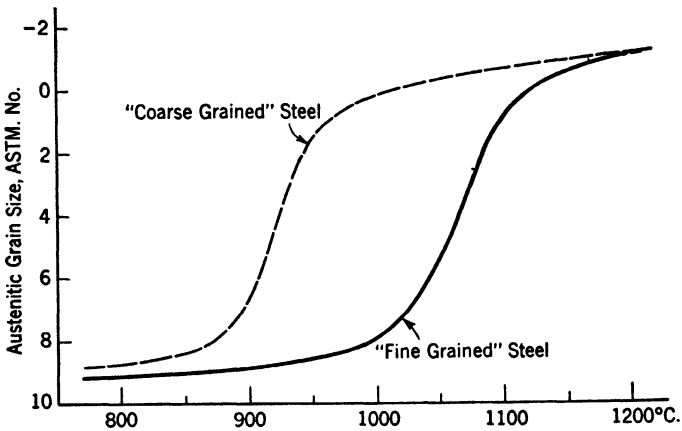

FIG. 9.3. Typical austenitic grain-growth curves of a "coarse-grained" steel (not deoxidized with aluminum) and a "fine-grained" steel (deoxidized with aluminum). The steels differ materially in austenitic grain size only in the usual pack carburizing range (*e.g.*, 950°C), not at hardening temperatures (800 to 850°C) or at forging temperatures (1150 to 1200°C).

of a dispersoid. Relatively insoluble or slowly soluble excess carbides and finely dispersed oxides such as Al_2O_3 will retard grain growth in the usual heat-treating temperature range above the A_{c_1} or A_{c_3}. Typical growth curves are shown in Fig. 9.3. It is evident that grain size differences are not great at temperatures just above the A_{c_1} range or at very high temperatures.

9.8 Engineering Applications, Low-carbon Steels

At the moment, discussion will be confined to steels that are used solely in the annealed or normalized conditions or, equivalently, in the hot-worked condition. Steels containing less than about 0.25% C are predominantly ferrite and only relatively small changes in properties are possible by altering the distribution of the carbide phase. With higher carbon contents, very great changes in properties may be effected

by quenching and thereby suppressing the normal eutectoid reaction. These changes will be covered in subsequent chapters, but here attention is directed to ingot irons and low-carbon steels, *i.e.*, those containing less than 0.25% C. (The two phrases are not quite synonymous since, if less than 0.03% C is present, the material is properly termed *iron* rather than steel.)

The low-carbon steels, used as hot-rolled or occasionally as cold-worked, constitute approximately 80% of the steel used. The reason is to a considerable extent economic; as such steels are not used primarily for strength, the chemical and physical specifications are not too strict and the metal can be produced in semifinished form—sheets, rods, etc.—at the comparatively low cost of 4 to 6 cents per pound. With the low cost are associated favorable factors such as plasticity, which permits severe forming operations to produce such shapes as automobile fenders, fairly good strength, ready machinability,[1] and ease of fusion welding by torch or electric arc.

Optimum machinability or free-cutting properties in low-carbon steels are obtained by increasing the sulfur and necessarily the manganese contents beyond the limits desired for structural uses. The manganese sulphide inclusions that are present in increased quantities reduce the continuity of the plastic ferrite and, therefore, embrittle the steel somewhat without increasing its hardness. The less ductile structure increases the ease of chip removal by the cutting tool. A new type of "free-cutting" steel contains lead, the effect of which is similar to that in the leaded brasses but, present in smaller amounts, the lead is not readily visible in the steel microstructure.

9.9 Cold-working, Annealing, and Aging of Low-carbon Steels

Micrographs 9.11 to 9.13 show structures of a 0.20% carbon steel after severe cold-rolling. As would be anticipated, the longitudinal section shows most clearly the elongation and thinning of both ferrite crystals and pearlitic areas. The rolling plane does not so visibly demonstrate the cold-rolling effects although ferritic grain boundaries and pearlitic areas are less well defined than in an annealed structure.

Microstructures after annealing 1 hr at 600°C (1110°F) show partial recrystallization of the ferrite but no evident change in the shape of the

[1] These low-carbon steels are a little too plastic for best machinability. Therefore cold-working, which hardens the metal and reduces ductility, improves machinability. Low-carbon steel castings that cannot be cold-worked show improved machinability by water quenching from the austenitic state, a process that makes higher carbon steels unmachinable but only slightly hardens the low-carbon metal.

pearlitic areas. This is predictable from the Fe:C phase diagram; recrystallization of *ferrite within pearlite* does not alter the carbide distribution and, although the pearlitic area is undoubtedly softened, it has not changed shape.

Annealing at 710°C (1300°F) causes complete ferritic recrystallization and some ferritic grain growth as shown in Micro. 9.14, but the pearlitic areas still show cold-worked shapes. However, this *process anneal* alters the shape of the carbide lamellae in the pearlite as well as softening the ferrite therein. Micrograph 9.16 at a higher magnification reveals that the pearlitic area, which at a low magnification seemed unaffected by cold-work, now is characterized by globular carbides. The lamellae of Fe_3C have a large surface and high interfacial energy. By changing to spheroids, the Fe_3C surface area and interfacial energy are reduced. This spheroidization of carbide below the A_1 temperature further softens the low-carbon steel and makes it even more plastic for subsequent cold-working. If the steel were heated above the A_1, normal austenite would form and subsequent cooling would reestablish the usual lamellar pearlite structure.

Cold-working of ordinary low-carbon steels hardens the structure and reduces ductility. Subsequent storage at room temperature is accompanied by marked further increases in hardness. This effect is known as *strain-aging;* the usual aging response here following plastic strain rather than quenching. It is believed that nitrogen in metastable solid solution in ferrite is responsible for the effect. Complete deoxidation of liquid steel with aluminum or similar metals that take nitrogen from iron (*e.g.*, zirconium) substantially eliminates this aging. The aging is undesirable since many articles are fabricated by cold-work, and it is not always feasible to avoid a delay between successive stages. If aging does occur and then further cold-work is attempted, much greater force is required and cracking is more likely to be encountered.

9.10 Low-alloy High-strength Steels

The advent in the steel industry of continuous rolling mills, with a high productive capacity for sheet steel at a low unit cost, has stimulated investigations into new means of utilizing the product. One innovation of this character has been the development of a new type of steel having a considerably greater strength than carbon steels in the equivalent hot- or cold-rolled condition. The increased physical properties are achieved in most cases by the same type of structural modifications that have been previously discussed, *i.e.*, by refinement of the ferrite grain size and solid-solution strengthening of the ferrite structure. The new aspect

of this development enters by reason of the use of small amounts of expensive alloys, such as nickel or chromium, and an extensive use of low-cost alloying elements, such as manganese, silicon, copper, or phosphorus. The effect of phosphorus on the properties of steel for many years was believed to be an embrittlement at low temperatures. This misconception arose originally from the many brittle failures encountered with high-phosphorus-content steel rails during the first winter of operation on the Trans-Siberian Railroad. In the latter part of the nineteenth century, phosphorus was known and utilized as a strengthener of steel. Recent work on the low-alloy (and relatively low-cost) high-strength steels has rediscovered this fact and outlined the conditions under which low-temperature embrittlement will or will not appear. In general, the phosphorus content of a steel may be considerably increased if the carbon content is low, and vice versa.

The increased strength of the low-alloy steels has permitted use of the thinner sections that may be readily produced by a continuous mill, and despite the higher steel cost per unit of weight, the lower weight of the final structure may result in direct metal-cost economies as well as obvious but less determinate savings possible when the lighter structure is one that is moved (*i.e.*, a freight car, truck body, etc.). However, the use of thinner sheet metal required a compensating improvement in corrosion resistance to prolong the useful life of the structure. The addition of copper (and phosphorus) is effective in somewhat improving the resistance to weathering as well as increasing strength, but generally painting must still be relied upon for adequate protection.

9.11 Carburizing and Decarburizing

If a hard steel surface is desired, a high-carbon steel can be used, or a much cheaper low-carbon steel may be heated in a carbonaceous atmosphere to increase the carbon content of the surface layers. The latter process, called *carburizing*,[1] may be done by heating the steel while it is packed in a mixture of charcoal and an energizer such as $BaCO_3$. At elevated temperatures, *e.g.*, 900°C, the following reactions occur:

(1) $C + O_2$ (initial air in charcoal) $\rightarrow CO_2$; $CO_2 + C \rightarrow 2CO$
(2) $Fe + 2CO \rightarrow Fe_{(C)} + CO_2$; $CO_2 + C \rightarrow 2CO$
(3) $BaCO_3 \rightarrow BaO + CO_2$; $CO_2 + C \rightarrow 2CO$

[1] Not *carbonizing*, which is a process driving the hydrocarbons from bituminous coal and thereby converting it to relatively pure carbon.

It is apparent that some oxygen atoms are required to transport the carbon atoms from solid pieces of charcoal to iron via gaseous CO. The energizer, here $BaCO_3$, functions to increase the rate of supply of carbon atoms or the amount of the active agent, CO.[1]

Carburizing of a large number of parts may be done more cheaply by heating in a closed furnace containing an atmosphere of hydrocarbon gas such as natural gas or methane. The reactions are as follows:

$$(4)\quad Fe + CH_4 \rightarrow Fe_{(C)} + 2H_2; \qquad CH_4 \rightarrow C + 2H_2$$

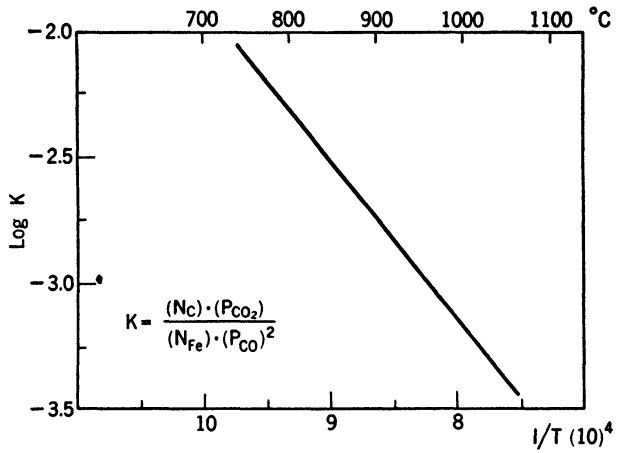

FIG. 9.4. Relation between temperature T and the equilibrium constant K for the reaction, $2CO + Fe \rightarrow C(\text{in Fe}) + CO_2$. The decrease in K with increase in temperature means that the per cent C in iron at equilibrium decreases for a fixed CO_2 : CO ratio.

The gas must flow over the work to remove the hydrogen, or the reaction would go to equilibrium and stop. Too rapid a flow might result in the decomposition of the gas at the iron surface at a rate faster than the carbon is dissolved, in which case free carbon deposits as a soot. The equilibria of reactions (2) and (4) at varying temperatures are shown in Figs. 9.4 to 9.6.

A most significant fact revealed by a comparison of these graphs pertains to the relative effect of temperature on reactions (2) and (4). As the temperature is increased, the equilibrium constant for reaction

[1] An investigation of carburizing using carbon that was artificially made radioactive (*Metal Progress*, **52**, 227, 1947) demonstrated conclusively that reactions (2) and (3) describe the carburizing process and the energizer reactions.

(2) decreases; *i.e.*, the carbon concentration in iron would decrease for a specific CO_2/CO ratio. In other words, to maintain the same carbon concentration in iron, the proportion of CO in the gas must increase. The effect of temperature on carburization with methane is the reverse.

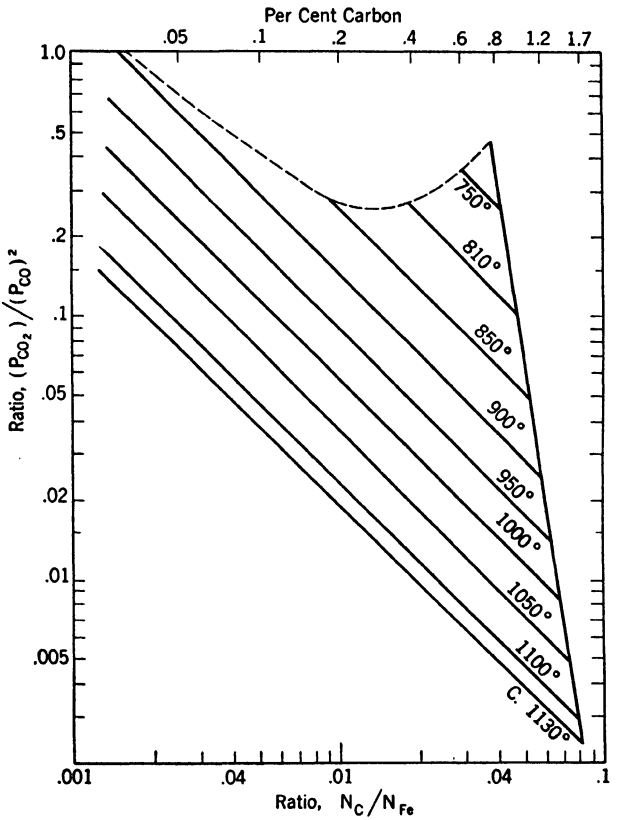

FIG. 9.5. Equilibrium between carbon content of iron, at austenitic temperatures, and ratio of partial pressure of CO_2 to the square of the partial pressure of CO. Carbon content of iron is expressed as molal concentration (*bottom*) or weight per cent (*top*). (*Stanley.*)

Figure 9.6 shows that for a specific CH_4/H_2 ratio, the carburizing power or the carbon concentration in iron increases with temperature.

Carburizing can also be done in a liquid salt such as a fused chloride mixture. Sodium cyanide is usually dissolved in the liquid and with iron in the bath, reacts as:

(5) $2NaCN + O_2$ (from air above bath[1]) $\rightarrow 2NaCNO$ (cyanate)

(6) $3NaCNO \rightarrow NaCN + Na_2CO_3 + C_{(to\ Fe)} + N_{(to\ Fe)}$

Thus cyaniding nitrides iron while it carburizes it, and the resulting surface layer is more brittle than a plain carburized surface zone.

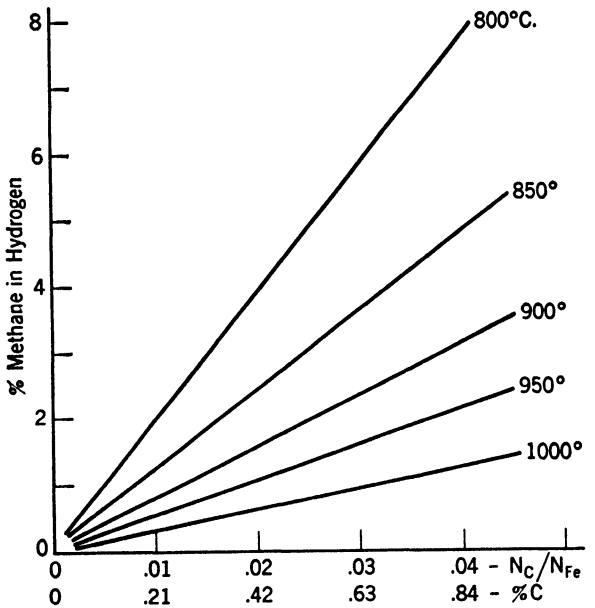

FIG. 9.6. Equilibrium relationships between per cent CH_4 in H_2 and carbon in Fe at different austenitic temperatures. At a specific methane content, the carbon content of iron increases with the temperature (opposite to temperature effect when CO is the carburizing agent; see Fig. 9.5).

$Ba(CN)_2$ is sometimes added with sodium cyanide to produce *activated* baths. This increases the carburizing part of the treatment by

(7) $Fe + Ba(CN)_2 \rightarrow Fe_{(C)} + BaCN_2$

If the steel is almost entirely ferrite, *i.e.*, pure iron or a low-carbon steel below the A_{c_1} temperature, the ferrite can absorb a maximum of 0.025% carbon, and the external carbon supplied to the surface can form

[1] One heat-treating shop wanted to make a cyaniding pot entirely safe by installing a hood that completely enclosed the top of the pot holding the liquid bath. It was an expensive, good-looking, and safe installation. Unfortunately iron treated in this bath did not surface-harden and reactions (5) and (6) give the reason.

only a very thin surface layer of Fe_3C. If the steel is above the A_{c_1} temperature but below the A_{c_3}, the surface carbide can eutectoidally react with any adjacent ferrite that is present to form austenite, but this intermediate reaction slows up carbon absorption, and carburizing in this temperature range results in thin, shallow cases with a very high surface-carbon content (up to 3.0% in the outer 0.004 in. layer). However, if the steel is initially in the austenitic condition, carbon at the surface is soluble to an amount exceeding 0.80% and is free to diffuse into the steel. The higher the temperature attained, the deeper is the carbon penetration and, correspondingly, the lower may be the surface carbon concentration, since the carbon diffusion rate into the steel generally increases more rapidly than the increase in rate of carbon supply to the surface. In most commercial carburizing, the surface may contain about 0.80 to 1.0% carbon with the concentration tapering off until, at a depth (usually 0.010 to 0.040 in.) determined by the time, temperature, and other carburizing-practice variables, the carbon content is that of the original low-carbon steel. The "Metals Handbook" contains articles devoted to carburizing as well as to other surface treatments. However, it should be emphasized here that the limitations of these surface treatments are to a considerable extent explicable on the basis of the pertinent phase diagrams, particularly the solid-solution fields, since *diffusion is impossible in the absence of solid solubility.* Thus the concentration limits away from the immediate surface of the steel being treated are set by the phasial solubility limits. The structures and properties attained after heat treatment of carburized steels follow the generalizations covered in Chap. 10 for steels of the appropriate range of carbon contents.

An important aspect of carburizing is the growth of the surface layer that results from the addition of carbon atoms. Even though the carbon dissolves interstitially, it is a little too large for the interstices and somewhat expands the iron lattice. Necessary dimensional adjustments with the core are readily made by plastic austenite at the carburizing temperatures. On cooling, however, the surface layer of higher carbon content expands more on transforming to pearlite than does the core, which transforms to ferrite, mostly, and pearlite. As a result, the surface layer is left with residual compressive stresses that are a desirable feature of carburized parts. Actually, carburized parts are practically always quenched and, although the effect of quenching has not yet been discussed, the same types of residual compressive stresses are then obtained.

The surface of steel may lose carbon to its surrounding atmosphere

as well as gain carbon. The previous reaction (2) $2CO + Fe \rightarrow Fe_{(C)} + CO_2$, is reversible and may proceed to the left, removing carbon from the surface layer if the steel is heated in CO_2. Whether this decarburizing reaction or carburizing occurs depends on the ratio of CO_2 and CO or their partial pressures as follows:

For the chemical reaction, $2CO + Fe \rightleftarrows Fe_{(C)} + Co_2$; the mass action law states that at a temperature T, an equilibrium state is reached where the equilibrium constant

$$K_T = \frac{[Fe_{(C)}] \times [CO_2]}{[Fe] \times [CO]^2}$$

Assuming that solid-state concentrations are constant and that the active concentrations of the gases CO and CO_2 are proportional to their partial pressures, the critical ratio becomes:

$$P_{(CO_2)}/P^2_{(CO)}$$

Some other possible *decarburizing* reactions are

$$Fe_{(C)} + H_2O \rightarrow Fe + CO + H_2$$
$$Fe_{(C)} + O_2 \rightarrow Fe + CO_2$$

Decarburization is chiefly a problem with higher carbon-content steels which are heat-treated *after* being fabricated to final shape. At the moment, it is sufficient to say that, if the surface has a low-carbon content, it will have the properties of a low-carbon steel.

QUESTIONS

Group A

1. Calculate the percentages of structural constituents in slowly cooled steels containing (*a*) 0.08% carbon, (*b*) 0.35% carbon, (*c*) 0.70% carbon, (*d*) 1.2% carbon, (*e*) 1.6% carbon.

2. Answer question 1 assuming that the *stable* system is achieved.

3. Why is a low-carbon-steel sheet preferred for automobile fenders, and why is it desirable to have this steel a "killed" type?

4. Why will a 0.20% carbon steel carburize very much more quickly at 875°C than will ingot iron?

5. What would be the difference in structure of a 1.2% carbon steel if (*a*) furnace-cooled from above the A_{cm} and (*b*) normalized from above the A_{cm}, reheated just above the A_{c_1}, and then furnace-cooled?

Group B

1. If the hypereutectoid steel of Micro. 9.10 had been strongly deoxidized with Al and then cooled very slowly from above the A_{cm}, the resulting microstructure would be *abnormal*, showing heavier carbide envelopes at the former austenitic

grain boundaries and then a zone of free ferrite between the carbide envelopes and pearlitic areas. Give a possible explanation of the mechanism of the development of this abnormal structure.

2. At austenitic temperatures, a decarburized 0.8% carbon steel has a smooth gradient of per cent carbon vs. distance, increasing smoothly from 0.00% at the immediate surface to 0.8% carbon at some depth (*e.g.*, 0.01 in.). Describe, in terms of the A_3 line of the Fe:C diagram, the redistribution of carbon on very slow cooling that results in a free ferrite band to perhaps 0.004 in. and, abruptly, a practically complete pearlitic structure of nearly 0.8% carbon.

CHAPTER 10

THEORY OF HEAT TREATMENT OF STEELS

Steels may be heat-treated in order to accomplish one or more of the following objectives: (1) the elimination of hydrogen, dissolved during pickling or electroplating, which causes brittleness; (2) relieving microstresses in the atomic lattice that increase brittleness (tempering or drawing); (3) relieving macrostresses that may cause distortion upon machining or failures in service (stress-relief annealing); (4) eliminating the effects of cold-work (subcritical or process annealing); (5) changing the structure to a more uniform condition (normalizing); (6) changing the structure to a softer or more machinable condition (annealing, full or spheroidizing types); (7) enhancing the strength and hardness properties to a marked extent (hardening, usually followed by a tempering treatment). Of these heat treatments, Type 1, performed at 250 to 450°F, is accompanied by no visible change in the microstructure and, with 4, is not included in this discussion.

10.1 Formation of Austenite

Almost all steels, except the highly alloyed austenitic types, consist of the stable phases, ferrite and carbide, when they are machined or otherwise formed to shape prior to final heat treatment. The first step in the heat treatment is to *austenitize* the steel; *i.e.*, heat the metal to a temperature above the A_{c_1}, or above the A_{c_3} if it is of hypoeutectoid composition. The austenite does not immediately form as a homogeneous phase throughout the structure. Some time is required for the initial austenite nuclei to grow by absorbing the surrounding ferrite and carbide crystals. Even after the structure has completely transformed to austenite, it is not necessarily homogeneous; areas that were formerly ferrite may be somewhat low in carbon, and those formerly carbide may be high in carbon concentration. In the case of a hypoeutectoid steel, some time may be required for carbon to diffuse into areas that were previously large masses of ferrite. Hypereutectoid steels are hardened from a temperature between the A_{cm} and the A_1 lines; hence, some undissolved carbides remain in the austenite, and the austenite in the

vicinity of these carbides does not immediately have the same carbon content as it has elsewhere.

The time required to obtain homogeneous austenite varies with the maximum temperature reached and the structural characteristics of the original ferrite-carbide matrix. The higher the temperature to which the steel is heated in the γ field, the shorter will be the time required for carbon diffusion to erase nonuniformities in carbon dis-

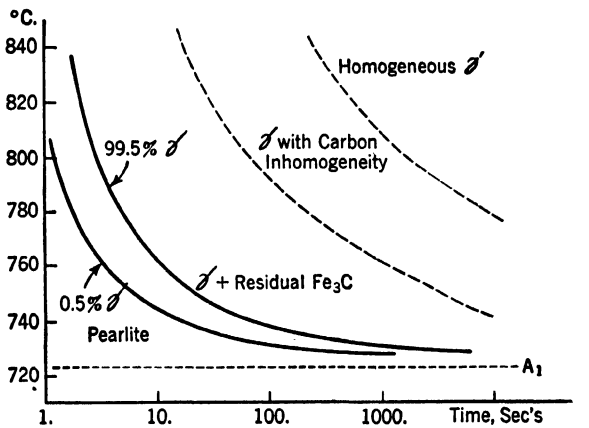

FIG. 10.1. Austenitization graph of a plain carbon eutectoid steel, starting with a pearlitic structure obtained by normalizing from 875°C. The first curve (0.5% –) represents the first visible evidence of austenite; the second curve (99.5% γ) represents the disappearance of pearlite although some residual carbides remain undissolved. The third line, dashed, represents the approximate time-temperature limits for solution of all residual austenite; and the last dashed curve represents the probable attainment of homogeneity in the austenite. (*Mehl.*)

tribution. For example, a normalized eutectoid carbon steel requires about 5 sec at 780°C or 100 sec at 730°C to transform about 99.5% to austenite. However, it requires about 200 sec at the 780°C to dissolve all carbides, and in the vicinity of 10,000 sec (nearly 3 hr) to attain a completely homogeneous austenite. At 810°C, homogeneous austenite is obtained in 1,000 sec (about 17 min).[1] A finely spheroidized carbide structure austenitizes most rapidly, next a fine pearlitic structure, then, most slowly, a coarse pearlitic or spheroidized structure. Typical time-temperature curves for austenitization are shown in Fig. 10.1.

If the prior structure consists of large masses of ferrite or contains coarse crystallites of cementite, the austenitizing time is noticeably longer at any specific temperature. If the carbide phase is not simply Fe_3C but contains chromium, molybdenum, vanadium, or tungsten

[1] Mehl, *Trans. ASM*, **29**, 813, 1941.

carbides which are relatively stable and slow to dissolve, then homogeneous austenite is rarely attained by the ordinary times and temperatures utilized in industrial practice. A higher temperature that would completely dissolve the alloy carbides and homogenize the austenite is undesirable for reasons of possible and undesirable austenitic grain growth or quenching stresses (page 281), or relatedly, danger of distortion or cracking upon quenching. However, the subsequent discussion of heat treatment is predicated upon starting with homogeneous austenite except when the contrary is explicitly stated. Furthermore, the discussion applies only to carbon steels except when otherwise specified.

10.2 Isothermal Transformation of Austenite to Pearlite

In the $Fe:Fe_3C$ diagram of Fig. 9.1 (page 236), the equilibrium line indicating the temperature at which austenite eutectoidally transforms to the ferrite-carbide aggregate known as *pearlite* is called the A_1 line. The diagram also shows a lower position of this same line labeled the A_{r_1}, where austenite transforms to pearlite upon cooling at a rate faster than that required to maintain equilibrium conditions. The A_1 temperature has a fixed equilibrium value, but the A_{r_1} temperature (and also the A_{r_2}), resulting from undercooling, varies with the speed of cooling.

A similar displacement of lines in phase diagrams has been mentioned, qualitatively, in every other system discussed so far. The effect in $Fe:Fe_3C$ alloys, however, is of such direct importance in practical heat-treating that a more quantitative treatment is desirable. Such a treatment is experimentally possible by quenching small sections, from a temperature in the homogeneous austenitic range, into a bath at a temperature below the A_1 line and noting the time required for transformation to start and the time necessary for completion. When this procedure, *isothermal* or *constant-temperature* transformation, is carried out at a number of temperatures from the A_1 line to room temperature, a temperature-time graph, such as that shown in Fig. 10.2, is obtained. To minimize the complexities, the discussion initially will be limited to a eutectoid steel, 0.8% carbon.

The horizontal line represents the A_1 temperature of 723°C. The roughly parallel C-shaped lines below the A_1 define the time required for the $\gamma \rightleftarrows \alpha + Fe_3C$ reaction to start (marked *s*) and be completed (marked *f*) at any specific temperature in the indicated range. The transformation is slow to start and be completed at temperatures just under the critical, but the delay in starting and the time required for completion decrease as the temperature drops to about 550°C (about 1000°F). In this range, the greater the degree of undercooling, the more

unstable austenite becomes or, in other words, the greater is the urge to transform. Down to about 550°C, this effect is dominant over the associated difficulty in transformation resulting from the formation of two phases of far different carbon contents, α (0.025% C) and Fe_3C

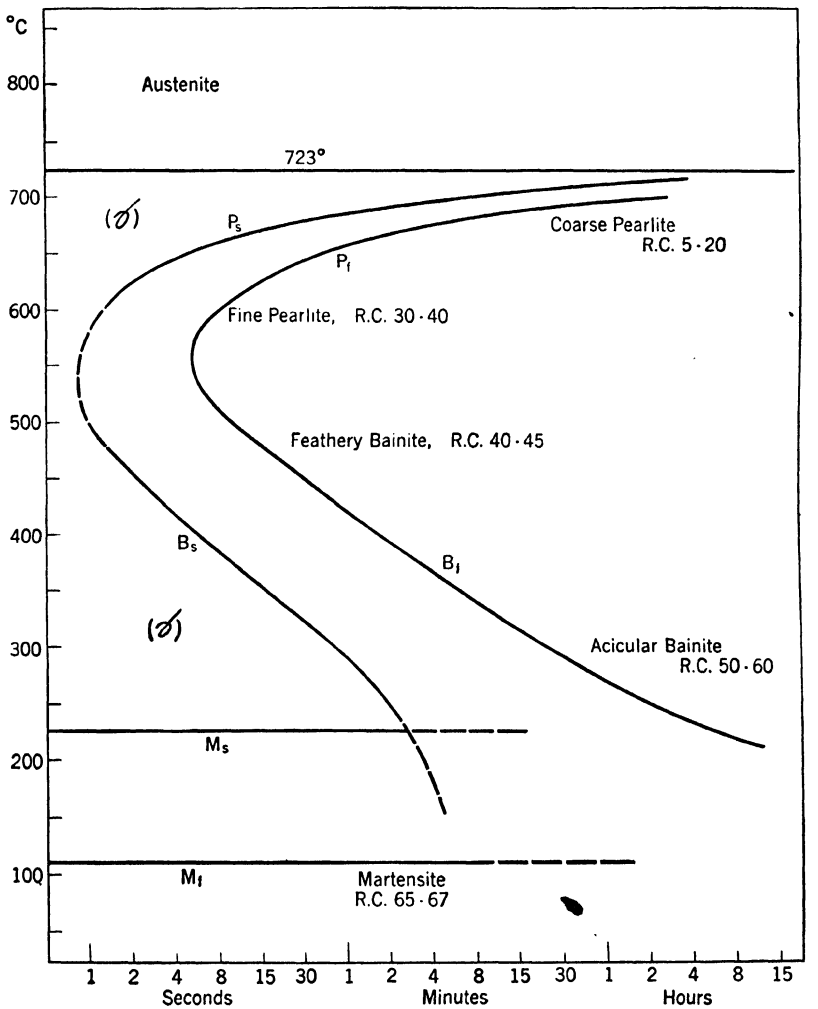

FIG. 10.2. Isothermal transformation diagram for 0.80% C, 0.76% Mn steel, austenitized at 900°C, austenitic grain size No. 6. P_s and P_f : start and finish of pearlite reaction; B_s and B_f: start and finish of bainite reaction; M_s and M_f: start and finish of martensite reaction. Abscissa, logarithmic time as indicated.

(6.7% C), from a homogeneous solution. The transformation in this range results in a pearlitic aggregate of the two phases, and their formation involves diffusion of carbon. If the degree of unstability is low and the rate of reaction slow, plenty of time is available for diffusion. The ferrite and carbide then form coarse, lamellar pearlite with an associated low hardness. As the temperature of austenitic transformation decreases (toward 550°C), the rate increases, the time available for carbon diffusion is less, and, consequently, the pearlite lamellae become increasingly finer, or closer together, with a related increase in hardness.

The mechanics of the transformation in this range are partly known. Carbide formation initiates the process, and presumably, as carbide forms, the adjacent austenite becomes depleted in carbon, thus less stable (*e.g.*, note the course of the A_3 line with carbon concentration), and ultimately an adjacent layer of ferrite forms. As the α phase forms with little (0.025%) carbon in solution, that element diffuses to the adjacent austenite that eventually becomes supersaturated, carbide again forms, and so forth. The formation of coarse pearlite at high temperatures seems to conform to this description in that the structure apparently develops by alternate deposition of ferrite and carbide, but finer pearlites seem to show simultaneous growth of both phases at their open ends in contact with austenite. Crystallographic relationships seem to be well defined for the coarse pearlite in which the carbide-ferrite lamellae are quite straight. As the lamellae become finer, they are subject to greater distortion and bending with a loss in obvious crystallographic relationships.

In eutectoid steels, with no excess phase at the austenite boundaries, the pearlite forms nodules, which tend to grow across the boundaries and become larger than the former γ grains. Upon more rapid cooling with the eutectoid reaction occurring near the Ar' point or in the 550°C range, pearlite grows from an austenitic boundary, in a roughly spherical form, into all adjacent austenite grains. The large number of nuclei now cause the pearlite nodules to be much smaller than the original austenite grains. In a polished section, the pearlite has a nodular form, and exceptional micrographic technique is required to resolve the individual ferrite-carbide lamellae.

10.3 Isothermal Formation of Bainite

At temperatures between about 550 and 200°C (1000 to 350°F), more time is required for the transformation of austenite to start, and the subsequent rate of transformation decreases. In this range of temperatures, while the degree of "unstability" of the austenite con-

tinues to increase, the retardation force, arising from very slow diffusion of carbon and the greater rigidity of the austenite lattice, becomes increasingly important and overbalances the increased urge to transform. Structures in this range vary from a feathery aggregate of ferrite and very fine carbides at around 450°C to groups of dark-etching, lens-shaped (but more angular) needles with no visible carbides at around 200°C. All these structures are called *bainite.* They are basically different from pearlites; *e.g.*, the ferrite in pearlite has one crystallographic relationship to austenite, while in bainite it has quite a different relationship, actually one similar to that shown by hypoeutectoid ferrite

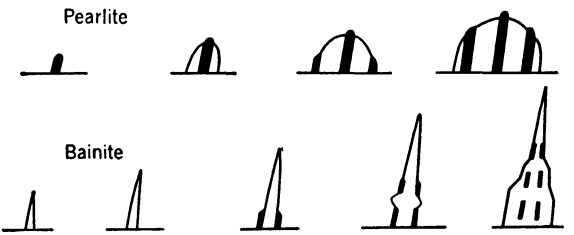

FIG. 10.3. Growth of pearlite, nucleated by a carbide crystal, and of bainite, nucleated by a ferrite crystal and with carbide rejected, after reaching a critical concentration, as discontinuous small crystallites. (*Hultgren.*)

separating from austenite. The difference indicates that, whereas pearlite formation is initiated by carbide separation, bainite is initiated by ferrite separation[1] (see Fig. 10.3).

10.4 Formation of Martensite

The structures formed directly from austenite at temperatures below about 200°C are also lens-shaped needles, similar in shape and appearance to the bainites formed at slightly higher temperatures, but they have slower etching characteristics and, therefore, are usually lighter in color. The structure, as freshly formed, is called *white martensite.* Whereas carbide is readily visible in pearlite and detectable by X rays in bainite, no carbides have been found in freshly formed martensite by any experimental means now available. The lens-shaped, angular needle structure of martensite is frequently called *acicular* (from the Latin word meaning needle-shaped). The structure shows an apparently clear-cut crystallographic relationship to a specific set of planes of the austenite, which, however, is not a simple plane such as the octahedral (plane of slip and twinning).[2]

[1] Smith and Mehl, *Trans. AIME,* **150,** 211, 1942.

[2] Greninger and Troiano, *Trans. AIME,* **140,** 307, 1940.

Freshly formed martensite has been found to have a body-centered structure that is not cubic but tetragonal. The transformation mechanism best accounting for the observed crystallographic relationship between martensite and the parent austenite is that proposed by

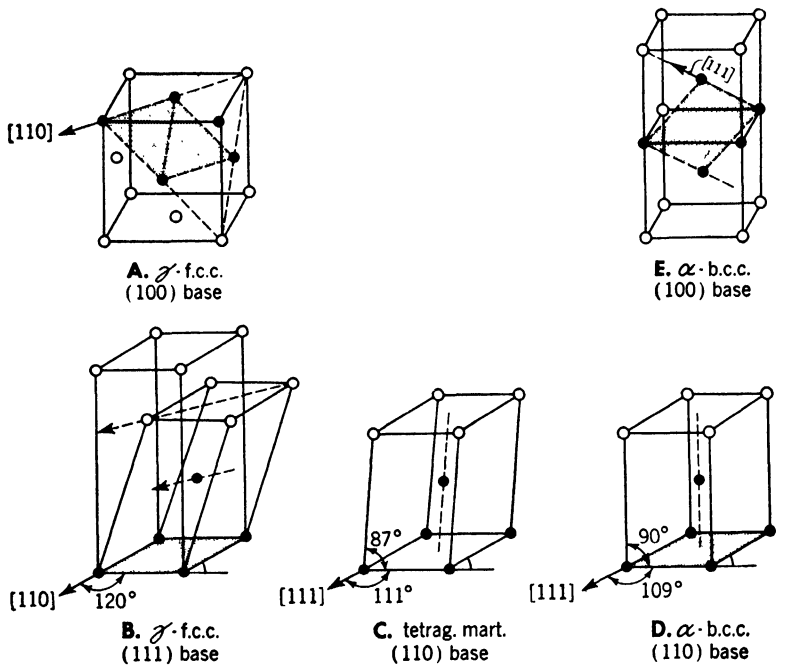

FIG. 10.4. Shearing movements of iron atoms involved in changing from face-centered cubic austenite to body-centered cubic ferrite via the martensite transformation. (*A*) normal austenite lattice, cube base, octahedral plane cross-hatched; (*B*) normal austenite lattice but with the cross-hatched octahedral plane drawn as the base; (*C*) atoms on the planes above move in the direction indicated by arrows in sketch *B* and atoms on the base move slightly to change the angle as shown. The movement results in a body-centered lattice but here has not gone to completion so structure is tetragonal; (*D*) completion of the movement results in a normal body-centered cubic lattice. The base plane which was octahedral in *B* becomes the dodecahedral plane of the body-centered lattice; (*E*) showing the section of *D* oriented in a normal body-centered cubic sketch. The same five atoms in black appear in all five sketches.

Kurdjumow and Sachs, which involves a shearing movement of atoms on specific planes of the austenite (Fig. 10.4) in a manner analogous to the shearing movements accompanying mechanical twinning.

In Fig. 10.4*A* the familiar face-centered cubic structure of austenite is reproduced in the normal form with cube faces. In *B*, the same structure is reproduced with four atoms of the octahedral (111) plane as the base; the same atoms in each sketch are blackened to show this

relationship. The sequence of planes parallel to the octahedral base is, as described in Chap. 2, *ABCA*. The light lines in Fig. 10.4*B* show a rhombohedron. The arrows show the shearing movement required to transform the face-centered cubic structure to body-centered cubic. In part *C*, the shearing movement has occurred but not completely, and the resulting structure is most simply described as body-centered tetragonal, the structure of white martensite with about 0.8% carbon. When the shear is completed, the structure becomes as shown in *D*. To demonstrate that this is body-centered cubic, the sketch of two normal body-centered cubes is shown in part *E*. The plane that was (111) in the face-centered cube becomes (110) in the body-centered cube, and the direction that was [110] in the face-centered cube becomes [111] in the body-centered cube.

Returning to Fig. 10.2, the isothermal transformation graph, it is apparent that, if the steel were quenched from the austenitic state to 150°C, a fixed amount of martensite would form and would not be increased by holding at temperature. If the steel were held ½ hr or so, the remaining austenite, according to the graph, would start transforming to bainite. *The martensite reaction, therefore, should, strictly speaking, not be shown on an isothermal transformation chart. The martensite reaction proceeds with temperature drop and stops when the temperature is held constant.*

The M_s temperature at which martensite starts to form is markedly altered by the carbon content of the austenite (not of the steel because not all carbides may be dissolved in the austenite). Experimental data show that other elements also have some effect. Confining the present discussion to plain-carbon steels, the M_s temperature can be expressed by the equation:

$$M_s(°C) = 550 - 361(\%\ C) - 39(\%\ Mn)$$

Thus pure ferrite, upon drastic quenching, would start to transform to the body-centered lattice at 550°C, an ordinary medium-carbon steel (0.4% C + 0.6% Mn) at 382°C and a eutectoid steel (*e.g.*, 0.8% C + 0.7% Mn) at 234°C.

10.5 Isothermal Transformation of Noneutectoid Steels

Superimposed isothermal transformation diagrams for two commercial steels, one hypoeutectoid and one hypereutectoid, are reproduced in Fig. 10.5. In comparison with Fig. 10.2 of a eutectoid steel, these have horizontal lines above the A_1, representing the upper critical temperature A_{cm} (top edge of diagram) or A_3 for the steels. Also there

is a line marked F_s, representing the start of ferrite separation or C_s, representing the start of excess cementite or carbide separation.

Further comparison of the superimposed diagrams reveals that carbon content has only a minor effect on the time required for the pearlite

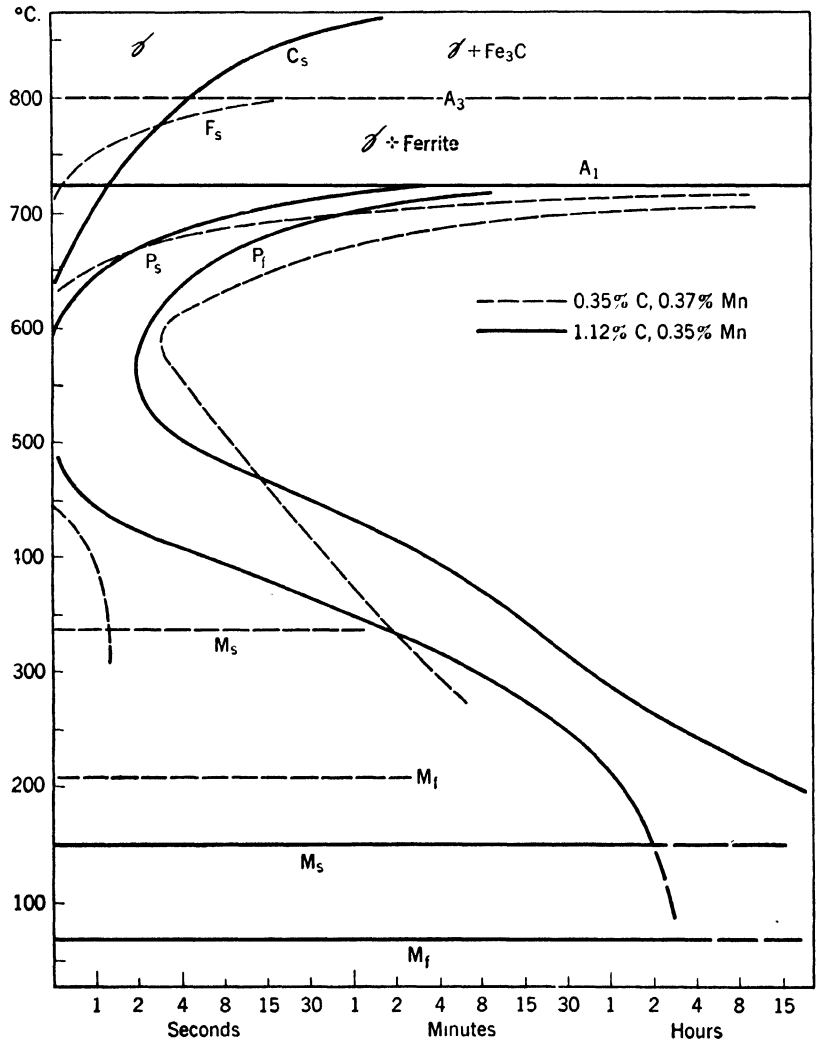

FIG. 10.5. Effect of carbon on austenite transformation as shown by isothermal transformation graphs of a hypoeutectoid steel (dashed lines) and a hypereutectoid steel (solid lines).

reaction, from the A_1 to the knee of the transformation diagram. However carbon does tend to stabilize austenite at lower temperatures. It greatly retards the initiation and completion of the bainite reaction, displacing this part of the C graph strongly to the right. As just mentioned, it also strongly decreases the martensite reaction temperatures, M_s and M_f. Thus the medium-carbon (0.35%) steel is completely martensitic at 200°C, whereas the high-carbon steel retains some austenite to the vicinity of room temperature.

The isothermal diagram for the hypoeutectoid steel should show an F_f line, representing the finish of pro-eutectoid ferrite separation at any specific temperature, but this line was omitted to simplify the graph. At temperatures near the "knee" of the C curve, the ferrite separation is not complete when the reaction starts; *i.e.*, the F_f line would be above the P_s line at 700°C, but below the P_s line near the knee of the graph. Under the latter conditions, both free ferrite and pearlite may be forming simultaneously in different parts of the austenitic grain upon transformation at 650 to 600°C. However, the ferrite separation rarely would be complete here; the pearlite would then contain less than 0.8% carbon and the amount of free ferrite would be less than that indicated by use of the lever rule and phase diagram:

$$\text{For } 0.35\%\text{ C; } \frac{0.8 - 0.35}{0.8 - 0.025}\ (100) = 58.5\%\text{ free ferrite}$$

This result is in accord with the discussion of the Fe:C phase diagram in Chap. 9. It is interesting to note that just below the A_1 temperature, ferrite separation is complete before the pearlite reaction starts. In some laboratory research on the F_f line, it was found that a steel with this 0.35% carbon showed approximately 65% free ferrite, *more* than the amount indicated by the phase diagram. Since decarburization did not occur, the obvious explanation is to use the principle discussed in the Al:Si system, metastably projecting the A_3 line to the transformation temperature, as in Fig. 10.6:

(1) Eutectoid composition at 0.95% C

(2) Amount of free ferrite $= \dfrac{0.95 - 0.35}{0.95 - 0.025}\ (100) = 63.2\%$

10.6 Transformation of Austenite on Continuous Cooling

Since the isothermal transformation diagrams (Figs. 10.2 and 10.5) are fundamentally time-temperature charts, it would seem possible to superimpose cooling curves and decide therefrom whether a given cooling rate would result in pearlite, martensite, or a mixture of the two. It is apparent that bainite could not form on continuous cooling of the plain-carbon steels since upon starting at the A_1 line, no continuous cooling curve could cross the B_s line from the metastable austenite field. However, it is not possible in any event to superimpose a cooling curve directly on an *isothermal* diagram. If the isothermal P_s time at 650°C

is 5 sec for a eutectoid steel, cooling from the A_1 to 650°C in 5 sec will not cause pearlite to start to form immediately. The isothermal diagram postulates an incubation time in this case of 5 sec *at* 650°C. Upon making certain simplifying assumptions, it is possible to construct a continuous cooling *transformation* diagram from an isothermal one.[1]

Assume that, with reference to Fig. 10.7,

1. The extent of transformation at a time-temperature point X is not greater than if quenched to X; in other words, more time will be required for measurable transformation.

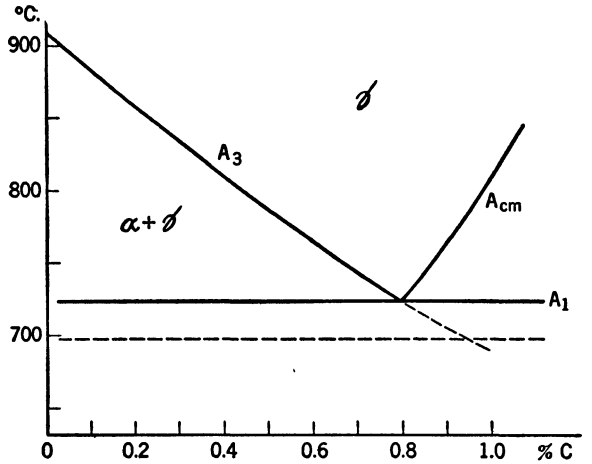

FIG. 10.6. Eutectoid region of the Fe : Fe_3C phase diagram, in solid lines, with a metastable prolongation of the A_3 line to a postulated Ar_1 line. By this diagram, more than the lever rule amount of ferrite could form at a subcritical temperature if the eutectoid reaction were delayed by an element which had little effect on ferrite separation.

2. On cooling through a limited temperature range, T_x to T_o, the amount of transformation equals that on the isothermal diagram at the mean temperature $\frac{1}{2}(T_x + T_o)$ for the cooling interval $t_o - t_x$.

Using these assumptions, it is shown in Fig. 10.7 that on continuous cooling to point O, conditions are equivalent to having isothermally reached the point (*) on cooling continuously to O, that lies on the P_s line; therefore, pearlite would just start to form. This point O was selected by trial and error to obtain the asterisk point that lies on the P_s line. Later arbitrary times may be selected to find the P_f point for this cooling rate. Other cooling rates may be selected to locate continuous cooling P_s and P_f curves. Then a derived cooling diagram may be drawn, such as Fig. 10.8, here applicable to a plain-carbon eutectoid steel.

[1] Grange and Kiefer, *Trans. ASM*, **29**, 85, 1941.

The uses of Fig. 10.8 are fairly self-evident. For example, if it was desired to normalize a very thin steel strip, upon cooling in air more rapidly than 35°C per sec, some martensite might be encountered and slower cooling would be necessary. On the other hand, normalizing a roll casting 3 ft thick and weighing several tons might require an oil quench to obtain a cooling rate as fast as from 5 to 20°C per sec.

The critical cooling velocity shown by this diagram is 140°C per sec. If a fully martensitic structure were desired, that cooling rate must be

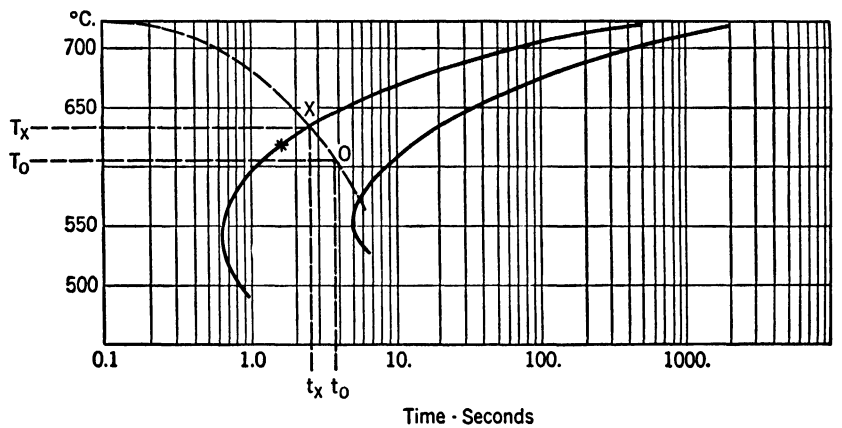

FIG. 10.7. Estimation of time of start of pearlite reaction upon continuous cooling from the isothermal diagram. Upon cooling at rate shown by dashed cooling curve, assume nothing happens until point X is reached. Cooling to O requires time $(t_o - t_x) = 1.4$ sec and it is assumed that the average temperature for this period is halfway between T_x and T_o, *i.e.*, 620°C. Since 1.4 sec at 620°C is at the asterisk, on the isothermal P_s line, then O is the P_s for continuous cooling.

met or exceeded to avoid some pearlite in the structure. An intermediate cooling rate, *e.g.*, 100°C per sec, would give a pearlite-martensitic mixture. From the earlier discussion, it should be remembered that the pearlite will be in the form of nodules distributed at the former austenitic grain boundaries.

If only a small amount of pearlite is present, *e.g.*, 15 to 25%, the black etching nodules in white martensite nicely reveal the former austenitic grain size. This is one method of determining austenitic grain size and is particularly appropriate for eutectoid steels where no free ferrite or carbide can form to show the high-temperature grain size. Experimentally, the effective amount of pearlite is achieved by a gradient quench. The bar of the steel is austenitized and quenched from one

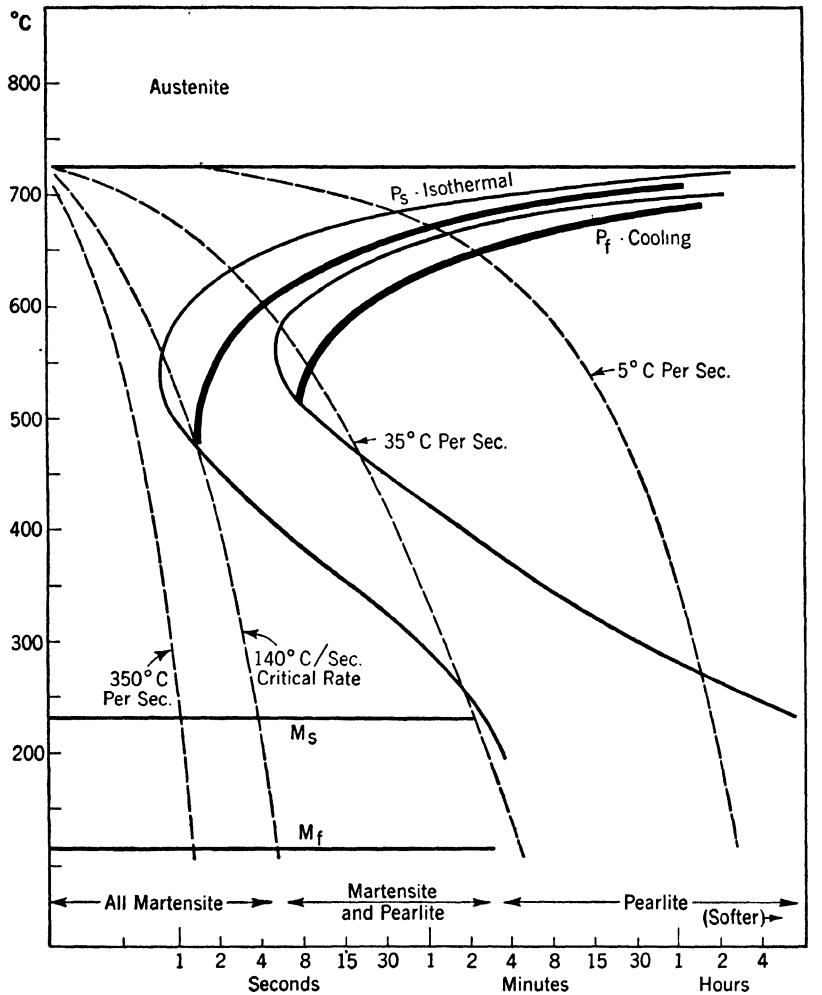

FIG. 10.8. Transformation diagram for continuous cooling (heavy P_s and P_f lines) of a eutectoid steel in comparison with the isothermal transformation lines. Four different cooling rate curves are superimposed and the structures so obtained are labeled at the bottom.

end. Somewhere between the quenched and the air-cooled ends, a cooling rate will have existed that resulted in just the right proportions of pearlite nodules and martensite.

10.7 Hardenability

It should now be clear that successful hardening requires cooling, *particularly from* 723 to 550°C, in a time less than that required for fine pearlite to form at the "nose" of the cooling transformation graph (Fig. 10.8). Since heat is abstracted directly by the cooling medium only from the surface of the steel, the cooling rate at various depths below the surface, in conjunction with the time position of the transformation graph, will determine the depth of the completely martensitic structure. The depth of hardening under controlled experimental conditions is called the *hardenability;* the word does not refer to *degree* of hardness but to the *depth* of useful hardness.

There are two presently accepted methods for quantitatively evaluating the hardenability of steels. One, developed by Grossman,[1] requires quenching from the austenitic state under controlled conditions a series of cylinders of increasing diameters. The cylinders are subsequently sectioned, and hardness traverses across the diameter made. The diameter of quenched rod that will just harden through in the sense of showing 50% martensite at the center is the *critical diameter* or D_c. A numerical value of $D_c = 1$ in. means that a $\frac{7}{8}$-in. rod would be completely martensitic while a $1\frac{1}{8}$-in. rod would show mostly fine pearlite at the core.

The second method, developed by Jominy,[2] involves a differential quench. A standard cylinder 1 in. in diameter by 4 in. long is austenitized and water of a specified temperature, pressure, and quantity directed against one end of the hot cylinder. The test jig is shown in Fig. 10.9. After the entire rod is cold, a flat surface is ground on the longitudinal surface of the rod and hardness measured at varying distances from the quenched end. The resulting data, typically as shown in Fig. 10.10, enable the specification of distance from the quenched end to the zone of half hardness (or 50% martensite) as the Jominy hardenability.

The entire control of hardenability is based on control of the time required for initiation of the transformation to fine pearlite at the A_r' temperature of about 550°C (1000°F). Factors affecting this time are as follows:

1. Austenitic Grain Size. Since the fine pearlite starts to form at austenitic grain boundaries, fine-grained austenite transforms more quickly at around 550°C. Steels with fine-grained austenite then tend

[1] Grossman, Asimow, and Urbon, "Symposium on Hardenability," *ASM*, 1939.

[2] Jominy, "Symposium on Hardenability," *ASM*, 1939.

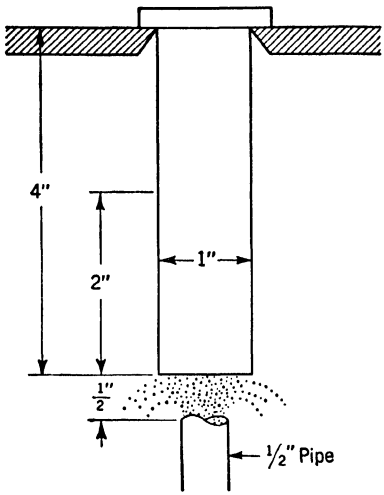

FIG. 10.9. Jominy hardenability test bar 4 in. long by 1 in. diameter held in jig centered ½ in. above a ½-in. pipe with water pressure such that, without the specimen, water would rise to a level 2 in. above the specimen end (or 2½ in. above the pipe).

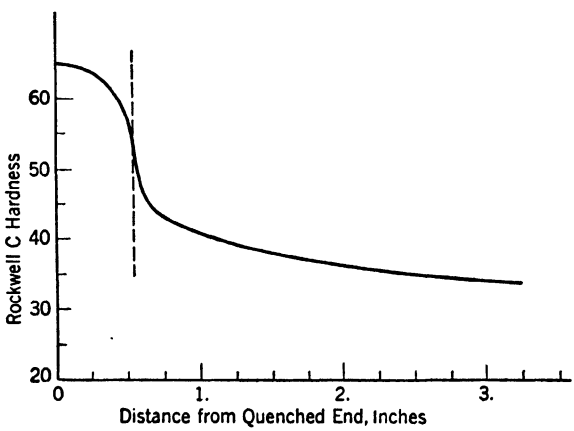

FIG. 10.10. Typical Jominy hardenability data on a steel with sufficient carbon to harden to Rockwell C65 at the martensitic quenched end (*e.g.*, above 0.6% C), and with sufficient manganese or other alloying agents to show a hardenability, indicated by the dotted line, of about ½-in. distance from the quenched end to the zone of 50% martensite, 50% fine pearlite.

to be shallow hardening while those with coarse-grained austenite harden to a greater depth.

2. Austenitic Homogeneity. Since the pearlite reaction is nucleated by carbide formation, residual carbides or localized areas of austenite rich in carbon cause the pearlite reaction to start sooner and thus contribute to shallow hardening. For example, it has been found[1] that the rate of nucleation at 680°C may vary by a factor of 1,000 between 5 and 90 min of austenitizing (at 900°C), resulting in a change of reaction time from 1 to 7 min. However, at the significant A_r' point, this factor is less important.

3. Austenitic Composition. Alloying elements which, in addition to carbon, must diffuse during pearlite formation, necessarily slow up the rate of its formation and increase the time required for diffusion to establish the conditions permitting the reaction to start. The chief distinction between water-, oil-, and air-hardening steels is in the position of the nose of the transformation diagram. In the graph shown here, Fig. 10.8, only water-cooling completely avoids the high-temperature transformation at the 550°C region. If some manganese, nickel or chromium is added, the P_s curve may be displaced to the right sufficiently for the slower cooling of an oil quench to exceed the critical cooling rate. Finally, appreciable amounts of these elements or combinations of them with perhaps others, such as molybdenum, might so slow up the rate at around 550°C that even air-cooling would permit the steel to form martensite. Isothermal transformation curves of these alloyed steels may be considerably more complicated[2] than the one shown for carbon steels (*e.g.*, the *bainite* structure can form upon direct cooling of some alloy steels), but their significance is similar.

10.8 Volume Changes and Related Stresses Accompanying Transformations

The transformation of austenite into pearlite or martensite is accompanied by an expansion of the steel and the release of thermal energy. The critical temperatures (A_r and A_c values) may be determined by measuring dimensional changes with temperature (by use of a dilatometer) or by cooling or heating curves (thermal analysis). A simple demonstration of both dimensional and thermal changes may be made by stringing a piano wire, which is always made of approximately eutectoid steel, between two supports with electrical contacts. (A 12-ft length of 0.034-in. wire can be used directly across an ordinary

[1] Mehl, *loc. cit.*

[2] Davenport, *Trans. ASM*, **27**, 837, 1939; or see Chaps. 11 and 12.

110-volt alternating-current power supply.) A current is passed through the wire to raise its temperature above the A_{c_1}, and then the current is shut off to permit the wire to cool in air. It sags during heating but, since the rate of heating is seldom uniform along its length, the transformation to austenite at the A_{c_1} temperature is not readily detected. As it cools, however, the sagging wire rises steadily as the austenite contracts with drop in temperature. Because of rapid cooling of the thin section in air, the steel does not transform until it reaches a dark-red color, corresponding to a temperature of about 550 to 600°C. As it then transforms to fine pearlite, the wire becomes visibly hotter, an effect commonly called *recalescence*. The expansion, resulting both from the transformation and the rise in temperature, causes the wire to sag suddenly. Then, as the transformed structure continues to cool, the suspended wire resumes its slow contraction and steady rise to its original position.

Upon slow cooling, as in a furnace, there is not any great temperature difference or gradient between the outside and center of even fairly heavy sections; all of the transformation occurs at a high temperature (the A_{r_1}), and the expansion accompanying the transformation is accommodated by deformation of the plastic metal. Under these circumstances, there cannot be any appreciable residual stresses. When a heavy section, such as a steel roll casting 1 ft thick, is cooled in air or a liquid medium, the outside may reach the transformation temperature and expand while the center is much hotter and still completely austenitic. To accommodate the surface expansion, the metal in the central region is pulled toward the surface, and the ends may be forced in and become slightly concave. Well after the surface section has transformed and resumed its normal contraction, the central section reaches its transformation temperature and starts expanding. In order to conform to an expansion of the interior, the surface layers must expand. Since they are contracting at this time, the enforced expansion takes place by plastic flow, but at a much lower temperature and in metal having less plasticity than was the case upon furnace-cooling. If the roll has been quenched, this stage of the cooling cycle may find the surface in a brittle martensitic condition, not able to deform plastically, and surface sections may spall off, sometimes with explosive violence. Assuming that the surface plastically conforms to the expanding core, the final stages of cooling find the center, which transformed at a higher temperature and consequently is hotter, contracting more than the surface and now tending to pull it inward. This tensile pull of the center is balanced by the compressive elastic strength

of the surface so that, when the metal is uniformly at room temperature, there is a residual tensile stress in the center and a residual compressive stress at the surface.

The presence of residual stresses is not confined to steel sections 1 ft in thickness; it may be found in all metals (see page 176 for aluminum alloys) and in sizes less than 1 in. thick, if cooling from a high temperature was sufficiently rapid to produce a marked temperature differential between the surface and center sections. A high quenching temperature usually results in greater temperature gradients and thus introduces greater stresses with a related increase in the danger of cracking or distortion. The stresses described above act in a circumferential direction on cylindrical specimens, but these are also accompanied by longitudinal (lengthwise on the surface) and radial (from surface to center) stresses. The stresses result in a displacement of the normal atomic spacing. If the crystal lattice is more or less uniform, they may be detected by X-ray measurements. They may also be detected mechanically by machining off surface layers (or splitting tubes, etc.) since, when part of the metal in a balanced elastic stress system is removed, the remaining unbalanced stresses cause some deformation or distortion.[1] This is frequently a problem of considerable magnitude in machine-shop work.

Residual stresses may be relieved thermally by heating to a temperature sufficiently high to permit plastic deformation. The elastic limit of metals decreases rapidly at elevated temperatures and, since stresses are elastically balanced, they are diminished by internal flow. They are also reduced by an external or gross deformation; stretching the rod causes more flow in sections previously under tensile stresses and may eventually reverse the stress in sections under originally compressive forces, resulting in an equalization effect upon release of the external force.

Martensite, forming in relatively cold austenite, may be subject to stress of a much greater magnitude (since the elastic limit is higher) but on a much smaller scale. The first plates of martensite forming in plastic austenite may expand without trouble. When the adjacent austenite later transforms to martensite, the accompanying expansion is opposed by contact with the previously formed martensite. Thus the first martensitic needles are under a high, localized, elastic tensile stress with their newer neighbors balanced in compression. Minute cracks have been detected in the martensitic structure after etching and examining at a high magnification. The cracks may be a stress-cor-

[1] Sachs and Van Horn, "Practical Metallurgy," *ASM*, 1940.

rosion (etching) effect, but they do suggest one cause for the brittleness of martensite.

10.9 Tempering of Martensite

Freshly formed martensite has been described as a body-centered tetragonal structure, under high microstresses, and greatly supersaturated with carbon or containing very disperse carbides. Reheating of martensite would be expected to permit a reversion to the stable body-centered cubic lattice, internal readjustments to relieve stresses, and, on the basis of the previous discussion of age-hardening, precipitation of carbide particles followed by growth or agglomeration of these carbides, as permitted by temperature and time. Upon *tempering* or *drawing* at successively higher temperatures for a constant time of 1 hr, the whole process, for carbon steels, can be divided up into stages on a rather arbitrary basis which, nevertheless, has a practical significance.

150 to 230°C (300 to 450°F). The tetragonal lattice becomes cubic, residual austenite transforms (probably on cooling from the draw), carbide precipitation causes the martensite to etch more rapidly and to a blacker structure called *tempered* or *black* martensite. Hardness may increase slightly in the lower end of the range, but, despite the transformation of residual austenite, growth of carbides in the upper temperature range decreases hardness slightly, from C65 to C60–63. Carbides remain too small, however, to be resolved by the microscope.

230 to 400°C (450 to 750°F). The growth of carbides in a globular form continues, although they still may be unresolvable by the microscope. Their general distribution causes the entire structure to etch rapidly and to a black mass which is called *troostite*. Hardness continues to decrease, from about C62 to about C50.

400 to 650°C (750 to 1200°F). The growth of carbides continues to the point where they can be resolved at high magnifications although the structure appears dark and indistinct at magnifications up to about ×500. The structure is called *sorbite* and includes hardnesses in the range C45–20.

650 to 723°C (1200 to 1335°F). Continued growth of carbides brings them to a size that may be resolved at ×500, although their form may be better seen at ×1,000. They appear as globular particles in a continuous ferrite matrix, which now becomes visible as a separate phase for the first time although grain growth of the ferrite has undoubtedly accompanied carbide growth in earlier stages. The structure is called *spheroidite*, and it is naturally soft, from C20–5, tough, and gummy to machine. (Spheroidal carbide structures may also be obtained by

heating pearlitic structures in the same temperature range, since carbides tend to assume the shape having least surface area or lowest energy. A long time is required to spheroidize pearlites, and the minimum size of the ultimate spheroids is limited by the size of the lamellae from which they develop.)

In the above discussion, time of tempering has been assumed to be constant. Since the softening resulting from the tempering process is primarily related to carbide particle growth, it should be possible to express softening in terms of the diffusion equation presented on page 70, or,

$$\text{Hardness} = f[t(e^{-Q/RT})]$$

where t = time
Q = activation energy for diffusion
R = gas constant
T = absolute temperature

Mathematical manipulation of this equation[1] has resulted in the expression:

$$\text{Hardness} = f[T(c + \log t)]$$

where c is a constant, expressed in units of time, that varies with steel composition and austenitization conditions.

All softening curves thus far studied can be plotted according to this equation, with hardness the ordinate and $T(c + \log t)$ as the abscissa. Thus both time and temperature variables are represented by a single curve. The hardness obtained for a given time and temperature of reheating martensite may also be obtained by a longer time at a lower temperature, or vice versa. Once the constant c has been evaluated, a convenient time can be chosen and the exact temperature required to obtain a specified hardness is readily calculated.

The constant c has been evaluated for carbon steels and found to vary linearly from about 15.9 (sec) for 0.30% carbon to 11.8 (sec) for 1.0% carbon steels. Typical tempering curves, in terms of hardness vs. temperature and hardness vs. $T(c + \log t)$ are given in Sec. 10.12.

10.10 Summarizing of Theory

Pearlite is the lamellar aggregate of ferrite and carbide *formed only from relatively homogeneous austenite* upon slow to moderate cooling rates or isothermal transformation between the A_1 and some temperature not more than about 250°C below the A_1. The faster the cooling rate, the more rapidly is the pearlitic structure developed, with a related

[1] Hollomon and Jaffe, *Trans. AIME*, **162**, 223, 1945.

increase in fineness of the lamellae and hardness of the aggregate. The more rapidly pearlite is formed, the less time is available for the separation of excess ferrite or carbide, with the result that pearlite is of a fixed carbon content only when formed under very slow cooling conditions. Further increase in the cooling rate of austenite causes at least some of it to remain unchanged until acicular white martensite forms at the M_s temperature, and, after attaining or exceeding a critical rate, only martensite is formed. Reheating of martensite causes precipitation and growth of *granular* carbides in a ferrite matrix with a continuous change in hardness. The terms, tempered martensite, troostite, sorbite, and spheroidite, apply to certain ranges of structural aggregates of ferrite and granular carbides, arbitrarily selected on the basis of hardness, etching behavior, and micrographic appearance.

10.11 Microstructures

Isothermal transformation diagrams may, with proper equipment, be readily determined experimentally using only a high temperature austenitizing liquid salt bath, a moderate- to low-temperature transformation salt bath, and a cold-water tank. Hardness tests and a microscope may be used to estimate the time of start and of completion of the austenite transformation.

Austenite never appears as such to an appreciable extent in any microstructure of a plain-carbon steel. Any austenite present will largely or completely transform to martensite upon quenching from the transformation bath to room temperature. The etching characteristics of martensite vary somewhat with the carbon content of the austenite from which it forms (Micros. 10.1*a* to 10.2*b*).

Pearlite appears micrographically as described in the previous chapter, with fine pearlite that forms near the nose of the transformation diagram being difficult to resolve except when the lamellae are nearly parallel to the surface of polish. Pro-eutectoid carbide or ferrite offer few or no difficulties as to polishing or identification (Micros. 10.1*a* to 10.2*b*, 10.3 to 10.12).

Bainite formed at around 400°C has a feathery appearance. The parallel "fins" branching from a stem resemble pearlite but are straighter and finer than ordinary pearlite. At 250 to 300°C, bainite has an acicular structure much like tempered martensite. In specimens partly transformed to bainite, however, the quenched structure shows martensite needles to be white while the bainite needles are black (Micros. 10.19 and 10.20).

The reason for martensite etching white while low-temperature bainite etches dark is probably related to the distribution of carbon.

During the formation of martensite there is neither time nor sufficient atomic mobility for crystals of the Fe_3C phase to form. The martensite transformation occurs with no measurable diffusion, and presumably the carbon atoms are trapped in a very supersaturated body-centered solid solution. Bainite, forming more slowly and at a higher temperature, contains the carbide phase in a disperse form which causes the structure to etch rapidly and have a black appearance.

General polishing and etching procedures for pearlitic structures were discussed in Chap. 9. Bainitic and martensitic structures are quite easy to polish in comparison with pearlites. Their greater hardness practically eliminates difficulties from surface flow. However, whereas Picral is preferred as an etchant for pearlite, Nital is preferred for etching bainite and martensite. This is reasonable inasmuch as Nital was specified earlier as more desirable for delineating ferrite.

The micrographs in this section do not attempt to show the full development of all parts of the transformation graphs. Steps in the separation of ferrite from austenite of a hypoeutectoid steel are shown in Micros. 10.1*a*, and 10.1*b*, 10.2*a*, and 10.2*b*.

This series, in addition to showing ferrite separation in hypoeutectoid austenite as grain boundary masses just below the A_1, shows very beautifully the effect of variable carbon content on the etching characteristics of martensite. As ferrite separates, the remaining austenite becomes richer in carbon, and the martensite, formed upon quenching, etches more slowly.

Similar partial transformation structures for a completely austenitized hypereutectoid steel are shown in Micros. 10.3 to 10.6 and for the same steel, austenitized between the A_{cm} and A_1, in Micros. 10.7 to 10.12.

A series of tempered 0.70% carbon martensitic structures are reproduced in Micros. 10.13 to 10.18. Finally, some representative bainite structures are shown in Micros. 10.19 and 10.20.

Tempered martensitic structures (Micros. 10.13 to 10.18) vary in etching characteristics according to the size of the carbide particles or the mean free path of ferrite between them. In a tempered series, it is desirable to etch all specimens for the same time to obtain a specific evaluation of density of blackness of tempered martensite vs. troostite, sorbite, or spheroidite.

10.12 Properties of Ferrite-carbide Aggregates

The presence of carbide envelopes in hypereutectoid carbon steels has already been mentioned as a source of brittleness. In the pearlitic

(*continued on page* 297)

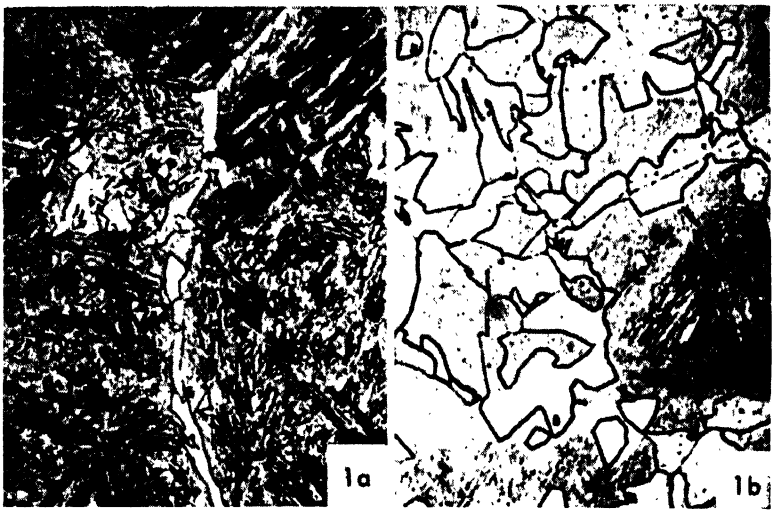

Micro. 10.1*a*. 0.40% C, 0.71% Mn steel, austenitized at 1000°C, quenched to 684°C, held 10 sec and quenched; Rockwell C50; ×1,000; Nital etch. After 10 sec at the subcritical temperature, ferrite has started to form at the austenitic grain boundaries. The quench from 684°C did not affect the ferrite but changed the austenite to coarse, acicular martensite.

Micro. 10.1*b*. As in Micro. 10.1*a* but held 36 sec at 684°C; Rockwell C48. During the interval from 10 to 36 sec, more ferrite grains have appeared and grown in size at the austenitic grain boundaries.

Micro. 10.2*a*. As in Micro. 10.1*a* but held 100 sec at 684°C; Rockwell C34. The separation of ferrite from austenite has accelerated as shown by the hardness change as well as by the microstructure. As ferrite separates, the remaining austenite becomes enriched in carbon. Again it transforms to martensite upon quenching, but this higher carbon martensite (as compared to that in 10.1*a*) shows a less marked acicular or needle structure. It also etches to a lighter color.

Micro. 10.2*b*. As in Micro. 10.1*a* but held 360 sec at 684°C; Rockwell C31. Ferrite separation is nearing completion here, but no sign of transformation of the remaining austenite to pearlite is yet visible. In fact, after 3,600 sec this particular steel had a Rockwell C29 and a structure practically identical to this. Here, the effect of carbon content of the austenite on the etching characteristics of the martensite derived from it is more evident than in Micro. 10.2*a*.

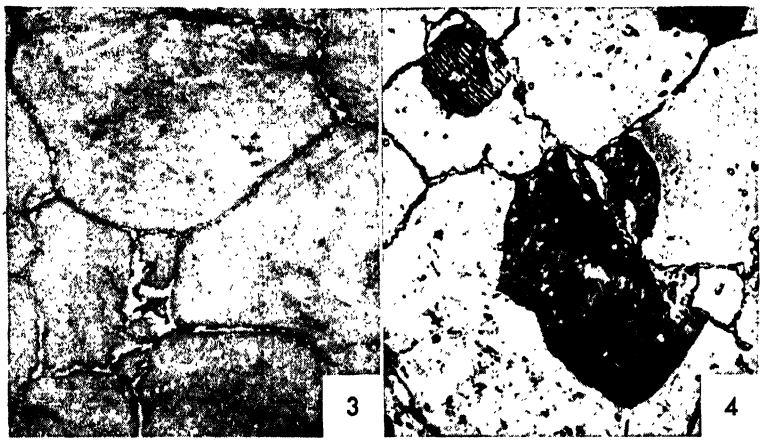

Micro. 10.3. Razorblade steel with 1.2% C, austenitized at 1000°C (1830°F), held 50 sec at 710°C (1310°F) and quenched in water; ×1,000; Picral etch; hardness C65. This specimen has been held long enough to cross the C_s line of the isothermal transformation graph (Fig. 10.5, page 272) but not to reach the line indicating the start of pearlite formation. Carbides outline the former austenitic grains, which transformed to white martensite in the water quench. Note the comparatively large size of the austenitic grains.

Micro. 10.4. Same 1.2% C steel, austenitized at 1000°C, held 100 sec at 710°C, and then quenched; ×1,000; Picral etch; hardness C40. The transformation of austenite to moderately coarse pearlite is about one-third completed. Note in the upper left corner of this structure that pearlite is growing into an austenitic grain in two directions, at the sides and at the ends of the lamellae. Pro-eutectoid (excess) carbide is visible at the austenitic boundaries.

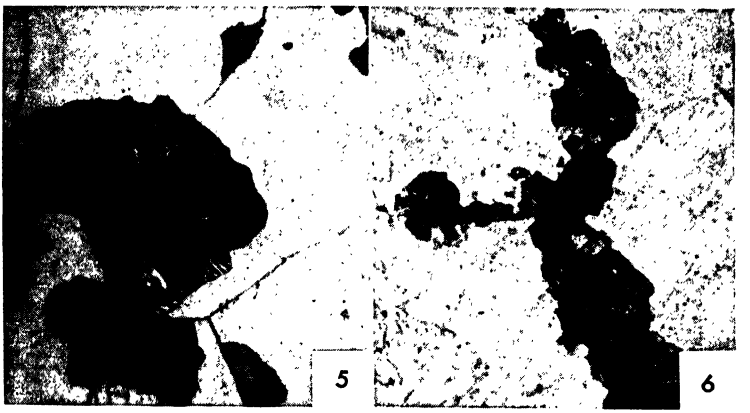

Micro. 10.5. Same 1.2% C steel, austenitized at 1000°C, held 20 sec at 680°C (1250°F), and then quenched; ×1,000; Picral etch; hardness C46. The reaction at this lower temperature, yielding a finer pearlite, is about one-third complete in a much shorter time. The front of the pearlite nodules shows that growth is chiefly at the *ends* of the pearlite lamellae at this temperature. Growth is mainly from the former austenite boundaries into one adjacent grain. At this temperature, only a trace of pro-eutectoid carbide has been able to form at the grain boundaries of the γ phase.

Micro. 10.6. Same 1.2% C steel, austenitized at 1000°C, held 5 sec at 610°C (1110°F), and then quenched; ×1,000; Picral etch; hardness C55. The transformation, here about 15% complete, has started much sooner at this temperature near the nose of the S curve, and the pearlitic structure is much finer, so fine that it is not resolved in this slightly overetched structure. The martensitic needles, in areas which were austenite before quenching, are more evident here because of the overetching. Note the nodular appearance of the fine pearlite areas (which formerly were called *primary troostite*) and their characteristic radiation into two austenitic grains from the boundary. This structure is typical of a steel quenched at somewhat less than the critical cooling rate. The short time at 600°C has not permitted excess carbide to form at the austenitic grain boundaries, but the austenite grain size is revealed by the fine pearlite nodules at the boundaries.

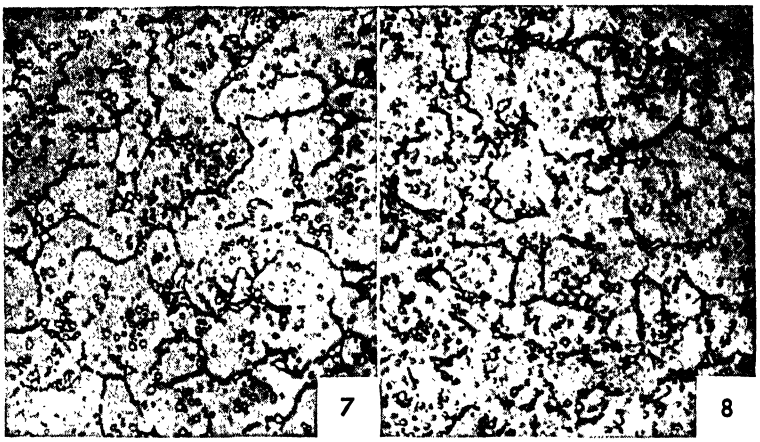

Micro. 10.7. Same 1.2% C steel, austenitized at 850°C (1540°F), held 5 sec at 710°C (1310°F), and quenched; ×1,000; Picral etch; hardness C65. In this and the following structures, the same steel was austenitized below the A_{cm} line, in a commercial hardening temperature range at which the spheroidized carbides are not completely dissolved. Cementite has started to form at the austenitic grain boundaries much sooner than in the comparable specimen (Micro. 10.3), which was austenitized at a much higher temperature. Note the fine austenitic grain size in the present specimen, austenitized at a lower temperature.

Micro. 10.8. Same 1.2% C steel, austenitized at 850°C, held 10 sec at 710°C, and quenched; ×1,000; Picral etch; hardness C65. After a somewhat longer holding time, cementite at the grain boundaries and residual particles have thickened, but the pearlitic reaction has not yet started.

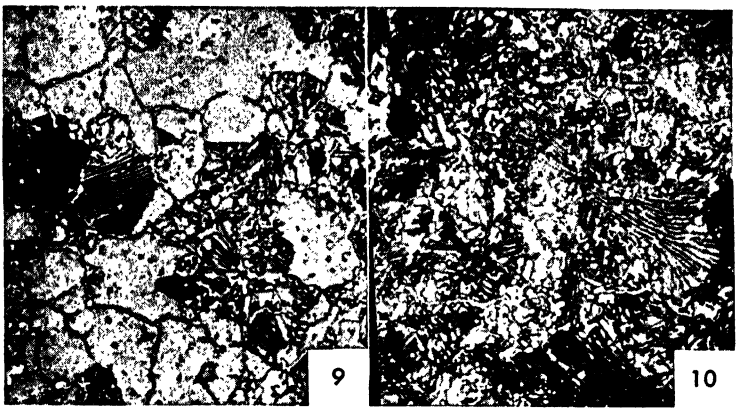

Micro. 10.9. Same 1.2% C steel, austenitized at 850°C, held 30 sec at 710°C, and quenched; ×1,000; Picral etch; hardness C41. By now, the pearlite reaction has reached a stage of about 40% completion. Note that coarse pearlite has grown from the grain boundary into just one austenitic grain. Comparison of this structure with that of Micro. 10.4 shows that although the fine-grained austenite transforms more quickly, the resulting pearlite spacing is similar.

Micro. 10.10. Same 1.2% C steel, austenitized at 850°C, held 100 sec at 710°C and quenched; ×1,000; Picral etch; hardness C21. The transformation is complete but not simply to pearlite. While some grains show this lamellar structure, others show merely coarse globular carbides. This is one form of a so-called *abnormal* but very frequently encountered type of structure. In the abnormal structure, carbides continue to form on carbides already present, which here were globular, so that the transformed structure contains large globular carbides and ferrite. Sometimes the excess grain-boundary carbides become very thick with a correspondingly thick ferrite envelope next to them and with perhaps a little pearlite in the center of the former austenite grains.

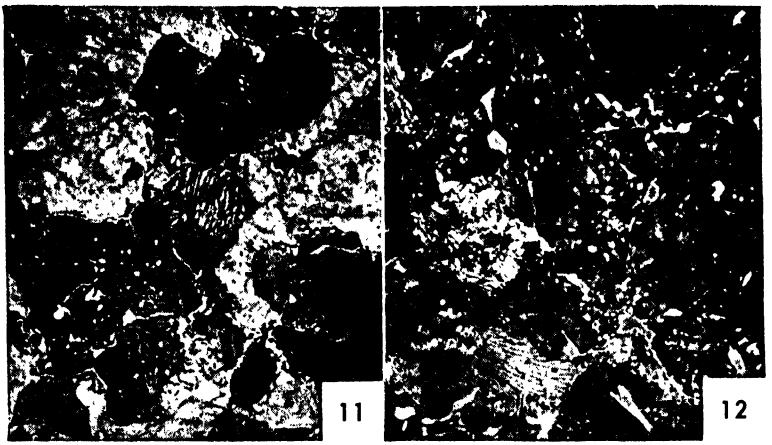

Micro. 10.11. Same 1.2% C steel, austenitized at 850°C, held 10 sec at 680°C (1250°F), and quenched; ×1,000; Picral etch; hardness C49. The austenite transformation is about 60% complete and, although some excess carbide formed first at the austenitic grain boundaries, considerably less is present than in the equivalent 710°C specimen. The pearlite is distinctly finer and not so well resolved.

Micro. 10.12. Same 1.2% C steel, austenitized at 850°C, held 50 sec at 680°C, and quenched; ×1,000; Picral etch; hardness C30. The steel has completely transformed to rather fine pearlite with some excess carbides. The pearlite is not resolved in some grains but is readily visible in others where the angle of the lamellae to the surface is more favorable.

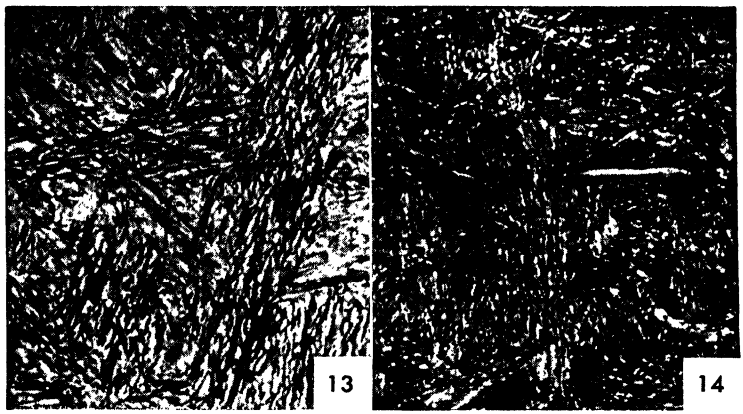

Micro. 10.13. Forged steel of 0.70% C (SAE 1070), quenched from 925°C (1700°F) in cold water and tempered 1 hr at 100°C (212°F); ×1,000; etched 2 min in 4% Picral; hardness C64. The structure after this very low tempering treatment is still essentially a *white martensite.* Only three directions of the acicular or needlelike martensitic plates are apparent in this micrograph, indicating that this entire field was only part of one austenitic grain. The temperature from which this specimen was quenched was about 250°F above that ordinarily employed in commercial practice. The high temperature results in a coarse structure, well adapted to show the nature of martensite but too brittle for most service applications (*cf.* Micro. 10.8, page 290).

Micro. 10.14. Same as Micro. 10.13, reheated 1 hr at 200°C (390°F); ×1,000; etched 40 sec in 4% Picral; hardness C60. The somewhat higher temperature draw has caused the martensitic structure to etch more rapidly and darker. It is now called *tempered martensite.* The horizontal line at the right center section represents a small oxide inclusion (see page 305).

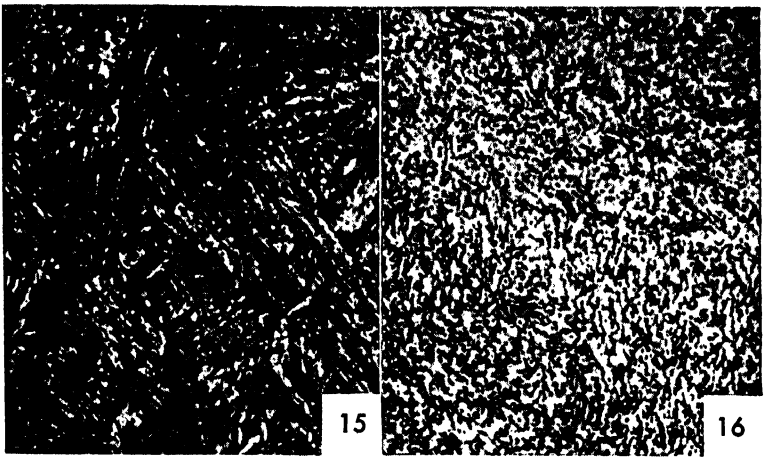

Micro. 10.15. Same as Micro. 10.13, reheated 1 hr at 350°C (630°F); ×1,000; etched 25 sec with 4% Picral; hardness C50. General precipitation of fine carbides, below a resolvable size, causes the specimen to appear to be a black aggregate in which the martensitic plate directions are still evident. This structure is normally called *troostite.*

Micro. 10.16. Same as Micro. 10.13, reheated 1 hr at 600°C (1080°F); ×1,000; etched 25 sec with 4% Picral; hardness C30. Carbides have grown to a size just about resolved at this magnification, and the ferrite matrix is now evident. The structure is termed *sorbite.*

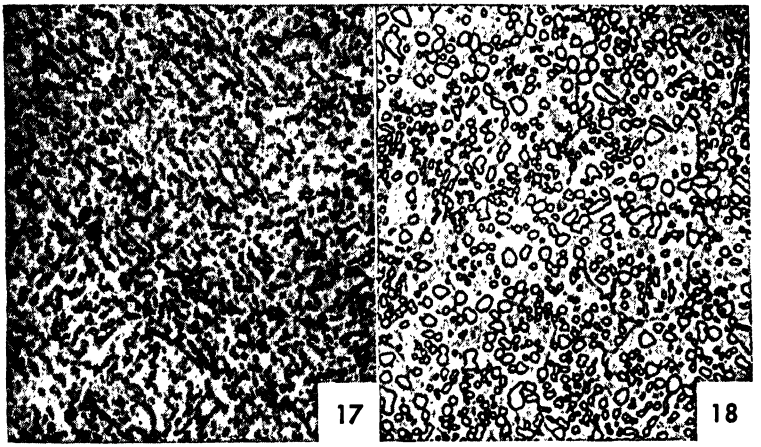

Micro. 10.17. Same as Micro. 10.13, reheated 4 hr at 720°C (1330°F); ×1,000; etched 25 sec with 4% Picral; hardness C8. The continued growth of carbides has made them clearly resolved so that this structure is much whiter and clearer than the preceding one. It would be called fine *spheroidite.* Note that alignment of the carbide particles still reveals the sites of the former martensitic needles.

Micro. 10.18. A commercial steel (SAE 52100) which gave machining difficulties; ×1,000; Nital etch. This structure, with its rather coarse carbide particles widely spaced in a ferrite matrix, could have originated only by an extremely long subcritical spheroidizing anneal.

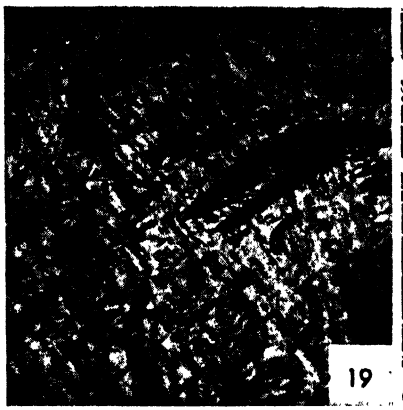

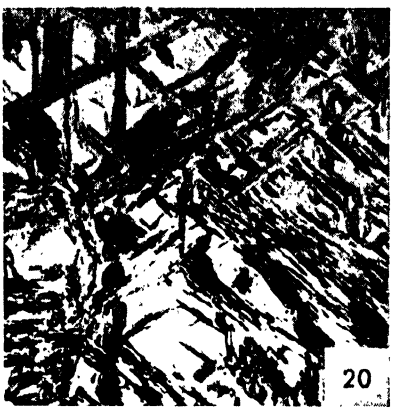

Micro. 10.19. Thin section of 0.6% C steel, austenitized at 1000°C, quenched to 350°C, held 30 sec at 350°C and quenched in water; ×1,000; Nital etch. The transformation of austenite to bainite has started with this structure showing about 2% bainite as scattered black needles in a martensitic background.

Micro. 10.20. Same steel and austenitization as Micro. 10.19, held 100 sec at 350°C and quenched; ×1,000; Nital etch. The bainite reaction has progressed with time and is here about 60% complete. Etched for the same time as the previous microstructure, details of the martensite here are not revealed. Presumably the bainite has less than the austenitic carbon content, and carbon enrichment of austenite, now martensite, results in a less etching effect.

structures, while the ferrite is continuous and occupies about 90% of the structure, the 10% carbide, disposed in thin lamellar plates, interrupts the continuity of the ferrite much more than the same amount of carbide disposed in the spherical or globular dispersion characteristic of sorbite. Consequently, although fine pearlite and sorbite may have the same hardness and appear to have similar black, unresolvable

TABLE 10.1. TENSILE PROPERTIES OF THE PRODUCTS OF AUSTENITE TRANSFORMATION*

Reaction temperature, °C	Rock. C hardness	Yield strength (0.2% offset), (000) psi	Tensile strength, (000) psi	% elongation in 2 in.	Reduction area, %	Pearlite spacing, A
700	19	50	120	13	20	6,300
650	30	95	155	16	35	2,500
600	40	135	190	14	40	1,000
550†	38	132	185	12	30	
500	36	130	180	16	46	
450	40	150	190	18	54	
400	44	170	210	16	52	
350	48	190	230	13	44	

* Data from Gensamer, Pearsall, Pellini, and Low, *Trans. ASM*, 30, 983, 1942. Obtained on a eutectoid plain-carbon steel (0.80% C, 0.74% Mn, 0.24% Si); corrected for recalescence during transformation.
† Data variable in this temperature range.

structures upon examination at moderate magnifications, the lamellar structure developed directly from austenite always shows less impact strength, particularly in the notch bar test, which requires good local plasticity, than the globular structure of the same phases, developed by quenching and tempering.

Some typical tension test data, on specimens with a 0.25-in. diameter and a 1-in. gauge length (comparable to the usual 0.505 by 2-in. specimen), are presented in Table 10.1. These show a linear increase in strength properties with decrease in the reaction temperature (or decrease in the logarithm of the pearlitic spacing), from the A_1 to the A_r' temperature. There is a discontinuity of property changes in the vicinity of the nose of the T graph at around 550°C, but in the bainite region there again is a linear increase in strength with decrease in temperature. There appear to be two maxima in ductility, as shown by elongation or reduction in area values: one in the middle of the pearlite range and one in the middle of the bainite range. No data are included

on martensitic specimens since it is almost impossible to get uniform loading and representative tensile test data for this brittle structure.

Martensitic structures are the hardest obtainable in ordinary steels. Reasons for the high level of hardness are speculative. In view of the discussion of work-hardening in Chap. 4 and of age-hardening in Chap. 6 where high hardness was attributed to high microstresses and related lattice distortions, it seems reasonable to infer that the hardness of

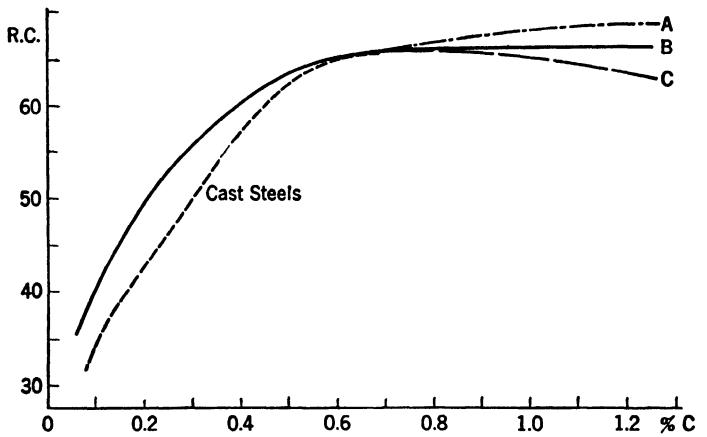

FIG. 10.11. Rockwell C hardness of quenched steels vs. carbon content. In the hypo-eutectoid range, solid-line data are for wrought steels, plain carbon, and alloy types (*Burns, Moore, and Archer*); dotted line is for cast steels (*Clark and Kowall*). In the hyper-eutectoid range, line *A* represents completely martensitic structures; line *B* represents hardness of steels quenched in the normal way (from between A_1 and A_{cm} temperatures; line *C* represents steels quenched from above the A_{cm} line to room temperature.

martensite is related to microstresses and lattice distortion resulting from the transformation at a low temperature with successive localized expansions at the site of each martensite needle as it forms. This is certainly a factor, and carbon content is another important factor, shown graphically in Fig. 10.11. The differences between parts *A*, *B*, and *C* at high-carbon levels are explicable in terms of the earlier Figs. 10.2 and 10.5, remembering that austenite is face-centered cubic and soft. The straightness of the part from 0.10 to about 0.40% carbon permits the percentage of carbon in a low- to medium-carbon cast steel to be fairly accurately determined by quenching it to martensite.[1]

The properties of tempered martensitic structures of plain-carbon steel are typified by the data of Table 10.2 (also Fig. 1.1 on page 16). No tensile data are given for the as-quenched or white martensitic

[1] Clark and Kowall, *Trans. AIME*, **158**, 328, 1944.

structure. This structure is so brittle that even slight nonaxial loading, ordinarily removed by localized plastic flow, builds up extremely high elastic stresses on one side of the test specimen, and fracture will be initiated on that side while the *average stress* is still well below the fracture strength.

The factor of time of tempering is taken into account in the graph of Fig. 10.12 where hardness is plotted against the function $T(c + \log t)$. It can be assumed that, eliminating the variables of retained austenite or carbides undissolved during the original austenitization, the mechanical properties of tempered martensite at a given hardness are the same no matter by what combination of time and temperature of tempering that hardness was obtained. The data of Fig. 10.13 show that bainite and pearlite soften along the same path as martensite although pearlite softening, by spheroidization, is slower.

More precise generalizations expressing the relation of structure to properties have been made (see Table 10.1) as shown in Table 10.2.

TABLE 10.2. PROPERTIES OF A MEDIUM-CARBON STEEL (0.38% C, 0.55% MN) IN THE FORM OF 1-IN. ROD, QUENCHED AND TEMPERED AS INDICATED*

Temper, °C	Tensile strength, psi	Yield strength, psi	% elongation in 2 in.	BHN
Oil-quenched, 815°C				
427	100,000	67,000	21	179
538	90,000	59,000	26	170
649	75,000	53,000	33	156
704	71,000	51,000	34	137
Water-quenched, 815°C				
427	110,000	81,000	19	223
538	95,000	68,500	23	187
649	82,000	57,500	30	156
704	73,000	51,000	34	143

* Data from "Making, Shaping, and Treating of Steel," U.S. Steel Corp. The oil-quenched steel was probably not martensitic throughout the cross section, hence its lower strength properties for a specific temper.

1. Strength properties vary linearly with the austenite reaction temperature and the logarithm of the lamellar spacing of the resulting pearlite, and this spacing is proportional to the diffusivity of carbon at the reaction temperature.

2. The resistance to deformation of a metallic aggregate consisting

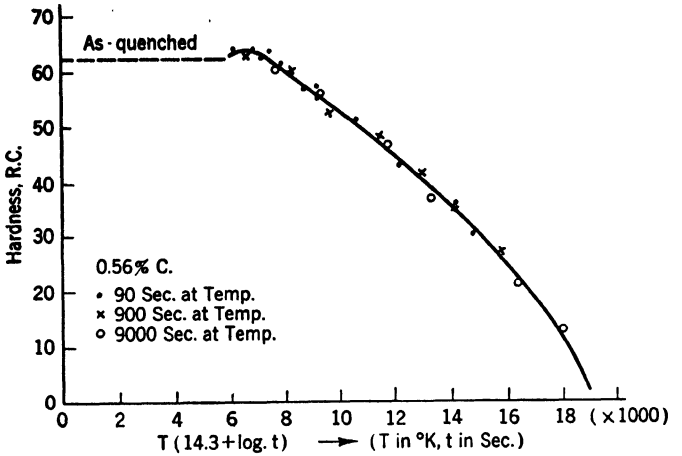

FIG. 10.12. Tempering data for a 0.56% carbon steel, quenched to martensite and tempered over a range of temperature for 90, 900, and 9,000 secs. The parameter $T(14.3 + \log t)$ permits all time-temperature data to be plotted as a single softening curve. (*Hollomon and Jaffe.*)

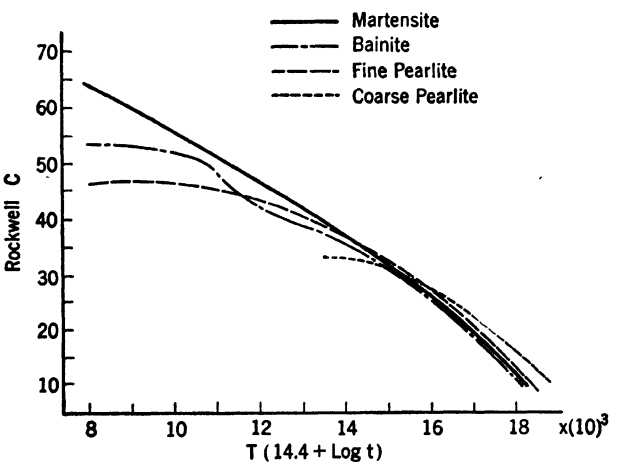

FIG. 10.13. Tempering data of a plain 0.94% C steel from four different initial structures: (1) martensitic; (2) bainitic, obtained by isothermal transformation of austenite at 300°C; (3) fine pearlitic, obtained by isothermal transformation of austenite at 490°C and (4) coarse pearlitic, obtained by isothermal transformation of austenite at 650°C. Softening of the pearlitic structures depends on agglomeration of lamellar carbides which is a slow process; thus the pearlitic-tempered structures have softened slightly less than martensitic or bainitic structures at $T(c + \log t)$ values of about 18,000. (*Hollomon and Jaffe.*)

of a hard phase dispersed in a softer one is proportional to the logarithm of the average length of straight path through the continuous phase. This rule has been found to apply to both pearlitic and spheroidized structures, and extrapolation leads to reasonable carbide particle sizes for the finest, unresolvable, spheroidal carbide (tempered martensite) structures.

10.13 Austempering

This is the name of a special heat-treating process that consists essentially of isothermally transforming austenite at a temperature between the range of fine pearlite formation (A_r' on the T graph) and martensite formation (M_s).[1] The structures developed in this range are called bainites (page 268) which, in carbon steels, cannot develop in any specimen *cooled continuously* from the A_1 line to room temperature, whatever the rate. The transformation graph (Fig. 10.2, page 267) shows the range of hardness of bainite structures. At least in the lower part of the temperature range, bainite has a hardness directly comparable to that of tempered martensite. Since this structure forms directly from austenite at an appreciably higher temperature than martensite, the microstresses developed in bainite are of a much lower magnitude (*cf.* microcracks in martensite, page 281). Bainite structures with a hardness of C50 have shown phenomenally high plasticity for hardened steel: 0.18-in. sections have shown a reduction of area of 35% in tensile tests or absorbed 35 ft-lb of energy in impact tests, whereas tempered martensite, at the same hardness, shows less than 1% reduction in area or only 3 ft-lb impact strength. However, it is only in this hardness range that the bainite structures show superior properties and then only in the case of carbon steels. In the range C40–45, the sorbitic structure is superior for the same reasons that it is superior to fine pearlite. In the hardness range required for cutting tools, C60–65, the bainite structures cannot be obtained. Other limitations of the process involve the size requirements; sections must be thin enough to cool past the A_r' point rapidly enough to avoid the formation of fine pearlite, more expensive equipment is required to quench into a bath at around 250 to 400°C and hold there a fixed time, and finally, normal variations among different heats of steel result in variable time requirements for transformation in the required temperature range.

10.14 Marquenching (Martempering)

It was pointed out in Sec. 10.12 that tempered martensitic structures are superior in ductility or toughness to direct transformation structures

[1] Legge, *Metals & Alloys*, **10**, 228, 1939.

in the frequently important range of hardness, Rockwell C25–45. This has increased the importance of *hardenability* by making it desirable to be able to quench to martensite throughout a thick section. At the same time, this effect brings into more frequent occurrence the troubles incident to quenching to martensite, namely distortion, residual stresses, and cracking. These result to a considerable degree from the thermal gradients necessarily accompanying rapid cooling.

Examination of Fig. 10.2 reveals a method of eliminating thermal gradients and most of the troubles incident thereto. Just above the M_s line, austenite is metastable and shows no hurry to transform to bainite. Therefore, instead of quenching to room temperature, it is possible to quench in a liquid at a temperature just above the M_s temperature of the steel and hold there until the temperature throughout the piece is uniform. Then the steel may be removed from the hot liquid and cooled relatively slowly through the M_s–M_f range. Thus no thermal macrostresses are superimposed on microstresses from the transformation of austenite to martensite at different times for different depths. Distortion, residual macrostresses, and cracking are almost completely eliminated.

The time of holding just above the M_s is not too critical for, if a small amount of bainite is formed, it will not substantially reduce the hardness or strength properties achieved. The most critical part of the process is cooling past the "nose" of the transformation graph to avoid fine pearlite formation. This is difficult since a hot bath gives a slower cooling rate than a cold liquid. This problem is the same as that encountered in austempering, but the two processes should not be confused—one aims at a bainitic structure, the other at a martensitic one.

The word *martempering* was chosen by the originator of the process, Shepherd,[1] presumably on the basis that the process resulted in a martensite with substantially less stresses than those in a fully quenched steel, and the lower stress was analogous to the stress reduction achieved by tempering martensite. However, the term is misleading inasmuch as martensite resulting from martempering is not tempered martensite in any sense of the word *tempered.* It is free of macrostresses resulting from thermal gradients, but it has a high level of microstresses resulting from volume changes accompanying transformation. Also martempering gives *white martensite,* tetragonal if the carbon content is high, and with no precipitated carbides. It still requires the usual subsequent tempering operation (unless it is a softer, low-carbon-content martensite).

[1] Shepherd, *Metal Progress,* **46,** 309, August, 1944.

QUESTIONS

Group A

1. How might a spheroidized structure in a 0.8% carbon steel be converted to (*a*) fine pearlite, (*b*) coarse pearlite, (*c*) a spheroidized structure appreciably finer than the original?

2. Why is a sorbitic structure preferable to pearlite of equal hardness, *e.g.*, Rockwell C30, for an automotive connecting rod?

3. What is the quantitative difference in time required for the transformation at 710°C of coarse austenite vs. fine austenite plus residual carbides (see micrographs in this chapter)?

4. Of the two austenitized structures of question 3, which, upon quenching, would show (*a*) greater quenched hardness and (*b*) greater hardenability?

5. Specify two methods other than chemical analysis for checking the carbon content of a hypoeutectoid steel.

Group B

1. How might an annealed 0.40% carbon steel be heat-treated to show (*a*) large areas of free ferrite plus areas of fine spheroidized carbides in ferrite, (*b*) uniformly distributed fine spheroidized carbides?

2. Suppose a quenched but untempered (martensitic) 0.8% carbon steel part were placed in a furnace at 800°C. What would be the effect of this structure on the austenization time at 800°C? If cracks in the part were found after the subsequent quench, explain their probable origin.

3. Explain the logical reason for anticipating the differing effect of austenitic carbon content on the pearlitic and bainitic parts of the transformation graph in Fig. 10.5.

4. If a 1.2% carbon steel were hardened from 950°C instead of the usual 790°C, why is it most important that it be tempered *twice* rather than the usual once? (Assume a 190°C temper for a tool.)

CHAPTER 11

HEAT-TREATED ENGINEERING STEELS; PLAIN CARBON AND ALLOY TYPES

The properties and the microstructures of steel are not necessarily identical for grades having similar thermal and mechanical treatments and compositions, as specified by the elements usually determined in chemical analyses performed by the mill. The variables in properties and structures are related to the ingot from which the particular shape was fabricated and, earlier than that, to the process by which the steel in the ingot was produced. Some significant variables may be traced to even earlier stages, particularly, the original raw materials. Some understanding of these effects is desirable in evaluating the steels available for specific applications.

11.1 Comparison of Steels by Production Processes

The preponderant amount of steel produced and consumed is of a grade termed *basic open-hearth* carbon steel. Basic open-hearth refers to the refining process, including refractories, furnace, and the associated slag and metal practices, by which the steel is produced from pig iron and scrap steel. The "Metals Handbook" includes a brief description of this process, as well as of the other two important types, acid bessemer and basic electric. In acid processes, both refractories and slags are highly siliceous which prevents any removal of phosphorus and sulfur from the metal during refining. Hence, only raw materials low in these elements can be treated by an acid process for the production of steels having a composition within the usual specifications ranges. Basic electric steel is usually made under two slags, one of an oxidizing character to remove phosphorus, and a second slag of a reducing nature, containing calcium carbide (except for low-carbon stainless steels), which removes sulfur and, more importantly, oxygen. For this reason and because of the use of selected scrap, electric steels ordinarily contain less phosphorus and sulfur than basic open-hearth grades. In addition to this difference in the content of normally reported impurities, phosphorus and sulfur, the three major types of steel can be differentiated

by the concentration of an impurity not usually determined analytically, *i.e.*, oxygen, present in the combined form as an oxide. Naturally, the oxygen content will vary inversely with the carbon content, no matter how the steel is produced. By processes, however, the degree of oxidation of the liquid steel and, relatedly, the amount of residual oxides in the final product, will decrease in this order: acid bessemer (high), basic open-hearth, and basic electric (low by reason of the finishing slag). A description of the skill and knowledge required to control the form, size, and dispersion of the solid oxide in the final steel is beyond the scope of this book, but the importance of this final form is paramount in many applications. Oxides or oxide mixtures (FeO, MnO, and SiO_2) with relatively low melting points are certain to segregate at the original austenitic grain boundaries of the cast metal and, if present in any considerable amount, impair the impact properties (see page 330). The same effect is true for sulfides or oxysulfides, both brittle compounds. The amount of oxides in the finished steel depends not only on the steelmaking process but also on the operating conditions for a given process. The physical form in which oxygen is present may vary in carbon or alloy steels according to its chemical form, *i.e.*, whether present as FeO and MnO, SiO_2, Cr_2O_3, Al_2O_3, TiO_2, or Zr_2O_3. Combinations of oxides forming low-melting-point constituents, particularly of an acid (SiO_2) and base (FeO), tend to agglomerate and form large "inclusions" while the highest melting-point oxides (Al, Ti, and Zr oxides) solidify while the steel is liquid and are ultimately dispersed in the much less objectionable, or, in respect to grain size, beneficial, form of very fine particles.

The size, amount, and dispersion of oxides (or sulfides) affect mechanical properties as previously mentioned. For example, bending properties may be adversely affected when the bending axis is parallel to elongated stringers of inclusions (bending with the "fiber"). In addition, the welding characteristics of a steel are markedly affected. Bessemer steel strip (skelp) welds much better than an equivalent open-hearth grade in pipe making by lap and butt welding, although it is not certain whether this is due to low-melting-point inclusions or some other characteristic. On the other hand, an unusually high oxide content in high-quality electric steel used for making aircraft propellers by welding may cause defects in the weld deposit as a result of the reaction between carbon and oxides in the liquid weld metal. Finally, a critical dispersion of very small oxide particles may inhibit grain growth in the austenitic state and considerably raise the temperature at which coarsening begins. Thus, when dispersed aluminum, titanium, or zirconium oxides are formed by additions of one of these elements to

the liquid steel containing dissolved oxygen as FeO, the final solid steel is usually fine grained. This condition is of importance in carburizing at high temperatures (page 257) or in attaining improved physical properties in either carbon or low-alloy structural steels (page 256).

11.2 Classification of Steels by Composition

Different groups of steel consumers and producers have separately classified the large number of steels of varying composition by specific numerical and letter designations. Thus the U. S. War Department has one set of specifications for the various steels. The Society of Automotive Engineers (SAE), representing an important consuming industry, has another set where the specifications may be identical but the identifying symbols are different. The American Iron and Steel Institute (AISI), representing the steel producers, also has a set of specifications. Fortunately, the AISI specifications generally follow the same numerical identification system as the SAE and, since the former listing is somewhat more extensive, it is coming into fairly general usage. Tables 11.1 and 11.2 reproduce a large part of the AISI coverage, including the most widely used steels. The listings may be abbreviated as below—the first two numbers showing the type and approximate amount of alloy elements and the last two numbers specifying the carbon content.

10*XX*—plain carbon steels
11*XX*—high S free-machining steels
13*XX*—1.75% Mn steels
23*XX*—3.5% Ni steels
25*XX*—5% Ni steels
31*XX*—1.25% Ni, 0.65% Cr steels
33*XX*—3.5% Ni, 1.5% Cr steels
40*XX*—0.25% Mo steels
41*XX*—0.90% Cr, 0.20% Mo steels
43*XX*—1.75% Ni, 0.80% Cr, 0.25% Mo steels
46*XX*—1.75% Ni, 0.25% Mo steels
51*XX*—0.80% Cr steels
52*XX*—1.25% Cr steels
61*XX*—0.90% Cr, 0.15% V steels
86*XX*, 87*XX*, 94*XX*—low Ni:Cr:Mo alloy steels

11.3 Alloying Effects on the Fe:C Phase Diagram[1]

Metallic elements added in moderately small amounts to medium-carbon steels do not introduce new phases into the system. The new

[1] Bain, "Functions of Alloying Elements in Steel," *ASM*, 1939.

TABLE 11.1. STANDARD CARBON STEELS, JULY 1946, SPECIFICATIONS

AISI No.*	% C	% Mn	% P†	% S†	SAE No.	Forms available‡
C1010	0.08–0.13	0.30–0.60	0.04	0.05	1010	All
C1015	0.13–0.18	0.30–0.60	0.04	0.05	1015	All
C1020	0.18–0.23	0.30–0.60	0.04	0.05	1020	All
C1022	0.18–0.23	0.70–1.00	0.04	0.05	X1020	All
C1025	0.22–0.28	0.30–0.60	0.04	0.05	1025	All
C1030	0.28–0.34	0.60–0.90	0.04	0.05	1030	All
C1035	0.32–0.38	0.60–0.90	0.04	0.05	1035	HB, CB
C1040	0.37–0.44	0.60–0.90	0.04	0.05	1040	All
C1045	0.43–0.50	0.60–0.90	0.04	0.05	1045	HB, CC
D1049	0.43–0.50	0.50–0.80	0.05	0.05	....	R, W
C1050	0.48–0.55	0.60–0.90	0.04	0.05	1050	HB, CB
C1055	0.50–0.60	0.60–0.90	0.04	0.05	1055	HB
C1060	0.55–0.65	0.60–0.90	0.04	0.05	1060	HB, R
D1064	0.60–0.70	0.50–0.80	0.05	0.05	1064	R, W
C1065	0.60–0.70	0.60–0.90	0.04	0.05	....	HB
C1066	0.60–0.71	0.85–1.15	0.04	0.05	X1065	R
C1070	0.65–0.75	0.60–0.90	0.04	0.05	1070	HB
C1075	0.70–0.80	0.40–0.70	0.04	0.05	....	R
C1078	0.72–0.85	0.30 0.60	0.04	0.05	1078	HB, R
C1080	0.75–0.88	0.60–0.90	0.04	0.05	1080	HB
C1085	0.80–0.93	0.70–1.00	0.04	0.05	1085	HB
C1095	0.90–1.05	0.30–0.50	0.04	0.05	1095	HB, CB, R
			Free-cutting Steels			
B1010	0.13 max.	0.30–0.60	0.07–0.12	0.05 max.	....	R, W
B1111	0.08–0.13	0.70–1.00	0.07–0.12	0.10–0.15	1111	B, R
C1111	0.08–0.13	0.60–0.90	0.045 max	0.16–0.23	....	R
C1115	0.13–0.18	0.70–1.00	0.045 max	0.08–0.13	1115	B, R
C1120	0.18–0.23	0.70–1.00	0.045 max	0.08–0.13	....	B, R
C1137	0.32–0.39	1.35–1.65		0.08–0.13	X1335	B, R

* Prefix AISI letters mean: B—acid bessemer carbon steel; C—basic open-hearth carbon steel; D—acid open-hearth carbon steel.

† Maximum values for basic open-hearth steels.

‡ HB—hot-rolled bars; CB—cold-finished bars; B—bars; R—rods; W—wire.

NOTE. This listing is not complete but represents most of the usual steels; others are of intermediate carbon contents. Si ranges for all basic open-hearth steels may be 0.10% max., 0.10 to 0.20%, or 0.15 to 0.30%.

atoms generally are soluble in austenite. Below the critical temperature, they may exist in solution in ferrite, in the carbide phase, or be dis-

tributed in both. Some of the common alloying elements are listed in Table 11.3 with their distribution classified.

TABLE 11.2. AISI STANDARD ALLOY STEEL COMPOSITIONS

AISI No. *	% C	% Mn	% Ni	% Cr	% Mo	SAE No.	Type
A1320	0.18–0.23	1.60–1.90	...	...	...	1320	Mn steels
A1330	0.28–0.33	1.60–1.90	...	...	...	1330	
A1340	0.38–0.43	1.60–1.90	...	...	...	1340	
A2317	0.15–0.20	0.40–0.60	3.25–3.75	...	...	2315	3% Ni steels
A2330	0.28–0.33	0.60–0.80	3.25–3.75	...	...	2330	
A2340	0.38–0.43	0.70–0.90	3.25–3.75	...	...	2340	
E2512	0.09–0.14	0.45–0.60	4.75–5.25	...	...	....	5% Ni steels
A2515	0.12–0.17	0.40–0.60	4.75–5.25	...	...	2515	
A3115	0.13–0.18	0.40–0.60	1.10–1.40	0.55–0.75	...	3115	Ni:Cr steels
A3130	0.28–0.33	0.60–0.80	1.10–1.40	0.55–0.75	...	3130	
A3140	0.38–0.43	0.70–0.90	1.10–1.40	0.55–0.75	...	3140	
A3141	0.38–0.43	0.70–0.90	1.10–1.40	0.70–0.90	...	X3140	
A3150	0.48–0.53	0.70–0.90	1.10–1.40	0.70–0.90	...	3150	
E3310	0.08–0.13	0.45–0.60	3.65–3.75	1.40–1.75	...	3310	
A4023	0.20–0.25	0.70–0.90	...	...	0.20–0.30	4023	Mo steels
A4032	0.30–0.35	0.70–0.90	...	...	0.20–0.30	4032	
A4130	0.28–0.33	0.40–0.60	...	0.80–1.10	0.15–0.25	X4130	Cr:Mo steels
E4132	0.30–0.35	0.40–0.60	...	0.80–1.10	0.18–0.25	....	
A4140	0.38–0.43	0.75–1.00	...	0.80–1.10	0.15–0.25	4140	
A4150	0.48–0.53	0.75–1.00	...	0.80–1.10	0.15–0.25	4150	
A4320	0.17–0.22	0.45–0.65	1.65–2.00	0.40–0.60	0.20–0.30	4320	Ni:Cr:Mo steels
A4340	0.38–0.43	0.60–0.80	1.65–2.00	0.70–0.90	0.20–0.30	X4340	
E4340	0.38–0.43	0.60–0.80	1.65–2.00	0.70–0.90	0.20–0.30	....	
A4620	0.17–0.22	0.45–0.65	1.65–2.00	...	0.20–0.30	4620	Ni:Mo steels
P4620	0.17–0.22	0.45–0.65	1.65–2.00	...	0.20–0.27	...	
A4640	0.38–0.43	0.60–0.80	1.65–2.00	...	0.20–0.30	4640	
A4820	0.18–0.23	0.50–0.70	3.25–3.75	...	0.20–0.30	....	
A5120	0.17–0.22	0.70–0.90	...	0.70–0.90	...	5120	Cr steels
A5140	0.38–0.43	0.70–0.90	...	0.70–0.90	...	5140	
A5150	0.48–0.53	0.70–0.90	...	0.70–0.90	...	5150	
E52100	0.95–1.10	0.25–0.45	...	1.20–1.50	...	52100	
E52101	0.95–1.10	0.25–0.45	...	1.30–1.60	...	....	
A6120	0.17–0.22	0.70–0.90	...	0.70–0.90	0.10 min. V	....	Cr:V steels
A6150	0.48–0.53	0.70–0.90	...	0.80–1.10	0.15 min. V	6150	
A8620	0.17–0.24	0.60–0.95	0.35–0.75	0.35–0.65	0.15–0.25	....	Low Ni:Cr:Mo steels
A8630	0.27–0.34	0.60–0.95	0.35–0.75	0.35–0.65	0.15–0.25	....	
A8640	0.37–0.45	0.70–1.05	0.35–0.75	0.35–0.65	0.15–0.25	....	
A8650	0.46–0.54	0.70–1.05	0.35–0.75	0.35–0.65	0.15–0.25	....	
A8720	0.17–0.24	0.60–0.95	0.35–0.75	0.35–0.65	0.20–0.30		
A8730	0.27–0.34	0.60–0.95	0.35–0.75	0.35–0.65	0.20–0.30		
A8740	0.37–0.45	0.70–1.05	0.35–0.75	0.35–0.65	0.20–0.30		
A8750	0.46–0.59	0.70–1.05	0.35–0.75	0.35–0.65	0.20–0.30		
E9315	0.13–0.18	0.40–0.65	3.00–3.50	1.00–1.40	0.08–0.15		
A9420	0.17–0.24	0.80–1.15	0.25–0.65	0.25–0.55	0.08–0.15		
A9430	0.27–0.34	0.85–1.25	0.25–0.65	0.25–0.55	0.08–0.15		
A9440	0.37–0.45	0.85–1.25	0.25–0.65	0.25–0.55	0.08–0.15		

* Prefix letters mean: A—basic open-hearth alloy stee ; E—electric furnace steel.
P and S are 0.04 max. each for basic open-hearth steel, 0.05 each for acid open-hearth or acid electric, and 0.025 each for basic electric steels. Si is between 0.20 and 0.35% for all these steels.

The alloying elements necessarily alter the thermodynamic properties of the three phases and thereby raise or lower the critical temperatures, A_3 and A_1 for medium-carbon steels. These always change

relatively in such a manner that their intersection comes at lower carbon contents; *i.e.*, the alloying elements reduce the carbon content of the eutectoid. These effects are shown in Fig. 11.1. From the steel classification of Table 11.1, it is apparent that for the ordinary alloy structural steels, the critical temperatures are not substantially changed. However, when the alloy is a strong carbide former such as vanadium,

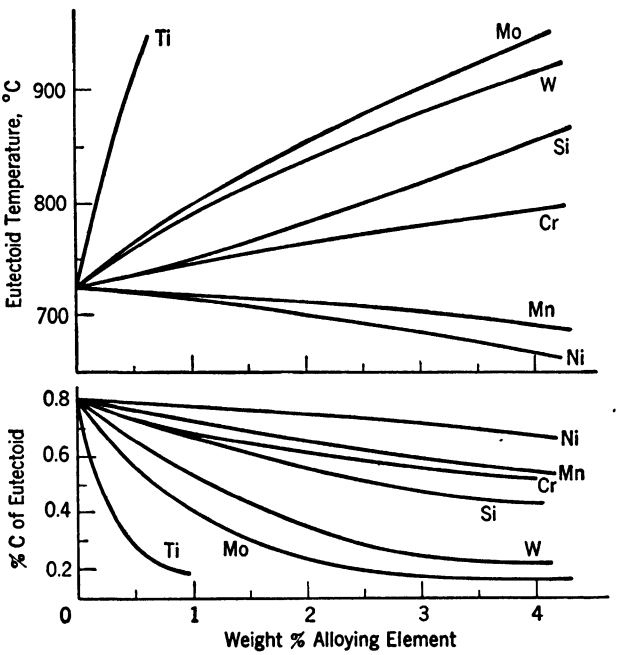

FIG. 11.1. Effect of some common alloying elements on the eutectoid temperature and the eutectoid carbon content. (*Bain.*)

the resulting carbide is usually more difficult to dissolve in austenite than Fe_3C. The austenitization temperature actually used may, therefore, be higher for, unless the alloy carbide is dissolved, neither the alloying element nor the carbon will have its desired effect on, for example, hardenability and hardness.

The effect on critical temperatures may appear to be anomalous in many steels; while nickel depresses both the A_c and A_r temperatures, molybdenum raises the A_c temperatures and depresses the A_r temperatures. The reason for the latter effect is related to the increased sluggishness of the eutectoid reaction in steels in which the alloying element both dissolves in ferrite and forms a stable carbide that is slow to dissolve

in, or precipitate from, austenite. Published data for critical points are generally based on the transformation temperatures obtained on fairly rapid heating or cooling. They do not apply for heat treatments in which the steel is held at temperature for an appreciable time. For example, a highly alloyed (British) aircraft steel of 4% Ni, 1.25% Cr, and 0.5% Mo with 0.25% C was reported to have an A_{c_1} of 1320°F and an A_{c_3} of 1395°F. It was found that, upon heating ½-in. sections to a series of temperatures and holding for 2 hr, the steel became a

TABLE 11.3. DISTRIBUTION OF ALLOYING ELEMENTS IN ANNEALED STEELS (BAIN)

In ferrite	In carbide	Inclusions
Cu		
P		
Ni		
Si	.....	SiO_2
Al	.....	Al_2O_3
Zr	.....	ZrO
Mn (strong)	Mn (weak)	MnO, MnS
Cr (mod.)	Cr (mod.)	Cr_xO_y
W (weak)	W (mod. strong)	
Mo (weak)	Mo (strong)	
V (very weak)	V (very strong)	V_xO_y
Ti (very weak)	Ti (very strong)	Ti_xO_y

mixture of austenite and ferrite at 1225°F (thus, it was above the A_1 temperature) and became completely austenitic at 1300°F (necessarily, it was above the A_3 temperature). A similar difference of from 25 to 100°F between the A_3 temperatures on a continuous heating cycle and those obtained on holding at temperature is found in most published temperature data on critical points of alloy steels.

11.4 Effects of Alloying Elements on Austenite Transformation Diagrams

Each of the alloy steels in the AISI classification of Table 11.2 has its own characteristic isothermal transformation diagram.[1] Their importance justifies the selection and discussion of a few typical and important diagrams here. The influence of 3% nickel is shown by Fig. 11.2, the diagram for steel No. 2340. The nickel, in solid solution in the austenite, lowers both critical temperatures and the temperature of

[1] The "Atlas of Isothermal Transformation Diagrams" by the U.S. Steel Corp., 1943, presents a large number of the useful diagrams.

most rapid transformation or "knee" of the graph. Also it displaces the entire diagram to the right and widens the spacing between the *start* and *finish* lines.

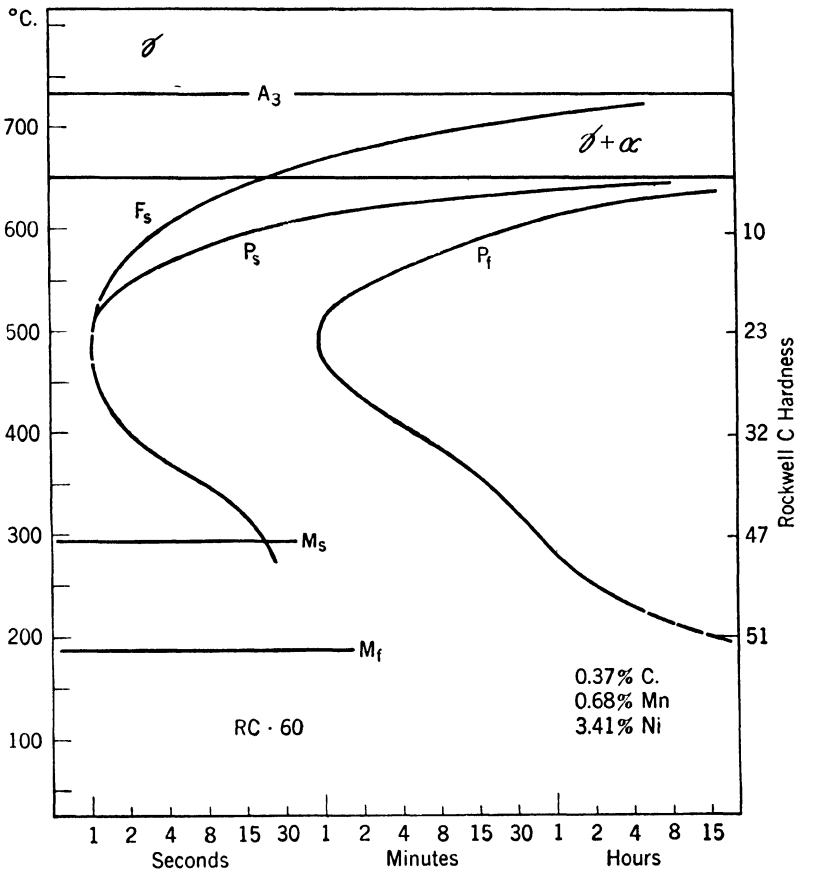

FIG. 11.2. Isothermal transformation diagram for steel AISI 2340; 0.37% C, 0.68% Mn, 3.41% Ni; austenitized at 790°C; grain size No. 7 to No. 8. Rockwell hardnesses of the completely transformed structures are shown.

The effect of manganese is shown by Fig. 11.3, the diagram for steel T1335, a 1.85% Mn steel. The diagram changes are similar to those for nickel except for a sluggish "finish" of the transformation at about 500°C. This presumably is related in an unknown way to the mildly carbide-forming tendencies of manganese. A comparable 1% Cr steel,

No. 5140 represented by Fig. 11.4, shows this characteristic more strongly with the delay now apparent in the *start* line for austenite transformation at 550°C.

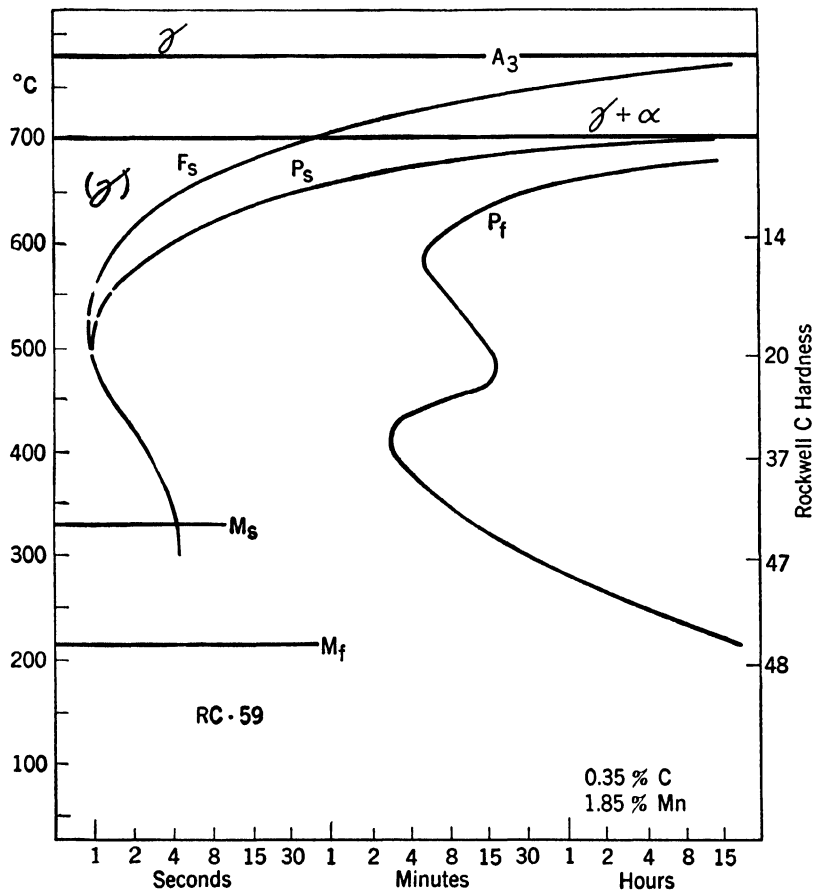

FIG. 11.3. Isothermal transformation chart for steel AISI T1335; 0.35% C, 1.85% Mn; austenitized at 845°C; 30% No. 2 grain size and 70% No. 7. Rockwell hardnesses of the completely transformed structures are shown.

More complex steels are represented by the Cr:Mo steel, No. 4140, whose isothermal transformation diagram is given in Fig. 11.5. It is similar to the plain chromium steel except that now the start of the transformation is still more delayed; to 3 sec at 500°C instead of 1.5 sec.

Triple alloy steels are represented by steel No. 4340 with the diagram

Fig. 11.6. Now ferrite separation preceding the pearlite reaction requires nearly 180 sec or 3 min to be initiated at 650°C, the temperature of the upper knee. The lower knee forms a horizontal shelf. It is

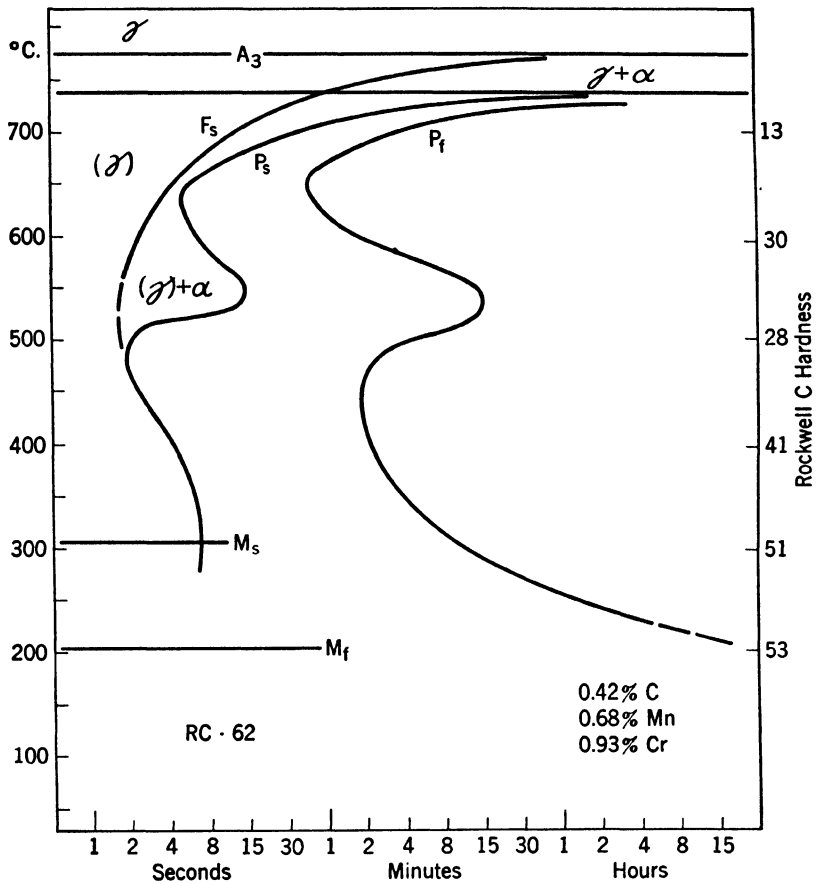

FIG. 11.4. Isothermal transformation diagram for steel AISI 5140; 0.42% C, 0.68% Mn, 0.93% Cr; austenitized at 845°C; grain size No. 6 to No. 7. Rockwell hardnesses of the completely transformed structures are shown.

clear that, here, it is easily possible to cool at such a rate that ferrite separation and fine pearlite formation are completely eliminated and yet have transformation starting at about 500°C and continuing during cooling with the formation of a bainite structure. This would typically occur upon air cooling of moderately thin sections. However almost

any section less than 2 in. thick could be oil-quenched and miss the bainitic "knee" just below 500°C to obtain a fully martensitic structure.

In accordance with the discussion in Chap. 10, it should be realized that all these alloy steel transformation diagrams are presented only as

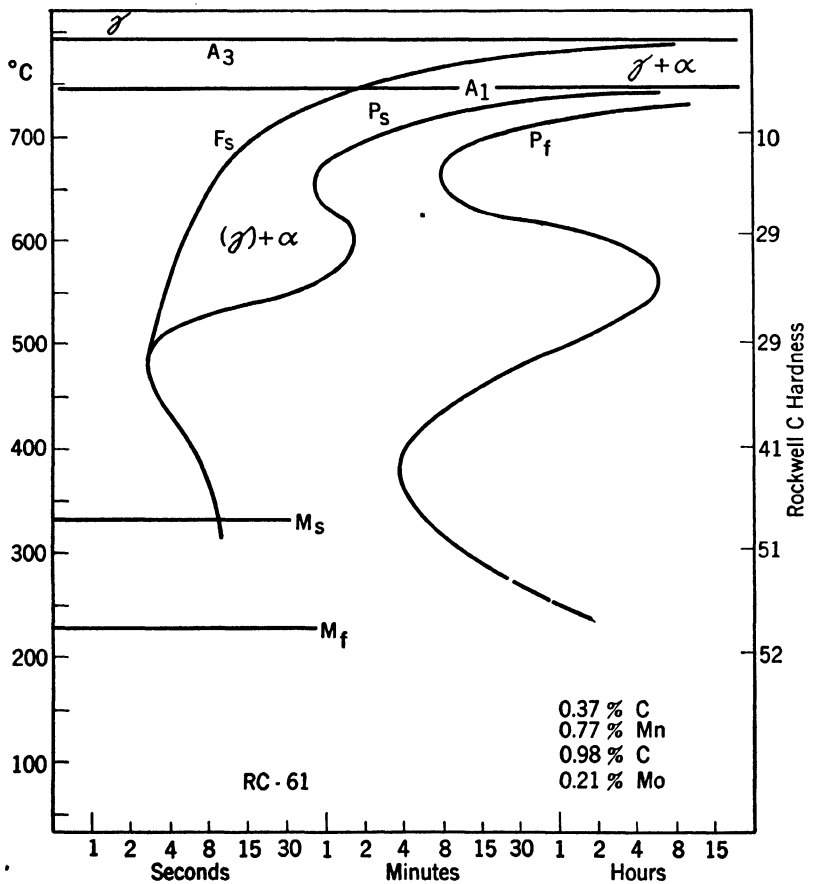

FIG. 11.5. Isothermal transformation diagram for steel AISI 4140: 0.37% C, 0.77% Mn, 0.98% Cr, 0.21% Mo; austenitized at 845°C; grain size No. 7 to No. 8. Rockwell hardnesses of the completely transformed structures are shown.

typical for steel in the middle of the permissible composition range and austenitized for usual times and temperatures. Alloy element content on the high side or high austenitization temperatures would displace all transformation lines to the right, increasing hardenability.

The effect of alloying elements is based upon their redistribution during the pearlite reaction, and it would be anticipated that this would be evident by a change in the pearlitic structure. Data reproduced in Fig. 11.7 show that nickel and manganese each result in an increased

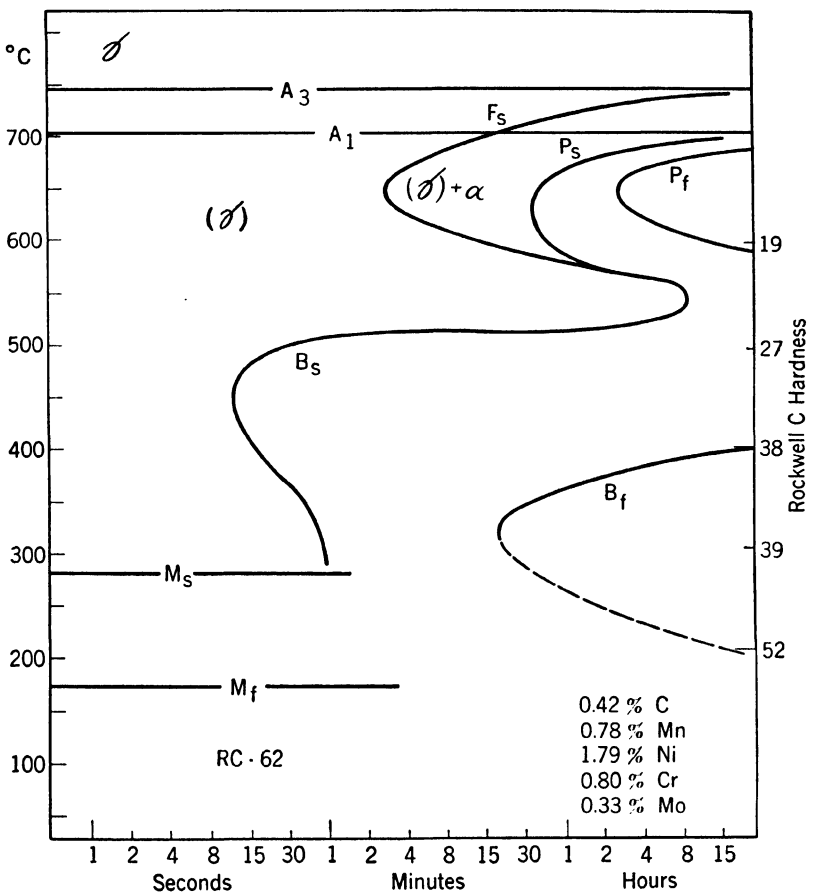

FIG. 11.6. Isothermal transformation diagram for steel AISI 4340; 0.42% C, 0.78% Mn, 1.79% Ni, 0.80% Cr, 0.33% Mo; austenitized at 845°C; grain size No. 7 to No. 8. Rockwell C hardnesses are shown.

spacing of pearlite at a specific austenitic transformation temperature. (The interlamellar spacing data could be replotted in terms of *temperature under the equilibrium A_1 temperature* to eliminate this variable, but then a further correction for variation in carbon diffusion rate would be

required.) The two compositional factors known to decrease hardenability, hypereutectoid carbon content or cobalt in solution in austenite, both decrease pearlitic spacing for a given transformation temperature.

The alloying elements affect not only the isothermal part of transformation diagrams but also the martensite reaction. The effect of carbon and manganese on the M_s temperature was given by the empirical equation on page 271. To this can be added the effects of additional

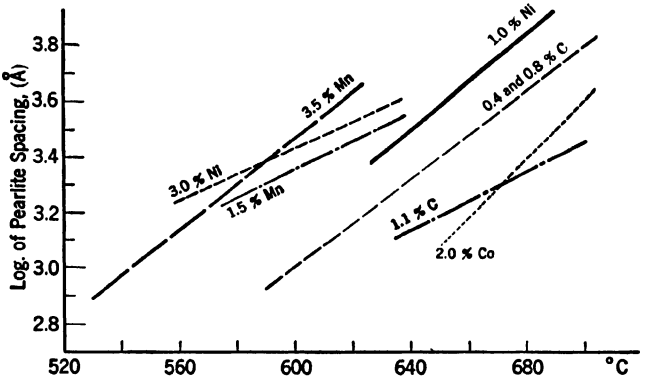

FIG. 11.7. Effect of the carbon, cobalt, nickel, and manganese content of austenite on the interlamellar spacing of pearlite formed upon subcritical transformation of the austenite. High-carbon content and cobalt decrease the pearlite spacing, therefore increase the transformation rates and decrease hardenability. Manganese and nickel have the opposite effect. (*Pellisier, Hawkes, Johnson, and Mehl, Trans. ASM* **30,** 1049, 1942.)

alloying elements. These generally are less potent in decreasing the M_s point than carbon, as is indicated by the expanded formula,[1]

$$M_s(°C) = 550 - 361(\%\ C) - 39(\%\ Mn) - 20(\%\ Ni) - 39[\%\ Cr] - 28[\%\ Mo]$$

Brackets for Cr and Mo indicate greater uncertainty resulting from the slower rates of solution in austenite of carbides containing these elements.

11.5 Hardenability of Medium-carbon Steels, Plain and Alloy Types

It is evident from Fig. 11.6 that small amounts of several alloying elements are more effective in increasing hardenability than a large amount of one element. Grossman[2] found that the increases in harden-

[1] Grange and Stewart, *Trans. AIME*, **167**, 467, 1946.
[2] Grossman, *Trans. AIME*, **150**, 227, 1942.

ability obtained by the addition of alloying elements are multiplicative. For example, Fig. 11.8 shows the increases in hardenability given by most of the common elements, assuming constant grain size and solution of all elements in austenite. If to a plain iron-carbon alloy were added 0.14% Mn, 0.16% Mo, 0.20% Cr, and 1.4% Ni, each separately increasing hardenability by 50%, the total hardenability would be

$$1.5 \times 1.5 \times 1.5 \times 1.5 = 5.1$$

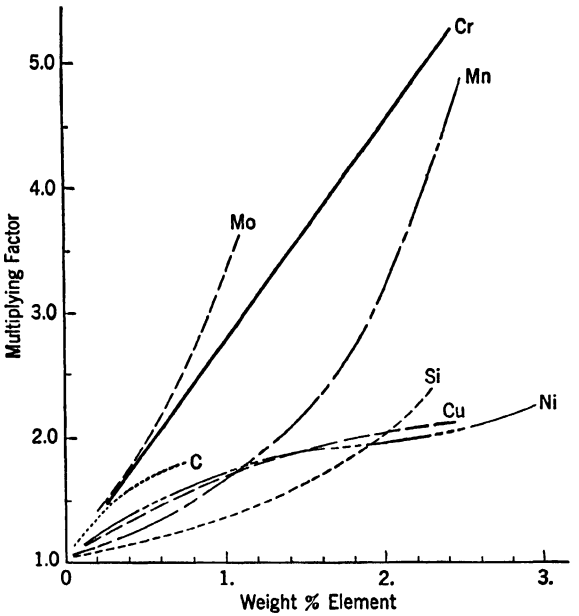

FIG. 11.8. Multiplying factors for calculating the hardenability of steels from the content of elements carbon, manganese, silicon, chromium, nickel, copper, and molybdenum. (*Kramer, Siegel, and Brooks, AIME* **167**, 670, 1946.)

This means that, if the comparable (in grain size, Si content, etc.) plain carbon steel had a critical diameter of ½ in., the size of rod that would harden to 50% martensite at the center upon a given water quench, a 2½-in. rod of the alloy steel would harden to the same degree at the center for the same severity of quenching.

Of the two hardenability tests discussed briefly on page 277, the Jominy test is the easier and cheaper to make and has become the more widely used. In certain types of work, steel is purchased on a hardenability specification replacing, or in addition to, a compositional specifi-

cation. There are groups of hardenability bands, and it may be specified that the steel shall have a Jominy hardenability within this band. This emphasis on hardenability has resulted in considerable research on the Jominy test and test variables.

An adherent oxide scale on the quenched end of the Jominy bar is one source of considerable error. This scale reduces heat transfer and, therefore, decreases cooling rates at varying points along the bar. Actual cooling rates have been experimentally determined under the

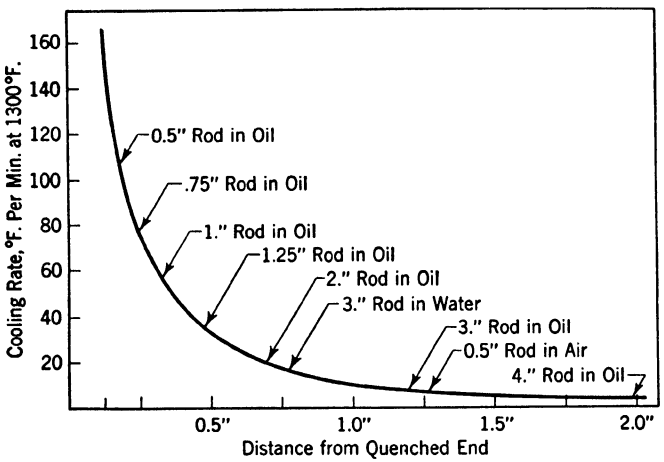

FIG. 11.9. The cooling rate at 1300°F of a Jominy end-quench test bar at various distances from the quenched end. Also shown are equivalent cooling rates for the centers of various sizes of rods as cooled in oil, water, or air.

specified test conditions with results as shown in Fig. 11.9. This graph also shows the center cooling rates for various sizes of ordinary steel bars to facilitate visualization of the use of Jominy data.

Typical Jominy hardenability curves are given in Fig. 11.10 for the steels whose transformation graphs were given in Figs. 11.2 to 11.7. The effects of austenitization temperature, time, and prior microstructure on hardenability of one of these alloy steels, No. 4340, are indicated by the Jominy data of Fig. 11.11. These variables are most significant in steels containing slowly dissolving carbides. The microstructural effect could be anticipated in view of the discussion of austenitization on page 265.

A cheaper means of attaining increased hardenability is to use "lean" alloy steels containing relatively small amounts of several alloy elements, particularly boron. The addition of a minute amount,

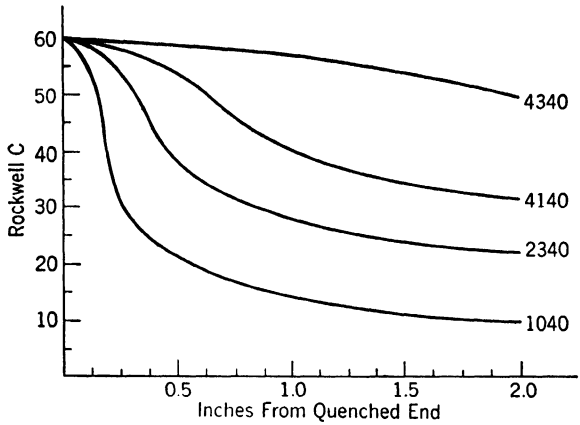

FIG. 11.10. Typical Jominy hardenability curves for four standard medium carbon steels austenitized at 845°C (1550°F) from an initial normalized condition.

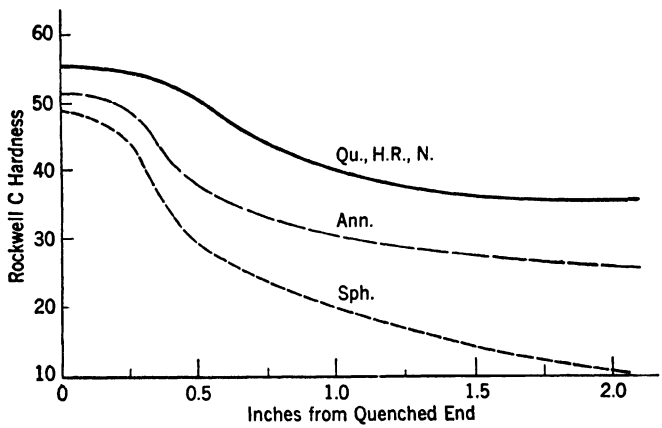

FIG. 11.11. Effect of prior structure on Jominy hardenability of AISI No. 4140 steel (0.40% C, 0.90% Cr, 0.20% Mo). The prior structures were: (*Qu*) quenched from 945°C; (*H.R.*) hot-rolled in austenitic state to 1-in. rod and air-cooled; (*N*) normalized by air cooling from 845°C; (*Ann.*) annealed by furnace cooling from 845°C; (*Sph.*) spheroidized by normalizing and reheating at 700°C for 24 hrs. All bars were then heated 10 min at 845°C and end-quenched. (When bars were heated 4 hr at 845°C and end-quenched, their hardenabilities were the same and corresponded to the top curve.) (*Welchner, Rowland, and Ubben, Trans. ASM* **32**, 521, 1944.)

approximately 0.001% by weight, of boron causes a marked increase in hardenability, as shown by Fig. 11.12. The effect is far greater for the medium-carbon steels than for high-carbon steels and may vanish for hypereutectoid steels. However in the 0.40% carbon type, this practically "trace" amount of boron may double the hardenable size of section. This is true only if the steel is austenitized at about 850°C; higher temperatures destroy the increased hardenability effect.

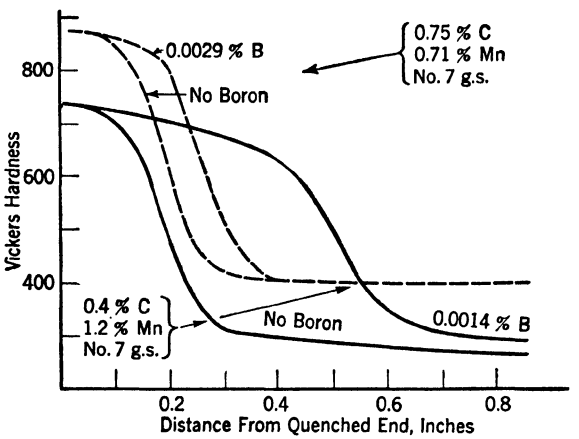

FIG. 11.12. Effect of boron additions on the Jominy hardenability of a medium (0.4%) carbon steel and a high (0.75%) carbon steel. (*Grange.*)

Boron-treated steels are frequently termed *needled* or *intensified* steels. The increased hardenability is associated with a boron constituent, which is found at austenitic grain boundaries. Only a trace amount is needed because of the grain boundary concentration. High austenitization temperatures remove the grain boundary concentration by solution and diffusion. The boron, in an unidentified form, increases hardenability by reducing fine pearlite nucleation at austenitic grain boundaries. In the pearlite-martensite region of end-quenched Jominy hardenability bars, austenitic grain boundaries are outlined by fine pearlite in the absence of boron but not in boron steels.[1]

11.6 Tempering of Medium-carbon Alloy Steels

The changes in properties of a medium-carbon steel upon tempering a fully martensitic structure were given in Chap. 10, page 299. The tempering curves for alloy steels are similar but not identical for the same reasons that their isothermal transformation graphs are not

[1] Grange and Garvey, *Trans. ASM*, **37**, 136, 1946.

identical. The tempering of martensite involves the precipitation and growth of carbide. If up to 3% Cr is present in the steel, for example, the stable carbide will not be Fe_3C but $(FeCr)_3C$ with chromium replacing iron up to 15% of the iron present in the carbide. Therefore, for the carbide to grow, not only must interstitial carbon atoms diffuse through ferrite but substitutional chromium atoms must also diffuse.

Chromium and the other carbide-forming elements diffuse slowly; therefore, in the early stages of tempering, *i.e.*, at low temperatures, only metastable Fe_3C may be formed. However, appreciable growth could occur only for the stable carbide phase. Therefore, growth and softening are slower. Typical martensitic tempering data for four alloy steels previously covered are presented in Fig. 11.15 on page 342. Apart from rate influences, the tempering of these moderate alloy steels is generally similar to that of the plain carbon steels.

11.7 Cast vs. Forged Medium-carbon Steels

Ordinary steel castings and also forgings are usually made of some grade of medium-carbon steel with or without alloying elements. As is implicit in the material of Chaps. 3 and 4, the cast steels initially have coarser grains, since their austenitic grains originate between the liquidus and the solidus at about 1500 to 1400°C, while in the forged steels the austenitic grains originate at around 1000°C, a typical forging temperature. Furthermore, nucleation in the solid state is far greater than in a liquid or, alternatively, grain growth, dependent on diffusion, is far slower in the solid. Both factors tend to give a finer austenitic grain in the forging and, relatedly, a finer grain in the final structure.

Steel castings, however, have one very definite advantage over nonferrous castings: their grain size can be altered by subsequent heating and cooling. The discussion of grain size on page 253 implicitly describes the means of refining the grain size of a medium-carbon steel. Reheating the casting above the A_1 temperature causes new and fine austenite grains to form in pearlitic areas. It is necessary to continue heating to above the A_3 line to eliminate the coarsely dispersed ferrite, formed at the as-cast austenitic boundaries. Just above the A_3 line, the structure will be relatively fine-grained austenite which, on cooling, gives a relatively fine-grained ferrite-pearlite aggregate. The process may be repeated to reduce the grain size further although repetitions give a diminishing return, and usually no further refinement can be observed after three treatments.

Unfortunately, however, carbon (or pearlitic areas surrounded by ferrite) is not the only element that needs to be redistributed. Man-

ganese is always present in these steels in quantities between 0.40 and 0.90%. Upon freezing of the steel, manganese dendritically segregates by a coring mechanism on cooling through the liquidus-solidus interval, just as does carbon. Carbon microsegregation or coring is readily eliminated because of the high diffusion rate of interstitial carbon, but manganese forms a substitutional solid solution in austenite and diffuses relatively slowly.

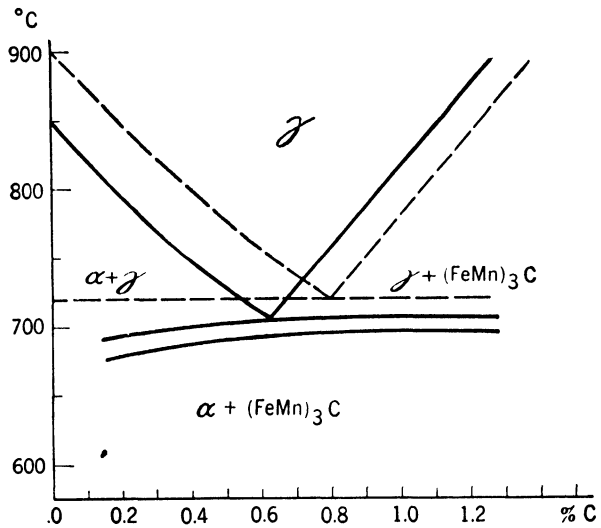

FIG. 11.13. Vertical section of the Fe:Mn:C ternary-phase diagram taken at a 2.5% Mn content, superimposed on the straight binary Fe-C eutectoid section (dashed lines). In the ternary alloys, the eutectoid horizontal line becomes a curved band with a short range of temperature in which ferrite, carbide, and austenite can coexist.

The dendritic segregation of manganese causes carbon to redistribute itself dendritically on going through the A_3-A_1 interval. Consider Fig. 11.13 where the normal A_3 and A_1 lines of the Fe:C diagram are given and also the A_3-A_1 lines of a 2.5% Mn steel. Assume a cast 0.4% carbon steel in which the centers of the original dendrites are nearly free of Mn and the interdendritic spaces attain a concentration of 2.5% Mn. Assume further that the anneal has not caused any substantial homogenization with regard to manganese. Then on cooling from just above the regular A_3 line, ferrite first starts to form, not at the new annealed austenitic boundaries but at those places where there is a low manganese content. Ferrite continues to grow in these low-Mn areas, necessarily displacing carbon into the Mn-rich interdendritic austenite. When

these areas cool to their indicated A_3 temperature, the carbon concentration is greater than 0.4 and, therefore, no ferrite forms there even at this later stage. Thus the final structure may show dendritic ferrite and interdendritic pearlite regardless of austenite grain boundaries.

Small castings usually consist of very fine dendrites that homogenize quite readily with respect to C and Mn. Large castings with coarser dendrites frequently need a special homogenization treatment at a high austenitic temperature in which, therefore, no grain refinement is achieved. Of course the effect of manganese in making a dendritic pattern observable is most evident upon slow cooling or full annealing. Normalizing will reduce the carbon redistribution from coring effects as discussed in relation to Fig. 11.13, and quenching to martensite will avoid them altogether. However, no heat treatment will affect the distribution of constituents not soluble in austenite such as oxides or sulfides (Micros. 5 and 6).

Forging of medium-carbon steels is primarily a shaping process, which reduces the amount of machining that might be required to produce a given shape from heavy bar stock. It usually starts with bars or billets, which in turn have been hot-rolled from cast ingots. The hot-rolling breaks up the as-cast dendritic structure, closes internal voids by a pressure-welding effect, and breaks up the grain-boundary distribution of oxides and sulfides, aligning them in the direction of hot-working.

Homogenization of the steel is not ordinarily achieved in hot-working and interdendritic high-manganese areas become elongated, parallel bands in the hot-rolled structure. These become pearlitic-rich bands in the final *annealed* forging by the same carbon redistribution mechanism discussed in relation to Fig. 11.13. The bands show the direction of flow of the metal in the forging operation. The forging can be cut parallel to the general direction of flow, ground smooth, and deeply etched. No microscope is required to see what had been the general flow of metal in the forging die. Of course, inclusions as well as pearlitic and ferritic grains will be aligned in the flow direction.

Since metal is stronger in the direction parallel to bands and stringers of inclusions and weaker in the transverse directions, forgings are designed to have highest service stresses in the flow direction. If this can be done, the forging will have a more uniform and somewhat higher strength and noticeably higher ductility (in the direction of stress) than is possible in a casting of the same steel, heat-treated to the same hardness. Typical data are given in Table 11.4. The forging will also be

stronger than the same part machined out of solid bar stock since, in this case, stresses at certain points might well be across the grain of the hot-rolled bar.

TABLE 11.4. COMPARISON OF FORGED VS. CAST ALLOY STEEL CRANKSHAFTS; CRANK CHEEK SECTIONS*

	Composition					Heat treatment, °F		
	% C	% Mn	% Cr	% Ni	% Mo	Normalize	Oil quench	Temper
Cast	0.30	0.74	1.07	0.71	0.99	1950	1600	1180
Forged	0.35	0.68	1.01	0.84	0.96	1650	1550	1225

TENSILE PROPERTIES

	BHN	Tensile strength, psi	% elongation in 2 in.	Endurance, psi	Notched endurance, psi
Cast	275	110,000–139,000	3–13	34,000	20,000
Forged	275	136,000–139,000	18–19	62,000	30,000

* *Drop Forging Topics*, **11**, 2, 1946. Forging tested in direction parallel to flow direction.

11.8 Machinability

Since cutting metal fundamentally involves cleavage of the structure, a metal is easily machined when the stress required for cleavage is relatively low and the stress required for flow is relatively high. Also, since the tool usually must indent the metal in order to initiate cleavage or shear fracture, the metal being cut must be noticeably softer than the cutting tool. These are not all the factors involved in the word "machinability" but, considering only the metal being cut, they suggest that a moderately soft structure with low ductility should be quite easy to cut.

Lower ductility is not usually the aim of the metallurgist or engineer, but where machining costs are more important than optimum properties, easily machinable steel may be produced by increasing the sulfur content from 0.04 to 0.10 or 0.15%. The accompanying insoluble sulfides in the structure increase the discontinuities in the metallic ferrite-pearlite aggregate. Such steel has practically the same yield and tensile strength, hardness, and nearly the same tensile elongation as comparable steels with low sulfur content. Low local ductility of the structure, though, enables machining at high speeds and to good surface finishes.

Changing the dispersion of carbide in ferrite can also alter local ductility. The heat treatment of steels to obtain great hardness or other desired properties was an art practiced for literally thousands of years before any scientific knowledge of the process was available. However, a knowledge of the theory of structural changes, *i.e.*, a correlation of the $Fe:Fe_3C$ diagram, the T graph, and the martensite tempering curve makes it possible to dispense with memorized formula for the treatment of each different type of steel. An appreciation of these three aspects of theoretical reasoning, as summarized on page 283, enables the metallurgist, confronted with a specific, undesirable microstructure, to prescribe a heat treatment, or an intelligently minimized series of tests for the determination of a treatment, that will produce any one of the large number of possible microstructures.

Some steels are heat-treated before machining if the desired physical properties do not require high hardness. Most machining operations cannot be readily performed on steels of hardnesses greater than Rockwell C20–25 (BHN 200–250) although, by use of rugged, modern equipment for holding the work and tool rigid, simple cutting operations have been successfully accomplished on steels at hardnesses of C45 (BHN 425). In most cases where final hardness is to be above C25 and in the manufacture of all cutting tools, the metal is first machined to shape, then hardened to a martensitic structure, and finally tempered or drawn by reheating to the temperature required to give the specified physical properties. In these cases, the structure of the steel prior to machining is of considerable importance in determining the ease of cutting, tool wear, and the final surface finish on the machined part. It is not proposed to discuss here the variables of tool design, physical characteristics of tool steels, the rigidity of the work-holding device, and tool lubricants or coolants, although these factors might affect machinability more than the structure of the steel being cut. If these conditions are all properly adjusted, a pearlitic structure will usually cut better than a sorbitic or a spheroidized structure. The lamellar structure is more brittle, the metal tends to shear immediately in front of the tool (along the line of cut), and the chips break off more readily, resulting in a cleaner type of cut. On the other hand, a very fine pearlitic structure is harder, requires more strength at the tool edge, and thus necessitates use of more powerful and rigid machines. The type of cutting operation is also a variable; the best structure for an intricate milling operation may not be best for drilling or thread-cutting operations.[1] A frequent

[1] Woldman, *Iron Age*, **147**, No. 25, p. 37, No. 26, p. 44, 1941.

compromise in structure is the use of a partially spheroidized pearlite, frequently called a *wormy* structure. The structures shown by Micros. 11.1 and 11.2 illustrate extreme divergences.

Methods of obtaining different types of structures are implicitly explained in Chap. 10, a coarse pearlitic structure by slow furnace-cooling of austenite and finer pearlites by somewhat more rapid cooling. Spheroidized structures may, of course, be obtained by tempering of martensite, but when this structure is desired for machining purposes it is usually obtained by reheating fine pearlite (normalized structure) below the A_1 temperature. This method depends on the surface tension forces of the carbide phase, which effectively break up the lamellar distribution and gradually agglomerate the carbide to approximately spherical shapes. Moderately short times only partly spheroidize the lamellae; quite long times are required to complete the process. The spheroids formed are somewhat related in size to the pearlite; specifically, a coarse pearlite cannot be treated to give a fine spheroidite. Heating slightly above the A_1 and then cooling below will naturally break up a coarse pearlitic structure more rapidly. Finally, isothermal transformation treatments have been successfully employed to obtain more machinable structures; *i.e.*, heating into the austenitic range, furnace-cooling to 1150 to 1250°F (620 to 680°C), holding there 1 to 4 hr, and then air-cooling.

11.9 Microstructures

The presence of alloying elements does not affect the hardness of martensite appreciably nor its micrographic appearance. Furthermore, tempered martensites of alloy steels appear identical to those of plain carbon steels, assuming the same initial grain size, carbon content, and tempered hardness. Therefore, practically no micrographs are included here of the medium-carbon, plain or alloy type, steels in the martensitic condition.

The most notable microstructural effect of alloying elements is evident in annealed and normalized steels. The lamellar form of carbide may not be developed upon full annealing, and this will affect machinability, *e.g.*, Micros. 11.1 and 11.2. Higher manganese content steels are susceptible to banding when annealed and, to a less degree, when normalized, as evidenced by Micros. 11.3 and 11.4.

A nontypical cast-steel structure is shown by Micro. 11.5 with the effect of remedial heat treatment shown by Micro. 11.6.

The effect of deep hardenability on susceptibility to underbead weld cracking is illustrated by Micros. 11.7 and 11.8.

The effect of alloying elements on annealed and normalized structures is shown by micrographs of the five alloy steels whose transformation graphs were shown earlier, *viz.*,

Micros. 9 and 10—steel No. 2340 (3% Ni)
Micros. 11 and 12—steel No. 1335 (1.8% Mn)
Micros. 13 and 14—steel No. 5140 (1% Cr)
Micros. 15 and 16—steel No. 4140 (1% Cr, 0.2% Mo)
Micros. 17 and 18—steel No. 4340 (1.8% Ni, 0.8% Cr, 0.3% Mo)
Micros. 19 and 20—steel No. 4640 (1.8% Ni, 0.3% Mo)

These micrographs show that the pearlitic microstructures of the chromium steels are like plain carbon steel while nickel, somewhat surprisingly, tends to result in broken-up lamellae. Nickel and molybdenum together completely destroy the lamellar character *for steels annealed below* 950°C. Heating to a very high austenitic temperature, *e.g.*, 1100°C or higher, dissolves all the carbides in these steels. Without the nucleating effect of undissolved carbides, normal pearlite is more likely to be obtained if a sufficiently slow cooling rate is employed.

Steels with as high hardenability as the 4140, or particularly the 4340, are likely to be quite hard upon normalizing thin sections. For example, the air-cooled 4340 of Micro. 11.18 shows a completely martensitic-bainitic structure of fairly high hardness.

11.10 Properties of Heat-treated Medium-carbon Steels

Some mechanical property data of the basic structures of steel, ferrite, pearlite, bainite, and tempered martensite, were given in Chap. 10 on page 297. Now having considered the use of alloying elements in medium-carbon steels to obtain increased hardenability, we should give consideration to the relative properties of these structures in alloy steels. Hollomon and coworkers[1] heat-treated a Ni:Cr steel (3135) and a Ni:Cr:Mo steel (8735) in three ways: (1) quenched to martensite, (2) isothermally transformed to a partially bainite structure and then quenched, and (3) isothermally transformed to a mixture of ferrite and pearlite in austenite and then quenched.[2] All structures were then tempered to comparably different hardnesses or tensile strengths and tested.

Their data show that *at a given tensile strength*, the specimens that before tempering were fully martensitic had the highest yield strength, the highest ductility, the highest endurance limit or fatigue strength,

[1] Hollomon, Jaffe, McCarthy, and Norton, *Trans. ASM*, **38**, 807, 1947.

[2] Some martensite was desired in the bainite and in the ferrite plus pearlite for property comparisons to be made over a wider range of hardnesses.

(*Continued on page* 341)

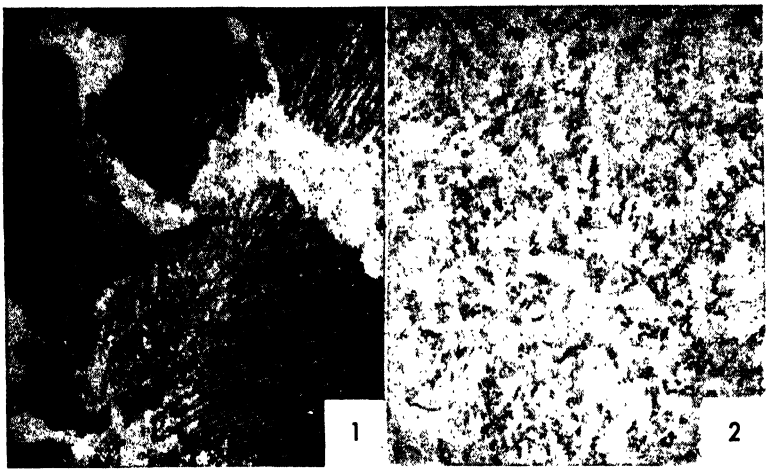

Micro. 11.1. Alloy steel (1.0% Ni, 0.5% Cr, 0.5% C); ×1,000; Picral etch. This steel is used for small screws in an aircraft engine. Specifications require an extremely good surface on the threads and at the base of the threads to ensure adequate fatigue strength. The structure shown represents stock which was readily cut and from which few parts were rejected. It shows excess ferrite surrounding moderately coarse pearlite, both derived by slow cooling of a coarse-grained austenite.

Micro. 11.2. Same alloy steel (1.0% Ni, 0.5% Cr, 0.5% C); ×1,000; Picral etch. Stock from a different source for the same aircraft screws machined with difficulty. Over 50% of the parts made were rejected as having an inferior finish, although tooling was identical to that employed for the previous steel. This spheroidized structure has exactly the same hardness (Rockwell B90) as that above, but the continuity of the ferritic structure here confers greater plasticity to the aggregate. The spheroidal structure can be changed to a pearlitic type, but a high temperature (1700°F for ½ hr) is required to dissolve the carbides in austenite, presumably because of the chromium content, although in any case a moderately coarse spheroidal structure must be heated to a higher temperature, or held a longer time, to transform to homogeneous austenite.

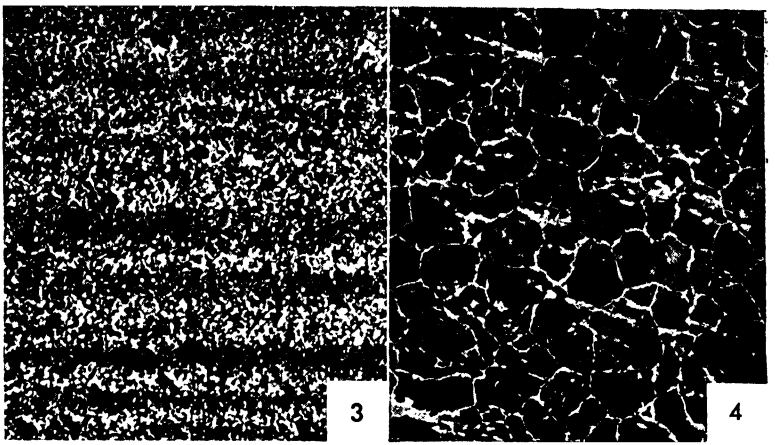

Micro. 11.3. Section from alloy structural steel (railway generator shaft) containing 1.25% Mn and 0.10% V; ×100; Nital etch. The alloying elements, particularly vanadium, have made this steel very fine grained, a desirable condition for its particular service. The carbon content appears to be about 0.40% but is actually only about 0.30%. The smaller amount of ferrite is partly a result of a rapid cooling rate through the critical temperature and partly a result of the lower equilibrium carbon content of the eutectoid when the manganese content is raised. Thus with 1.25% Mn, the equilibrium concentration of the eutectoid is displaced from 0.80 to 0.72% C.

The structure of the rod is not uniform in respect to ferrite; some areas contain more ferrite and less pearlite than others. The high- and low-ferrite areas are both parallel to the rolling direction. The resulting *banded* structure is frequently encountered in slowly cooled steels.

Micro. 11.4. Section from a steel rail; ×100; Nital etch. Rails require greater strength and hardness than ordinary structural steels and are generally made of steels approaching the eutectoid in carbon content. This particular rail appears to contain about 0.75% C, although actually somewhat less than that is present (0.68 %); the abnormally small amount of ferrite resulted from fairly rapid cooling in air with a related depression of the A_{r_3} temperature (page 236). There are a few elongated streaks of ferrite not completely confined to an austenitic grain boundary. These show the direction of rolling of the rail and are related to phosphorus segregation as in the banded structure of the Mn:V steel. Some of the ferrite bands show elongated nonmetallic inclusions of either sulfides or oxides (of a darker color than the ferrite).

Micro. 11.5. Section from a large steel casting; ×50; Nital etch. This structure represents a *defective casting*, not one found in good cast steels. It contains about 0.35% C and has probably been given one heat treatment, since in some areas a moderately fine-grained ferrite and pearlite structure is visible. However, other areas have large aggregates of ferrite and, in the midst of these, a string of small globules is visible. At one point, there is a eutectic-appearing mixture of particles at the intersection of three former austenitic grains. These are oxysulfide inclusions that formed in the last part of the structure to freeze, the austenitic boundaries. The large sections of ferrite probably resulted from phosphorus segregation in the same, last-freezing areas. The appearance of ferrite inside the former austenite grains suggests that one heat treatment, an inadequate one, was given the casting. The gross ferrite areas cause this steel to have poor strength properties while inclusions at the original austenitic grain boundaries are conducive to poor impact and fatigue strength.

Micro. 11.6. Same casting as Micro. 11.5 after double heat-treatment; ×50; Nital etch. The poor structure has been eliminated by a double anneal. First, the steel was heated 200°F above the Ac_3 to 1750°F (950°C), and held for 2 hr to homogenize the austenite. After furnace-cooling, the structure was uniform but not particularly fine-grained because of coarseness of the high-temperature austenite grains. The steel was then reheated to about 25°F above the Ac_3 held only long enough to ensure completely austenitizing the structure, and subsequently air-cooled. The final structure is uniformly fine-grained and would show good strength. However, the distribution of inclusions has not been changed; they are not readily visible now but still retain an envelope type of dispersion. Although the resistance to impact stresses and the fatigue strength of this structure are superior to the values shown by the original steel, they are inferior to those of good castings. The form of the inclusions can be changed only by modifying the original melting, deoxidizing, and casting procedure. For example, the addition of an element that would raise the freezing point of the inclusions and cause them to solidify before the steel would produce a uniform rather than intergranular dispersion.

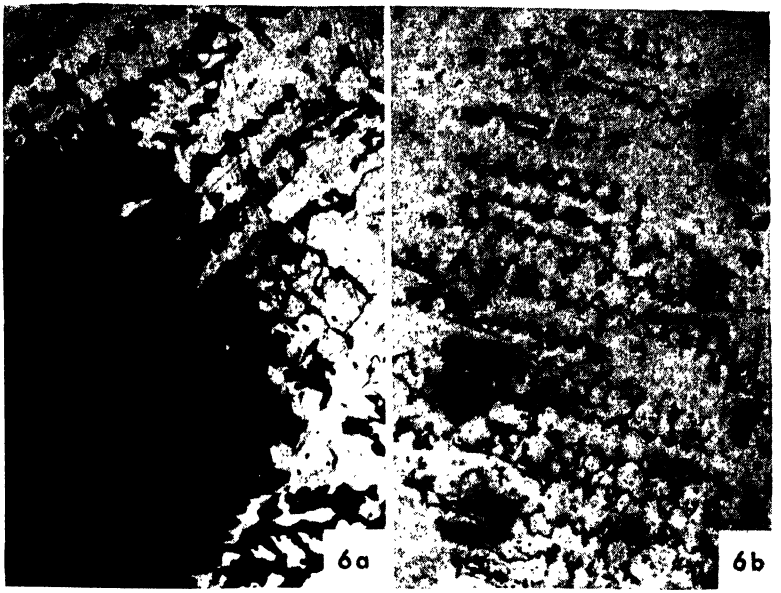

Micro. 11.6*a*. Centrifugally cast 0.80% C steel in the as-cast condition; ×100; Nital etch. This was a section only ⅛ by ¼ in. in size, which could be produced more cheaply by centrifugal casting. The micrograph represents a section adjacent to a corner (upper right). Either coring gave a surface of low-carbon content or, more probably, the mold material resulted in local surface decarburization. The point of interest is the dendritic shape of the hypoeutectoid ferritic crystals.

Micro. 11.6*b*. Centrifugally cast 0.80% C steel; zone near the center of ⅛ by ¼ in. section; ×100; unetched. In the centrifugal casting of the thin section, it was not possible to feed the last part to solidify with liquid metal. Therefore, the volume change on solidification resulted in shrinkage porosity, which very clearly outlines the dendritic crystals of austenite. Some larger pores here are probably the result of gas evolution in the last stages of solidification.

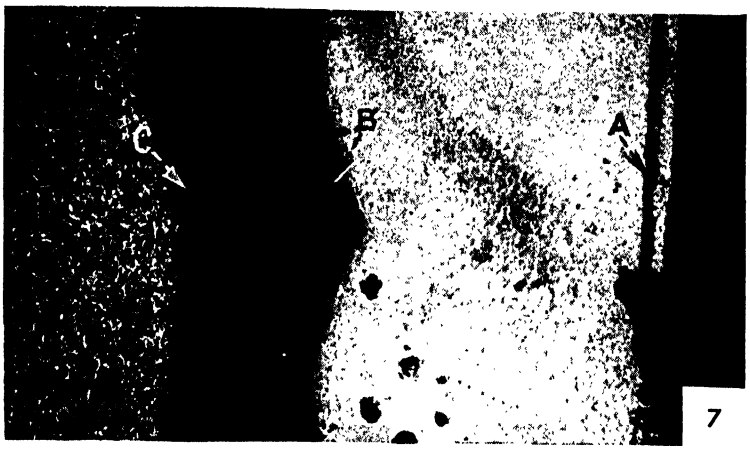

Micro. 11 7. SAE 3140 steel (0.40% C, 0.75% Mn, 1.25% Ni, 0.60% Cr), section from a generator axle broken in service; ×10; Nital etch. This macrograph, taken at the base of a keyway notch on a 2-in. shaft, may be interpreted as follows: The original keyway was cut somewhat oversize. To correct the error, a layer of ordinary low-carbon steel was deposited by welding at the base. Subsequent machining apparently disclosed porosity, or other defects, in the first deposit, so a second layer of metal was welded over the first. The right-hand edge of the micrograph represents the base of the keyway, and ¼ in. to the left of this, an open line *A* shows the poor junction of the first and second weld deposits (weld metal, of low-carbon steel, is white). About 2 in. farther to the left, at *B*, a sharp discontinuity in shading indicates the junction between the alloyed steel base and the first weld deposit. To the immediate right of *B*, a higher magnification disclosed evidence of carbon diffusion from the base metal into the low-carbon weld metal. To the left of B, there is a dark zone that shows a sharp transverse crack, followed at *C* by the normal base metal. This zone (*B* to *C*) was heated to the austenitic state by the first welding operation, and cooled rapidly by the mass of the main section. It became martensitic and probably highly stressed as well. The second weld deposit and thermal gradients related to the rapid localized heating probably initiated the crack in the martensitic structure, which also was tempered to its present dark etching state before finally cooling again to room temperature.

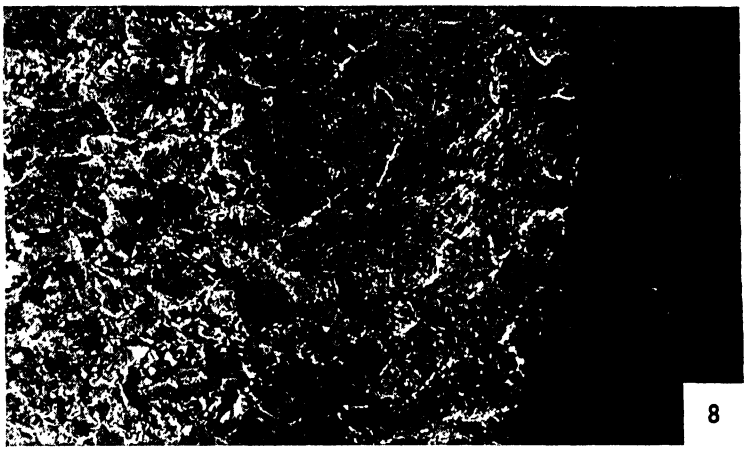

Micro. 11.8. Section in vicinity of *C* from Micro. 11.7; ×1,000; Nital etch. A higher magnification of a section in the vicinity of *C* shows an area to the right in which the alloy became completely austenitic and cooled rapidly enough to become martensitic. It is in this section (although farther to the right, beyond this field) in which the crack shown in the micrograph above was formed. In between the martensitic section and the unaffected base metal at the left, there is a zone of metal that apparently became austenitized at a sufficiently high temperature for grain growth to have occurred, as evidenced by the ferrite that separated at the austenitic boundaries on cooling. The separation of the ferrite is in itself evidence that this narrow zone cooled slowly enough to avoid martensitization. Here, within a narrow zone of about 0.003 in., relatively unaffected metal, an area of grain growth, and an area of tempered martensite are visible.

Micro. 11.9. Steel 2340 (0.37% C, 3.4% Ni), furnace-cooled from 950°C; ×1,000; Nital etch. This annealed microstructure shows ferrite and "pearlite" with the carbide in the latter structure only partly lamellar, part being spheroidal. Hardness of RG72, Brinell 202, is appreciably higher than that of an equivalent plain carbon steel (RG58).

Micro. 11.10. Steel 2340, ½ in. section air-cooled from 950°C; ×1,000; Nital etch. The normalized structure shows only traces of free ferrite, and the pearlitic structure is too fine to be resolved. Hardness of RG85, Brinell 247, is again appreciably higher than that of a plain carbon steel.

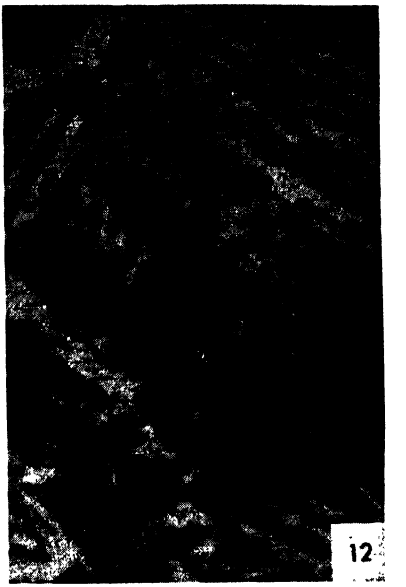

Micro. 11.11. Steel T1335 (0.35% C, 1.85% Mn); furnace-cooled from 950°C; ×1,000; Nital etch. The annealed structure shows finer pearlite than would a plain carbon steel and also less ferrite, because of the decrease in eutectoid carbon content and also, probably, some slight undercooling. Hardness RG75, Brinell 210, nearly the same as annealed 2340.

Micro. 11.12. Steel T1335, ½-in. section, air-cooled from 950°C; ×1,000; Nital etch. The normalized structure shows some Widmanstätten ferrite plates and a fine, somewhat nonlamellar, pearlite. The hardness of RG84, Brinell 242, is again nearly the same as normalized 2340.

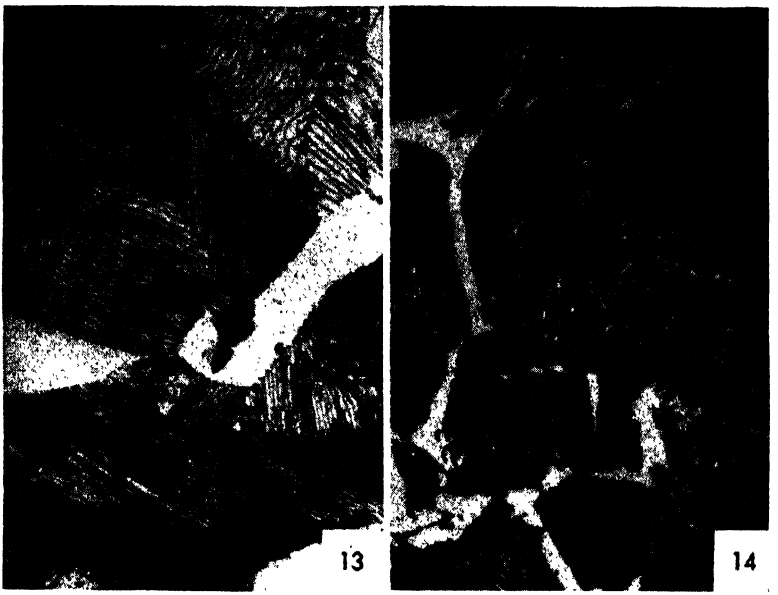

Micro. 11.13. Steel 5140 (0.42% C, 0.93% Cr), furnace-cooled from 950°C; ×1,000; Nital etch. This annealed structure shows well resolved pearlite and free ferrite, with only about 30% of the structure α. Hardness RG72, Brinell 202, is practically identical to that of 2340 and 1335.

Micro. 11.14. Steel 5140, ½-in. section air-cooled from 950°C; ×1,000; Nital etch. The normalized structure is practically identical to that of normalized 2340 with just traces of ferrite outlining the former austenitic grain boundaries and only vaguely resolved fine pearlite. The hardness of RG90, Brinell 272, is slightly higher than that of 2340 and 1335.

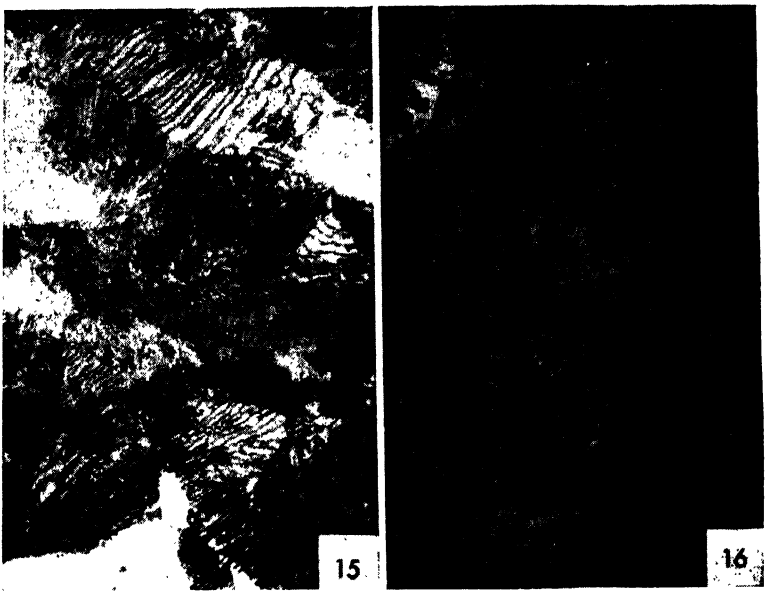

Micro. 11.15. Steel 4140 (0.40% C, 0.95% Cr, 0.20% Mo), furnace-cooled from 950°C; ×1,000; Nital etch. This annealed structure shows some resolved and some unresolved pearlite and less free ferrite than the single alloy steels. It is harder than the 2340–5140 group, *i.e.*, RG84 or Brinell 242.

Micro. 11.16. Steel 4140, ½-in. section air-cooled from 950°C; ×1,000; Nital etch. This duplex alloy steel shows quite a different normalized structure; Widmanstätten ferrite and apparently carbide nodules rather than ordinary pearlite. The high hardness of RG105, RC45, or Brinell 429, and the transformation graph suggest that the structure may be partly bainitic.

Micro. 11.17. Steel 4340 (0.42% C, 1.78% Ni, 0.80% Cr, 0.33% Mo), furnace-cooled from 950°C; ×1,000; Nital etch. This high hardenability triple-alloy steel upon annealing identical to that of the previous 2340–4140 group, shows a very different microstructure. Globular carbides rather than pearlite suggest that not all the alloy-type carbides were dissolved upon austenitization at 950°C. The Widmanstätten ferrite form is analogous to the normalized structure of T1335 and suggests an equivalent transformation temperature, lower than that obtaining upon annealing the lower alloy steels. The high hardness, RG97 or Brinell 350, supports this view as does the transformation diagram (page 315).

Micro. 11.18. Steel 4340, ½-in. section air-cooled from 950°C; ×1,000; Nital etch. This structure appears to be practically identical to that of tempered martensite (*cf.* Micro. 10.15 on page 294). Actually, reference to the transformation diagram indicates that the structure is bainite, and the hardness RC52 or Brinell 508 supports this conclusion. The heat treatment, although in accord with the definition of normalizing, could hardly be called that in view of the structural result obtained.

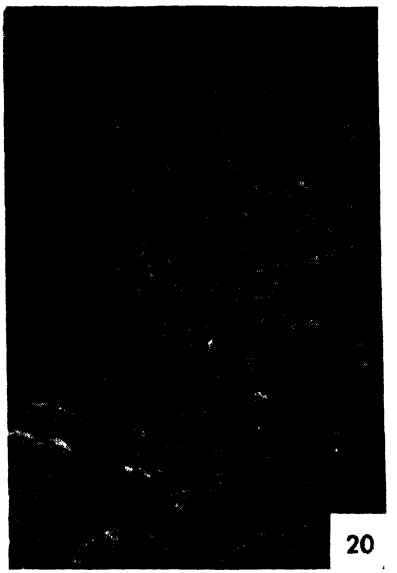

Micro. 11.19. Steel 4640 (0.36% C, 1.84% Ni, 0.23% Mo), furnace-cooled from 950°C; ×1,000; Nital etch. This Ni:Mo steel shows an extreme divergence from the normal pearlitic structure upon annealing. The rather coarse but nonlamellar carbides do not result in much hardness, *i.e.*, the RG71 or Brinell 196 is a little less than annealed 2340, etc. The structure is pertinent in connection with the matrix of high-tensile Ni:Mo cast iron (page 454).

Micro. 11.20. Steel 4640, ½-in. section, air-cooled from 950°C; ×1,000; Nital etch. This structure represents an extreme also, here in the development of Widmanstätten ferrite plates. However, distribution of the carbide phase again is such that the hardness is only moderate, RG83, Brinell 235, or equivalent to normalized 2340, etc.

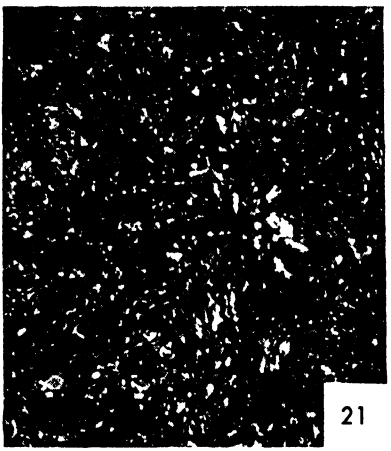

Micro. 11.21. SAE 4335 steel (1.8% Ni, 0.8% Cr, 0.3% Mo, 0.35% C); ×1,000; Nital etch. This structure is that of the steel after quenching in oil from 1550°F and tempering to a hardness of C50. Employed in an antiaircraft gun, this steel is used for a part subjected to battering impact loads. The section is too large to be "austempered," yet hardness is vital and as much toughness as possible is desired. This Ni:Cr:Mo steel has greater toughness at a Rockwell of C50 than most other available carbon or alloy types.

the greatest resistance to overstressing in fatigue, and the greatest toughness under severe conditions. When the steels did fail, the energy absorbed in fracturing was greater than that absorbed in the same steels with the other structures. The curves of Fig. 11.14 showing the energy required to break notched impact specimens at temperatures within the useful range, −80 to +200°C, show that the presence of bainite in the tempered martensite is less detrimental at room temperatures and above than pearlite.

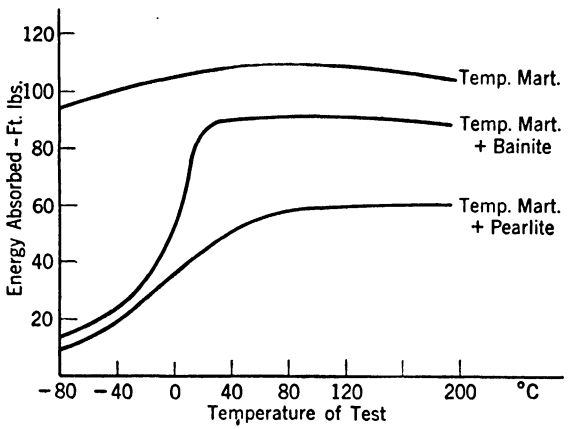

FIG. 11.14. Variation of impact strength with temperature for medium-carbon steels heat-treated in two cases by isothermal transformation to part bainite or part pearlite, quenched to transform remaining austenite to martensite, and then tempered so that all three kinds of structures had the same tensile strength, 125,000 psi.

The above comparisons are of different structures for the same steel. What of the properties of tempered martensites of the same hardness for different alloy steels? Assumption of the same hardness would predict the same distance between carbide crystallites, according to Gensamer's law (page 291). Another factor to be considered in the case of alloy steels would be the properties of the ferrite matrix containing the carbides. Ferrite is subject to solid-solution strengthening (see page 79) but, more importantly, its inherent plasticity is altered and the change may be an increase or a decrease according to the principles of Chap. 3.

Tempering curves for four medium-carbon alloy steels of the types already considered in some detail are given in Fig. 11.15. The plain manganese (1340) and nickel (2340) steels soften at about the same rate. The sharp increase in hardness at 700°C is caused by the formation of some austenite, which becomes martensite upon quenching from the

tempering operation. Both nickel and manganese lower the A_1 temperature so that at 700°C the structure is austenite and ferrite rather than all austenite.

The chromium and Cr:Ni:Mo steels, 5140 and 4340, soften less rapidly, and both show an inflection at temperatures in the range 400 to 500°C. Presumably, the carbide phase formed at lower temperatures is Fe_3C, while at the higher temperatures the more stable phase $(FeCr)_3C$ or $(FeCrMo)_3C$ forms.

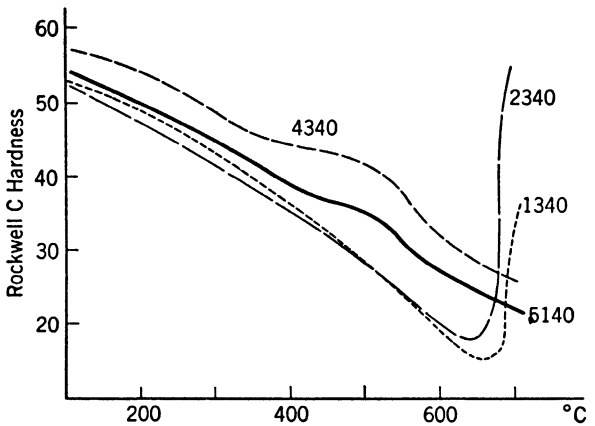

FIG. 11.15. Tempering curves for four medium-carbon alloy steels (1340–1.7% Mn; 2340–3.0% Ni; 5140–1.0% Cr; 4340–1.7% Ni, 0.8% Cr, 0.3% Mo). Tempering time for all curves was 20 hr.

A comparison of the property changes upon tempering of a plain carbon steel (1045), a chromium steel (5130) and a Cr:Mo steel (4130) is available in the data of Table 11.5. Particularly noteworthy is the higher tensile, yield, *and impact strength* of the Cr:Mo steel as quenched and tempered to a sorbitic structure. A further comparison of the properties of a plain carbon and several alloy steels, as annealed to ferrite + coarse pearlite and as quenched and tempered to sorbite of the same hardness, is available in the data of Table 11.6. Since all specimens were oil-quenched, it is probable that the plain carbon steel was not fully hardened. The pearlite formed upon quenching may be responsible for the very low notched impact strength of the plain carbon steel. This factor somewhat vitiates the comparison.

The particularly important property of local ductility or resistance to notch brittleness is the most significant difference between different medium-carbon steels, heat-treated to the same structure of tempered

martensite and the same hardness. Data by Sachs[1] and others show that, in general, nickel alloy steels have somewhat higher notch toughness, particularly at high hardness levels, Rockwell C40–50. For example,

TABLE 11.5. MECHANICAL PROPERTIES OF A CARBON STEEL, A CHROMIUM STEEL AND A CR:MO STEEL IN VARIOUS CONDITIONS. CARBON CONTENTS AND TEMPERING TREATMENTS WERE SELECTED TO GIVE COMPARABLE HARDNESSES IN EACH CONDITION*

Steel	% C	% Mn	% Cr	% Mo
C, open hearth.....	0.45	0.57		
Cr, elec. furnace.....	0.33	0.41	0.72	
Cr:Mo, elec. furnace .	0.32	0.72	0.80	0.27

Steel	Heat treatment	Tensile strength, psi	Yield strength, psi	% elonga-tion in 4 in.	BHN	Izod impact
C	As rolled	82,100	50,100	28		16
Cr	As rolled	82,800	52,000	31	230	20
Cr:Mo	As rolled	113,700	86,110	20		5
C	Annealed	77,100	41,900	28		10
Cr	Annealed	78,200	46,700	29	189	15
Cr:Mo	Annealed	96,900	64,100	24		12
C	H_2O qu 850°C; temper. 400°C	127,300	100,400	12		27
Cr	H_2O qu 845°C; temper. 418°C	138,500	118,100	13	381	10
Cr:Mo	H_2O qu 845°C; temper. 400°C	190,100	171,300	13		37
C	H_2O qu 860°C; temper. 500°C	114,600	81,100	16		26
Cr	H_2O qu 845°C; temper. 500°C	127,400	99,800	17	355	21
Cr:Mo	H_2O qu 845°C; temper. 500°C	172,300	150,300	16		49
C	H_2O qu 860°C; temper. 600°C	101,300	70,500	23		30
Cr	H_2O qu 845°C; temper. 600°C	109,200	87,500	22	292	85
Cr:Mo	H_2O qu 845°C; temper. 612°C	141,900	122,200	20		76

* "The Making, Shaping, and Treating of Steel," U.S. Steel Corp., 968, 1940.

in Table 11.7 tensile test data on notched bars are tabulated, some notches being concentric and others eccentric. Among the three steels listed, the nickel steel 2340 shows noticeably superior ductility and eccentric notch strength (depending on notch ductility). The data are

[1] Sachs, Ebert, and Brown, *Trans. AIME*, **171**, 605, 1947.

also interesting in that they show that, at a tensile strength of 200,000 psi measured in the usual way, the concentrically loaded notched bar requires a greater fracture stress and an eccentrically loaded bar breaks at a much lower stress. Less tempering or a higher tensile strength of 250,000 psi decreases ductility so much that both notched strengths are

TABLE 11.6. MECHANICAL PROPERTIES OF A PLAIN CARBON AND SEVERAL ALLOY STEELS, AS ANNEALED AND AS QUENCHED AND TEMPERED TO THE SAME HARDNESS*

Steel	% C	% Mn	% Cr	% Ni	% Mo
C	0.62	0.45			
Cr	0.49	0.53	0.60		
Ni	0.40	0.65	....	3.60	
Cr:Ni	0.43	0.57	0.46	1.60	
Cr:Mo	0.32	0.72	0.80	....	0.27

Steel	Heat treatment	Tensile strength, psi	Yield strength, psi	% elongation in 2 in.	BHN	Izod impact
C	Annealed, 775°C	103,000	62,400	19	196	
Cr	Annealed, 775°C	116,200	74,100	20	217	
Ni	Annealed, 775°C	104,700	71,000	22	205	
Cr:Ni	Annealed, 775°C	111,700	70,300	22	212	
Cr:Mo	Annealed, 775°C	109,400	89,390	21	217	
	Oil-quenched, 845°C					
C	Temper., 565°C	126,200	84,400	18	235	5
Cr	Temper., 612°C	125,300	105,200	18	228	66
Ni	Temper., 540°C	128,000	112,500	19	248	54
Cr:Ni	Temper., 600°C	128,000	111,000	20	248	54
Cr:Mo	Temper., 618°C	125,600	112,200	21	235	90

* "The Making, Shaping, and Treating of Steel," U.S. Steel Corp., 969, 1940.

lower. The data also show a slight superiority of 2340 made in the electric furnace (EF) over that made in the open hearth (OH).

11.11 Temper Brittleness

Notch bar tests of the alloy steels have revealed one occasionally serious difficulty found in alloy steels, particularly Ni:Cr (3140, etc.) types. When the alloy steel is tempered in the vicinity of 500 to 680°C and slowly cooled, the steel is severely embrittled; if quenched, it shows the full ductility to be anticipated for that hardness. This condition is

known as *temper brittleness.* Microstructure and tensile strength, hardness, and other properties are unaffected by the cooling rate from the tempering operation and only localized ductility as shown by a notch test indicates the embrittlement. Considerable study[1] of this phenomenon has shown ways of avoiding it, *e.g.*,

1. The presence of molybdenum in amounts of 0.20 to 1.0%
2. A fast cool from the tempering operation

Data supporting these conclusions are given in the references cited, *e.g.*, a 0.55% C, 3.6% Ni, 2.25% Cr steel when air-cooled from 680°C

TABLE 11.7. NOTCH TENSILE PROPERTIES OF QUENCHED AND TEMPERED ALLOY STEELS*

Steel	Tensile strength 200,000 psi, RC40			Tensile strength, 250,000 psi, RC49		
	Concentric notch strength	Notch ductility, %	Eccentric notch strength	Concentric notch strength	Notch ductility, %	Eccentric notch strength
2340, EF	285,000	3.0	135,000	260,000	0.8	90,000
2340, OH	280,000	2.5	120,000	230,000	0.7	85,000
5140	265,000	1.7	90,000	180,000	0.3	55,000
T1340	265,000	1.4	90,000	125,000	0.1	35,000

* Sachs, Ebert, and Brown, *Trans. ASM*, 1946.

had a Charpy impact strength of only 15 ft-lb, but when water-quenched from 680°C, it showed a Charpy value of 70 ft-lb.

The cause of temper brittleness is not known with certainty. The data of Pellini and Queneau show that the phenomenon is reversible; *i.e.*, an embrittled steel can be reheated to 550°C and quenched, and it will then show the anticipated ductility. Furthermore, the effect is observed upon tempering pearlitic structures to a somewhat less degree, as well as in tempered martensite or bainite. These observations suggest that carbide precipitation from ferrite, resulting from the solubility decrease from 0.02% carbon at 600°C to 0.007% carbon at room temperature, may be the fundamental cause of temper brittleness.

11.12 Quenching Rates

The effect of cooling rate is of sufficient importance to demand inclusion of the following table (from Grossman) in which the higher numbers represent more severe quenching. The table demonstrates,

[1] Greaves and Jones, *J. Iron Steel Inst.*, **111**, 231, 1925. Hollomon, *Trans. ASM*, **36**, 473, 1946. Pellini and Queneau, *Trans. ASM*, **39**, 139, 1947.

more or less quantitatively, the value of movement of the cooling medium in speeding up the quenching rate, particularly the rate in the important temperature range of 723 to about 550°C.

	Oil—60°C	Water—20°C	Brine—20°C
No circulation of liquid or agitation of piece.	0.2	1.0	2.0
Mild circulation (or agitation)	0.3	1.1	2.1
Good circulation	0.4	1.4	
Strong circulation	0.6	1.8	
Violent circulation	1.0	4.0	5.0

Differences in the efficiency of the several types of quenching baths in conducting heat from the metal are related to the "wetting" tendency of the liquid, to its vaporization characteristics or tendency to form vapor blankets that insulate the steel, to its ability to remove scale that also acts as an insulator, and to other physical variables. Naturally the temperature of the medium is of importance, particularly with reference to its boiling point; *e.g.*, hot water cools steel more slowly than does hot oil.

There are noticeable differences among various types of oils, depending on their relative viscosities, vapor-forming characteristics, and the chemical changes occurring with continued use. There are differences between waters, particularly between fresh tap water that contains dissolved air and water that has been used for some time (or distilled water) with little or no air to come out of solution at the steel surface and thereby slow up heat transfer. Finally, the concentration of a brine or caustic solution is of importance, and tests have shown that 9% sodium chloride or 3% sodium hydroxide solutions are most favorable for elimination of soft spots caused by vapor pockets at the steel surface in the early stages of cooling. Incidentally, the increased speed of cooling of brines does not depend on the use of lower temperatures of the bath, but it is related to its action in removing surface oxide or scale and in suppressing vapor formation at the steel surface.

These factors are illustrated by Fig. 11.16, which reproduces some typical cooling curves of alloys quenched in air, water, and oil. In general there are three stages of cooling:

1. *Vapor.* The hot metal instantly transforms the liquid in contact with it to vapor so that the metal actually cools slowly in a hot, gaseous

blanket. (This stage is not evident in Fig. 11.16 because of the low quenching temperature of 850°F or 460°C.)

2. *Vapor-liquid.* Slightly cooler metal still loses heat by converting liquid to gas, but the rate of vapor formation is slower and the gas escapes as rapidly as it forms. The escaping vapor or local boiling gives a local agitation that brings fresh, cool liquid to the metal surface. Therefore, this is the most active or rapid cooling stage.

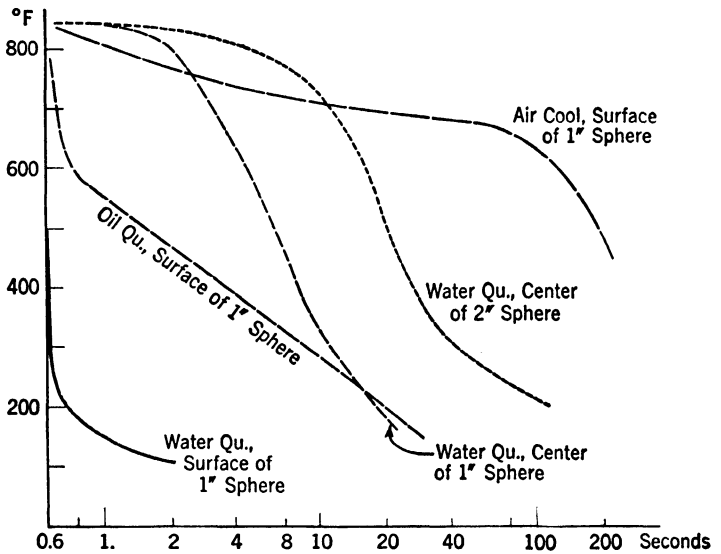

FIG. 11.16. Temperature-time curves showing the surface cooling rate of 1-in. steel spheres quenched in water, mineral oil, and air; also, the center cooling rate for 1- and 2-in. spheres quenched in water. (*French.*)

3. *Liquid.* The relatively cool metal does not have sufficient heat to form gas and, as liquid contacts the metal surfaces, the liquid is heated, rises, and is replaced by cooler liquid. Heat transfer is best here, but the thermal gradient is too small for rapid cooling. The effect of movement of the quenching liquid is to reduce the vapor stage. High-pressure sprays practically eliminate this stage. Different mediums may not have the same relative duration of each stage. From the metallurgical requirement of achieving martensite with minimum macrostresses of thermal origin, it is obvious that fast cooling is desirable from the A_1 temperature to about 450°C and slow cooling thereafter. There are many special procedures, apart from marquenching (page 301) that attempt to approach this ideal. It suffices here to say that quenching is an all-important part of hardening heat treatments.

11.13 Flame, Induction, and Weld Hardening

The theoretical discussion of structural and property changes accompanying the heating and cooling of steels applies not only to heat treatment of complete sections but also to intentional heating of localized surface areas, as in induction-hardening[1] and flame-hardening processes. No structures are reproduced here for they would be found nearly to duplicate those produced by normal heat treatments of similar steels. In both processes, uniform control of actual temperatures in the austenitic field may be somewhat difficult to achieve, but the very short time at temperature minimizes grain growth of the structure. Hardenability is seldom an important factor since a depth of hardening of about ¼ in. is the maximum usually desired. Distortion is frequently troublesome in flame hardening since the entire surface to be hardened cannot always be brought to temperature at once. When large sections are treated, the flame proceeds slowly over the surface with the quenching liquid following closely behind the torch. Considerable experience is required in regulating flame intensity, rate of movement, and sequence of movement over the surface so as to austenitize to a sufficient depth for proper hardening, to minimize distortion, and to avoid overlapping with a structural discontinuity at the junction of two successive passes.

The induction-hardening process, where applicable, avoids overlap difficulties by heating the entire surface simultaneously. This method is limited by the cost of the requisite electrical equipment and by the simplicity of shape required in parts to be treated. It is being very successfully employed for rounds, particularly the bearing surfaces of automotive or aircraft crankshafts. The process is also applicable to irregular sections and even parts with sharp corners. However, difficulty is then encountered in obtaining uniform heating; corners may be severely overheated before reentrant sections are austenitized and considerable experimentation with the induction current, frequency, time, and other variables may be necessary before satisfactory results are obtained.

In general, lower frequencies give slower heating and a deeper hardened section. Very high frequencies, correspondingly, tend to give very localized but extremely fast heating.

The martensitic structures observed in shallow induction-hardened parts are particularly interesting. Since the heating time is a matter of 15 to 60 sec, homogeneous austenite is not obtained. In fact, a pearlitic structure of 0.8% carbon may be induction-hardened to a full

[1] Cone, *Metals & Alloys*, **9**, 1, 1938.

martensitic hardness of Rockwell C65 or 66 and still *appear* to be pearlite. The carbide apparently mostly dissolves, but concentration gradients approaching those of the pearlitic structure remain in the austenite. Upon quenching, the structure becomes martensitic but, when polished and etched, the low-carbon martensite, originally ferritic areas, etches rapidly and the higher carbon martensite, originally carbide lamellae, etches slowly thereby giving a pearlitic appearance but with shading reversed.

The use of induction- or flame-hardening procedures requires special consideration since most of this chapter has emphasized the necessity for high hardenability in order to obtain tempered martensitic structures throughout the section. There are at least three justifications for employing surface hardening by localized heating:

1. The engineering service may require high hardness at the surface to resist wear and good strength with plasticity in the core. A carburized and heat-treated low-carbon steel would have better wear resistance at the surface (Chap. 12) but less core strength than an induction-hardened medium-carbon steel.

2. Residual stresses upon proper induction hardening show compression at the surface. Although balancing tensile stresses necessarily exist beneath the surface, the surface stresses are in the right direction to resist the service stresses most frequently causing failure.[1]

3. The cost of induction hardening, *when a large number of identical sections are treated*, is very much less than in the case of the usual through hardening. The direct saving is in time, labor, and fuel. A further advantage is the fact that induction hardening eliminates decarburization and minimizes surface oxidation or scaling.

Welding is essentially a chill-casting process involving small amounts of liquid metal, which, in contrast to ordinary castings, is fused to the "mold" or, in this case, the section being welded. The fusion requirement means that the base metal in contact with the weld deposit is at least momentarily heated to the proximity of its melting point with a consequent temperature gradient from this zone to a distant point in the base section at which the temperature rise is insignificant. Thermal gradients have already been mentioned as sources of distortion or internal stresses, or both, and it is for this reason that welded joints are given a stress-relief anneal if service requirements are severe. When possible, the entire welded section may be heated into the stress-relief annealing temperature range (1100 to 1300°F), but in large assemblies, it is possible only to "flame-anneal," *i.e.*, reheat locally with a torch.

[1] Almen, *Metal Progress*, **46**, 1263, December, 1944.

If the steel has air-hardening characteristics resulting from the presence of alloying elements, the zone adjacent to the weld may become partially martensitic as a result of being heated into the austenitic field and cooled rapidly by the flow of heat into adjacent cooler sections. High stresses in a localized martensitic zone are very likely to cause crack formation and failure under ordinary service conditions (see Micro. 11.7). This difficulty can be avoided by preheating the entire structure, before welding, to about 500 to 700°F. The warm base metal slows up the quenching effect of heat flow from the zone next to the weld into the adjacent colder metal.

11.14 Civil Engineering Applications

In the fields of civil engineering and building construction, large structures, such as bridges and buildings, require steels of moderate cost, as specified by the ASTM, in structural grades of plain carbon, so-called (low) silicon steel, and the more expensive 3.5% nickel steel. The yield point of the nickel structural steel is at least 50% greater, and of the silicon steel about 40% greater, than that of the carbon steel. This is, of course, partly because around 0.4% carbon is specified in the former steels while only 0.2 to 0.3% carbon would be used in the plain carbon steel to obtain the properties designated.

Medium-manganese steel containing, *e.g.*, 1.60% Mn with 0.33% C and 0.18% Si, as used in the main compression members of the Kill van Kull Bridge,[1] is in competition with the other high-strength structural steels used in the as-rolled condition. On cooling after hot-rolling, it tends to develop an extremely fine pearlite structure, which probably accounts in large measure for its strength—yield point over 58,000 psi and tensile strength over 100,000 psi.

In addition to the structural steels used in the as-rolled condition, heat-treated mild carbon grade steels, of comparatively high strength, have been available to bridge engineers since 1915. Heat-treated I bars, for use at a unit stress 50% higher than that specified for ordinary structural steel, were adopted for the principal tension members of the Carquinez Strait cantilever bridge in California. Their cost was approximately 1 cent a pound above the cost of ordinary structural steel I bars. Silicon steel was used for the towers and compression members of this bridge and for the towers, floor, and anchor girders of the George Washington Bridge over the Hudson River at Fort Lee. It

[1] Additional information on the steels employed in bridge structures may be obtained by consulting the article from which these data were abstracted, *viz.*, D. B. Steinman, *Metal Progress*, June, 1931.

also cost about 1 cent per pound more than ordinary structural steel as against some 2.5 cents per pound for the standard 3.5% nickel steel, which, in spite of high cost, has been specified for important members in many bridges, such as stiffening trusses in the Manhattan Bridge (8,000 tons from a total of 44,000 tons of steel in the entire bridge).

Heavy steel rails are typically of eutectoid composition, with a minimum of about 0.50% carbon for the lighter rails. They were formerly always used in the approximately normalized condition produced by air-cooling after hot-rolling. In recent years, however, rails subject to particularly heavy service have come to be heat-treated. They are usually allowed to cool from the hot-rolling operation to below the critical temperature, then reheated to the austenitic condition and the ends quenched in an air blast. Subsequently, the entire rail is permitted to cool slowly in air and, in this stage, heat flows from the main body of the rail and tempers the air-cooled ends. Structural variations, from moderately coarse to fine pearlite, will be found in the various parts of the rail, *i.e.*, the head, web, and flange, according to the differing cooling tendencies in these regions, while a very fine pearlitic structure is found at the ends (page 329). The heat-treated structure shows a somewhat higher hardness at the rail ends, which are subjected to a greater battering effect by the passage of trains. In addition, the main part of the rail, although slightly softened by the slow cooling, shows very much increased resistance to impact loads and to failures from transverse fissures and other internal defects.

Specifications for steel castings cover a rather wide range including carbon steels and alloy steels for general industrial, or railroad and marine, structural purposes, as well as alloy steels for valves, flanges, and fittings for service at temperatures up to about 600°C (dull red).

The carbon content of the plain carbon steel castings is left to the discretion of the manufacturer, but it is not intended that heat treatment (such as liquid quenching or spraying, and tempering), other than annealing or normalizing, shall be required in order to develop the specified strength properties. On this basis, the carbon would normally run from 0.2 to 0.3% in the soft castings to 0.5 or 0.6% in the hardest. The chemical compositions range from 0.5 to 1.0% Mn and from 0.2 to 0.75% Si to ensure satisfactory deoxidation of the liquid steel, while phosphorus and sulfur are not allowed above 0.05 and 0.06%, respectively, by reason of their embrittling effect.

The alloy steel castings specified by ASTM for structural purposes are divided into three classes according to the following criteria:

The tension requirements for Class A castings are intended to apply

to castings of such design and dimensions that they may be regarded as unsuitable for any method of heat treatment other than one that includes slow furnace-cooling from above the critical temperature. In Class B castings, the properties are obtained by air-cooling, which is regarded as a safe procedure for the great majority of alloy-steel castings, developing in them the highest tensile-strength and yield-point values that can be obtained from the materials by any method of heat treatment except liquid quenching. In Class C castings, liquid quenching followed by tempering is the approved treatment.

The chemical specifications limit only the phosphorus and sulfur to 0.05 and 0.06%, respectively, and the manufacturer may use carbon, silicon, and manganese, and other alloying constituents at his discretion in obtaining the requisite physical properties in all three classes of castings, which range from 75,000 to 150,000 psi tensile strength, and from 40,000 to 125,000 psi yield point, with elongation in 2 in. never below 10% and reduction of area never below 25%.

Under these specifications, many types of low-alloy steel may be offered, such as vanadium, chromium, chromium-vanadium, nickel, nickel-chromium, chromium-molybdenum, or manganese steel.

QUESTIONS

Group A

1. Specify the steel and the heat treatment to be used for the connecting rod of a small engine where (*a*) the cost is important but not weight, *e.g.*, a lawnmower engine, (*b*) the weight and reliability are all important, *e.g.*, a small plane motor.

2. Why is it simpler to weld a plain carbon steel than an alloy steel, both containing about 0.40% carbon? If they contained only 0.15% carbon, why would the difference in weldability be insignificant?

3. Why are induction-hardened steels never decarburized to a noticeable degree, while the same steel hardened in the usual way, in an air atmosphere, is usually decarburized to some extent?

4. Describe the probable microstructures of the AISI steel No. 2340 at distances 1/16, 1/4, 1/2, 1 and 3 in. from the quenched end of the Jominy test bar in Fig. 11.9.

Group B

1. Take the isothermal transformation graph for steel No. 2340 in Fig. 11.2 and determine the continuous cooling transformation diagram using the method of Grange and Kiefer (page 274).

2. Determine the continuous cooling transformation graph of the No. 4340 steel in Fig. 11.7, using the same procedure.

3. Calculate the Jominy hardenability curves for the two steels in questions 1 and 2, using the derived continuous cooling diagrams and the cooling rate data for the Jominy test given in Fig. 11.8 with the assumption (unwarranted) that the specified cooling rate is constant with time and temperature.

4. Oil quenching is known to result in more residual austenite than the faster cooling of water quenching. Explain why (see page 176 of Chap. 6).

CHAPTER 12

CARBON AND ALLOY TOOL STEELS

There are several thousand different tool steels, if enumerated by their trade names; several hundred, if classified by their composition, and perhaps twenty or so, if classified by the *types* of alloy composition. In the aggregate, they represent a very small fraction of the steels produced on a tonnage basis or even in terms of dollar value despite their considerably greater cost per pound. Their importance, however, is of first rank since tools are essential for production. There are many large and small manufacturing units that make and heat-treat their own tools. It is not unusual for thousands of dollars to be spent in designing and machining a special tool for which the cost of the steel is only a few dollars. If the heat treater then cracks the tool while hardening it, harsh words are going to be spoken!

12.1 Classification of Tool Steels

Steels used for tools generally have high carbon content to ensure hardness and abrasion resistance. If no other alloying elements are added or if the amount added is insufficient to affect hardenability very noticeably, the steel will have to be hardened by water quenching, unless in very thin sections. Typical steels of this character are included in Group A of the abbreviated listing in Table 12.1.

Enough alloying elements may be added to increase hardenability notably, and the steel can be hardened by quenching in oil and then classified as an oil-hardening steel, Group B of the table. Finally, sufficient alloying elements may be present for even thick sections to cool in air and become fully martensitic. These air-hardening steels are classified in Group C and include types known as *high-speed steels.*

The table indicates that the important alloying elements for tool steels are those which have a strong affinity for carbon and form alloy carbides. Elements, such as nickel and silicon, which dissolve in ferrite and tend to convert carbide to graphite, are seldom added to tool steels. In most cases, alloying elements are used in tool steels to obtain abrasion resistance and resistance to softening at higher temperatures; the

TABLE 12.1. CLASSIFICATION OF SOME COMMON TOOL AND DIE STEELS

Group A—Water-hardening Tool and Die Steels

No.	Composition			Hardening temp., °F	Draw temp., °F	Typical uses
	% C	% Mn	% other			
1	0.70	0.70	....	1450	500–1000	Flat dies, chisels
2	1.10	0.30	....	1450	300– 450	Punches and cutting tools
3	1.30	0.30	0.20V	1500	300– 450	Punches and cutting tools
4	1.10	0.30	1.00Cr	1500	300– 450	Punches and cutting tools
5	1.30	0.30	3.50W	1550	300	Finishing cuts

Group B—Oil-hardening Tool and Die Steels

No.	Composition					Hardening temp., °F	Draw temp., °F	Typical uses
	% C	% Mn	% Cr	% Mo	% other			
1	0.85	1.2	0.5	..	0.5W	1450	350–450	Nondeforming
2	0.40	0.8	1.0	0.2	....	1575	1200	Zn die-casting dies
3	0.50	0.3	1.7	0.5	2.5W	1750	1200	Hot-trim dies
Graph Mo	1.50	1.2	..	0.5	1 2Si	1500	1000	Draw dies
52100	1 00	..	1.2	..	..	1500	350–450	Bearings
C:Cr*	2.2	..	12.0	..	..	1800	900	Cold-work dies

Group C—Air-hardening and High-speed Steel Types

Type name	Composition						Hardening temp. °F	Draw temp. °F	Typical uses
	% C	% W	% Mo	% Cr	% V	% Co			
C:Cr	0.3	..	1.5	5	0.5	..	1800	1100	Al die-casting dies
High C:Cr	1.5	..	1.0	12	0.2	..	1800	900	Cold-form dies
Cr air hard	1.0	..	1.0	5	0.2	..	1850	900	Cold-form dies
Cr:W hot work	0.4	7.5	..	7.5	..	..	2150	1200	Hot-work dies
Cr:W hot work	0.4	12	..	12	..	..	2350	1200	Brass die-casting dies
18-4-1	0.7	18	..	4	1.2	..	2350	1050	Cutting tools
18-4-2	0.8	18	..	4	2.0	..	2350	1050	Cutting tools
18-4-1 Co	0.7	18	..	4	1.2	5	2350	1050	Cutting tools
18-4-4	1.2	18	..	4	4.0	..	2350	1050	Cutting tools
6-5-4-1	0.7	5.5	4.5	4	1.2	..	2250	1050	Cutting tools
6-5-4-2	0.8	5.5	4.5	4	2.0	..	2250	1050	Cutting tools
6-5-4-1 Co	0.7	5.5	4.5	4	1.2	5	2225	1050	Cutting tools
Mo Max.	0.7	2	8	4	1.2	..	2200	1050	Cutting tools

* Austenitized at 1850°F, this steel may be hardened by air-cooling.

associated hardenability effects, although important, are to some degree incidental.

High carbon content, corresponding to a large amount of the carbide

phase, does not appreciably increase martensitic indentation hardness as was evident in Chap. 10. However, undissolved carbide particles greatly increase the resistance to abrasion or wear and, therefore, all cutting tools or parts subjected to sliding wear will have a longer life when made from a hypereutectoid steel. The gain in wear resistance is at the sacrifice of ductility or toughness; a 0.60% carbon steel can readily be heat-treated to the same Rockwell C64 hardness as a 1.20% carbon steel. It will then have less wear resistance but greater toughness. Therefore, a razor blade would be made from the 1.2% carbon steel, and a cold chisel, subjected to pounding and requiring ease of sharpening, would be made from the 0.6% carbon steel.

Small amounts of vanadium or tungsten make the carbide phase still harder and permit the addition of extra carbon tied up in the form of undissolved carbides. Thus wear resistance is further increased, grain growth during austenitization more restricted, and at the same time insufficient alloying elements enter the austenite to alter hardenability noticeably.

Steels used for forging or extrusion dies are subjected to impact stresses and, therefore, have medium-carbon contents, as noted in Chap. 11. However, the dies may be subjected to high operating temperatures and rapid changes in temperature and, for this type of service, alloys are added to restrict carbide growth and softening during use and to minimize thermal or "fire" cracking.

Also in the Group C steels, it is apparent that 1% Mo is used to replace about 2% W (*e.g.*, 6% Mo + 5% W in place of 18% W). Cobalt, not previously discussed as an alloying element, confers increased abrasion resistance to the Group C steels while decreasing toughness. It also decreases hardenability, but this effect is not significant in these air-hardening steels. All the Group C high-speed steels, the 18:4:1 type particularly, may be produced with a much lower carbon content, *e.g.*, 0.40 to 0.50, for use as hot-work die steels.

12.2 Phase Diagram of High-speed Steels

It is not possible to present phasial relationships for a complex alloy such as Group C, 18:4:1, by the conventional two-dimensional temperature-composition phase diagram. However, by taking a few liberties with details, a quasi-binary diagram such as Fig. 12.1 may be drawn, which will be useful in discussing heat treatment temperatures. It should be emphasized that the diagram suggests temperatures but not phasial compositions except for carbon content.

The presence of 18% W, 4% Cr, and 1% V raises the A_1 temperature

from 723 to approximately 840°C and the eutectic temperature from 1135 to about 1330°C.[1] At the same time, the eutectoid composition is reduced from 0.80 to about 0.25% carbon, and the maximum solubility of carbon in austenite is reduced from 1.70 to approximately 0.70%. Substantially the same changes are observed if the steel is any one of the Group C high-speed steels.

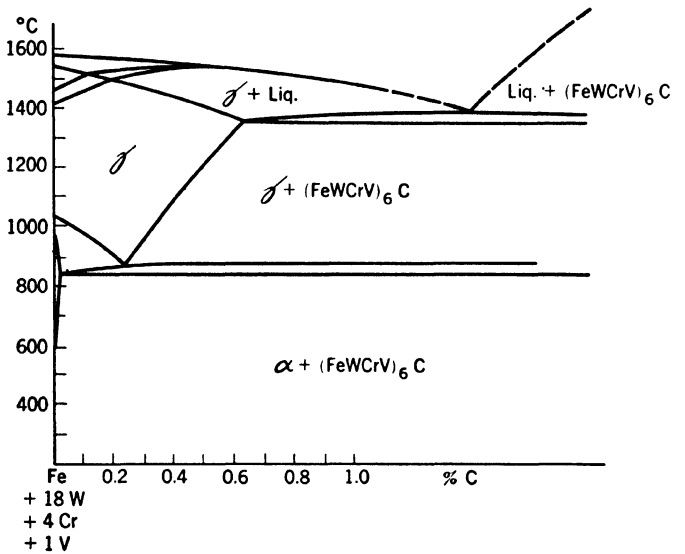

FIG. 12.1. Pseudo-binary phase diagram for alloys of iron plus 18% W, 4% Cr and 1% V with varying carbon contents. Eutectic and eutectoid transformations occur over a range of temperatures in these complex alloys and the compositions of ferrite, austenite, and carbide are not necessarily fixed. The diagram shows only the approximate saturation carbon contents of austenite at various temperatures between the eutectic and eutectoid.

These pronounced changes in temperature and composition of important parts of the diagram naturally lead to pronounced modifications in heat treatment of the steel. For example, the increase in A_1 temperature means a necessary increase of the austenitization temperature to at least above the A_{c_1}. Suppose that, analogously to a plain 1.2% carbon steel, the 18:4:1 steel were heated just above its A_1, held until equilibrium were reached, and quenched to convert the austenite

[1] According to Gibbs's phase rule, the addition of two more components, *e.g.*, tungsten and chromium, means that the eutectoid and eutectic in the Fe:C system are no longer invariant. Rather, two independent variables are possible so that the eutectoid and eutectic can each occur, at equilibrium, over a range of temperatures, and the composition of one phase may independently vary.

to martensite. Instead of the Rockwell C65 to be expected from the 0.75% carbon content, the steel would have a Rockwell C42 hardness. The diagram shows that at 850°C, the austenite would contain only about 0.25% carbon. Recalling Fig. 10.11 (page 298) and knowing that only carbon affects the hardness of martensite, we should expect this result.

It is now apparent that to obtain the desired 0.60 to 0.70% carbon in this alloyed austenite, it is necessary to heat to within the range of 1250 to 1300°C. Can that be done without excessive grain growth? The answer is suggested by the diagram. Some undissolved alloy carbides will be present at even the highest austenitization temperatures, and it would be only in the vicinity of the eutectic or 1330°C that extensive grain growth would be encountered unless the time at a slightly lower temperature was extremely long.

It is interesting as a historical note that steels of this approximate composition were made in the period 1890–1900 and that, after heat treatment and tests, they were considered to be of no interest or practical value. There was no knowledge of the phasial relationships, and the heat treatments that were tried were of the conventional type used for plain carbon steels. In 1907 two young metallurgists, still with no phasial knowledge but with plenty of curiosity, tried very high austenitization temperatures close to the melting point. After subsequent tempering, the steel was found to maintain a hardness of C65 even when heated to a dull-red heat. A tool treated in this way could cut at such a high rate of speed that it glowed at a dull-red heat (visible in a dark room) and not immediately lose its sharp edge. An astonishing achievement at that time, it earned the alloy its present name, high-speed steel, and was an important factor in the great industrial developments of this century.

12.3 Transformation Diagrams of Tool Steels and Their Uses

The transformation diagrams of some of the more frequently used tool steels are presented in Figs. 12.2 to 12.6.[1] Since these are being reproduced for their value in understanding the normal heat treatments, the diagrams are generally drawn for austenitization conditions employed in industrial heat treatments but with some discussion of the effects of overheating or underheating, *i.e.*, austenitizing at too high or too low a temperature.

[1] Payson and Klein, *Trans. ASM*, **31**, 218, 1943, is the source of much of the material in this section.

The upper portions of Fig. 12.2 indicate that plain carbon steel must be cooled rapidly past 500°C to avoid the formation of fine pearlite.

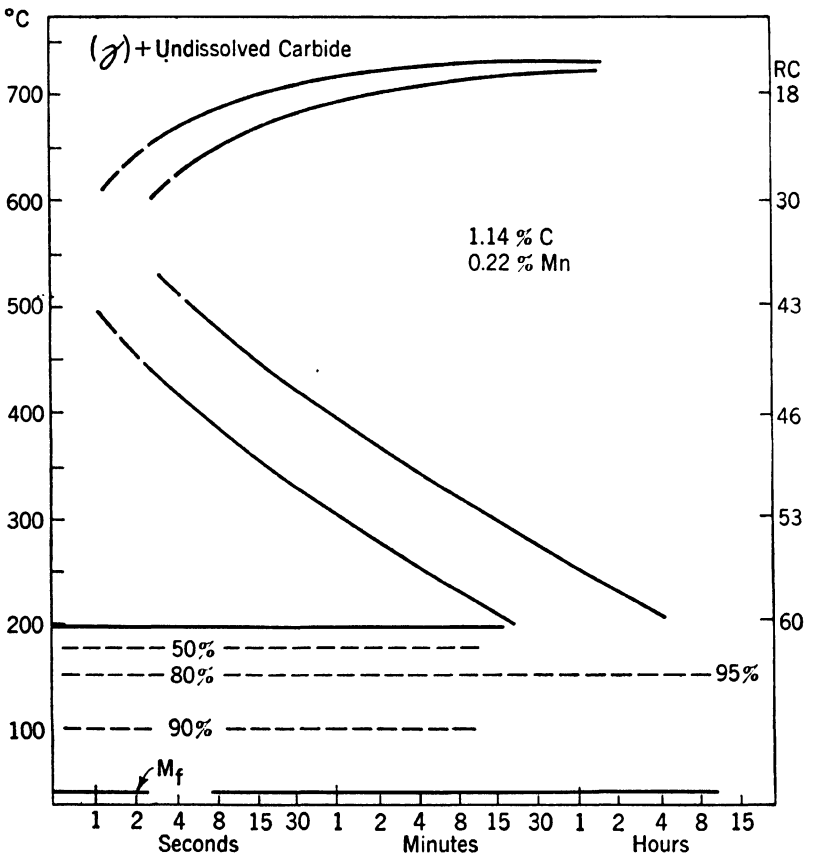

FIG. 12.2. Isothermal transformation diagram for a water-hardening plain carbon tool steel (1.14% C, 0.22% Mn) austenitized according to the usual hardening treatment at 790°C; therefore from the $\gamma + Fe_3C$ field with undissolved carbides in the structure. Rockwell hardnesses of transformation structures are shown. The degree of transformation of austenite to martensite, shown by dashed lines may vary with cooling rate (or relatedly, cooling stresses) in large sections. The 95% transformed at the right end of the 80% horizontal (150°C) means 80% martensite + 15% bainite since long holding here would cross the bainite transformation line if that were extended below 200°C. (*Payson and Klein.*)

The tungsten "finishing" steel, Group A5, has a similar transformation diagram. These are essentially water-hardening steels, although a somewhat higher manganese content (*e.g.*, 0.50 instead of about 0.25%)

may permit thin sections such as saw blades to be hardened by oil quenching. The effect of higher austenitizing temperatures on the martensite reaction is given in Table 12.2. These data show that higher quenching temperatures give a coarser grain structure, fewer residual carbides to resist abrasion, and more retained austenite upon cooling to room temperature.

The value of these transformation diagrams may be illustrated by considering the hardening of a 6-in. block of carbon tool steel. Suppose it is quenched by a high-pressure spray that will cool the surface layers rapidly to about 65°C, permitting their complete transformation to

TABLE 12.2. EFFECT OF AUSTENITIZATION TREATMENT ON MARTENSITE REACTION OF CARBON TOOL STEEL*

	Austenitization treatment		
	790°C, 1 hr	830°C, ½ hr	870°C, ½ hr
γ grain size, ASTM	No. 9	No. 8	No. 6
Amount of undissolved carbides	Very many	Many	Some
% martensite at 150°C	80	40	5
% martensite at 100°C	90	80	50
% martensite at 30°C	100	95	85

* Payson and Klein, *Trans. ASM*, **31**, 218, 1943.

martensite. The center of the block will cool much more slowly and transform at about 550°C to fine pearlite. Somewhere between the center and the surface will be a zone which at a specific time will have missed the pearlite reaction but which would not have cooled below the M_s line. In this zone, the austenite will remain untransformed for some time. If the block is transferred to the tempering furnace while the surface is still warm (the recommended procedure) and tempered 1 hr at 200°C, some austenite will remain in this subsurface zone and finally transform upon cooling of the entire block to room temperature.

The volume expansion accompanying the transformation if it occurs at this time, upon cooling from tempering, will result in high surface tensile macrostresses. These may well cause the corners of the block to chip off, sometimes many hours after final cooling from the tempering furnace.

This difficulty could be avoided if thermal gradients were eliminated during original martensite formation or if the block were allowed to transform completely before tempering. However, marquenching (martempering) of such a large block of carbon tool steel could not be

accomplished because of the rapid cooling required past 550°C. If the normally quenched steel were allowed to stand around too long at room temperature to permit complete transformation before tempering, the surface would become too cold and might chip or crack from quenching stresses combined with transformation stresses. A successful com-

TABLE 12.3. EFFECT OF AUSTENITIZATION TREATMENT ON MARTENSITE REACTION IN OIL-HARDENING NONDEFORMING STEEL*

	Austenitization treatment			
	790°C, 1 hr	870°C, ¾ hr	980°C, ¾ hr	1095°C, ½ hr
γ grain size, ASTM	No. 9	No. 6	No. 5	No. 2
Undissolved carbides	Very many	Few	None	None
% martensite at 150°C	80	10	10	10
% martensite at 100°C	95	40	40	40
% martensite at 30°C	99	90	80	80

* Payson and Klein, *Trans. ASM*, **31**, 218, 1943.

TABLE 12.4. EFFECT OF AUSTENITIZATION TREATMENT ON MARTENSITE REACTION IN AIR-HARDENING HIGH-CARBON–HIGH-CHROMIUM STEEL*

	Austenitization Treatment			
	1010°C, 1 hr	1070°C, ½ hr	1110°C, ¼ hr	1150°C 5 min
γ grain size, ASTM	No. 11	No. 10	No. 9½	No. 9
% martensite at 95°C	95	20	Trace	0
% martensite at 30°C	100	85	30	Trace
Rockwell hardness as quenched	C65	C59	C47	C36

* Payson and Klein, *Trans. ASM*, **31**, 218, 1943.

promise is to quench as before to about 65°C and then, if a heavy mass is involved, hold at this temperature in a warm oil bath until the temperature is uniform.

For the oil-hardening steels of Figs. 12.3 and 12.4, slower cooling means less thermal gradients and more uniform transformations throughout cross sections. The 52100 grade is not strictly a tool steel, having been developed originally for ball bearings. It and the "nondeforming" steel are about 95% transformed to martensite by the time they reach 95°C, if austenitized at the normal temperature. The effect of higher

austenitizing temperatures on the martensite reaction of the 52100 ball-bearing steel is shown by Fig. 12.3*a*, and the comparable data for

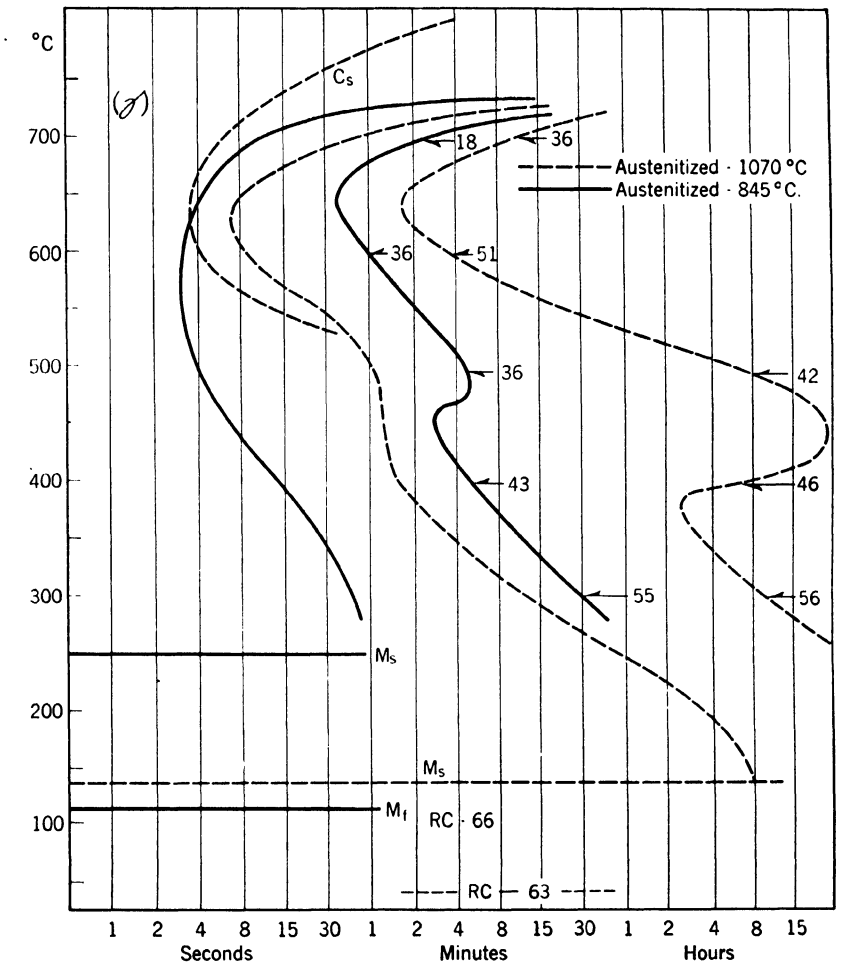

FIG. 12.3. Isothermal transformation diagram for steel AISI 52100 (1.02% C, 1.41% Cr) austenitized at the normal hardening temperature, 845°C (solid line) and at a temperature of 1070°C, sufficiently high to dissolve all carbides. The 845°C gave a very fine No. 9 grain size while the 1070°C treatment resulted in a No. 3 grain size. Rockwell hardness data are shown; the quenched RC 63 for the 1070°C treatment represents martensite plus soft retained austenite. (*Atlas of Isothermal Diagrams, U.S. Steel Corp.*)

the nondeforming steel are given in Table 12.3. As in the case of the plain carbon steel and as is predictable from material considered in

earlier chapters, higher austenitization temperatures result in more complete solution of hypereutectoid carbides, a corresponding austenitic grain growth, and a related depression of the M_s and M_f temperatures.

Finally, transformation diagrams of two typical air-hardening tool steels are reproduced in Figs. 12.5 and 12.6. Notable is the degree to which the "knee" of the reaction, corresponding to fine pearlite formation in carbon steels, is displaced upward and to the right, to about 780°C and 600 sec as compared to 550°C and less than 1 sec. In addition, there is a temperature interval of from about 600 to about 350°C, in which metastable austenite shows no indication of transform-

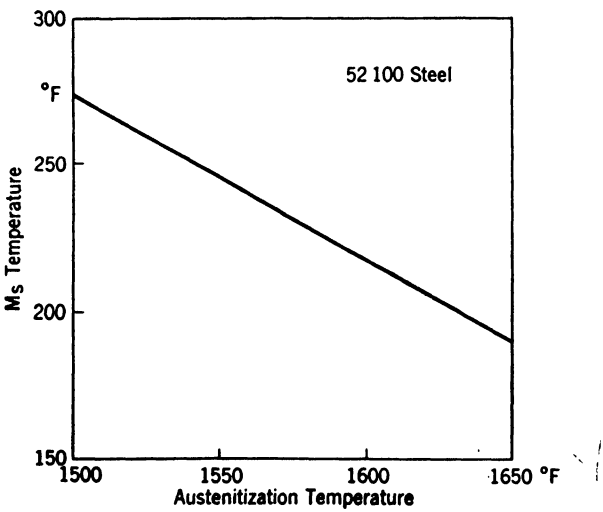

FIG. 12.3a. The M_s temperature for 52100 steel (1% C, 1¼% Cr) as a function of the austenitization temperature; increased carbon solution lowers the M_s temperature.

ing even when held a period of weeks! However, the carbide precipitation that may occur upon holding austenite at these temperatures (see C_s line in Fig. 12.6) will change the M_s and M_f temperatures and affect tool properties.

Transformation diagrams of this type permit a quenching process equivalent to martempering although much older in usage and known as *hot-quenching*. After austenitizing, the steel is quenched in a liquid salt bath at about 550 to 500°C, held until the temperature is uniform, and then quenched in oil. The chief advantage of doing this as contrasted with air cooling is economic. Moderate-sized sections of the steel will harden quite successfully upon air-cooling as is obvious from

the transformation diagram. However, if a heat-treating shop is processing a large number of parts in this way, a room of normal size is

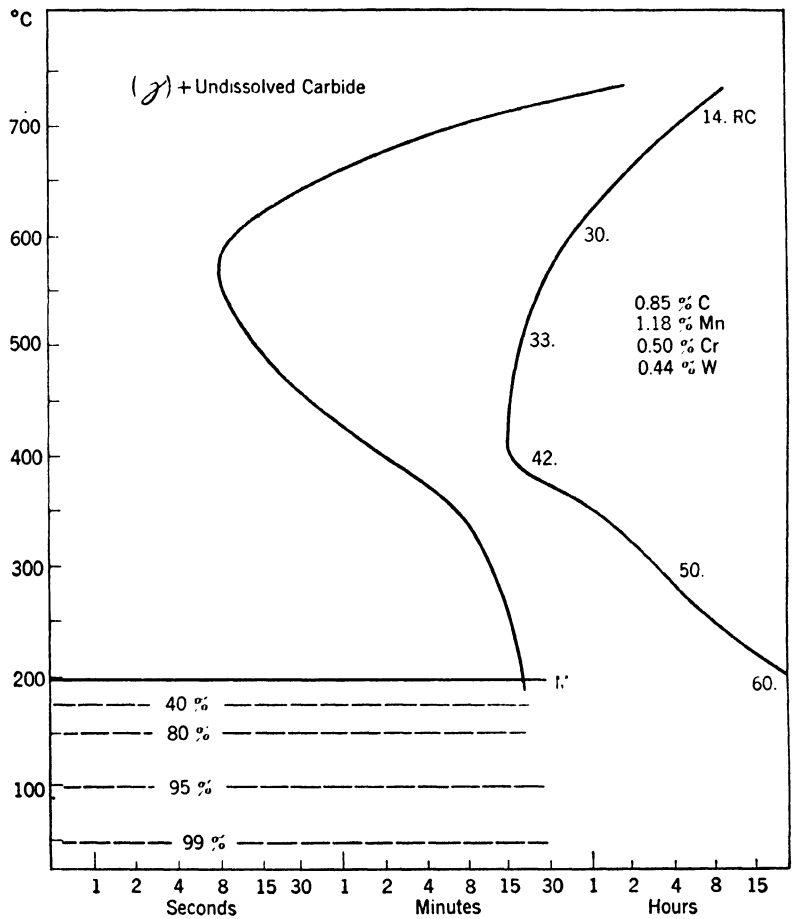

FIG. 12.4. Isothermal transformation diagram for an oil-hardening, nondeforming tool or die steel as austenitized at the usual hardening temperature of 790°C. Not all carbides would be dissolved in the austenite at this temperature.

soon filled up with hot steel and no further processing, *i.e.*, tempering, is possible until the parts are nearly at room temperature. On the other hand, an oil quench directly from the high austenitization temperature is certain to give more distortion and also result in severe thermal

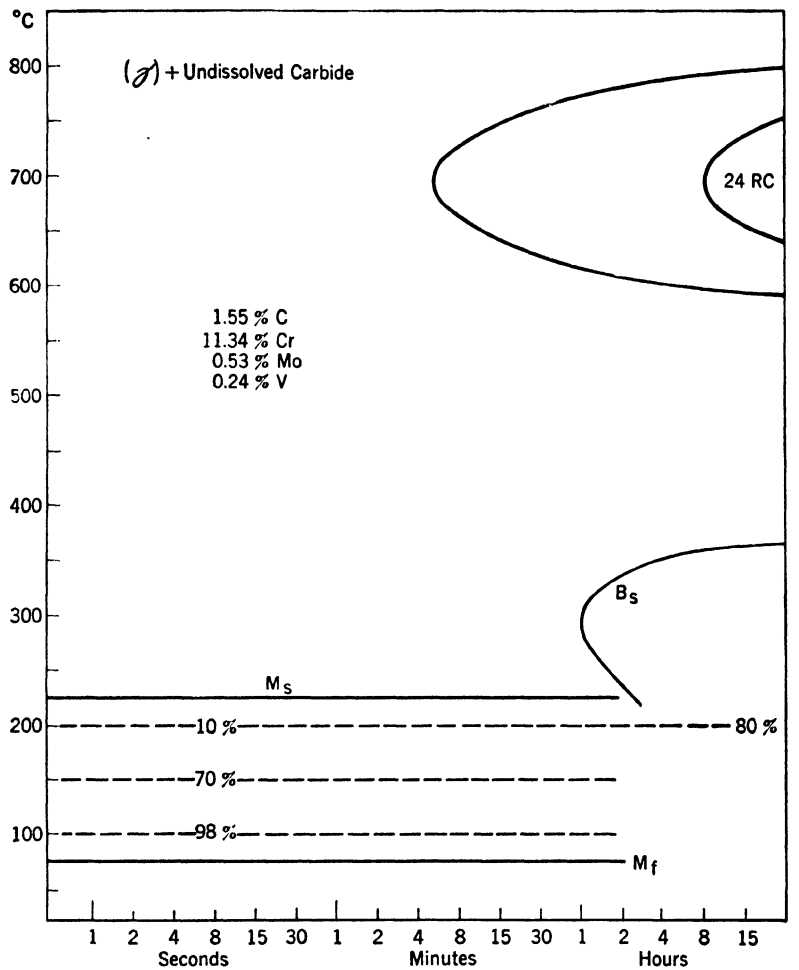

FIG. 12.5. Isothermal transformation diagram for high-carbon, high-chromium die steel as austenitized at the usual hardening temperature of 1000°C from an annealed (spheroidized) structure. In the martensitic formation range, long time holding will cause bainite to form as shown by the horizontal at 200°C (*e.g.*, 10% martensite, 70% bainite after 15 hr).

gradients with accompanying macrostresses and potential cracking. The hot quench is a successful compromise between the economic and the metallurgical difficulties.

The effect of increased austenitization temperature on the formation of martensite is shown in the case of the high-carbon–high-chromium steel

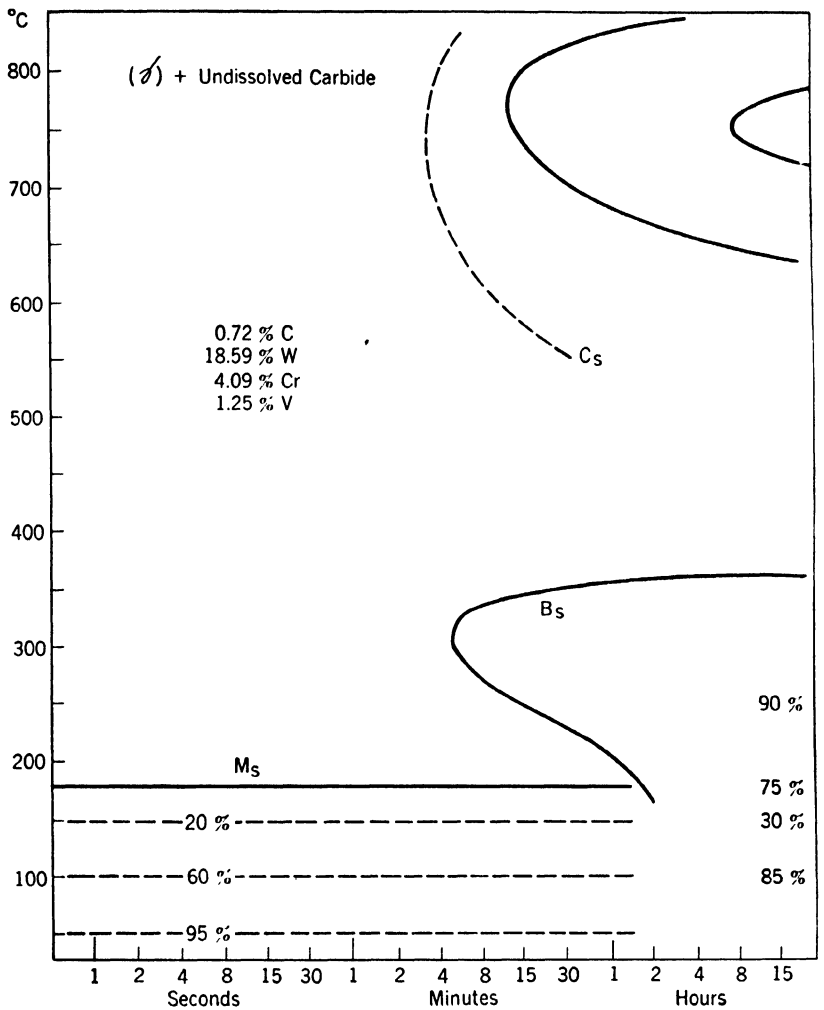

FIG. 12.6. Isothermal transformation diagram for 18-4-1 high-speed steel as austenitized at the usual hardening temperature of 1290°C from an annealed structure. In the martensitic formation range, long time holding permits bainite to form as indicated by the increased percentage transformation at long times (15 hr). The dashed C_s line indicates approximate start for carbide precipitation from supersaturated austenite prior to the eutectoid reaction.

by the data of Table 12.4. The pronounced drop in M_s and M_f temperatures upon overhardening is typical of the higher chromium content steels. The related large increase in the amount of retained austenite

upon cooling to room temperature is the obvious cause for the decrease in as-quenched hardness. If, immediately after quenching, such steels are cooled to well below room temperature, *e.g.*, −120°F, the austenite retained upon cooling to room temperature almost completely transforms to martensite. When returned to room temperature, the steel will be harder than before the subzero treatment and, if careful dimensional measurements are made, it will be found that the steel has "grown" or increased in volume. These effects, to be anticipated upon the trans-

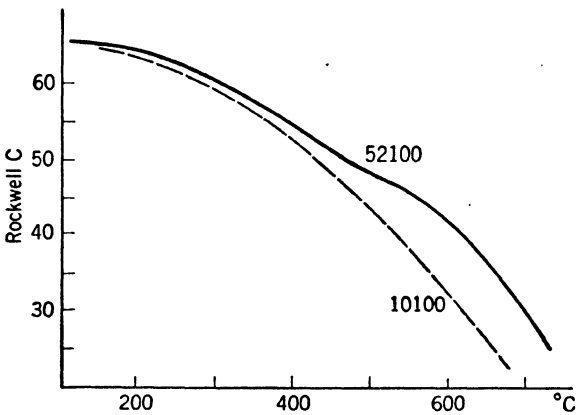

FIG. 12.7. Tempering data for a plain high-carbon steel, water-quenched from 790°C, and for 52100 (1% C and 1.2% Cr) after being quenched in oil from 845°C. Tempering time for both curves was 1 hr.

formation of austenite to martensite, would not be observed if the steel were underhardened with only a relatively small amount of carbide dissolved in austenite.

If these higher alloy steel tools warp or distort upon heat treatment and must be straightened, this plastic deformation should be performed while the steel is relatively soft, *i.e.*, partly austenitic. The transformation diagrams show that while the steel is still warm, immediately after quenching, a normally hardened high-speed steel may contain 30 or 40% austenite. This is the stage when slight deformation for straightening can best be performed.

12.4 Tempering of High-speed Steels

When high-alloy steels such as those of Group C are quenched and tempered, typical hardness vs. tempering temperature curves obtained are shown in Fig. 12.8 in comparison with tempering curves of plain

carbon tool steel and the 52100 chromium steel as given in Fig. 12.7. The sequential changes for the plain carbon steel have already been described—precipitation of carbide in martensite and change from tetragonal to cubic body-centered lattice, precipitation of carbide in retained austenite and conversion of austenite to martensite, growth of carbides in a globular form accompanied by softening. Microstresses associated with the transformation of retained austenite and the related localized expansions cause a decrease in torsional impact strength of plain

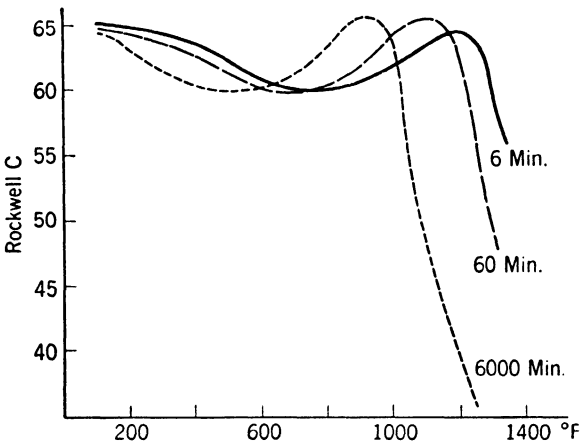

FIG. 12.8. Tempering curves of 18-4-1 high-speed steel, quenched in oil from the usual hardening temperature of 2350°F; curves for hardness after tempering 6, 60 and 6,000 min are reproduced. Almost identical tempering curves are obtained for the 6-5-4-2 high speed steel when oil-quenched from its usual hardening temperature of 2225°F. (*Roberts, Grobe and Moersh.*)

carbon tool steel at about 200°C, as shown by the data of Fig. 12.9. In properly hardened carbon steel or 52100 steel, there is insufficient retained austenite to cause any strong inflections in the hardness tempering curve. The slight inflection at 500°C and the subsequent slower softening of the 52100 steel are associated with formation of the stable carbide, $(FeCr)_3C$ since, for its formation and growth, chromium must substitutionally diffuse as well as the interstitial carbon.

Three tempering curves of a high-speed steel are shown in Fig. 12.10. Of the three curves the dashed line represents an underhardened steel, *i.e.*, austenitized at 2100°F. Its hardness is highest initially because, assuming that the steels were all cooled just to room temperature after hardening, this steel would have the least dissolved carbon and alloy in the austenite, therefore, the least amount of soft austenite in the structure before tempering. Conversely, the overhardened specimen, the

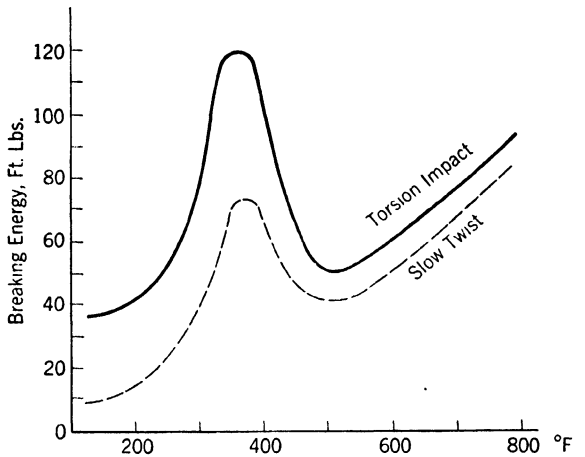

FIG. 12.9. Energy required to break tempered martensitic structures as a function of the tempering temperature. The 1.1% C tool steel was quenched in brine from 1450°F and tempered for 1 hr at the indicated temperatures. The breaking energy for the specimens given a slow twist was obtained by integrating the area under the torsional stress vs. torsional strain curve for each test specimen. The peak at about 375°F (190°C) presumably corresponds to stress-relief of martensite with no change of retained austenite; the low values at about 500°F result from the stresses generated by retained austenite transforming to martensite upon cooling from the tempering operation.

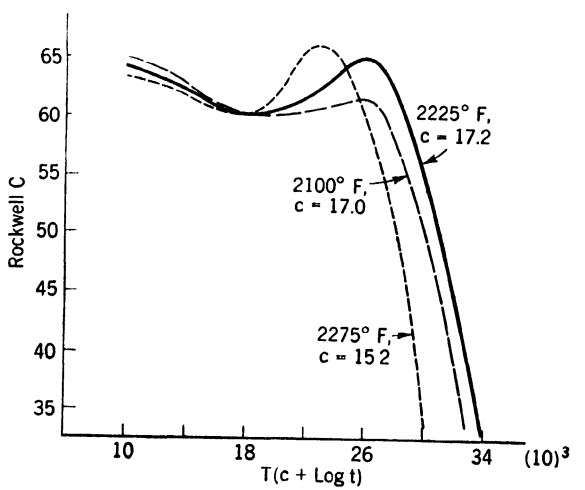

FIG. 12.10. Tempering curves for 6-5-4-2 high-speed steel austenitized at three different temperatures. Tempered hardness is plotted against the parameter $T(c + \log t)$ where T is the tempering temperature, t the tempering time and c a constant for a specific steel and austenitization treatment. (*Roberts, Grobe and Moersh.*)

dotted line representing austenitization at 2275°F, would have the most retained austenite and be softest after quenching. This steel would be even softer, initially, if it were tempered before being cooled to room temperature. If, for example, it were cooled only to 100°C, almost half the structure would be austenite and the hardness might be in the Rockwell C50–60 range.

Before tempering, these steels consist of varying proportions of undissolved highly alloyed carbide, an alloyed martensite, and an alloyed retained austenite. No tempering temperature will affect the alloy carbide that was not dissolved at the high temperature. The effect of tempering the martensite is best shown by the dashed line in Fig. 12.10 for the underhardened steel. As usual, the first tempering effect, here at temperatures up to about 450°C, is a precipitation of carbide and reversion of the tetragonal lattice to a cubic structure. However, in this temperature range, the large tungsten atom and perhaps the chromium and vanadium atoms are too sluggish to diffuse to form the alloy carbide. Instead, the simplest carbide forms, substantially Fe_3C, while microstresses are partly relieved and slight softening occurs. As the temperature is raised, increased activity of the alloying atoms permits the gradual disappearance of Fe_3C and the formation in its place of stable highly alloyed carbide. Correspondingly, the ferrite (tempered martensite) matrix is depleted of alloying elements. Beyond 550°C, the alloy carbides grow, and softening occurs fairly rapidly.

The retained austenite that is normally present in quantities of from 10 to 20% (unless the steel were underhardened or cooled to subzero temperatures) is metastable at all temperatures up to almost 600°C for the customary tempering times. From the isothermal transformation diagram, it is apparent that little will happen at the tempering temperature except for precipitation of some alloy carbides above about 500°C. This, however, makes the austenite less stable, *i.e.*, raises the M_s and M_f temperatures and thus permits the retained austenite to transform *when the steel is cooled from the tempering operation.* Thus, the increase in hardness of the normally hardened high-speed steel, and more pronouncedly of the overhardened steel, after tempering in the range 500 to 550°C, is caused by the formation of new martensite from retained austenite.

The formation of new martensite in a hard and moderately brittle tempered martensite, upon cooling from the tempering operation, results in high microstresses. If the steel is quenched from the tempering operation or high macrostresses are present from other sources (*e.g.*, sharp corners, sharp changes in section size, or an originally too drastic

quench), the steel may crack upon cooling from the first tempering operation. It is more likely to crack at this time than during the hardening quench because there is no soft cushion of retained austenite to deform and reduce the stress level. For these reasons, it is the practice of most shops to employ two tempering treatments. The second heating tempers the martensite formed from the first tempering and, more importantly, reduces the micro- and macrostresses in the tool and also the likelihood of brittle failure in service.

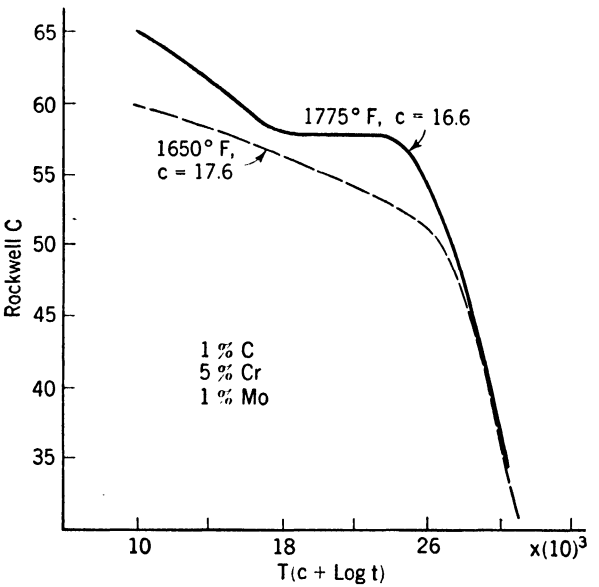

FIG. 12.11. Tempering curves for Cr:Mo die steel austenitized from two different temperatures. Tempered hardness is plotted against the parameter $T(c + \log t)$ where T is the tempering temperature, t is the tempering time and c a constant for a specific steel and austenitization treatment. (*Roberts, Grobe and Moersh.*)

The effect of time at tempering temperature has not been discussed, but it is obviously a significant variable inasmuch as diffusion is the primary requisite for carbide precipitation and growth. The graphs of Fig. 12.8 showed the effects of tempering time of an 18-4-1 high-speed steel. It is clear that the character of the tempering curve is unchanged, only the temperature of the secondary hardness peak is lowered or displaced to the left by longer tempering times. As in the case of medium-carbon steels, a single parameter has been found to express the two variables of tempering time and temperature.[1] This parameter, of the form,

[1] Roberts, Grobe, and Moersh, *Trans. ASM*, **39**, 521, 1947.

$$T(c + \log t)$$

where T = temperature
t = time
c = a constant whose value depends on the composition of the austenite

was used as the abscissa in the tempering curves of Fig. 12.10 and is also employed to describe the tempering of two Cr:Mo die steels in Figs. 12.11 and 12.12. The graphs for the air-hardening Cr:Mo die steel of

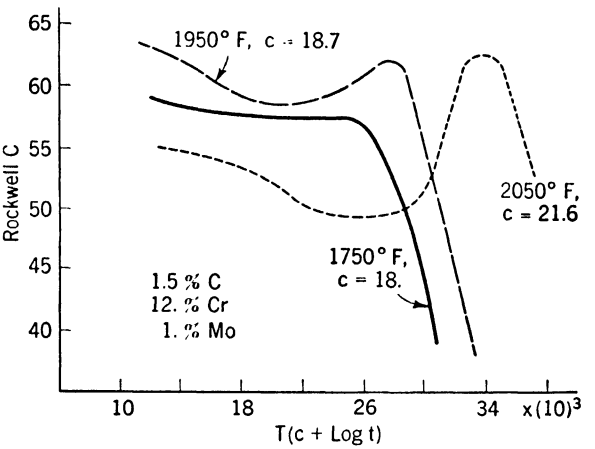

FIG. 12.12. Tempering curves for an air-hardening die steel austenitized at three different temperatures as indicated on each curve. Tempered hardness is plotted against the parameter $T(c + \log t)$ where T is the tempering temperature, t is the tempering time and c is a constant for each curve whose value depends on the austenitization temperature. Hardening from the lowest temperature results in no secondary hardening; hardening from the highest temperature results in low initial hardness because of retained austenite and then a related pronounced secondary hardening. (*Roberts, Grobe and Moersh.*)

Fig. 12.12 show in a particularly noteworthy way the effect of austenitization temperature. The 1750°F (950°C) treatment gives a quenched hardness of C64 since, with more carbides dissolved, the martensite is harder although some retained austenite is now encountered as is shown by the secondary hardening upon tempering. The 2050°F (1125°C) austenitization gives a low-quenched hardness of only C55 because too many carbides have dissolved, resulting in a very large amount of retained austenite. On tempering, a pronounced peak results from transformation of retained austenite upon cooling from tempering. The displacement of the peak to the right is somewhat misleading in this graph since the *temperature* of maximum secondary hardening does not increase

noticeably; the high austenitization temperature changes the constant c used in plotting abscissa values.

The use of the parameter for abscissa is this: Suppose the hardness desired shows a $T(c + \log t)$ value of 30,000. A convenient time could be chosen and the corresponding required temperature immediately calculated if the constant c is known. Thus, data of this sort enable the heat treater to choose convenient times, overnight or otherwise, and calculate the exact temperature required to achieve the desired hardness.

12.5 Surface Effects upon Hardening Tool Steels

The working parts of a tool are the edges or the surfaces. It is readily possible unintentionally to carburize or decarburize this part of the tool during heat treatment. Annealed stock usually will have a surface decarburized during hot-working and annealing treatments at the steel mill. This is not objectionable in most cases since machining of the tool will expose a fresh, representative surface. Decarburization during the hardening heat treatment will, however, require grinding of the surface to remove the soft, low-carbon surface layer. Grinding of a hardened tool requires leaving enough stock on the tool before hardening to permit meeting specified dimensions. Furthermore grinding is expensive and in some cases, *e.g.*, hack-saw blades, impracticable. Finally, grinding of a martensitic structure, if not performed with care, may cause the formation of cracks. Local overheating and local expansions followed by contractions, all within a hard and brittle structure, result in cracks. Whenever cracks are observed on a tool at right angles to the direction of grinding, it is fairly certain that they originated in grinding not in the heat treatment.

Schlegel[1] has shown that heating 18:4:1 high-speed steel at the usual austenitizing temperatures for short times in most gaseous atmospheres results in surface carburization followed by decarburization over longer periods (Fig. 12.13). This is true whether the atmosphere is oxidizing, *i.e.*, contains oxygen from excess air in the combustion mixture, is neutral (gas completely burned to CO_2 and H_2O with no O_2 or CO), or is reducing (contains some CO and H_2). Actually, equilibrium at 1290°C in the reaction $C + CO_2 \rightarrow 2CO$ is far to the right; *i.e.*, CO_2 will burn carbon and also oxidize iron. How then can carburization occur in oxidizing or "neutral" atmospheres?

Presumably CO_2, H_2O, or O_2 present in the gas oxidizes iron very rapidly at 1290°C. As oxygen atoms can diffuse through the thin oxide

[1] Schlegel, *Trans. ASM*, **29**, 541, 1941.

scale more quickly than carbon atoms, carbides are less rapidly oxidized. Rapid oxidation of the metal surface raises the temperature locally and permits solution in austenite of carbides that were in the scale. Thus the austenite adjacent to the scale may briefly contain up to 1.0% C although the steel contains only 0.7% C.

Oxygen diffusion through the scale, required for continued scaling, decreases in rate very rapidly with thickening of the scale. However,

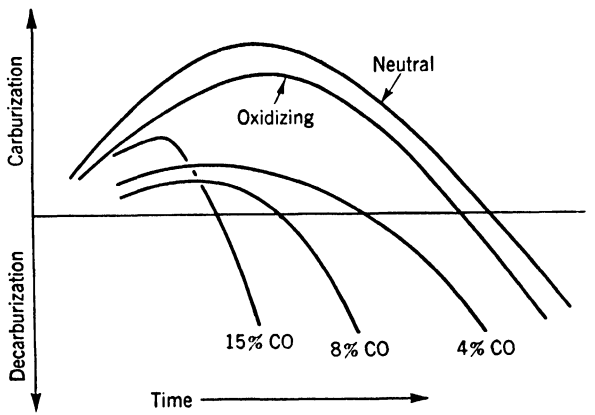

FIG. 12.13. Surface carbon effects on high-speed steel of different atmospheres with increasing time at the austenitizing temperature. The "neutral" atmosphere would be completely burnt gas with no excess oxygen. The oxidizing atmosphere would be gas burnt with an excess of air. The varying percentages of carbon monoxide would be atmospheres of gas burnt with insufficient air. Therefore, all atmospheres for this schematic graph contain CO_2 and H_2O as well as CO or oxygen. (*Schlegel.*)

carbon can diffuse interstitially, and its rate is less affected by scale thickness. Therefore, increased time and thicker scales permit carbon to diffuse to the surface and oxidize at a rate faster than scaling of the iron. The result is decarburization.

Decarburization produces a soft surface layer on the hardened steel, often best detected by a file test after tempering. Carburization at the high heat may also cause the surface to be file-soft by reason of the large amount of retained austenite that would be found there.

Steels of the high-speed type are usually preheated at from 700 to 850°C and held there to attain a uniform temperature and thereby reduce the time of exposure to the high heat. Although surface oxidation or scaling during the preheat may cause slight decarburization, severe decarburization can occur only at the high temperature. Although no data have been published showing decarburization during

the tempering operation at about 550°C, it apparently can also occur at this relatively low temperature.

Protection from surface chemical changes is most necessary at the high hardening temperature. It may be readily achieved by packing the steel part in cast-iron chips, but this slows up the heating and prevents close control of the time at the high temperature since it is difficult to determine when the steel reaches the proper temperature. Protection is also achieved by using a carbon block to hold the steel. Above 1000°C, the atmosphere within a carbon block is nearly 66% N_2 + 34% CO, and scaling and decarburization will not occur *if there is no oxide scale that was formed during the preheat.*

Suitable liquid baths adequately prevent surface changes if the bath is properly protected from dissolved oxygen. At high temperatures, this may be achieved by a surface covering of silicon carbide or by comparable conditioners.

Extremely hard cutting edges may be obtained by nitriding the hardened high-speed steel in ammonia or in a liquid cyanide bath. The basis for these treatments was discussed earlier.

12.6 Cast vs. Forged Tool Steels

The higher carbon content of tool steels, the effect of accompanying alloying elements on the phase diagram (*e.g.*, Fig. 12.1), and the metastable coring that occurs during freezing are factors that cause the presence of *eutectic* structures in high-alloy tool steels upon solidification from the liquid state. From concepts that were introduced in Chap. 5, it is evident that more rapid solidification results in smaller primary austenite dendrites and a finer austenite-carbide eutectic. The diagram of Fig. 12.1 indicates that the eutectic contains a relatively high proportion of the brittle carbide phase. Therefore, the carbide phase will be continuous in the eutectic and, since the eutectic is inevitably continuous in the total structure, the as-cast structure of steels such as high-speed steel is brittle.

It is not practical, or even possible in some cases, to dissolve all carbides in austenite; therefore, forging is the only practical means of breaking up the brittle carbide network of these steels. At proper hot-working temperatures, deformation causes fractures of undissolved, brittle eutectiferous carbide. The plastic austenite flows around the carbide fragments and pressure-welds as it flows into the carbide cracks. If the deformation is solely an extension in one direction, as in hot-rolling, the continuity of the carbide network is destroyed, but the cellular pattern of coarser eutectic particles merely becomes strung out in the direction of metal flow. The cast pattern is still evident as elongated

cells, and there is some evidence that, as might be expected, this structure is not so tough as a random distribution of the carbides. It is not possible to achieve a *completely* random dispersion, but it can be approached by repeatedly hammer forging so as to cause flow first in one direction and then at right angles, or even in the reverse direction.

The more rapid the solidification, the finer will be the eutectic network carbide structure. Rapid freezing is encouraged by casting of smaller sections or ingots. However, the smaller the ingot, the less the forging that can be done before reducing the section size to final dimensions, *e.g.*, 1-in. rod. Thus tool steel ingots in size are necessarily a compromise between a small size to ensure rapid freezing and a large size to permit extensive forging.

In some cases, the steel may be cast in a mold shaped to give the finished tool, *e.g.*, a milling cutter. If a low-carbon-content surface is avoided or removed by machining, such tools, although very brittle, may have extremely good cutting characteristics after proper heat treatment. Since it is apparent that cast high-speed-steel tools must have low shock resistance, their utility will depend considerably on the cutting service conditions.

12.7 Microstructures

Annealed tool steels are almost always supplied by the producer with spheroidized carbide structures. This structure is softer and, at high-carbon contents, enables the steel to be more readily machined to the desired shape. Quenched and drawn structures are easily polished with proper abrasives because the surface is not very susceptible to localized flow and distortion.

Etching of martensitic high-speed-steel structures is usually quite slow, probably because of the alloying elements present. It is sometimes questionable whether white areas in such steels are ferritic decarburized zones or austenitic areas retained as such because of high carbon content. However, a few black (tempered) martensitic needles intruding into a white area are fairly clear evidence of retained austenite. Subzero cooling followed by retempering will conclusively differentiate between ferrite and retained austenite.

The high-temperature austenitic grain size is always important as an indicator of proper or improper heat treatment. The size of the martensitic needles is an indicator of austenitic grain size, and the amount of undissolved carbides in a hypereutectoid steel also suggests whether or not excessive austenitizing temperatures were used.

Steels of the high-speed type before tempering may be etched with Nital to reveal the austenitic grain size. After tempering, martensitic

needle size will be suggestive, but for quantitative grain-size measurements, a special etch such as the Snyder reagent (3% HCl and 7% HNO_3 in alcohol) can be used to bring out the austenitic grain size.

Structures reproduced in this chapter fall into the following groups:

Micro. 12.1—Annealed carbon tool steel; carbide "bead" envelopes.

Micros. 12.2 and 12.3—Steel 52100; properly and improperly heat-treated.

Micros. 12.4 to 12.9—W:Cr steel, which responds to heat treatment like a high-speed steel; cast vs. forged structures.

Micros. 12.10 to 12.16—High-speed steel of the 6% W, 5% Mo type; as-hardened, hardened, and tempered, "burnt," carbide network structures.

Micros. 12.17 to 12.19—Carburized and nitrided structures.

Micros. 12.20 and 12.21—Graph-Mo tool steel, annealed structure; "bull's-eye" structure.

Micros. 12.22 to 12.31—Isothermal transformation of the W:Cr steel, which resembles high-speed steels in its response to heat treatment.

Micros. 12.32 to 12.33—Structural effect of subzero cooling of the W:Cr steel.

Micro. 12.34—Structural effect of electric stencil marking of a martensitic (W:Cr) steel.

12.8 Subzero Treatments of Tool Steels

Tool steels having high-carbon contents, and frequently high-alloy contents as well, are likely to have retained austenite in the structure after cooling from the hardening heat treatment. A higher-than-normal austenitization temperature or failure to cool the steel sufficiently (*i.e.*, to the vicinity of room temperature) is conducive to abnormally large quantities of retained austenite for, by now, obvious reasons. This results in a greater secondary hardness for high-speed steels, a greater change of dimensions upon tempering, more chances of cracking upon cooling from tempering, and a more brittle structure.

Three means for minimizing retained austenite are available: (1) under hardening, *i.e.*, a low austenitization temperature, (2) cooling the steel to such a low temperature, *e.g.*, −80°C, that the M_f line is passed, or (3) double or triple tempering. The significance of underhardening has already been covered; it may be particularly undesirable in high-speed steels since it means less secondary hardness.[1]

[1] Slight underhardening of high-speed steel is regular practice for tools subjected to shock and mistreatment. Here the slightly less secondary hardness is less important than a corresponding greater toughness.

(*Continued on page* 396)

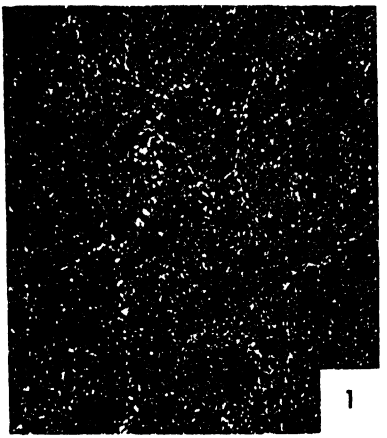

Micro. 12.1. Carbon tool steel (1.20% C); ×500; Nital etch. This structure of the raw stock, before hardening, shows finely spheroidized carbides in a ferritic matrix although details are not too evident at this relatively low magnification. However, traces of the former austenitic grain boundaries are visible by reason of a greater carbide concentration at these areas. This structure must have originated as follows: The steel was normalized (from above the A_{cm} line) and then reheated below the critical temperature for spheroidization of the fine, lamellar carbides. Probably cooling from the austenitic field through the critical temperature was too slow to prevent the separation of excess carbide in the form of envelopes around the austenitic grains. The subsequent spheroidization treatment broke up the continuity of the carbide envelopes but left a "string of beads" of carbide in a network form. This structure is not eliminated by hardening from the usual temperature between the A_{c_1} and A_{cm} lines; the coarser carbides, aligned as grain-boundary envelopes, are not dissolved, and their residual presence in a network results in a more brittle tool, subject to chipping at the cutting edge or other difficulties that are summarized in the words "poor tool performance."

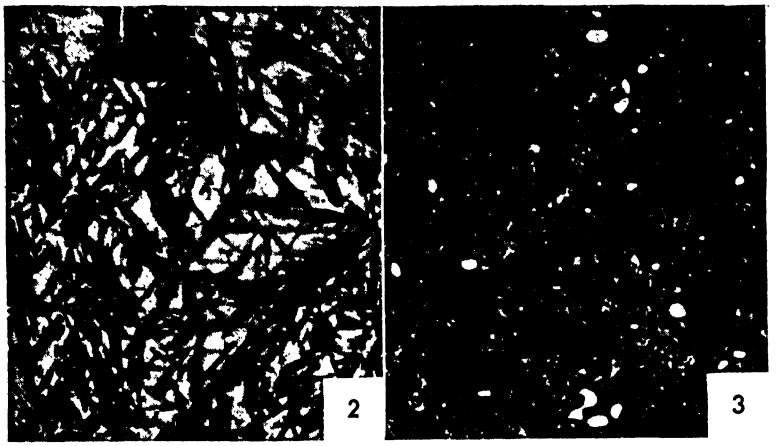

Micro. 12.2. Overhardened SAE 52100 steel (1.25% Cr, 1.00% C); ×1,000; Nital etch. This steel, originally developed for ball bearings, is now widely used where high hardness and good depth of hardening are essential. The structure shown was from a defective part in an aircraft-engine clutch. This section showed brittle chipping of corners that had been designed with rounded edges to avoid such trouble. The brittleness is undoubtedly related to the extremely coarse martensite that must have been derived from very coarse austenite. The steel had been heated in a salt bath, and it is hypothesized that the salt bath was used shortly after hardening some high-speed steel and that insufficient time was allowed for cooling of the bath from the high-speed temperature (about 2300°F) to the proper temperature for this steel (about 1550°F). This structure shows no residual carbides although it is strongly hypereutectoid (1.25% Cr lowers the eutectoid carbon content to about 0.70%), and it is believed the part was heated above 1800°F.

Micro. 12.3. Properly hardened SAE 52100 steel; ×1,000; Nital etch. This structure is of the same steel when the original stock was quenched in oil from 1550°F and drawn to the same hardness as above, Rockwell C62. The background is extremely fine black martensite (it might be called *troostite* except for the high hardness), which would be much tougher than the overheated coarse martensite. In addition, the presence of residual, undissolved carbides (the white spheroids) considerably increases resistance to abrasion.

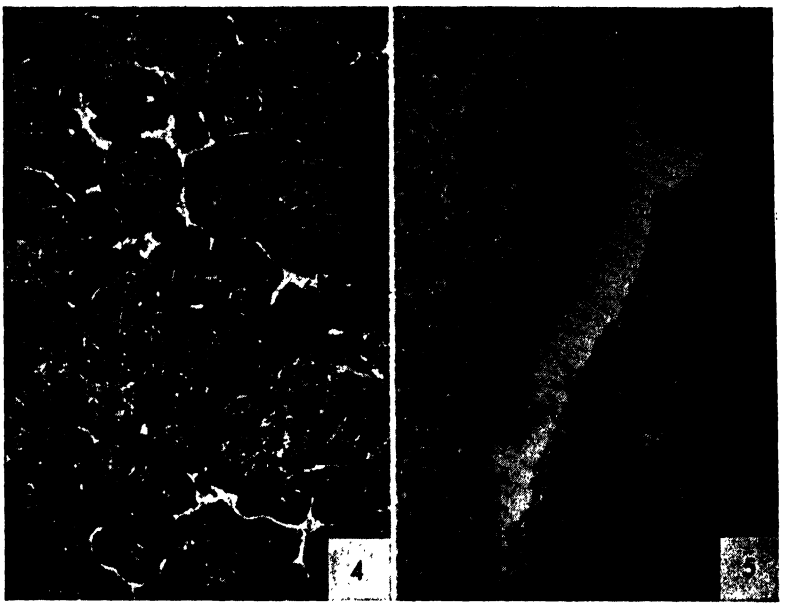

Micro. 12.4. 0.5% C, 7% W, 7% Cr steel; section 1 in. thick, as-cast and then annealed (12 hr at 1,000°C, furnace-cooled); ×100; Nital etch. This cast structure has a typical dendritic pattern evident even after annealing. Heavy interdendritic carbides of eutectiferous origin are white. Former austenitic dendrites now consist of alloyed ferrite and carbide with a few needles of pro-eutectoid carbide visible. (With 0.5% C, this alloy steel is hypereutectoid.)

Micro. 12.5. Same as Micro. 12.4 but at ×1,000. Details of the massive eute*ctic* carbide and the finely dispersed spheroidized eute*ctoid* carbide are evident at this higher magnification.

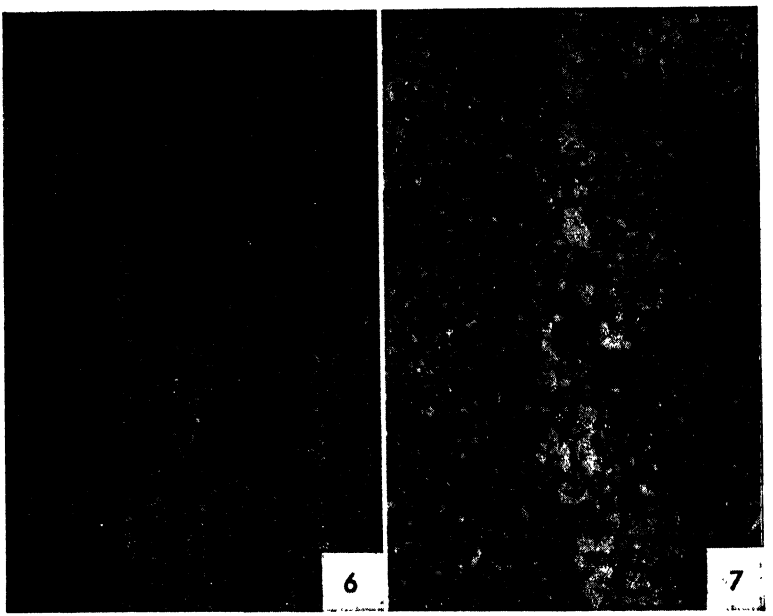

Micro. 12.6. 0.5% C, 7% W, 7% Cr steel; section hot-rolled from ingot to billet, hot-forged from billet to ring shape, and then annealed (12 hr at 1000°C, furnace-cooled); ×100; Nital etch. The faint horizontal lines represent coarser carbides of eutectic origin, which, after being broken up by hot-working, are now aligned in what was the flow direction.

Micro. 12.7. Same as Micro. 12.6 but at ×1,000. The difference in particle size of coarser carbides here as compared to their original size is evident by a comparison of this structure with Micro. 12.5. The alignment here is too marked to represent the most desirable structure but is not generally considered detrimental unless the stress direction is perpendicular to the carbide stringers.

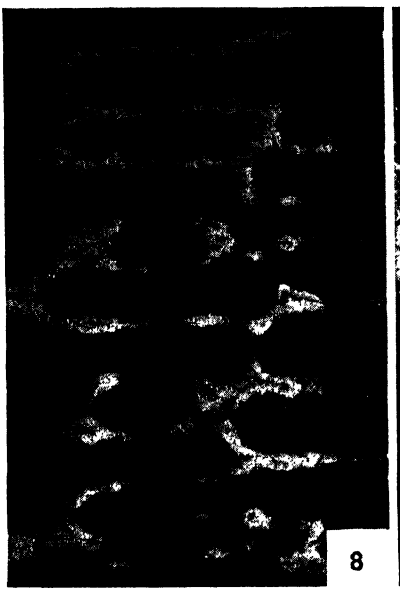

Micro. 12.8. The cast W:Cr steel of Micro. 12.4 after hardening and double tempering (1150°C, oil quench, tempered twice at 550°C) to a Rockwell C62 hardness; ×100; Nital etch. The black dendritic structure represents tempered martensitic needles, formed in austenitic dendrites that were lower in carbon content than the interdendritic zones. The white interdendritic zones contain some undissolved eutectiform carbides (slightly different in color from the retained austenite surrounding them). The higher carbon content of the interdendritic zone is responsible for the retained austenite.

Micro. 12.9. The forged W:Cr steel of Micro. 12.6 after hardening and double tempering (as in Micro. 12.8); ×100; Nital etch. The carbide stringers of the forged structure result in a higher carbon content of adjacent austenite upon heating to 1150°C. This results in austenite retained to some degree even after double tempering. In the wrought structure, however, the white areas are discontinuous "lenses" or short bands rather than continuous interdendritic zones.

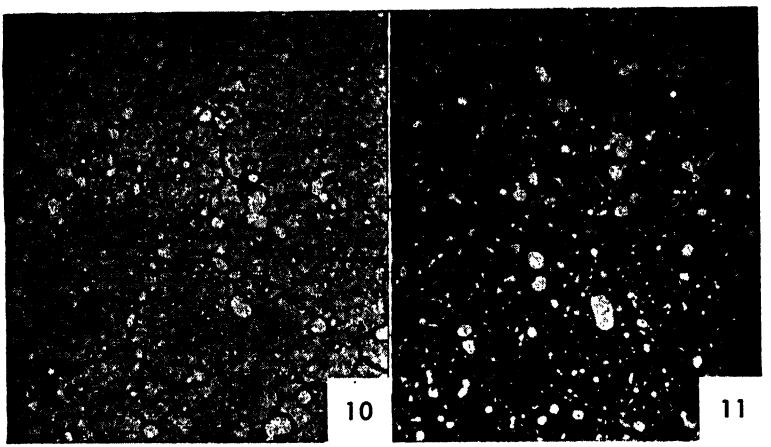

Micro. 12.10. Fine-grained high-speed steel (Type 6:5:4:1), quenched from 2250°F; ×1,000; Nital etch; C66. After quenching from this hardening temperature, slightly below the normal value of 2275°F, many residual, undissolved alloy carbides of (Fe, W, Mo, Cr, V)$_6$C are present in the structure, and the austenite grain size is considerably smaller than for the specimen shown in Micro. 12.12. Although this structure is predominantly martensitic, the needlelike or acicular characteristic is not noticeable.

Micro. 12.11. The fine-grained high-speed steel (Micro. 12.10) after tempering 2 hr at 1050°F; ×1,000; Nital etch; C64. The precipitation of alloy carbides and decomposition of residual austenite result in this structure etching more rapidly than Micro. 12.10 and to a black aggregate in which the martensitic needles are too small to be evident. The white spheroids are the residual, undissolved alloy carbides, unaffected by the tempering treatment. Since a Nital etch of a tempered high-speed steel will not reveal the size of the former austenitic grains, a special etch (Snyder's reagent, 7% HCl and 3% HNO_3 in alcohol) may be used to show the former austenitic grain boundaries and yield evidence as to the actual temperature attained in hardening a specific part.

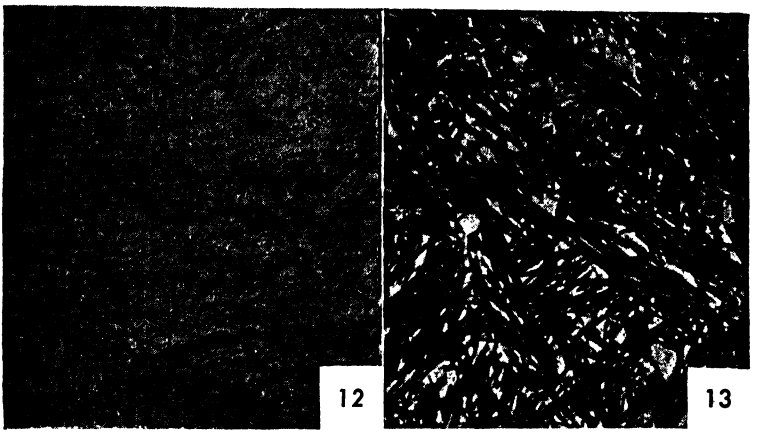

Micro. 12.12. Coarse-grained high-speed steel (Type 6:5:4:1), as-quenched from 2325°F; ×1,000; Nital etch; C61. There are only a few undissolved alloy carbides in this martensitic-austenitic structure. Some traces of eutectic melting are visible at the austenitic grain boundaries although the burning is not very pronounced and would not be detectable in the tempered structure (Micro. 12.13). Quenched from a higher temperature than the specimen of Micro. 12.10, and thus with more carbon in solution in the austenite, this specimen has more retained austenite and is, therefore, softer.

Micro. 12.13. The coarse-grained high-speed steel after tempering 2 hr at 1050°F; ×1,000; Nital etch; C66. Martensite needles forming in a coarse-grained austenite are always more readily resolved than the needles in a fine-grained structure. Although more evident and preferable for demonstrating the nature of martensite, they are decidedly not preferable for most uses. This structure is evidence that the tool was *overhardened, i.e.*, heated at the upper limit of the permissible range. It would have better cutting properties than Micro. 12.11, if the greater brittleness of this structure did not cause chipping or crumbling of the cutting edge or if the tool did not snap under an impact load. The special etch (Snyder's reagent) would reveal the grain size of this structure better than it would that of a fine-grained aggregate and would also reveal the incipient melting.

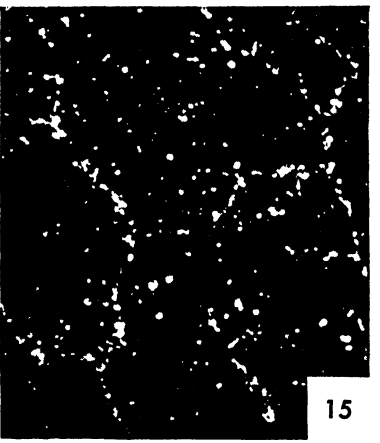

Micro. 12.14. Overheated or burned high-speed steel (Type Mo-Max) quenched from 2350°F and tempered at 1050°F; ×1,000; Nital etch; C65. When high-speed steel is heated above its eutectic temperature, the liquid phase that forms at grain boundaries is of nearly eutectiferous composition and upon quenching, solidifies as a brittle eutectic in which the carbide is the continuous phase. This structure, formed by quenching, is naturally much finer than, and readily distinguished from, the eutectic present in the cast alloy or in inadequately hot-worked metal. As in all cases of *burning*, the eutectic is predominantly located at grain boundaries, particularly at the junction of three grains, although some spherical liquid pools, formed within the grains, now show a *rosette* eutectic structure. Note the coarse austenitic grain size (now, largely coarse martensite). The brittle eutectic network makes the entire structure brittle, and the metal is ruined as a tool. It cannot be readily reclaimed and is ordinarily useful only as scrap for remelting.

Micro. 12.15. Properly hardened (2275°F) and tempered (1050°F) high-speed steel (Type 6:5:4:1); ×1,000; Nital etch; C64. This structure shows an undesirable distribution of the coarse carbides, present originally in the form of a eutectic network that surrounded the austenitic grains during solidification. Since these carbides cannot be completely dissolved in the solid alloy, hot-working (forging and upsetting) must be relied upon to break up this distribution and, in this specimen, the hot-working apparently was insufficient. In some very inadequately hot-worked (or cast) structures, these carbides may be seen in the form of a coarse eutectic. This is a transverse section of a broach made from a 2-in. diameter bar.

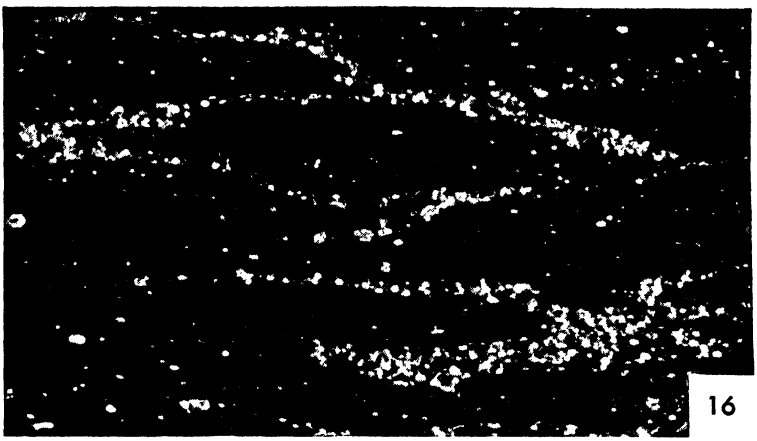

Micro. 12.16. A longitudinal micrograph of the same specimen as Micro. 12.15; ×1,000; Nital etch. The transverse section of the tool showed an equiaxed grain boundary distribution of undissolved carbides. This is a view of the same tool but with the polished section parallel to the long axis of the broach (longitudinal). The carbide distribution is, of course, an indication of the direction of hot-working, and here the envelopes, instead of indicating an equiaxed structure, show characteristically elongated grains. The structure is frequently termed *hooked* carbides.

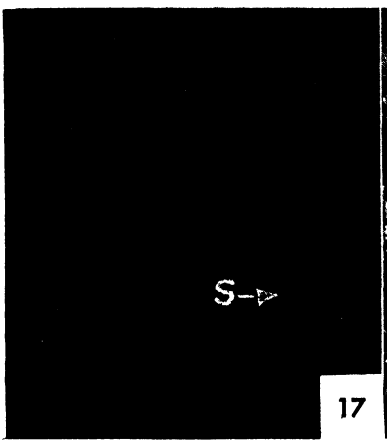

17

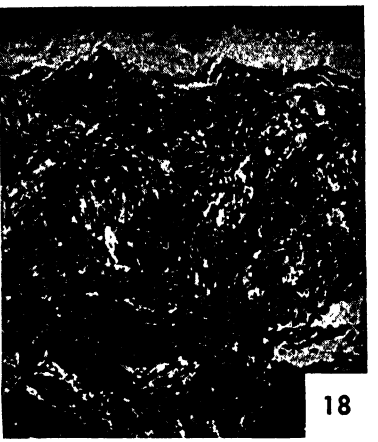

18

Micro. 12.17. Carburized free-machining steel, SAE-X1315 (0.15% C, 1.5% Mn, 0.128% S); the case after hardening and tempering; ×500; Nital etch; C60. This low-C, high-Mn, free-cutting steel after carburizing, quenching, and drawing shows a typical tempered martensitic structure in the case, together with some Mn sulfide inclusions (*S*).

Micro. 12.18. Case of nitrided steel (0.24% C, 0.55% Mn, 1.20% Al, 1.10% Cr, 0.25% Mo, 3.50% Ni) after normal ammonia treatment of 48 hr at 975°F; ×200; Nital etch. This represents a good nitrided case with an extremely high degree of hardness. The immediate surface shows a characteristic white layer of somewhat less hardness than the nitrided zone immediately below it. It is believed that the atomic nitrogen that diffuses into the metal during the ammonia treatment, forms an aluminum nitride with a high degree of dispersion (aluminum is always present in amounts of about 1% in steel that is to be nitrided). This particular grade of steel for nitriding has age-hardening characteristics that seem to be associated with the combination of nickel and aluminum. Not only does the long nitriding treatment at 975°F increase the hardness of the surface to an extent comparable with other grades but, simultaneously, precipitation of a phase (of unknown character) occurs in the body of the metal not reached by nitrogen. This results in an increase of mechanical strength and hardness of the core that accompanies the surface hardening (*e.g.*, tensile strength of 130,000 psi increased to 190,000 psi Brinell hardness from 275 to 415).

Micro. 12.19. Nitrided case of same grade of steel as Micro. 12.18 but on an originally severely decarburized surface; ×200; Nital etch. A decarburized steel, slowly cooled from above the A_1 temperature, usually shows columnar grains of ferrite extending until they encounter the normal pearlitic structure. This does not mean that decarburization removes all the carbon to a certain depth at which it suddenly increases to the normal value, but, when a structure with a carbon gradient cools slowly, ferrite forms first at the point in the structure that has the highest A_3 point (compare with banding, page 329) and continues to grow, forcing carbon away from the austenite-ferrite interface, until the entire structure transforms. When the decarburized, columnar ferrite grains are subsequently nitrided, *growth* of the structure causes a strong outward force to develop. If the structure is weak, as in this case, the net result may be *spalling* of the case. Note how spalling (or cracking of the case) follows the grain boundaries at the decarburization interface. The very large ferrite grains permitted very coarse nitride needles to form during cooling from the treatment.

Micro. 12.20. Graph-Mo tool steel, annealed state; ×800; Nital etch. The structure of this tool steel shows spheroidized carbides indicative of about 1.0% carbon in the combined state, as $(FeMo)_3C$. Temper graphite nodules are also present, randomly distributed in the ferritic matrix, and these bring the total carbon content to the vicinity of 1.5%. The molybdenum is present in relatively small quantities, 0.4 to 0.6%, and serves chiefly, with the silicon, to control the graphitization tendencies (see pearlitic malleable, page 457). Quenched from 790°C (1450°F), this steel would show a structure of martensite containing some undissolved carbides and also the graphite nodules.

Micro. 12.21. Graph-Mo tool steel heated to 1000°C and furnace-cooled with a rate of 1°C per min from 820 to 550°C; ×1,000; Nital etch. At 1000°C, all spheroidal carbides were in solution in austenite and probably some of graphite as well. Upon slow cooling past the A_{cm} line, extra carbon precipitated from the austenite *on the graphite nodules*, not at austenitic grain boundaries. On further slow cooling past the A_1 temperature, the eutectoid reaction occurred in the normal manner, *i.e.*, to pearlite, at points away from the graphite nodules. In their vicinity, preferred nucleation caused the stable eutectoid, $\gamma \rightarrow \alpha$ + graphite with the eutectoidal graphite depositing on the graphite nodules, again because of their powerful preferred nucleation effect. This results in the clear ferrite islands around each graphite nodule, a structure that in the analogous pearlitic malleable cast iron (page 457) is called a *bull's-eye* structure.

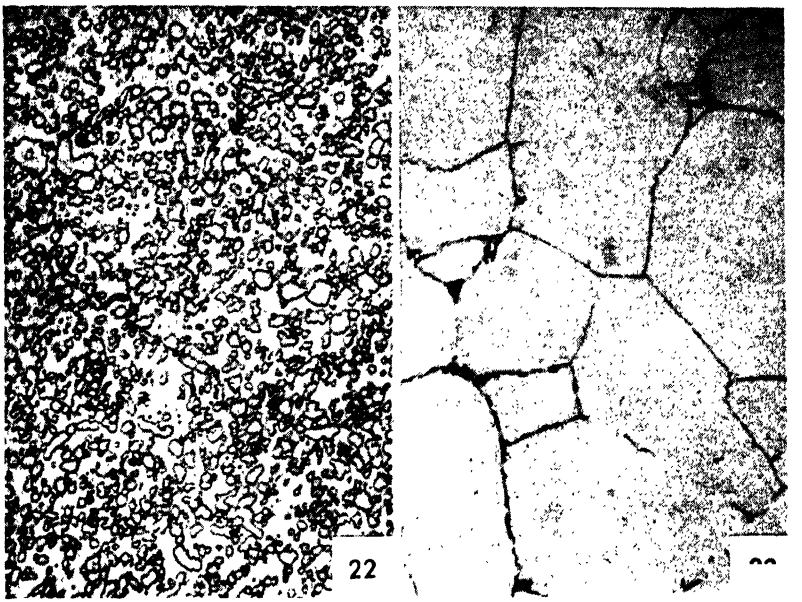

Micro. 12.22. 0.5% C, 7% W, 7% Cr steel; forged and annealed structure; ×1,000; Nital etch. The standard spheroidite, alloyed carbide in alloyed ferrite, structure typical of properly annealed tool steels.

Micro. 12.23. W: Cr steel austenitized 10 min at 1150°C, quenched to 790°C, held there 30 min, and quenched; ×1,000; Nital etch. Most of the spheroidal carbides of Micro. 12.22 have dissolved in the austenite although a few remain after the 1150°C treatment. Some carbides have precipitated from austenite at the grain boundaries during the isothermal 790°C treatment, and these cause the austenitic grain boundaries to be clearly evident. At a few grain-boundary points, the eutectoid transformation has started.

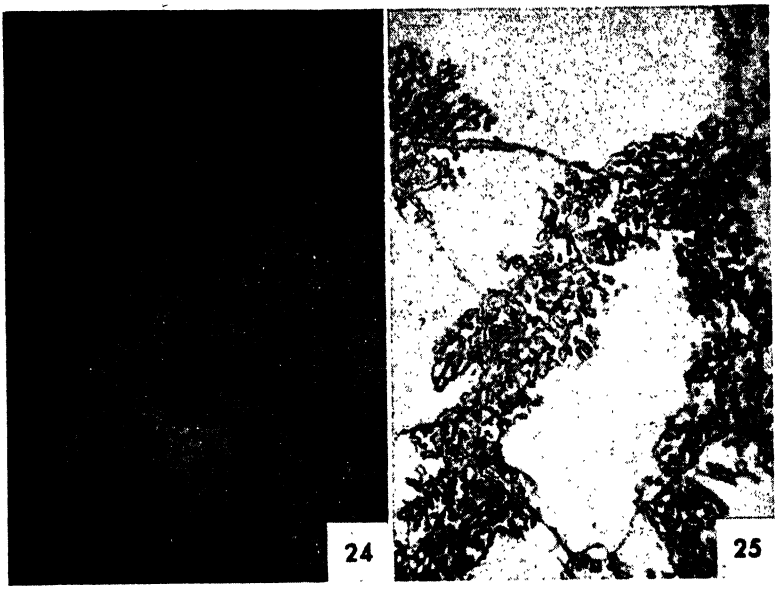

Micro. 12.24. W:Cr steel austenitized 10 min at 1150°C, quenched to 790°C, held there 70 min, and quenched; ×1,000; Nital etch. Longer holding at the subcritical temperature than in Micro. 12.23 has permitted further eutectoid transformation, here about 10% complete.

Micro. 12.25. W:Cr steel treated as in Micro. 12.24 but held 150 min at 790°C; ×1,000; Nital etch. Continued holding at the subcritical temperature has permitted the eutectoid transformation to proceed isothermally to about 30% completion. Note that in this steel, which in many ways is comparable to high-speed steel, the eutectoid structure is not lamellar pearlite but a spheroidal alloyed carbide-ferrite aggregate. With this Nital etch, no interface is visible between the alloyed ferrite (in with the carbide in transformed zones) and the untransformed austenite. No further micrographs of this series are shown because, upon completion of the transformation, the structure is similar to the initial annealed structure of Micro. 12.20.

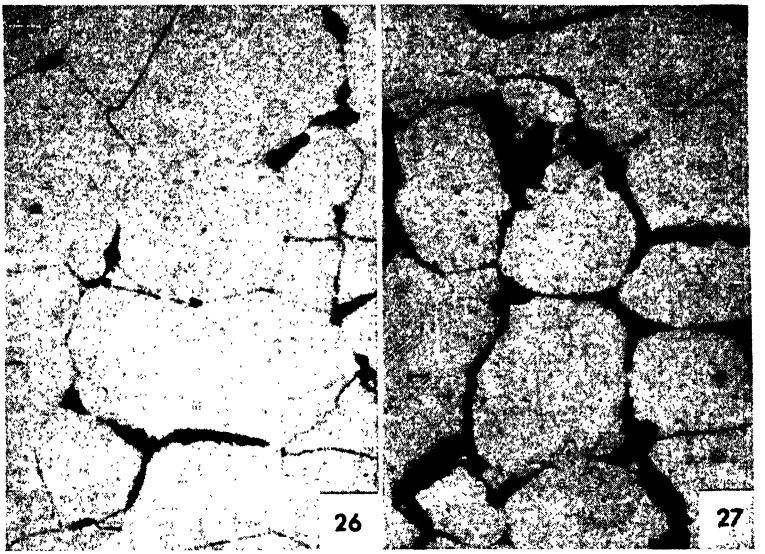

Micro. 12.26. W:Cr steel austenitized 10 min at 1150°C, quenched to 760°C, held 15 min, and quenched; ×1,000; Nital etch. This structure should be compared with Micro. 12.23 (30 min at 790°C). A few undissolved carbides again are evident. The eutectoid transformation at this temperature of 760°C has proceeded somewhat further in half the shortest time used at 790°C. An examination of a large area disclosed that the transformation here is about 5% complete. This temperature of 760°C is that of most rapid eutectoid (nonbainitic) transformation for this steel, corresponding to the "nose" of the transformation graph.

Micro. 12.27. W:Cr steel, treated as in Micro. 12.26 but held 30 min at 760°C; ×1,000; Nital etch. After 30 min of isothermal treatment, the transformation is about 10% complete.

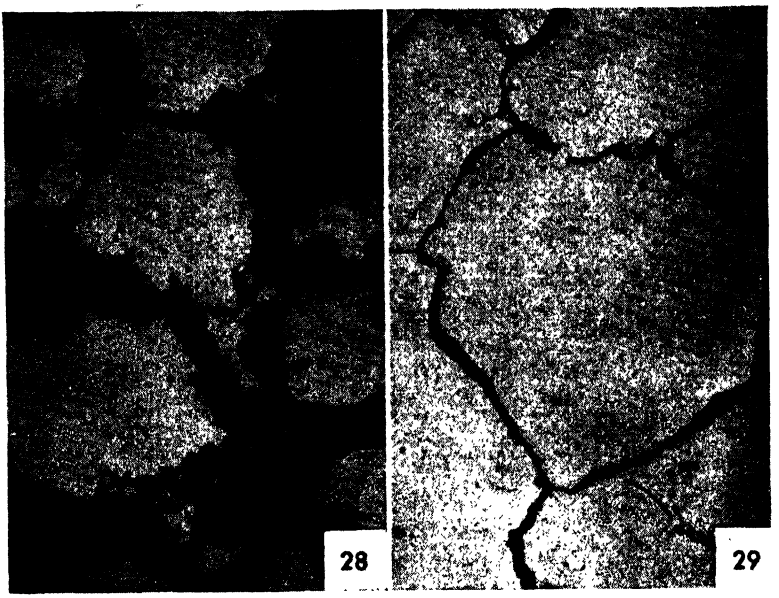

Micro. 12.28. W:Cr steel austenitized 10 min at 1150°C, quenched to 760°C, held 60 min, and quenched; ×1,000; Nital etch. Still further holding (*cf.* Micro. 12.26) has permitted about 25% completion of the isothermal transformation. Note that at this 760°C temperature, the eutectoid transformation produced is very much finer than that formed at 790°C (Micro. 12.25). The coarser white carbides inside the black transformation structure are undissolved carbides, which here become visible by color contrast.

Micro. 12.29. W:Cr steel austenitized at 1150°C, quenched to 710°C, held 60 min, and quenched; ×1,000; Nital etch. The same transformation time as in Micro. 12.27 but at a lower temperature has resulted in very much less transformation. This is clear evidence of the sluggish transformation in these steels at temperatures between that of the regular eutectoid transformation and the bainitic reaction zone.

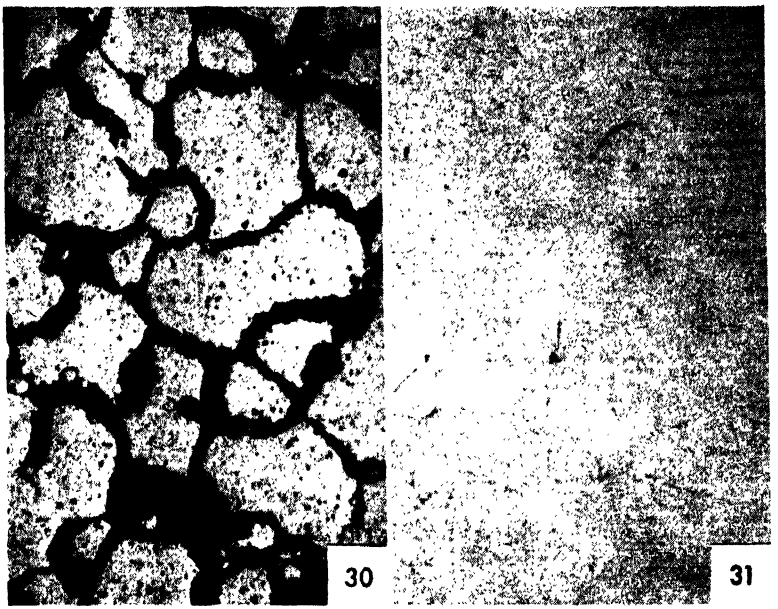

Micro. 12.30. W:Cr steel austenitized only 2 min at 1150°C, and held 60 min at 710°C; as in Micro. 12.29; ×1,000; Nital etch. The shorter austenitization time has resulted in a finer austenitic grain size and more undissolved carbides (the small black dots). More austenitic grain boundaries to nucleate the eutectoid transformation and a less homogeneous austenite have resulted in more transformation than in the case of Micro. 12.29 with the same isothermal treatment.

Micro. 12.31. W:Cr steel austenitized 10 min at 1150°C, quenched to 550°C, held there 24 hr, and quenched; ×1,000; Nital etch. Prolonged holding at this subcritical temperature has resulted in no perceptible transformation. The very great sluggishness of transformation at this temperature makes it suitable for hot-quenching. The 24-hr holding has resulted in the austenitic grain boundaries just becoming visible (specimen etched 10 min in 4% Nital) because of a slight amount of carbide precipitation at these places.

Micro. 12.32. 0.5% C, 7% W, 7% Cr steel, austenitized 4 min at 1150°C, oil-quenched, double tempered at 540°C; ×1,000; etched 3 min in 2% Nital. The few moderately coarse-tempered martensitic needles in a white background are evidence of a large amount of austenite present even after cooling from the first tempering operation. This structure has a rather low hardness of C59 because of the retained austenite. Undissolved carbides are present but not visible because of the lack of contrast.

Micro. 12.33. Same steel and heat treatment as Micro. 12.32 except that, immediately after the oil quench and before tempering, the steel was cooled to −80°C in a dry ice-acetone mixture; ×1,000; again a 3-min etch in 2% Nital. Subzero cooling before tempering cooled the steel to the proximity of its M_f temperature and resulted in the transformation of most of the austenite to martensite. Subsequent tempering has blackened the martensitic needles. Here, undissolved carbides are visible by contrast although the small ones may be confused with slight traces of white retained austenite between black martensitic needles. This structure like Micro. 12.32 has a hardness of C59. However, a third temper of 540°C would soften this structure (*e.g.*, to C57) but would increase the hardness of the previous structure (*e.g.*, about C61), which contains an appreciable amount of retained austenite.

Micro. 12.34. Bearing ring made of W:Cr steel, hardened and tempered, then given an identification number, marked on with an electric stencil. This surface was lightly polished to remove all traces of the stencil mark, then etched with Nital; ×100. The electric "stencil" marks the surface by a minute electric arc. This micrograph shows that immediately below the mark the steel is locally heated to its melting point. Around the central hole, an extremely fine as-cast hypoeutectic structure is present although not readily visible at this magnification. The white zone in general is the part made austenitic during stenciling. The crack along one straight edge of the mark was formed by the rapid local heating and associated volume changes in the originally hard-tempered martensitic structure.

Subzero treatments are particularly effective in transforming austenite to martensite when performed immediately after the hardening quench. If the quenched steel is held at room temperature for some hours before cooling, less austenite is transformed to martensite although no certain explanation is available at present for the stabilizing effect of room temperature "aging." If the subzero treatment follows the first tempering operation, less retained austenite is present than prior to tempering, but most of that remaining will be converted to martensite.

The Cr:W steel of Table 12.5 is particularly susceptible to retained austenite. This steel responds to heat treatment much like high-speed

TABLE 12.5. EFFECT OF SUBZERO TREATMENT (AT −80°C) ON THE HARDNESS AND GROWTH OF A 0.5% C, 7% CR, 7% W STEEL

Sequential heat treatments	Steel not chilled			Steel chilled after quench		
	Rockwell C	% γ*	Growth	Rockwell C	% γ*	Growth
As-quenched from 2050°F	56	40	−0.0021	56	40	−0.0021
Chilled, cooled to −80°F	..	..	.....	63	5	+0.0018
Tempered 1 hr, 1000°F	63	20	+0.0012	61	2	+0.0004
Retempered 1 hr, 1000°F	62	10	+0.0007	59	0	+0.0000
Retempered 10 hr, 960°F	59	5	+0.0004	56	0	+0.0000
Retempered 10 hr, 960°F	59	2	+0.0002	56	0	+0.0000

* Per cent retained austenite, estimated from microstructure.

steel (see Micros. 12.20 to 12.32). It is used for thrust bearing faces in hydraulically actuated pitch aluminum aircraft propellers. Rings of this steel must be put on the hub of the propeller before the forging of the propeller neck and subsequent solution heat treatment of the aluminum alloy. The steel is, therefore, subjected to several hours at about 515°C. In service, the bearing race takes the full thrust, about 150,000 lb, of the rotating propeller and must have a minimum hardness of Rockwell C58, or the bearings would indent the bearing race and variable pitch control would be lost. Hence the steel must withstand several hours at 515°C without softening.

The data of Table 12.5 show that, upon normal austenitization and cooling, a very large amount of austenite is retained upon reaching room temperature, and an appreciable amount may remain after even the first and second temper (see Micro. 12.30). The data on retained austenite, based on metallographic examination, are supported by the dimensional changes, since expansion or growth indicates $\gamma \rightarrow M$ trans-

formation. It is also clear from other experimental work that the subzero treatments are most effective after the original quench.[1] Finally, it is apparent from the table that the subzero treatment appreciably diminished the tempered hardness although the hardness before tempering increased. This is in accord with the previous section attributing most of secondary hardening to the transformation of retained austenite to martensite upon cooling from the tempering operation.

The effect of the subzero treatment then is like that produced by underhardening; it reduces the resistance to softening during tempering. In the case of the bearing races, subzero treatments were abandoned because, although they conferred much improved dimensional stability (and probably improved toughness in the final product), the complete elimination of retained austenite permitted softening to below RC58 during the aluminum alloy solution treatment at 515°C.

Subzero treatments of high-speed steel have been acclaimed as increasing tool life and cutting performance. Such results could be anticipated if the steel had been overhardened, tempered only once, or had a carburized surface zone—in other words, if retained austenite were present and if shock resistance were not a factor. However, careful studies of the effect of this treatment on properly hardened and tempered high-speed-steel tools have shown no improvements in their cutting performance or life.[2]

When high-alloy steels are used for gauges where dimensional stability is all important, subzero treatments are used to ensure the complete absence of retained austenite. Here, the frequently recommended procedure of repeated cooling, *e.g.*, to −80°C, and heating to room temperature seems to be absurd. Once the steel has been cooled to −80°C or lower, repetition of the treatment could not achieve anything until the martensite formed on the first cooling is tempered.

12.9 Dimensional Changes upon Heat Treatment

The volumes of ferrite + carbide, of austenite, and of martensite are all somewhat different. The annealed structure of alloyed ferrite and carbide contracts upon austenitization since the face-centered cubic lattice is more close-packed. There is an expansion when austenite changes to martensite on cooling but, even when this transformation is

[1] In these tests, the heat treater fully expected complete cracking of the bearing races when all old-time "rules" were violated by putting the steel in a dry ice–acetone mixture before tempering. With a complex shape and less retained austenite, it is possible that the subzero cooling at this time might be dangerous.

[2] Kennedy, *Trans. ASM*, **34**, 250, 1945.

complete, the expansion does not exactly coincide with the prior contraction upon heating. The atomic dispersion of carbon in martensite and perhaps the presence of microstresses result in a greater volume than corresponds to the original ferrite and carbide. Therefore, tempering of martensite is accompanied by a slight contraction. Dimensional changes for an 18:4:1 high-speed steel upon cooling through the M_s temperature are shown by the graph of Fig. 12.14. This graph also

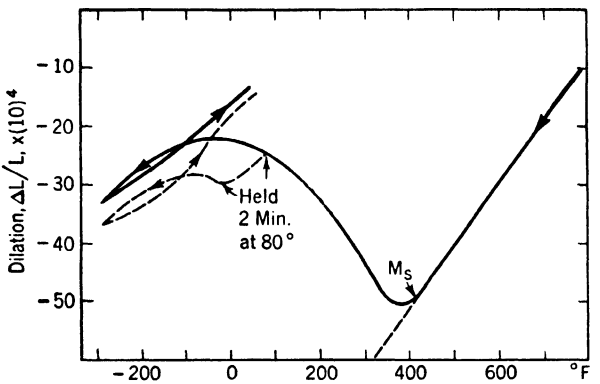

FIG. 12.14. Volume changes as indicated by length changes upon cooling of an 18-4-1 high-speed steel from 2350°F. The solid line shows the length changes upon *continuous cooling from 2350 to −310°F.* Expansion begins at 405°F, the M_s point, and continues until at about −100°F, all austenite has transformed to martensite. The dotted line represents a case where cooling was interrupted by holding the specimen at room temperature for 2 min. This noticeably stabilized the austenite still present so that the austenite-martensite transformation did not again start until the specimen cooled to a temperature of about −100°F. In this latter case, the dimensions upon reheating to room temperature show that not all austenite is transformed to martensite even upon cooling to −310°F. (*Cohen.*)

shows that holding at room temperature before subzero cooling stabilizes the retained austenite and reduces the effectiveness of the subsequent cooling.

If the dimensional changes in a specific tool take place at greatly different times as a result of thermal gradients, not only macrostresses result but also greater volume changes. The maximum thermal gradients encountered upon water, oil, and air cooling of several diameter steel rods have been calculated by Scott and are shown in Table 12.6. It is clear that the difference between oil-quenching and air-cooling is far greater than the difference between oil- and water-quenching. Table 12.7 shows the increases in volume that were found upon hardening four common tool or die steels. It would be expected that distortion and stresses would be greatest in the steel with the greatest volume change.

Shrinkage occurs upon tempering of the air-hardening chromium die steel. Complete stability of dimensions is not obtained until all martensite has been tempered to the point of precipitation of the *stable* carbide, here $(CrFe)_7C_3$ and some $(FeCr)_3C$. Transitional carbides that form at temperatures below 600°C may cause some shrinkage but not to the original annealed dimensions.

TABLE 12.6. CALCULATED MAXIMUM TEMPERATURE DIFFERENCE BETWEEN CENTER AND SURFACE OF STEEL CYLINDERS QUENCHED FROM 930°C IN MEDIUM AT 30°C*

Cylinder diam., in.	Temperature difference, °C		
	Water	Oil	Air
4	846	567	55
2	801	414	30
1	734	277	16
0.5	617	171	9

* Scott and Gray, *Trans. ASM*, **29**, 503, 1941.

TABLE 12.7. INCREASE IN VOLUME OF TOOL STEELS ON HARDENING*

	Composition						Heat treatment, °F	% increase in volume
	% C	% Mn	% Cr	% Mo	% W	% V		
	0.9	1.1	0.5	...	0.5	...	1440 to water	0.69
	1.0	0.2	1.3	...	...	...	1470 to water	0.52
No. 21	1.0	0.6	5.2	1.0	...	0.2	1730 to gas†	0.30
No. 15	1.5	0.2	11.5	0.8	...	0.2	1850 to gas	0.11

* Scott and Gray, *Trans. ASM*, **29**, 503, 1941.

† Quenched in dissociated ammonia to preserve a bright, scale-free surface.

No. 15 showed directionality of dimensional change; on tempering, it contracted in the rolling direction and showed little change in the transverse direction.

12.10 Characteristics of Water-hardening Tool Steels

When high-speed steel was developed, some prophets foresaw the obsolescence of plain carbon tool steels. However, a greater amount of carbon tool steel is produced now than when it was the sole steel available for tools. The chief uses are for purposes where shallow hardening or a soft core is desirable for reasons of toughness or energy absorption under shock and where service temperatures are not appreciably above room temperature. A typical example is drill rod, used particularly for rock drills and punches for deep drawing.

Chromium up to about 0.6% increases hardenability for use in larger

sizes of drills. Likewise, up to about 0.25% V is frequently present in the steel. This carbide-forming element widens the permissible hardening range because the relatively insoluble vanadium carbide restricts grain growth upon overheating. Therefore, temperature control is less critical. The extremely fine grain of the C:V tool steel also improves the shock resistance of the steel. To compensate for the carbon tied up as undissolved vanadium carbide, C:V steels contain about 0.10% extra carbon and also *less* manganese if it is desirable to retain shallow hardening characteristics. For example, two equivalent water-hardening carbon steels for dies might be (1) 0.60% C, 0.70% Mn or (2) 0.70% C, 0.30% Mn, 0.20% V.

Carbon tool steel is usually marketed in the annealed condition with a completely spheroidized carbide structure. When properly hardened, *i.e.*, from 790°C (1450°F), there is not much retained austenite although there may be enough to cause difficulties. For example, the torsion impact test data[1] of Fig. 12.9 show a decrease in toughness of carbon steels when tempered in the range 240 to 275°C. As another example, consider the case of a purchaser of carbon-steel punches for the deep drawing of brass cartridge cases. Samples of all punches bought were Rockwell tested and then deep-etched in hot HCl solution. Any brittleness in the steel caused cracking from the combined action of stress concentration by the Rockwell Brale indentation and hydrogen pressure from pickling. One punch manufacturer found that single-tempered carbon-steel punches always cracked in this test while double-tempered punches of the same hardness did not crack. In this case, retained austenite transforming to austenite martensite upon cooling from the tempering treatment was not the sole source of stresses because the punches were lightly ground and polished after tempering. The second temper would relieve stresses from these operations as well as those from the transformation of retained austenite.

12.11 Uses of Oil-hardening Tool Steels

The Group B tool steels of Table 12.1 are intermediate in general properties and cost between the carbon tool steels and high-speed steels. The presence of relatively small quantities of chromium, molybdenum, manganese, and/or vanadium does not impart air-hardening characteristics except to thin sections and also does not ordinarily contribute secondary hardening. The chief advantage frequently is that a tool or

[1] Torsion tests are superior to tension tests for fully hardened steels since plasticity involves shear stresses and fracture involves normal stresses. In torsion, the shear stress τ is equal in intensity to the normal stress σ whereas in tension, τ is only one-half the value of σ for a specific load. Gensamer, "Strength of Metals," ASM, 1941.

die upon relatively mild quenching in oil does not distort or deform so much as a carbon steel that must be drastically quenched in water or brine.

The alloying elements increase resistance to wear but slightly, and cutting tools are not frequently made from this class of steel. It is useful for large dies where the greater depth of hardening increases the resistance of the die to deformation under pressure or concentrated loads. The steels, therefore, are well suited for hot-forging dies that do not become too hot in service. In all uses such as forging dies where shock resistance is important, the carbon content is kept low, *i.e.*, 0.40 to 0.60%. If wear resistance is more significant, as in trimming dies, the carbon content will be higher, 0.70 to 1.10%.

Graphitic tool steels have the usual tool-steel structure plus nodules of graphite. This phase contributes some lubrication characteristics that fit these steels for certain uses, particularly dies, where maximum wear resistance is not required.

The last steel in the oil-hardening Group B of Table 12.1 is a 2.25% C, 12% Cr steel. The presence of some molybdenum or the use of a high hardening temperature would confer air-hardening properties. Examination of the Fe:12% Cr:C diagram shows that this steel is almost *eutectic* in structure and that at the usual hardening temperature of 1000°C, most of the carbides are undissolved. The large amount of $(CrFe)_4C$ in this steel gives it unusually great resistance to abrasion or wear although, as could be expected, it is rather brittle and does not retain hardness to so high temperatures as the high-speed grades. It sometimes shows 50% longer life in drawing dies than the 18:4:1 high-speed steel.

The presence of undissolved eutectiferous carbides requires hot-forging of this and similar high-carbon high-alloy steels. The eutectic network is not otherwise broken up and, unless its continuity is destroyed, ductility will be low. After hot-working, carbides are distributed in the direction of flow. This means that the properties of the steel will not be the same in the longitudinal and transverse directions. This condition of directionality includes dimensional changes; *e.g.*, an originally round hole will be elliptical after heat treatment. Scott (see Table 12.7) shows that tempering of the high-C:high-Cr steel causes the usual shrinkage in the flow direction but practically none in the transverse direction.

12.12 High-speed Type and Air-hardening Steels

The 0.30% C, 5% Cr steel with small amounts of molybdenum and vanadium in Table 12.1 hardens in air, is tough because of the low-

carbon content, resists cracking from temperature changes, and resists softening at moderate service temperatures. Among its many uses, then, are extrusion dies for aluminum and magnesium alloy shapes, or molds for pressure die castings of these metals.

The high-C:high-Cr steels with small amounts of molybdenum are air hardening but are not high-speed types; *i.e.*, they do not maintain hardness at 1000°F and, therefore are used chiefly for cold-forming operations requiring wear resistance.

The 7 to 12% Cr with 7 to 12% W steels have high-speed-steel characteristics, *i.e.*, comparable transformation diagrams, hardening, and tempering characteristics. They are more prone than high-speed steel to retained austenite as was brought out in discussion of Micros. 12.20 to 12.32. These steels tend to be tougher and more resistant to fire checking with the "cushions" of retained austenite; in addition, the high chromium content confers oxidation resistance. Therefore, the steels are suitable for some of the severest die service, *e.g.*, extrusion dies for brasses operating at 700 to 800°C.

The high-speed steels are sometimes used in the cast and heat-treated state. From the prior discussion, it should be evident that a brittle eutectic network will then be present. Chill casting in small sections minimizes but does not eliminate this network. However, ample evidence has been accumulated that brittleness in a cutting tool may be associated with very desirable cutting properties. It depends on the type of tool and service stresses; in general, if shock is absent, the more brittle structure may cut better and dull less rapidly. The chief drawback to precision-cast high-speed steels is the decarburization usually found on the cast surface. Proper selection of mold material or machining of the surface could obviate this difficulty.

The transformation diagram for high-speed steel (Fig. 12.6) indicates that bainitic structures can be obtained, or at least part bainite, part martensite. Payson[1] claims that this structure improves tool life under conditions of intermittent or shock cutting.

Among the various high-speed steels of Table 12.1, the 18:4:1 is still the standard type for general use. Increasing the vanadium content to 2%, accompanied by an increase in carbon content, improves cutting performance but increases the cost of the steel. The 4% V grade carries these dual effects further, but the cost increase has prevented any wide use of this steel. The presence of cobalt increases the tendency for decarburization of the steel, narrows the heat treatment temperature range, and increases brittleness. The increased wear resistance, how-

[1] Baer and Payson, *Trans. ASM*, **39**, 488, 1947.

ever, makes use of the cobalt-bearing steel economical for machining cast iron that has abrasive sand particles embedded on the surface or for heavy first cuts of forgings and the like with an abrasive surface oxide scale.

Substitution of about 4 to 5% Mo for 10 to 12% W gives the 6:5:4:2 type of high-speed steel. The heat treatment and properties are very similar to standard 18:4:1. The steel is somewhat more subject to decarburization, but the surface can be protected with borax in gas- or oil-fired furnaces as well as by use of carbon block muffles or liquid baths. Certain specialized tools, *e.g.*, high-speed-steel hack-saw blades, are produced chiefly from this type of steel. Increased vanadium content or addition of cobalt causes the same effects in 6:5:4:2 as with 18:4:1 high-speed steel.

Use of about 8% Mo with little or no tungsten results in a lower cost steel (Mo-Max) since molybdenum is cheaper than tungsten and the steel is less dense; therefore, a greater volume of steel is obtained for the same number of pounds purchased. However, it is more subject to decarburization than the 6:5:4:2 type and requires even closer temperature-time control at the hardening heat treatment. Although widely used when tungsten was scarce, its normal uses are restricted to a few tools such as drills where its performance practically equals that of 18:4:1.

In 1947, the molybdenum types of high-speed steel accounted for about 50% of the total high-speed steel produced in the United States. Of the molybdenum steels, the 6:5:4:2 (M-2) is by far the most important from the standpoint of both production and general acceptance as a general-purpose high-speed steel. In general, the choice of type of steel is based on considerations that include tool performance, cost of the steel (base prices in 1947, 82, 63, and 59 cents per pound for 18:4:1, M-2, and Mo-Max, respectively) density (8.72, 8.14, and 8.00, respectively) and the relative heat-treating costs.

It is impossible to distinguish between the structures of these three different types of high-speed steel *when each has been properly heat-treated.* The difference in properties, particularly cutting performance, is also minute or absent. Long studies in plants of large users have indicated a tendency for one grade to be superior for one type of cutting operation while a different grade might show a slight superiority for a different operation. The differences are usually small, apparent only from statistical studies, and might be far outbalanced by variability in the heat treatment or structure of any one type or by improper tool design and maintenance.

Other materials besides high-speed steel are available for cutting operations at elevated temperature. The *Stellite* type of alloy containing cobalt, chromium, and tungsten must be cast and ground to shape and is more expensive than the steels. It requires no heat treatment and maintains useful cutting hardness at temperatures far above those permitted by the use of high-speed steel.

Carbide compositions, such as Carboloy or Firthite, generally contain approximately 94% WC particles, held in position by about 6% cobalt. The alloy cannot be produced with a useful structure by melting and casting, but powders of the constituents, tungsten (or tantalum, boron, etc.) carbide, and cobalt are mixed, pressed to approximately final shape, and then sintered by heating to a high temperature in a hydrogen atmosphere. The aggregate possesses great hardness (closely approaching that of the diamond, which is the hardest material known), high compressive strength, but a relatively low order of toughness. Tools made of carbides have often been seen machining glass or porcelain in popular demonstrations. These tools are almost requisite in cutting abrasive materials of relatively low strength that rapidly dull the edges of other tools, such as Al:Si alloys (page 165), white cast iron, graphite, hard rubber, slate, or asbestos compositions. Carbide tools will cut cast irons at exceptionally high speeds, which produce very high temperatures at the tool edge. In many types of machining work, they will remove metal from forgings, castings, etc., at rates far surpassing the best attainable with high-speed-steel tools. The brittleness of the material, however, sometimes limits its applicability since a high clearance angle cannot be employed. It has occasionally been found inferior to high-speed steels in machining some types of highly alloyed steels, and it is usually inferior on machines subject to excessive vibration by either tool or work.

QUESTIONS

Group A

1. A coarsely spheroidized 1.0% carbon steel gives trouble in an intricate machining operation. It is desired to test the machinability of specimens with the following structures: (*a*) coarse pearlite + some spheroidized carbides, (*b*) entirely fine pearlite, (*c*) entirely fine spheroidal carbides, (*d*) moderately coarse pearlite + ferrite, (*e*) partially spheroidized moderately fine pearlite. Describe the heat treatments required, in terms of temperatures and cooling rates, to produce these structures (if they can be obtained).

2. What quenching mediums are used for cooling steels from the austenitic range? (Arrange in order of decreasing cooling rates.) (*b*) What advantages would be gained by quenching a ½-in. section of carbon steel into brine, then, as soon as the exterior has cooled below 1000°F, transferring the section into an oil

bath? (*c*) After removing from the brine, holding in air a few seconds, and then replacing in the brine, what might the final surface structure be?

3. How might a large screw driver be treated, using an external source of heat but once, to develop a fine pearlitic structure in the shank and a troostitic structure at the tip?

4. What difficulties are associated with the hardening of dies used for cutting threads? How would you suggest heating a large high-speed-steel wedge so as to bring the heavy section up to the proper hardening temperature without "burning" the thin edge?

5. Since neither the hardness nor the toughness of a high-speed-steel cutting tool is usually increased by tempering at 1050°F, why should it be given this treatment?

Group B

1. How could you reduce the hole diameter by heat treatment of a wire-drawing die of high-C:high-Cr steel after it was worn to too large a hole?

2. Specify in detail a heat treatment of a hardened high-speed steel, based on the transformation diagram of Fig. 12.6, designed to achieve maximum softness for remachining.

3. Why does steel 52100, after a spheroidizing anneal, sometimes show at the immediate surface *columnar* ferrite grains, then a zone of *pearlite* between the pure ferrite and the spheroidized carbide structure? Explain, particularly, why the ferrite is columnar in structure and why the intermediate zone is pearlite rather than spheroidite.

CHAPTER 13

SPECIAL CORROSION- AND HEAT-RESISTANT ALLOYS

The most important ferrous alloys that resist corrosion have not yet been studied, namely, stainless steels. Austenitic alloys of this type are also well suited for extremely low-temperature service, *e.g.*, at the liquid-air temperatures used for oxygen production. They show their

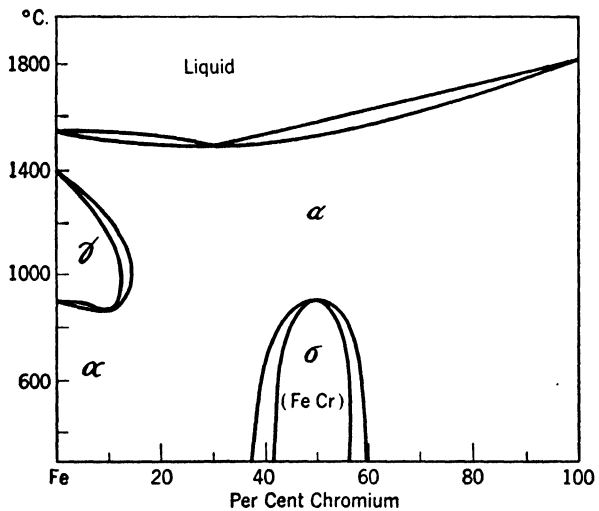

FIG. 13.1. Binary Fe:Cr phase diagram showing the closed γ loop as body-centered chromium and body-centered iron form ferrite solid solutions.

versatility by also being well suited for high-temperature service since their resistance to corrosion includes resistance to oxidation and fairly good strength at temperatures up to 600°C. Special alloys are now being made for the 800°C or higher temperature required for gas turbines and some parts of jet engines.

13.1 Phase Diagrams for Stainless Steels

Stainless steels generally contain chromium, or chromium and nickel, always with some carbon and other elements, deliberately added

or as unavoidable impurities. The Fe:Cr diagram of Fig. 13.1 shows that body-centered cubic chromium tends to stabilize body-centered cubic α iron and its high-temperature counterpart δ, which merge to form what is called the *closed* γ *loop*. Thus beyond 16% Cr, no austenite will be found in binary alloys and, for this reason, they resemble most nonferrous alloys; *e.g.*, they show no transformation hardening by quenching, no grain refinement by heat treatment, etc. Thus binary

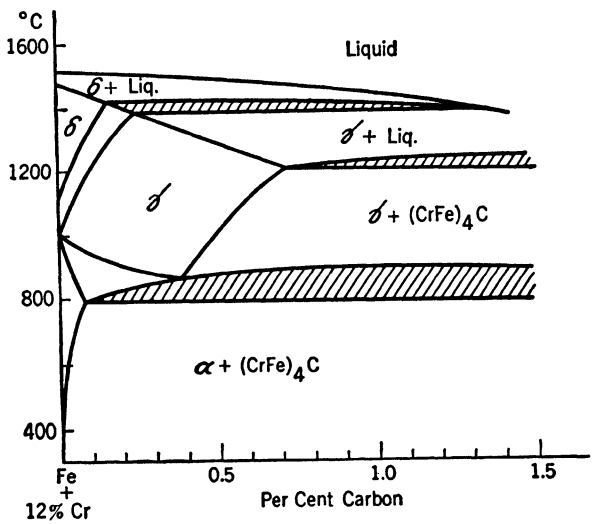

FIG. 13.2. Pseudo-binary phase diagram of iron plus 12% Cr with varying percentages of carbon. Tie lines in two-phase fields do not show compositions of the two phases nor relative proportions. The cross-hatched areas are three-phase fields. A second carbide may exist at the higher carbon contents (see Fig. 13.3).

Fe:Cr alloys, free of carbon, are not properly called steels but stainless *irons*. The σ phase of the binary system, which may be formed by ordering in high-chromium content alloys, is of specific importance in certain stainless steels.

The binary Fe:Cr diagram does not show the effect of carbon, which is soluble in austenite and increases the chromium limit of the γ loop. For a discussion of the hardenable chromium steels, *e.g.*, the so-called *stainless cutlery* grades, the pseudo-binary diagram Fig. 13.2 is useful, (Fe + 12% Cr):C. Chromium constricts the γ field of the Fe:C diagram, decreasing the eutectoid composition to about 0.35% C and the maximum carbon solubility in austenite to 0.7%. The eutectoid temperature is considerably higher, and the eutectoid reaction is no longer represented by a line but by a field (dotted) since Gibbs's phase

rule for this three-component system permits one degree of variability for the $\gamma \rightarrow \alpha +$ carbide reaction; *i.e.*, $F = 3 - 3 + 1 = 1$.

The chromium in fully annealed steels is present in both the ferrite and the carbide phases. The distribution in terms of the identity of the carbide phase is shown in Fig. 13.3 as varying with chromium and carbon

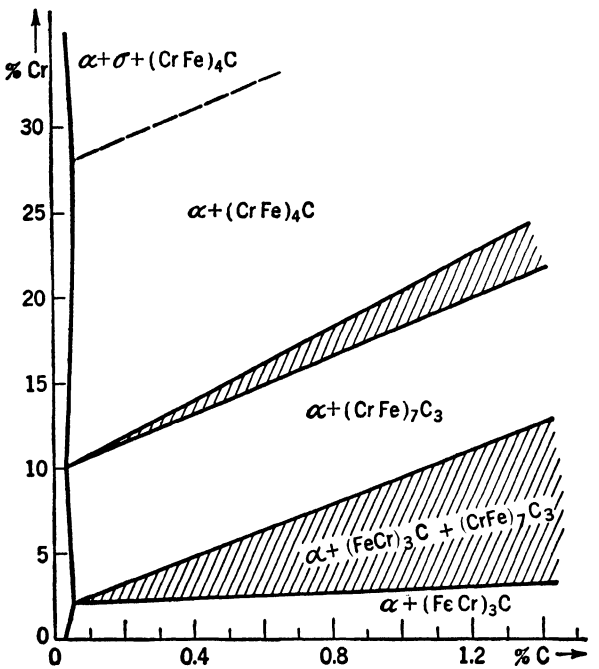

FIG. 13.3. Diagram showing the phases present in slowly-cooled Fe:Cr:C alloys as a function of chromium and carbon content. Chromium can enter Fe_3C in amounts up to 15% Cr without changing its structure and this carbide is designated as $(FeCr)_3C$. The next carbide is $(CrFe_7)C_3$ which contains a minimum of 36% Cr. The $(CrFe)_4C$ is the carbide usually found in stainless steels and contains over 70% Cr.

content. The medium-carbon alloy steels discussed in Chap. 11 contain normal orthorhombic Fe_3C with chromium replacing iron up to 15% by weight of the carbide, *i.e.*, $(FeCr)_3C$. In the high-C:high-Cr tool steels of Chap. 12, the carbide phase is $(CrFe)_7C_3$ which contains at least 36% Cr. The 12% Cr stainless steels may contain this same carbide, but most stainless grades have the next carbide in the series, $(CrFe)_4C$, which contains a minimum of 70% Cr by weight.

When face-centered cubic nickel is added to iron, it tends to depress the A_3 temperature, as shown in Chap. 11, and stabilize face-centered cubic austenite. With 30% nickel or more, binary Fe:Ni alloys are

completely austenitic at all temperatures. The effect of increasing nickel contents in Fe:Cr alloys is shown by the diagrams of Figs. 13.4 and 13.5. Like Fig. 13.2, these are pseudo-binary diagrams of (Fe + 18% Cr + 4% Ni):C and (Fe + 18% Cr + 8% Ni):C, respectively. They show that with 4% Ni, the stainless steels containing less than about 0.4% C can become a mixture of ferrite and carbide but only in the vicinity of room temperature. With 8% Ni present, the three-phase

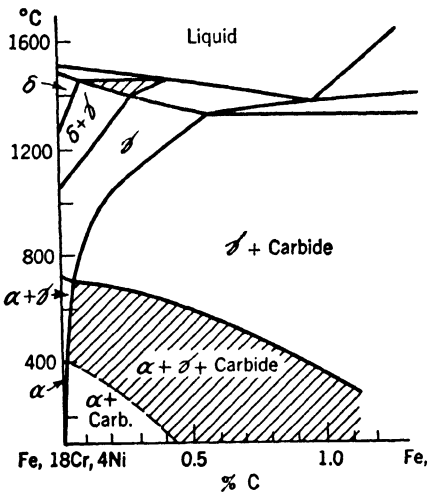

FIG. 13.4.

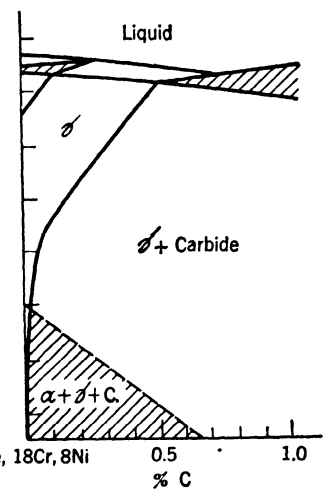

FIG. 13.5.

FIGS. 13.4 and 13.5. Pseudo-binary phase diagrams of Fe + 18% Cr + 4% Ni against varying carbon content (13.4) and Fe + 18% Cr + 8% Ni against varying carbon content (13.5). The carbide in both cases is $(CrFe)_4C$ at least up to 0.5% C. Note how increasing nickel content stabilizes austenite, restricting the high-temperature δ and room-temperature α. The three-phase fields are cross-hatched. Phase compositions and relative proportions cannot be obtained from tie lines in two or three phase fields in these diagrams.

eutectoidal field is pushed to still lower temperatures and carbon contents. As the ferrite formation is further restricted, the high-temperature equivalent phase, δ, is also similarly restricted. Diagrams for higher nickel contents are not given, but the diagrams shown clearly indicate that low-nickel content in an Fe + 18% Cr base would be conducive to hardening by martensite formation while high-nickel contents would tend to give a more stable austenite.

The carbide solubility line of Fig. 13.5, equivalent to the A_{cm} line of the Fe:C diagram, is of great importance with regard to the heat treatment and properties of the 18:8 types of stainless steel. Unfortunately, these pseudo-binary diagrams do not indicate compositions of the various phases, but Fig. 13.3 shows that the stable carbide in an 18%

Cr, 0.10% C steel is $(CrFe)_4C$. Since nickel is not a carbide-forming element, this may be presumed to be the carbide in 18:8 stainless steel. With a minimum of 70% Cr in the carbide phase and with only 18% Cr in the austenite at temperatures above the A_{cm}, precipitation of the carbide phase inevitably results in depletion in chromium content of the remaining austenite. As in almost every case yet studied, the new phase precipitating from a solid solution does so preferentially at the solid-solution grain boundaries. This commonly occurs in the 18:8 steels heated in the range 500 to 800°C after the steel has been rapidly cooled from above the A_{cm}. An exception is when the structure has been cold-worked; then precipitation is just as rapid on planes of slip as at grain boundaries. The significance of grain-boundary precipitation of carbide and localized depletion in chromium content of the austenite is discussed on page 426.

13.2 Microstructures

Most of the stainless and high-temperature alloys contain iron as their major component and structurally show the familiar phases, ferrite, austenite, and carbide. Austenitic structures in the annealed state offer considerable difficulty to the metallographer. Surface flow occurs during ordinary polishing, and localized transformation along scratches or other sites of more severe flow greatly alter the appearance of the structure. Electrolytic polishing of these steels is particularly desirable since it minimizes difficulties of this character.

The resistance to corrosion of the stainless steels includes a resistance to attack by the usual etching reagents, *e.g.*, Nital, which is oxidizing and passivates stainless-steel surfaces. One widely used reagent is aqua regia in glycerine, called Glyceregia (1 part HNO_3, 2 parts HCl, 3 parts glycerin). Etching may be done electrolytically, using a dry cell with the specimen as anode and a 10% oxalic solution as the electrolyte.

All the micrographs in this chapter were supplied by the Universal Cyclops Steel Corporation. They include the following:

Micros. 13.1 to 13.2—Stainless Type 410 (14% Cr), annealed and "hardened."

Micros. 13.3 to 13.4—Stainless Type 430 (18% Cr), annealed at 790 and 845°C.

Micros. 13.5 to 13.6—Stainless Type 302 (18% Cr, 8% Ni, 0.11% C), annealed at 985 and 1150°C.

Micros. 13.7 to 13.9—Stainless Type 302 (18:8), showing carbides or

ferrite precipitated at grain boundaries of the annealed structure upon heating at 650°C.

Micros. 13.10 to 13.12—Stainless Type 310 (25% Cr, 20% Ni) as hot-rolled and annealed and welded.

Micros. 13.13 to 13.19—High-temperature alloy (Uniloy 19-9 DL with 19% Cr, 9% Ni, and small quantities of Mo, W, Cb, and Ti). A series showing the appearance of ferrite at grain boundaries upon reheating hot-rolled stock with the amount first increasing with temperature then later decreasing until the structure becomes fully austenitic.

Micro. 13.20—Vitallium alloy (28% Cr, 5% Mo, 61% Co) as hot-rolled.

13.3 Mechanical Properties of Stainless Steels

The stainless steels are never chosen for a given use solely because of their strength or ductility. However, if a steel with the high corrosion resistance of the stainless types is required, then mechanical properties may be quite significant in choosing from among the stainless types listed in Table 13.1. The 400 series includes alloys in which chromium is the essential alloying element; of these, the first three may be austenitic at high temperatures and ferritic at low temperatures and are, therefore, amenable to heat treatment.

Types 410, 418, and 420 are all of the 12 to 14% Cr group. They will discolor slightly in normal atmospheres but, after the formation of a visible film, the metal is protected from further attack. The approximately 0.35% carbon in Type 420 permits hardening to a Rockwell C55 which is sufficient for cutlery purposes. The basic type, No. 410, also is hardenable but to a less degree. In fact, the best reason for heat treatment of Type 410 is to dissolve the chromium carbide in austenite and, therefore, have it in solution in the martensite. From the discussion of the Fe:Cr:C diagram, it should be recalled that the chromium will preferentially go to the carbide phase in, for example, the annealed structure and, therefore, full corrosion resistance of the matrix ferrite will not be obtained. Of course, if solution of the chromium carbide in austenite is attained, hardenability is no problem in any of these steels, and they may be oil-quenched or, in thinner sections, air-cooled.

Type 418 is a modification of the 410 analysis with 3% W added for improved high-temperature strength and resistance to softening. The carbon content should be increased somewhat beyond that of 410 to compensate for that tied up with tungsten. Whereas Type 410 in the

(*Continued on page* 422)

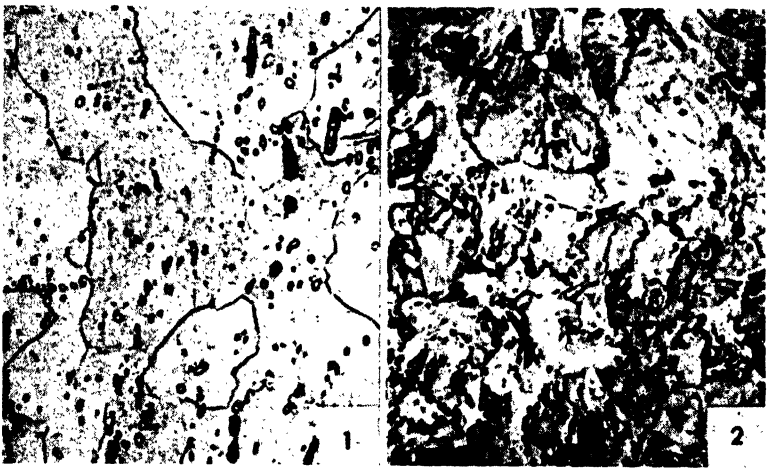

Micro. 13.1. Stainless 410 (14% Cr, 0.09% C); annealed by air-cooling from 790°C (1450°F); Rockwell B67 hardness; ×1,000; Glyceregia etch. This structure is ferritic from room temperature to 790°C, hence cooling rate upon annealing is unimportant. The alloyed ferrite grains do not contain as much as 14% Cr since the carbide phase (clear, rounded particles) is $(CrFe)_4C$ containing up to 70% Cr. The black spots are oxide inclusions, or holes that contained oxides before etching.

Micro. 13.2. Stainless 410 as in Micro. 13.1; heated to 955°C (1750°F) for 3 min and air-cooled; Rockwell B100 hardness; ×1,000; Glyceregia etch. With 14% Cr and 0.09% C, the structure was completely austenitic at 955°C, and there is ample alloying agent to make the steel air-hardening. Therefore, the structure is now a low-carbon martensite, containing 14% Cr and with no separate carbide phase.

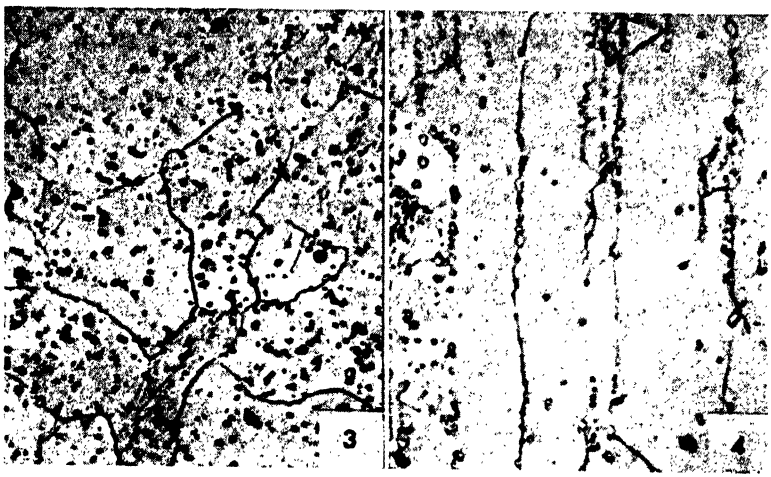

Micro. 13.3. Stainless 430 (18% Cr, 0.09% C); hot-rolled and annealed by air-cooling from 790°C (1450°F); ×1,000; Glyceregia etch. As in the 14% Cr alloy, the structure is completely ferritic with carbides of the $(CrFe)_4C$ type.

Micro. 13.4. Stainless 430; heated to 845°C (1550°F) and air-cooled; Rockwell B85 hardness; ×1,000; Glyceregia etch. This section parallel to the rolling direction shows elongated ferrite grains whose lateral or transverse growth is restrained by undissolved $(CrFe)_4C$ particles. Here the carbides are noticeably concentrated at ferritic grain boundaries. With the higher chromium content, little or no austenite can form in this alloy at any temperature so that it is not hardenable except by cold-working.

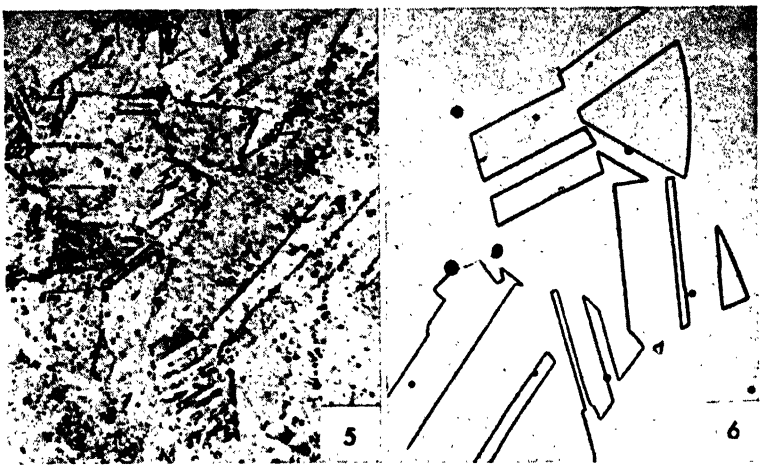

Micro. 13.5. Stainless 302 (18% Cr, 8% Ni, and 0.11% C); annealed at 985°C (1800°F) and quenched; ×1,000; Glyceregia etch. The structure consists of austenitic grains showing numerous annealing twins. In addition, some undissolved carbide particles of $(CrFe)_4C$ are present in a random distribution.

Micro. 13.6. Stainless 302, same as Micro. 13.5 but annealed at 1205°C (2100°F) and quenched; ×1,000; electrolytic etch with 10% oxalic acid. The austenitic grain size is very much coarser here, and annealing twin bands show up very sharply with this etch. Solution of carbides and homogenization of the austenite give a clearer background.

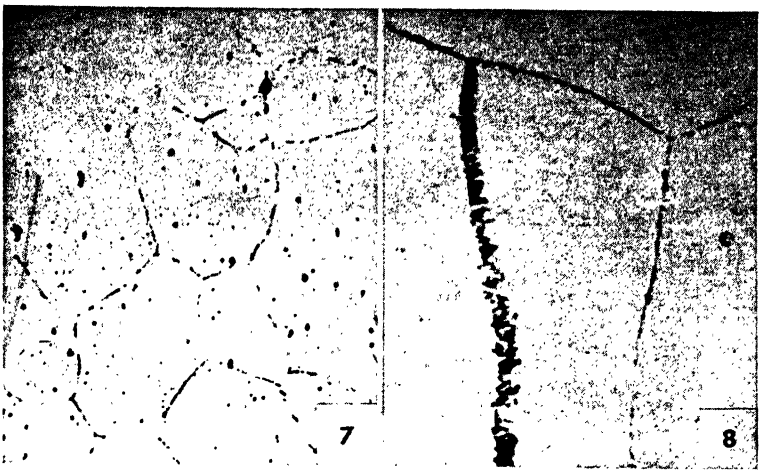

Micro. 13.7. Stainless 302, annealed 1150°C (2000°F), quenched and reheated 24 hr at 650°C (1200°F); ×240; Glyceregia etch. The grain boundaries of the austenite show up here with a dotted appearance, related to the presence of precipitated carbides.

Micro. 13.8. Same specimen as Micro. 13.7 but at ×1,000. Even at this high magnification, the grain-boundary precipitated carbides are quite small. The broad dark band of particles is probably a zone where the polished surface intersects an austenitic grain boundary in an almost parallel manner, *i.e.*, at a very small acute angle.

Micro. 13.9. Stainless 302 (18:8) annealed at 1050°C (1910°F), quenched and reheated 20 hr at 680°C (1250°F); ×1,000; Glyceregia etch. Not only has carbide precipitation occurred in the usual manner, *i.e.* at grain boundaries, but a new phase—ferrite—has appeared at these same locations. No analysis of the steel was made, but it is probable that the nickel content was on the low side, perhaps only 7.5%, in this particular case. Low-nickel content is conducive to ferrite formation in the 18:8 steels.

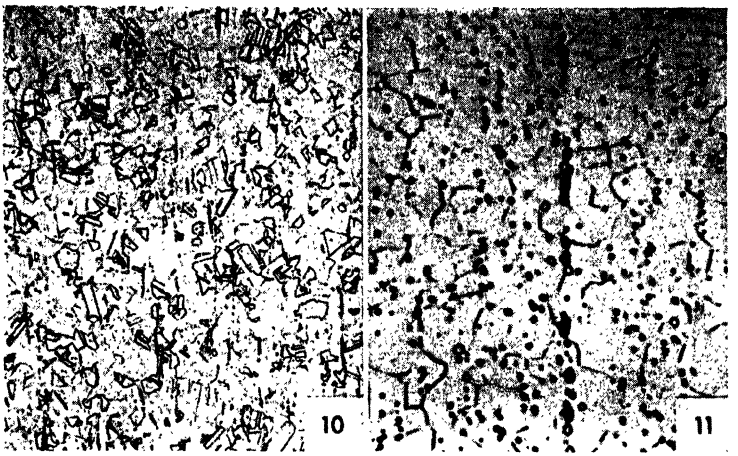

Micro. 13.10. Stainless 310 (25% Cr, 20% Ni, 0.15% C max.); hot-rolled and annealed by air cooling from 1150°C (2000°F); ×100; electrolytic etch. At this low magnification, the structure shows only face-centered cubic austenite with annealing twins. The few short black streaks are probably sites of oxide inclusions removed by the etch.

Micro. 13.11. Same hot-rolled and annealed 25:20 stainless at ×1,000. At this high magnification the spheroidal carbides undissolved by the anneal are clearly resolved as well as a stringer of oxides and the fine-grained austenitic matrix.

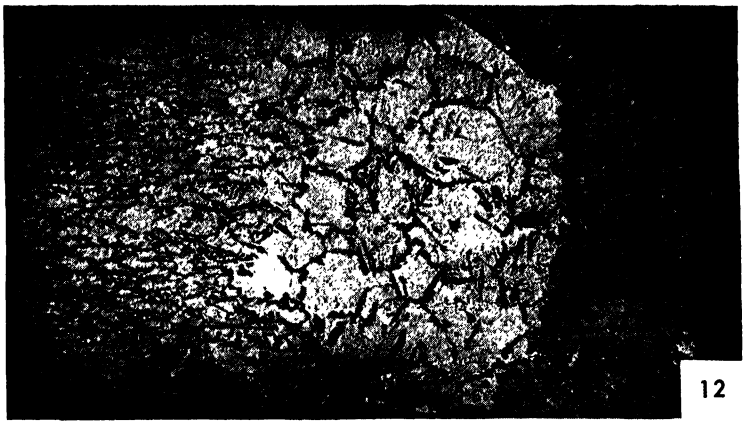

Micro. 13.12. Oxidation-resistant stainless steel (20% Cr, 12% Ni) at a welded joint; ×50; etched with 1:2:3 parts of HNO_3, HCl, and glycerin. In this micrograph, the dark, fine-grained structure at the right side represents the weld deposit (also of 20:12 steel); at the left the original structure of the base metal sheet is visible. In the intermediate zone, the structure shows the effect of being heated close to its melting point. This steel is largely austenitic, although some alloyed ferrite or body-centered iron is visible at the darker structure, showing a grain-boundary network distribution. In the heat-affected zone there has been a pronounced grain growth and, associated with this, a weakening of the structure. This is why in most tests of sound, welded specimens, fractures occur in the coarsened structure adjacent to the weld, rather than in the fine-grained, or equivalently, the chill-cast weld deposit.

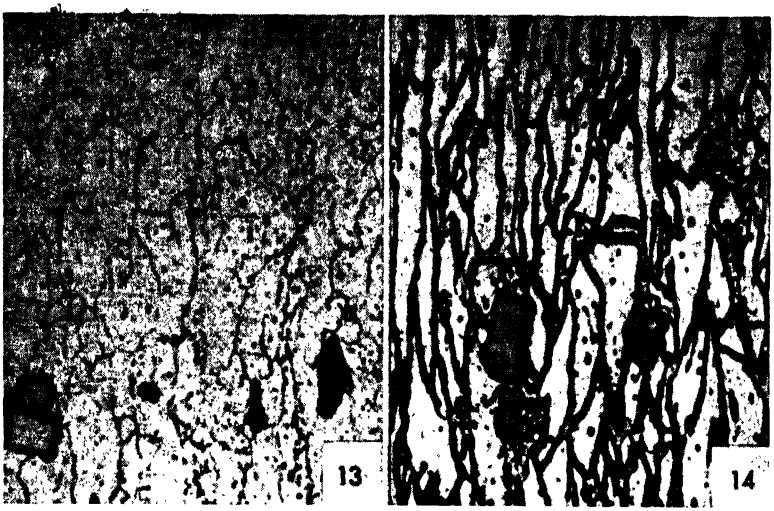

Micro. 13.13. High-temperature stainless steel (Uniloy 19-9 DL) of composition: 0.30% C, 1.0% Mn, 0.5% Si, 19.2% Cr, 9.0% Ni, 1.2% Mo, 1.2% W, 0.37% Cb, 0.35% Ti; hot-rolled; ×1,000; electrolytic etch. The large angular light-gray particles of Ti nitride appear pink when examined on the microscope. Slightly smaller rounded gray particles are chromium oxide inclusions. The black specks in the matrix are carbides, probably of complex composition since the molybdenum, tungsten, columbium, and titanium present in the alloy are all strong carbide formers. The matrix of elongated crystals is austenite.

Micro. 13.14. Same 19-9 DL stainless, heated to 650°C and air-cooled; ×1,000; electrolytic etch. The large gray inclusions were unaffected by heating, but ferrite formed at the austenitic grain boundaries giving a thick "veined" appearance.

Micro. 13.15. Same 19-9 DL as Micro. 13.13, reheated to 825°C for 1 hr and air-cooled; ×1,000; electrolytic etch. The amount of ferrite present has increased, and a carbide phase has precipitated within the ferrite.

Micro. 13.16. Same 19-9 DL, reheated to 875°C for 1 hr and air-cooled; ×1,000; electrolytic etch. At this somewhat higher temperature, the ferritic structure has reverted to austenite although chemical homogeneity has not yet been attained.

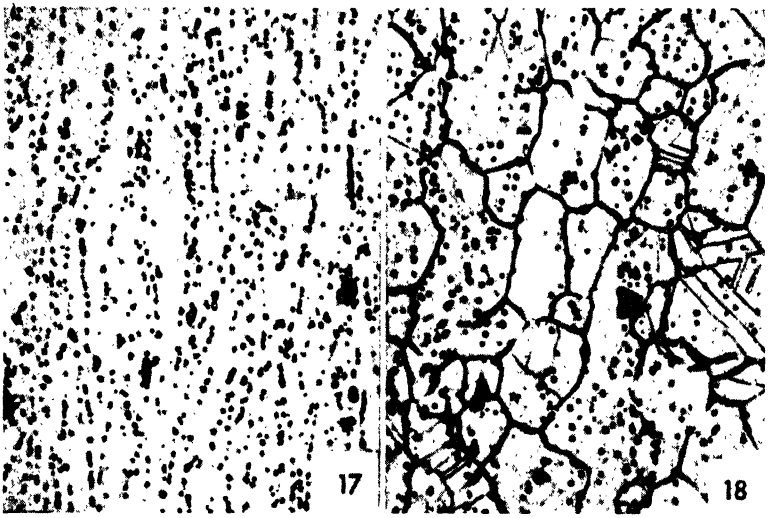

Micro. 13.17. Same 19-9 DL as Micro. 13.13, reheated to 930°C for 1 hr and air-cooled; ×1,000; electrolytic etch. Carbides in the austenitic matrix have coarsened considerably. The austenitic matrix is very fine-grained although grain size is not revealed here.

Micro. 13.18. Same 19-9 DL, reheated to 1100°C for 1 hr and air-cooled; ×1,000; electrolytic etch. Annealing twins are visible in the coarser grained austenite. Some carbides have redissolved, and the titanium nitride as well, at this temperature. The width of grain boundaries is probably an etching effect.

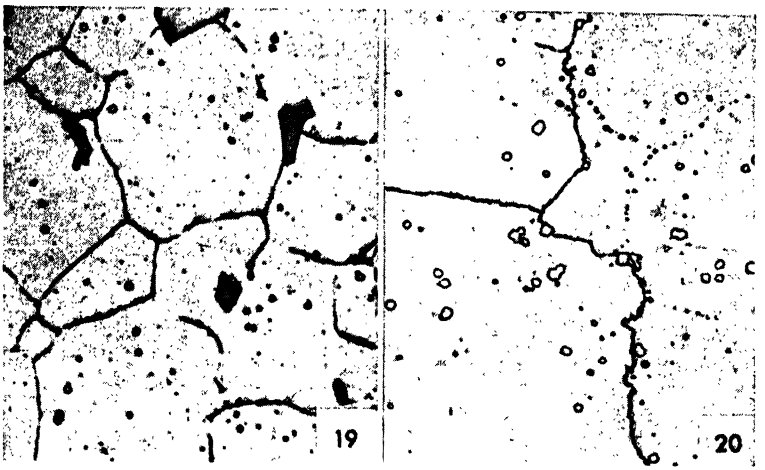

Micro. 13.19. Same 19-9 DL as Micro. 13.13, reheated to 1150°C for 15 min and air-cooled; ×1,000; electrolytic etch. Further austenitic grain growth and solution of carbides are evident upon comparison of this structure with Micro. 13.18.

Micro. 13.20. Vitallium alloy (0.29% C, 0.56% Mn, 28.75% Cr, 3.01% Ni, 5.52% Mo, 61.08% Co, 0.33% Fe); as hot-rolled; ×500; electrolytic etch with 10% oxalic acid. This is not a steel but a nonferrous alloy of cobalt base. It is more frequently used in the cast condition in which case the carbide phase shows a eutectic structure. Here the carbide phase (perhaps a CrMo carbide) is dispersed in a coarse-grained solid-solution alloyed cobalt matrix. Note carbides along former austenitic grain boundaries (upper right); the boundary has migrated.

martensitic state gradually softens with time at 350°C, the 418 grade resists softening almost indefinitely at 450°C.

The 16 to 18% Cr series exhibit improved tarnish and oxidation resistance. With low-carbon contents, they are predominantly ferrite at all temperatures. Thus alloy 430 does not respond noticeably to

TABLE 13.1. TYPICAL MECHANICAL PROPERTIES OF STAINLESS STEELS*

AISI alloy No.	Composition				Condition	Yield strength, psi (000)	Tensile strength, psi (000)	% elongation in 2 in.	BHN	Creep strength§ (000)
	% C	% Cr	% Ni	% other†						
410	<0.15	12.5	..	....	Annealed	40	75	30	150	11.0
					Heat-treated	115	150	15	300	
418	<0.15	12.5	..	3 W	Annealed	80	100	22	217	21.0
					Heat-treated	150	200	17	387	
420	0.35	13	..	....	Annealed	60	98	28	180	
					Heat-treated	200	250	8	480	
430	<0.12	16	..	....	Annealed	40	70	35	165	8.5
					Cold-rolled	95	110	10	225	
446	<0.35	28	..	....	Annealed	50	80	30	165	6.5
301	0.11	17	7	....	Annealed	30	100	65	160	18 0
					Cold-rolled	165	200	15	385	
302	0.10	18	8	....	Annealed	30	90	55	160	18 0
					Cold-rolled	165	190	8	400	
304	0.08	19	9	....	Annealed	30	85	50	160	18 0
					Cold-rolled	160	185	8	400	
309	<0.20	23	13	....	Annealed	30	82	50	165	17 0
					Cold-rolled	120	150	4	275	
310	<0.25	25	20	...	Annealed	40	100	50	165	17.0
316	<0.10	18	11	2.5 Mo	Annealed	30	90	50	165	24.0
347	<0.10	18	10	0 8 Cb‡	Annealed	30	85	50	160	19.0
312	...	29	9	...	Hot-rolled	45	90	30	170	
330	...	36	16	. ..	Hot-rolled	55	100	35	200	
					Cold-drawn	...	150			

* Data from "Handbook on Stainless Steels," Allegheny-Ludlum Steel Corp.

† 1% Mn in No. 400 series, 2% Mn in No. 300 series.

‡ Minimum columbium is eight times the % carbon.

§ Stress giving 1% flow in 10,000 hr at 540°C. *Caution:* The alloy having best creep strength for 10,000 hr at 540°C may not be best at other temperatures or times.

heat treatment although it may be hardened by cold-work. The carbon content may be increased to about 1% (Type 440-C not listed here) and, as mentioned earlier, the Fe:Cr austenitic loop will be displaced enough to the right for the alloy to be hardenable by heat treatment. In fact, this 440-C alloy will have good stainless characteristics *only when hardened,* for otherwise too much chromium would be tied up with the carbide phase.

The 25 to 28% Cr alloy, No. 446, is completely ferritic at all temperatures. Its sole use is based on the oxidation and scaling resistance characteristic of the high chromium content. The alloy is subject to

normal grain growth when used continuously at high temperatures and, if then cooled slowly, will be extremely brittle from a carbide phase precipitated at the boundaries of coarse ferrite grains.

The Cr:Ni steels of the 300 series are all predominantly austenitic and cannot be hardened by heat treatment. The alloys are annealed, for example, by quenching from a high temperature, 1050 to 1100°C. They are hardened by cold-working. The degree of strain-hardening is greater than that to be expected from purely plastic deformation. Figures 13.4 and 13.5 show that, under equilibrium conditions, the austenite should start transforming to ferrite at some temperature near 500°C. Quenching from 1050°C not only prevents carbide precipitation upon crossing the A_{cm} line but prevents this ferrite formation at lower temperatures. However, plastic deformation assists the slightly metastable austenite to transform at least partially and, at room temperatures, to a low-carbon-content martensite. Whereas the quenched fully austenitic alloys are nonmagnetic, the cold-worked steels of the 300 series become strongly attracted by a magnet.

The degree of strain-hardening of the austenitic steels is related to the stability of the austenite and, therefore, to the nickel content. Type 301 with only 7% Ni, typically, becomes extremely hard at machined edges as a result of local cold-work. Further cutting through this hardened zone results in a relatively rapid tool wear. Type 302 with 8% Ni hardens somewhat less rapidly and, therefore, can be cold-worked somewhat more before re-annealing becomes necessary. The slightly higher nickel content, typically 9%, of Type 304 is accompanied by a further slight decrease in strain-hardening.

Assuming that quenching from the anneal prevents precipitation of carbides on cooling, the diagram of Fig. 13.5 indicates that the austenite is supersaturated with carbon, and a carbide will precipitate if given opportunity by heating in the range 500 to 800°C. The most damaging effects of carbide precipitation are apparent in a susceptibility to intercrystalline corrosion but, in addition, strength is increased (in the absence of corrosion) and ductility decreased, particularly notch ductility. The room-temperature Izod impact strength may be reduced from about 120 ft-lb to about 30 ft-lb when Type 302 18:8 is annealed and reheated 3,000 hr at 650°C.[1] Type 304 is characterized by a lower carbon content and, therefore, suffers less in this regard.

It is impractical to produce 18:8 steel with less than the 0.02% C that is required for immunity to grain-boundary carbide precipitation. The low carbon of Type 304, usually about 0.07% C, causes appreciably

[1] Thum, "Book of Stainless Steels," ASM, p. 395.

higher production costs than Type 302 with about 0.12% C. Immunity is necessary in all welded structures subject to corrosion or notch stresses since the temperature of fusion at one place inevitably creates a near-by zone of temperature permitting carbide precipitation, and it is seldom feasible to anneal the entire welded assembly at 1050°C and quench. To achieve immunity, therefore, it is necessary to add an element with a considerably greater affinity for carbon than chromium. Both titanium and columbium may be used but columbium, as in Type 347, is preferred since, during fusion welding, it is less subject to loss by oxidation. The formation of a columbium carbide is assured by having at least eight times as much (by wt. %) of Cb as there is carbon.

The other grades of stainless steels listed in Table 13.1 are employed for specific corrosion- or oxidation-resistant characteristics, not for their mechanical properties. Types 309 and 310 are as oxidation resistant as the ferritic 446, but in addition they are much more resistant to grain growth and related embrittlement. Both alloys cost more than No. 446, and No. 310 is necessarily more expensive than No. 309. The higher nickel-content alloy, No. 310, has a more completely austenitic structure and withstands fluctuating temperatures better than No. 309. In addition to the standard grades listed in Table 13.1, many other types of stainless steels are produced for special requirements. There are "free-machining" grades that contain an increased amount of sulfur or selenium. These grades have very considerably improved machinability with only a slight loss in corrosion resistance and mechanical properties.

13.4 Corrosion Resistance of Stainless Steels

Stainless steels owe their name and uses to the phenomenon of passivity, which is a condition of negligible corrosion in spite of a chemical tendency to react with the metal's surroundings. The good corrosion resistance of aluminum, in spite of its great affinity for oxygen, is a result of the oxide film that quickly forms, is adherent, and is nearly impervious to the passage of more oxygen atoms. Analogously, the passivity of stainless steels is always found in association with oxidizing conditions, and the oxide film theory of corrosion resistance here again is useful. In connection with stainless steels, several broad generalizations are possible:[1]

1. Corrosion resistance depends on passivity.
2. Chromium is the basis element for attaining passivity.
3. Corrosion resistance generally increases with chromium content of the matrix phase.

[1] Zapffe, *Metal Progress*, **48**, 693, 1945.

4. Strongly reducing conditions, *i.e.*, an absence of oxidizing conditions, cause a susceptibility to attack.

5. Strongly oxidizing conditions cause extraordinary resistance to attack.

6. The chlorine ion is destructive to chromium steels.

7. Nickel not only improves the engineering properties but increases resistance to corrosion in neutral chloride solutions and acids of low oxidizing capacity.

8. Molybdenum expands the passivity range and improves resistance to corrosion in hot sulfuric and sulfurous acids as well as neutral chlorides including sea water.

9. Intergranular attack of austenitic types is one of the foremost characteristics of these steels. It is avoided by low-carbon contents, by proper heat treatment, or by alloying with columbium or titanium.

Expanding a few of these generalizations, the requirement of chromium in the matrix is exemplified by the improved corrosion resistance of the No. 410 and No. 420 straight chromium alloys when in the martensitic condition. The grain growth that may occur in the completely ferritic No. 446 (28% Cr) alloy does not affect its corrosion resistance which is comparable to the austenitic steels. However, grain growth, *e.g.*, upon welding as shown by Micro. 13.12, makes the straight chromium alloy less desirable from the standpoint of mechanical properties.

In contact with salt solutions that are freely exposed to air, surface oxidation of stainless steels produces passivity and substantial immunity to corrosion. However, stainless steels cannot be recommended for storage tanks or other contacts with stagnant solutions. The original oxygen in the solution may be quickly used up and, if its oxidizing capacity is not maintained, *e.g.*, by aeration, then pitting attack is possible. A minute activated or anodic area and a large passivated or cathodic area result in a small total corrosion but destructive solution or pitting at the anodic spots. A high-nickel content and the presence of molybdenum, as in Type 316, are conducive to minimizing general corrosion and pitting, respectively, in neutral chlorides. However, this steel cannot be relied upon for all service conditions, *e.g.*, in the least oxidizing acids, HF and HCl, which attack all stainless steels at almost all concentrations and temperatures.

The chief service difficulty encountered with 18:8 stainless steel has been intergranular corrosion made possible by precipitation of $(CrFe)_4C$ at austenitic grain boundaries. The basis for this condition is shown by the schematic drawing of Fig. 13.6. Chromium diffuses from the

immediate vicinity of grain boundaries to form the carbide phase at these sites. The resulting depletion of the matrix lowers chromium content below the 12% required for corrosion resistance. The low chromium content grain-boundary metal is anodic to the rest of the grain and solution in a corrosive medium is localized at the grain boundaries. If a strip is *sensitized*, *i.e.*, treated to obtain grain-boundary carbide precipitation, and then boiled for 72 hr in the Strauss test

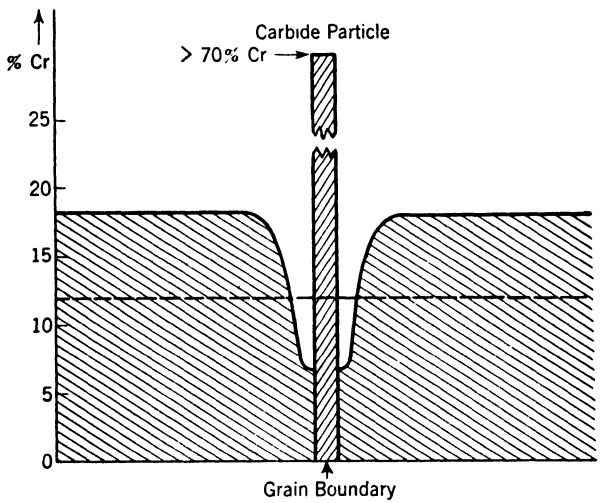

FIG. 13.6. Schematic section through boundary of two austenitic grains of 18:8 stainless steel with a carbide particle $(CrFe)_4C$ precipitated at the boundary. This plot of chromium content through the section shows chromium depletion of austenite adjacent to the carbide particle. The amount of chromium left in solution at the boundary is below the 12% Cr (dashed horizontal) required for corrosion resistance.

solution (47 cc H_2SO_4 and 13 g $CuSO_4.5H_2O$ in 1 liter of solution), the individual austenitic grains in the corroded zone are almost completely disconnected. If the strip is bent, the surface grains may fall out as individual crystallites.

The effect of temperature and time variables is shown by the graphs of Fig. 13.7 from Bain.[1] An 18:8 steel with 0.08% C was solution-treated at 1050°C, quenched, and different specimens reheated 3 min, 1 hr, and 1,000 hr at constant temperatures from 200 to 800°C. Intergranular penetration after boiling in the Strauss solution for 100 hr was measured by the decrease in electrical conductivity, a sensitive measurement since the zone of penetration tends to become a nonconductor.

[1] Bain, Aborn, and Rutherford, *Trans. ASST*, **21**, 481, 1933.

Deterioration is greater and comes at a lower temperature for longer times of heating. In the same graph, a comparison is made between sensitivity of annealed and cold-rolled metal upon precipitation treatments of 1,000 hr. The cold-rolled metal is only slightly affected in comparison with the annealed, and the temperature of sensitization is lower. This should be anticipated in view of the discussion of precipita-

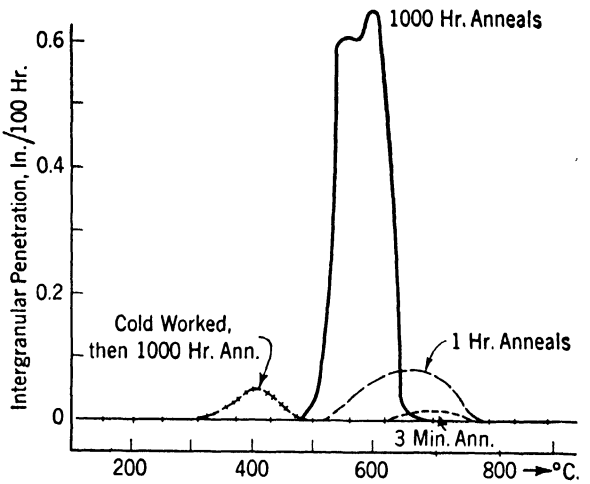

FIG. 13.7. Effect of variation in annealing or reheating time of stainless steel at temperatures in the carbide precipitation range as shown by intergranular attack in modified Strauss solution (47 cc H_2SO_4 and 13 g $CuSO_4 \cdot 5H_2O$ diluted with water to 1,000 cc). Intergranular attack is greatest and at lower temperatures for long heating times. Cold-working prior to heating induces precipitation at a lower temperature and more uniformly through the structure, reducing relative intergranular penetration. (*Bain, ASST*, 1933.)

tion in cold-worked Al:Cu alloys. Precipitation is sooner and more general.

The curves of Fig. 13.7 also show that at 650°C, for example, little intergranular penetration occurs after 3 min, a large amount occurs after 1 hr, and almost none is found again after 1,000 hr. This does not mean that the carbide precipitate redissolves after 1,000 hr at 650°C. Rather it should be interpreted as (1) carbide particle growth, which interrupts continuity of the boundary precipitate and (2) diffusion of chromium from the matrix into the impoverished boundary zone (Fig. 13.6), raising the chromium content there to at least the 12% minimum requirement and diminishing the anodic-cathodic difference between boundary and matrix.

13.5 Alloys for High-temperature Service

No detailed discussion of high-temperature mechanical testing can be included here. An important chief difference from ordinary tensile tests is with respect to the effect of time. Above a temperature that is roughly equivalent to the recrystallization temperature, most metals can flow continuously at comparatively low constant stresses. At just below this specific temperature, strain-hardening during initial flow will increase strength, and the flow will decrease and stop. Right in the range, flow may start rapidly, then continue slowly and uniformly for a period of years. This flow is called *creep*, and the unit stress required to cause a given rate of flow at a specific temperature is called the *creep strength* (see Table 13.1). If the stress is too high, the rate of flow may at some stage increase and proceed to fracture. Relatively high stresses may be used in testing and the hours to fracture at each stress measured. From such data, the *stress-rupture* properties may be obtained, *i.e.*, the hours required for rupture and the elongation at a given stress level. Creep properties are most important for structures designed for extremely long life with close dimensional tolerances, *e.g.*, for steam turbines. Stress-rupture data are more important for metals whose expected life is short, *e.g.*, 50 to 100 hr in a jet engine.

Certain generalizations in regard to high-temperature properties are made below without specifying the occasional exceptions:[1]

1. A coarse-grained structure is stronger than a fine-grained structure. This is the opposite of the room-temperature property effect.
2. Cast structures are stronger than wrought (really another expression of point 1).
3. Stable structures are stronger than metastable ones. Flow seems generally to occur more readily if a structural or phasial change is also taking place at the test temperature. Actually high-temperature flow seems to involve movement of activated atoms as in diffusion, and theoretical analyses have been made using similar mathematical equations.[2]
4. Austenitic-type structures are stronger than the ferritic type.
5. A stable eutectiform network, in small quantities and with the second phase (*e.g.*, carbide) of a growth-resistant type, strengthens the matrix phase appreciably (see Chap. 7 and the Mg:Ce alloys).
6. High-melting-point elements, sometimes called *refractory* metals, give best high-temperature alloys. Alloys of these metals have higher recrystalliza-

[1] ASTM Symposium on Materials for Gas Turbines, 1946. Grant, *Trans. ASM*, **39**, 281, 335, 368, 1947.

[2] Kauzman, *Trans. AIME*, **143**, 57, 1941.

tion temperatures and require higher temperatures for phase changes involving diffusion (points 3 and 5).

7. A longer life at a high temperature (*e.g.*, in the stress-rupture test) usually results in rupture with less ductility. An alloy that is ductile in a short-time, high-temperature test may fail in a brittle manner after stressing for several hundred or thousand hours at temperature.

8. Failures at high temperatures are usually intercrystalline in contrast to transcrystalline fractures ordinarily observed at room temperatures. The approximate temperature at which the mode of fracture changes is called the *equicohesive* temperature. Below this, the grains are ordinarily weaker than the grain boundaries; above this temperature, the reverse is considered to be true.[1]

9. The data of secondary creep or of stress-rupture tests give straight-line plots of log(stress) vs. log(rupture time), or log(stress) vs. log(minimum creep rate).

10. The best alloy at one temperature or creep rate will not usually be the strongest alloy at some other temperature or creep rate.

The preceding generalizations are based on a considerable amount of experimental work carried on in 1940 to 1947. Prior to 1940, there was no great need for alloys to withstand stresses at very high temperatures. When the need arose, the strongest alloy available was Type 316 stainless steel (18:11, Mo). Its high-temperature strength properties, *i.e.*, creep and stress rupture, relative to other alloys in the field, are shown in Fig. 13.8.[2]

Among the first of the newer alloys to be developed was the Timken 16:25:6 alloy. Its development was as follows: 16% Cr and about 1% Si were judged to be necessary for corrosion and oxidation resistance. Molybdenum, needed for high-temperature strength, was limited to about 6% by steelmaking and hot-working difficulties. Nickel was required in amounts of about 25% to obtain a completely austenitic structure. Nitrogen rather than carbon was employed for stabilization and strengthening effects.

The 16:25:6 alloy falls in Group A of Fig. 13.8 as does the 19-9 DL shown in Micros. 13.13 to 13.19, Gamma-Cb and several other chromium, nickel, iron alloys containing molybdenum, tungsten, titanium, and columbium. These alloys are used for wheels in turbosuperchargers or

[1] Another possible factor is that high-temperature oxidation proceeds more rapidly at grain boundaries, known to be the case in stainless steels (Bayertz, *Trans. ASM*, **24**, 420, 1936. Grain-boundary oxidation plus stress would then result in another form of stress-corrosion intercrystalline failure.

[2] Symposium on "Super Alloys for High Temperature Service," *Metal Progress*, **50**, 97, July, 1946.

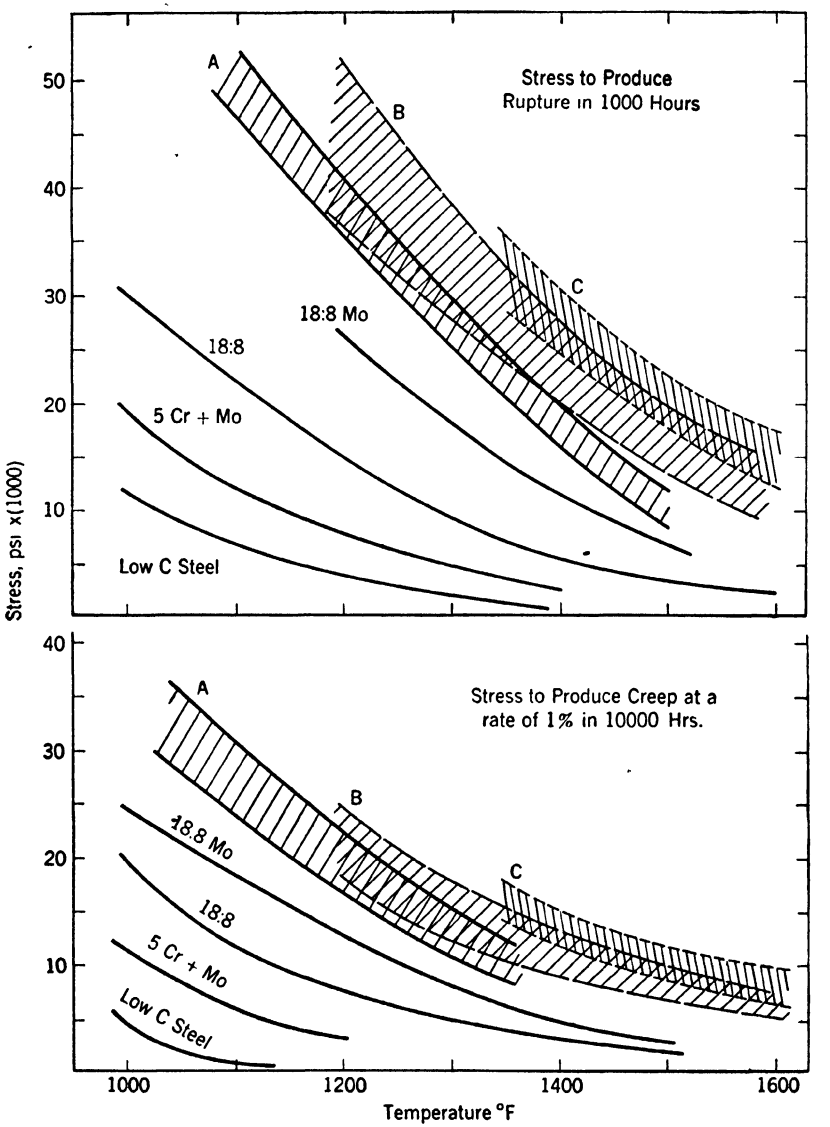

FIG. 13.8. The creep strength (for 1% flow in 10,000 hr) and rupture strength (for 1,000 hr) of some of the standard steels of 1940 and newer "superalloys." Class *A* alloys include Cr:Ni:Mo types that are not usually heat-treated such as 16:25:6, 19:9 DL, Gamma-Cb, etc. Class *B*-type alloys are normally heat-treated and include wrought Ni:Cr and Co:Cr compositions such as Inconel, N155, and S816. Class *C* alloys, usually employed in the cast form, include Vitallium and other cobalt, chromium, molybdenum types. Class *C* alloys usually contain more carbon than the comparable wrought alloys in Class *B*.

gas turbines with relatively low operating temperatures, *e.g.*, about 650 to 750°C (1200 to 1380°F).

The heat-treated Group B alloys of Fig. 13.8 are more highly alloyed and include Inconel, an alloy commonly designated as N155, and a newer alloy called S816 (see Table 13.3 for compositions). These alloys are precipitation hardenable, and the heat treatment of S816, for example, involves water quenching from a solution treatment at 1300°C followed by aging for at least 10 hr at 800 to 850°C. This heat treatment is designed to achieve stability of structure at service temperatures rather than maximum hardness.

Finally, the Group C alloys of Fig. 13.8 are in general cobalt-base alloys chiefly used in the form of precision castings.[1] These also are subject to aging or precipitation phenomena. Some remarkably good high-temperature properties have been obtained, but the status of developments here ranks the topic as an art rather than a science. Little or nothing is known about the pertinent constitutional relationships or phase diagrams although research is proceeding in an attempt to develop this scientific background.

Creep data in the literature show that the 25:20 stainless steel is weaker than the 18:8 stainless alloy for a creep rate of 1% per 10,000 hr at 540°C while, for a lesser creep rate of 0.1% per 10,000 hr, it is stronger. Table 13.4 shows that Timken 16:25:6 alloy is likewise stronger or requires a higher stress to rupture in 1,000 hr than the Gamma Cb type at 1200°F, but it is weaker than the latter type at 1500°F and higher. Vitallium type alloys are stronger but less ductile as the carbon content increases up to about 1%, creating in cast alloys a eutectiferous interdendritic carbide network in a solid-solution matrix. Beyond this, added carbon makes the network too massive and continuous with a diminution in rupture strength.[2]

13.6 Alloys for Low-temperature Service[3]

Aircraft and equipment used in polar areas are subjected to temperatures as low as −70°F. Equipment employed to liquify hydrocarbons, such as propane, for storage or to liquify air for oxygen production is subjected to temperatures in the vicinity of −300°F. Oxygen in large quantities and at a low cost is of vital importance in the production of synthetic gasoline from natural gas or coal. The development of low-cost oxygen is stimulating the tonnage use of this element for

[1] Focke, *Metal Progress*, **48**, 487, 1945.
[2] Grant, *ibid.*
[3] Seigle and Brick, *Trans. ASM*, **40**, 813, 1948.

iron and steel production. These considerations have considerably increased the interest in the properties of metals at low temperatures.

As the temperature decreases, the yield strength, tensile strength, and hardness of *all* metals and alloys increase[1] (excluding phase or structural changes with temperature). The ductility of all face-centered cubic metals is relatively unaffected but, in the case of all other structures, ductility is adversely affected. In the case of the pure metals, no phase changes are involved, and the loss in ductility at low temperatures is reversible; *i.e.*, iron may become very brittle at liquid-air temperatures but upon heating to room temperature, it again becomes as ductile as it was before being cooled.

The ductility of face-centered cubic metals makes aluminum- or copper-base alloys completely satisfactory at any subzero temperature, but the difficulty of soldering aluminum makes it expensive to fabricate certain structures such as complex heat exchangers. Austenitic stainless steels are also quite ductile at low temperatures, but they are fairly expensive, not readily soldered, and their thermal conductivity is too low for best heat-exchange properties.

The regular steels are cheap and comparatively easy to fabricate, but they lose ductility at low temperatures. The temperature at which embrittlement of steels appears as the temperature decreases is affected by the following variables:

Mechanical Test Variables:

1. Rate of Loading. In the temperature range of embrittlement, increased rate of loading (impact) makes embrittlement appear at a higher temperature.

2. Ratio of Principal Stresses. In torsion where the shear stress equals the normal stress, embrittlement of a plain carbon steel may not appear until −300°F is reached. In ordinary tension, embrittlement may be observed at −200°F. In notched bend tests, the embrittlement may appear at −50°C, unless the notch is very sharp or the bar is wider than normal. In these cases, the multiaxial stress ratio increases ($\sigma_1 : \sigma_3$; see page 20) and embrittlement may appear at room temperature. Incidentally, the notch by reducing the effective gauge length multiplies the strain rate by a factor of roughly a million times. Thus notches have a double effect.

[1] The magnitude of the strength increase is shown by the following figures for ultimate tensile strengths at room temperature and at liquid-air temperature: copper, from 30,000 to 50,000 psi; ingot iron, from 40,000 to 100,000 psi; annealed 18:8 stainless steel, from 80,000 to 200,000 psi.

Metallurgical Variables:

1. Ferritic Grain Size. Fine-grained steels retain toughness to a lower temperature.

2. Composition. *Oxygen* is detrimental and aluminum deoxidized steels show notable superiority although this may also be due to a finer grain and to excess aluminum in ferrite.

Carbon, above 0.10% clearly decreases toughness or raises embrittlement temperatures. Below 0.10%, this effect is probably also true if the steel is otherwise deoxidized. The form and dispersion of the carbide phase are important; as discussed in Chap. 10, pearlite with lamellar Fe_3C is inherently more brittle than sorbite with finely spheroidized carbide. Low temperatures accentuate this difference (Fig. 11.14, page 341).

Nickel is the only element that clearly increases toughness at low temperatures or decreases the temperature of embrittlement. The martensite that readily occurs in high-nickel alloys (8% nickel or more) is quite tough if the carbon content is low.

Molybdenum, Chromium, Etc. The carbide formers improve low-temperature toughness in the presence of carbide by reducing any tendency for the coarse lamellar structure.

Summing up, for structural service down to −70°F, a fine-grained, aluminum deoxidized, normalized low-carbon steel is suitable. For temperatures down to about −150°F, a similarly treated steel with about 4% Ni, or one with about 0.5% Cu and Cr, will usually be satisfactory. For liquid-air temperatures, higher nickel steels appear to be suitable if notches can be avoided; otherwise stainless steel, a copper-base alloy or an aluminum-base alloy, would be better.

The tin solders are of particular interest since many heat exchangers of copper, for example, are assembled with 50% Pb:50% Sn solder. There is reason to believe that these solders are suitable at constant low temperatures in the absence of stress. However they,[1] and all tin-base alloys, become brittle at temperatures of −100°C (−150°F). Moreover, a triaxial tensile stress at below 13.2°C, which tends to facilitate the expansion required for the transformation from white to gray tin, may also cause marked deterioration of properties. This type of stress on the solder can originate from temperature fluctuations of flat sheets soldered together.

QUESTIONS

1. Why does cast-aluminum alloy 142 (see Chap. 6) have better elevated temperature properties than cast-aluminum alloy 195 and why is aluminum alloy 142 "overaged" for service as, for example, pistons in internal-combustion engines?

[1] Kalish and Dunkerley, *Trans. AIME*, **176**, 1948.

2. An alloy frequently used for high-temperature high-pressure steam lines (*e.g.*, about 500°C) contains 5% Cr, 1% Mo. After several years of service, graphitization is frequently found to have occurred. Explain why this would be conducive to brittle failures.

3. A failure is a failure; the structure (*e.g.*, a steam line) must be repaired to be used. Why does the engineer care whether it is a brittle or a ductile failure?

4. Why is it that structures constructed from stainless-steel sheet overlapped and properly spot-welded, do not usually require use of 18:8 stabilized with titanium or columbium?

5. Cast austenitic stainless-steel parts do not usually exhibit so good resistance to corrosion as wrought stainless-steel parts of the same composition. Explain why not, and estimate the effect of heat treatment in changing this relatively poorer resistance.

TABLE 13.2. SOME TYPICAL CREEP-STRENGTH DATA FOR SEVERAL OF THE ALLOYS EMPLOYED FOR HIGH-TEMPERATURE SERVICE*

Alloy and condition	At 1350°F		At 1500°F		At 1600°F	
	Stress, psi	Creep rate†	Stress, psi	Creep rate†	Stress, psi	Creep rate†
19-9DL forged, qu., aged....	15,000	1.8‡	6,500	8.2		
	12,000	0.8	5,000	0.4		
19-9DL cast, qu., aged.....	15,000	1.1‡				
	12,000	0.4				
N-155 (0.14% C) forged, qu., aged.....	15,000	1.1	10,000	2.5		
N-155 (0.32% C) forged, qu., aged.....	15,000	0.8	10,000	0.9		
	12,000	0.2	7,000	0.4		
S-590 forged, qu., aged.....	20,000	1.2	10,000	0.5	7,000	0.5
	15,000	0.4	8,000	0.2	5,500	0.1
S-816 forged, qu., aged.....	20,000	0.6	10,000	1.0	9,000	37.5‡
	15,000	0.3	8,000	0.8	5,500	0.6
Vitallium 0.2% C, cast, aged.	15,000	4.4	10,000	3.6	10,000	1.3
			7,000	2.0	7,000	0.4
422-19 0.4% C, cast, aged...	15,000	1.0	12,000	0.7	12,000	2.3
			10,000	0.4	11,000	0.2

* Cross and Simmons, "Symposium on Materials for Gas Turbines," ASTM, 1946. Discrepancies between 1500 and 1600°F data for Vitallium probably result from specimen and test variables.

† Creep rate in per cent per 10,000 hr measured at 1,000 hr.

‡ Specimen fractured.

TABLE 13.3. APPROXIMATE COMPOSITIONS OF SOME OF THE ALLOYS USED FOR HIGH-TEMPERATURE SERVICE

Common alloy designation	Type (Fig. 13.8)	% Cr	% Ni	% Co	% W	% Mo	% other	% C
18-8	..	18	8	..	...	...	.....	0.10
18-8 Mo	..	18	11	..	...	2.5	.....	0.10
25-20	..	25	20	..	...	...	.....	0.20
19-9 DL	A	19	9	..	1.2	0.4	0.4Ti, 0.4Cb	0.10
Gamma Cb	A	16	25	..	...	3	3.Cb	0.20
16-25-6	A	16	25	..	...	6	0.15 N_2	0.10
Hastelloy B	B	..	66	..	...	28	5Fe	0.1
Inconel W	B	14	75	...	...	...	2.5Ti, 0.6Al	0.1
N155	B	20	20	20	2	3	1Cb	0.15
N155	B	20	20	20	2	3	1Cb	0.40
S590	B	20	20	20	4	4	4Cb	0.40
S816	B	20	20	43	4	4	4Cb	0.40
Vitallium	C	28	2	Bal.	...	6	.....	0.25
Vitallium	C	28	2	Bal.	...	6	.....	1.00
N155	C	20	20	20	2	3	1Cb	1.00
422-19	C	28	12	Bal.	7.5	...	.....	0.40

NOTE. Unless otherwise specified, the balance of all alloys is iron with probably small amounts of Si, Mn, etc.

TABLE 13.4. TYPICAL STRESS-RUPTURE DATA OF SOME TYPICAL ALLOYS EMPLOYED FOR HIGH-TEMPERATURE SERVICE

Alloy	Condition	Stress to cause rupture in 1,000 hr				
		1200°F	1350°F	1500°F	1600°F	1700°F
18-8	Wrought, qu., aged	11,500	7,800	3,500	2,700	
18-8 Mo	Wrought, qu., aged	25,000	14,000	7,000	4,000	
19-9DL	Wrought, qu., aged	37,000	18,000	10,000	7,500	
GammaCb	Wrought, qu., aged	36,000	18,000	11,000	8,000	
16-25-6	Wrought, qu., aged	38,000	19,000	10,000	7,000	
Inconel W	Wrought, qu., aged	38,000	16,500			
N-155	(0.15C) qu., aged	38,000	22,000	13,500	9,500	
N-155	(0.40C) qu., aged	.....	24,000	16,500	10,000	5,000
S-590	Qu., aged	42,000	25,000	15,000	10,000	5,500
S-816	Qu., aged	.....	31,000	18,000	10,000	6,000
Vitallium	(0.2C) cast	44,000	27,000	16,000	13,000	10,000
Vitallium	(1.0C) cast	.....	.....	24,000	20,000	13,000
422-19	Cast	.....	37,000	22,000	14,500	11,500

CHAPTER 14

CAST IRONS

In a radio quiz show, a presumably well-informed inquisitor asked which of the following were alloys and which metals: copper, brass, bronze, cast iron, and aluminum. The contestant correctly named brass, bronze, and cast iron as alloys, only to be informed that he was wrong—cast iron was a metal! The engineer knows cast iron as a cheap structural material. It has always been that, but recently it has also become, with metallurgical control, an alloy that can be produced with high strength and certain particularly desirable properties not readily obtained with other alloys.

14.1 Fe:C:Si Phase Diagram

Cast irons are essentially pig iron from a blast furnace, remelted with additions of cast-iron scrap and, occasionally, of steel scrap and perhaps some ferroalloys to modify the composition to that finally desired. The original pig iron is usually made particularly for foundry use. Analyses of some typical grades are as shown in the accompanying table.[1]

Trade name	% C	% Si	% S	% P	% Mn
No. 1—soft	3.00	3.00	0.05	0.3–1.5	0.1–1.0
No. 1—foundry	3.25	2.50	0.05	0.3–1.5	0.1–1.0
No. 2—foundry	3.50	2.00	0.06	0.3–1.5	0.1–1.0
No. 3—foundry	3.75	1.50	0.065	0.3–1.5	0.1–1.0

It is evident that silicon as well as carbon is an important alloying agent. Rather than present the complex ternary phase diagram, a vertical section of a 2% Si content has been reproduced in Fig. 14.1. As shown in the two previous chapters, a third component changes the eutectic and eutectoid from an invariant reaction at a single temperature to a univariant reaction occurring over a range of temperatures, even

[1] Stoughton, "Metallurgy of Iron and Steel," McGraw-Hill, 1934.

under equilibrium conditions. The carbon contents of austenite at the eutectoid and the eutectic are reduced by the silicon from 0.8 and 1.7 to about 0.6% and 1.5% C respectively. The carbon content of the eutectic is also reduced from 4.25 to 3.65%. Since this reduction in eutectic carbon content is linear with silicon content over the range of interest here, it can be expressed as

$$\text{Eutectic carbon } \% = 4.25 - 0.30\ (\% \text{ Si})$$

This relationship is in common use as a means for determining the closeness to eutectic composition of a gray cast iron.[1]

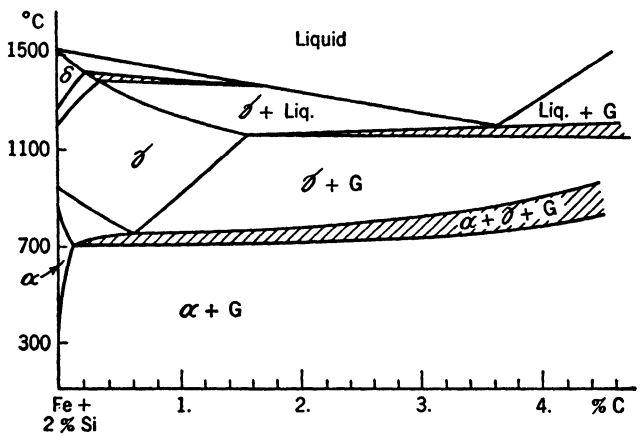

FIG. 14.1. A vertical section of the Fe : C : Si system at a constant 2% Si concentration. Cross-hatched fields are three-phase areas. (*Greiner, Marsh, and Stoughton.*)

14.2 Graphitization upon Solidification of Gray Cast Iron

When cast iron is melted, poured, and allowed to solidify in a mold and then broken, the fractured surface may be gray, white, or a mixture of the two. A sooty gray appearance of the fracture means that the structure consists of graphite flakes in a metallic aggregate. The graphite being weak, fracture progresses from flake to flake with ultimately a broken surface consisting mostly of graphite. If the fracture

[1] Rehder (*Trans. AFA*, 1947) shows that if it is assumed that one silicon atom ties up three iron atoms as Fe_3Si, then removing the proper quantity of Fe as Fe_3Si for a specific silicon cencentration leaves the carbon content of the eutectic in the remaining *free* iron at 4.25%. The Fe_3Si is not a separate phase but is in solution. Other data cited by Rehder support the postulation of Fe_3Si as a molecular compound in solution.

is white, then the structure consists solely of carbide and ferrite, and fracture has occurred along or through the brittle white masses of eutectiferous Fe_3C. A mottled color means that, in some places, graphite flakes are present and, elsewhere, eutectiferous carbide.

The main factors influencing the formation of graphite rather than Fe_3C upon freezing of the eutectic in an Fe:C alloy are

1. Solidification rate
2. Composition

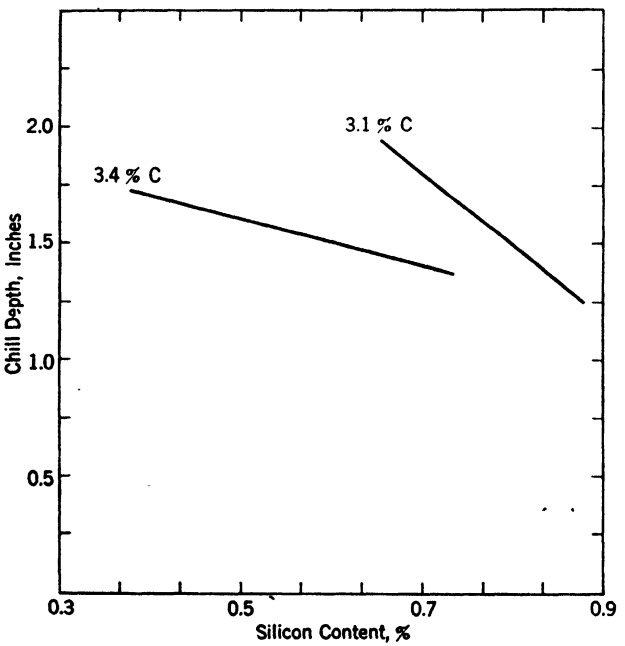

FIG. 14.2. Chill depth (depth of white cast iron from a chilled surface) upon solidification of a cast iron as diminished by increasing silicon content for two constant carbon contents. (*Schuz and Pohl.*)

Since the stable Fe:C system involves iron and graphitic carbon, it is reasonable that slow solidification favors the stable iron-graphite system and rapid solidification favors the metastable system, iron and iron carbide. Most iron foundrymen are familiar with the practice of using metal "chill" plates at certain parts of a sand mold. These plates induce rapid solidification at these points, which results in a hard wear-resisting structure of $Fe:Fe_3C$ eutectic. Elsewhere, slower freezing may result in a softer iron-graphite structure.

The most important elements present in cast irons of ordinary

composition are carbon and silicon, and a high content of either element or both is conducive to solidification of the iron according to the stable system, *i.e.*, with graphitic carbon. Figures 14.2 and 14.3 show that an increase in the concentration of either element, keeping the other constant, decreases the depth of white or carbidic iron when the alloy is

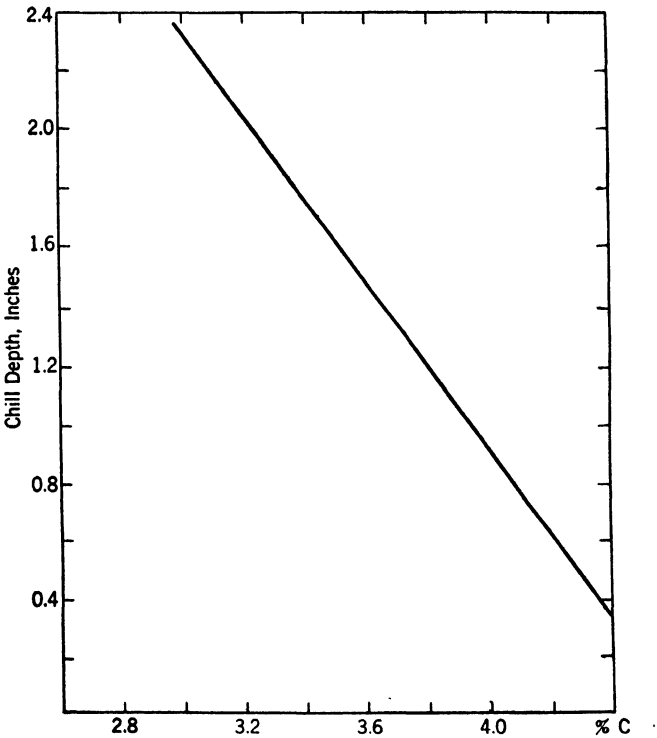

FIG. 14.3. Chill depth upon solidification of a cast iron as diminished by increasing carbon content for an approximately constant silicon content of 0.81 to 0.89%. (*Schuz and Pohl.*)

solidified under conditions of constant surface chilling (somewhat analogous to the Jominy end-quench for hardenability of steels). Other elements that promote graphitization if present in the cast iron are nickel, aluminum, titanium, zirconium, and copper.

Manganese is in itself a moderately strong carbide-forming element, and its presence in cast iron tends to stabilize carbide or prevent graphitization. For example, if just enough silicon is present to give a completely graphitic structure under specific controlled conditions, a slight increase in manganese may make the iron "mottled" (partly carbide in

the eutectic) or a large increase in manganese may cause the iron to solidify completely in the metastable or carbide condition. This effect is postulated on the absence of sulfur.

Sulfur chemically acts to stabilize iron carbide although it does not participate in the carbide formation. It has a very strong influence; it is ordinarily considered that each 0.01% sulfur is sufficient to neutralize the graphitizing influence of 0.15% silicon. However, sulfur has a strong affinity for manganese to form a manganese sulfide compound (page 52) which has little influence on carbide or graphite formation. Therefore, the first additions of sulfur to an iron with a moderately high manganese content have an indirect graphitizing tendency by removing the carbide-stabilizing manganese; vice versa, the first additions of manganese to a moderately high sulfur iron remove some of the sulfur from an active to an inactive role and thus promote graphitization. Although the sulfur content of foundry pig iron may be in the vicinity of 0.05%, sulfur present in the coke enters the iron with which it is in contact. This may result in a considerable increase in sulfur content when high-sulfur coke is used and, in setting up a furnace charge, necessitates a compensating adjustment in silicon or manganese contents.

Phosphorus chemically acts to promote carbide formation. Physically, it forms a phosphide eutectic with a melting point below that of iron and carbon. This causes the $\gamma + Fe_3C$ eutectic to solidify over a temperature range which increases the critical time available for silicon to promote graphitization. With moderately low phosphorus contents, the physical effect predominates and graphitization is encouraged, but large amounts of phosphorus cause it to act chemically as a carbide stabilizer.

Gaseous elements, particularly hydrogen and oxygen, may enter cast iron during melting and affect the cast structure. Hydrogen seems to stabilize carbides (Boyles[1]) and, when combined with oxygen as steam or moisture, is quite active in preventing graphitization during solidification but does not seem to have any effect on graphitization of the solid iron. Oxygen, as iron oxide, seems to promote graphitization during solidification and retard the process in the solid alloy[2] (during malleabilizing, page 444).

Of the *alloying elements*, nickel, which like silicon dissolves completely in ferrite, also acts as a graphitizer while the carbide-forming elements, specifically chromium and molybdenum, tend to stabilize the carbide phase. Thus, by adding these elements in proper relative quantities,

[1] Boyles, The Structure of Cast Iron, *ASM*, 1946.

[2] Boegehold, *Trans. ASM*, **26**, 1084, 1938.

the graphitizing characteristics of the original unalloyed cast iron will be relatively unaffected. The desirable properties obtained by the addition of alloying elements will then be related to their effect on graphite flake size and on the transformation characteristics of the austenite present with graphite after solidification.

Graphitization has so far been used to refer to eutectic solidification, a choice between one of the two following eutectic reactions:

(1) Liquid $\rightarrow$ austenite + Fe_3C

or

(2) Liquid $\rightarrow$ austenite + graphite

A third possibility is that the reaction is according to the metastable system, *i.e.*, to γ + Fe_3C, with an almost immediate decomposition of the Fe_3C, *i.e.*,

(3) Liquid $\rightarrow \gamma + Fe_3C$, then $Fe_3C \rightarrow \gamma$ + graphite

Some recent work by Eash[1] suggests that this last reaction is the origin of distinctly hypoeutectic structures such as Types D or E of the AFA chart, Fig. 14.4 (see also Micro. 14.7). The melting and casting conditions that lead to this type of structure include superheating and the resultant undercooling effect.

Graphite nuclei may exist in liquid cast iron and, if present at the time of solidification, they will promote solidification directly as graphite. Superheating destroys these graphitic nuclei and induces greater undercooling. Since the γ:Fe_3C eutectic temperature is a few degrees below the γ:graphite eutectic, the undercooled liquid solidifies according to the metastable system. However, a high silicon and carbon content induces immediate subsequent graphitization. Inoculation of the superheated iron may permit attainment of the normal and usually more desirable graphite structure Type A of Fig. 14.4.

Rapid solidification in general results in a finer grain size and a finer eutectic structure, and cast iron is no exception to this rule. Figure 14.5 shows the AFA graphite flake-size chart. The finest flakes, size 8, are not shown here but size 6 represents a structure where the longest flakes are from $\frac{1}{8}$ to $\frac{1}{4}$ in. long at $\times 100$. At the other extreme, size 1 represents a structure where the longest flakes are from 2 to 4 in. long

[1] Eash, *Trans. AFA*, **49**, 887, 1941.

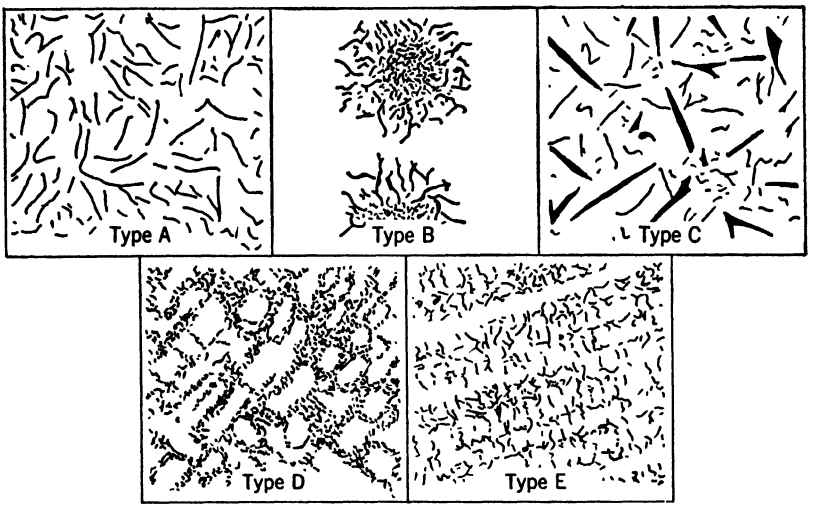

FIG. 14.4. Graphite flake types in gray cast iron according to joint recommendations of the AFA and ASTM: Type A—uniform distribution, random orientation; Type B—rosette groupings, randomly oriented; Type C—superimposed different flake sizes, random orientation; Type D—interdendritic flakes, random orientation; Type E—interdendritic flakes, preferred orientation.

at ×100. Mahin and Lownie[1] have shown that a given soft iron cast as 1.2-in. diameter bars showed a graphite flake size 4; cast as 2-in. diameter bars, the flake size was 3; cast as 6-in. diameter bars the flake size was 1.

14.3 Graphitization in the Solid State

An Fe:C alloy may solidify as a white, carbidic cast iron or as a gray graphitic iron. In either case, the major part of the structure is austenite, primary and eutectiferous. Upon slow cooling in a mold from the eutectic to the eutectoid temperature, the austenite will reject excess carbon. In a hypoeutectic cast iron, there are no, or comparatively few, austenitic grain boundaries since the structure consists of primary dendrites completely surrounded by interdendritic eutectic. However, the eutectic carbon exerts a powerful preferred nucleation effect, and the precipitation of excess carbon from austenite, as required by the A_{cm} line slope, results in the growth of eutectic Fe_3C in the white iron or of graphite in the gray iron.

[1] Mahin and Lownie, *Am. Foundryman*, January, 1946.

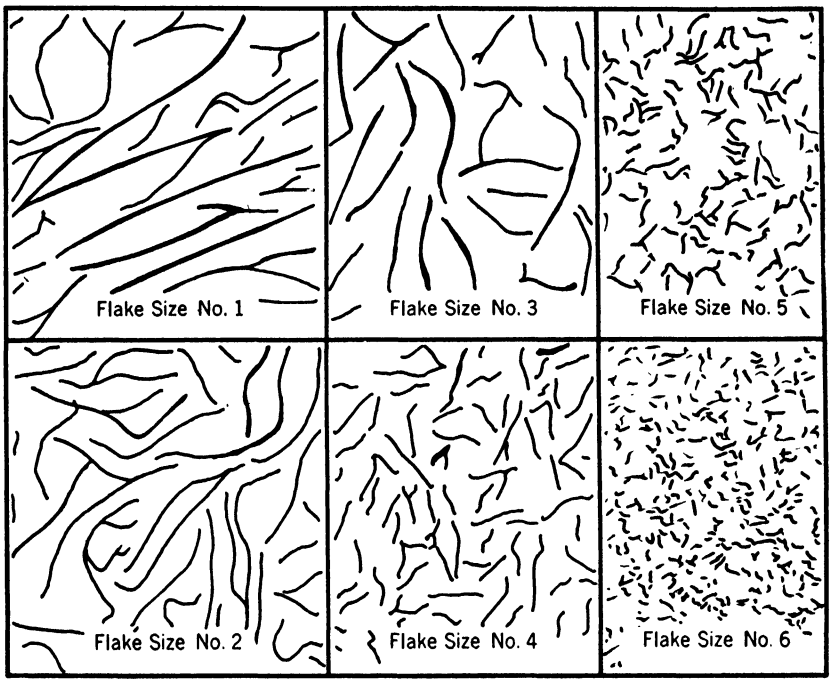

FIG. 14.5. Graphite flake size in gray cast iron according to joint recommendations of the AFA and ASTM (reduced 50% in reproduction). No. 1—longest flakes greater than 4 in. at × 100; No. 2—longest flakes 2 to 4 in. at × 100; No. 3—longest flakes 1 to 2 in. at × 100; No. 4—longest flakes ½ to 1 in. at × 100; No. 5—longest flakes ¼ to ½ in. at × 100; No. 6—longest flakes ⅛ to ¼ in. at × 100; No. 7—(not shown)—1/16 to ⅛ in. long at × 100; No. 8—(not shown)—less than 1/16 in. at × 100.

Upon cooling in air or in the mold to the eutectoid or A_1 temperature, the austenite will transform and, like the eutectic, two alternative eutectoid reactions are possible:

$$(1)\ \gamma \rightarrow \alpha + Fe_3C$$

or

$$(2)\ \gamma \rightarrow \alpha + \text{graphite}$$

The normal pearlite reaction (1) will generally occur in white cast irons, although in the eutectiferous austenite no pearlite may appear. Again, the massive eutectic Fe_3C exerts a nucleation effect and the eutectoidal Fe_3C may form integrally on the massive carbide leaving a structure of ferrite and eutectic carbide (see Micro. 14.4, page 448).

If it is a gray cast iron, the type of eutectoid reaction will depend on the carbon and silicon content, the possible presence of other alloying elements in the austenite and, of course, on the cooling rate. The specific composition may result in a completely graphitic eutectic structure but a regular pearlitic carbide eutectoid structure. Therefore, of a total 3.50% C, 2.70% may be in the form of graphite and 0.80% as Fe_3C in pearlite.

A fairly strongly graphitizing composition, *e.g.*, containing more silicon and less rapid cooling may cause the eutectoid to form ferrite and graphite. This may occur only at points of preferred nucleation adjacent to graphite flakes, with the eutectoidal graphite a part of the flakes and ferrite bands alongside the flakes. Elsewhere a pearlitic structure may be present so that of a total of 3.50% C, 3.10% may be present as graphitic flakes and only 0.40% as Fe_3C in pearlite. This structure would naturally be softer than a completely pearlite-graphite structure. Maximum softness is achieved by a composition and cooling rate that result in complete graphitization of the eutectoid carbide as well as that of the eutectic; therefore, a structure of ferrite (containing silicon in solid solution) and graphite flakes.

The discussion thus far is concerned with graphitization upon continuous cooling from the original solidification. It is possible, of course, to have a composition which would result in graphitization upon extremely slow cooling but which would form a completely carbidic or white cast iron upon ordinary cooling as of a sand casting. In this case, reheating of the casting and holding at an elevated temperature will result in a decomposition of the iron carbide. For example, a 2.50% C, 1.5% Si alloy would probably solidify as a white iron. Upon heating the casting to 900°C, the structure would be austenite with about 1.1% C in solution plus eutectiferous Fe_3C. This would, with time, graphitize as

$$Fe_3C \rightarrow 3Fe \text{ (austenite, 1.1\% C)} + \text{graphite}$$

There is a considerable difference in the structure of graphite formed in a solid alloy previously completely free of graphite and graphite formed in a solidifying iron or in an iron already containing flakes. Flakes are brittle and disrupt continuity of plastic ferrite, and their edges constitute sharp internal notches. Graphite formed by the above reaction with no flakes present grows in all directions, thereby forming a nodule. A nodule disrupts the ferrite much less and greatly diminishes

the internal notch effect. Therefore, the alloy with nodular graphite is malleable and shows some ductility while, with flake graphite, it is fairly brittle.

Cooling from the graphitizing temperature of about 900°C again permits carbon to separate from austenite on to the nodules already present. At the A_1 temperature, very slow cooling or a strongly graph-

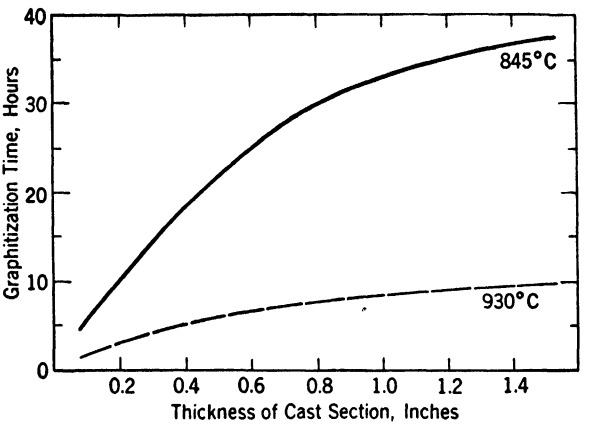

FIG. 14.6. Effect of annealing temperature and prior solidification rate, *i.e.*, thickness of cast section, on the time for complete graphitization of a white cast iron at two annealing temperatures. (*Schneidewind, Reese, and Tang.*)

itizing composition will result in a graphitic eutectoid reaction with the eutectoidal graphite forming on the nodules already present. Faster cooling or a less graphitizing reaction can give a pearlitic eutectoid and a final structure of graphite nodules in pearlite.

The factors affecting the rate of graphitization of a white cast iron are

1. Basic composition, particularly carbon and silicon.
2. Rate of cooling of the original casting upon solidification. The finer grain size and eutectic structure of a more rapidly solidified iron give more interfacial surfaces for the initiation of graphitization (Fig. 14.6).
3. Rate of heating to the annealing or graphitizing temperature.
4. The temperature of annealing (Fig. 14.6).
5. The atmosphere in the annealing furnace.
6. Hereditary effects from the original pig iron or the melting process. This includes compositional effects not ordinarily measured, *i.e.*, the oxygen and hydrogen contents, etc.

14.4 Microstructures

Although white cast irons offer no difficulties to the metallographer, gray cast irons are anything but easy to polish. Until quite recently, most micrographs of gray cast iron showed apparently great quantities of graphite as thick flakes. The thickness of the graphite was exaggerated by polishing with the usual long-napped cloths. The cloth fibers dug out soft graphite, and the abrasive particles cut the resulting narrow channels to broad valleys. Polishing with short-napped cloths such as silk results in more scratches but gives a truer picture of the size and distribution of graphite flakes. Lead- or paraffin-covered laps with carefully sized abrasive particles embedded in the surface can prepare the surface prior to final polishing so as to minimize the time required on the cloth.

Even with the best polishing technique some graphite flakes will apparently be quite wide or thick, *e.g.*, specimen Type B of the chart in Fig. 14.4. In these cases, the graphite flake must be nearly parallel to the surface of polish.

The charts prepared by the AFA, Figs. 14.4 and 14.5, offer standards for description of graphite flake distribution and size. The charts and comparisons with them are made on unetched specimens at $\times 100$. Graphite flakes show up better against the white polished matrix before etching; otherwise black pearlitic areas may diminish contrast between graphite and matrix.

14.5 Properties of Cast Irons

Structurally, the matrices of gray cast irons resemble steels in that they contain varying proportions of ferrite and pearlite. The ferrite may be a little stronger than that of most carbon steels because of the dissolved silicon, but the pearlitic part of the structure may be softer as a result of its somewhat greater coarseness. Overbalancing both of these factors is the weakening and embrittling effect of a relatively large amount (3% by weight corresponds to 12% by volume) of the soft, brittle graphite flakes that disrupt the continuity of the plastic matrix. The edges of the flakes are likely to be comparatively sharp, and each acts as an internal notch which, upon deformation, tends to initiate a crack in the plastic matrix. For this reason, gray cast irons break with a brittle fracture and, until the past decade, at stresses of only 20,000 to 30,000 psi. In recent years, strengths have been increased until around 60,000 psi is a common value. Some foundries have been pouring iron for several years with no test bars in the 60,000-psi class ever breaking below this value. There are classifications of 30,000, 40,000, 50,000, and

(*Continued on page* 456)

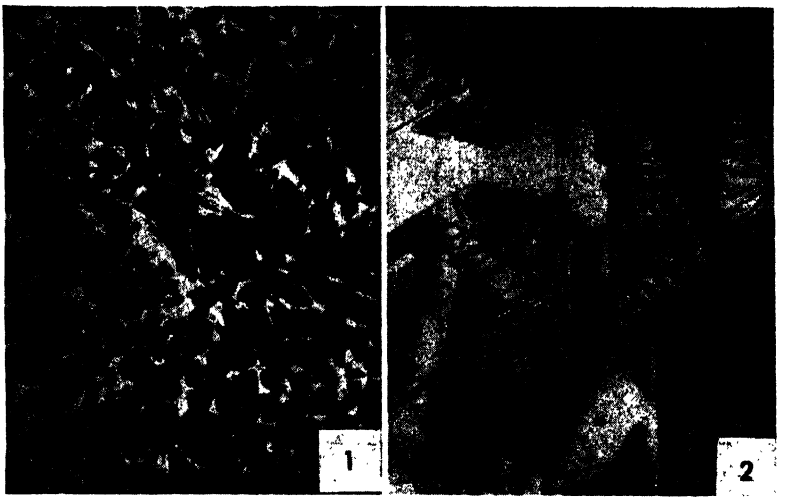

Micro. 14.1. Commercial white cast iron (about 2.50% C); ×50; Picral etch. This specimen shows a hypoeutectic structure in which the gray background was chiefly primary austenite but transformed on later cooling to pearlite. The white masses are iron carbide. The eutectic structure of γ and Fe_3C is not very evident since the austenite part of the eutectic was alongside, and indistinguishable from, the primary austenite. Although white iron is ordinarily considered to be brittle, hard, and unmachinable, this structure is sufficiently low in carbide for the pearlite to be nearly continuous. The iron showed a slight ductility in the tension test and could be machined.

Micro. 14.2. Same white iron; ×1,500; Picral etch. At a high magnification, details of the pearlitic background and massive carbides become readily visible. Although in this hypoeutectic structure three different forms of carbide should exist, specifically, eutectic Fe_3C, Fe_3C separating out from γ along the A_{cm} line, and eutectoid carbide, only the first and last are visible. Presumably, Fe_3C separating out from austenite along the A_{cm} line formed on the massive, eutectiferous Fe_3C already present rather than at the austenitic boundaries. This form of preferred nucleation, or in reality, growth of present large nuclei, is rather frequently encountered in all alloys where a comparable condition may exist. Here, the eutectoid reaction was normal, and all of the eutectoid carbon apparently formed pearlitic carbide.

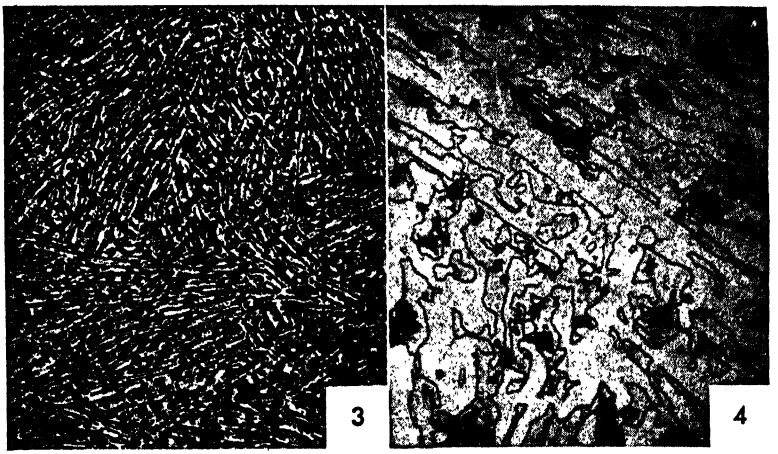

Micro. 14.3. High-carbon white cast iron (about 4.0% C); ×50; Picral etch. This structure appears to be completely eutectiferous, showing only ledeburite. Again the white structure is carbide, appearing in this chill-cast structure in a needlelike form. The background was austenite as the eutectic solidified.

Micro. 14.4. Same white iron; ×800; Picral etch. At a higher magnification, details of the ledeburite structure become evident. The white carbides stand in relief with ferrite in between, since the intervening austenite did not normally transform to pearlite. The carbide forming from austenite along the A_{cm} line built up on the eutectiferous carbide masses, as in Micro. 14.2, but in addition, carbide from the pearlite reaction also tended to form on the Fe_3C already present. In some areas, this has resulted in a completely abnormal structure (see page 291) where only ferrite and massive carbides are visible while, in other places, some small areas of fine pearlite (dark masses) are visible.

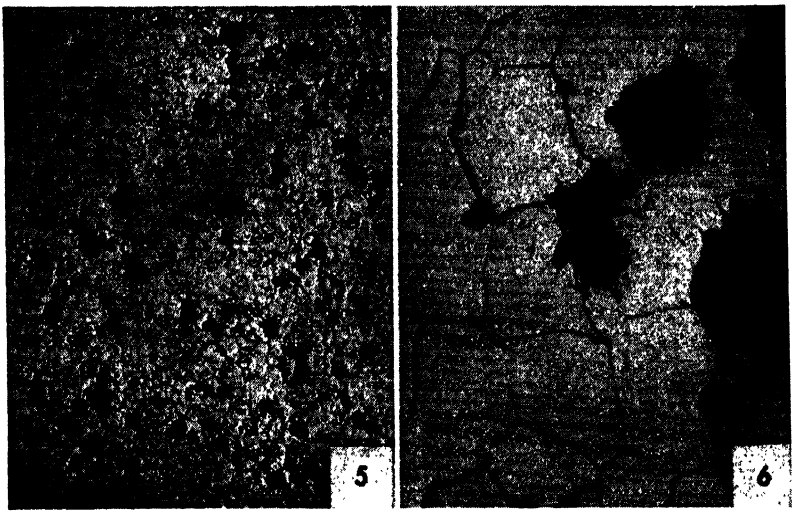

Micro. 14.5. Standard malleable cast iron; ×50; Nital etch. If the white cast iron of Micro. 14.1 were heated long enough below the eutectic temperature, the carbide would decompose to graphite by the reaction $Fe_3C \rightarrow 3Fe\ (\gamma) + C$ (graphite). The graphite forming in a solid structure grows in all directions from nuclei in the carbide to form *nodular graphite* or *temper carbon* particles in austenite. Very slow cooling through the eutectoid, with sufficient amounts of dissolved silicon present, causes the eutectoid reaction to be in the form, $\gamma \rightarrow \alpha + C$ (graphite), and this additional graphite forms on the nodules already present. The end structure shown here consists of a continuous, moderately fine-grained ferrite containing irregular, randomly dispersed graphite nodules.

Micro. 14.6. Malleable cast iron; ×300; Nital etch. At a higher magnification, details of the ferritic matrix and nodular (or "temper") carbon particles are more evident.

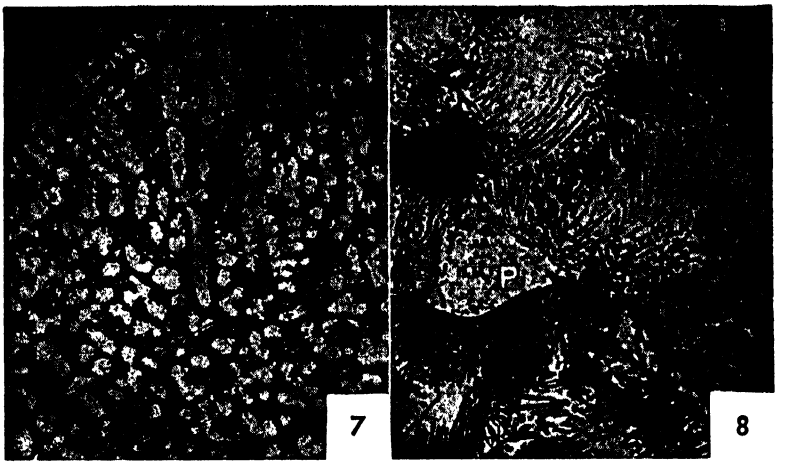

Micro. 14.7. Chill-cast gray iron from an automotive hydraulic brake cylinder; ×100; Nital etch (very light). This structure is recognizable immediately as hypo-eutectic, with primary dendrites surrounded by a continuous eutectic structure. The primary dendrites were austenite, which subsequently transformed to pearlite, but the light etch has not darkened the pearlitic structure. The black eutectic structure is of pearlite (γ during the eutectic reaction) and very small graphite flakes. The eutectic structure is fine as a result of the chill casting. In order to chill-cast the iron and still obtain a graphitic structure, the silicon content must be quite high, with manganese and sulfur low or balanced.

Micro. 14.8. Chill-cast iron (Micro. 14.7) at ×1,000; light Nital etch. This high magnification shows the pearlitic character of the primary dendrites (which solidified as austenite) and the very fine (as compared to normal cast iron, Micro. 14. 9) graphitic carbon flakes. The white structure *P* with small holes is a eutectic structure of iron phosphide, called *steadite.*

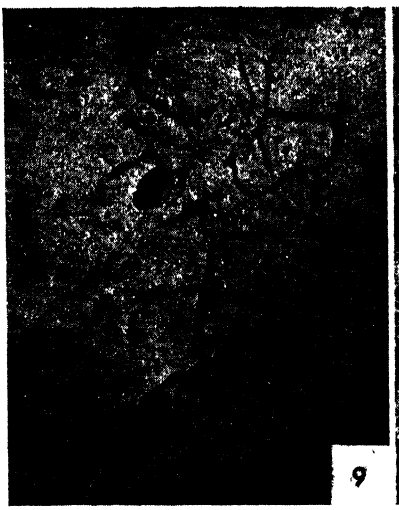

Micro. 14.9. Gray cast iron at ×50; as polished with no etch. The graphite flake structure of ordinary cast irons is most readily visible in the unetched structure since the black "grooves" representing the graphite show up best against a white background. The size of these flakes is evidently about twenty times those of the chill-cast iron (Micro. 14.8).

Micro. 14.10. Gray cast iron at ×50; light Nital etch. This is a somewhat different iron from Micro. 14.9, having more and larger graphite flakes. The white area adjacent to the graphite is generally ferrite (with silicon, etc., in solid solution). Light-gray areas are pearlite.

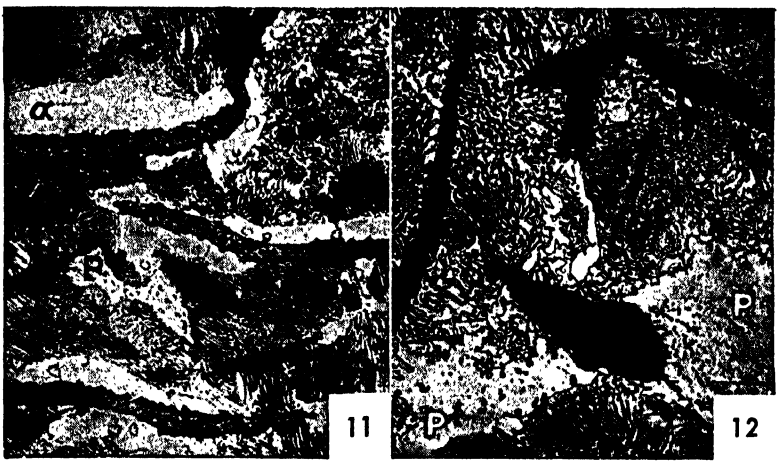

Micro. 14.11. Soft gray cast iron at ×300; Nital etch. At this high magnification, the pearlitic part of the background of the iron is resolved. The pearlite in ordinary moderately soft cast irons is coarser than in steels, because of slower cooling through the critical temperature and the higher silicon content and coarser grain size of the austenite. The white structure adjacent to the graphite is ferrite (α) and, in addition, some steadite is visible (P).

Micro. 14.12. Relatively hard roll iron at ×300; Nital etch. This iron is used for cast-iron rolls employed in rubber mills. It is noticeably harder and more abrasion resistant than ordinary soft iron, for two reasons: there is more carbon in the combined form as pearlite, and there is a much higher phosphorus content and the iron contains large areas of the hard, white phosphide eutectic (marked P).

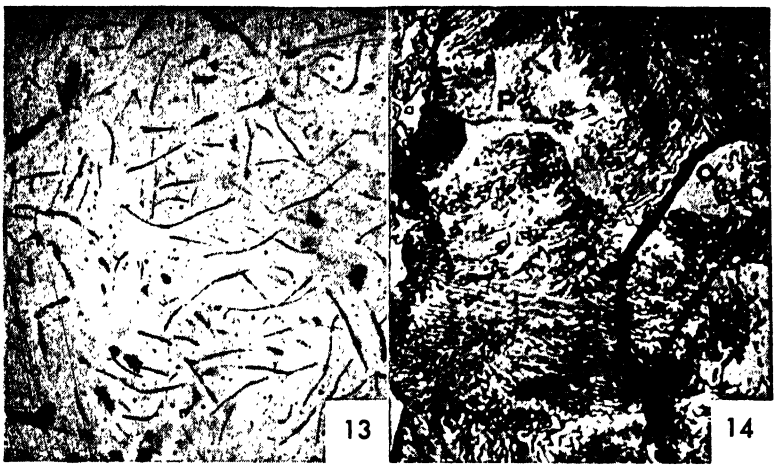

Micro. 14.13. High-strength gray cast iron; ×100; unetched. This iron with a low Si content was melted in a special (Bracklesburg) furnace and then treated with powdered ferrosilicon just before casting. The structural effect is similar to that of sodium added to Al:Si alloys before casting (see page 133), but the mechanism is different. Here, the total silicon content is sufficient to cause the iron to be graphitic and relatively free from large carbides, even in thin sections, and the addition of the ferrosilicon at the proper time provides many more nuclei for solidification with a resultant refinement in structure. The size of these graphite flakes should be compared with those of Micros. 14.9 and 14.10.

Micro. 14.14. High-strength cast iron (Micro. 14.13) at ×1,000; Nital etch. The matrix structure of the high-strength iron is almost completely pearlitic although a few small ferrite areas are visible (α), as well as some steadite, (P).

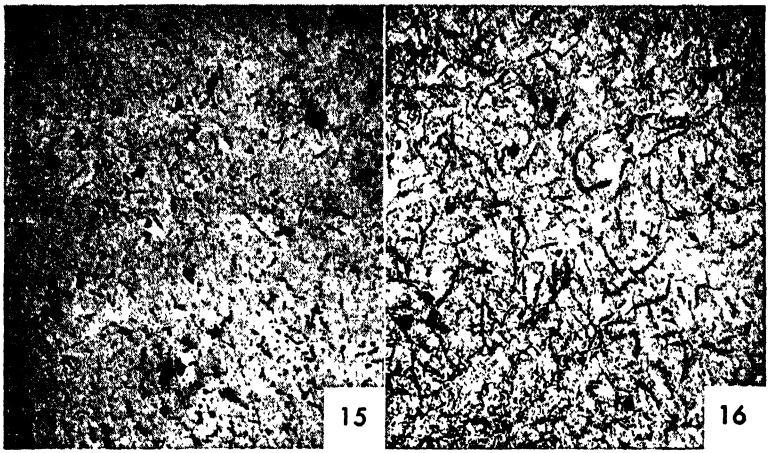

Micro. 14.15. High-strength alloy (Ni, Cr, and Mo) cast iron; ×100; unetched. Additions of nickel, chromium, and molybdenum, with the carbide-stabilizing effect of the chromium and molybdenum balanced by the graphitizing effect of nickel and silicon, result in a greater refinement of graphite flakes than can be achieved by Fe:Si inoculation. Note in this structure that the graphite shows an interdendritic form of dispersion. This iron at ×1,000 has a structure very similar to that of Micro. 14.14; pearlite, a few ferrite areas, and fine graphite.

Micro. 14.16. Alloy cast iron; ×50; Picral etch. This iron has less alloy content than Micro. 14.15; it contains 3.0% C, 1.70% Ni, and 0.6% Mo (trade name, Ni-Tensyl). The graphite flake size is decidedly smaller than ordinary gray iron, while the matrix is a eutectoidal ferrite-carbide aggregate.

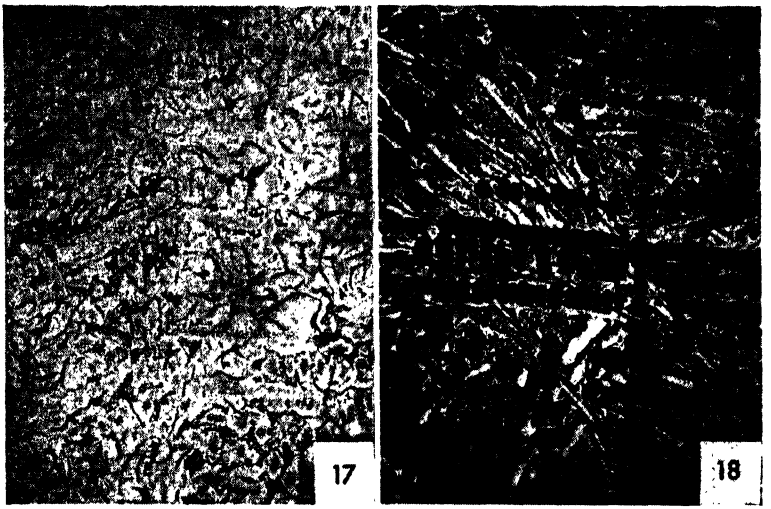

Micro. 14.17. Heat- and corrosion-resistant alloy cast iron; ×50; Nital etch. This is a highly alloyed austenitic iron of the following composition: 2.75% C, 14% Ni, 2% Cr, 6% Cu (trade name, Ni-Resist). Variations in shading of the austenite (from white to light brown) show coring in the solid-solution austenitic dendrites. The small, bent, black streaks are graphite flakes, and the fine eutectiferous network represents carbides.

Micro. 14.18. Abrasion-resistant alloy cast iron (Ni-Hard); 3.5% C, 4.5% Ni, 1.7% Cr; ×100; Nital etch. This structure is also clearly hypoeutectic with primary dendrites surrounded by a fine eutectic structure. The highly alloyed austenite is so sluggish in transformation that it becomes martensitic at ordinary cooling rates in the mold after casting. In addition, the eutectic structure contains an alloy carbide. The aggregate is hard and unmachinable; it can be cut only by grinding.

60,000 psi cast iron. The higher strengths have been achieved in two ways; by greatly refining the graphite flake size (*e.g.*, Micros. 14.13 and 14.15) and by attaining a fine, completely pearlitic matrix. Success in achieving this structural condition is dependent on close control of the chemical composition of the iron and of pouring temperatures.

Aside from strength properties, gray cast irons have several other features that fit them particularly well for certain applications. The relatively low melting point and ready castability of irons make them relatively cheap, although, naturally, costs will be increased if high-strength specifications require laboratory control and use of alloying elements. More important in some applications is the fact that the internal structural discontinuities offer sites for the local dissipation of vibrational energy. This is equivalent to saying that gray cast irons have a high internal friction or damping capacity. Used as a base for machinery or any equipment subject to vibration, the structure of the iron permits the vibrations to be absorbed internally. Machine bases, or piano frames, could be made of welded steel assemblies, but these assemblies would not so readily absorb external vibrations and, at frequencies approaching the natural vibration period of the structure, the amplitude of vibration might well increase to the point where the structure would break by fatigue stressing. The great importance of this feature of cast irons is just coming to be recognized and more fully utilized, *e.g.*, in the Ford cast crankshaft.

Malleable iron castings are of intermediate cost and properties between gray iron and steel.[1] The nodular form of graphite, or temper carbon, does not interrupt the continuity of the ferritic matrix, and the aggregate may show strengths of around 55,000 psi combined with elongation values in the vicinity of 12 to 18%. Two fairly recent developments have been of engineering significance. Closer control of composition and pouring temperatures (sometimes achieved by the use of special melting furnaces) has given a metal that is consistently white in the as-cast form and yet quickly graphitizes upon reheating. This possibility of quicker graphitization has been successfully utilized by the development of new annealing furnaces in which castings need not be packed in an insulating carbonaceous material (to protect them from excessive scaling) and require a week to heat, to hold, and to cool from

[1] In many applications, pearlitic malleable cast iron and cast steel may be used interchangeably, and in these cases, malleable iron enjoys a competitive advantage. Although its heat treatment may be more expensive, there is a lesser cost from (1) scrap lost in risers and (2) cost of removing risers (the risers can be knocked off the original white iron castings with a hammer while they must be cut from steel castings).

the annealing temperature but in which the malleabilizing treatment can be completed in 48 hr or less. Uniform results can be achieved only by uniformity of heating during annealing, a requirement best met by long, continuous furnaces of small cross section. A second development has been of malleable cast iron containing temper carbon nodules in a pearlitic rather than a ferritic matrix. The pearlitic structure enables the iron to show strengths in the vicinity of 70,000 to 80,000 psi and good elongation, 6 to 12%. Some foundries call this material *semisteel*, but the disrepute of this meaningless word has led to the use of the more exact descriptive term *pearlitic malleable*.

Heat treatment of cast irons will not affect the graphite structure, at least not that representing carbon in excess of the amount soluble in austenite. (This is the reason that malleable cast iron must be entirely "white" as cast; graphite forming as flakes at a high temperature cannot be changed to the nodular form.) However, reheating of pearlitic malleable or gray cast iron above the critical temperatures develops austenite of eutectoidal carbon content. This austenite will behave on cooling in a manner nearly identical to that of a eutectoid steel (see Chap. 10); it may be quenched to martensite and then tempered, it may be "austempered" to hard but tough bainite structures, it may be air-cooled to develop a finer pearlite than was originally present, or it may be very slowly cooled to effect a more complete graphitization and, consequently, a softer structure.

There are several cast irons for special applications. A high silicon cast iron (trade name, Duriron) resists sulfuric acid attack at all concentrations as well as many other chemicals. The martensitic cast iron (Micro. 14.18) shows particularly high resistance to wear and is applicable for many uses in which white cast iron or Hadfield manganese steels do not show sufficient service life.

QUESTIONS

1. What structural characteristics and consequent properties may be developed by the use of "chills" on the treads of freight-car wheels during casting of a normally gray iron?

2. What factors are responsible for the widespread use of cast-iron pipe for water or gas conduction?

3. In what respect might the structure of gray cast iron be considered suitable for use as a bearing material?

4. Cast-iron brake linings for busses may show cracks after hard service, in which localized frictional heat momentarily raises the surface layer to a temperature well above the critical (A_1) point. Where would the cracks be likely to appear in relation to the surface structure? What other features might be expected to be visible in this surface structure?

5. Compare the normal and optimum mechanical properties of unalloyed gray cast iron, malleable cast iron, and cast steel.

6. If chromium or molybdenum is added to iron, why is nickel usually added also and in somewhat greater amounts?

7. Compare a Ni:Mo cast iron with plain gray iron with regard to (*a*) machinability, (*b*) strength, (*c*) structure, (*d*) applications.

REFERENCES

MERICA, Progress in Improvement of Cast Iron and Use of Alloys in Iron, *Trans. AIME*, **125**, 13, 1937. "Metals Handbook," Cast Iron, Malleable Iron, Pearlitic Malleable Iron.

CHAPTER 15

MONOTECTICS; SINTERED METAL POWDERS

There are many binary alloy systems in which the component metals do not show complete mutual solubility in the liquid form. Examples of this type include Fe:Sn, Cu:Pb, Ni:Pb, Cu:Cr, Cu:Co, Cu:Mo, Cu:W, Cu:S, Cu:Se, Cu:Te, Ag:Ni, Ag:W, Ag:Mo, Al:Cd, Al:Pb, Zn:Pb, Zn:Bi. In a few of these, such as the Ag:Mo system, the metals seem to show almost no liquid solubility. In most of the others, however, the two liquid metals show some mutual solubility at temperatures near the melting point of the more refractory constituent and form a homogeneous liquid if the temperature is increased to a sufficiently high value.

15.1 Monotectic Phase Diagram; Ag:Ni

The Ag:Ni phase diagram (Fig. 15.1) shows two horizontal lines, at 960.5°C (0.5° above the melting point of silver) and at 1435°C (17° below the melting point of nickel). At 960.5°C, an α solid solution consisting of almost pure silver (containing only about 0.1% Ni) forms by a peritectic reaction between liquid silver and the $\alpha_{(Ni)}$ phase. The peritectic concentration is so near to pure silver in composition that it cannot be shown in the figure. At 1435°C, a liquid of 95% Ni reacts to form a small amount of liquid containing about 97% Ag and a large amount of the $\alpha_{(Ni)}$ phase, containing 4% Ag in solid solution. The reaction, written in the form

$$\text{Liquid}_{(95\%\ \text{Ni})} \rightarrow \text{liquid}_{(3\%\ \text{Ni})} + \alpha_{(Ni)}$$

is called a *monotectic*. It consists, essentially, of a considerable change in the composition and proportionate amount of a liquid phase, occurring at a constant temperature, as a result of the rejection of a solid phase. Above the monotectic horizontal, there is always a dome-shaped field (not reproduced completely in the figure), and alloys at temperatures and concentrations within this field consist of two liquid phases. Since there is usually a considerable difference between the specific gravity of

the two liquids, they tend to separate into two liquid layers in a manner similar to oil and water. Thus, binary alloys of compositions under the "dome" cannot usually be melted and cast, particularly in large sections, without serious liquid segregation, which results in a nonuniform distribution of the ultimate solid phases. Alloys of this type are success-

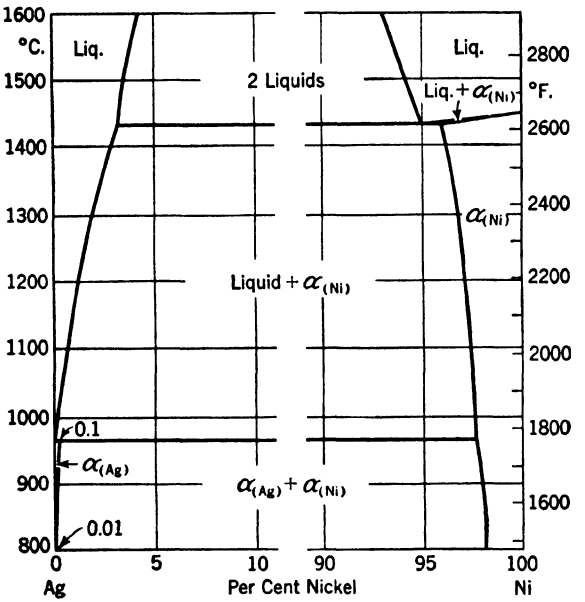

FIG. 15.1. Phase diagram of the silver-nickel system showing a monotectic at 1435°C and a peritectic at 960.5°C.

fully produced by mixing metal powders and sintering at a temperature under that of the monotectic (although this is not the only field of application of powder metallurgical methods).

15.2 Pressing of Metal Powders

The compacting of a metallic powder into a desired shape may be accomplished by pressing at room temperatures in a die and then sintering or by pressing at an elevated temperature. Variables in the pressing process are

1. Metal powder particles: sizes, shapes, and hardness
2. Pressing temperature, time, and pressure

3. Lubrication, to permit flow of particles along die walls and past each other

Metal powders may be produced by chemical, mechanical, or thermal processes, and the properties of a given metal powder will depend somewhat on its origin. However, all particles are usually uneven and are presumed to touch opposing surfaces only at points even after considerable compression. In addition, the particles may be covered with oxide films that interfere with bonding, upon compression, to a degree depending on the thickness of the oxide film.

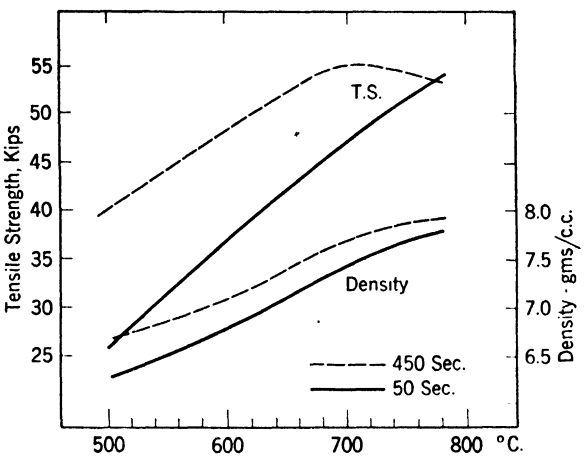

FIG. 15.2. Tensile strength and density as a function of the hot-pressing temperature of electrolytic iron for two different times of pressing. The pressure was 10 tons per sq in. and the atmosphere hydrogen. (*Henry and Cordiano, AIME*, **166**, 520, 1946.)

Fine powders require higher pressures to produce a given strength and density. Generally, mixed powder sizes give higher densities than any uniform particle size. Irregular shapes give the densest compacts, flakes the least dense.

Harder particles, lower pressures, and lower temperatures all contribute to weaker and less dense pressed shapes. The effect of the temperature and time of hot pressing of electrolytic iron powder upon the tensile strength of the compact is shown by the data of Fig. 15.2. These data indicate that hot pressing in a hydrogen atmosphere may give a product that is almost as dense and even stronger than pure iron produced by normal methods. However, expensive equipment is required to hot-press in hydrogen on a commercial scale, and it is usually simpler to press at room temperature and then separately heat in

hydrogen to obtain true bonding of the particles. However, hot pressing produces a compact of higher density than when like pressure and temperature are applied separately.

Cold-bonding or cold-welding upon pressing at room temperatures may be achieved to a certain degree, sufficient to enable the compacted shape to be removed from the die and placed in a sintering furnace. The pressures involved are frequently quite high, and if the unit pressure, for example, is 25 to 50 tons per sq in., a very large press is required to produce a shape of any size. Large presses are expensive so, again, an economic factor is involved in the selection of a hot- or cold-pressing process.

The flow of particles during compression is facilitated by lubrication. As pressure is applied to the top, movable plunger, it is transmitted from particle to particle. The effective pressure on particles near the bottom, fixed plunger, will be less than that on particles near the top, the loss resulting from friction.[1] Densities in different parts of the object will vary in accordance with the local pressure. Since pressure is transmitted by particles, interparticle lubrication is a significant variable. Side-wall die lubrication is of greater importance, however, except in thin, wide compacts. The lubricant used may be of the type that would volatilize upon sintering, *e.g.*, stearic acid, or it may be something that will alloy with the metal, specifically, graphite with iron powders.

15.3 Sintering of Metal Powders[2]

Upon heating of an aggregate of metal powder particles, the first increase in adhesion of particles or of strength of the compact is at about 150 to 200°C except for refractory metals such as tungsten and molybdenum. Presumably this is associated with the removal of adsorbed gases. When a compact is heated gradually from room temperature to just below its melting point, a second marked change occurs at approximately the recrystallization temperature of the major metal present. In the absence of insoluble impurities and porosity, rapid grain growth across particle interfaces begins at a temperature approximately two-thirds of the melting point (three-fourths of the absolute temperature of melting). Excessive grain growth can result in less strength even though density of the compact continues to increase.

At high sintering temperatures, pores tend to diminish in size and disappear with long sintering times. This may not occur at temperatures in the recrystallization range because of gas evolution at internal

[1] Kamm, Steinberg, and Wulff, *Trans. AIME*, **171**, 439, 1947.
[2] Rhines, *Trans. AIME*, **166**, 474, 1946.

surfaces, *i.e.*, into the pores. Actually, a decrease in density or growth of the compact is frequently observed at the recrystallization temperature.

The diminution in size of pores at high temperatures must be caused by lateral growth of the initial "point bonds" or localized welds. This lateral growth depends upon diffusion and plastic flow within the

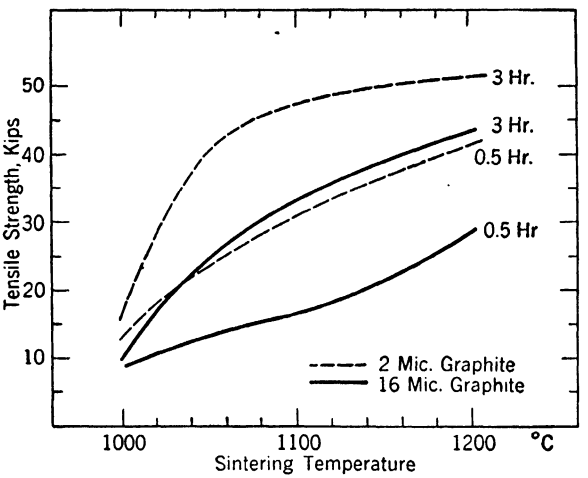

FIG. 15.3. Tensile strength as a function of sintering temperature and time for compacts of electrolytic iron powder plus 1% graphite, using two different sizes of graphite powders. The sintering atmosphere was hydrogen and the compacts were cooled slowly in the hydrogen. (*Squires, Trans. AIME*, **171**, 473, 1947.)

compact. The usual tendency for the system to lower its internal energy by a reduction in surface area would supply the force tending to sinter the mass of particles. The extent of the force will vary with, among other things, the shape of the pores or their radii of curvature.

In many cases, unlike powders are compacted and sintered. Here, sintering must produce not only bonding but also diffusion toward a homogeneous alloy structure. For example, Fig. 15.3 gives data on sintering of iron-graphite powders and, in this case, the final compact was a steel. The graphite lubricant and alloy agent dissolved completely in the austenitic iron powder during sintering.

15.4 Microstructures

The preparation of pressed and sintered objects for metallographic examination involves no unusual difficulties except in cases of extreme

porosity. This latter condition is characteristic of cold-pressed objects prior to sintering. Such structures can be polished by employing laps with very short-napped cloths. However, etching in the normal manner is almost impossible since the etchant will tend to penetrate the compact and, after drying, ooze out to stain the surface. In these cases, heat etching in a vacuum may give satisfactory results although it will tend also to change the structure.

Polishing of carbide compacts cannot be accomplished with the usual abrasives since the carbide particles are harder than all abrasive particles except diamond dust. Therefore, only diamond dusts or proprietary compounds containing this abrasive will be satisfactory. The micrographs in this section, together with pertinent information regarding preparation of the specimens, were supplied by Professor G. J. Comstock of the Stevens Institute of Technology.

15.5 Properties and Applications

The Ag:Ni and Ag:Mo alloys shown here cannot be produced with the proper distribution of the two phases except by powder metallurgical methods. The alloys have particular application as contact materials in electrical circuit breakers and other similar uses. The silver, constituting the continuous phase, has a very high electrical conductivity and is present in amounts sufficient to prevent heating of the contacts under closed-circuit conditions. At the same time, the silver areas are so small that, even though they fuse in spots, the contact-opening mechanism can readily break these small, fused areas. The second phase of a refractory metal prevents fusion of large areas under the action of an accidental electrical arc.

The tungsten carbide material represents another specific structure that cannot be obtained by ordinary melting and casting procedures. This alloy can be melted and cast without segregation, but the brittle tungsten carbide phase solidifies to form a *continuous* structure. Thus, the aggregate is too brittle to be used in the cast form, and the structure cannot be hot-worked or modified by heat treatment. When powders are mixed and sintered, the *cobalt* forms a practically continuous structure enveloping each carbide particle. It is possible to modify the thermal conductivity and other properties of the sintered carbides by altering the amount or composition of the matrix cobalt. Other sintered carbides than tungsten have been produced by similar techniques and successfully employed as cutting tools (*cf.* page 404).

The other structures reproduced here are of alloys customarily prepared by normal metallurgical methods. However, powdered iron

(*Continued on page* 470)

Micro. 15.1. Alloy of 60% Ag, 40% Ni; ×1,000. Powders of the two metals were mixed in the specified proportions, pressed into the desired shape, and then sintered at a temperature slightly below the melting point of the silver. The gray irregular shapes represent the original nickel powder, while the continuous, dark matrix is the silver phase. (The relative areas of α_{Ni} and $\alpha._{Ag}$ shown in this small section are not representative.) Slow cooling from the sintering temperature permitted nickel, which had dissolved (up to 0.1%) in the silver, to precipitate as the α_{Ni} phase and caused the silver-rich phase to appear dark *except* for light areas adjacent to the nickel; here nucleation for precipitation was furnished by the nickel particles (an effect discussed in several previous sections, *e.g.*, *abnormal* steel structures).

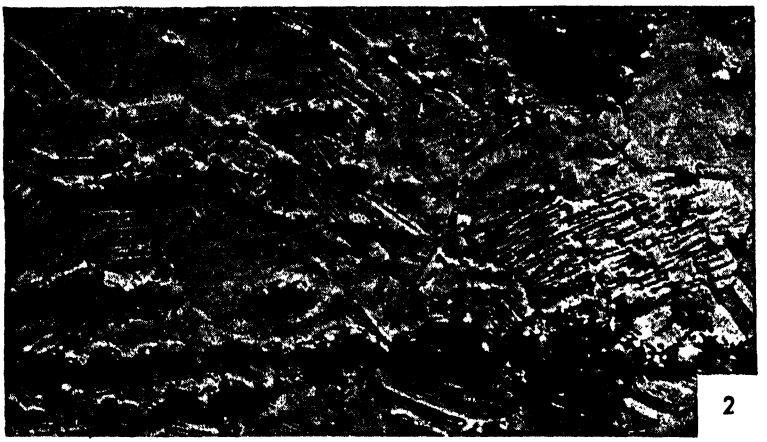

Micro. 15.2. Alloy of 60% Ag, 40% Ni; rolled; ×1,000. The continuous ductile silver matrix of the previous specimen permitted the specimen to be rolled, after which it was reheated to the sintering temperature and rapidly cooled. This micrograph of a section transverse to the rolling direction shows much less than the expected amount of nickel, perhaps because of segregation resulting from inadequate mixing of the powders. The harder, gray nickel particles stand in relief while the annealing twins in the silver matrix are evidence of the working and heating. The primary purpose of rolling the original sintered aggregate was to eliminate porosity and attain a sound, dense structure.

Micro. 15.3. Alloy of 60% Ag, 40% Mo; ×1,000. Powdered metals of these two components were mixed, pressed, sintered, rolled, and resintered. In this system, there is practically no mutual liquid solubility. The silver again forms a continuous ductile matrix phase, which permitted the sintered compact to be rolled without breaking. Twins in the silver phase again are evidence of the deformation and subsequent reheating. In addition, the elongated stringers of the gray molybdenum phase are evidence of deformation (*cf.* slag stringers in wrought iron, page 41).

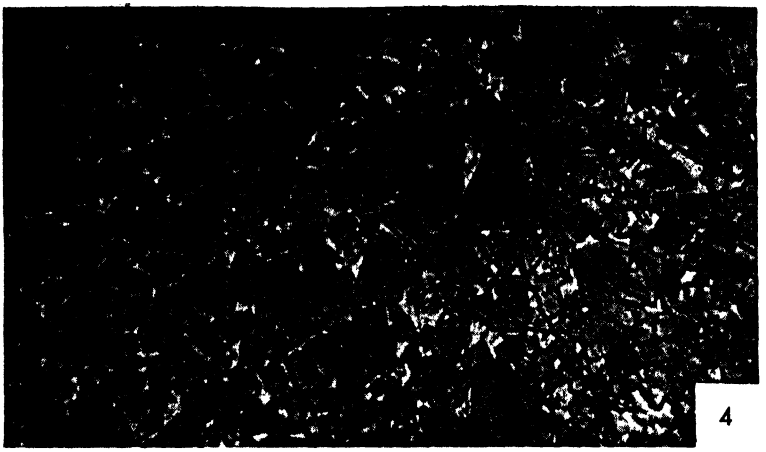

Micro. 15.4. Alloy of 94% tungsten carbide, 6% Co; ×2,000. Powders of the carbide (dark gray) and cobalt (light matrix) were mixed by grinding together in a ball mill for many hours. After grinding, the external shape of the carbide particles is quite different from that shown here; the milling of the brittle carbide resulted in a form characteristic of such materials, with little evidence of crystallinity. The milled powder mixture was then pressed to approximate final shape and sintered in a hydrogen atmosphere at a temperature above the melting point of the cobalt but below that of the carbide. There were too many of the solid, interlocking carbide particles for any "floating" segregation to occur, but the liquid cobalt phase dissolved tungsten carbide to an amount of about 18% of its own weight (thus, the proportion was about 93% solid carbide and 7% liquid). On cooling, most of the carbide that was dissolved in the liquid cobalt precipitated on the undissolved carbides already present (again, preferred nucleation) and left the final particles in this characteristic crystalline form.

Micro. 15.5. Sintered carbon steel; ×1,000. Carburized iron powder was compacted at 50,000 psi, sintered 1 hr at 1120°C (2050°F), and slowly cooled. The structure is that of an annealed steel containing about 0.30% carbon; it shows ferrite and coarse pearlite. In addition, a few oxides are visible and some small pores.

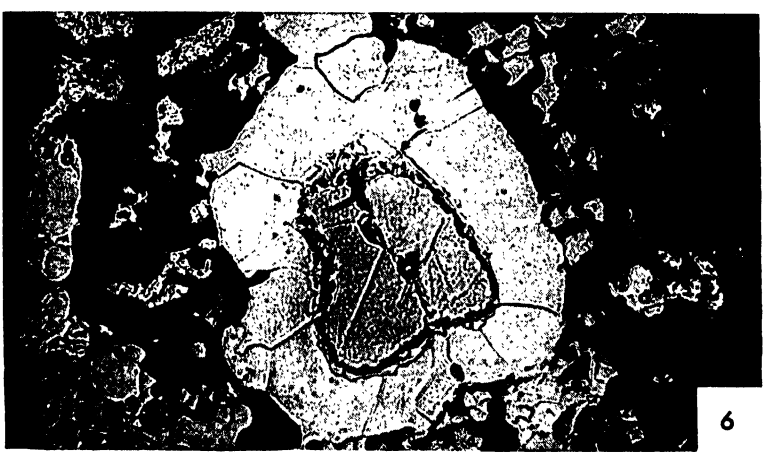

Micro. 15.6. Diffusion of Zn into Cu powder; ×1,000. Zn and Cu powders were heated together (without pressing) at a temperature at which no melting occurred and the loose powders did not sinter. The large particle shows a core of copper, a narrow zone of α and a wide zone of β brass. Small particles in this photograph have been completely converted to the β phase. All these structures resulted from an inward diffusion of zinc, in the form of a vapor, from the surface of the copper particles.

(sometimes in a slightly carburized condition) is being processed by pressing and sintering to make gears and other similar parts. The basis of this application is purely economic; powder methods can produce a large number of articles to a close dimensional tolerance at a low unit cost if the metal powders are not too expensive. The additional cost of metal in a powdered form and of pressing and sintering equipment may frequently be more than offset by the saving in the gross weight of metal and the costs of removing excess by machining of forgings or castings.

Although brass is ordinarily cast or wrought, the micrograph showing diffusion of zinc into copper particles is illustrative of the diffusion process occurring during sintering, which converts pure metal powders into alloyed aggregates. Powdered copper-base alloys were mentioned previously as being of importance in the field of bearings, and, in this application, structures can be obtained with a degree of porosity greater than any foundry can produce. Of course, the important aspect is a *controlled* dispersion of porosity for soaking up oil without having large areas with no supporting metal underneath. The spot-welding industry owes its economic usefulness very largely to the development of a Cu:Mo alloy, necessarily produced from powders, for tips on the contact electrodes. As in the Ag:Mo alloy, the copper is continuous and supplies the required conductivity while the refractory molybdenum prevents the material being welded from fusing to the electrodes with an associated sticking, tearing, and necessity for frequent tip-redressing.

Finally, it is possible to produce from powders aggregates of metals and nonmetals, such as asbestos, to meet specific service requirements not attainable otherwise. It is not within the scope of this book to discuss all these possibilities or to dwell on the actual forming and sintering methods employed in producing the structures. The size and shape of the original metal-powder particles, the pressing temperature and pressure, the sintering temperature and time, are all factors affecting the final density and structure and are subjects of active experimentation. It is sufficient to say here that, under optimum conditions, dispersions of two or more phases can be created in a form not attainable by normal methods of casting, working, and heat-treating. Consequently the aggregates may have unusual and very valuable properties for specific applications. However, the structures are still amenable to reasoning based on phasial relationships, deformational characteristics, etc., as covered in this book.

REFERENCE

JONES, "Principles of Powder Metallurgy," Longmans, 1937.

CHAPTER 16

GENERALIZATIONS

Nonferrous metals differ among themselves, as well as from irons and steels, in their response to alloying and to mechanical and thermal treatments. However, the differences are essentially in the degree, not in the kind, of reactions encountered; all metals and alloys have been found to follow the same general pattern of behavior. Variations in the details of the pattern are shown to a considerable extent by the specific alloy phase diagrams although, it should be emphasized, these deal with the constitutional or phasial relationships and not directly with structures. Structures may be varied, by mechanical or thermal treatments, without disturbing the phasial equilibrium in a chemical sense (*e.g.*, cold-working, or spheroidization of carbides in a steel). In other cases, a high-temperature treatment may be required to change the number or kind of phases present in order to obtain a new and controlled distribution of these phases. The constitutional diagrams are highly useful in disclosing the basic structural elements available, as a function of the alloy composition, and frequently are useful in realizing the potential values of the alloy.

16.1 Binary-phase Diagrams

1. Between two separate single-phase fields, there is always a region, in concentration and temperature, of alloys containing a mixture of the two phases.

2. At a given temperature T in a two-phase field, the *equilibrium* composition of each of the two phases is given by the intersections of a horizontal line, drawn at T, with the two-phase field boundary lines. By Gibbs's phase rule, when the temperature of an alloy in this field is varied, the composition of each phase is automatically fixed.

3. The relative proportions of the two phases for a specific alloy at T are given by the lever rule (see page 59).

4. At all compositions along a horizontal line of the diagram, three (and only three) phases can coexist. The situation is most simply represented by an equation in which the phase meeting the horizontal

in the form of a notch somewhere along its length is in equilibrium with the two phases at the ends of the horizontal (*e.g.*, eutectic, Chap. 5; peritectic, Chap. 8; eutectoid, Chap. 9; monotectic, Chap. 15). In a binary alloy, the coexistence of three phases is possible only for specific fixed compositions of each phase and at a fixed temperature; *i.e.*, the period of their coexistence is indicated by a constant temperature on a cooling curve.

5. Equilibrium conditions may be attained only upon extremely slow heating or cooling and, in general, time may approach temperature in importance when metallurgical reactions are considered. The phase diagram enables one to predict qualitatively the direction of departures from equilibrium encountered in commercial alloys.

6. The degree to which a phase change in the solid state can be suppressed depends on the degree of the compositional readjustments that are involved, as shown by the phase diagram. A phase change in the solid state can be completely suppressed by rapid cooling when and only when the change involves solely a considerable compositional readjustment requiring diffusion, *e.g.*, precipitation from supersaturated solid solution. If a lattice change also is involved, the diffusional part of the phase change may be suppressed, but shearing movements of atoms upon decreasing temperature will generally enable the lattice change to take place to some degree, *e.g.*, martensite transformations.

16.2 Microstructures

1. Homogeneous single-phase alloys show a uniform structure with grain boundaries (or twins) as the only distinguishable detail. In etched nonhomogeneous (cored) solid solutions, the dendrites in the cast structure may efface grain boundaries (see Chap. 3).

2. In hypo- or hypereutectic alloys, the eutectic, if present in sufficient amounts (usually 5 to 10% of the structure is enough), appears as a continuous, two-phase structure surrounding primary dendrites of the excess phase.

3. When a second phase forms in a solid alloy under circumstances requiring diffusion, it appears first, or in greatest quantities, at grain boundaries of the phase already present, unless the alloy is in an unstable or cold-worked condition, when nucleation may be quite general. If formation of the new phase does not involve diffusion, as in the martensite transformation, nucleation is general throughout the structure.

4. Preferred nucleation may considerably alter the structure resulting from eutectoid and similar reactions. Thus carbide spheroids in eutectoidal austenite transforming at 700°C may induce the formation of spheroidal carbides in ferrite rather than lamellar carbides; graphite

nodules in the austenite may induce the eutectoidal formation of ferrite and more graphite.

5. The orientation of a new solid phase must be crystallographically related to that of its parent solid phase as a result of the necessity of lattice matching during nucleation of the new phase. When the new structure grows in the form of plates, needles, or polyhedra, these form a geometrical pattern called a *Widmanstätten structure.*

6. Undercooling tends to increase the nucleation rate of a reaction, whether it is a solidification process or the separation of one or more new phases from the solid state, with a corresponding decrease in grain or particle size. Reactions involving diffusion of two elements may be entirely suppressed by rapid cooling with the appearance of metastable or transitional phases. The alloy concentration of eutectics and eutectoids may be increased, decreased, or widened to a range by undercooling.

7. The structure obtained by heating any alloy to a specific temperature T is stable and will remain unchanged for any lower temperature, regardless of the cooling rate, *unless* the phase diagram indicates a change of composition or structure occurring between T and room temperature. Thus, a structure may be stabilized by heating to a temperature slightly above that encountered in service.

8. Disperse particles of a second phase are subject to growth, generally in a spherical form, if heated for long periods of time at a high temperature unless (*a*) the phase is completely insoluble, or (*b*) it is completely soluble, in which case, the particles disappear.

16.3 Properties

1. The strength and hardness of metals are increased by

a. Decreasing the grain size (effect small, except for extremely fine grains, see Chap. 4).

b. Cold deformation (effect moderately strong, see Chap. 4).

c. Adding another element in solid solution (effect generally small but variable for different solute elements and concentrations and greatest when the solution is inhomogeneous or cored, see Chap. 3).

d. The presence of a second phase in a moderately coarse form (effect moderate, see Chaps. 5 to 9).

e. The presence of a second phase in an extremely fine dispersion (effect very strong, see Chaps. 6, 7, and 10).

2. Ductility properties generally decrease to an extent proportional to the increase in strength (important exceptions; a few solid solutions such as α brass, Chap. 3, certain age-hardenable alloys, Chap. 6, and a part of the range of *pearlite* and *bainite* structures, Chap. 10).

3. In two-phase alloys, the mechanical properties (particularly

plasticity) are basically determined by those of the *continuous* phase in the structure even though it is present in relatively small proportions (for example, hypoeutectic Al:Si and Al:Cu alloys, Chap. 6). A general quantitative law has been proposed[1] stating that the resistance to deformation of a two-phase structure consisting of a plastic matrix and a disperse hard constituent varies linearly with the logarithm of the average length of uninterrupted path through the continuous phase.

4. Physical as well as mechanical properties are affected by structural variations. For example, both thermal and electrical conductivities are decreased by addition elements in solid solution. When an element is added in amounts exceeding the solubility limit, the effect of the second phase appearing in the structure will depend on the conductivity of that phase and its dispersion; if it has a low conductivity and forms a *continuous* structure, it will have an effect disproportionate to the amount present. Other physical properties, such as magnetism, are frequently more related to atomic structure than to the visible microstructure.

5. Corrosion properties are not amenable to many generalizations, but one of considerable importance, associated with structure, is as follows: the localized precipitation of a second phase at grain boundaries of the matrix solid solution may result in a severe, electrolytic-cell type of corrosion at the boundary areas with a considerably more serious diminution in strength properties than an equivalent corrosion distributed uniformly over the entire surface.

6. Failure to achieve the expected service life from a metal may often be traced to faulty mechanical details rather than to internal flaws or improper microstructures. Considerable internal porosity may be tolerated in a casting if the porosity occurs in areas subjected to low stresses, *e.g.*, in the center of a section subjected to bending forces. Surface defects, such as scratches, tool marks, or intergranular corrosion "notches," cause high localized stress concentrations; if the surface is a very plastic material, such as annealed copper or aluminum on Duralumin (Alclad), localized plastic flow may reduce the stress concentration to the point where it is insignificant. An equivalent stress concentration at the surface of a less plastic material may seriously reduce the impact or fatigue strength of the metal even when there is no apparent reduction in the ordinary tensile strength.

[1] Gensamer *et al.*, *ASM Preprint*, 1941.

INDEX